UNIVERSITY OF TEXAS ARLINGTON

COASTAL MANAGEMENT PROGRAM – CYCLE 26

BEST PRACTICES IN MODELING SEDIMENT TRANSPORT AND BUDGET ALONG THE TEXAS COAST

Final Report

(CONTRACT NO. 23-020-018-D867)

Prepared for:

Texas General Land Office

1700 N. Congress Avenue, Mail Code 158

Austin, TX 78701

Submitted by:

The University of Texas at Arlington, Arlington, Texas, USA

September 2024

ACKNOWLEDGMENT

This report was funded by a Texas Coastal Management Program grant approved by the Texas Land Commissioner, providing financial assistance under the Coastal Zone Management Act of 1972, as amended, awarded by the National Oceanic and Atmospheric Administration (NOAA), Office for Coastal Management, pursuant to NOAA Award No. NA21NOS4190136. The views expressed herein are those of the author(s) and do not necessarily reflect the views of NOAA, the U.S. Department of Commerce, or any of their subagencies.

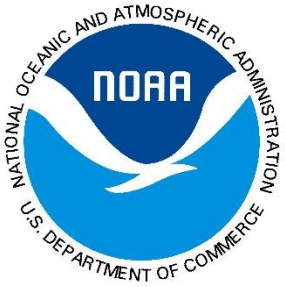

EXECUTIVE SUMMARY

This report presents the findings of the COASTAL MANAGEMENT PROGRAM – CYCLE 26 BEST PRACTICES IN MODELING SEDIMENT TRANSPORT AND BUDGET ALONG THE TEXAS COAST project. The study explores uncertainties and errors in current sediment transport and budget practices, aiming to provide recommendations for best practices in sediment transport modeling in support of coastal sediment management. It includes a comprehensive literature review of sediment supply to the Texas coast and a survey of modeling practices for sediment transport and budget estimations. In addition, the project features case studies on two significant river systems: Brazos-San Bernard and Colorado. Finally, the project findings advocate for key considerations in sediment transport modeling towards a holistic coastal management approach.

This report is structured into two main sections, a main body and four appendices, each corresponding to a key task of the project. The first appendix provides a comprehensive review of recent literature on sediment budget studies along the Texas Coast, analyzing assessments of major waterbodies and identifying gaps in existing research. The second appendix explores current practices in sediment dynamics modeling in coastal areas, comparing various hydro-morphodynamic models and their applications. The third appendix details morphodynamical scenario analyses for the Brazos and Colorado Rivers, employing advanced numerical modeling techniques to investigate the complexities of sediment transport in these areas. The final appendix consolidates the findings from previous tasks, presenting case studies that demonstrate real-world implications of sediment transport modeling and offering recommendations for best practices, including the importance of analyzing multiple scenarios and choosing appropriate modeling platforms while setting realistic expectations for model capabilities. The study emphasizes accurate representation of flow-sediment load relationships and addresses the challenges of scale issues between short-term and long-term processes. It also highlights the significance of integrating local coastal features and determining sources and sinks. The research recognizes the limitations of stationarity assumptions in sediment transport regimes and stresses the need to incorporate sea level rise in modeling efforts. Additionally, the study underscores the importance of addressing wave input and nearshore transformation in understanding sediment dynamics. The report concludes with a synthesis of our findings and their implications for coastal management strategies. It provides guidance for researchers, coastal managers, and policymakers on improving sediment transport modeling practices and developing more effective, sustainable approaches to coastal management along the Texas coast and in similar environments worldwide.

Table of Contents

EXECUTIVE SUMMARY 3

1. INTRODUCTION 5

2. OVERVIEW OF THE KEY CONSIDERATIONS IN SEDIMENT TRANSPORT MODELING 7

3. CONCLUSIONS 8

List of Appendices

APPENDIX A: TASK 1 REPORT

APPENDIX B: TASK 2 REPORT

APPENDIX C: TASK 3 REPORT

APPENDIX D: TASK 4 REPORT

1. INTRODUCTION

Coastal environments, particularly sedimentary coasts and barrier systems found along the Gulf of Mexico, are dynamic and complex interfaces between land and sea. The intricate interaction of hydrodynamics, sediment movement, and geomorphological changes presents significant challenges in coastal management. Understanding and predicting sediment transport is necessary for sustainable coastal development and protection, as it fundamentally influences coastal behavior and evolution. This document is the final report for the project "COASTAL MANAGEMENT PROGRAM – CYCLE 26 BEST PRACTICES IN MODELING SEDIMENT TRANSPORT AND BUDGET ALONG THE TEXAS COAST." This GLO Sediment Management Plan project examined the complexities of sediment transport estimates and modeling, the uncertainties involved and challenges in accurately predicting sediment delivery to the Gulf which thereby affects coastal projects.

As highlighted in this study, current sediment analysis methods often rely on simplified assumptions that limit accuracy. Key limitations include: applying Load Duration Curves (LDCs) from upstream to downstream without accounting for spatial variations in sediment regime; neglecting sediment contributions from lateral flow and bank erosion, especially during high-flow events; overlooking hysteresis effects and reverse flows in sediment-discharge relationships; failing to address supply-limited sediment budgets, particularly for fine sediments; and ignoring salinity impacts on cohesive sediment deposition at the estuary-ocean interface. Additionally, climate change and sea-level rise further complicate these processes, altering coastal hydrodynamics and increasing erosion risks. To address these limitations, this study explored utilizing advanced numerical modeling techniques and incorporating the latest developments in sediment transport theory and coastal hydrodynamics. These models help assess uncertainties and potential inaccuracies in current practices, providing coastal managers and stakeholders with more accurate information for future planning.

Task 1 of this project conducted a comprehensive review of recent literature on sediment budget studies along the Texas Coast. This review aimed to analyze assessments of major waterbodies, scrutinize methodologies, and identify gaps in existing research. The study focused on eleven waterbody systems that drain into the Gulf of Mexico, including major rivers flowing into the Texas Coast and natural and built passes. For each system, the review provided detailed descriptions of watershed characteristics, daily flow statistics, annual sediment yield, and information on sediment input from rivers. It also examined sediment input from shoreline erosion and deposition rates where available. The study identified three distinct approaches used for sediment budget analysis along the Texas Coast: quantitative methods, geomorphological models, and field surveys and sampling. Key findings highlighted significant gaps and uncertainties in sediment data, including limited historical sediment data from USGS gauges, uncertainties in

estimating sediment inputs from fluvial sources and coastal shoreline erosion, and limited available data on sediment outputs due to dredging and longshore transport. The review emphasized the need for enhanced methodologies, data integration, and collaborative research efforts to improve the accuracy of sediment budgeting along the Texas Coast, which is crucial for informed coastal management strategies in the face of ongoing environmental changes and anthropogenic activities. Task 2 of this project conducted a literature review on the current state of practice in sediment dynamics modeling in coastal areas. The study examined common frameworks for modeling sediment dynamics in coastal rivers and estuaries, identified the advantages and shortcomings of widely used hydro-morphodynamic models, and explored uncertainties and errors in current sediment transport modeling practices. The review compared quantitative sediment budget models with hydro-geomorphological models, highlighting their respective strengths and limitations. It provided a detailed assessment of nine widely-used hydro-geomorphological models (Delft3D, TELEMAC, MIKE 21, ADCIRC, XBeach, LITPAK, CoSMoS, GENESIS, and SBEACH), focusing on their application in coastal settings and their ability to simulate complex interactions between hydrodynamics, sediment transport, and morphological changes. The study emphasized the importance of selecting appropriate models based on project requirements and environmental conditions. It also identified potential areas for future improvement in sediment dynamics modeling. This review offers valuable insights for researchers and coastal managers in choosing and applying suitable models for sediment transport studies in coastal areas. Task 3 of this project focused on morphodynamical scenario analyses for the Brazos River and the Colorado River, contributing to the Texas General Land Office (GLO) Sediment Management Program. The study employed advanced numerical modeling techniques, specifically the Delft3D Flexible Mesh software, to investigate the complexities of sediment transport modeling in these coastal areas. The research explored various scenarios to highlight uncertainties and potential variability in the results of current sediment transport modeling practices. Key findings included the significant impact of factors such as morphological acceleration, selection of representative flow, sediment type (mud versus sand), and the use of lumped versus spatially variable sediment influx on sediment transport patterns. The study demonstrated that current morphodynamical models can simulate complex phenomena like the opening of a river mouth during a hurricane, but also discussed remaining challenges. It highlighted the limitations of current approaches to determining representative flows and proposed using duration-based flow values with morphological acceleration as a potentially more robust method for long-term simulations. Importantly, the research emphasized the need for caution when interpreting results from morphologically accelerated models and recommended more comprehensive data collection efforts, particularly for sediment composition and distributed sediment inputs along river reaches. These findings provide insights to inform future studies and improve decision-making processes for coastal management projects in Texas and similar coastal environments.

Task 4 consolidated the previous tasks and findings that confirmed the considerable variability in sediment budget and yield estimates, highlighting how different methods, analyses, and assumptions can lead to divergent results, complicating decision-making for coastal managers and

engineers. It presented a series of case studies that demonstrate the real-world implications and the consequences of inadequate understanding sediment transport processes or modeling. These examples serve as cautionary tales, showing how coastal projects built without sufficient data or understanding of coastal processes can lead to unforeseen and often problematic outcomes. It also addressed the shortcomings of purely data-driven management efforts, noting that while more data is an obvious solution, most collection campaigns provide only snapshots of the dynamic and non-stationary nature of coastal system. This limitation underscores the importance of modeling in complementing data, while also acknowledging the challenges inherent in modeling such complex systems. This task concluded with recommendations for best practices in sediment transport modeling. These include adopting a comprehensive approach that integrates thorough data collection with thoughtful, scenario-based modeling techniques. By considering multiple scenarios and employing state-of-the-art modeling approaches, coastal managers and engineers can use their best available tools to better recognize the uncertainties inherent in coastal systems and work towards more effective and sustainable coastal management strategies.

The following section is developed based on findings from previous this project and outlines general guidelines for modeling sediment transport and budget processes to support sustainable decision-making along the Texas coast.

2. OVERVIEW OF THE KEY CONSIDERATIONS IN SEDIMENT TRANSPORT MODELING

Sediment transport modeling is a complex field with numerous important considerations. Analyzing multiple scenarios is crucial, allowing modelers to explore a range of potential outcomes from baseline conditions to gradual environmental changes and extreme events. This approach provides a comprehensive understanding of how different factors interact over time, enabling planners to identify robust strategies and anticipate unexpected consequences.

Choosing the appropriate modeling platform is essential, as different models suit different scales and purposes. Watershed-scale models like SWAT are designed for long-term simulations at low spatial resolutions, making them suitable for modeling sediment at the watershed level. However, they struggle with event-based simulations and complex flow dynamics, particularly in coastal regions. Hydrodynamic and morphodynamic models are better at simulating detailed sediment transport dynamics in specific water bodies, including rivers, estuaries, and coastal areas. An ideal approach may involve combining watershed-scale models with hydrodynamic models, though this is challenging and heavily dependent on data availability.

Setting realistic expectations for model capabilities is essential. Sediment transport processes are inherently complex and difficult to simulate precisely. While process-based models often prove more capable than those relying solely on data, they still have significant limitations. These models should be used with a clear understanding of their limitations and not be mistaken for infallible

predictive tools in complex coastal systems. Selecting relevant processes for modeling is also very important, as is determining sediment influx entry points and sinks.

The transport of sediment in most rivers is affected by many interdependent factors along the main stem and tributaries, basin hydrology, water-resource development, and human activities. Representing flow-sediment load relationships accurately is challenging, as Load Duration Curves (LDCs) can oversimplify complex flow patterns and sediment transport processes.

Addressing scale issues is also necessary, particularly when bridging the gap between short-term hydrodynamic processes and long-term morphological changes. Modelers can tackle this by implementing a "morphological acceleration factor" and simulating "morphological tide" to understand and predict long-term effects of tidal forces on coastal morphology.

Recognizing the limitations of stationarity assumptions is also crucial, as sediment transport regimes can change over time due to various factors such as reservoir construction, changes in land use, and instream sand and gravel mining. Incorporating sea level rise into models is increasingly important for long-term coastal management, as it fundamentally alters coastal environments and amplifies the challenges of non-stationarity.

Integrating local features such as tidal inlets, barrier islands, coastal structures, nearshore bathymetry, and coastal vegetation is vital for accurate predictions. These features significantly influence sediment dynamics and create complex patterns of wave breaking and nearshore currents.

Finally, addressing wave input and nearshore transformation is critical for understanding how waves interact with coastal topography and affect sediment transport and shoreline morphology. This often involves coupling different types of models, such as wave, current, and morphological models, to develop targeted coastal management strategies.

3. CONCLUSIONS

This comprehensive study on sediment transport modeling along the Texas coast underscored the complexity and importance of understanding coastal sediment dynamics. The project, spanning multiple tasks, has revealed significant challenges in accurately predicting sediment delivery to the Gulf of Mexico and its effects on coastal projects.

Key findings highlight the limitations of data and current sediment analysis methods, including oversimplified assumptions and the neglect of critical factors such as spatial variations in sediment regimes, lateral flow contributions, and the impacts of climate change and sea-level rise. The study emphasizes the need for advanced numerical modeling techniques and the incorporation of the latest developments in sediment transport theory and coastal hydrodynamics to address these limitations.

Furthermore, the project highlights the non-stationary nature of coastal systems and the need for continuous data collection and model refinement. It cautions against over-reliance on purely data-driven management efforts and emphasizes the complementary role of modeling in understanding complex coastal processes.

The research also stresses the importance of a holistic approach to coastal sediment management. This includes combining quantitative data, numerical models, and field surveys, as well as integrating watershed-scale with hydrodynamic and coastal processes. The study advocates for scenario-based modeling techniques to account for uncertainties involved.

Ultimately, this study provides valuable insights and recommendations for best practices in sediment transport modeling. It calls for a more nuanced, comprehensive approach to coastal management that acknowledges inherent uncertainties while targeting for more accurate predictions. By adopting these practices, coastal managers and engineers can work towards more effective and sustainable coastal management strategies, vital for the long-term health and resilience of the Texas coastline.

UNIVERSITY OF TEXAS ARLINGTON

COASTAL MANAGEMENT PROGRAM – CYCLE 26

BEST PRACTICES IN MODELING SEDIMENT TRANSPORT AND BUDGET ALONG THE TEXAS COAST

Task 1: Literature Review of Sediment Supply to Texas Coast

(CONTRACT NO. 23-020-018-D867)

Prepared for:

Texas General Land Office

1700 N. Congress Avenue, Mail Code 158

Austin, TX 78701

Submitted by:

Habib Ahmari, Ph.D., P.E.

Nabila Khandaker, M.Sc.

Yu Zhang, Ph.D.

Behzad Nazari, Ph.D., P.E.

The University of Texas at Arlington, Arlington, Texas, USA

February 2024

EXECUTIVE SUMMARY

The Texas coastline faces ongoing challenges related to coastal erosion, a process influenced by factors such as storm events, sea-level rise, and human activities such as coastal development. Hurricanes and tropical storms contribute significantly to erosion, causing the gradual wearing away of land. Rising sea levels, associated with climate change, exacerbate erosion by increasing the frequency and severity of flooding events. Human interventions, including infrastructure projects and navigation channels, can alter natural sediment dynamics, impacting erosion rates.

Sediment budgets, accounting for sediment sources, transport, and sinks, play a crucial role in understanding coastal systems. Various agencies, such as the Texas General Land Office (TGLO) and the U.S. Army Corps of Engineers (USACE), are involved in coastal shoreline monitoring and managing. Strategies include beach nourishment, dune restoration, and protective structures. Ongoing research and collaborative efforts aim to develop effective mitigation strategies and adapt to the dynamic coastal environment in Texas.

This study conducts a comprehensive review of recent literature on sediment budget studies along the Texas Coast, aiming to analyze assessments of major waterbodies, scrutinize methodologies, and identify gaps in existing research. The focus of the review extends to major rivers flowing into Texas Coast and natural and built exchange points. Eleven waterbody systems are considered, maintaining consistency with previous research. For each system, the review provides detailed descriptions of watershed characteristics, encompassing size, rivers, major creeks, reservoirs, and climate details. Additionally, it presents daily flow statistics, annual sediment yield, and information on sediment input from rivers within the watershed, drawing from sources such as USGS gauges, previous studies, and watershed sediment yield studies. The review also examines sediment input from shoreline erosion and sediment deposition rates, where available, to comprehensively assess contributions to each waterbody's sediment budget. Finally, the study quantifies sediment delivery from each waterbody to the Gulf of Mexico based on developed sediment budgets for adjacent coastal areas.

In this review, approaches used for sediment budget analysis along the Texas Coast are identified, and their pros and cons are presented. Regardless of the method employed, accurate estimates of sediment sources and sinks are crucial and remain a major gap. The review presents available information on primary sediment sources (fluvial sources and shoreline erosion) and sinks (dredging and longshore transport), addressing gaps and uncertainties in sediment data.

The key findings from this review and possible gaps in the sediment budget analysis of the Texas Coast could encompass the following:

- Three distinct approaches used for sediment budget analysis along the Texas Coast are identified: quantitative methods, geomorphological models, and field surveys and sampling. Hydro-geomorphological models, considered the most accurate approach to sediment budgeting in coastal areas, have been utilized only for the Brazos River Estuary, Laguna Madre system, and Rio Grande Estuary. Quantitative methods have been applied to the

sediment budget analysis of the East Texas Coast from Sabine Pass to San Luis Pass, as well as coastal areas between Freeport Entrance and Matagorda Ship Channel. However, such analyses have not been undertaken for other parts of the Texas Coast. Field surveys and sampling have been conducted for the entire Texas Coast; however, many of these studies were carried out several decades ago, and their findings may not accurately represent the current status of sediment dynamics in these areas.

- The sediment inputs from fluvial sources to the Gulf of Mexico (either directly or through coastal bays and lagoons) have been estimated from historical sediment data collected at gauge stations or by utilizing empirical formulas for calculating overland erosion and sediment yield for a given point in a watershed. Limited historical sediment data from USGS gauges and ungauged watersheds in the study area introduce uncertainties into sediment inputs, which are necessary for an accurate sediment budget analysis. Moreover, at the majority of gauge stations, only suspended load has been measured, leaving the contribution of bedload to the total load unknown. Estimating sediment load into the Gulf of Mexico from sediment yield empirical formulas is based on a study prepared more than four decades ago, and various factors influencing soil erosion may have changed since the completion of this study, affecting the sediment load. The inherent uncertainty of soil erosion empirical formulas, coupled with the lack of a comprehensive examination of the accuracy of their results through field observations, contributes to the uncertainty surrounding sediment yield estimates. The comparison between the annual sediment load calculated from historical sediment data from USGS gauges and empirical overland erosion methods showed significant differences. For the Sabine River, the estimate from the sediment yield empirical formula is as much as 3-4 times higher than the annual sediment loads estimated using USGS data.

- The sediment inputs from coastal shoreline erosion have been estimated by tracking the long-term movement of the Texas Gulf shoreline from aerial photos, satellite images, and other sources. Factors such as the scale and resolution of aerial photos, the dynamic nature of coastal processes, and potential human errors in interpretation may contribute to uncertainties in shoreline measurements. While the rate of shoreline movement is available for the Texas Gulf Coast between Sabine Pass and the Rio Grande, such information is available only for some bays, including Galveston Bay, Matagorda Bay, San Antonio Bay, and Aransas Bay. The lack of shoreline erosion rates in other bays adds to the uncertainties in the sediment budget of the Texas Coast.

- The sediment outputs from the coastal area include sediment loss due to dredging and wave-driven longshore sediment transport. The primary sources of uncertainty in the volume of dredged material within the Gulf Intracoastal Waterway (GIWW) are attributed to the method of estimating the quantity of dredged material, sediment characteristics such as density and composition, and incomplete or inaccurate documentation of dredging activities. The accuracy of the quantity of dredged material was reported to vary between 10 and 100%.

Sediment loss due to longshore sediment transport has not been thoroughly investigated along the Texas Coast. This analysis requires utilizing geomorphological models to determine sediment fluxes and transport pathways. Such modeling is conducted only for the Laguna Madre and Rio Grande Estuary areas, as well as the Brazos-San Bernard Estuary area.

While substantial progress has been made in understanding sediment dynamics along the Texas Coast, the study underscores the need for enhanced methodologies, data integration, and collaborative research efforts to fill existing gaps. Accurate sediment budgeting is essential for informed coastal management strategies, particularly in the face of ongoing environmental changes and anthropogenic activities impacting the Texas coastline. This study addresses the critical need to comprehend and manage sediment dynamics and budgets along the Texas Coast, emphasizing the ecological, economic, and societal implications of coastal sediment processes. The findings offer valuable insights and recommendations for enhancing sediment management practices in the region, providing best practices recommendations for the Texas General Land Office's Sediment Management Plan.

TABLE OF CONTENTS

EXECUTIVE SUMMARY **1**

1. Introduction **11**
1.1 Coastal Sediment Dynamics 11
1.2 Objectives 11
1.3 Significance of the Study 12
1.4 Overview of Methodology and Approach 12
1.5 Structure of the Report 13

2. Overview of Sediment Budget Analysis **14**
2.1 Basics of Sediment Budget Analysis 14
2.2 Sediment Budget Analysis at Watershed Scale 15
2.3 Sediment Budget Analysis in Coastal Area 15
2.4 Methods of Sediment Budget Analysis 17

3. Sediment Budget of Texas Coast **19**
3.1 Study Area 19
3.2 Sabine Lake System 21
3.2.1 Sabine Lake System Watershed Characteristics 21
3.2.2 Sabine Lake System Sediment Budget 25
3.2.3 Sediment Delivery from Sabine Lake to Gulf of Mexico 29
3.3 Galveston Bay System 31
3.3.1 Galveston Bay System Watershed Characteristics 31
3.3.2 Galveston Bay System Sediment Budget 38
3.3.3 Sediment Delivery from Galveston Bay to Gulf of Mexico 43
3.4 Brazos-San Bernard Estuary System 45
3.4.1 Brazos River Watershed Characteristics 45
3.4.2 Brazos River Estuary Sediment Budget 47
3.4.3 Sediment Delivery from Brazos River to Gulf of Mexico 50
3.4.4 San Bernard River 51
3.4.5 San Barnard River Estuary Sediment Budget 53
3.4.6 Sediment Delivery from San Bernard River Estuary to the Gulf of Mexico 55
3.5 East Matagorda Bay System 57
3.5.1 East Matagorda Bay System Watershed Characteristics 57
3.5.2 East Matagorda Bay System Sediment Budget 59
3.5.3 Sediment Delivery from East Matagorda Bay to Gulf of Mexico 61
3.6 Matagorda Bay System 62
3.6.1 Matagorda Bay Watershed Characteristics 62
3.6.2 Matagorda Bay System Sediment Budget 68
3.6.3 Sediment Delivery from Matagorda Bay to Gulf of Mexico 73
3.7 San Antonio Bay System 76

3.7.1 San Antonio Bay System Watershed Characteristics 76
3.7.2 San Antonio Bay Sediment Budget 82
3.7.3 Sediment Delivery from San Antonio Bay to Gulf of Mexico 85
3.8 Aransas Bay System 86
3.8.1 Aransas Bay System Watershed Characteristics 86
3.8.2 Aransas Bay Sediment Budget 89
3.8.3 Sediment Delivery from Aransas Bay to Gulf of Mexico 91
3.9 Corpus Christi Bay System 92
3.9.1 Corpus Christi Bay System Watershed Characteristics 92
3.9.2 Corpus Christi Bay Sediment Budget 95
3.9.3 Sediment Delivery from Corpus Christi Bay to Gulf of Mexico 100
3.10 Baffin Bay System 100
3.10.1 Baffin Bay System Watershed Characteristics 100
3.10.2 Baffin Bay Sediment Budget 103
3.10.3 Sediment Delivery from Baffin Bay to Gulf of Mexico 105
3.11 Laguna Madre System 106
3.11.1 Laguna Madre System Watershed Characteristics 106
3.11.2 Laguna Madre Sediment Budget 109
3.11.3 Sediment Delivery from Laguna Madre to Gulf of Mexico 113
3.12 Rio Grande System 119
3.12.1 Rio Grande System Watershed Characteristics 119
3.12.2 Rio Grande Estuary Sediment Budget 121
3.12.3 Sediment Delivery from Rio Grande Estuary to Gulf of Mexico 125
4. SUMMARY, GAP ANALYSIS, AND Recommendations 128
4.1 Methodologies, Associated Assumptions, Input Datasets, and Modeling Tools Involved in Sediment Budget Analysis Studies for Texas Coast 128
4.1.1 Quantitative Methods (Mass Balance) 128
4.1.2 Hydro-geomorphological Models 129
4.1.3 Field Surveys and Sampling Approaches 132
4.2 Potential Gaps in the Existing Studies on Sediment Budgets in the Texas Coast 135
4.2.1 Potential Gaps in Sediment Sources 135
4.2.2 Sediment Inputs from Fluvial Sources 135
4.2.3 Sediment Inputs from Coastal Shorelines Erosion 140
4.2.4 Potential Gaps in Sediment Sinks 145
4.3 Key Findings and Recommendations for Future Studies 148
REFERENCES 150

LIST OF FIGURES

Figure 1.1 Major Texas Rivers Discharging to Gulf of Mexico 13

Figure 2.1 Schematic of Sediment Budget Analysis with a Single Cell 14

Figure 2.2 Sediment Sources and Sinks in a Watershed [1] 15

Figure 2.3 Sediment Exchange in Coastal Areas [3] 16

Figure 2.4 Sediment Cell for Budget Analysis and Sediment Sources and Sinks [4] 17

Figure 3.1 Study Area and Eleven Waterbody Systems 20

Figure 3.2 Sabine Lake System Watershed 21

Figure 3.3 Sabine River Watershed and USGS Monitoring Stations 22

Figure 3.4 Neches and Angelina Rivers Watershed and USGS Monitoring Stations 24

Figure 3.5 Sabine Pass Sediment Budget (Reproduced from Ref. [25]) 30

Figure 3.6 Net Rates of Long-term Movement for the Upper Texas Gulf Shoreline Between Sabine Pass and San Luis Pass Between the 1930s and 2019 [27] 31

Figure 3.7 Galveston Bay System Upper Watershed 32

Figure 3.8 Galveston Bay System Sub-watersheds 32

Figure 3.9 Trinity River Watershed and USGS Monitoring Stations 33

Figure 3.10 San Jacinto River Watershed and USGG Monitoring Stations 36

Figure 3.11 Galveston Bay Sediment Budget (Reproduced from Ref. [25]) 44

Figure 3.12 Brazos River Watershed and USGS Monitoring Stations 46

Figure 3.13 Suspended Sand Concentration in the Brazos River at USGS Richmond Station for the Period of 1969-1995 [53] 48

Figure 3.14 Sediment Budget for the Brazos River Estuary Based on Accumulation Rates Over a Period of 50 Years (before 2013). The values in White Boxes Show Sediment Deposition Rate (Thickness Change and Mass Rates) in Different Areas of the Estuary, and Red Arrows Indicate Sediment Loss from the Estuary Area [66] 50

Figure 3.15 Brazos River Delta Sediment Depositional Areas [67] 51

Figure 3.16 San Bernard River Watershed and USGS Monitoring Stations 52

Figure 3.17 Locations of Transects for Suspended Sediment Sampling [73] 55

Figure 3.18 Locations of Cells for Sediment Budget Analysis Along Coastal Area between Freeport Entrance and Matagorda Ship Channel (Modified from Ref. [74]) 56

Figure 3.19 Net Rates of Long-term Movement for the Texas Gulf Shoreline Between San Luis Pass and Pass Cavallo from 1930s to 2019 [27] 57

Figure 3.20 East Matagorda Bay System and its Sub-watersheds (Redeveloped from Ref. [76]) 58

Figure 3.21 Shoreline Change in East Matagorda Bay Area (Data Developed by the Texas Bureau of Economic Geology (Adopted from Ref. [84]) 60

Figure 3.22 Grainsize Distribution from Shallow Bed Grab Samples Collected from Matagorda Bay in 2021 (Circles) Overlain with the Sediment Distribution Map Modified from Ref. [85] (Area Marked by the Red Box is Where Sand is Found by Both Studies (Figure 4 in Ref. [86])) 61

Figure 3.23 Matagorda Bay System Watershed 63

Figure 3.24 Colorado River Watershed and USGS Monitoring Stations 64

Figure 3.25 Lavaca River Watershed and USGS Monitoring Stations 66

Figure 3.26 Sediment Rating Curve for the Lavaca River at Edna Station [101] 71

Figure 3.27 Net Long-term (1930s to 2010s) Shoreline Movement Rates in the Copano, San Antonio, and Matagorda Bay Systems [106] 73

Figure 3.28 Depositional Areas in the Colorado River Locks Project Site Study [108] 75

Figure 3.29 San Antonio Bay System Watershed 77

Figure 3.30 Guadalupe River Watershed and USGS Monitoring Stations 78

Figure 3.31 San Antonio River Watershed and USGS Monitoring Stations 80

Figure 3.32 Net Rates of Long-term Movement for the Middle Texas Gulf Shoreline Between Pass Cavallo and the Packery Channel Area (Matagorda Island, San José Island, and Mustang Island) Calculated from Shoreline Positions Between the 1930s and 2019 [27] 86

Figure 3.33 Aransas Bay System Watershed and USGS Monitoring Stations 87

Figure 3.34 Corpus Christi Bay System Watershed 93

Figure 3.35 Nueces River Watershed and USGS Monitoring Stations 94

Figure 3.36 Baffin Bay Watershed and USGS Monitoring Station 101

Figure 3.37 TCEQ Water Quality Stations on Los Olmos, San Fernando, and Petronila Creeks 104

Figure 3.38 Laguna Madre System Watershed 107

Figure 3.39 Arroyo Colorado Watershed and USGS and TCEQ Monitoring Stations 108

Figure 3.40 Total Suspended Solids (TSS) concentrations at TCEQ Stations Located (a) Upstream (TCEQMAIN-13074) and (b) Downstream (TCEQMAIN-13072) on the Arroyo Colorado Tidal Segment Boundary [175] 111

Figure 3.41 Monthly Sediment Load for Arroyo Colorado near Harlingen (TCEQMAIN-13074/USGS-08470400) [170] 112

Figure 3.42 Conceptual Sediment Budget for the Southern Part of the Lower Laguna Madre for the Period of 1980-2008 [176] 113

Figure 3.43 Net Rates of Long-term Movement for the Lower Texas Gulf Shoreline Between Packery Channel and the Rio Grande (Padre Island and Brazos Island) Calculated from Shoreline Positions from the 1930s to 2019 [27] 114

Figure 3.44 Sediment Budget of Laguna Madre System (Cells 1 to 7) in Ref. [177] 117

Figure 3.45 Sediment Budget of Laguna Madre System (Cells 7 to 14) in Ref. [177] 117

Figure 3.46 Sediment Budget of Laguna Madre System (Cells 14 to 21) in Ref. [177] 118

Figure 3.47 Sediment Budget of Laguna Madre System (Cells 21 to 27) in Ref. [177] 118

Figure 3.**48** Rio Grande River Watershed and USGS Monitoring Stations..... 119

Figure 3.49 Suspended Sediment Concentration in Rio Grande at Brownsville (1966-2019) [189] 123

Figure 3.50 TCEQ Monitoring Stations on the Lower Rio Grande..... 124

Figure 3.51 Sediment Budget for Rio Grande Estuary System (Cell 27b A and B) [177] 127

Figure 4.1 East Texas Coast Sediment Budget from Sabine Pass to High Island (Right) and from Bolivar Peninsula and Galveston Island 129

Figure 4.2 Annal Sediment Load of the Brazos River at Richmond and Rosharon Stations Estimated Based on (a) Daily Average Sediment Load, and (b) Sediment Load Rating Curves (**Section 3.4.2.1**) 139

Figure 4.3 Annal Sediment Load to Sabine Lake Estimated Based on (a) Sediment Load Measured at USGS Stations, (b) Sediment Yield Empirical Formulas, and (c) Field Study of Sediment Deposition Rate in Sabine Lak (**Section 3.2**) 141

Figure 4.4 Annal Sediment Load from Brazos River to Gulf of Mexico Estimated Based on (a) Sediment Load Measured at USGS Stations, and (b) Sediment Yield Empirical Formulas (**Section 3.4**) 142

Figure 4.5 Net Rates of Long-term Movement for the Texas Gulf Shoreline Between Sabine Pass 143

Figure 4.6 USACE Galveston District Annual Average Dredged Material by River System (1991-2015) [52]..... 147

LIST OF TABLES

Table 3.1 Sabine and Neches Rivers Annual Daily Discharges at USGS Stations 23

Table 3.2 Sabine and Neches Rivers Suspended Sediment Concentration and Load at USGS Stations..... 28

Table 3.3 Trinity and San Jacinto Rivers Annual Daily Discharges at USGS Stations..... 35

Table 3.4 Trinity and San Jacinto Rivers Suspended Sediment Concentration and Load at USGS Stations..... 41

Table 3.5 Lower Brazos River Annual Daily Discharges at USGS Stations..... 46

Table 3.6 Lower Brazos River Suspended Sediment Concentration and Load at USGS Stations 50

Table 3.7 San Bernard River Annual Daily Discharges at USGS Stations..... 53

Table 3.8 San Bernard River Suspended Sediment Concentration and Load at USGS Station . 54

Table 3.9 Annual volume change in each cell and the net and gross sediment transport rates for Cells 1 to for used in sediment budget calculations [74,75]..... 56

Table 3.10 Annual Volume Change in Each Cell and the Net and Gross Sediment Transport Rates for Cells 1 to for used in the Sediment Budget Calculations in East Matagorda Bay Area [74,75] 62

Table 3.11 Colorado River Annual Daily Discharges at USGS Stations..... 65

Table 3.12 Lavaca River Annual Daily Discharges at USGS Stations..... 66

Table 3.13 Colorado River Annual Suspended Sediment Concentration and Load at USGS Stations..... 70

Table 3.14 Lavaca River Annual Suspended Sediment Concentration and Load at USGS stations 70

Table 3.15 Annual volume change in each cell and the net and gross sediment transport rates for Cells 1 to for used in sediment budget calculations [74,75]..... 76

Table 3.16 Guadalupe River Annual Daily Discharges at USGS Station..... 78

Table 3.17 San Antonio River Annual Daily Discharges at USGS Station..... 80

Table 3.18 Guadalupe and San Antonio Rivers Suspended Sediment Concentration and Load at USGS Stations 83

Table 3.19 Mission River and Aransas River Annual Daily Discharges at USGS Stations..... 88

Table 3.20 Mission River and Aransas River Suspended Sediment Concentration and Load at USGS Stations 90

Table 3.21 Nueces River Annual Daily Discharges at USGS Stations..... 94

Table 3.22 Nueces River Suspended Sediment Concentration and Load at USGS Stations 96

Table 3.23 San Fernando, Petronila, and Los Almos Creeks Daily Discharges at USGS Stations 103

Table 3.24 San Fernando, Petronila, and Los Almos Creeks Total Suspended Solids (TSS) Concentration at TCEQ Stations 104

Table 3.25 Arroyo Colorado Annual Instantaneous Discharges at USGS Station 108

Table 3.26 Arroyo Colorado Suspended Sediment Concentration and Load at USGS Station 110

Table 3.27 Rio Grande Annual Daily Discharges at USGS Stations 120

Table 3.28 Rio Grande Suspended Sediment Concentration and Load at USGS Station..... 123

Table 3.29 Rio Grande River Total Suspended Solids (TSS) Concentration at TCEQ Stations 124

Table 4.1 Summary of the Sediment Budget Analysis Method Employed in Waterbody Systems Along Texas Coast 129

Table 4.2 Samples Studies that Utilized Field Surveys and Sampling Approaches to Assess Sediment Budget in Waterbodies Along Texas Coast 133

Table 4.3 Summary of Available Sediment Data for Streams Discharging into the Gulf of Mexico 137

Table 4.4 Net Shoreline and Land-area Loss between the 1930s and 2019 for the Texas Gulf 144

Table 4.5 Net Shoreline and land-area change between the 1930s and 2019 for the 11 Waterbody System Along Texas Gulf Shoreline (**Figure 3.1**) [27] 144

1. INTRODUCTION

1.1 Coastal Sediment Dynamics

Coastal regions represent dynamic interfaces where land and sea converge, shaping unique ecosystems and providing vital habitats for diverse flora and fauna. Central to the intricate balance of these ecosystems is the perpetual movement and interaction of sediments along the coastline. Sediments, comprising a mix of sand, silt, and clay particles, play a pivotal role in shaping coastal morphology, influencing shoreline stability, and sustaining the delicate equilibrium of marine and terrestrial environments.

The dynamic nature of coastal sediment regime is underscored by the continuous processes of erosion, transport, and deposition. Waves, tides, and currents, driven by meteorological and oceanographic forces, constantly reshape coastlines. Understanding these processes is not only crucial for comprehending the evolving physical characteristics of coastal areas but also for elucidating their broader ecological and societal implications.

Coastal sediments serve as the building blocks of beach systems, barrier islands, and estuarine environments. Their movement is intricately linked to the health of ecosystems, providing essential habitats for marine life and supporting biodiversity. Moreover, sediments act as natural buffers against coastal hazards, mitigating the impact of storms and contributing to the overall resilience of coastal communities.

The Texas Coast encompasses a diverse set of landforms, climates and drainage systems, and the coastal sediment processes are correspondingly varied. Excessive sediment depositions and shoreline erosion are simultaneously challenging the economic vitality of coastal communities, and in many locations, these are shaped by processes taking place off the coast and affected by human-induced disturbances such as damming and land development.

Over the past few decades, many studies have been conducted related to the sedimentation processes along the Texas Coast or inland streams that impact the coast. As the Texas General Land Office (TGLO) is in the process of developing a coordinated plan for sedimentation management in Texas Coast, there is a pressing need to review the current state of the knowledge with respect to sediment budget along the coastal zone, identify gaps in information as well as methodologies that need to be filled to inform the formulation of the plan. The present report summarizes the outcomes of a comprehensive literature survey on coastal sediment budget undertaken by a UTA sponsored by TGLO.

1.2 Objectives

The primary objective of this study was to undertake a comprehensive literature review, examining recent studies that document sediment budgets on the Texas Coast. By conducting this review, our aim was to achieve the following key goals:

- Analyzing documented assessments of major waterbodies, river mouths, and both natural and constructed exchange passes.

- Reviewing the methodologies, associated assumptions, input datasets, and modeling tools employed in each of these studies.
- Compiling a detailed summary of the outcomes while identifying potential gaps in the existing research.

1.3 Significance of the Study

Quantifying and predicting sediment dynamics in coastal zones poses inherent challenges due to the complexity of erosion processes on land and sediment transport in various waterbodies. Consequently, sediment budget estimates are frequently burdened by significant uncertainties arising from deficiencies in transport models and a lack of precise information on sediment supply. The primary contributor to sediment influx in Texas coastal areas is the sediment supplied by runoff and transported by rivers into the Gulf of Mexico. This supply is influenced by climate conditions, freshwater dynamics, land-use changes, and morphological alterations in river channels and floodplains. Current sediment budget analyses often rely on simplistic assumptions about sediment sources, composition, and volume along channels draining into the coastal zone. These assumptions include:

- Direct utilization of load duration curves (LDCs) established at upstream monitoring stations for downstream inlets, without considering longitudinal variations in the LDCs.
- Neglecting sediment supply from lateral flow and bank erosion.
- Overlooking hysteresis, with sustained high sediment loads observed even months after major flood events.
- Inability to specifically address fine, cohesive particles like silt and clay, limited by supply rather than flow magnitude.
- A lack of specific treatment of the impacts of salinity on the deposition of cohesive sediments along the estuary-ocean interface.

This study was initiated to investigate the uncertainties in current practices related to understanding sediment transport and budgets. It aims to provide recommendations for best practices to inform the Texas General Land Office (TGLO) Texas Sediment Management Plan.

1.4 Overview of Methodology and Approach

The research team conducted an extensive literature search using various widely utilized databases and the Google search engine, resulting in the collection and indexing of over 190 references for review. This review encompasses the analysis and summarization of publicly available documents from federal and state agencies (including USACE, USGS, TWDB, GLO, TCEQ, etc.), academic journals, and consulting firms' reports.

The examined documents pertain to the sediment budget of major rivers flowing into the Gulf of Mexico, both directly and indirectly. Specifically, the rivers under review include Sabine, Neches, Trinity, San Jacinto, Brazos, San Bernard, Colorado, Lavaca, Guadalupe, San Antonio, Nueces,

and Rio Grande. Additionally, the review covers natural exchange points such as Sabine Lake, Galveston Bay, Pass Cavallo, Cedar Bayou, Aransas Bay, San Antonio Bay, and Brazos Santiago. **Figure 1.1** visually represents these river systems, their surrounding areas, and the natural exchange passes. To maintain consistency with previous studies, the project area is divided into eleven waterbody systems, as shown in **Figure 1.1**.

Figure 1.1 Major Texas Rivers Discharging to Gulf of Mexico

1.5 Structure of the Report

Chapter 1 functions as an introductory section to this report. Chapter 2 provides an overview of sediment budget analysis in coastal regions. Chapter 3 offers an in-depth literature review on sediment studies relevant to sediment budget analysis along the Texas coast, with a particular emphasis on the sediment transport pathway from the watershed to the Gulf of Mexico. Chapter 4 consolidates the project's findings and highlights potential gaps in sediment data required for sediment budget analysis for Texas Coast areas.

2. OVERVIEW OF SEDIMENT BUDGET ANALYSIS

Sediment budget analysis is a systematic examination of the dynamic interactions governing the transport, deposition, and erosion of sediment within a specified geographical area or environmental system. This process involves assessing the inputs, outputs, and storage of sediment over time, providing a comprehensive understanding of the sedimentation processes at play. Key components of sediment budget analysis include the identification of sediment sources, quantification of transport mechanisms, and evaluation of deposition and erosion patterns. By employing various techniques such as field measurements, remote sensing, and numerical modeling, sediment budget analysis contributes vital insights into the geomorphic evolution of landscapes, coastal areas, and river systems. This holistic approach is essential for effective natural resource management, environmental conservation, and the sustainable development of ecosystems influenced by sediment dynamics.

2.1 Basics of Sediment Budget Analysis

A sediment budget is the process of keeping track of where sediment comes from and where it goes in a drainage basin. It means measuring or estimating how much sediment is gained and lost in a specific area over a set time. The difference between the amount of sediment coming in and going out should exactly match how the sediment volume changes in that area. **Figure 2.1** shows a basic system with just one cell for studying sediment budget. In mathematical terms, we can express the most basic sediment budget with Equation 2.1:

$$I \pm \Delta S = O \tag{2.1}$$

Here, I and O correspond to the sediment coming into and going out of the cell, and ΔS represents the change in sediment within the cell.

The units for I, O, and ΔS typically represent the mass of sediment over time (e.g., kg/yr), although volumes (m^3/yr) can also be employed in a sediment budget. Given that sediment transport often occurs during significant floods, the chosen time scale for each source and sink component becomes crucial. Therefore, whether the sediment budget is calculated over a single storm, multiple years, or decades is a key consideration. Additionally, the measurements used to quantify erosion and deposition (I and S) may involve linear (m), cross-sectional (m^2), or volumetric (m^3) dimensions. For source apportionment, it is essential to have a volumetric or mass rate for all components [1].

Figure 2.1 Schematic of Sediment Budget Analysis with a Single Cell

2.2 Sediment Budget Analysis at Watershed Scale

A sediment budget at the watershed scale refers to a comprehensive assessment of the sources, movement, and deposition of sediment within an entire watershed or river basin. This analysis involves tracking the input and output of sediment across the various components of the watershed, including rivers, tributaries, hillslopes, and floodplains. A sediment budget at the watershed scale takes into account natural processes like soil erosion, transport, and deposition, as well as human activities such as construction, agriculture, and land use changes (**Figure 2.2**), which can significantly impact sediment dynamics.

By quantifying sediment sources and sinks within the watershed, this sediment budget analysis provides valuable insights for managing soil erosion, preserving water quality, and understanding the overall health of the watershed ecosystem. It often involves the use of field measurements, remote sensing, and modeling techniques to assess the complex interactions influencing sediment transport within the watershed.

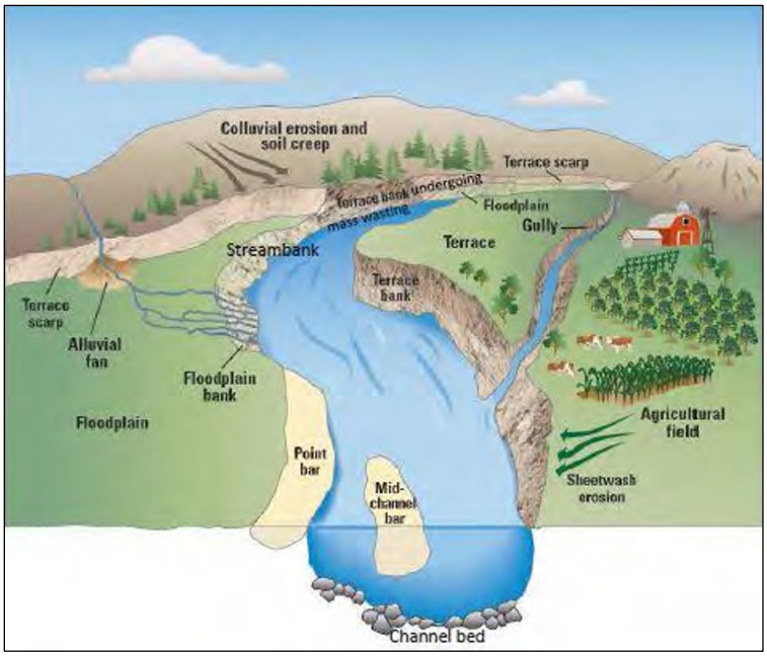

Figure 2.2 Sediment Sources and Sinks in a Watershed [1]

2.3 Sediment Budget Analysis in Coastal Area

Similar to sediment budget analysis in any system, the evaluation of sediment budgets in coastal areas involves examining the equilibrium between changes in the sediment volume stored within the system and the total volumes of sediment entering or exiting the system. Examples of coastal systems include estuarine regions composed of fine (mud-size) sediments to open-coast littoral systems primarily made up of sand-sized sediments [2]. In coastal settings, sediment budget analysis is of particular significance due to the dynamic nature of these areas, often influenced by

factors like tides, waves, and human activities. The sediment exchange in coastal areas is shown schematically in **Figure 2.3**.

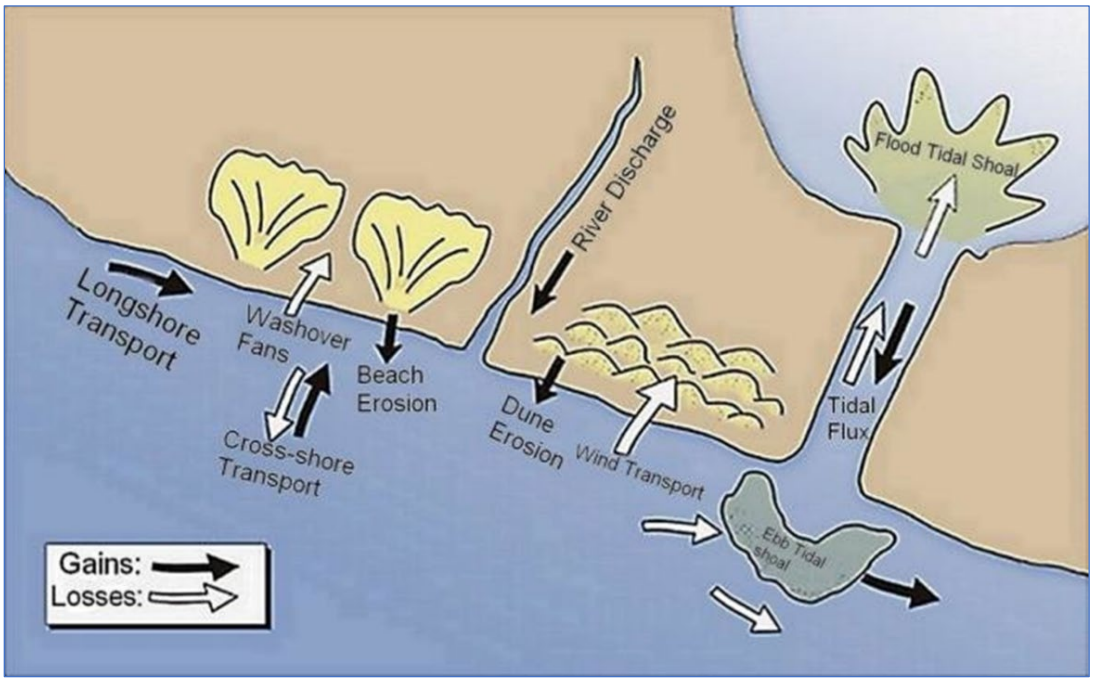

Figure 2.3 Sediment Exchange in Coastal Areas [3]

Defining a series of cells is a standard practice for conducting sediment budgets in coastal areas. Once these sediment cells are defined, it is essential to establish appropriate boundaries for both the overall sediment budget and internal boundaries that separate sub-cells within the designated area. Equation 2.2 may be used to conduct sediment budget calculation within each defined cell [4]. The parameters in Equation 2.2 are shown in **Figure 2.4**. In this figure LST denotes longshore sediment transport.

$$\sum Q_{source} - \sum Q_{sink} - \Delta V + P - R = Residual \qquad (2.2)$$

where:

Q_{source}: sources of sediment to the control volume (cell)

Q_{sink}: sinks of sediment in the control volume (cell)

ΔV: net change in volume within the cell

P and R: amounts of material placed in and removed from the cell, respectively

Residual: degree to which the cell is balanced

To achieve equilibrium in a cell, the *Residual* should be zero. If it deviates from zero, it indicates a potential error in calculating inputs or losses, or there may be an unidentified factor influencing a change in volume.

A sediment budget should reflect a specific time span. When analyzing gradual sediment processes like the formation of a river delta, it is advisable to extend the timeframe to several decades or even a century. This extended duration provides a more precise understanding of sediment dynamics, necessitating the availability of long-term historical data. On the other hand, if the focus is on evaluating the impact of a coastal structure, such as a jetty, a shorter duration can be chosen. However, a budget limited to a few years may be disproportionately affected by atypical physical events, such as unusually severe winter storms or the El Niño-Southern Oscillation [5].

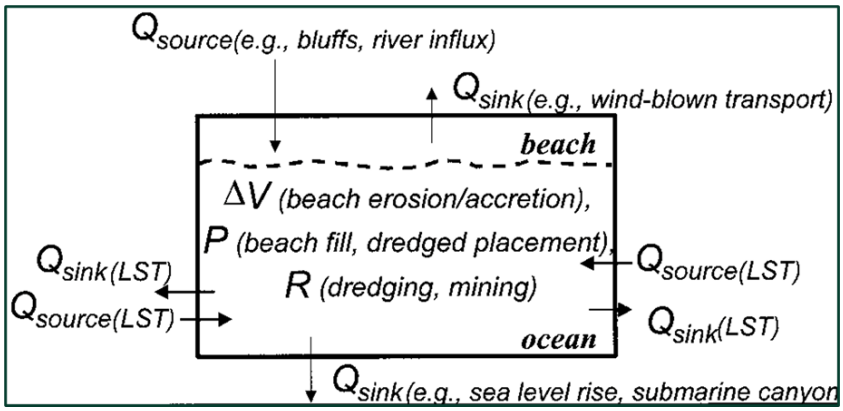

Figure 2.4 Sediment Cell for Budget Analysis and Sediment Sources and Sinks [4]

2.4 Methods of Sediment Budget Analysis

Coastal area sediment budget analysis involves various methods to assess the sources, transport, and sinks of sediment within a given coastal system. Followings are some common methods used in coastal sediment budget analysis:

- ***Quantitative Sediment Budget Models***: The U.S. Army Corps of Engineers, actively involved in coastal and sediment management, has developed tools to aid in the analysis of sediment budgets. Examples of these tools include Sediment Budget Analysis System (SBAS), Sediment Budget Analysis System-A (SBAS-A), and Sediment Budget Calculator (SBC). The SBAS is a PC-based application for calculating and displaying local and regional sediment budgets including single and multiple inlets, estuaries, bays, and adjacent beaches [6]. The SBAS-A is the modified version of SBAS for application within the ArcGIS platform [7]. The SBC is an online webtool that calculates a family of viable solutions for an inlet and adjacent beach sediment budget given site-specific parameters as defined by the user [8].
- ***Hydro-geomorphological Models:*** Several numerical models have been developed that can be used for sediment budget analysis in coastal areas. These models are designed to simulate the various processes involved in sediment transport, erosion, and deposition along coastlines.

Some well-known models include Delft3D, MIKE21, TELEMAC, XBeach, LITPACK, CoSMoS, GENESIS, SBEACH, ADCIRC, etc. When conducting sediment budget analysis, the selection of a model is based on the specific characteristics and processes of the coastal area under study. It is important to note that model selection should be tailored to the goals and scope of the analysis, considering factors such as the scale of the study area, data availability, and the nature of sedimentation processes. These models and their applications in coastal area sediment budget analysis are discussed in Task 2 of the project.

- ***Field Surveys and Sampling***:
  - *Sediment Sampling*: Collecting sediment samples from different locations within the coastal area to analyze their characteristics, including grain size, composition, and organic content, as well as sediment deposition rate and origin.
  - *Bathymetric Surveys*: Measuring and mapping the underwater topography of the seabed to understand changes in sediment distribution and rate of deposition.
  - *Sediment Tracers*: Introducing radioactive and geochemical tracers to track the movement of sediments and identify their sources and sinks.
- ***Remote Sensing***:
  - *Satellite Imagery:* Utilizing satellite data to monitor coastal changes, including shoreline shifts, erosion, and sediment transport patterns.
  - *Aerial Photography:* Analyzing historical and recent aerial photographs to identify changes in coastal morphology over time.

The integration of various methods in sediment budget studies enables the development of a comprehensive understanding of sediment dynamics in coastal areas.

3. SEDIMENT BUDGET OF TEXAS COAST

3.1 Study Area

This review primarily examines the sediment budget of the major rivers that flow into the Gulf of Mexico, either directly or indirectly. These rivers include Sabine, Neches, Trinity, San Jacinto, Brazos, San Bernard, Colorado, Lavaca, Guadalupe, San Antonio, Nueces, and Rio Grande. Additionally, it covers the natural exchange points such as Sabine Lake, Galveston Bay, Pass Cavallo, Cedar Bayou, Aransas, San Antonio, and Brazos Santiago. **Figure 3.1** illustrates these rivers, their surrounding areas, and the exchange passes. To maintain consistency with previous studies, the study area is divided into eleven waterbody systems, as shown in **Figure 3.1.**

In the following sections, for each waterbody system, a description of the watershed characteristics is provided. This section offers information on the size and extent of the watershed, rivers, major creeks, and reservoirs within the watershed, along with climate details (precipitation and temperature statistics), daily flow statistics for rivers and major creeks, and annual sediment yield.

Next, the available information on the quantity of sediment input to the waterbody from the rivers within the watershed is presented. This information is collected from various sources, including USGS gauges, previous studies on stream sediment loads, and watershed sediment yield studies. The study on sediment input from shoreline erosion and sediment deposition rates in the waterbodies, wherever available, was also reviewed, and the contribution to the sediment budget of the waterbody is presented.

Finally, the sediment delivery from the waterbody to the Gulf of Mexico was quantified based on the available sediment budget developed for the coastal area adjacent to the waterbody.

It should be noted that all the quantities presented in this report, including flow and sediment values, are expressed in both the U.S. conventional system of units and the SI system of units. The reason for using a dual system of units is that the flow and sediment quantities are cited from different references that use either of these systems. Presenting the values in both systems would assist those who may use this report in future work and need to refer to the original sources.

Figure 3.1 Study Area and Eleven Waterbody Systems

3.2 Sabine Lake System

3.2.1 Sabine Lake System Watershed Characteristics

The Sabin Lake system encompasses the Sabine River, Neches River, Sabine Lake Estuary, and various reservoirs. These rivers serve as drainage systems for a wide array of landscapes, including forests, wetlands, as well as rural and urban regions. The watershed of the Sabine Lake system holds significant importance from both ecological and economic perspectives. It sustains a diverse range of wildlife and plant species, some of which are rare or endangered. Moreover, the Sabine River and its reservoirs offer recreational opportunities like fishing, boating, and birdwatching, which attract tourists and contribute to the local economies. **Figure 3.2** depicts the Sabine Lake system and its associated features.

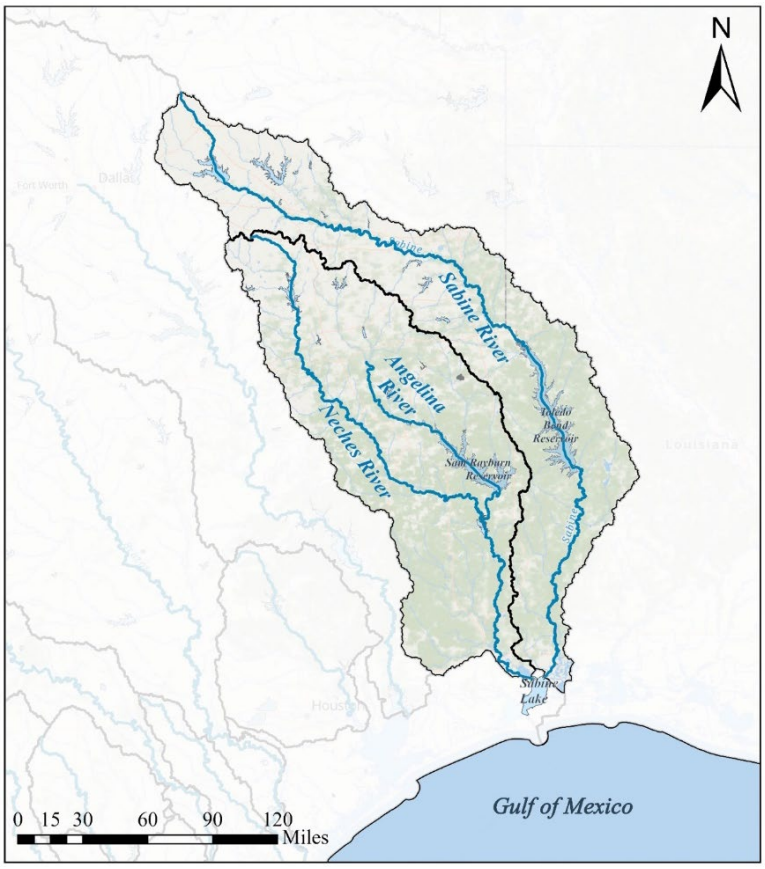

Figure 3.2 Sabine Lake System Watershed

3.2.1.1 Sabine River

The Sabine River traverses the state of Texas and serves as a boundary between Texas and Louisiana. The Sabine River watershed encompasses parts of northeastern Texas, western Louisiana, and southwestern Arkansas, covering an approximate area of 9,756 mi^2 (25,267 km^2). Originating in northeast Texas, the main stem of the Sabine River flows southeast before

eventually reaching Sabine Lake and subsequently the Gulf of Mexico (GoM). The Sabin River watershed and the United States Geological Survey (USGS) gauge stations on this river is shown in **Figure 3.3**. The region experiences a humid subtropical climate, characterized by an average annual precipitation ranging from 43 to 47 inches (1,100-1,200 mm) [9]. The precipitation patterns in this area can fluctuate from year to year are influenced by various factors such as seasonal variations and climate patterns.

Figure 3.3 Sabine River Watershed and USGS Monitoring Stations

The Sabine River exhibits an average daily discharge of approximately 7,963 cfs (225 m^3/s) (**Table 3.1**) at the Deweyville/Ruliff station located about 29 miles (47 km) upstream from its mouth (**Figure 3.3**). Given that this discharge constitutes 95% of the total flow, the estimated river flow at its mouth, where it meets Sabine Lake, is approximately 8,934 cfs (253 m^3/s) [9]. This value represents the long-term average discharge derived from several years of recorded data. It is important to acknowledge that the discharge can vary considerably throughout the year to seasonal fluctuations in rainfall and other contributing factors. The Sabine River is susceptible to high flows during periods of intense precipitation, particularly during tropical storms and hurricanes, which can temporarily elevate the discharge significantly. Additionally, the Sabine River features several dams along its course, and its lower estuary, namely Sabine Lake.

In 1979, an assessment was conducted to determine the erosion, caused by water, and sediment yield in the Sabine River basin. The study estimated the annual sediment yield in the basin to range from 0.1 to 1.02 tons/acre (22 to 229 tonnes/km^2), with an average of 0.21 tons/acre (47 tonnes/km^2) specifically in the Lower Sabine River basin. These figures provide an indication of the amount of sediment carried by water erosion within the specified areas during that particular time period [10].

3.2.1.2 Neches River

The Neches River originates in Van Zandt County, Texas, near Rhine Lake. It flows for approximately 416 miles (669 km) through the lush piney woods of east Texas before ultimately reaching Sabine Lake (**Figure 3.4**). The Neches River watershed encompasses a significant portion of eastern Texas, spanning an area of approximately 9,937 mi^2 (25,736 km^2) [11]. The climate in the Neches River basin is generally mild, although it is prone to various extreme weather events such as hurricanes, tornadoes, droughts, heat waves, cold waves, and intense precipitation [12]. The average annual precipitation in the Neches River watershed ranges from 48 to 60 inches (1,219-1,524 mm) [13].

The average streamflow of the Neches River Saltwater Barrier at Beaumont station, approximately 25 miles (40 km) upstream the location where it empties into Sabine Lake, is 11,100 cfs (314 m^3/s) [14]. For the Evadale station, the average daily discharge is 5,923 cfs (168 m^3/s), ranging from 2,090 to 9,940 cfs (59 to 281 to m^3/s) (**Table 3.1**).

In the Neches River basin, an assessment conducted in 1979 estimated the annual sediment yield to range from 0.08 to 1.08 tons/acre (18 to 242 tonnes/km^2), with an average of 0.16 tons/acre (25 tonnes/km^2) specifically in the Lower Neches River basin [10].

Table 3.1 Sabine and Neches Rivers Annual Daily Discharges at USGS Stations

Station	Drainage Area, mi^2 (km^2)	Period	Discharge, cfs (m^3/s)		
			Max	Average	Min
Sabine River Ruliff [1] (USGS-08030500)	9,329 (24,162)	1924 - 2023	14,800 (419)	7,963 (225)	2,070 (58.6)
Neches River Evadale [2] (USGS-08041000)	7,951 (20,593)	1904 - 2023	9,940 (281)	5,923 (168)	2,090 (59)

[1] https://waterdata.usgs.gov/nwis/inventory/?site_no=08030500&agency_cd=USGS
[2] https://waterdata.usgs.gov/nwis/inventory/?site_no=08041000&agency_cd=USGS

3.2.1.3 Angelina River

The Angelina River is situated in the eastern part of Texas and is primarily located within the Angelina National Forest. Serving as a tributary of the Neches River, it has a watershed that spans approximately 3,070 mi^2 (7,951 km^2) (**Figure 3.4**). The region is characterized by dense forests, wetlands, and a rich diversity of wildlife. The Angelina River is formed by the convergence of

Shawnee and Barnhart Creeks in southwestern Rusk County, near Henderson, Texas. From this point, it flows in a southeasterly direction until it merges with the Neches River on the left bank near Jasper, Texas. The average annual precipitation in the Angelina River watershed falls within the range of approximately 45 to 55 inches (1,143 to 1,397 mm) [13].

In the Angelina River basin, an assessment conducted in 1979 estimated the annual sediment yield to range from 0.46 tons/acre (103 tonnes/km^2) in Upper Angelina River to 0.1 tons/acre (22 tonnes/km^2) in Lower Angelina River [10]. Also, the annual sediment yield was reported as 0.009 to 0.31 tons/acre (2-70 tonnes/km^2) in forested areas [15] and 0.085 to 1.31 tons/acre (19 to 294 tonnes/km^2) in logged areas of the watershed [16].

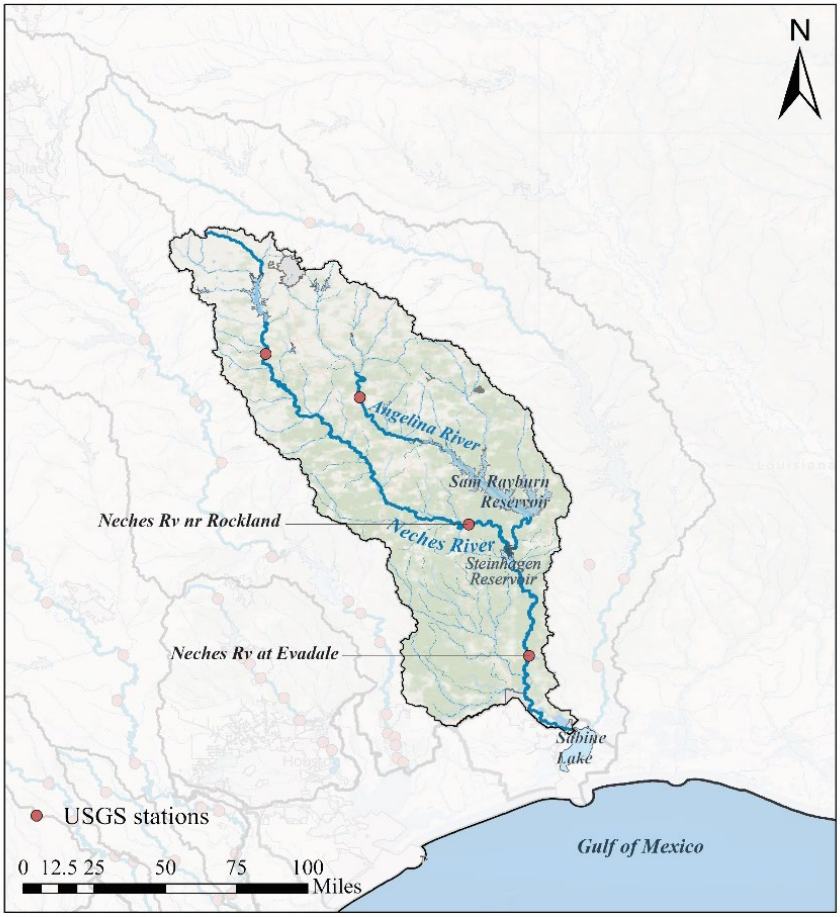

Figure 3.4 Neches and Angelina Rivers Watershed and USGS Monitoring Stations

3.2.1.4 Reservoirs

There are several dams constructed on the Sabine River and its tributaries (**Figure 3.2** to **Figure 3.4**), serving diverse purposes such as flood control, hydroelectric power generation, water supply, and recreational activities. Some of the significant dams on the Sabine River system include:

- *Toledo Bend Dam*: Located on the Sabine River between Texas and Louisiana, Toledo Bend Dam was built in 1967. It has a surface area of about 284 mi^2 (735 km^2) and a capacity of more than 4.5 $\times 10^6$ acre-ft (5.5 $\times 10^9$ m^3) at normal water levels. The Toledo Bend reservoir is one of the largest reservoirs in the United States and serves multiple purposes, including flood control, water supply, hydroelectric power generation, and recreation [9].
- *Sam Rayburn Dam*: Situated on the Angelina River, a tributary of the Sabine River, the Sam Rayburn Dam forms the Sam Rayburn Reservoir. This reservoir is primarily used for flood control, water supply, and recreation.
- *Town Bluff Dam*: Located on the Neches River, a major tributary of the Sabine River in Texas, the Town Bluff Dam creates the B. A. Steinhagen Reservoir (also known as Town Bluff Reservoir). It serves as a flood control structure and offers recreational opportunities.

3.2.1.5 Sabine Lake

Sabine Lake, situated on the Gulf Coast at the Texas-Louisiana border, is an estuary created by the merging of the Sabine River and the Neches River. Both rivers contribute freshwater and sediment to the lake. With an area spanning approximately 45,320 acres (184 km^2) [17], Sabine Lake is linked to the Gulf of Mexico through the Sabine Pass. The estuarine nature of Sabine Lake fosters a wide range of marine and coastal ecosystems, supporting a diverse array of flora and fauna. The combination of freshwater inputs and tidal influence creates a unique and dynamic environment within the lake.

The water in Sabine Lake is brackish, which means it has a mix of both freshwater and saltwater. The level of salinity and turbidity in the lake can vary depending on rainfall, tidal influence, and other factors. The lake is known for its rich biodiversity as the lake and its surrounding marshes and wetlands are home to numerous species of fish, shellfish, and waterfowl. It serves as an important nursery area and feeding ground for various fish species, including redfish, flounder, and speckled trout. The lake also supports migratory bird populations and serves as a vital stopover point during their migration routes.

3.2.2 Sabine Lake System Sediment Budget

The Sabine Lake receives sediment input from the rivers and other sources within its watershed. The dynamics of sediment budgets in estuarine environments can be complex due to factors such as tidal currents, wave action, and the interaction between freshwater and saltwater. Estuaries like Sabine Lake typically act as sediment sinks, meaning they accumulate sediment brought in by rivers and other sources. Sediment entering the estuary tends to settle out due to reduced water velocities and the influence of tides. The amount of sediment that accumulates in Sabine Lake depends on various factors, including the sediment load of the Sabine River and Neches River, tidal dynamics, wind and wave action, and human activities in the area.

Human activities such as channelization, dredging, or land-use changes in the watershed can affect sediment budgets in estuaries. These activities may alter sediment transport patterns, increase erosion, or impact the natural sedimentation processes.

In order to assess the sediment budget of Sabine Lake accurately, it is necessary to conduct a detailed analysis of the sediment input originating from the Sabine River, Neches River, and other contributing sources.

3.2.2.1 Sabine River Sediment Load

The Sabine River carries a significant amount of sediment due to its diverse watershed, including areas with erodible soils and upstream land use practices. However, determining the exact amount of sediment carried by the river is challenging due to variations in flow rates, channel conditions, and sediment transport dynamics. The sediment load can vary significantly from year to year and is influenced by factors such as rainfall patterns, land use changes, and human activities in the watershed. During periods of heavy rain or extreme weather events, the sediment load can increase due to erosion and increased runoff. Dams that are built on the Sabine River and its tributaries trap sediment and have altered the natural sediment transport dynamics of the river system.

The USGS collected data on suspended sediment concentration from 1974 to 1995 at the Deweyville station (USGS-08030500 on Sabine River near Ruliff), located 65 miles (105 km) downstream of the Toledo Bend Dam, and 29 miles (47 km) upstream of Sabine Lake (**Figure 3.3**). It is worth mentioning that approximately 26% or 2,578 mi^2 (6,676 km^2) of the Sabine River watershed lies downstream of the Toledo Bend Dam. During this period, the following sediment quantities in the Sabine River at Deweyville were estimated [9]:

- mean suspended sediment concentration: 39 mg/L,
- mean daily suspended sediment load: 649 ton/day (589 tonnes/day),
- mean annual suspended sediment yield: 237,142 tons (215,132 tonnes),
- mean annual specific suspended sediment yield: 0.04 tons/acre/yr (8.9 tonnes/km^2/yr).

According to a study conducted to investigate the impact of the Toledo Bend Reservoir on sediment transport in the lower Sabine River, no evidence was found to suggest a reduction in sediment transport or alluvial sedimentation in the lower Sabine River as a result of the dam. However, it should be noted that a short scour area was observed immediately downstream of the dam [18]. This indicates that while sediment transport and alluvial sedimentation remained largely unaffected, there was a localized area of increased erosion immediately downstream of the dam.

The total suspended sediment yield from the Sabine River to Sabine Lake was estimated for the period of 1990-2009. The data on suspended sediment were collected at the Merryville station (LDEQ LA110201_00), which is situated approximately 37 miles (60 km) downstream of the Toledo Bend Reservoir (**Figure 3.3**). To estimate the total suspended solids (TSS) concentration, a TSS-discharge relationship specifically developed for the lower Sabine River was utilized. Based on the analysis, the long-term minimum, average, and maximum TSS concentrations during this period were estimated to be 1, 17, and 88 mg/L, respectively. The annual average sediment yield was determined to be 234,902 tons (213,100 tonnes), exhibiting a decreasing trend from 1990 to 2009. The sediment yield ranged from 17,637 tones (16,000 tonnes) in 1996 to 459,664 tons (417,000 tonnes) in 2001 [19]. The study concluded that the construction of the Toledo Bend Dam

did not alter the Sabine River regime, indicating that sediment in the lower Sabine River originates from sources located in the lower part of the river. This finding suggests that the dam did not significantly impact sediment transport from the lower Sabine River to Sabine Lake.

The gradation analysis of sediment data collected from the Deweyville station indicates that the suspended sediment in the lower Sabine River primarily consists of fine particles. On average, approximately 81% of the suspended sediment particles are finer than 0.063 mm in size. However, no specific bedload data is available for the lower Sabine River [9].

The presence of a sandy bed in this particular segment of the river and the occurrence of downstream-migrating sand bars suggested that sediment transport in the form of bedload could potentially be significant in the lower Sabine River [18]. This implies that in addition to the suspended sediment, there is a likelihood of substantial sediment movement along the riverbed, potentially contributing to the overall sediment transport dynamics of the lower Sabine River.

The suspended sediment concentrations and loads in Sabine River for the period of 1974-1995 at the USGS-08030500 station located near Ruliff are summarized in **Table 3.2**.

3.2.2.2 Neches River Sediment Load

Sediment transport in the Neches River occurs as a natural process where sediment particles are transported downstream by the river flow. Several factors influence sediment transport in Neches River, including discharge, channel morphology, sediment characteristics, and human activities such as urbanization, agriculture, and construction of reservoirs.

The USGS collected suspended sediment concentration data downstream of Town Bluff Dam from 1989 to 2000. Additionally, data was collected at the Evadale station (USGS-08041000), located approximately 47 miles (76 km) downstream of the Toledo Bend Dam and 50 miles (80 km) upstream of Sabine Lake (refer to **Figure 3.4**) from 1960 to 2021. It is worth noting that around 21% (817 mi^2 (2,116 km^2)) of the Neches River watershed lies downstream of the Evadale station. For this period, the minimum, average, and maximum suspended sediment concentrations were estimated as 11, 47, and 190 mg/L, respectively. The daily average sediment yield was calculated as 817 tons/day (737 tonnes/day). Furthermore, utilizing a streamflow and sediment load relationship developed specifically for the Neches River at Evadale, the mean annual suspended sediment yield was estimated as 245,437 tons (222,657 tonnes) [20].

The suspended sediment concentrations and loads in Neches River at Evadale station (USGS-080410000) for the period of 1960-2021 are summarized in **Table 3.2**.

Table 3.2 Sabine and Neches Rivers Suspended Sediment Concentration and Load at USGS Stations

Station	Period	Suspended Sediment Concentration, mg/L (Suspended Sediment Load, tons/yr)		
		Max	Average	Min
Sabine River near Ruliff (USGS-08030500)[1]	1974 - 1995	523 (3,920)	39 (782)	7 (10)
Neches River near Evadale (USGS-08041000)[2]	1960 - 2021	190 (6,560)	47 (817)	11 (10)

[1] https://mywaterway.epa.gov/monitoring-report/NWIS/USGS-TX/USGS-08030500/
[2] https://mywaterway.epa.gov/monitoring-report/NWIS/USGS-TX/USGS-08041000/

3.2.2.3 Sediment Delivery to Sabine Lake

The Sabine and Neches Rivers contribute a substantial amount of sediment to Sabine Lake. The average annual suspended sediment loads of the Sabine River at Deweyville and the Neches River at Evadale were reported as 2,370,000 and 1,058,000 cu yd (1,811,995 and 808,899 m^3), respectively [21]. However, the method and the sediment specific weight used to calculate these volumes are not explicitly mentioned in the report. It can be inferred that the reported values were employed to estimate the cost of dredging at the mouth of the Sabine River, suggesting that the specific weight of the dredged sediment was assumed. Assuming a solids (dry) density of 33.4 lb/ft^3 (535 kg/m^3) for dredged materials [22], the average annual suspended sediment loads of the Sabine River at Deweyville and the Neches River at Evadale can be estimated as 1,068,633 and 477,052 tons/yr (969,448 and 432,775 tonnes/yr), respectively. These estimated values differ significantly from those reported in other studies mentioned in **Sections 3.2.2.1** and **3.2.2.2**. It should be noted that the rates of bedload carried by these rivers remain unknown due to a lack of measurements or data availability.

In the absence of accurate estimates of sediment load from rivers and other sources, alternative methods have been employed to estimate sediment delivery to Sabine Lake. One approach utilized $^{239, 240}Pu$ profiles to estimate the sediment deposition rate in the upper and lower estuary of Sabine Lake, which was found to be around 0.16 to 0.2 inches/yr (4-5 mm/yr) [23]. Using this deposition rate, the surface area of the lake, 71 mi^2 (184 km^2), and assuming a sediment density of 48.2 lb/ft^3 (700 kg/m^3), the average annual sediment yield to Sabine Lake is estimated to be 638,900 tons (579,600 tonnes). Considering the total mean annual suspended sediment yield from the Sabine River and Neches River as 480,340 tons (435,757 tonnes (= 213,100 tonnes + 222,657 tonnes)), it is apparent that the remaining sediment, 158,560 tons (143,843 tonnes), must enter the lake from other sources. These additional sources may include sediment from unmonitored areas between the monitoring stations and the points of entry of the Sabine and Neches Rivers into the lake. Furthermore, autochthonous organic matter, shoreline erosion, marine and coastal sources, reworking of bed sediments, and local fluvial inputs from coastal watersheds can contribute to the sediment input to Sabine Lake [24].

3.2.3 Sediment Delivery from Sabine Lake to Gulf of Mexico

Most of the sediment delivered to the Sabine Lake by the Sabine and Neches Rivers deposit in the lake and do not enter the Sabine Pass (**Figure 3.5**) which is the natural outlet of Sabine Lake into the Gulf of Mexico. However, the Sabine Pass is dredged regularly. Since this material is placed on land in a confined disposal facility and is no longer available to the littoral system, some mechanism must be replenishing sand in this channel.

The sediment delivery rate from the Sabine Pass to the Gulf of Mexico was estimated using a regional sediment budget [25,26]. The Sabine Pass area was divided into three cells: Sabine Pass Channel, Sabine Jetty Channel, and Sabine Bar Channel (**Figure 3.5**). Sediment budgets were calculated for each of these cells to determine the rate of sediment delivery.

The total sediment entering the Sabine Pass Channel is estimated as 863,250 cu yd/yr (660,000 m^3/yr), based on the quantity removed by dredging and the computed balance with the adjacent areas. Assuming a solids (dry) density 33.4 lb/ft^3 (535 kg/m^3) for dredged materials [22], the mean annual sediment delivery to the Sabine Pass Channel is 389,238 tons/yr (353,110 tonnes/year). Annual dredging from this channel is approximately 588,578 cu yd/yr (450,000 $m^{3/}$yr), equivalent to 267,862 tons/yr (243,000 tonnes/yr) meaning that the remaining materials 274,670 cu yd/yr (210,000 m^3/yr), equivalent to 125,000 tons/yr (113,400 tonnes/yr) move downstream the Sabine Jetty Channel. In this calculation, only materials transported as bedload are considered, as the quantity of the suspended load is unknown. Observations from satellite imagery have shown that plumes of fine sediment exiting the Sabine Pass disperse over the continental shelf and do not contribute to the littoral sediment budget.

The sediment deposition in the Jetty Channel is due to silt and sand delivery from upstream Sabine Pass Channel 274,670 cu yd/yr (210,000 m^3/yr) and some minor contribution from adjacent littoral system. The Jetty Channel has been dredged on a regular base at an average rate of 287,749 cu yd/yr (220,000 m^3/yr); therefore, no sediment is discharged from this channel to the downstream Bar Channel.

The Bar Channel receives a minimal amount of material from the Jetty Channel; however, it is regularly dredged at a rate of 1,831,131 cu yd/yr (1,400,000 m^3/yr). It is speculated that the sand and silt materials that are dredged and placed in disposal areas quickly migrate back into the channel [25].

Figure 3.5 Sabine Pass Sediment Budget (Reproduced from Ref. [25])

It should be noted that, in the sediment budget analysis discussed above, the contribution from shoreline erosion was not considered. The coastal area west of Sabine Pass exhibits a net shoreline retreat rate as high as 33 ft/yr (10 m/yr) observed between the 1930s and 2019. The coastal area spanning from Sabine Pass to Rollover Pass exhibits a net shoreline retreat at the rate of 9.9 ft/yr (3.03 m/yr) between the 1930s and 2019. Over this period, the cumulative net land loss is estimated to be approximately 4,482 acres (18.1 km^2) [27] (**Figure 3.6**).

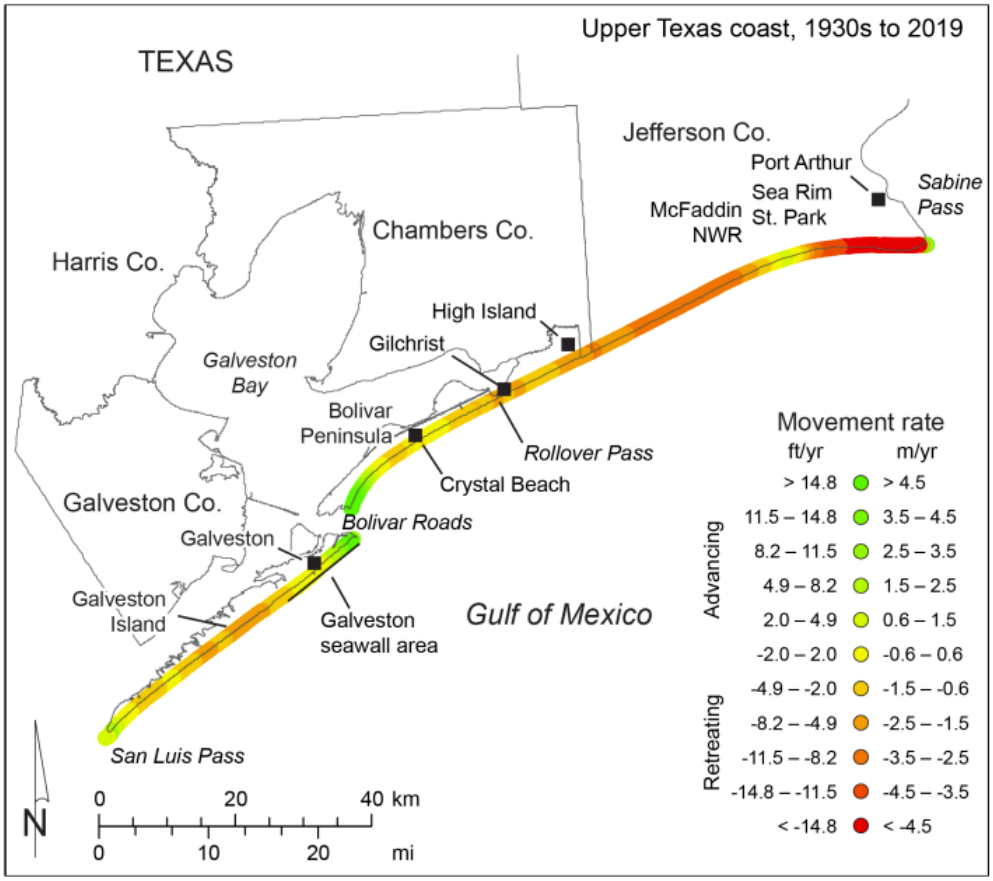

Figure 3.6 Net Rates of Long-term Movement for the Upper Texas Gulf Shoreline Between Sabine Pass and San Luis Pass Between the 1930s and 2019 [27]

3.3 Galveston Bay System

3.3.1 Galveston Bay System Watershed Characteristics

The Galveston Bay watershed is a vast area, spanning approximately 24,000 mi^2 (62,160 km^2) of land. It encompasses Galveston Bay and its surrounding estuaries. The Galveston Bay watershed can be divided into two main sections: the upper and lower portions. The upper portion of the watershed extends upstream of the Lake Livingston Dam on the Trinity River and the Lake Houston Dam on the San Jacinto River (**Figure 3.7**). It encompasses an area of approximately 20,000 mi^2 (51,800 km^2), constituting a significant portion of the entire Galveston Bay watershed. On the other hand, the lower Galveston Bay watershed covers an area of about 4,000 mi^2 (10,000 km^2). It consists of several sub-watersheds that directly or indirectly drain into Galveston Bay (**Figure 3.8**). These sub-watersheds play a vital role in the overall water flow and ecological dynamics of the lower Galveston Bay region [28]. Galveston Bay watershed faces significant environmental challenges. Water pollution is a primary concern, stemming from urban runoff, industrial activities, and agricultural practices. These factors pose risks to water quality and the overall health of the bay's ecosystems.

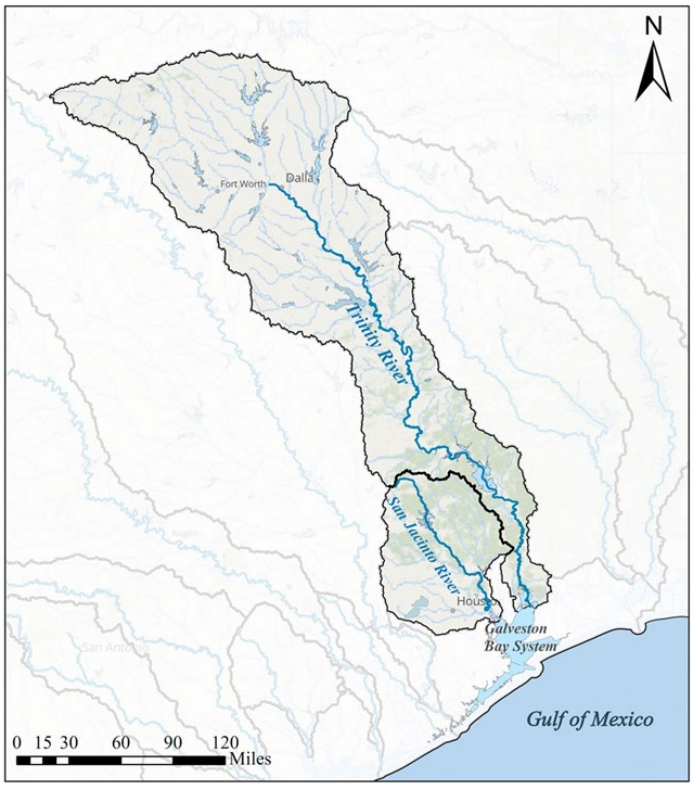

Figure 3.7 Galveston Bay System Upper Watershed

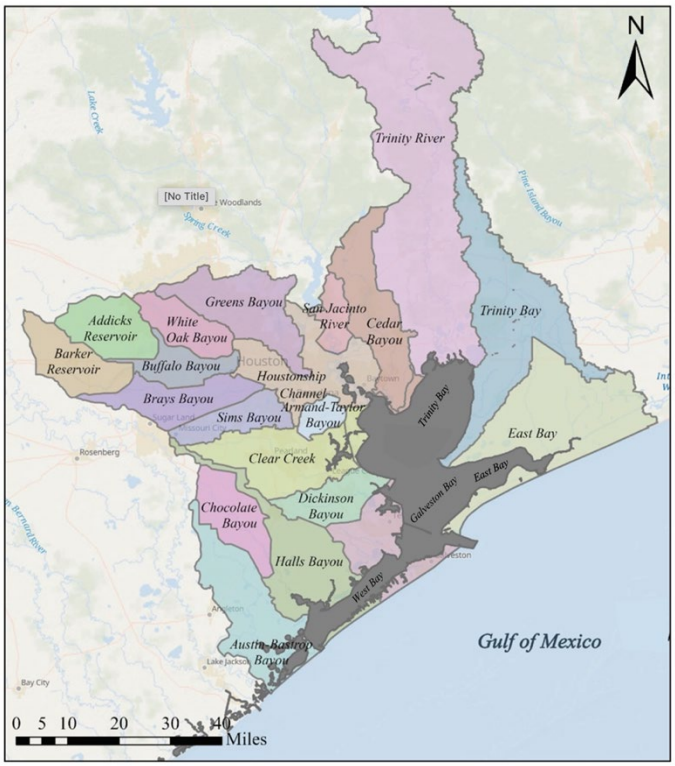

Figure 3.8 Galveston Bay System Sub-watersheds

3.3.1.1 Trinity River

The Trinity River, originating in north Texas that stretches about 715 miles (1,150 km) southeast before reaching Trinity Bay, which is part of the Galveston Bay system. Along its course, it passes through several major cities, most notably Dallas and Fort Worth. The Trinity River watershed covers a vast area of approximately 18,000 mi^2 (46,620 km^2) [29] and encompasses a diverse range of landscapes, including forests, grasslands, wetlands, and urban areas (**Figure 3.9**).

The Trinity River provides important water resources for municipal, industrial, and agricultural use in the region. The river and its tributaries also support a variety of wildlife and plant species, making it ecologically significant. The watershed area has a humid subtropical climate with a mean annual precipitation from 29 to 53 inches (737 to 1,350 mm) that increases from west to east. Average annual temperature increases from north to south across the watershed from 63 to 70°F (17 to 21 °C) [30].

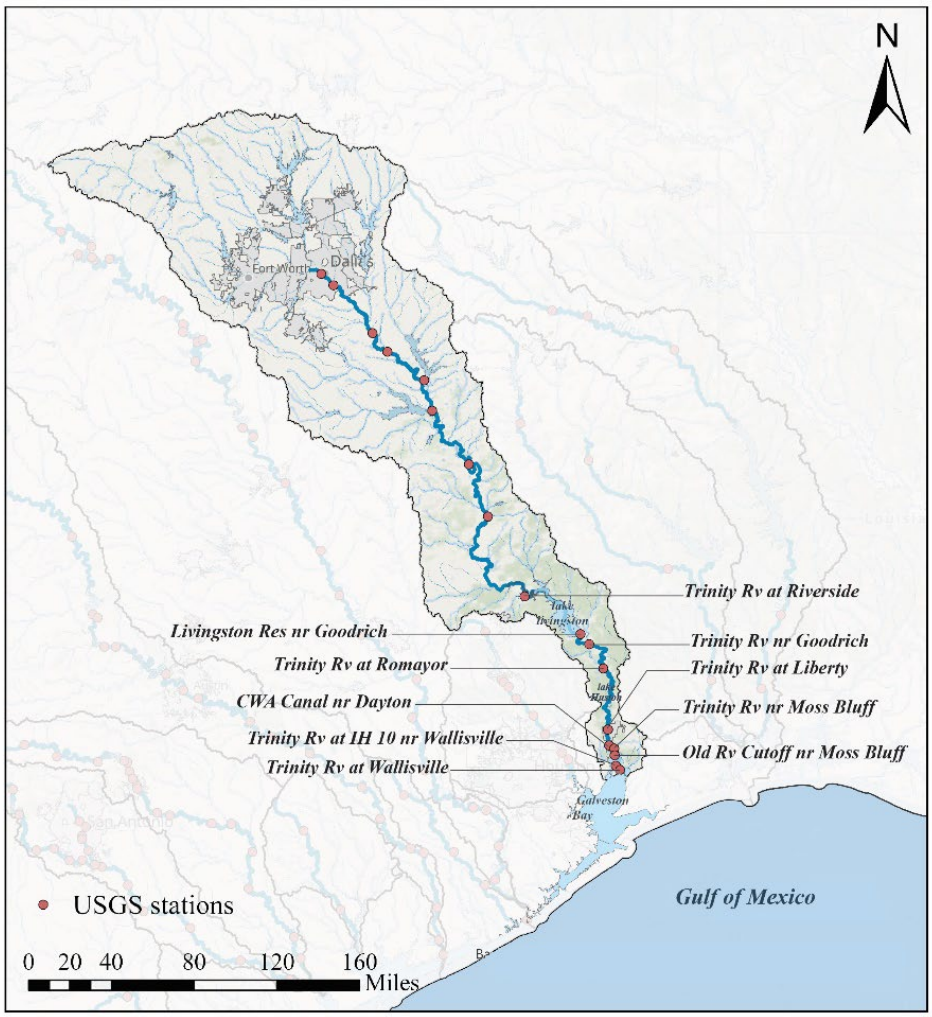

Figure 3.9 Trinity River Watershed and USGS Monitoring Stations

The USGS operates four streamflow gauging stations in the lower Trinity River watershed. These stations are: 08066250 (near Goodrich), 08066500 (at Romayor), 08067000 (at Liberty), and 08067252 (at Wallisville). The Wallisville site is approximately 4 river miles (6.4 km) upstream from where the Trinity River enters Galveston Bay. The Liberty site is approximately 30 river miles (48 km) upstream from the Wallisville site; the Romayor site is approximately 40 river miles (64.4 km) upstream from the Liberty site; and the Goodrich site is approximately 20 river miles (32.2 km) upstream from the Romayor site. The Goodrich site is about 10 river miles downstream from the Livingston Dam (16.1 km) (**Figure 3.9**) [29]. Based on a study conducted in 2007, the mean annual daily discharge of the Trinity River at the Goodrich, Romayor, and Liberty stations are 8,163, 8,687, and 17,986 cfs (231, 246, and 509 m^3/s), respectively [31].

For the Romayor station, the maximum, average, and minimum daily discharges for the period of 1923 - 2023 were reported as 16,900 cfs (479 m^3/s), 8,085 cfs (229 m^3/s), and 1,790 cfs (51 m^3/s), respectively (**Table 3.3**).

According to a study conducted by the USGS between January 2016 and December 2019, approximately 55% of the overall water volume discharged from Lake Livingston could be accounted for at the Wallisville station. The variation in water volumes between the release point at Lake Livingston and the measurement point at the Wallisville site suggests that a significant portion of the water released from Lake Livingston does not flow directly to Galveston Bay through the primary pathway of the Trinity River. Instead, it follows multiple distributary channels and passes through Old River Lake [32].

In 1979, calculations were made to determine the erosion, caused by water, and the sediment yield in the Trinity River basin. The annual sediment yield was estimated to range from 0.3 to 1.99 tons/acre (67 to 446 tonnes/km^2) in the entire Trinity River basin. In the Lower Trinity River basin, the average annual sediment yield was found to be approximately 0.42 tons/acre (94 tonnes/km^2) [10]. Sediment yields in the Trinity River basin for the period of 1964 -1989 were also estimated using daily suspended sediment data collected at the Texas Water Development Board (TWDB) and USGS stations. The analysis showed an annual sediment yield of 0.34 tons/acre (76 tonnes/km^2) at Romayor station and 0.007 tons/acre (1.6 tonnes/km^2) at Liberty located 35 miles (56 km) upstream from where it enters Galveston Bay (**Figure 3.9**), respectively [33].

3.3.1.2 San Jacinto River

The San Jacinto River basin covers an area of approximately 5,089 mi^2 (13,180 km^2) [34]. It encompasses two significant streams, namely Buffalo Bayou and the San Jacinto River, which are the main waterways in the basin. The San Jacinto River receives water from seven major tributaries. These tributaries are Cypress Creek, Spring Creek, West Fork San Jacinto River, Caney Creek, Peach Creek, East Fork San Jacinto River, and Luce Bayou.

The San Jacinto River basin experiences warm to hot conditions. Summers are typically hot and humid, with average high temperatures ranging from the upper 80s °F (27 °C) to the mid-90s °F

(32 °C). Winters are relatively mild, with average high temperatures ranging from the upper 50s °F (10 °C) to the mid-60s °F (16 °C) [30].

The San Jacinto River basin receives an average of around 44 to 56 inches (1,117 to 1,422 mm) of rainfall per year [35]. This rainfall is relatively evenly distributed throughout the year though there may be some seasonal variations. The region can experience heavy rainfall events, especially during the summer months when tropical systems and thunderstorms are more common.

Several USGS gauges monitor flow in the San Jacinto River and its tributaries. The average streamflow at the USGS gauge stations near Conroe and Humble (**Figure 3.10**) are approximately 537 and 1,161 cfs (15.2 and 33 m^3/s) [36]. For Conroe station, the maximum and minimum daily discharges for the period of 1924 - 2023 were reported as 2,290 cfs (65 m^3/s) and 51 cfs (1.4 m^3/s), respectively (Error! Reference source not found.).

Calculations were made in 1979 to determine the erosion caused by water and the sediment yield in the San Jacinto River basin. According to the analysis conducted, the annual sediment yield in the basin was estimated to range from 0.09 to 0.65 tons/acre (20 to 146 tonnes/km^2). In the Lower San Jacinto River basin specifically, the average annual sediment yield was found to be approximately 0.65 tons/acre (146 tonnes/km^2) [10].

Table 3.3 Trinity and San Jacinto Rivers Annual Daily Discharges at USGS Stations

Station	Drainage Area, mi^2 (km^2)	Period	Discharge, cfs (m^3/s)		
			Max	Average	Min
Trinity at Romayor[1] (USGS-08066500)	17,186 (44,511)	1923 - 2023	16,900 (479)	8,085 (229)	1,790 (51)
San Jacinto at Conroe[2] (USGS-08068000)	828 (2,145)	1924 - 2023	2,290 (65)	537 (15.2)	51 (1.4)

[1] https://waterdata.usgs.gov/nwis/inventory/?site_no=08066500&agency_cd=USGS
[2] https://waterdata.usgs.gov/nwis/inventory/?site_no=08068000&agency_cd=USGS

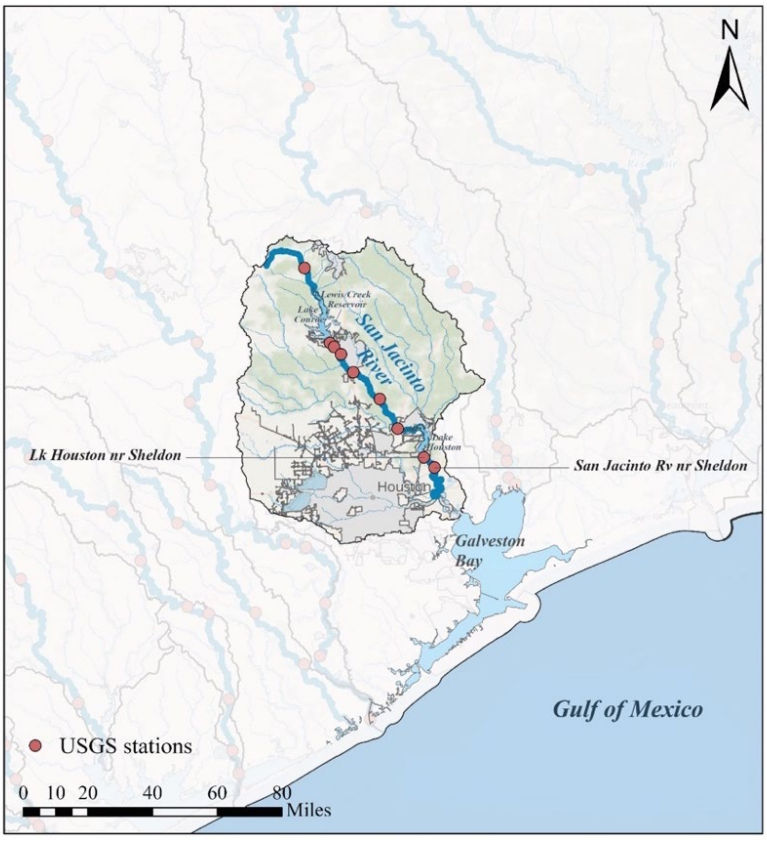

Figure 3.10 San Jacinto River Watershed and USGG Monitoring Stations

3.3.1.3 Reservoirs

Several dams and reservoirs have been constructed on the Trinity River and its tributaries to serve various objectives such as flood control and water supply [37]. Among the notable dams and reservoirs situated on the Trinity River and its tributaries are:

- *Lake Livingston:* Lake Livingston is a reservoir on the Trinity River, located in East Texas. It is one of the largest reservoirs in the state, covering approximately 90,000 acres (364 km^2). The Livingston Dam forms this reservoir with a total storage capacity of 2.83 $\times 10^9$ cu yd (2.16 $\times 10^9$ m^3).
- *Lake Ray Roberts:* Lake Ray Roberts is a reservoir located in North Texas on the Elm Fork of the Trinity River. The reservoir covers approximately 29,000 acres (117 km^2) and was created by the construction of Ray Roberts Dam. It serves as a water supply source for the cities of Denton and Dallas, as well as for recreational activities. It has a storage capacity (water supply and flood control) of 8.0 $\times$ 10^5 acre-ft (9.86 $\times 10^8$ m^3).
- *Lewisville Lake:* Lewisville Lake is another reservoir on the Elm Fork of the Trinity River, located near the city of Lewisville, Texas. With a surface area of around 29,000 acres (117 km^2) and total storage capacity (water supply and flood control) of 6.2 $\times 10^5$ acre-ft (7.63 $\times 10^8$ m^3) and it is primarily used for water supply, flood control, and recreational purposes.

The San Jacinto River Basin comprises several reservoirs, including the following [38]:

- *Lewis Creek Reservoir:* Located in Liberty County, Texas, Lewis Creek Reservoir is a relatively small reservoir with a storage capacity of approximately 16,400 acre-ft (2.02×10^7 m^3). It was constructed for water supply and flood control purposes.
- *Lake Conroe:* Situated on the west fork of the San Jacinto River in Montgomery County, Lake Conroe is a large reservoir with a storage capacity of around 411,022 acre-ft (5.07×10^8 m^3). It serves as a major water supply source for the City of Houston and surrounding areas, as well as providing recreational opportunities.
- *Lake Houston:* Positioned on the east fork of the San Jacinto River in Harris County, Lake Houston is another significant reservoir in the San Jacinto River Basin. It has a storage capacity of about 134,122 acre-ft (1.65×10^8 m^3) and serves as a municipal water supply source for the city of Houston.
- *Sheldon Reservoir:* Sheldon Reservoir, also known as Lake Houston Wilderness Park, is a small reservoir with a capacity of 4,224 acre-ft (5.21×10^6 m^3) located in northeast Harris County. While it is not as large as Lake Conroe or Lake Houston, it provides recreational opportunities and helps manage stormwater and runoff.

The dams and reservoirs on the Trinity and San Jacinto Rivers play essential roles in water supply, flood mitigation, and providing recreational opportunities for the surrounding communities. They also interrupt the delivery of sediment from upper part of the watersheds to lower regions and Galveston Bay.

3.3.1.4 Galveston Bay

Galveston Bay is a large estuary located along the Texas Gulf Coast. It is an important ecological and economic resource for the region. It receives freshwater input from various sources, including the Trinity River, San Jacinto River, and other smaller tributaries (**Figure 3.7**). These rivers contribute to the freshwater inflow and overall water circulation within the bay. Tides and wind-driven currents also play a significant role in shaping the hydrology of the bay. The Galveston Bay is composed of four major sub-bays: Galveston, Trinity, East, and West bays (**Figure 3.8**). The Trinity River, San Jacinto River, and other stream and creeks in lower Galveston Bay transport freshwater and sediment to Galveston Bay.

Galveston Bay is characterized by a salinity gradient due to the mixing of freshwater inflows and seawater from the Gulf of Mexico. The salinity levels vary spatially and temporally within the bay, influencing the distribution of different plant and animal species.

Galveston Bay receives sediment from various sources, including riverine input, coastal erosion, and storm events. Sediment transport and deposition are influenced by tidal and wave energy, as well as human activities such as dredging and shoreline modifications. The sediment composition within Galveston Bay can vary, including sand, silt, clay, and organic material.

The hydrodynamic processes in the bay, including tides and currents, can result in erosion and deposition of sediment. Erosion is more prevalent along certain areas of the bay's coastline, while

deposition can occur in sheltered areas or along river channels. These processes can impact the bay's shoreline and habitats.

3.3.2 Galveston Bay System Sediment Budget

Factors influencing Galveston Bay sediment budget include sediment input from the Trinity River, San Jacinto River, and other tributaries, coastal erosion, human activities (e.g., dredging, or land-use changes in the watershed), and sediment transport, deposition, and resuspension due to tides, currents, and wind-driven processes.

To establish sediment budget of Galveston Bay, a comprehensive assessment is needed to estimate the sediment input from the Trinity River, San Jacinto River, and other relevant sources.

3.3.2.1 Trinity River Sediment Load

The daily suspended sediment samples collected by TWDB over the 1964-1989 period at three locations along the lower Trinity were used to estimate the sediment load carried by the river [33]. These stations included Crockett, situated upstream, and Romayor and Liberty, positioned downstream of Lake Livingston (refer to **Figure 3.9** for the location of the lake). The sediment load carried by the river at these stations estimated as 5.6×10^6, 3.71×10^6, 0.077×10^6 tons/yr (5.11×10^6, 3.37×10^6, and 0.07×10^6 tonnes/yr), respectively. According to a sediment budget analysis, the sediment load transported by the Trinity River to its delta is estimated to be 0.082 tons/yr (0.74 tonnes/yr). This amount aligns with the estimated sediment yield for the Lower Trinity River at Wallisville Lake, which is reported as 0.08 tons/yr (0.073 tonnes/yr) [10]. The significant difference in sediment yields between Liberty and Romayor indicates a substantial presence of alluvial storage between these two locations. This suggests that minimal sediment makes its way downstream to the lower river at Liberty, regardless of the presence of Lake Livingston [30].

The sediment load in Trinity River at Romayor (**Figure 3.9**) was estimated for the period of 1936 to 1986 using data collected by the USGS and TWDB [39]. The findings showed that the amount of sediment carried by the river at that location varied during different time periods. Specifically, it was 7.52×10^6 tons/yr (6.82×10^6 tonnes/yr) between 1936 and 1946, 3.08×10^6 tons/y (2.79×10^6 tonnes/yr) from1947 to 1968, and 0.8×10^6 tons/yr (0.73×10^6 tonnes/yr) from 1969 to 1986. The decrease in sediment load after 1968 was attributed to the construction of Lake Livingston. Following the construction of Lake Livingston, the average sediment concentration at this station decreased from 538 mg/L to 112 mg/L [39]. The sediment loads at the Liberty station, on the other hand, do not exhibit any indications of a shift in sediment patterns or regime [33].

Data collected by the USGS from May 2014 to December 2015 was used to estimate the suspended sediment concentration and suspended sediment load (SSL) in the Trinity River at Wallisville station. Throughout this period, the suspended sediment concentrations varied from 5 to 453 mg/L, with a median concentration of 65 mg/L. The minimum monthly SSL was estimated to be 100 tons (91 tonnes) in October 2014, while the maximum monthly load reached to 0.44×10^6 tons (0.40×10^6 tonnes) in November 2015. Over the course of the study, the total SSL at the Wallisville site

amounted to approximately 2.2 $\times 10^6$ tons (2 $\times 10^6$ tonnes). Notably, around 96% of this load was measured during seven high-flow events that occurred in 2015 [29].

Suspended sediment concentration data collected at the Liberty station by USGS were utilized to develop a discharge-sediment load rating curve. This curve was then used to estimate the average daily suspended sediment load and the annual total suspended load of the Trinity River at this station for the period of 1960 to 2017. The estimated values for the average daily load and annual total load are 3,163 tons/day and 1.16 $\times 10^6$ tons/yr (2,869 tonnes/day and 1.05 $\times 10^6$ tonnes/yr), respectively [40].

The USGS, in collaboration with the TWDB, collected streamflow and water quality information at USGS monitoring stations located in the Lower Trinity River basin. The purpose was to assess the characteristics of streamflow, nutrients, and suspended sediment that enter Galveston Bay from the Trinity River. The findings regarding suspended sediment concentration and sediment load from three distinct survey periods are outlined as follows.

- *2009 Campaign*

  During this campaign, the sampling took place during two periods of high flows. At the Wallisville station, the measurements of suspended sediment load in April 2009 ranged from a maximum of 31,142 tons/day to a minimum of 11,672 tons/day (28,252-10,589 tonnes/day). In September to November 2009, the suspended sediment load varied from a maximum of 23,905 to a minimum of 2,805 tons/day (21,686 to 2,545 tonnes/day) [41].

- *2014-2015 Campaign*

  Throughout the study, the measured suspended sediment concentrations at the Wallisville site ranged from 5 to 453 mg/L with a median concentration of 65 mg/L. These concentrations were observed to vary in response to changes in discharge, with the highest suspended sediment concentrations occurring 1 to 2 days prior to the peak discharge for each event. The total suspended sediment load at the Wallisville site from May 2014 to December 2015 estimated approximately 2.2 $\times 10^6$ tons (2.0 $\times 10^6$ tonnes). During this period, the monthly suspended sediment load reached its minimum of 100 tons (91 tonnes) in October 2014 and its maximum of 441,000 tons (400,000 tonnes) in November 2015. Notably, around 96% of this sediment load was measured during seven high-flow events in 2015, with one particular high-flow event contributing approximately 27% to the overall sediment load [29]. According to the findings of this study, the water volume recorded at the Wallisville site during high-flow events represents a proportion of the volume measured at the Goodrich, Romayor, and Liberty sites. As a result, the total suspended sediment load (SSL) measured in the primary channel of the Trinity River is just a portion of the overall SSL transported from the Trinity River watershed into Galveston Bay. It is hypothesized that the remaining volume and SSL are redirected into nearby wetlands and channels within the delta area. This diversion may account for a significant majority of the SSL, particularly during certain high-flow events [32].

- *2016-2019 Campaign*

  In this study, suspended sediment concentrations and loads were calculated at both Wallisville and Liberty sites for a series of 11 hydrologic events that represented different streamflow. The study found that the Liberty site had higher daily mean suspended sediment concentrations and total suspended sediment loads compared to the Wallisville site. During the high-flow events, the suspended sediment concentrations were estimated to range from 130 to 275 mg/L at the Liberty site and from 70 to 232 mg/L at the Wallisville site. The total suspended load for this period was estimated to be 4.9×10^6 tons (4.44×10^6 tonnes) at the Liberty site and 1.2×10^6 tons (1.1×10^6 tonnes) at the Wallisville site, indicating that only 25% of the sediment load measured at the Liberty site was observed at the Wallisville site. This suggests that only a portion of the suspended sediment load observed at the Liberty site reached Galveston Bay through the main channel of the Trinity River during the events that were measured, and that the Lower Trinity River likely serves as a sink of suspended sediment. Based on the discrete samples and collected data, it was observed that a portion of the sediment load was redirected from the main channel of the Trinity River to Old River Lake and the associated distributary channels. Suspended sediment loads during high flow events ranged from 6,510 to 26,900 tons/day (5,906 to 24,403 tonnes/day) at the Wallisville site and from 5,780 to 46,100 tons/day (5,244 to 41,821 tonnes/day) at the Old River Lake site [32].

The suspended sediment concentrations and loads in Trinity at Romayor station (USGS-08066500) for the period of 1960-2021 are summarized in **Table 3.3**.

3.3.2.2 San Jacinto Sediment Load

The USGS, in partnership with the Houston-Galveston Area Council and the Texas Commission on Environmental Quality, conducted a study during the period of July 2008 to August 2009. The study involved the measurement of streamflow and the collection of continuous and discrete water quality data in the West Fork San Jacinto River basin downstream from Lake Conroe. The sediment data were collected at two stations: USGS-08067650 below Lake Conroe and USGS-08068000 near Conroe. In the West Fork San Jacinto River basin, the suspended sediment concentrations ranged from 3 to 133 mg/L, with a median concentration of 7.6 mg/L. On the other hand, at station 08068000, the concentration varied from 1.5 to 268 mg/L, with a median concentration of 14 mg/L [42].

The total estimated suspended sediment load during study the period was about 1,900 tons (1,724 tonnes) at station USGS-08067650 and about 72,000 tons (65,317 tonnes) at station USGS-08068000 near Conroe. Because the estimated concentrations derived from the regression equations contained large error components, the computed load estimates are inferred to also include large errors. The suspended sediment load were about 40 times larger at station 08068000 compared with load at station USGS-08067650, likely because station USGS-08067650 is 2.5 miles (4 km) downstream from a reservoir (Lake Conroe) with controlled releases, and station USGS-08068000 is 11 miles (18 km) downstream from station USGS-08067650. Flow at station

USGS-08068000 is more representative of water quality properties in the West Fork San Jacinto River Basin compared with station 08067650, which is more representative of water quality properties of releases from Lake Conroe [42].

The suspended sediment concentrations and loads in West Fork San Jacinto River at a station near Conroe (USGS-08068000) for the period of 1965-2011 are summarized in **Table 3.4**.

Table 3.4 Trinity and San Jacinto Rivers Suspended Sediment Concentration and Load at USGS Stations

Station	Period	Suspended Sediment Concentration, mg/L (Suspended Sediment Load, tons/yr)		
		Max	Average	Min
Trinity River at Romayor (USGS-08066500)[1]	1960 - 2021	1,270 (195,000)	79 (5,677)	4 (9)
West Fork San Jacinto near Conroe (USGS-08068000)[2]	1965 - 2011	1,270 (18,800)	60 (286)	1 (0.28)

[1] https://mywaterway.epa.gov/monitoring-report/NWIS/USGS-TX/USGS-08066500/
[2] https://mywaterway.epa.gov/monitoring-report/NWIS/USGS-TX/USGS-08068000/

3.3.2.3 Sediment Delivery to Galveston Bay

Sediment delivery to Galveston Bay typically occurs through natural processes such as riverine input, coastal erosion, and tidal movements. Human activities also affect sediment delivery to Galveston Bay. For example, construction projects, channel dredging, and land development have altered natural sediment transport patterns and has led to changes in the sediment dynamics of the bay.

A sediment budget for Galveston Bay was developed by evaluating the quantities of sediment sinks, sources, and movements [43]. This study took into account fluvial inputs, which encompassed runoff from the Trinity River, San Jacinto River, and local tributaries experiencing land erosion, as well as shoreline erosion, as the primary sediment sources. Additionally, the dredged materials from the navigational channels were identified as major sediment sinks. The analysis showed that the total mass of sediment contributed by fluvial sources amounted to roughly 2.2 $\times 10^6$ tons/yr (2 $\times 10^6$ tonnes/yr) while shoreline erosion added approximately 0.2 $\times 10^6$ tons/yr (0.18 $\times 10^6$ tonnes/yr). On the other hand, the calculated sink volume resulting from channel dredging records was 12.1 $\times 10^6$ tons/yr (11 $\times 10^6$ tonnes/yr). Consequently, there was a deficit in the total source volume, amounting to approximately 9.7 $\times 10^6$ tons/yr (8.8 $\times 10^6$ tonnes/yr). The identified factors contributing to this deficit included:

- Underestimation of fluvial inputs (including the Trinity River),
- Aeolian input,
- Coastal and marine sources derived from barrier island overwash,

- Fine grain suspended sediment transported into Galveston Bay from the Gulf of Mexico through Bolivar Roads,
- Dredged material from navigation channels may have a significantly lower density than the assumed 0.84 ton per cu yd (1 tonnes/m^3). This would lead to an overestimate of the actual mass of solids being removed,
- Shoreline erosion may be underestimated based on a greater active profile height,
- Channel wall and shoulder erosion due to ship and storm-induced wave action,
- Bed load transport particularly from the San Jacinto River,
- Dredged material may be escaping from some beneficial use sites and be transported back into navigation channels,
- Navigation channels may be undergoing side-slope adjustment (localized transport) contributing to higher sedimentation rates,
- Sediment being resuspended by waves and currents within the Bay system and transported into navigation channels.

To address the deficit volume in the sediment budget, it was assumed that the difference is attributed to the resuspension of sediments within Galveston Bay caused by waves and currents with a net vertical erosion rate of approximately 0.2 in/yr (5 mm/yr). However, this contradicts the findings of Phillips (2004) [44] which estimate a net accumulation rate of 0.14 to 0.15 ft/yr (3.5 to 3.7 mm/yr).

The depth of Galveston Bay system has also been impacted by changes in sediment influx and other factors. It experienced a decrease at an average rate of approximately 16.8 in/100 yrs (426 mm/100 yrs) between 1854 and 1933 [45], but later underwent an increase. Between 1968 and 1977, depth measurements revealed a rise of 0 to 4.9 ft (0-1.5 m) in Galveston, Trinity, and East bays, primarily attributed to groundwater and mineral extraction [46]. Although West Bay also deepened, the extent was comparatively lesser than the other bays.

The conversion of certain marsh areas into open water in the interior sections of the Trinity River delta is reported [47]. This conversion could indicate the influence of subsidence or decreased sediment inflow as potential factors. The U.S. Army Corps of Engineers [48] found that Lake Livingston, about 100 river miles (161 km) upstream, traps almost 98% of the sediment that enters the reservoir. Other studies also confirm that the present sediment load is significantly less than the long-term load that provided material for delta construction [39]. However, based on the observation of a decline in the area of deltaic wetlands, it was found that relative sea level rise is outpacing sedimentation [49].

Sediment accumulation rates of 0.05 and 0.07 in/yr (1.2 and 1.8 mm/yr) were attained in the Trinity River delta by radiocarbon dating method. However, modern fluvial sediment input from the Trinity River to the delta is occurring at a rate of approximately 0.016 in/yr (0.4 mm/yr), which is insufficient to balance subsidence and wetland loss and keep pace with future sea level rise [50]. This rate of annual sediment load is consistent with the estimated low sediment yield for the Lower Trinity River at Wallisville Lake, which is reported as 0.08 tons/yr (0.073 tonnes/yr) [10].

3.3.3 Sediment Delivery from Galveston Bay to Gulf of Mexico

Using a regional sediment budget, the sediment delivery rate from Galveston Bay to the Gulf of Mexico was estimated [25]. The Galveston Bay area, spanning from High Island to San Luis Pass, was divided into 16 cells for analysis (**Figure 3.11**). Sediment budgets were calculated for each of these cells to determine the rate of sediment delivery. The estimated total sediment entering the Gulf of Mexico from Galveston Bay is 6.02×10^5 cu yd/yr (4.60×10^5 m^3/yr). This estimation was based on the quantity of sediment removed through dredging in the Entrance Channel (Cell 11) and the calculated balance with the adjacent cells (**Figure 3.11).** Assuming a solids (dry) density of 33.4 lb/ft^3 (535 kg/m^3) for the dredged materials [20], the sediment transport to the Gulf of Mexico is 270,540 tons/yr (245,429 tonnes/yr). Conversely, sediment also enters from the Gulf into the bay. Specifically, a total of 88,000 m^3/yr (47,221 tonnes/yr) of littoral sediment enters the Bay. Out of this, 11,800 m^3/yr (6,331 tonnes/yr) comes through the Rollover Pass (Cell 7), and 76,200 m^3/yr (40,889 tonnes/yr) enters through San Luis Pass (Cell 18). Based on these estimates, the net sediment delivery from Galveston Bay to the Gulf of Mexico is approximately 220,00 tons/yr (200,000 tonnes/yr).

In the sediment budget analysis discussed above, the sediment contribution from shoreline erosion was not considered. This omission can be justified, given that the Bolivar Peninsula and Galveston Island shoreline experienced a relatively low net retreat rate up to 5 ft/yr (1.5 m/yr) from the 1930s to 2019 (**Figure 3.6**) [27].

As mentioned in **Section 3.3.2.3** and highlighted in other studies (e.g., Ref. [44]), the sediment budget analysis of Galveston Bay shows an annual deficit of 9.7×10^6 tons/yr (8.8×10^6 tonnes/yr). The fluvial sediment inputs are insufficient to account for observed sediment deposition rates in Galveston Bay. A major sediment source is the transport of sediment through the Bolivar Roads inlet. Satellite imagery reveals the presence of sediment plumes entering and exiting Galveston Bay via the inlet, which is influenced by tides and wind conditions. Once the sediment enters the bay, its fate depends on the oceanographic factors such as currents and wave energy. It is expected that a substantial portion of the incoming sediment, particularly fine-grained material, will be retained within the Bay, especially beyond the flood-tidal delta [44].

Extreme hydrologic events, such as Hurricane Harvey in 2017, can have a significant impact on sediment dynamics in Galveston Bay. During this event, a substantial amount of freshwater, estimated to be 9×10^6 acre-ft (11.1×10^9 m^3), about 3 times the bay volume, flowed into the bay. Additionally, approximately 10.9×10^7 tons (9.9×10^7 tonnes) of sediment were delivered into the bay, equivalent to 18 years of average annual sediment load. The sediment deposits resulting from Hurricane Harvey were observed through sediment cores, with the thickest deposit found in the San Jacinto estuary, exceeding 19.7 inches (500 mm) in thickness. The mouth of Clear Lake, Trinity Bay, and East Galveston Bay experienced sediment deposit thicknesses of 8.7, 7.9, and 3.5 inches (220, 200, and 89 mm), respectively. In one particular site within the San Jacinto Estuary, the sediment cores revealed 18.9 inches (48 cm) of erosion followed by the deposition of 8.7 inches (220 mm) of new sediment [51].

Hurricane Ike also resulted in a substantial amount of sediment being deposited in East Galveston Bay. Instead of originating from fluvial inputs, the sediment was carried into the bay system by the storm surge from the Gulf of Mexico, specifically from Bolivar Peninsula. As the surge subsided, the water transported the surface soil from the surrounding land into East Bay. The thickness of the newly deposited sediment varied, with some areas near Rollover Pass and south of Wallis Lake on Smith Point experiencing up to 4.6 ft (1.40 m) of sediment accumulation. It is estimated that Hurricane Ike deposition amounted to at least 209 $\times 10^6$ cu yd (160 $\times 10^6$ m^3) in the bay. This is roughly equivalent to a 3.3 ft (1 m) thick layer of sediment in East Bay. Based on post-Ike bathymetric profiles, a significant portion of these sediments either returned to the Gulf of Mexico through Bolivar Roads or were redistributed to other areas within Galveston Bay [52].

Figure 3.11 Galveston Bay Sediment Budget (Reproduced from Ref. [25])

3.4 Brazos-San Bernard Estuary System

3.4.1 Brazos River Watershed Characteristics

The Brazos River watershed is the second largest river basin by area within Texas. Originating in eastern New Mexico, the Brazos River courses through Texas before ultimately reaching the Gulf of Mexico (**Figure 3.12**). The total drainage area of the Brazos River and its tributaries is approximately 45,600 mi^2 (118,000 km^2). The upper part of the watershed, totaling 9,570 mi^2 (24,786 km^2) does not contribute to the downstream flows [53].

The lower region of the watershed experiences a humid subtropical climate. Although precipitation is distributed across the year, it frequently encounters summer droughts and extended periods of low-flow due to significant evapotranspiration. On average, annual precipitation ranges from 29 to 51 inches (750 to 1,300 mm) [54]. The predominant land use in this region is agriculture, with the focus on cattle grazing. Approximately 3,000 mi^2 (7,689 km^2) spread across the 27 counties in the lower half of the basin are dedicated to agricultural and open rangeland purposes [53].

An assessment conducted in 1979 estimated the annual sediment yield in the Brazos River basin to range from 0.14 to 2.52 tons/acre (31 to 565 tonnes/km^2), and 0.87 tons/acre (192.6 tonnes/km^2) in Lower Brazos River [10].

3.4.1.1 Brazos River

The Brazos River flows into the Gulf of Mexico near Freeport, Texas, on the central Texas coast, south of Houston. It is best described as a meandering, incised sand bed with fragile banks. The lowest 300 miles (482 km) of the Brazos River has a channel slope of 0.7 ft/mile (0.13 m/km) [53]. It has the highest flow and sediment discharge of any Texas rivers, with an annual suspended sediment yield of approximately 0.17 tons/acre (39 tonnes/km^2) [55].

The USGS operates several streamflow gauging stations on the main stem of the Brazos River (**Figure 3.12**). Two of these stations are located downstream in the lower reach of the river: USGS-08114000 near Richmond 93 river miles (150 km) upstream from the mouth, and USGS-08116650 near Rosharon 57 river miles (92 km) upstream from the mouth. **Table 3.5** provides the most recent discharge data for these two lowermost USGS stations, with sediment data, on the Brazos River.

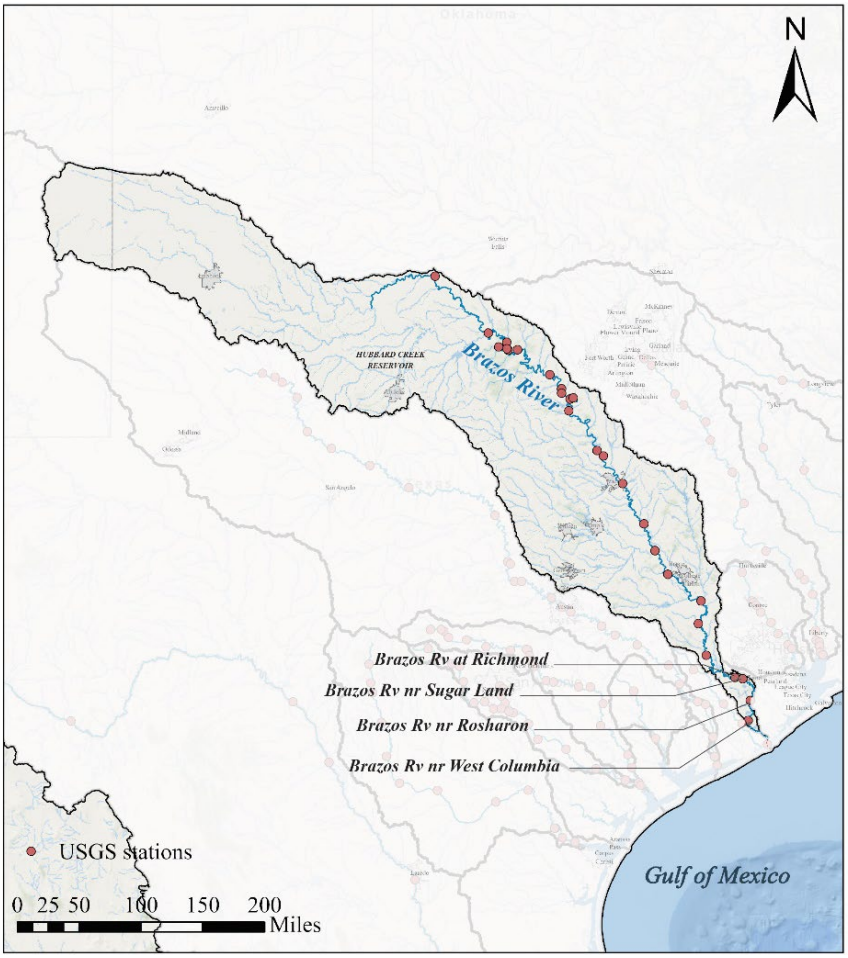

Figure 3.12 Brazos River Watershed and USGS Monitoring Stations

Table 3.5 Lower Brazos River Annual Daily Discharges at USGS Stations

Station	Drainage Area, mi² (km²)	Period	Discharge, cfs (m³/s)		
			Max	Average	Min
Richmond[1] (USGS-08114000)	45,107 (116,827)	1940 - 2023	15,900 (753)	7,641 (217)	2,310 (23)
Rosharon[2] (USGS-08116650)	45,339 (117,428)	1966 - 2023	15,500 (822)	8,177 (237)	2,200 (24)

[1] https://waterdata.usgs.gov/tx/nwis/inventory?site_no=08114000
[2] https://waterdata.usgs.gov/nwis/inventory/?site_no=08116650

3.4.1.2 Reservoirs

Reservoir construction has been a significant undertaking on the Brazos River since the early 1900s, and it has had a substantial impact on both river discharge and sediment load. Within the basin, there are a total of 1,178 reservoirs, with thirteen of them collectively accounting for 88% of the managed storage. Lake Whitney, the largest among these reservoirs, is located along the

main stem of the Brazos River, with a drainage area of 27,189 mi^2 (70,420 km^2) and a total storage capacity of approximately 2×10^6 acre-ft (2.47×10^9 m^3). The second-largest reservoir on the Brazos River is Possum Kingdom Lake, with a drainage area of 23,596 mi^2 (61,113 km^2) and a storage capacity of 0.72×10^6 acre-ft (0.89×10^9 m^3) [53,56].

3.4.2 Brazos River Estuary Sediment Budget

The Brazos River estuary is one of the few riverine estuaries along the Texas coast. It receives sediment from rivers and other sources within its watershed. The current Brazos River delta is classified as a wave-dominated delta, which extends approximately 1.25 miles (2 km) into the Gulf of Mexico. The process of deposition and the enlargement of the delta are primarily driven by significant flood events. These large flood events contribute to the accumulation of sediment in the delta area, leading to its growth and development over time.

The estimation of sediment budgets for estuarine environments can be complex due to factors such as tidal currents, wave action, and the interaction between freshwater and saltwater. Also, human activities such as channelization, dredging, and land-use changes in the watershed have affected sediment budget. In the 1990s, sediment buildup occurred at the mouth of the San Bernard River on the Texas central coast. This issue resulted from two major projects: the diversion of the Brazos River channel in 1929 and the construction of the Gulf Intracoastal Waterway (GIWW) in the 1940s. These projects have changes sediment dynamics in the estuary, leading to the closure of the San Bernard River mouth by accumulated sediments, which had various impacts on navigation and the local ecosystem [57].

It is reported that the Brazos River does not experience a typical seasonal flood wave. Instead, it tends to swing between extended periods of multi-year drought and flood conditions [58]. As a result, the rate of sediment transported by the Brazos River to the Gulf of Mexico (GoM) is influenced by the climate cyclicity in the Brazos River watershed. Approximately 85% of the time, sediment export from the river to the GoM is minimal and is trapped in the estuarine area. However, during periods of high flows, the sediment that has been trapped can be mobilized and subsequently exported to the GoM. When high-discharge sediment loads coincide with the remobilization of deposited sediments, the combined effect can lead to sediment flux during an event that exceeds what would be expected based solely on discharge [59]. The intermittent behavior of the Brazos River has led to alternating layers in sediment deposition, with periods dominated by sediment from the Brazos River itself and background sedimentation from the GoM during non-event periods [60]. These sedimentation patterns provide valuable information in estimating the sediment budget within the Brazos River estuary.

There are several other factors that influence the sedimentation patterns in the Lower Brazos River's delta. Within the river delta, prevailing southeast winds drive beach sediments in a one-sided alongshore transport pattern toward the southwest. This region frequently faces extratropical northers and occasional hurricanes events that result in substantial change to coastal deposits [61]. The presence or absence of a salt wedge in the lower reaches of the Brazos River also influences sediment transport dynamics toward the Gulf of Mexico [59].

3.4.2.1 Brazos River Sediment Load

Historical sediment load carried by the Brazos River is available from the Texas Water Development Board (TWDB) (early 1900s to 1980) and USGS (1966-present). Analysis of this data shows that the sediment transport in the river has changed, particularly since 1982. These changes in sediment dynamics can be attributed to a combination of factors including reservoir construction, land use transformations, and sand and gravel mining activities within the Brazos River basin. The total area of harvested acres of non-hay crops in the lower Brazos River Basin during 1924-1992 decreased more than 75% from about 32% to about 8% of the total area. Correspondingly, erosion potential has decreased substantially. Instream sand and gravel mining activities within the Brazos River account for 11 to 25% of the total sand delivery. Despite the decrease in sand transport and change in distribution of both daily and annual peak discharges, the computed annual suspended sand load does not show significant changes [53].

There are several reservoirs in operation within the Brazos River watershed, each serve multiple purposes, including flood control, industrial and agricultural needs, and human consumption, while also retaining sediment carried by the river [53]. For example, the installation of the Somerville Dam on a major Brazos tributary resulted in a significant reduction in the river's sediment loading capacity [62]. Notably, a decline in suspended sand concentrations in the Brazos River at the Richmond station can be observed for the period 1969 to 1995, with a particularly pronounced decrease after 1982 (**Figure 3.**). These decrease in sand transport are likely the result of extensive reservoir construction, land use changes, and sand and gravel mining activities within the Brazos River basin [53].

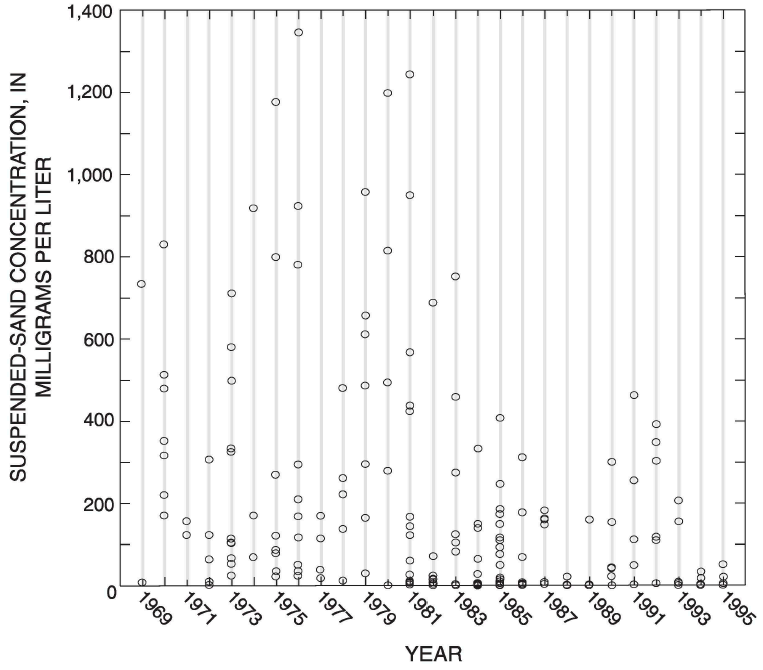

Figure 3.13 Suspended Sand Concentration in the Brazos River at USGS Richmond Station for the Period of 1969-1995 [53]

For the period of 1966-1986, the mean monthly suspended sediment loads for the Brazos River at Richmond stations were reported to vary from 2,500 to 91,000 tons (2,268 to 82,554 tonnes). In this period, the annual suspended sediment load averaged 10.9 $\times 10^6$ tons (9.9 $\times$ 10^6 tonnes). The minimum annual load of 0.4 $\times 10^6$ tons (0.36 $\times 10^6$ tonnes) occurred during the1984 water year, and the maximum annual load of 30.8 $\times 10^6$ tons (27.9 $\times 10^6$ tonnes) occurred during the 1968 water year [63].

In the absence of sediment measurements at the Richmond station since 1995 (except for a few measurements in 2020-2021), the average daily suspended sediment load at this station was estimated using a discharge-sediment load rating curve. According to this curve, the average daily suspended sediment load for the Brazos River at Richmond was estimated as 17,216 tons/day (15,618 tonnes/day) for the period of 1960 to 2017 [40]. The average annual suspended sediment load estimated from the daily load calculations amounts to 6.2 $\times 10^6$ tons (5.6 $\times 10^6$ tonnes) for this period. This figure is 43% smaller compared to the average annual load for the earlier period from 1966 to 1986, which was reported as 10.9 $\times 10^6$ tons/yr (9.9 $\times 10^6$ tonnes/yr) [56].

Further insights into sediment dynamics are provided in **Table 3.6** by summarizing the minimum, average, and maximum suspended sediment concentrations and load measured at the two lowermost stations with sediment data (Richmond and Rosharon) on the Brazos River. At the Richmond station, the average and daily suspended sediment load is calculated as 126,140 tons/day (114,435 tonnes/day) for the period of 1966 to 2021. At the Rosharon station the average daily suspended sediment load is estimated as 22,064 tons/day (20,015 tonnes/day) for the period of 1973-2023. Based on the daily sediment load, the average annual suspended sediment load at this station is estimated as 8 $\times 10^6$ tons/yr (7.3 $\times 10^6$ tonnes/yr).

The Brazos River transports both suspended sediment and bedload, but the dominant mode of transport is suspended sediment. The average delivery of suspended sediment to the Gulf of Mexico by the Brazos River was estimated at approximately 27.5 $\times 10^6$ tons (25 $\times 10^6$ tonnes), while the bedload delivery was estimated at about 2.5 $\times 10^6$ tons (2.3 $\times 10^6$ tonnes). This indicates an 11 to 1 ratio between suspended sediment and bedload transport [64].

The annual sediment yield at Rosharon station was also calculated using the daily flow data and the rating curves developed for bed load, suspended load, and total suspended material (suspended load + wash load). For the period of 1990-2009, the maximum suspended load and bedload at this station were reported as approximately 18 $\times 10^6$ and 1$\times 10^6$ tones (16.4 $\times 10^6$ and 0.82 $\times 10^6$ tonnes). The minimum suspended load and bedload in this period were 1$\times 10^6$ and 0 tones (0.9 $\times 10^6$ and 0 tonnes), respectively [65].

Table 3.6 Lower Brazos River Suspended Sediment Concentration and Load at USGS Stations

Station	Period	Suspended Sediment Concentration, mg/L (Suspended Sediment Load, tons/day)		
		Max	Average	Min
Richmond[1] (USGS-08114000)	1966 - 2021	9,440 (1,230,000)	1,545 (126,140)	12 (23)
Rosharon[2] (USGS-08116650)	1973 - 2023	4,740 (341,000)	414 (22,064)	15 (4)

[1] https://mywaterway.epa.gov/monitoring-report/NWIS/USGS-TX/USGS-08114000/
[2] https://mywaterway.epa.gov/monitoring-report/NWIS/USGS-TX/USGS-08116650/

3.4.3 Sediment Delivery from Brazos River to Gulf of Mexico

The Brazos River plays a significant role in sediment transport, ranking first in sediment load among Texas rivers. It delivers substantial amounts of water and sediment into the Gulf of Mexico. The Brazos River estuary receives sediment from various sources including the Brazos River and its tributaries, shoreline erosion, dredging activities, etc. The sediment load entering the river estuary is estimated to range between 11-17.6 $\times 10^6$ tons (10-16 $\times 10^6$ tonnes) annually [66].

The sediment budget calculation for the Brazos River estuary was conducted in 2013 using sediment cores collected from the area and estimating sedimentation rates through ^{137}Cs analysis. The sedimentation rate for the study area was determined over a 50-year period. **Figure 3.14** illustrates the results of this analysis for the Brazos River estuary area. Based on the accumulation rates over approximately 50 years, the budget estimates that approximately 1.43 $\times 10^6$ tons/year (1.3 $\times 10^6$ tonnes/year) of sediment entering the estuary are retained (8-13%), while 9.6-16.2 $\times 10^6$ tons/yr (8.7-14.7 ×tonnes/yr) (87-92%) are transported outside of the estuary area [66].

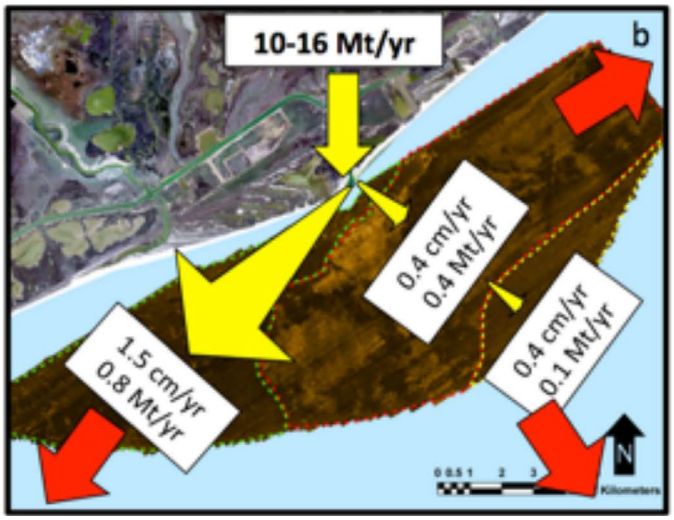

Figure 3.14 Sediment Budget for the Brazos River Estuary Based on Accumulation Rates Over a Period of 50 Years (before 2013). The values in White Boxes Show Sediment Deposition Rate (Thickness Change and Mass Rates) in Different Areas of the Estuary, and Red Arrows Indicate Sediment Loss from the Estuary Area [66]

A numerical modeling effort conducted to assess the impact of the construction of Brazos River Floodgates showed an annual sedimentation rate of 44 $\times 10^6$ cu yd (34 $\times 10^6$ m^3) in the Brazos delta (highlighted in green in **Figure 3.15**) [67]. When considering the surface area of the Brazos delta in this figure, an estimated annual deposition rate of 20 inches (50 cm) is calculated. This rate is significantly higher than those obtained from sediment cores, as illustrated in **Figure 3.14**.

Figure 3.15 Brazos River Delta Sediment Depositional Areas [67]

3.4.4 San Bernard River

3.4.4.1 San Bernard River Watershed Characteristics

The San Bernard River watershed covers approximately 900 mi^2 (2,331 km^2). This watershed is located in central Texas along the Texas Gulf Coast, and it extends across five counties: Austin, Colorado, Wharton, Fort Bend, and Brazoria. It is situated between the Brazos River Basin to the north and the Colorado River Basin to the south, making it an important geographical feature in the region (**Figure 3.16**). The San Bernard River watershed is primarily characterized by small-town urban areas, without any significant major municipalities. The river and its watershed play a significant role in the local ecosystem and water management in these counties [68].

Several climate zones can be found along the central Texas coast, ranging from humid in the north to dry subhumid in the south. There are significant differences between droughts and the precipitation brought by tropical storms [65]. The annual average precipitation in the San Bernard watershed ranges from 40 to 54 inches (1,016 mm to 1,372 mm). The average monthly temperature varies from 54 °F (12.2 °C) in winter to 84 °F (28.7 °C) in summer [68].

In the San Bernard River basin, an assessment conducted in 1979 estimated the annual sediment yield of 0.76 tons/acre (170 tonnes/km^2) [10].

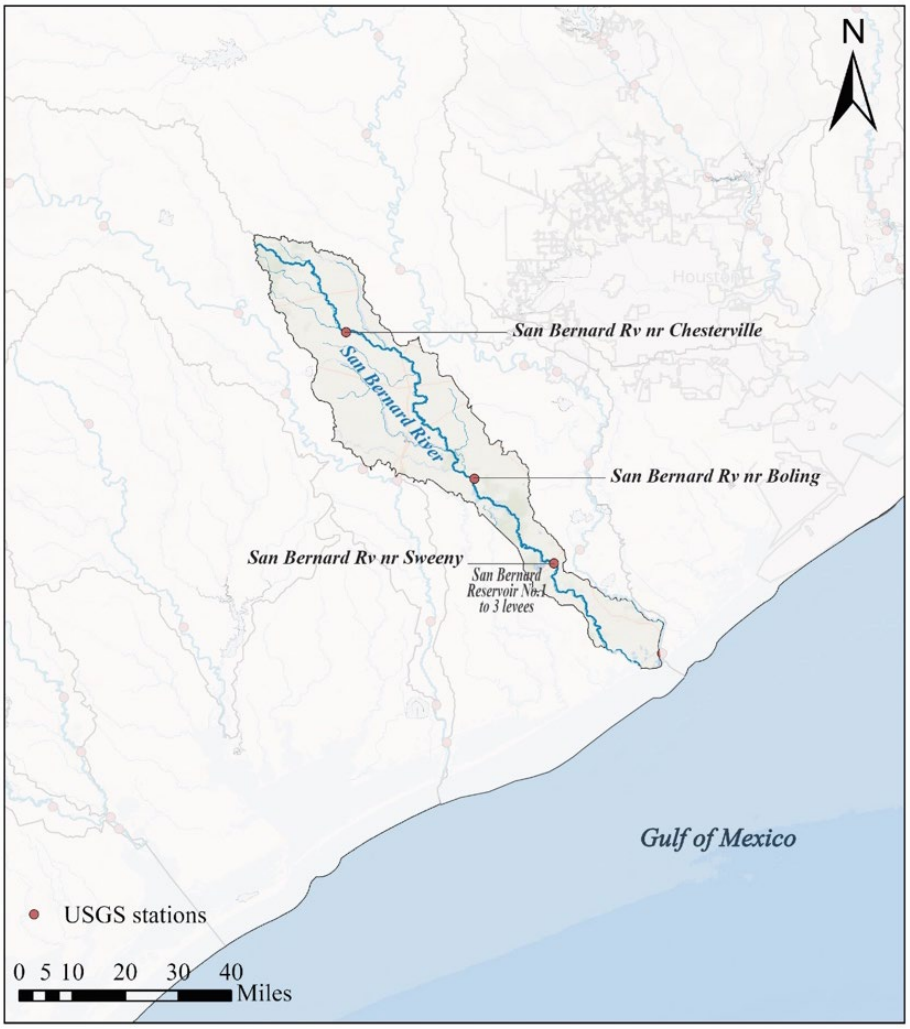

Figure 3.16 San Bernard River Watershed and USGS Monitoring Stations

3.4.4.2 San Bernard River

The San Bernard River begins near New Ulm in Southwest Austin County and flows southeast for 105 miles (168 km) through the Colorado River and Brazos River alluvial valleys. It drains into Cedar Lake and ultimately into the Gulf of Mexico 7.5 miles (12 km) southwest of Freeport (**Figure 3.16**) [69]. The streamflow is mainly produced by local storms, and the resultant sediment discharge is small [70].

The USGS operates several streamflow gauging stations on the main stem of the San Bernard River including Sweeny station (USGS-08117705), Boling station (USGS-08117500), and Chesterville station (USGS-08117370). These stations are located 25-river miles (40 km), 47-river miles (75 km), and 83-river miles (134 km) upstream from the river mouth (**Figure 3.16**). A summary of discharge data for these three stations is provided in **Table 3.7**.

Table 3.7 San Bernard River Annual Daily Discharges at USGS Stations

Station	Drainage Area, mi^2 (km^2)	Period	Discharge, cfs (m^3/s)		
			Max	Average	Min
Chesterville (USGS-08117370)[1]	135 (350)	2018 - 2023	5,730 (162.3)	1,845 (52.2)	33 (0.94)
Boling (USGS-08117500)[2]	727 (1,883)	1953 - 2023	1,330 (38)	533 (15)	150 (4.2)
Sweeny (USGS-08117705)[3]	878 (2,274)	2016 - 2023	3,260 (92)	589 (17)	41 (1.2)

[1] https://waterdata.usgs.gov/nwis/inventory/?site_no=08117370&agency_cd=USGS
[2] https://waterdata.usgs.gov/nwis/inventory/?site_no=08117500&agency_cd=USGS
[3] https://waterdata.usgs.gov/nwis/inventory/?site_no=08117705&agency_cd=USGS

3.4.4.3 Reservoirs

There are no major reservoirs or dams directly on the main stem of the San Bernard River. However, there are smaller water control structures and diversions in the basin, such as San Bernard Reservoir No. 1 to No. 3 Levees. In 1929, the San Bernard River was dammed on the Wharton-Fort Bend County line to create New Gulf Reservoir with a capacity of 2,150 acre-ft (2.65×10^6 m^3). This lake is owned by Texas Gulf Sulphur, and its water is used for municipal supply and irrigation [71].

3.4.5 San Barnard River Estuary Sediment Budget

The San Bernard River estuary is located within Brazoria County, and it is characterized by an average depth of 2.1 ft (0.64 m). This estuary, situated along the mid-Texas coast, receives its annual freshwater inflow primarily from the San Bernard River and the adjacent coastal watershed runoff, totaling an average of 683,753 acre-ft (8.4×10^8 m^3) annually [72].

Sediment input from other tributaries, coastal erosion, human activities (like dredging or changes in the watershed's land use), and sediment transport, deposition, and resuspension due to tides, currents, and wind-driven processes are all factors that affect the sediment budget of the San Bernard River estuary. The shape and configuration of the San Bernard River estuary is highly dynamic. Wind-driven waves typically approach the southeastern shore of the Brazos River delta, causing a pronounced asymmetrical alongshore transport of beach sediments towards the southwest. This predominant wave environment directs the general southwestward transport of both Brazos River and coastal sediments along the shore to the San Bernard River mouth. This natural coastal process, coupled with the excessive sediment discharge into the Gulf of Mexico by the Brazos River and the diversion of the Brazos River by 6 miles (10 km) from its historical mouth, has resulted in frequent blockage at the mouth of the San Bernard River.

3.4.5.1 San Bernard River Sediment Load

The San Bernard River drains a significantly smaller area than either the Colorado River or the Brazos River, and as a result, its flows and sediment discharge are much less [73]. The sediment load in the San Bernard River is available for the period of 1978-2021 at the USGS station near Boling (USGS-08117500) (**Figure 3.16**). For this period, the suspended sediment concentration ranged from 7 mg/L to 366 mg/L, with an average value of 70 mg/L. The average of suspended sediment load was 157 tons/day (142 tonnes/day). The minimum and maximum daily suspended sediment load are estimated as 0.32 tons/day (0.29 tonnes/day) and 1,770 tons/day (1,600 tonnes/day), respectively (**Table 3.8**).

Table 3.8 San Bernard River Suspended Sediment Concentration and Load at USGS Station

Station	Period	Suspended Sediment Concentration, mg/L (Suspended Sediment Load, tons/day)		
		Max	Average	Min
Boling[1] (USGS-08117500)	1978 - 2021	366 (1,770)	70 (157)	7 (0.32)

[1] https://mywaterway.epa.gov/monitoring-report/NWIS/USGS-TX/USGS-08117500/

The average daily suspended sediment load at Boling station was estimated using a discharge-sediment load rating curve. According to this curve, the average daily suspended sediment load for the San Bernard River at this station was reported to be 127 tons/day (115 tonnes/day) and annual total suspended load equal to 46,000 tons (41,730 tonnes), for the period of 1960-2017 [40].

The suspended sediment concentration in San Bernard was measured in 1999 at three sites close to its mouth (Stations 1, 4, 5 in **Figure 3.17**). These sites were located approximately 1, 2, 7 river miles (1.6, 3.3, and 11.3 km) from the river delta. The samples were collected at 2 ft (0.6 m) below surface, mid-depth, and close to bottom. The suspended sediment concentration varied between 16 and 149 mg/L, near surface, 14 and 165 mg/L at mid-depth, and between 27 and 272 mg/L near bed. There were differences in sediment concentration along the depth. The near-bottom sediment concentration was usually higher than that at mid-depth and close to the surface. Overall, the suspended sediment concentration increased from Section 5 (upstream) to Section 1 (river mouth) at all three measuring depths [73].

It is reported that Hurricane Harvey mobilized a substantial amount of sediment in the San Bernard estuary area. The monthly average suspended sediment load delivered by the San Bernard River during Harvey was estimated at 772 tons/day (700 tonnes/day). In total, during this month, the river transported 21,000 tons (19,000 tonnes) of sediment, accounting for 50% of the annual average suspended sediment load [40].

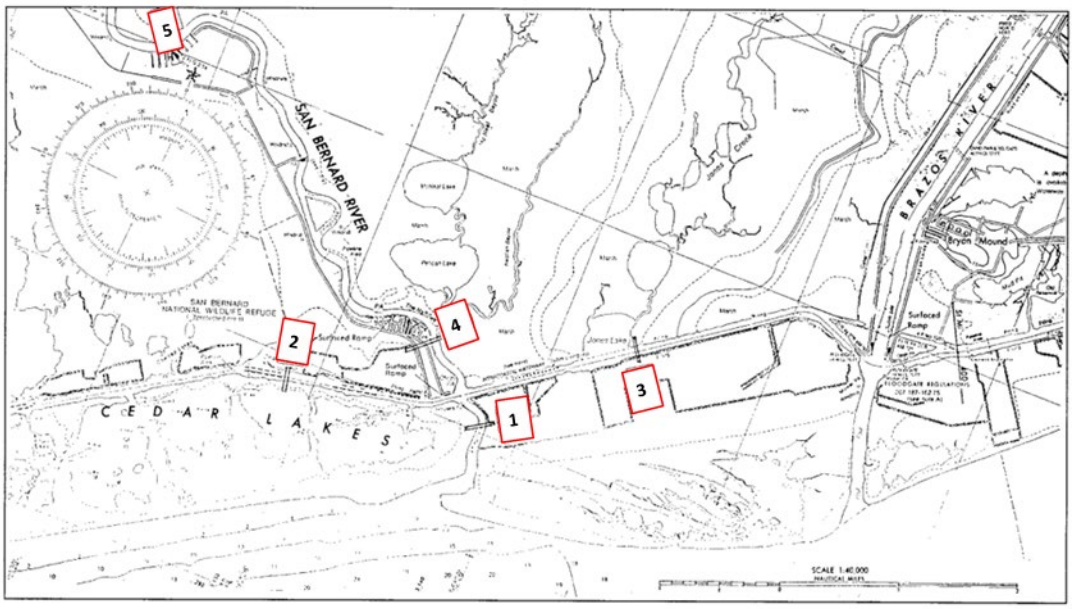

Figure 3.17 Locations of Transects for Suspended Sediment Sampling [73]

3.4.6 Sediment Delivery from San Bernard River Estuary to the Gulf of Mexico

The limited fluvial flow and a moderate tidal range contribute to the San Bernard River's relatively weak flushing capacity [70]. Consequently, sediments transported by the river tend to rapidly accumulate within its inactive channel. These conditions, coupled with the Brazos River's redirection to within 6 miles (10 km) of the San Bernard, result in frequent blockages at the river mouth. This lack of a direct connection to the Gulf of Mexico has led to significant changes in sediment and flow patterns, giving rise to multiple hazards and necessitating expensive corrective dredging initiatives [57].

The San Bernard Navigation Channel was dredged 20 times for the period of 1943-2002, with a frequency of 2.3 years and a shoaling rate of roughly 14,000 cu yd/yr (10,700 m^3/yr) [70].

A preliminary sediment analysis was conducted for the GoM costal area between Freeport Entrance and Matagorda Ship Channel [74,75]. The area was divided into 10 cells, and sediment budget for each cell was calculated (**Figure 3.18**). Cells 1 to 4 represent the area considered for the sediment budget analysis of the Brazos-San Bernard estuary area. In this analysis, the following sediment quantities were considered:

- average annual dredging from Freeport Entrance = 1,047,000 cu yd/yr (800,490 m^3/yr) based on the 1951-2006 dredging record and from San Bernard River mouth = 14,000 cu yd/yr (10,700 m^3/yr) based on the 1943-2009 dredging record.
- sand supplied to the system by the Brazos River = 1,850,000 cu yd/yr (1,414,426 m^3/yr) and by the San Bernard River = ~ 0. Based on this analysis, the sand delivery from the San Bernard River to the GoM is negligible.

– The annual volume change in each cell and the net and gross sediment transport rates for each cell are summarized in **Table 3.9**. The alongshore sediment transport in the vicinity of the Brazos-San Bernard estuary area is shown on **Figure 3.18**.

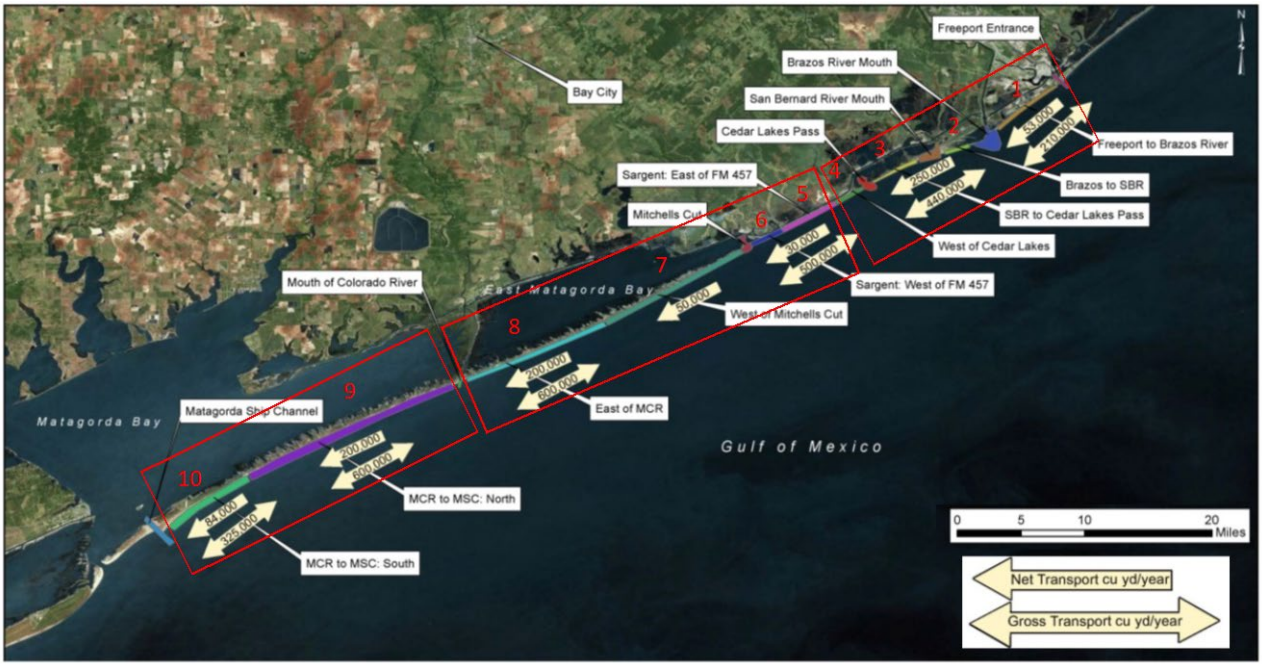

Figure 3.18 Locations of Cells for Sediment Budget Analysis Along Coastal Area between Freeport Entrance and Matagorda Ship Channel (Modified from Ref. [74])

Table 3.9 Annual volume change in each cell and the net and gross sediment transport rates for Cells 1 to for used in sediment budget calculations [74,75]

Cell No. and Extent of the Cell	Annual Volume Change (ΔV)[2] (cu yd/yr)	Alongshore Net Westward Sediment Transport (cu yd/yr)	Alongshore Gross Sediment Transport (cu yd/yr)
1- Freeport to Brazos Beach	–39,430	53,000	210,000
2- Brazos to San Bernard River	54,000	250,000	440,000
3- San Bernard River to Cedar Lakes	276,920	250,000	440,000
4- West of Cedar Lakes	–166,080	(-)[1]	(-)[1]

[1] No readily available potential transport rate.
[2] Quantiles presented in this column is from Ref. [75]

The contribution from the shoreline erosion was not considered in the sediment budget discussed above. According to **Figure 3.19**, the region between Freeport Channel and the Brazos River mouth has been eroding at the rate of 5-20 ft/yr (1.5-6 m/yr) while the area from the Brazos River mouth to mouth of the San Bernard River is advancing at the rates up to 21 ft/yr (6.3 m/y). Between the San Bernard estuary and Cedar Lake Pass, the shoreline is eroding at the rate of 2-30 ft/yr (0.6-9 m/yr) [27].

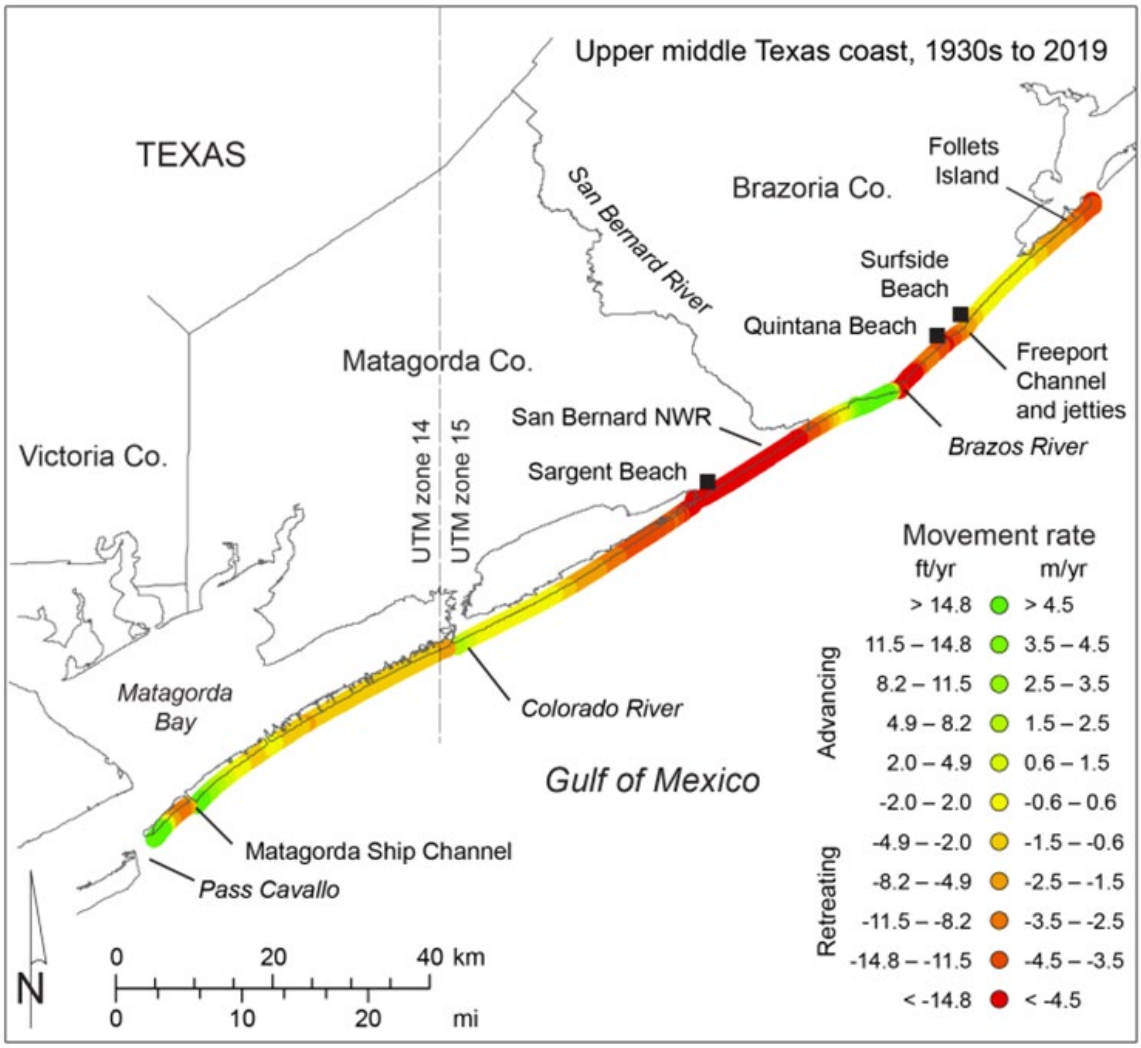

Figure 3.19 Net Rates of Long-term Movement for the Texas Gulf Shoreline Between San Luis Pass and Pass Cavallo from 1930s to 2019 [27]

3.5 East Matagorda Bay System

3.5.1 East Matagorda Bay System Watershed Characteristics

The East Matagorda Bay system, located within Matagorda County along the mid-coast of Texas, is an integral component of the Matagorda Bay system. It is enclosed by the Matagorda Peninsula and the tidal flats at the entrance of the Colorado River. The East Matagorda Bay does not have any major rivers flowing into it, and it receives only the runoff from the adjacent coastal watershed. Within the East Matagorda Bay watershed, there are nine ungauged watersheds that contribute inflow into the bay, as depicted in **Figure 3.20** [76]. The only connections from the bay to the Gulf of Mexico is through Brown Cedar Cut, situated near the northern tip of the peninsula, and Three Mile Cut east of mouth of the Colorado River. However, the exchange between the bay and the Gulf may occur only during high water levels. Mitchell's Cut, located on the easternmost edge of the bay, is a tidal inlet connecting the Gulf of Mexico with the GIWW and East Matagorda Bay.

The East Matagorda Bay watershed supports a diverse range of ecosystems, including marshes, estuaries, and coastal habitats. These ecosystems are important for a variety of wildlife species, including fish, birds, and other aquatic organisms.

The primary land cover types in this watershed are open water (72.2%) and wetlands (15.9%). Between 2008 and 2018, agriculture land cover has increased by 388%, from approximately 575 acres (1.05%) to 2,804 acres (5.1%). Developed land cover has increased by 256%, from 335 acres (0.6%) to 1,192 acres (2.2%) [77].

The Matagorda, Texas, experiences warm to hot conditions. Summers are typically hot and humid, with average high temperatures ranging from 86 to 89 °F (30 to 32 °C). Winters are relatively mild, with average high temperatures ranging from the upper 62 to 64 °F (17 to 18 °C). The average annual precipitation at Matagorda station is 44.6 inches (1,133 mm) [78].

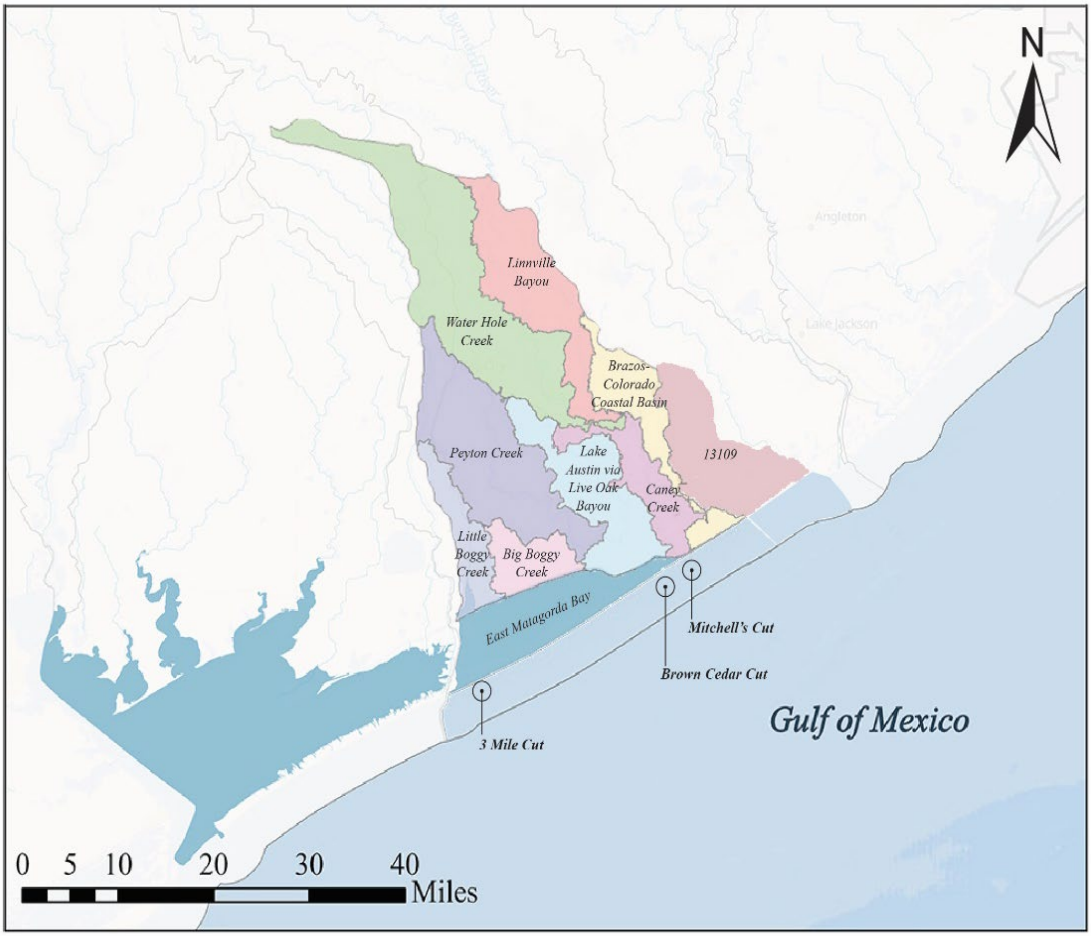

Figure 3.20 East Matagorda Bay System and its Sub-watersheds (Redeveloped from Ref. [76])

3.5.1.1 Caney Creek

Caney Creek begins northwest of Wharton, Texas, and meanders 155 miles (249 km) southeastward before reaching its confluence with the Gulf Intracoastal Waterway (GIWW),

located 5.5 miles (8.9 km) to the southeast of Sargent (**Figure 3.20**). Initially, Caney Creek is intermittent, but its flow becomes continuous upon receiving contributions from other streams at the Matagorda County line. The land along the creek is utilized for rice and cotton cultivation, as well as cattle ranching. The dominant land use categories in the Caney Creek watershed are agriculture, heavy woods (dense understory), light woods (relatively thin, no under story), public, residential, and water. Approximately 80% of the area land use is agricultural, 15% woods, and 5% residential [79].

The climate within the Caney Creek watershed is characterized by hot and humid conditions during the summer months, with average temperatures reaching 92 °F (33 °C) in July. Winters are comparatively mild, with average temperatures around 41 °F (5 °C) in January. The annual average rainfall for the area is recorded at 42.3 inches/yr (1,074 mm/ yr) [80].

The majority of the watershed features relatively flat to gently sloping terrain, which results in the gradual movement of runoff across the landscape. The surface geology of the watershed is complex, primarily due to the cyclic deposition of sediments. This geological process has led to the formation of discontinuous layers of sand, silt, clay, and gravel within the region [81].

During floods, floodwater from the Colorado will sometimes cross into the Caney Creek watershed due to the creek's proximity to the Colorado near the town of Glen Flora [82].

3.5.1.2 East Matagorda Bay

East Matagorda Bay is a minor estuary located on the mid-Texas coast in Matagorda County, just northeast of the Colorado-Lavaca Estuary. This minor bay system covers approximately 57 mi^2 (147.6 km^2) and has an average depth of 3.4 ft (1 m). Due to both natural and man-made factors, East Matagorda Bay now experiences reduced freshwater inflow as compared to earlier periods when the Colorado River used to flow directly into Matagorda Bay. The east bay now receives freshwater inflow only from runoff of surrounding coastal watersheds and from direct precipitation on the bay. Average surface inflow to East Matagorda Bay, based on estimates of runoff from surrounding coastal sub-watersheds, is 0.6 $\times 10^6$ acre-ft/yr (741 $\times 10^6$ m^3/yr) [83].

The bay's hydrodynamics are influenced by wind patterns, water temperature, and circulation patterns. These processes can impact water movement and the distribution of sediments and nutrients within the bay. The bay's salinity levels can vary depending on the balance between freshwater inflow and evaporation. Salinity is an important factor for the bay's ecosystem and the species that inhabit it.

3.5.2 East Matagorda Bay System Sediment Budget

The amount of sediment entering East Matagorda Bay can vary significantly over time due to natural processes and human activities. The sediment input into the bay is influenced by factors such as rainfall, creek discharges, coastal erosion, and human-made changes to the watershed. Additionally, sediment input can fluctuate seasonally and in response to specific weather events, such as storms. However, no flow and sediment data have been collected from creeks discharging

to the bay, which poses challenges for understanding sediment dynamics and calculating the bay's sediment budget.

Caney Creek does not flow into the East Matagorda Bay; instead, it discharges into the GIWW. The sediment yield from Caney Creek is also unknown due to the absence of stream gauging or sediment transport data collection.

3.5.2.1 Sediment Delivery to East Matagorda Bay

In the East Matagorda Bay basin, an assessment conducted in 1979 estimated an annual sediment yield of 0.0023 tons/acre (0.52 tonnes/km^2) [10]. This estimate is equivalent to 157,000 tons/yr (142,000 tonnes/yr) representing the amount of sediment that may annually enter the bay from upstream. This sediment inflow could result in an average sedimentation rate of 0.055 in/yr (1.4 mm/yr) in the bay, assuming no sediment would be transported to the Gulf of Mexico. This rate is significantly lower than the historical rate of 0.19 inches/yr (4.8 mm/yr) reported for the period between 1856 and 1934, i.e., before the completion of the Gulf Intracoastal Waterway (GIWW) construction [45].

Another potential sediment source for East Matagorda Bay and the navigation channel is lateral input resulting from bay shoreline erosion. The erosion rates along the perimeter of East Matagorda Bay were estimated to be up to 10 ft/yr (3 m/yr) (**Figure 3.21**). Furthermore, due to the degraded condition of the islands that previously provided shelter to the GIWW from the open bay, there is now an unobstructed pathway for sediment from within the bay to be deposited in the navigation channel [84].

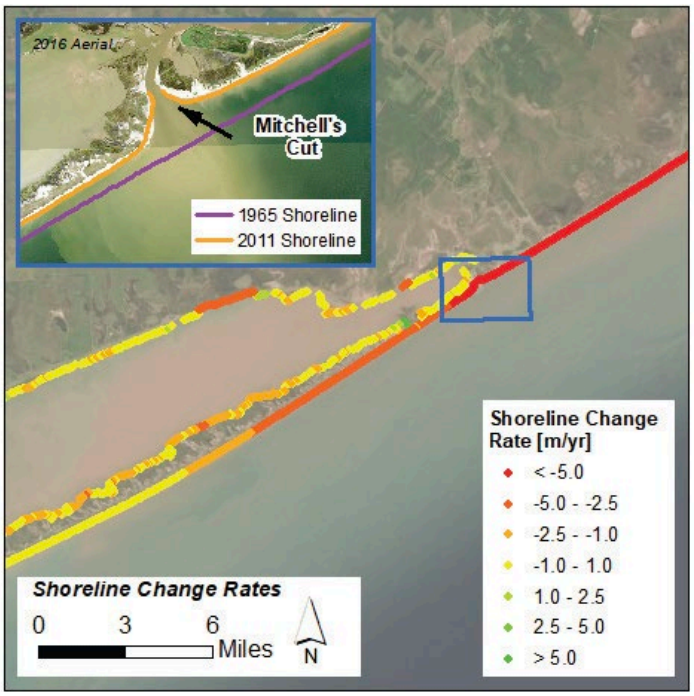

Figure 3.21 Shoreline Change in East Matagorda Bay Area (Data Developed by the Texas Bureau of Economic Geology (Adopted from Ref. [84])

3.5.3 Sediment Delivery from East Matagorda Bay to Gulf of Mexico

Although Mitchell's Cut connects the GIWW and East Matagorda Bay with the Gulf of Mexico, sediment entering the bay from its watershed and shoreline erosion does not reach the Gulf. It is even possible that some sand materials enter the GIWW and the bay through wind action in the shoreline area. The results of a field sampling published in 1979 [85] and recent investigations in 2021 [86] show that sediment regime vary in East Matagorda Bay. Different grain size distribution patterns can be found in different locations within the bay, but silt dominates. However, an area with fine sand can be found on the east side of the bay, closer to Mitchell's Cut (area highlighted with the red box in **Figure 3.22**). The source of this material might be the sand in Sargent Beach area transported through Michell's Cut [84]. It can be concluded that no sediment is delivered from the East Matagorda Bay to the Gulf of Mexico.

As shown in **Figure 3.21**, the shoreline between Mitchell's Cut and peninsula is eroding at the rate of 0.3 to 1.5 ft/yr (1 to 5 m/yr) with the highest erosion rate occurring in the area west of the Mitchell's Cut. The annual volume change (ΔV) in this area varies from 19,775 to 514,480 cu yd/yr (15,119 to 393,348 m^3/yr) [74,75]. The net sediment transport along the shore changes from 50,000 cu yd/yr (38,228 m^3/yr) west of Michell's Cut to 200,000 cu yd/yr (152,911 m^3/yr) east of mouth of Colorado River (**Figure 3.18**).

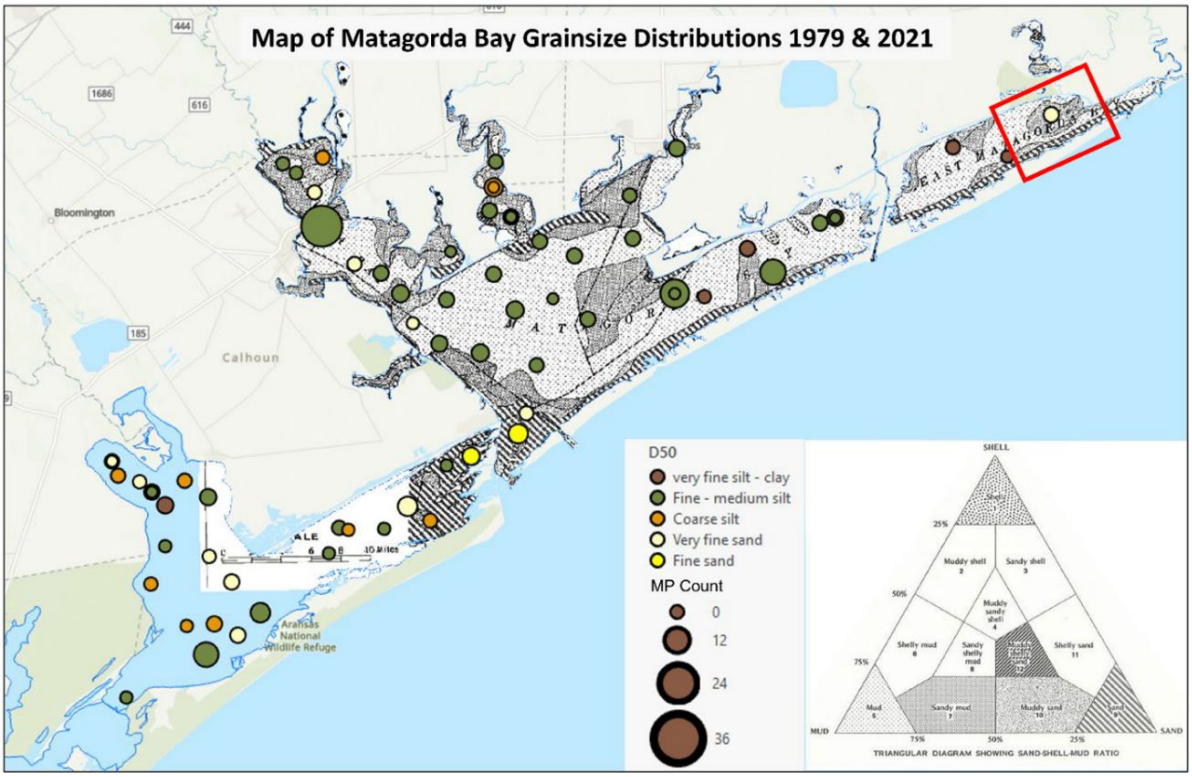

Figure 3.22 Grainsize Distribution from Shallow Bed Grab Samples Collected from Matagorda Bay in 2021 (Circles) Overlain with the Sediment Distribution Map Modified from Ref. [85] (Area Marked by the Red Box is Where Sand is Found by Both Studies (Figure 4 in Ref. [86]))

A preliminary sediment budget analysis was conducted for the GoM costal area between Freeport Entrance and Matagorda Ship Channel [74,75]. The area was divided into 10 cell, and sediment budget for each cell was calculated (**Figure 3.18**). Cells 5 to 8 represent the area considered for the sediment budget analysis of East Matagorda Bay area. The annual volume change in each cell and the net and gross sediment transport rates considered in sediment budget calculations are summarized in **Table 3.10**. The alongshore sediment transport rates the East Matagorda Bay area is shown on **Figure 3.18**.

Table 3.10 Annual Volume Change in Each Cell and the Net and Gross Sediment Transport Rates for Cells 1 to for used in the Sediment Budget Calculations in East Matagorda Bay Area [74,75]

Cell No. and Extent of the Cell	Annual Volume Change (ΔV)[1] (cu yd/yr)	Alongshore Net Westward Sediment Transport (cu yd/yr)	Alongshore Gross Sediment Transport (cu yd/yr)
5- Sargent: East of FM 457	–242,775	30,000	500,000
6- Sargent: West of FM 457	–167,440	30,000	500,000
7- West of Mitchells Cut	–514,480	50,000	-
8- East of Colorado River Mouth	–19,775	200,000	600,000

[1] Quantiles presented in this column is from Ref. [75]

3.6 Matagorda Bay System

3.6.1 Matagorda Bay Watershed Characteristics

The Matagorda Bay system (or the Colorado-Lavaca Estuary) is one of the oldest bay systems in Texas. It encompasses the Colorado River, Lavaca River, Lavaca Bay, Matagorda Bay, Carancahua Bay, Tres Palacios Bay, and other smaller creeks and bays (**Figure 3.23**). It is situated within a sub-tropical humid climate characterized by an average annual rainfall of approximately 42 inches (1,072 mm) [87]. The total drainage area of the Matagorda Bay watershed is approximately 4,480 mi^2 (11,600 km^2) [88].

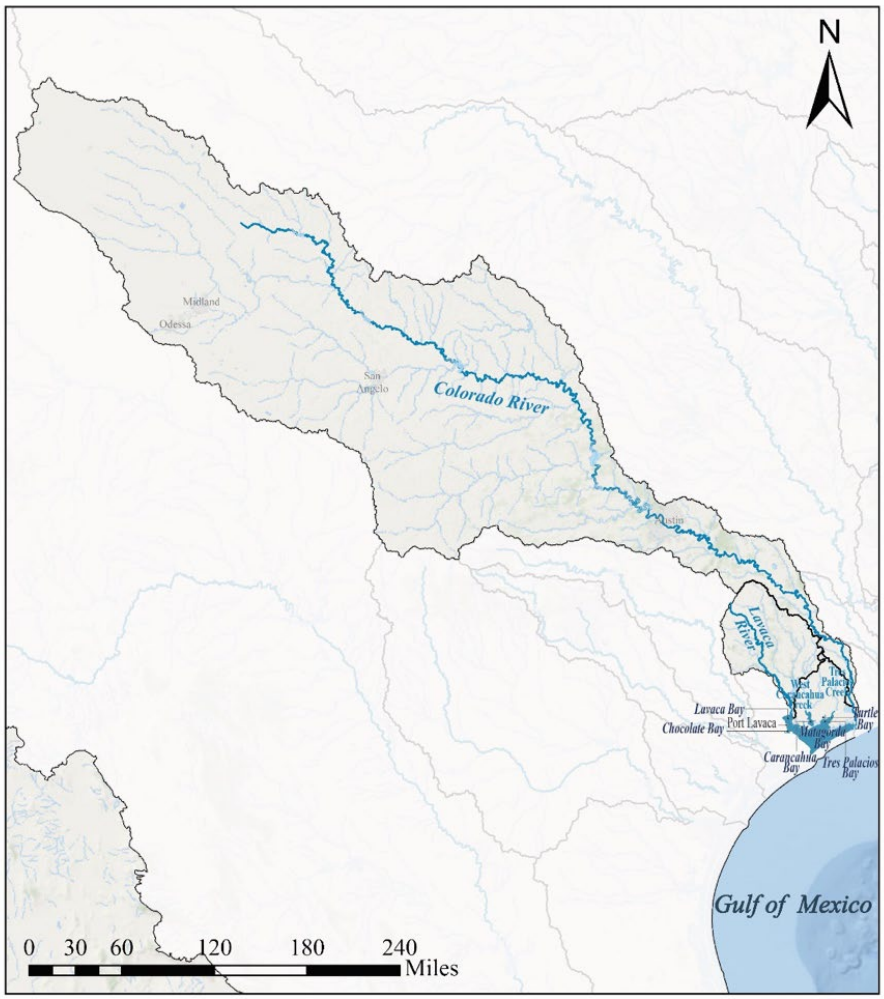

Figure 3.23 Matagorda Bay System Watershed

3.6.1.1 Colorado River

The Colorado River is a vital watercourse in Texas, extending over approximately 862 miles (1,387 km) from its origin in Dawson County to its terminal point at the Gulf of Mexico. Its path takes it in a generally southeast direction, passing through various cities and towns, including Ballinger, Marble Falls, Lago Vista, Austin, Bastrop, Smithville, La Grange, Columbus, Wharton, and Bay City, before ultimately discharging into the Gulf of Mexico at Matagorda Bay (**Figure 3.24**). The watershed is approximately 42,300 mi^2 (109,560 km^2) [89] and incorporates diverse ecosystems such as forests, grasslands, wetlands, and urban zones.

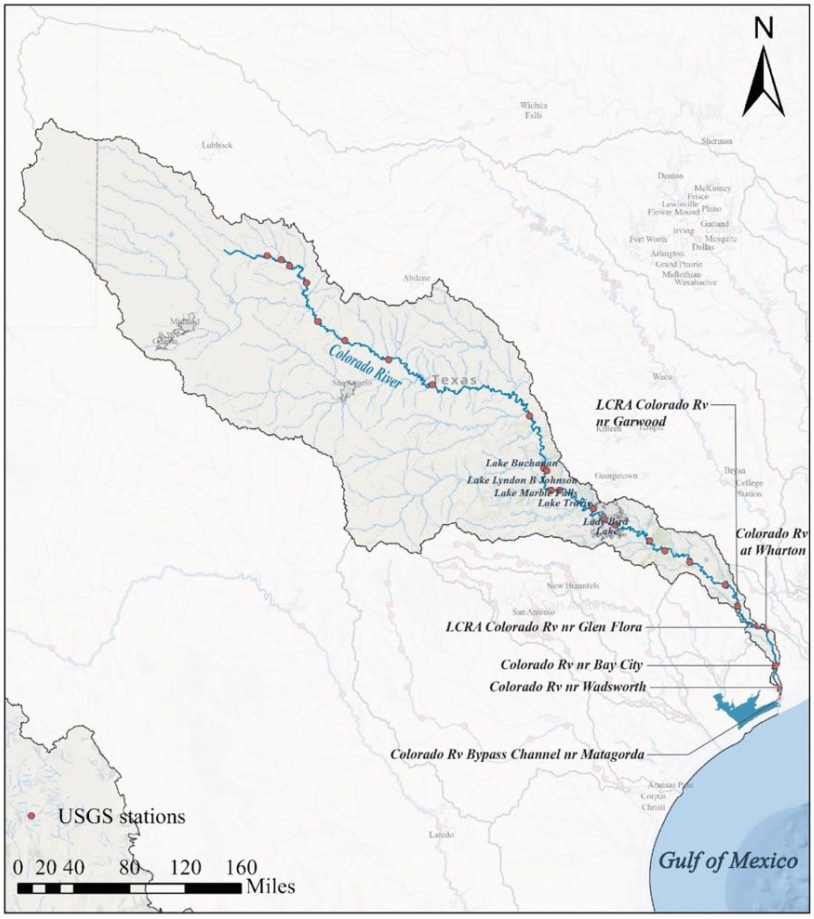

Figure 3.24 Colorado River Watershed and USGS Monitoring Stations

The Colorado River watershed experiences a semi-arid climate, with average monthly precipitation ranging about between 0.27 to 1.96 inches (7 to 50 mm) in lower Colorado basin region. The precipitation rates generally increase from the western parts towards the eastern parts of the watershed. The average monthly temperature across the lower Colorado region varies between around 41 to 79°F (5 to 26 °C) [90].

The USGS maintains numerous streamflow gauging stations across the Colorado River watershed. Stations in lower Colorado River include Wharton, Wadsworth, and the Bay City (**Figure 3.24**). The mean annual discharges at the Wharton, Wadsworth and Bay City stations are approximately 2,604, 2,340 and 2,683 cfs (74, 66, and 76 m^3/s), respectively (**Table 3.11**).

In 1979, erosion and sediment yield within the Colorado River basin were estimated. The yearly sediment yields varied, with rates of 0.35 tons/acre (78.5 tonnes/km^2) in the upstream area, 0.25 tons/acre (56 tonnes/km^2) in the middle area of the watershed, and 1.12 tons/acre (251 tonnes/km^2) in the lower part of the basin [10].

Table 3.11 Colorado River Annual Daily Discharges at USGS Stations

Station	Drainage Area, mi^2 (km^2)	Period	Discharge, cfs (m^3/s)		
			Max	Average	Min
Wharton[1] (USGS-08162000)	42,003 (108,787)	1938 - 2023	5,180 (147)	2,604 (74)	1,110 (31)
Bay City[2] (USGS-08162500)	42,240 (109,401)	1947 - 2023	5,300 (150)	2,683 (76)	746 (21)
Wadsworth[3] (USGS-08162501)	42,307 (109,574)	2015 - 2023	14,100 (400)	2,340 (66)	406 (11.5)

[1] https://waterdata.usgs.gov/nwis/inventory/?site_no=08162000
[2] https://waterdata.usgs.gov/nwis/inventory/?site_no=08162500
[3] https://waterdata.usgs.gov/nwis/inventory/?site_no=08162501

3.6.1.2 Lavaca River

The Lavaca River begins in the northeastern part of Gonzales County and travels generally southeast for 117 miles (188 km) until it empties into Lavaca Bay, which is a component of Matagorda Bay. The river flows through Lavaca and Jackson counties, passing through cities such as Hallettsville, Edna, and Vanderbilt (**Figure 3.25**). The watershed area of the Lavaca River covers approximately 2,309 mi^2 (5,980 km^2), including diverse habitats like forests, grasslands, and urban areas [91].

The Lavaca River watershed experiences a humid subtropical climate. The mean annual precipitation across the basin is 5.1 inches (129 mm). The average annual temperature varies from 59 to 80 °F (15 to 26.6 °C) [92].

The USGS operates several stream flow gauging stations across the Lavaca River watershed, including the Edna and Hallettsville stations (**Figure 3.25**). The mean annual discharges at Hallettsville and Edna stations are approximately 49 and 361 cfs (1.7 and 13 m^3/s), respectively (**Table 3.12**).

In 1979, a study estimated the sediment yield within the Lavaca River basin. In the Lavaca River basin, the average annual sediment yield was approximately 0.66 tons/acre (148 tonnes/km^2) [10].

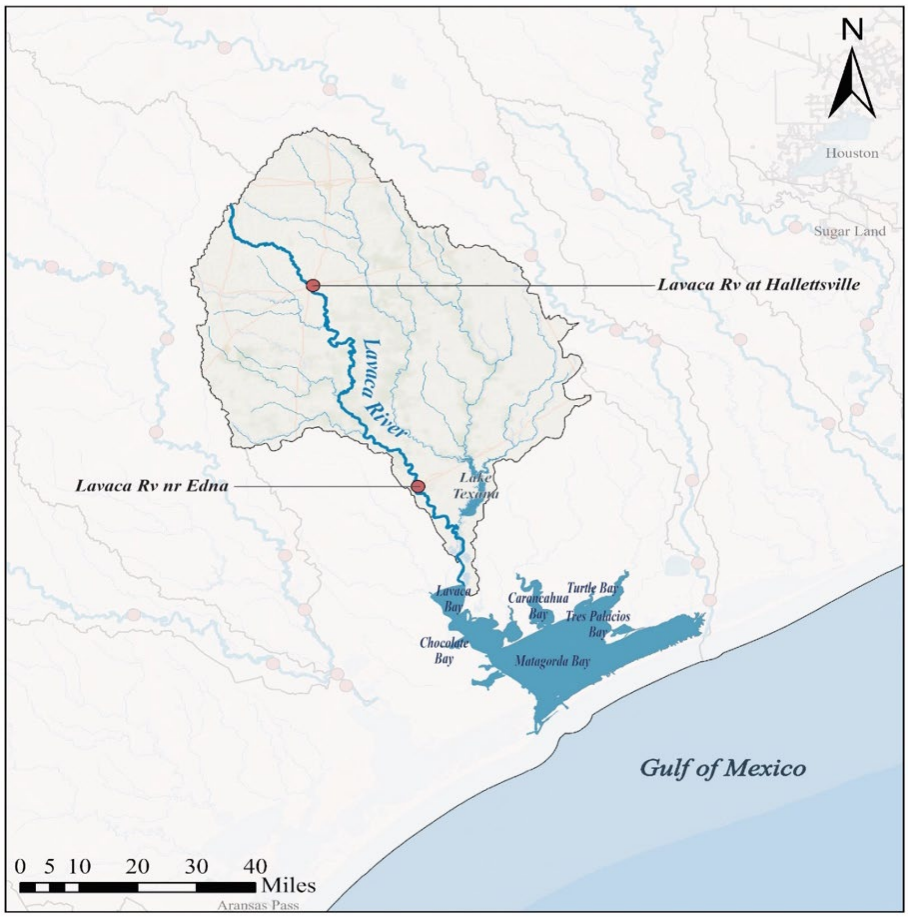

Figure 3.25 Lavaca River Watershed and USGS Monitoring Stations

Table 3.12 Lavaca River Annual Daily Discharges at USGS Stations

Station	Drainage Area, mi² (km²)	Period	Discharge, cfs (m³/s)		
			Max	Average	Min
Edna[1] (USGS-08164000)	817 (2,116)	1937 - 2023	2,380 (67.4)	361 (10)	33 (0.93)
Hallettsville[2] (USGS-08163500)	108 (280)	1966 - 2023	944 (26.7)	49 (1.4)	2 (0.06)

[1] https://waterdata.usgs.gov/nwis/inventory/?site_no=08164000&agency_cd=USGS
[2] https://waterdata.usgs.gov/nwis/inventory/?site_no=08163500&agency_cd=USGS

3.6.1.3 Reservoirs

Several dams and reservoirs have been constructed on the Colorado and Lavaca Rivers and their tributaries, serving a variety of purposes, such as flood control, hydroelectric power, water supply, and recreation.

Some of the notable dams and reservoirs located along the Colorado River and its tributaries are as follows [93].

- *Lake Travis:* Lake Travis is located on the Colorado River in Travis County, 13 miles (21 km) northwest of Austin. It has a total reservoir capacity of 1,134,956 acre-ft (1.4×10^9 m^3) encompassing a surface area of 19,297 acres (78 km^2) at conservation pool elevation.
- *Lake Marble Falls:* Starcke Dam and Lake Marble Falls are located on the Colorado River in Burnet County, near Marble Falls, Texas. The reservoir was built primarily for hydroelectric power. It has a total reservoir capacity of 7,486 acre-ft (9.2×10^6 m^3) encompassing a surface area of 608 acres (2.5 km^2) at the elevation of 738 ft (224.9 m) above mean sea level.
- *Lady Bird Lake:* Formerly known as Town Lake, Lady Bird Lake was formed by the construction of Longhorn Dam in 1960. Although it is not used for water supply or flood control, it provides recreational opportunities for residents of Austin. It covers an area of about 465 acres (1.89 km^2) at conservation pool elevation and has a storage capacity of around 7,151 acre-ft (8.8×10^6 m^3).
- *Lake Buchanan:* Lake Buchanan is the second largest of the Highland Lakes in Central Texas. The lake covers an area of about 22,137 acres (89.6 km^2), and the reservoir storage capacity is approximately 886,626 acre-ft (1.09×10^9 m^3).
- *Lake Lyndon B. Johnson:* Formed by the construction of Granite Shoals Dam (also known as Wirtz Dam) in 1950. Lake Lyndon B. Johnson covers an area of about 6,273 acres (25.4 km^2) at an operating elevation of 825.68 ft (251.67 m) above mean sea level. Its storage capacity is approximately 133,090 acre-ft (1.64×10^8 m^3).

The only reservoir in the Lavaca River watershed is Lake Texana [94].

- *Lake Texana:* Lake Texana is a reservoir on the Navidad River, a major tributary to the Lavaca River. It was created by the construction of the Palmetto Bend Dam. The lake covers approximately 9,676 acres (39.1 km^2) at the conservation pool elevation and has a total storage capacity of about 159,845 acre-ft (1.98×10^9 m^3). Lake Texana serves as a critical water supply source for the region, including cities such as Corpus Christi and Victoria. It also provides recreational opportunities, including boating and fishing.

3.6.1.4 Matagorda Bay

Matagorda Bay is separated from the Gulf of Mexico by the Matagorda Peninsula, and water exchange occurs through several principal tidal inlets, including Pass Cavallo, Matagorda Ship Channel, Greens Bayou, and the Colorado River. The Matagorda Bay has an area of 244,490 acres (990 km^2) and typically receives 3.5×10^6 acre-ft (4.3×10^9 m^3) of freshwater inflow from its major rivers: the Colorado River, Lavaca River, and the Tres Palacios River, as well as from numerous creeks and surrounding coastal watersheds [95]. The annual surface inflow to the bay ranged from a minimum of 441,162 acre-ft (0.54×10^9 m^3) in 1954 to a maximum of 14.9×10^6 acre-ft (18.4×10^9 m^3) in 1992 [96].

Matagorda Bay constitutes a shallow, depositional environment with depths of roughly 10 ft (3 m) observed at the confluence of the Colorado River. Lavaca Bay, situated to the northwest where it converges with the Lavaca River, maintains an approximate depth of 8 ft (2.4 m). The sediment composition of both bays stems from a combination of natural and human-made tidal inlets, coastal erosion, and the drainage basins of the Colorado and Lavaca Rivers. Overall, it appears that the modern Colorado River Delta serves as the primary source of sediment for the bay system [52].

The flow of freshwater into Matagorda Bay has undergone significant anthropogenic changes over the past century. These alterations include the construction of over 20 reservoirs and dam systems along tributaries within the Matagorda Bay system watershed. Additionally, the primary source of inflow into the estuary, the Colorado River, has experienced a shift in its discharge point. Instead of entering the eastern arm of Matagorda Bay, the river's water was redirected to flow directly into the Gulf of Mexico. The volume of inflow from the Colorado River into Matagorda Bay during the period of 1950s to the 1990s exhibited substantial variability. Efforts to restore and manage the inflow into Matagorda Bay were initiated in the early 1990s. This involved the completion of a diversion channel connecting the Colorado River and Matagorda Bay in May 1990, which led to an increase in inflow. Further restoration efforts included the construction of dams in two locations: the Tiger Island Cut dam in May 1991 and a dam across the Colorado River in July 1992. These measures effectively blocked the temporary entrance of the Colorado River into the Gulf of Mexico, fully restoring the natural flow pattern into Matagorda Bay [87].

3.6.2 Matagorda Bay System Sediment Budget

The Colorado River, initially flowing into a shared estuary with the Brazos River, altered its course around 1,000 years ago to discharge into Matagorda Bay near Matagorda, Texas, [97]. However, during the 1800s, the flow of sediment to the bay was blocked due to log and brush jams, resulting in the creation of a lake located 46 miles (74 km) upstream from Matagorda [98]. These obstructions significantly limited sediment discharge to the bay. In late 1920s a channel was excavated through the log jam, freeing the trapped sediment. This action led the rapid expansion of the Colorado River delta within Matagorda Bay, reaching as far as the Matagorda Peninsula by 1935 [99]. To establish a direct link to the Gulf, a straight channel was dredged through Matagorda Peninsula from one of the river outlets in the delta [97].

In addition to the Colorado River, the Matagorda Bay system receives both water and sediment from a variety of sources, including natural and human-made tidal inlets, storm channels, major and minor streams running through the upland areas, as well as runoff from the uplands. Additionally, sediment is contributed through the erosion of mainland shorelines. The exchange of water between the bay system and the Gulf of Mexico occurs through Greens Bayou, Matagorda Ship Channel, and Pass Cavallo. Larger rivers, including the Colorado and Lavaca Rivers, along with Garcitas Creek, have formed deltas along the edges of the bay. Among these, the Colorado River delta is the most extensive, and it has extended its reach across Matagorda Bay over time [85].

Tropical storms and hurricanes play a significant role in the transport and deposition of sediment within the Matagorda Bay system. The impact of these weather events depends on the location of the storm center. During these events, sediment can be transported from the Gulf shoreface, beaches, and barrier islands into the estuaries, bays, and lagoons. Conversely, sediment may also be carried from these waterbodies seaward through tidal inlets and storm channels as hurricanes approach, make landfall, and move further inland. Some hurricanes bring heavy rainfall, causing extensive flooding in coastal lowland areas. Under these flood conditions, rivers transport large volumes of water and sediment to estuaries and bays. Also, in tidal pass areas, tidal currents play a crucial role in transporting sand. However, within the Matagorda Bay system, astronomical tides have a relatively minor impact on sediment transport. Wind generates waves, typically ranging from 2 to 3 ft (0.6 to 0.9 m), resuspend bottom sediment. This suspended sediment can then be carried by wind-generated currents [85].

3.6.2.1 Colorado River Sediment Load

The USGS collects sediment data at many locations on the Colorado River. The closest station to the Matagorda Bay with sediment data is Wadsworth (USGS-08162501) (**Figure 3.24**). Sediment data at this station is available only for the period of 2012-2022. For this short period, the minimum, average, and maximum suspended sediment concentration were 6, 634, and 2,230 mg/L. The corresponding daily suspended sediment load were estimated as 4.1, 54,641, and 335,000 tons/day (3.7, 49,570, 303,900 tonnes/day) (**Table 3.13**).

At the Wharton station (USGS-08162000), located upstream of the Wadsworth station (**Figure 3.24**), sediment data is available for the period of 1974-2021. For this period, the minimum, average, and maximum suspended sediment concentration were 5, 90, and 5,530 mg/L. The corresponding daily suspended sediment load were estimated as 4, 4,456, and 358,000 tons/day (3.7, 4,042, 303,900 tonnes/day) (**Table 3.13**).

Given the small area and narrow width of the Colorado River basin between Wharton station and the river delta, it is reasonable to consider the sediment load measured at this station as the sediment load entering the river delta. Therefore, the annual sediment yield for the basin can be calculated as 0.083 tons/acre (18.6 tonnes/km^2) considering the contributing drainage area (1.96 $\times 10^7$ acre (79,253 km^2)) [100] and annual sediment load at this station (4,456 tons/day × 365 days = 1,626,440 tons/yr (1,475,480 tonnes/yr). This rate is significantly lower than the annual sediment yield values reported for the Colorado River basin, which range from 0.25 to 1.12 tons/acre (56 to 251 tonnes/km^2) [10].

Table 3.13 Colorado River Annual Suspended Sediment Concentration and Load at USGS Stations

Station	Period	Suspended Sediment Concentration, mg/L (Suspended Sediment Load, tons/day)		
		Max	Average	Min
Wadsworth[1] (USGS- 08162501)	2012 - 2022	2,230 (335,000)	634 (54,641)	6 (4.1)
Wharton[2] (USGS- 0816200)	1974 - 2021	5,530 (358,000)	90 (4,456)	5 (4)

[1] https://mywaterway.epa.gov/monitoring-report/NWIS/USGS-TX/USGS-08162501/
[2] https://mywaterway.epa.gov/monitoring-report/NWIS/USGS-TX/USGS-08162000/

3.6.2.2 Lavaca River Sediment Load

The USGS collects sediment data at on the Lavaca River at Edna (USGS-08164000) (**Figure 3.25**). Sediment data at this station is available for the period of 1977-2020. For this period, the minimum, average, and maximum suspended sediment concentration were 3, 103, and 745 mg/L. The corresponding daily suspended sediment load were estimated as 0, 190, and 10,800 tons/day (0, 172, 9,800 tonnes/day) (**Table 3.14**). The annual sediment yield for the basin is calculated as 0.13 tons/acre (29.7 tonnes/km^2) considering the contributing drainage area (5.2 $\times 10^5$ acres (2,116 km^2)) (**Table 3.12**) and annual sediment load at this station (190 tons/day $\times$365 days = 69,350 tons/yr (62,913 tonnes/yr)). This rate is significantly lower than the annual sediment yield value reported for the Lavaca River basin, which is documented as 0.66 tons/acre (148 tonnes/km^2) [10]. Nevertheless, these estimates are closer to the annual sediment load and sediment yield calculated for the period of 1958-1986 at the Lavaca River at Edna station, with values of 147,000 tons/year (1.3 $\times 10^5$ tonnes/year) and 0.28 tons/acre (63 tonnes/km^2) [39].

Table 3.14 Lavaca River Annual Suspended Sediment Concentration and Load at USGS stations

Station	Period	Suspended Sediment Concentration, mg/L (Suspended Sediment Load, tons/day)		
		Max	Average	Min
Edna[1] (USGS- 08164000)	1977 - 2020	745 (10,800)	103 (190)	3 (0)

[1] https://mywaterway.epa.gov/monitoring-report/NWIS/USGS-TX/USGS-08164000/

The sand transport load in the Lavaca River at Edna station was estimated using a sand load-discharge relationship that was developed using both measured and computer-modeled sediment discharge data. This relationship is shown in **Figure 3.**. To produce this relationship, flow and sediment data from the period of 1977-1993, obtained from the USGS gauge at Edna, and bed material gradations collected by the Texas Water Development Board (TWDB), were employed. The SAMWin model was utilized to compute the sediment rating curve [101].

With an average daily discharge of 361 cfs (10 m^3/s) at the Edna station (**Table 3.12**), the sand load estimated from **Figure 3.** is approximately 35 tons/day (32 tonnes/day) or 12,775 tons/yr (11,589 tonnes/yr).

It is important to note that the sediment load at the Edna station does not represent the total sediment discharge into Matagorda Bay, as only 35% of the Lavaca River watershed contributes to the flow and sediment at this location. Downstream of the Edna station, the Navidad River, a tributary of the Lavaca River, joins the Lavaca River. The Navidad River has a contributing watershed of 1,370 square miles (3,550 km^2) at Texana Dam, which accounts for 60% of the Lavaca River basin.

In the absence of sediment data for the Navidad River, both upstream and downstream of the dam, it remains unclear how much sediment is contributed from this river to the river delta and Matagorda Bay. Nevertheless, various studies have estimated Lake Texana's sediment trap efficiency to be between 32% and 43%. By using the 43% trap efficiency and considering the sediment yield from the Lavaca River and the Lake Texana basin, it has been estimated that the sediment load to the wetlands, delta, and Lavaca Bay may be reduced by as much as 32% when compared to the loading before Lake Texana was constructed [39].

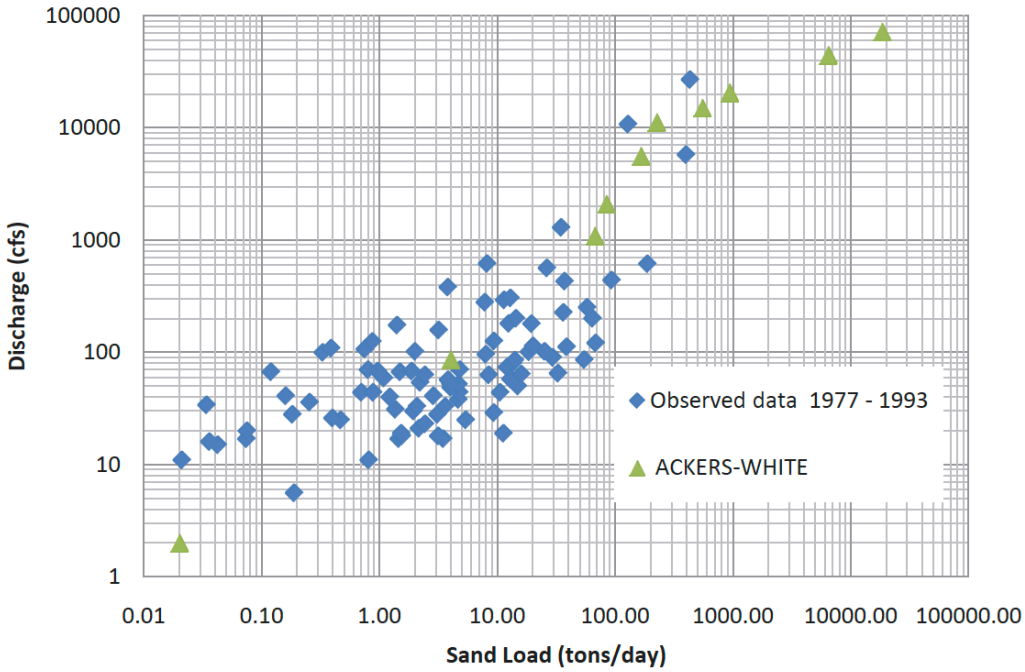

Figure 3.26 Sediment Rating Curve for the Lavaca River at Edna Station [101]

3.6.2.3 Sediment Delivery to Matagorda Bay

Matagorda Bay System encompasses several bays including Lavaca Bay, Tres Palacios Bay, Matagorda Bay, and some smaller bays. Sediment is delivered to these bays from rivers, creeks,

surface runoff from the uplands, shoreline erosion, and through natural and man-made tidal inlets and storm channels.

Following the removal of a log raft that obstructed its mouth, the Colorado River Delta underwent rapid development, expanding into the eastern arm of Matagorda Bay over approximately six years (from 1929 to 1935) [102]. This delta expansion was triggered by an increased sediment load transported into the bay, and it was anticipated to continue shifting due to a diversion project. However, a significant portion of the river's bedload, primarily consisting of sand, became trapped upstream in the navigation channel and silting basin [103]. In 1992, the Colorado River was rerouted to Matagorda Bay to provide a freshwater supply for the bay. This rerouted river became one of the primary sources of freshwater flow and sediment input into the Matagorda Bay system. The newly formed delta is likely a substantial contributor of muddy material to the bay system. The exact quantity of sediment contributed to the system remains unknown, but it is undoubtedly significant [104].

For the Colorado River, the suspended sediment load based on USGS data was estimated as 1.47 $\times 10^6$ tonnes/yr (**Section 3.6.2.1**). Also, it was reported that the Colorado River contributes approximately 5,756 acre-ft/yr (7.1×10^6 m^3/yr) suspended sediment and 462 acre-ft/yr (0.57×10^6 m^3/yr) sand to Matagorda Bay and the Gulf of Mexico [97]. Using sediment density of 965 kg/m^3 for suspended sediment and 2,700 kg/m^3 for sand, this results in a suspended sediment load and sand load of 7.5 $\times 10^6$ and 1.7 $\times 10^6$ tons/yr (6.85×10^6 and 1.53 $\times 10^6$ tonnes/yr), respectively.

The historical sediment delivery to Lavaca Bay was investigated by estimating sedimentation rate in the Lavaca River Valley for the past 10,000 years. Three primary sediment sources were identified including: suspended sediment carried by the Lavaca River and Garcetas Creek, which are categorized as fluvial sources; sediment eroded by wave action from Pleistocene clay bluffs along the bay margin; and sediment delivered from Matagorda Bay to the southern end of Lavaca Bay and transported up the Lavaca River valley. The estimated annual sediment delivery from these sources is as follows: 292, 97, and 11 acre-ft/yr (3.6×10^5, 1.2×10^5, and 0.14×10^5 m^3/yr), totaling 400 acre-ft/yr (4.94×10^5 m^3/yr) [105]. Using a sediment density of 965 kg/m^3, this results in a total sediment load of 460,000 tons/year (512,00 tonnes/year). The study concluded that 30% of the sediment entering Lavaca Bay from different sources was deposited within the bay, while the remaining 70% was transported to Matagorda Bay. Based on the annual volume of sediment deposited in Lavaca Bay, the long-term sediment deposition rate was estimated at 0.025 inches/yr (0.64 mm/yr). This rate is significantly lower, approximately half, when compared to the rate reported for the period of 1870-1934, which was 0.55 inches/yr (14 mm/yr) [45]. The discrepancy between these two estimates could be attributed to various factors, including the accuracy of the methods employed, the use of potentially inaccurate sediment density for converting sediment mass to volume, and potential changes in sediment and flow discharge rates into Lavaca Bay over the past century.

Sediment also enters the bay system from other freshwater contributors including Placedo Creek, East and West Carancahua Creeks, and Palacios Creek [104], however; the quantity of sediment load from these sources are unknown.

The Matagorda Bay shoreline is eroding at high rates due to strong waves and currents in the different sections of the bay [106] (**Figure 3.27**). However, the sediment removed from the shorelines across the bay does not show indicators of large accumulation on the bay bottoms. It appears that the modern Colorado River Delta serves as the primary source of sediment for the bay system [52].

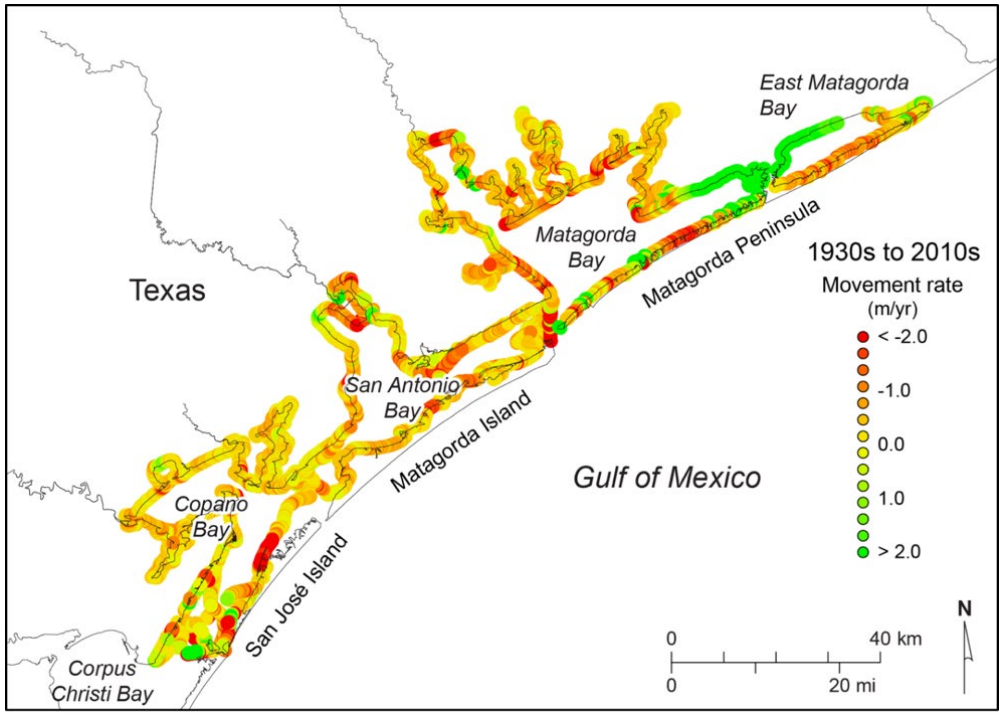

Figure 3.27 Net Long-term (1930s to 2010s) Shoreline Movement Rates in the Copano, San Antonio, and Matagorda Bay Systems [106]

The role played by tropical storms and hurricanes is significant in sediment transport and deposition with respect to the Matagorda Bay system [85]. Hurricanes, like Hurricane Gilbert, can significantly influence sediment deposition, with one year of the study attributing over 95% of sediment deposition at a levee site to this hurricane. During storm-free periods, sedimentation rates in the Colorado Delta were inversely related to marsh elevations, indicating changes in marsh area in the Colorado River Delta over time [49].

3.6.3 Sediment Delivery from Matagorda Bay to Gulf of Mexico

A study conducted by the U.S. Army Corps of Engineers (USACE) in this area emphasized regional sediment management strategies within the Matagorda Bay system, with a specific focus on addressing excessive shoaling in the upper reach of the Matagorda Ship Channel (MSC). However, the exchange of sediment between the Matagorda Bay system and the Gulf of Mexico

was not evaluated in this study. Additionally, the sediment budget analysis conducted in this study was limited to the inner bay system and did not extend beyond the MSC Entrance Jetties. Therefore, the study did not include an assessment of shoreline response and longshore sediment transport along the Matagorda Peninsula [104].

Water and sediment exchange between Matagorda Bay and the Gulf of Mexico takes place through several inlets, including Pass Cavallo, Greens Bayou, the Matagorda Ship Channel (MSC), and the Colorado River. Pass Cavallo, situated to the west of the MSC Jetty Entrance Channel, serves as the natural inlet. Sediment in and around this pass predominantly consists of sand and muddy sand, originating from the flood-tidal delta and transitioning bayward into sandy mud. Despite numerous studies focused on examining the pass's stability, the specific quantity of material entering or leaving the bay system remains unquantified [104]. Greens Bayou serves as a storm channel that becomes active only during hurricanes. It typically operates as an inlet for a few months in the aftermath of a storm and subsequently closes once the event has passed. The rate of sediment exchange between Matagorda Bay and the Gulf of Mexico through this channel is unknown. Sediment is introduced into the MSC's Entrance Channel from the Gulf of Mexico (GoM). The sand transport rate through this channel is quite low, but at the narrowest point, where the channel passes through the peninsula, powerful tidal currents have caused significant erosion.

The Entrance Channel has been regularly dredged at the rate of 259,000-346,000 cu yd/yr (198,020-264,536 m^3/yr) [104,107], whereas the average dredging for the section of the Main Channel located in the Matagorda Bay is approximately 1,156,000 cu yd/yr (883,825 m^3/yr) [104]. Starting in 1992, the Colorado River has been discharging into Matagorda Bay, resulting in the formation of a delta within the bay. This delta is likely a notable source of sediment in the bay system. Although the exact quantity of sediment introduced into the system remains uncertain, it is evidently substantial.

A numerical model study was conducted to investigate the intersection of the Gulf Intercoastal Waterway (GIWW) and the Colorado River. This study estimated the anticipated rate of sediment deposition in the Colorado River Lock project area, which encompasses the Bypass Channel, Colorado River Delta, GIWW, East and West Matagorda Bays. The depositional areas are shown in **Figure 3.28**. The findings of the study revealed that out of the 5×10^6 cu yd/yr (3.8×10^6 m^3/yr) of sediment inflow from the Colorado River, approximately 89% is deposited in the new delta areas of the river (Deltas 1 to 3 in **Figure 3.28**). Additionally, about 5.7% of the sediment is deposited in the old river delta area before rerouting to Matagorda Bay (Offshore area shown in **Figure 3.28**). The remaining 5.3% of the sediment is deposited in the GIWW West and East, Bypass Channel, and the Intersection area [108].

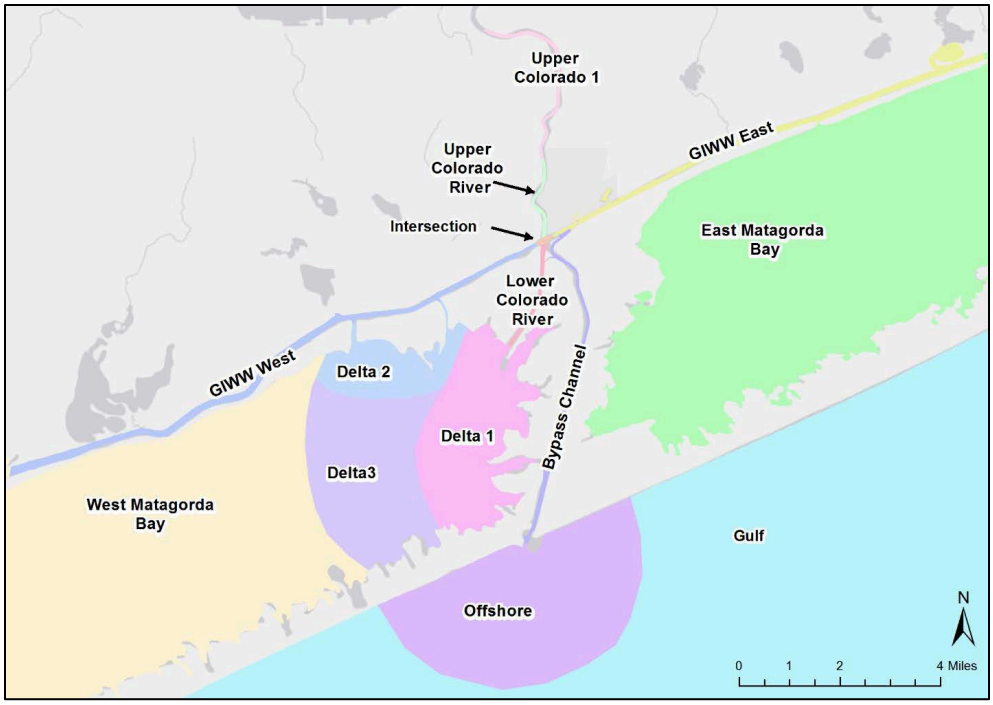

Figure 3.28 Depositional Areas in the Colorado River Locks Project Site Study [108]

A preliminary sediment analysis was conducted for the GoM costal area between Freeport Entrance and Matagorda Ship Channel [74,75]. The area was divided into 10 cell, and sediment budget for each cell was calculated (**Figure 3.18**). Cells 9 and 10 represent the area considered for the sediment budget analysis of the Matagorda Bay area. In this analysis, the following sediment quantities were considered:

- average annual dredging from Colorado River mouth (CRM) = 560,000 cu yd/yr (428,150 m^3/yr) based on the 1990-2003 dredging record and from Matagorda Ship Channel Entrance = 334,000 cu yd/yr (255,361 m^3/yr) based on the 1971-2004 dredging record,
- sand supplied to the system by the Colorado River = ~ 0. As detailed in **Section 3.6.2**, between 1934 and 1992, the Colorado River flowed directly into the Gulf of Mexico at the MCR. However, after redirecting the river to Matagorda Bay, a bypass channel was constructed to divert as much as 10% of the river's discharge back into the Colorado River Navigation Channel (CRNC) leading to the MCR. Consequently, no sediment input was considered at MCR in the sediment budget for the Matagorda Bay area.

The annual volume change in each cell and the net and gross sediment transport rates for each cell are summarized in **Table 3.15**. The alongshore sediment transport in the vicinity of the Brazos-San Bernard estuary area is shown on **Figure 3.18**.

In the sediment budget analysis of the Matagorda Bay area the sediment from shoreline erosion was not considered. The shoreline movement analysis shows that, on Matagorda Peninsula, the average long-term retreat rates are relatively small. For considering net shoreline change rates

calculated from the 1930s to 2019, Matagorda Island experienced an average retreat at a rate of 3.0 ft/ yr (0.91 m/yr), while Matagorda Peninsula retreated at 2.8 ft/yr (0.84 m/yr). The annual rates of land loss, estimated from these rates, are 12.5 acres/yr (0.05 km^2/yr) on Matagorda Island. The estimated total land loss along the Gulf shoreline since 1930 is 1,116 acres (4.5 km^2) on Matagorda Island [27] (**Figure 3.19**).

Table 3.15 Annual volume change in each cell and the net and gross sediment transport rates for Cells 1 to for used in sediment budget calculations [74,75]

Cell No. and Extent of the Cell	Annual Volume Change (ΔV)[1] (cu yd/yr)	Alongshore Net Westward Sediment Transport (cu yd/yr)	Alongshore Gross Sediment Transport (cu yd/yr)
9- Mouth of Colorado River to Matagorda Ship Channel: North	–123,120	200000	600,000
10- Mouth of Colorado River to Matagorda Ship Channel: South	355,680	84,000	325,000

[1]Quantiles presented in this column is from Ref. [75]

3.7 San Antonio Bay System

3.7.1 San Antonio Bay System Watershed Characteristics

San Antonio Bay system is one of seven major estuaries along the Gulf Coast of Texas, located at the confluence of the San Antonio and Guadalupe Rivers. It is protected from the Gulf of Mexico by Matagorda Island, leaving only relatively small and distant outlets to the Gulf, resulting in limited mixing of bay and Gulf waters. The San Antonio Bay system encompasses several waterbodies, including Ayres Bay, Espiritu Santo Bay, Guadalupe Bay, Hynes Bay, Mission Lake, Pringle Lake, and San Antonio Bay (**Figure 3.29**). A ship channel has been dredged from the Seadrift area to the Gulf Intracoastal Waterway, which provides the only major shipping access to the bay. The southwestern shoreline of San Antonio Bay is the northeastern boundary of the Aransas National Wildlife Refuge [109].

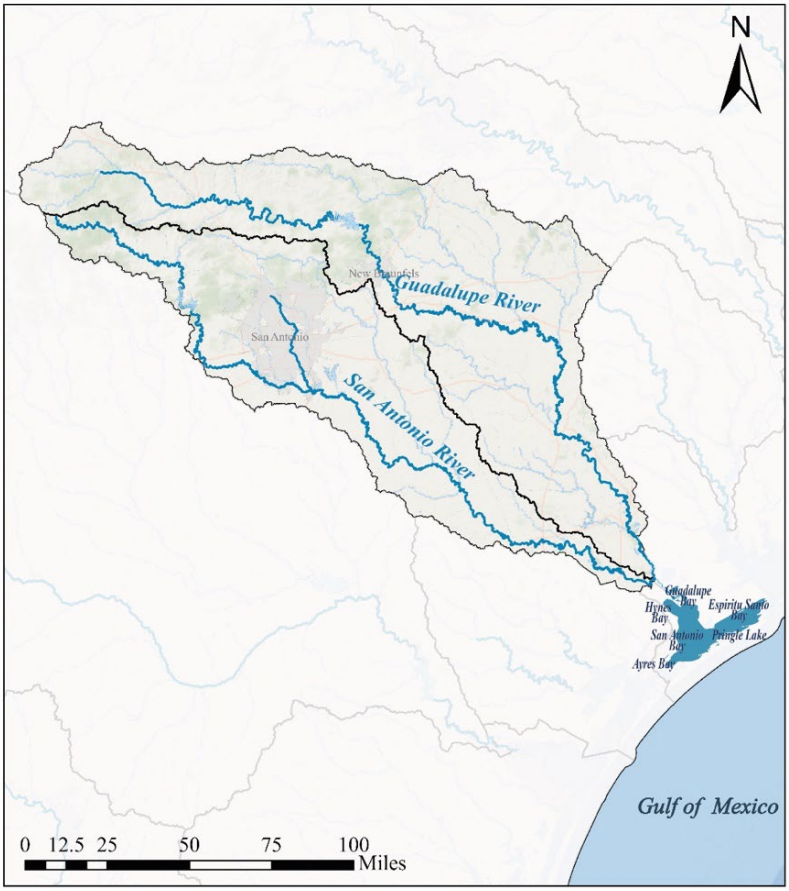

Figure 3.29 San Antonio Bay System Watershed

3.7.1.1 Guadalupe River

The Guadalupe River originates in southwestern Kerr County and flows eastward for approximately 250 river miles (402 km) to Gonzales. From there, it continues in a southeasterly direction for another 150 river miles (241 km) until it converges with the San Antonio River, situated 11 river miles (18 km) upstream from Guadalupe Bay, which is part of the San Antonio Bay system. The drainage area of the Guadalupe River encompasses about 10,200 mi^2 (26,418 km^2) including the San Antonio River watershed. Upstream from the confluence of the Guadalupe and San Antonio Rivers, the Guadalupe River watershed area covers 5,974 mi^2 (15,473 km^2), excluding the San Antonio River Basin. The major tributaries of the Guadalupe River are the Blanco River and the San Marcos River (**Figure 3.30**) [110]. The land use within the broader Guadalupe watershed is diverse and include urban areas, ranchland, pasture, forest, woody wetland, etc. [111].

The watersheds experience an average annual precipitation ranging from 30 inches (762 mm) at its headwaters to 40 inches (1,016 mm) near the coast in Victoria. The average monthly low temperatures range from 35.5 °F (1.9 °C) in January to 70.6 °F (21.4 °C) in July. Average monthly high temperatures range from 61.7 °F (16.5 °C) in January to 95.3 °F (35.2 °C) in August [110].

Several USGS streamflow gauges are located on the Guadalupe River as shown in **Figure 3.30**. The average daily discharge for the Guadalupe River is 1,897 cfs (54 m^3/s) at Victoria station. (**Table 3.16**).

In a study performed in 1979, the sediment yield in the lower Guadalupe River basin was estimated as 0.51 tons/acre (114 tonnes/km^2) [10].

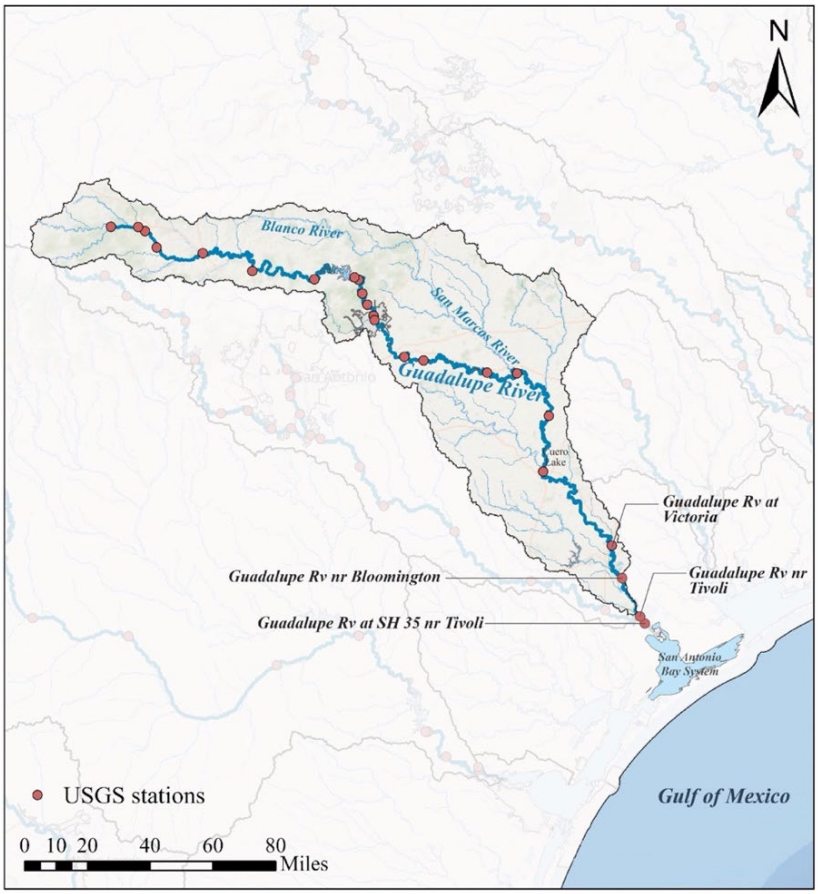

Figure 3.30 Guadalupe River Watershed and USGS Monitoring Stations

Table 3.16 Guadalupe River Annual Daily Discharges at USGS Station

Station	Drainage Area, mi^2 (km^2)	Period	Discharge, cfs (m^3/s)		
			Max	Average	Min
Victoria[1] (USGS-08176500)	5,198 (13,463)	1934 - 2023	5,690 (161)	1,897 (54)	931 (26)

[1] https://waterdata.usgs.gov/nwis/inventory/?site_no=08176500S

3.7.1.2 San Antonio River

The San Antonio River watershed is a dynamic ecosystem, characterized by rivers, creeks, and streams that can be rapidly affected by rainfall events and other weather conditions. Human activities within the basin can also have an impact on water conditions. This watershed covers a vast land area of 4,180 mi^2 (10,826 km^2), stretching from Kerr and Medina counties in the Texas Hill Country southeastward toward the Gulf of Mexico (**Figure 3.31**). The major sub-watersheds within this basin include the Medina River watershed, Leon Creek watershed, Upper San Antonio River watershed, Salado Creek watershed, Cibolo Creek watershed, and Lower San Antonio River watershed [112].

The San Antonio River main channel spans approximately 240 miles (386 km) in length, encompassing a drainage area of 934 mi^2 (2,419 km^2). The convergence of the San Antonio River with the Guadalupe River takes place within the delta region influenced by tides, situated just upstream of the Guadalupe-Blanco River Authority Saltwater Barrier near Tivoli. This confluence is located roughly 6.5 miles (11 km) upstream from the point where the Guadalupe River merges with the San Antonio Bay [113].

The lower part of the San Antonio River watershed experiences a humid subtropical climate, characterized by hot summers and mild winters. In Victoria, the mean annual temperature is around 70 °F (21.1 °C). The hottest and coldest months are August and January, with average highs of 94 °F (33.4 °C) and 63 °F (17.1 °C), respectively. Precipitation is distributed fairly evenly throughout the year, with March being the driest month and September the wettest, on average. Occasional summer droughts are not uncommon. Average annual precipitation varies across the region, ranging from approximately 30 inches (762 mm) in the northern basin sections to around 40 inches (1,016 mm) in the southern areas closer to the coastline. In Victoria, the mean annual precipitation measures 37 inches (950 mm), while in Goliad, it reaches 39 inches (980 mm). Regarding land cover, the predominant landscape is primarily composed of brush and grassland [113].

There are multiple USGS streamflow gauges situated along the San Antonio River as shown in **Figure 3.31**. The Goliad station records an average mean discharge of 768 cfs (22 m^3/s) for the San Antonio River (**Table 3.17**).

In 1979, a study estimated the sediment yield within the San Antonio basin. The average annual sediment yield in the upper and lower part of the basin was estimated as 0.87 tons/acre (195 tonnes/km^2) and 0.78 tons/acre (175 tonnes/km^2), respectively [10].

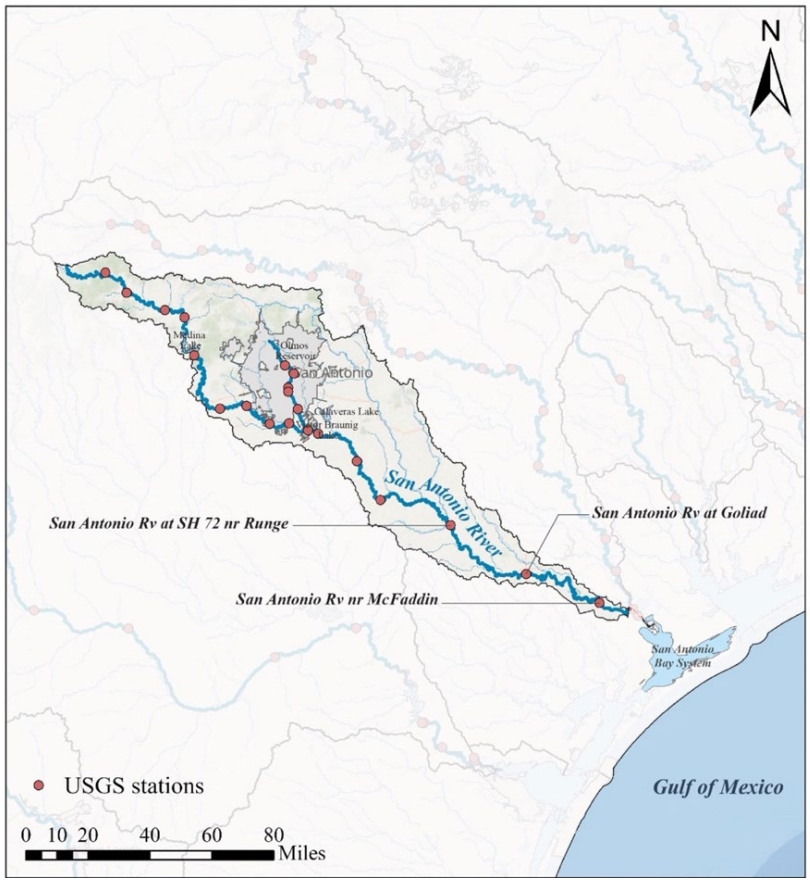

Figure 3.31 San Antonio River Watershed and USGS Monitoring Stations

Table 3.17 San Antonio River Annual Daily Discharges at USGS Station

Station	Drainage Area, mi² (km²)	Period	Discharge, cfs (m³/s)		
			Max	Average	Min
Goliad[1] (USGS-08188500)	3,921 (10,155)	1924 - 2023	1,890 (53.5)	768 (22)	343 (10)

[1] https://waterdata.usgs.gov/nwis/inventory/?site_no=08188500&agency_cd=USGS

3.7.1.3 Reservoirs

The Guadalupe River Basin has five primary reservoirs including [114]:

- *Canyon Lake:* Located approximately 12 miles (19.3 km) northwest of New Braunfels in Comal County, Canyon Lake is situated on the Guadalupe River. The lake has a total storage capacity of 378,852 acre-ft (4.7 ×10^8 m^3), encompassing a surface area of 8,308 acres (33.6 km^2) at a conservation pool elevation of 909 ft (277 m) above mean sea level. The dam controls a drainage area of approximately 1,432 mi^2 (3,708 km^2).

- *Coleto Creek Reservoir:* Coleto Creek Reservoir is situated 15 miles (24 km) southwest of Victoria in Victoria County, along Coleto Creek, which is a tributary of the Guadalupe River. The reservoir has a capacity of 35,084 acre-ft (4.3×10^7 m^3), covering a surface area of 3,100 acres (12.6 km^2) at the conservation pool elevation of 98 ft (30 m) above mean sea level. The dam effectively manages a drainage area spanning approximately 507 mi^2 (1,313 km^2).
- *Lake Dunlap*: Lake Dunlap, also known as TP-1 Dam, is situated 9 miles (14.5 km) northwest of Seguin in Guadalupe County, along the Guadalupe River. The lake boasts a capacity of 5,900 acre-ft (7.3×10^6 m^3), covering a surface area of 410 acres (1.7 km^2) at the conservation pool elevation of 575.2 ft (175.3 m) above mean sea level. The drainage area above the dam encompasses 1,653 mi^2 (4,281 km^2).
- *Lake Gonzales:* Lake Gonzales, also known as H-4 Dam or H-4 Reservoir, is situated 6 miles (9.6 km) northwest of the City of Gonzales in Gonzales County, along the Guadalupe River. The lake has a capacity of 6,500 acre-ft (8×10^6 m^3), covering a surface area of 696 acres (2.8 km^2) at the conservation pool elevation of 332 ft (101.2 m) above mean sea level. The drainage area above the dam spans 2,048 mi^2 (5,304 km^2).
- *Lake McQueeney:* Lake McQueeney, also known as TP-3 Dam or Abbott Dam, is situated five miles northwest of Seguin in Guadalupe County, along the Guadalupe River. The lake has a capacity of 5,000 acre-ft (6.2×10^6 m^3), covering a surface area of 396 acres (1.6 km^2) at the conservation pool elevation of 528.7 ft (161 m) above mean sea level. The drainage area above the dam spans 1,697 mi^2 (4,395 km^2).

Several dams have been constructed in the San Antonio River basin for different purposes. For example, in the San Antonio area, then Olmos Dam is used solely for flood control and the Lake Blue Wing reservoir is used for irrigation [115]. The major lakes in San Antonio River basin include [116]:

- *Calaveras Lake:* Calaveras Lake, located about 15 miles (24.1 km) southeast of San Antonio in Bexar County, along Calaveras Creek, a tributary of the San Antonio River, has a capacity of approximately 63,200 acre-ft (7.8×10^7 m^3). It encompasses a surface area of approximately 3,624 acres (14.7 km^2) at the conservation pool elevation of 485 ft (148 m) above mean sea level. The drainage area above the dam is only 65 mi^2 (168 km^2).
- *Medina Lake:* Medina Lake, located approximately 8 miles (12.9 km) northwest of Riomedina in Medina County, along the Medina River, a tributary of the San Antonio River, has a capacity of about 2,555 acre-ft (3.15×10^6 m^3). It encompasses a surface area of roughly 169 acres (0.68 km^2) at a normal elevation of 926.5 ft (282.2 m) above mean sea level. The drainage area above Medina Dam spans approximately 634 mi^2 (1,641 km^2).
- *Olmos Reservoir:* Olmos Reservoir is situated 4 miles (6.4 km) north of San Antonio in Bexar County, along Olmos Creek, a tributary of the San Antonio River. The reservoir has a capacity of 12,600 acre-ft (1.56×10^7 m^3) and a surface area of 889 acres (3.6 km^2) at the top

of the flood control pool, with an elevation of 725 ft (221 m) above mean sea level. The drainage area above the dam spans 32 mi^2 (82.9 km^2).

- *Victor Braunig Lake:* Victor Braunig Lake, formerly known as East Lake, is situated approximately 15 miles (38.8 km) southeast of San Antonio in Bexar County, along Arroyo Seco, a tributary of the San Antonio River. The reservoir has a capacity of 26,500 acre-ft (3.27×10^7 m^3) and covers a surface area of 1,350 acres (5.5 km^2) at the conservation pool elevation of 507 ft (154.5 m) above mean sea level. The drainage area above the dam is relatively small, spanning only 9.4 mi^2 (24.4 km^2).

3.7.1.4 San Antonio Bay

The San Antonio Bay estuarine complex is situated along the Texas coast, positioned to the south of Matagorda Bay and to the north of Copano-Aransas Bays. San Antonio Bay is the largest component of this system, which also encompasses Mission Lake, Hynes Bay, Guadalupe Bay Espirito Santo Bay, and Mesquite Bay. The primary sources of freshwater inflow into this complex include the San Antonio and Guadalupe Rivers, along with the Green Lake/Victoria Ship Channel. Matagorda Island serves as the barrier between this system and the Gulf of Mexico, allowing water exchange to occur through Pass Cavallo to the north and Cedar Bayou to the south. Consequently, there is limited direct exchange between the waters of San Antonio Bay and those of the Gulf. Most of the land surrounding San Antonio Bay retains its rural characteristics and is conducive to farming and ranching activities. In the southwest, the Aransas National Wildlife Refuge plays a crucial role in providing habitat for numerous species [117,118].

The bay receives an average of 2.5×10^6 acre-ft (3.08×10^9 m^3) of freshwater inflow per year from its major contributing rivers, the Guadalupe and San Antonio Rivers, as well as runoff from surrounding coastal watersheds [119].

3.7.2 San Antonio Bay Sediment Budget

San Antonio Bay is situated at the confluence of the San Antonio and Guadalupe Rivers, giving rise to a substantial bayhead delta known as the Guadalupe Delta. This delta, predominantly occupying the northwest portion of San Antonio Bay, has experienced considerable progradation over the past century, although it has somewhat stabilized in recent decades. The bay is less than 6.6 ft (2 m) deep on average and is brackish [120].

In terms of exchanges within San Antonio Bay, the primary pathways involve the Pass Cavallo complex (including the Matagorda Entrance Channel) and Aransas Pass. The closest inlet to the bay, however, is Cedar Bayou. When Cedar Bayou is open, it serves as an effective passage for migratory organisms [121] as well as sediment.

Because of the lack of a direct inlet, San Antonio Bay experiences relatively slow exchange with the Gulf of Mexico. As a result, the sediment characteristics of the bay, including texture and accumulation patterns, are not significantly influenced by tidal flux. Instead, the sediment deposited in the bay is primarily determined by the sediment load entering the bay from the San

Antonio and Guadalupe Rivers, along with contributions from other sources. There are some low bluffs along the shoreline that produce sand when eroded. It is reported that the sediments within the Guadalupe delta consist of more than 60% plant remains, whereas the sediments in the bay contain only approximately 4% plant remains. The entire bay is dominated by mud composed primarily of clay minerals [120].

In the San Antonio River delta, approximately half of the surface area features clay soil, while the other half consists of silty clay soil. This distinction seems to be more closely linked to the sediment carried by the rivers rather than the texture of the mapped deltaic and alluvial soils. Notably, both the San Antonio and Guadalupe Rivers have substantial portions of their drainage areas within the Texas Blackland Prairie region, known for its clayey, vertic soils [113].

San Antonio Bay is the second most productive oyster region on the Texas coast. The majority of the bay is regularly dredged by oystermen using their trawlers. The dredging activity disturbs the sediment at the bottom, resulting in a slightly coarser grain size due to the suspension of fine sediment, which then disperses to other areas of the bay.

In order to assess the sediment budget of San Antonio Bay accurately, it is necessary to conduct a detailed analysis of the sediment input originating from the Guadalupe River, San Antonio River, and other contributing sources.

3.7.2.1 Guadalupe River and San Antonio River Sediment Load

The USGS collects sediment data for the Guadalupe River at Victoria and the San Antonio River at Goliad. These stations are situated upstream of the confluence of the San Antonio and Guadalupe Rivers. Sediment data were also collected for a brief period from the Guadalupe River at SH 35 near Tivoli, which is located 1 mile (1.61 km) downstream of the confluence (**Figure 3.30** and **Figure 3.31**). In **Table 3.18**, the suspended sediment concentration and load at these stations are summarized.

Table 3.18 Guadalupe and San Antonio Rivers Suspended Sediment Concentration and Load at USGS Stations

Station	Period	Suspended Sediment Concentration, mg/L (Suspended Sediment Load, tons/yr)		
		High	Average	Low
Guadalupe at Victoria (USGS-08176500)[1]	1973 - 2020	2,390 (27,400)	141 (1,413)	9 (20)
San Antonio at Goliad (USGS-08188500)[2]	1974 - 2021	2,450 (28,000)	291 (1,486)	5 (4.7)
Guadalupe at SH 35 near Tivoli (USGS-08188810)[3]	2013 - 2018	1520 (8,990)	251 (1,860)	16 (2)

[1] https://mywaterway.epa.gov/monitoring-report/NWIS/USGS-TX/USGS-08176500/
[2] https://mywaterway.epa.gov/monitoring-report/NWIS/USGS-TX/USGS-08188500/
[3] https://mywaterway.epa.gov/monitoring-report/NWIS/USGS-TX/USGS-08188810/

According to the data collected at the Victoria and Goliad stations between 1972 and 1990, both rivers were found to transport a significant amount of fine sediment in suspension. The mean percentage of sediment finer than 0.0625 mm (silt and clay fractions) was 92% for the San Antonio River and 83% for the Guadalupe River. Furthermore, it was reported that for a given flow rate, the suspended sediment concentrations were approximately five times higher for the San Antonio River at Goliad compared to the Guadalupe River at Victoria station. Consequently, even though the flows of the Guadalupe River at Victoria are approximately twice as large as those of the San Antonio River at Goliad, the total sediment load of the Guadalupe River is only slightly greater. The sediment loads transported by the Guadalupe and San Antonio Rivers were estimated using suspended sediment concentration-discharge relationships developed from historical data (1973-1988). The calculated average sediment loads for the Guadalupe River and the San Antonio River were 630,000 tons/yr (571,530 tonnes/yr) and 700,000 tons/year (635,000 tonnes/yr), respectively [122].

In a comprehensive study conducted by the USGS, sediment carried by the San Antonio and Guadalupe Rivers was characterized using historical sediment data collected during 1966-2004 and 2011-2013. The study area for the Guadalupe River was situated between San Antonio and the Tivoli station on Guadalupe River, located approximately 1 mile (1.61 km) downstream from the confluence of the San Antonio and Guadalupe Rivers. The study area for the San Antonio River extended approximately 190 river miles (306 km) from Elmendorf, Texas, to the confluence of the San Antonio and Guadalupe Rivers [123]. The following are the findings of this study:

- The samples collected between 2011 and 2013 encompassed a broad range of suspended sediment concentrations (SSC), including some of the highest concentrations ever recorded at certain gauge stations. In contrast, most historical samples collected at these stations were routine samples, resulting in a relatively limited range of sediment concentrations. However, for the San Antonio River at Goliad, the SSC ranged from 69 to 1,970 mg/L, which is comparable to the historical range of 40-2,500 mg/L observed during the period of 1974-1994. The SSC varied from 67 to 1,400 mg/L in the Guadalupe River at Tivoli during 2011-2013. There is no historical sediment data available for this location.
- In the suspended sediment samples collected during 2011-2013, an average of about 94% of the particles was less than 0.0625 mm (silt and clay particles). This result supports the historical observations that theses river systems are primarily influenced by the transport of fine sediment particles.
- In the bedload samples collected during 2011-2013, an average of 51% of sediment particles was sand-sized particles in the range of 0.25-0.5 mm. The sediment loads calculated from the samples indicated that bedload typically composed less than 1% percent of the total sediment load.

The field data from the 2011-2013 campaign, along with historical sediment data, were used to develop and calibrate a watershed model. This model was employed to simulate hydrological conditions and suspended sediment loads during the period of 2000-2012 in the San Antonio River

basin downstream of San Antonio [124]. The modeling results indicated that at the outlet of the study area, the confluence of the San Antonio River with the Guadalupe River, the simulated daily mean suspended sediment load during 2006-2012 was 1,230 tons/day (1,116 tonnes/day). This rate is lower than the long-term suspended sediment load at this location, as shown in **Table 3.18**. The study acknowledged that suspended sediment loads are likely to vary for periods other than the years evaluated.

3.7.2.2 Sediment Delivery to San Antonio Bay

The primary source of sediment for the San Antonio Bay is from the San Antonio and Guadalupe Rivers. The combined sediment load supplied by these rivers to the bay system was reported as 694 acre-ft/yr (0.86×10^6 m^3/yr). This estimation was based on suspended sediment measurements taken at Goliad and Victoria during the period of 1943-1984 [49]. A study focusing on the Guadalupe River delta estimated that the average amount of suspended sediment transported to the delta is approximately 1×10^6 tons/year (0.91×10^6 tonnes/yr). It should be noted that this rate is nearly equal to the sediment delivered by the Guadalupe River (461,214 tons/yr (418,400 tonnes/yr)) for the period of 1945-1954 and the San Antonio River (568,218 tons/yr (515,480 tonnes/yr)) for the period of 1942-1954 [125]. These estimates are in line with those reported in **Section 3.7.2.1**.

A secondary source of sediment to the San Antonio Bay system is lateral input from shoreline erosion. The shoreline along most of the bay has been eroding, with the rate being higher in the upper part of the system (**Figure 3.27**). The area along the Guadalupe delta eroded at an average rate of 5 ft/yr (1.5 m/yr) between 1930 and 1982, with erosion rates locally reaching as high as 9 ft/year (2.7 m/yr) [126]. The rate of shoreline erosion between 1930 and 2010 in the Mission Lake area was as high as 10 ft/yr (3 m/yr) (**Figure 3.27**).

3.7.3 Sediment Delivery from San Antonio Bay to Gulf of Mexico

The sediment delivered by the San Antonio and Guadalupe Rivers primarily deposits in the upper bay areas, with shoaling occurring less frequently in the lower bays. It has been reported that approximately 21% of the sediment load entering the bay system is deposited in Mission Lake or as part of the Traylor Cut delta. This sediment load is composed of 2% sand, 27% silt, and 71% clay. Sand and silt first deposit in the Mission Lake area, while the finer sediments, i.e., clay particles, travel further downstream to San Antonio Bay. Most of this material deposits in the bay, but some may find their way to the Gulf of Mexico through passes such as Cedar Bayo. The deposition rate in San Antonio Bay was estimated to be 0.35 in/yr (9 mm/yr) [45]. In contrast, Espirito Santo Bay, located west of San Antonio Bay, receives an insignificant fluvial sediment load. Therefore, the deposition rate in this bay is significantly smaller than that in San Antonio Bay. Based on a trap efficiency curve, it was estimated that approximately 95% of the incoming sediment load would be trapped in San Antonio Bay, with the remaining 5% being transported into the Gulf of Mexico [49]. If the sediment load entering San Antonio Bay is approximately 1×10^6 tons/yr (0.97×10^6 tonnes/yr), the sediment load carried to the passes and into the Gulf of Mexico amounts to 50,000 tons/yr (45,359 tonnes/yr).

Long-term net shoreline recession rates have been calculated for the central Texas Gulf shoreline, spanning from Pass Cavallo to the Packery Channel area. The net shoreline change rates calculated up from the 1930s to 2019 showed an average retreat of 3.0 ft/yr (0.91 m/yr) for Matagorda Island (**Figure 3.32**), with an estimated annual land loss rate of 12.5 acres/yr (0.05 km^2/yr) [27].

In this region, there is limited data available concerning sediment pathways and the sediment budget. Consequently, the rate of sediment delivery from shoreline erosion or the San Antonio Bay System to the Gulf of Mexico remains unknown.

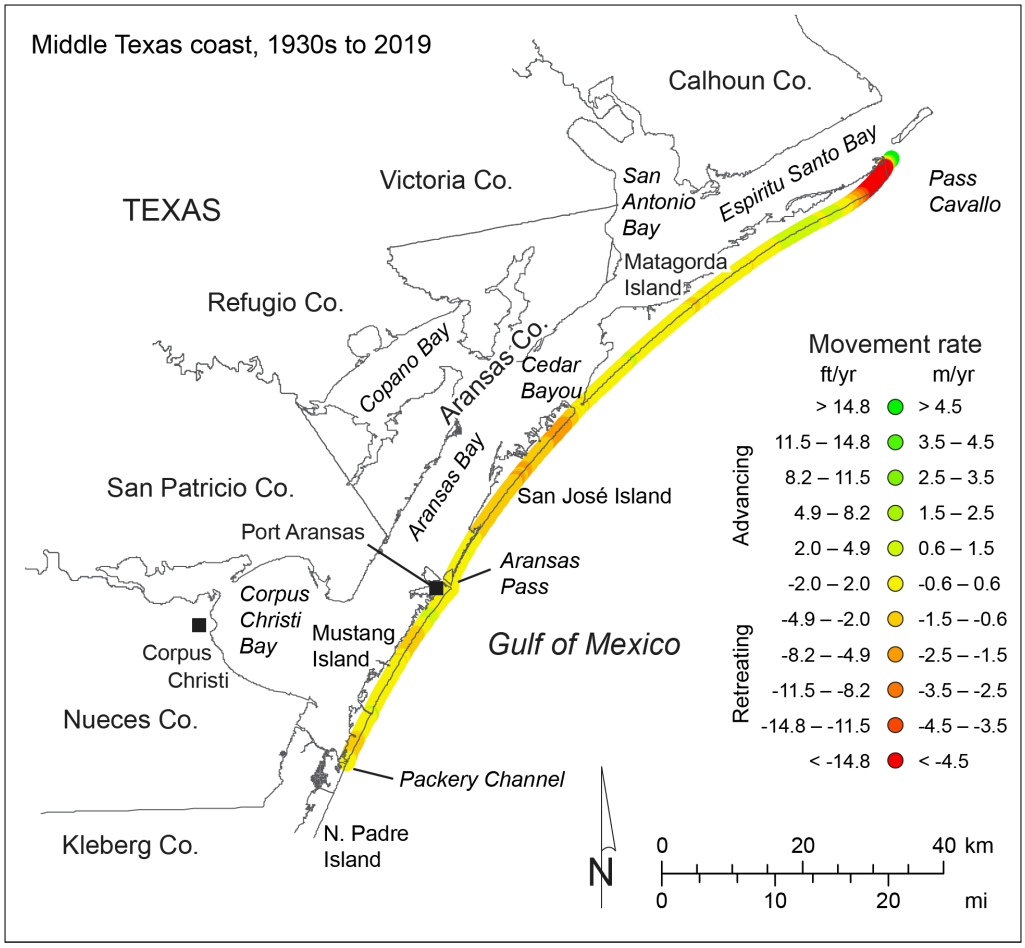

Figure 3.32 Net Rates of Long-term Movement for the Middle Texas Gulf Shoreline Between Pass Cavallo and the Packery Channel Area (Matagorda Island, San José Island, and Mustang Island) Calculated from Shoreline Positions Between the 1930s and 2019 [27]

3.8 Aransas Bay System

3.8.1 Aransas Bay System Watershed Characteristics

The Aransas Bay System or Mission-Aransas Estuarian system encompasses 223 mi^2 (577 km^2) [127]. It is situated along the Texas coast, positioned between the estuarine complexes of Corpus Christi Bay and San Antonio Bay. This system primarily comprises Aransas Bay, Copano Bay,

Mission Bay, and St. Charles Bay. To the south, Redfish Bay is closely associated with this system and is typically considered a part of it, although at times, it is categorized within the Corpus Christi Bay complex (**Figure 3.33**). Freshwater inflow into the system is contributed by the Aransas and Mission Rivers, along with Copano Creek, although the overall influence of freshwater is relatively limited. These bays are geographically separated from the Gulf of Mexico by San Jose Island, and water exchange occurs through Cedar Bayou and Aransas Pass [117,118].

The Aransas Bay system drainage basin is relatively undeveloped, and no dams or reservoirs have been constructed or proposed within the watershed [128].

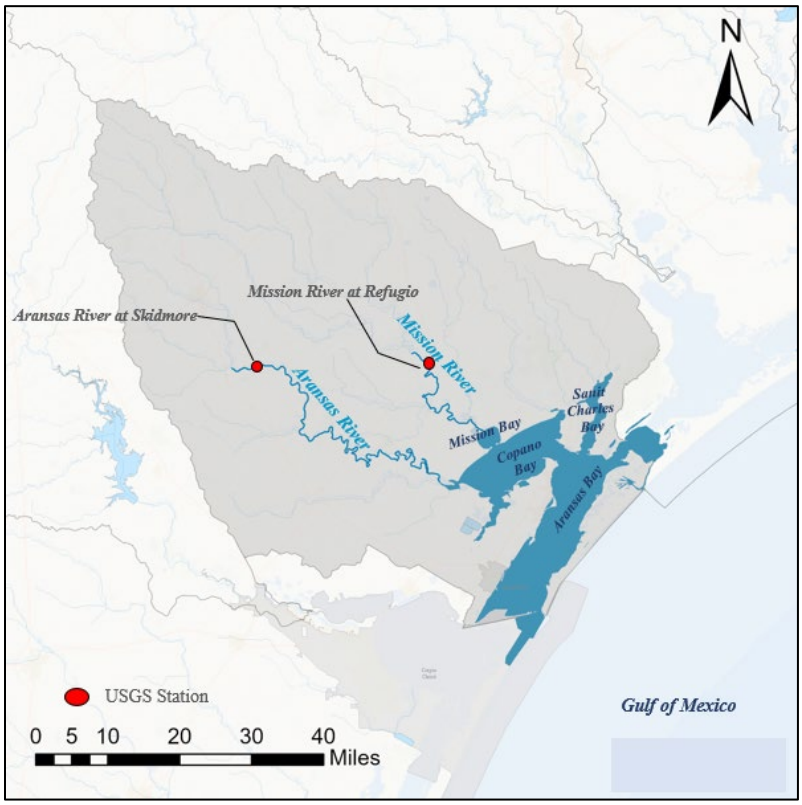

Figure 3.33 Aransas Bay System Watershed and USGS Monitoring Stations

3.8.1.1 Mission River

The Mission River originates from the confluence of Blanco and Medio Creeks in central Refugio County, Texas, and flows approximately 24 miles (39 km) southwest until it reaches its mouth at Mission Bay, an inlet of Copano Bay. The Mission River basin covers aa area of 1,029 mi^2 (2,665 km^2), which is distributed among Bee, Refugio, Goliad, and Karnes counties. Dominant land uses in the Mission River watershed include scrub/grassland (47.3%) and pasture (31.5%) [129].

The Mission River region is marked by annual temperatures fluctuating between 47 and 98 °F (8 to 37°C). Historical data covering the period from 1981 to 2010 indicates an average annual precipitation of 33.2 in (843 mm) within the Mission River's drainage area [129].

The river maintains an average daily flow of 119 cfs (3.4 m^3/s) as recorded at the USGS Refugio gauge station (**Figure 3.33**). This flow rate can vary due to a range of environmental and seasonal factors. A summary of flow record at this station is presented in **Table 3.19**.

The annual sediment yield for the Mission River basin is estimated as 0.29 tons/acre (65 tonnes/km^2) [10].

3.8.1.2 Aransas River

The Aransas River has its origin at the confluence of the Olmos, Aransas, and Poesta Creeks, located two miles north of Skidmore in southern region of Bee County. It runs for about 40 miles (64.4 km) south and southwest into Aransas County and eventually merges into Copano Bay, situated around ten miles to the northwest of Rockport [130]. The watershed area is 843 mi^2 (2,184 km^2) and is dominated by cultivated crops (44.7%) and scrub/grassland (24.3%) [129].

Within the river watershed, the average annual precipitation amounts to 32.3 inches (820 mm). In Beeville, where the meteorological station most accurately reflects the Aransas River watershed, the wettest month typically occurs in September with an average of 3.8 inches (97 mm), while the driest month usually falls in February with around 1.6 inches (41 mm) of precipitation [129].

In Beeville, the average high temperatures typically peak at 95 °F (35 °C) in August, but temperatures exceeding 100 °F (38 °C) have been recorded from April through September. In the winter, the average low temperature drops to 43 °F (6 °C) in January, with temperatures below freezing observed from September through April [129].

The Aransas River demonstrates an average daily flow of 34 cfs (0.96 m^3/s) at the USGS Skidmore gauge station (**Figure 3.33**). A summary of flow record at this station is presented in **Table 3.19**.

The annual sediment yield for the Aransas River basin is estimated as 0.28 ton/acre (62.8 tonnes/km^2) [10].

Table 3.19 Mission River and Aransas River Annual Daily Discharges at USGS Stations

Station	Drainage Area, mi^2 (km^2)	Period	Discharge, cfs (m^3/s)		
			Max	Average	Min
Mission River at Refugio[1] (USGS-08189500)	690 (1,787)	1938 - 2023	1,020 (29)	119 (3.4)	14 (0.4)
Aransas River at Skidmore[2] (USGS-08189700)	247 (640)	1963 - 2023	856 (24)	34 (0.96)	4.2 (0.74)

[1] https://waterdata.usgs.gov/nwis/inventory/?site_no=08189500S
[2] https://waterdata.usgs.gov/nwis/inventory/?site_no=08189700S

3.8.1.3 Reservoirs

Neither the Mission River nor the Aransas River is dammed or utilized as a water source for cities in the area. Consequently, both rivers flow directly into the Aransas Bay System [128].

3.8.1.4 Aransas Bay

The Aransas Bay system includes one tertiary bay (Mission Bay), three secondary bays (Copano, Port, and St. Charles Bays), and three primary bays (Aransas, Mesquite, and the northern section of Redfish Bay). Although these bays are geographically separated from the Gulf of Mexico by San Jose Island, they remain hydraulically connected through Aransas Pass and Cedar Bayou. The bay system is also hydraulically connected to San Antonio Bay to the north and Corpus Christi Bay to the south [127]. These bays are characterized by their shallow depths, with mean low water depths ranging from 2 ft (0.6 m) in Mission Bay to 10 ft (3 m) in Aransas Bay [131].

Aransas Bay is a large estuary located on the Texas Gulf Coast. Like many other bays in the area, it is a crucial ecological and economic asset. The bay receives freshwater from Copano Bay, which is connected to it through a navigational channel, and from various creeks such Aransas Creek. The GIWW runs along the Aransas Bay which plays an important role in water exchange between the neighboring bay systems along the Texas coast.

The primary factors influencing hydrological conditions in the Aransas Bay system encompass climatic conditions, freshwater inflows, and to a lesser degree, tidal fluctuations [132]. Tidal flow in Copano and Aransas bays is influenced by astronomical tides, meteorological conditions, and density stratification [117]. Due to the relatively shallow depths of the bays, ranging from 3.3 to 13.2 ft (1-4 m) at mid-tide, and the relatively small tidal prism, wind has a more significant impact on bay circulation than astronomical tides [46,117]. Wind-driven tides also facilitate substantial water exchange between the Gulf of Mexico and Aransas Bay [133].

In the period of 1941-1996, the Aransas Bay system annual inflows ranged between 7,503 and 1.54×10^6 acre-ft/yr (9.2×10^6 and 1.9×10^9 m^3/yr) with a mean inflow of 439,389 acre-ft/year (5.42×10^8 m^3/year) [127].

3.8.2 Aransas Bay Sediment Budget

Sediment delivery to Aransas Bay primarily occurs through natural mechanisms, including the inflow from rivers and creeks, coastal erosion, and tidal movements. Although there is no historical sediment data available for the Aransas Bay system, the USGS has collected suspended sediment information at monitoring stations along the Mission River at Refugio station and Aransas River at Skidmore station (**Figure 3.33**). These monitoring sites cover approximately 70% and 30% of their respective drainage areas, leaving a significant portion of the watershed ungauged [127].

3.8.2.1 Mission River Sediment Load

Suspended sediment data was collected for the Mission River at Refugio station (USGS-08189500). The suspended sediment concentration (SSC) at this site is available for the period of 1973-1993. For this period the minimum, average, and maximum SSC are reported as 6, 102, and 2,770 mg/L. The corresponding daily minimum, average, and maximum suspended sediment loads are estimated as 0, 30.5, and 1,680 tons/day (0, 28, 1,524 tonnes/day), respectively (**Table 3.20**).

Based on a sediment load-discharge relationship, the annual suspended sediment load for this site was calculated as 12,000 tons/yr (10,886 tonnes/yr) for the period of 1973-1993. However, the estimated yearly sediment load might not be entirely precise due to the limited availability of sediment data for flow rates above the 5% exceedance range (approximately 300 cfs (8.5 m^3/s)) [127].

3.8.2.2 Aransas River Sediment Load

Suspended sediment data was collected for the Aransas River at Skidmore station (USGS-08189700). The suspended sediment concentration (SSC) at this site is available for the period of 1966-1975. For this period the minimum, average, and maximum SSC were reported as 11, 236, and 1,640 mg/L. The daily minimum, average, and maximum suspended sediment load for this period were 0.1, 752, and 14,900 tons/day (0.09, 682, 13,517 tonnes/day), respectively (**Table 3.20**).

Based on a sediment load-discharge relationship, the annual suspended sediment load for this site was roughly 25,000 tons/yr (22,679 tonnes/yr) for the period of 1966-1975 [127]. These values match very well with the reported value of 100 tons/mi^2 (35 tonnes/km^2) for the corresponding period [134]. However, if the annual suspended sediment load is calculated using average daily suspended load of 752 tons/day (682 tonnes/day), the result would be ten times higher.

Table 3.20 Mission River and Aransas River Suspended Sediment Concentration and Load at USGS Stations

Station	Period	Suspended Sediment Concentration, mg/L (Suspended Sediment Load, tons/day)		
		Max	Average	Min
Mission River at Refugio[1] (USGS-08189500)	1973 - 1993	2,770 (1,524)	102 (28)	6 (0)
Aransas River at Skidmore[2] (USGS-08189700)	1966 -1975	1,640 (14,900)	236 (752)	11 (0.1)

[1] https://mywaterway.epa.gov/monitoring-report/NWIS/USGS-TX/USGS-08189500/
[2] https://mywaterway.epa.gov/monitoring-report/NWIS/USGS-TX/USGS-08189700/

3.8.2.3 Sediment Delivery to Aransas Bay

The sediment contribution to the Aransas Bay system is mainly from rivers and creeks inflow, local runoff, and shoreline erosion. Gulf of Mexico deposits from storms and inlets, and dredge spoil from channels are also other source of sediment to the bay system [128].

Sediment reaching the Aransas Bay system comes from the Rio Grande Prairie primarily via the Mission and Aransas Rivers [135]. The annual sediment production rates for Mission and Aransas Rivers are 0.29 tons/acre (65 tonnes/km^2) and 0.28 ton/acre (62.8 tonnes/km^2), respectively. These values correspond to annual sediment loads that are significantly higher than those measured at the USGS gauges on these rivers (**Sections 3.8.2.1** and **3.8.2.2**). The difference between these two

is five times for the Mission River and 2 times for the Aransas River, respectively. A portion of these differences can be attributed to the ungauged areas between the USGS gauge locations and the rivers' delta. However, for the Mission River, this ungauged area constitutes only 30% of the total basin area, and such a large difference in sediment load between the two different methods cannot be justified solely by this reasoning.

As sediments enters the bays, they deposit and form bay-head deltas, primarily due to reduced flow velocities and sediment transport capabilities. The landward shorelines of the estuaries within the Aransas Bay system are distinctive, featuring nearly vertical bluffs carved into Pleistocene sand, silt, and mud. The erosion of these bluffs contributes sediment to the neighboring lakes, marshes, and bays. The type of sediment deposited depends on whether the adjacent bluff consists predominantly of sand or mud. For example, Copano and Aransas Bays have the typical pattern of sediment texture distribution with fines in the middle and becoming coarser near the shoreline. Copano Bay has some low bluffs that are exposed to the prevailing wind and therefore are subject to some erosion. St. Charles Bay is sand dominated as compared to other bays [120].

The erosion in the Aransas Bay estuaries is primarily influenced by wind action, as the range of astronomical tides measures only about 0.5 ft (0.15 m) in the bays to a maximum of about 2 ft (0.6 m) along the Gulf shoreline. The landward shores of Copano and Aransas Bay primarily experience erosion, whereas the barrier island of Aransas Bay remains in a state of equilibrium or accretion. On the Gulf side of the barrier island, the shoreline is generally stable. This suggests that the sediment supply is adequate to counteract the erosion caused by wave action and longshore drift, maintaining a balance in sediment dynamics[135]. As an example, the landward edge of Copano Bay experienced an average net shoreline retreat of 0.8 ft/yr (0.24 m/yr) between 1930 and 1982. Rates of shoreline erosion for the most recent monitoring period from late 1950's to 1982 were even higher, reaching an average of 2.5 ft/year (0.76 m/yr) [136].

From this review, it can be concluded that sediment delivery to Aransas Bay has not been estimated or documented. However, since the navigational channels in the bay area have been frequently dredged [52], it can be assumed that the Aransas Bay is a depositional system during normal hydrological conditions. Like other salt-wedge estuaries, Copano Bay exhibits sediment deposition primarily dominated by suspended fluvial material rather than suspended marine sediments [137].

3.8.3 Sediment Delivery from Aransas Bay to Gulf of Mexico

The flow and sediment exchange between the Aransas Bay and Gulf of Mexico occur only through Cedar Bayou and Aransas Pass. During normal flows, sediment entering the Aransas Bay system may entirely deposit in bays due to the presence of the salt wedge that block the suspended marine sediment from enring these bays [137]. During high flow evens, however, sediment can transport from the river deltas to the Gulf of Mexico. For instance, during Hurricane Harvey, a powerful outflow surged through Aransas Pass near Port Aransas, causing substantial erosion in its wake. Moreover, substantial amounts of sediment, ranging from 3.3 to 19.7 ft (1 to 6 m) in thickness, deposited in Aransas Pass and the Lydia Ann Channel. Despite the sediment buildup within these

channels, the suspended sediment, carried in high concentrations, might have reached the Gulf of Mexico beyond the Port Aransas jetties [138].

Another source of sediment that could be transported to the Gulf comes from shoreline erosion. As mentioned earlier, the barrier island of Aransas Bay remains in a state of near-equilibrium or accretion. Landward surges play a vital role in preserving the barrier island under conditions of rising sea levels, due to overwash/rollover processes. However, the seaward surges, as seen during events like Hurricanes Harvey, are highly destructive, as they transport barrier island sediments out to sea, potentially causing irreversible loss [138].

The long-term net shoreline recession rates have been calculated for the central Texas Gulf shoreline between Pass Cavallo and the Packery Channel area (**Figure 3.32**). Net shoreline changes rates calculated from the 1930s to 2019 averaged retreat at 2.8 ft/yr (0.84 m/yr) for San Jose Island, with an estimated annual land loss rate of 6.4 acres/year (0.03 km^2/yr) [27].

There is limited data regarding sediment pathways and the sediment budget in this region. As a result, the rate of sediment delivery from shoreline erosion or the Aransas Bay system to the Gulf of Mexico remains unavailable.

3.9 Corpus Christi Bay System

3.9.1 Corpus Christi Bay System Watershed Characteristics

The Corpus Christi Bay system encompasses a vast area that drains into the bay and its associated estuaries. Corpus Christi Bay is located along the Gulf of Mexico in the southeastern part of the state of Texas. The watershed of Corpus Christi Bay covers a large region, including parts of several counties in South Texas. The bay is primarily fed by the Nueces River and its tributaries, which bring a significant amount of freshwater and sediment into the bay, influencing its hydrology and ecology. The bay is connected to the Gulf of Mexico through several natural and constructed channels, such as Fish Pass, Packery Channel, Wilson Cut, and Aransas Pass. Major reservoirs in the Corpus Christi Bay system watershed are Upper Nueces Lake, Choke Canyon Reservoir, and Lake Corpus Christi. **Figure 3.34** illustrates the Corpus Christi Bay watershed.

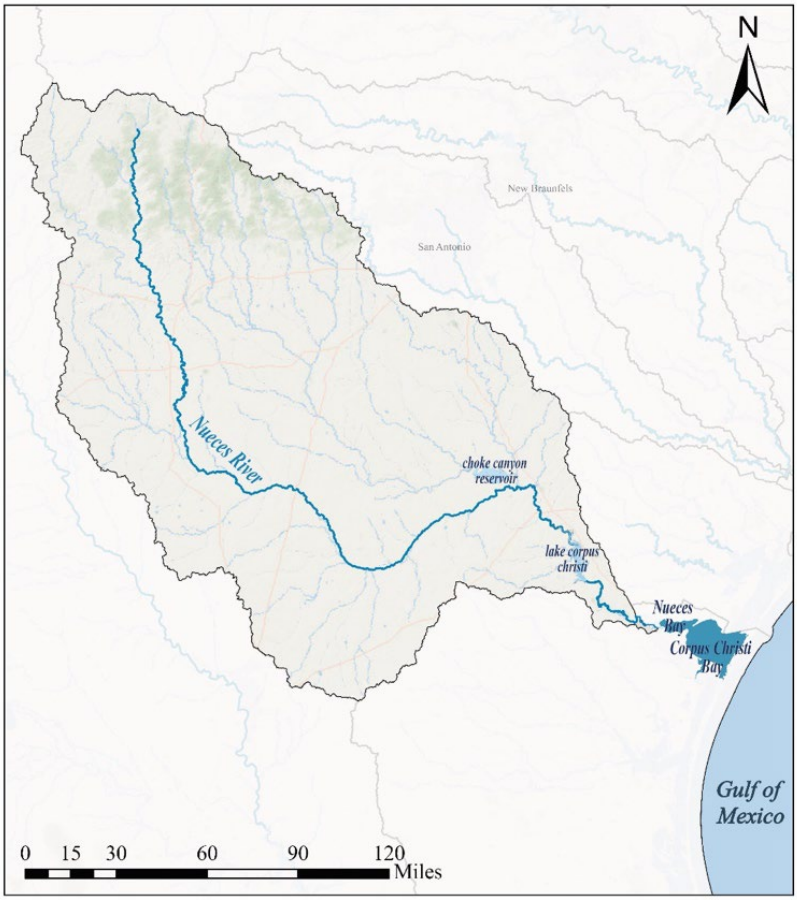

Figure 3.34 Corpus Christi Bay System Watershed

3.9.1.1 Nueces River

The Nueces River rises in Edwards and Real counties and follows a southerly and southeasterly course of 315 miles (506 km) to its mouth on Nueces Bay, which drains to the Gulf of Mexico. The Nueces River is one of the largest watersheds Texas, covering approximately 16,800 mi^2 (43,500 km^2) [139]. Other streams within the basin include the Leona, Frio, Sabinal and Atascosa Rivers and San Casimiro, Seco, Hondo, and San Miguel Creeks [140]. The Nueces River watershed and the USGG gauge stations on this river is shown in **Figure 3.35**.

The Nueces Basin is situated in a relatively arid area of Texas, which contributes to it having the third lowest average annual watershed yield among the major river basins in Texas [140]. Also, the river's hydrology is characterized by rapid flow and occasional flooding, primarily attributable to the semi-arid climate prevailing in the region [141].

The climate of the area is classified as subtropical with short, mild winters and long, hot, and humid summers with temperature varying between 39 to 97 °F (3.7 to 36 °C). Precipitation varies from about 40 inches/yr (1,016 mm/yr) in the coast to 25 inches/yr (635 mm/yr) further in land

and south [142]. The mean annual discharge of the Nueces River at the Tilden, Bluntzer and Calallen stations are 350, 227, and 396 cfs (10, 6.4, 11.2 m^3/s) (**Table 3.21**).

In the Nueces River basin, the annual sediment yield was reported as 0.1 to 2.08 tons/acre (22 to 466 tonnes/km^2) in upper and lower Nueces River [10].

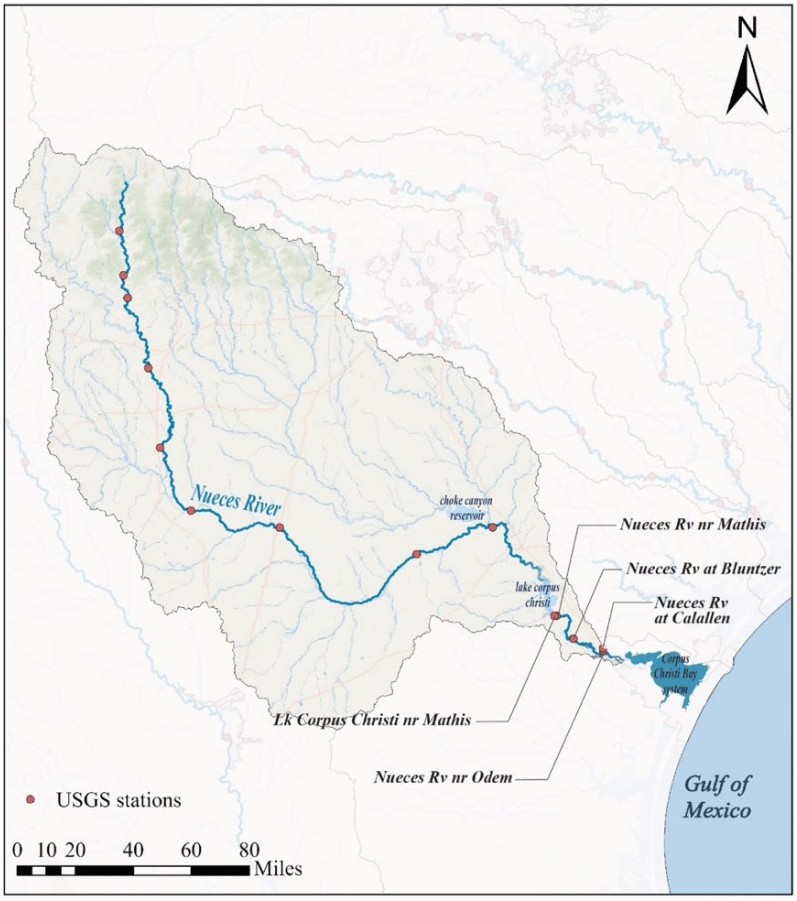

Figure 3.35 Nueces River Watershed and USGS Monitoring Stations

Table 3.21 Nueces River Annual Daily Discharges at USGS Stations

Station	Drainage Area, mi^2 (km^2)	Period	Discharge, cfs (m^3/s)		
			Max	Average	Min
Tilden[1] (USGS-08194500)	8,093 (20,960)	1942 - 2023	1,430 (40)	350 (10)	43 (1.2)
Bluntzer[2] (USGS-08211200)	16,611 (43,022)	1966 - 2023	472 (13.4)	227 (6.4)	99 (2.8)
Calallen[3] (USGS-08211500)	16,684 (43,211)	1999 - 2023	2400 (68)	396 (11.2)	29 (0.82)

[1] https://waterdata.usgs.gov/nwis/inventory/?site_no=08194500&agency_cd=USGS
[2] https://waterdata.usgs.gov/nwis/inventory/?site_no=08211200&agency_cd=USGS
[3] https://waterdata.usgs.gov/nwis/inventory/?site_no=08211500&agency_cd=USGS

3.9.1.2 Reservoirs

The Nueces River, like many rivers in Texas, is a managed system. Three major reservoirs have been constructed along the river and its tributaries: Upper Nueces Lake, Choke Canyon Reservoir, and Lake Corpus Christi [140]:

- *Upper Nueces Lake:* Upper Nueces Lake, situated 6 miles (9.7 km) to the north of Crystal City in Zavala County along the Nueces River, had an initial storage capacity of 7,590 acre-ft (9,362,113 m^3), covering a surface area of 316 acres (1.27 km^2) at the conservation pool elevation of 598 ft (182 m) above mean sea level. The storage capacity has reduced since the reservoir was impended, and the current capacity is approximated at 5,200 acre-ft (6.41 $\times 10^6$ m^3) at the same elevation. The drainage area upstream of the dam is estimated to span 2,160 mi^2 (5,594 km^2).
- *Choke Canyon Reservoir:* It is located about 65 miles (105 km) south of San Antonio and 4 miles (6.4 km) west of the community of Three Rivers. Just before the Frio River joins the Nueces River, it impounds water from San Miguel Creek and the Frio River. Choke Canyon Reservoir has a surface area of 25,438 acres (103 km^2) and a storage capacity of about 662,821 acre-ft (8.2 $\times 10^8$ m^3) at top of the conservation pool elevation, 220.5 ft (67 m) above mean sea level. The drainage area above the dam is approximately 4,667 mi^2 (12,087 km^2).
- *Lake Corpus Christi:* Lake Corpus Christi is located 4 miles (6.4 km) west of Mathis, at the intersection of the Live Oak, San Patricio, and Jim Wells County lines, on the Nueces River. The reservoir has a capacity of 254,732 acre-ft (3.14 $\times 10^8$ m^3) encompassing a surface area of 18,700 acres (76 km^2) at the conservation pool elevation of 94 ft (29 m) above mean sea level. The drainage area above the dam is approximately 16,656 mi^2 (43,140 km^2).

3.9.1.3 Corpus Christi Bay

Corpus Christi Bay, situated along the Gulf of Mexico, is where freshwater from the Nueces River and additional sources mixes with the seawater from the Gulf. It is separated from the Gulf by Mustang Island although a direct connection to the Gulf exists through the Entrance Channel of the Corpus Christi Ship Channel (Aransas Pass). The bay, averaging a depth of 10 ft (3 m), spans an area of roughly 192 mi^2 (497 km^2) [143]. Corpus Christi Bay receives freshwater inflow from the Nueces River, Oso Creek, and surrounding coastal watersheds. The Nueces River contributes an average of 587,000 acre-ft/yr (7.24 $\times 10^8$ m^3/yr) freshwater inflow to the Nueces estuary [144].

Corpus Christi Bay is known for its ecological importance, supporting a wide variety of plant and animal species. It is also significant for recreational activities like boating, fishing, and birdwatching, and it contributes to the local economy through tourism and commercial fisheries.

3.9.2 Corpus Christi Bay Sediment Budget

Various factors contribute to the Corpus Christi Bay system's sediment budget. These factors encompass sediment inflows from Nueces River, coastal erosion, anthropogenic activities, and

land-use alterations in the watershed. Additionally, sediment movement, accumulation, and suspension due to tidal, current, and wind-induced mechanisms play a pivotal role.

3.9.2.1 Nueces River Sediment Load

The Nueces River functions as the primary source of both sediment and freshwater for the Nueces River delta and the Corpus Christi Bay system. Prior to dam construction, the river annually transported a sediment load of 750,000 tons/yr (680,000 tonnes/yr) to the delta. However, due to the reservoirs built in the lower stretches of the river, the sediment supply to the delta and the bay has reduced significantly, accounting for only 4% of the annual load [39]. Lake Corpus Christi, situated in the lower Nueces River, functions as an efficient sediment trap. According to reports, the lake retained 97% of the sediment that entered it between 1977 and 1985 [145].

The USGS collects sediment data for the Nueces River at several locations (**Figure 3.35**). The Three Rivers station, located 21 mile (34 km) upstream of the Lake Corpus Christi, has the longest with recorded of sediment data in lower Nueces River that is from 1970 to 1995. Other stations downstream of the dam have very limited sediment data in the period of 2006-2010, with Bluntzer station having the highest number of data points. The suspended sediment concentration (SSC) and daily sediment load at these two stations are summarized in **Table 3.22**.

Table 3.22 Nueces River Suspended Sediment Concentration and Load at USGS Stations

Station	Period	Suspended Sediment Concentration, mg/L (Suspended Sediment Load, tons/day)		
		Max	Average	Min
Three River[1] (USGS-08210000)	1970 - 1995	1,730 (17,800)	140 (693)	2 (0.03)
Bluntzer[2] (USGS-08211200)	2006 - 2010	1,070 (3,040)	271 (911)	25 (5.5)

[1] https://mywaterway.epa.gov/monitoring-report/NWIS/USGS-TX/USGS-08210000/
[2] https://mywaterway.epa.gov/monitoring-report/NWIS/USGS-TX/USGS-08211200/

The sediment measurements were also taken in the Nueces River estuary area at the TCEQMAIN-18866 station from April 2005 to June 2014. The data collected revealed a median TSS value of 33.5 mg/L, with minimum values recorded at 5 mg/L and maximum value at 169 mg/L [146].

The USGS conducted a study aimed at modeling streamflow and suspended sediment concentrations and loads in the lower Nueces River watershed from 1958 to 2010, spanning from downstream of Lake Corpus Christi to the Nueces Estuary [147]. This study used historical sediment data collected between 1942 and 1982 and data periodically gathered by the USGS during 2006-2007 and 2010. Data were collected from three USGS stations: the Nueces River near Mathis (USGS-08211000), the Nueces River at Bluntzer (USGS-08211200), the Nueces River at Calallen (USGS-08211500), and an ungauged location on a Nueces River tributary, Bayou Creek at Farm Road 666 near Mathis (USGS-08211050). The findings of this study are as follows:

- Annual suspended sediment loads at the Mathis station, situated downstream of Wesley E. Seale Dam (**Figure 3.35**), decreased significantly following the impoundment of Lake Corpus Christi in 1958. Most suspended sediment transported by the Nueces River downstream from the dam occurred during high-flow releases from the dam or during floods.
- From 1958 to 2010, estimated annual suspended sediment loads at the Mathis, Bluntzer, Calallen, and Odem stations in the Lower Nueces River watershed (**Figure 3.35**) were 94, 207, 260, and 278 tons/day (85, 188, 236, and 252 tonnes/day), respectively.
- On average from 1958 to 2010, an estimated 288 tons/day (261 tonnes/day) of suspended sediment were delivered to the Lower Nueces River, with an estimated 278 tons/day (252 tonnes/day) delivered to the estuary. Annual total sediment load to the estuary varied from an estimated 3.8 to 2,490 tons/day (3.4 to 2,259 tonnes/day) during this period.
- Of the 288 tons/day (261 tonnes/day) of suspended sediment delivered to the Lower Nueces River, various sources contributed: 113 tons/day (103 tonnes/day) (39%) from cropland in the study watershed (i.e., downstream of Lake Corpus Christi to the Nueces Estuary), 94 tons/day (85 tonnes/day) (33%) from Lake Corpus Christi releases, 44 tons/day (40 tonnes/day) (15%) from the erosion of stream-channel bed and banks, and 36 tons/day (33 tonnes/day) (12%) from all other land categories except cropland. An estimated 10 tons/day (9 tonnes/day) (3%) of suspended sediment load delivered to the Lower Nueces River were removed by water withdrawals before reaching the Nueces Estuary.

The effects of freshwater inflow on sediment transport and nutrients supply to the Nueces River and its estuary were studied [148]. Sediment and water samples were collected from the Nueces River and the Nueces Estuary near the river mouth. The river water samples were obtained from a station within LaBonte Park, situated below the Calallen Dam at the confluence point between the ephemeral Hondo Creek and the Nueces River, in close proximity to the USGS-08211500 station near Calallen. Sampling of the estuary stations occurred quarterly between April 2011 and October 2013, while river samples were collected in July 2012, October 2012, and February 2013. The study's findings are as follows:

- The average TSS in the estuary ranged from 16.6 to 249 mg/L during 2011-2013 study period.
- TSS was significantly different between near stations (close to river mouth) and far stations (in Corpus Christi Bay close to GoM). It was speculated that wind and cold front events could have significant role to have high TSS concentration in the primary bay of the Nueces Estuary.
- TSS in the Nueces River estuary was higher than the Nueces River in October and January.
- Both the Nueces Estuary and the Nueces River predominantly contained coarser particles, characterized by a larger surface area. However, during July, the sediments in the Nueces Estuary were mainly composed of fine particles. Despite the variance in grain size

distributions between the Nueces Estuary and Nueces River, there was no significant difference observed in the adsorption surface area which represents the particles' capacity to bind with other substances.

- Typically, the Nueces River maintains base flow conditions, preventing water from overflowing the Calallen Dam. On September 22, 2013, the average TSS concentration was 52 mg/L at the station above the Calallen Dam in the Nueces River, 508 mg/L at the station near the confluence of Hondo Creek and the Nueces, and 53 mg/L further downstream. This discrepancy indicates that the ephemeral stream, Hondo Creek, contributes significantly to the TSS concentration in the river. Nevertheless, in the Nueces Estuary, TSS levels rarely surpass 50 mg/L. Lake Corpus Christi retains most of the sediments, resulting in lower TSS levels downstream.

3.9.2.2 Sediment Delivery to Corpus Christi Bay

Corpus Christi Bay receives freshwater inflow from the Nueces River, Oso Creek, and surrounding coastal watersheds. Based on the USGS study, the average suspended sediment load delivered to the Nueces Estuary is 278 tons/day (252 tonnes/day) [147] (see **Sections 3.9.2.1)** or 101,470 tons/yr (92,000 tonnes/yr). However, most of the sediment sourced from the Nueces River and its tributaries deposit in the Nueces Delta and Bay, and Corpus Christi Bay.

Lithogenic (^{226}Ra, ^{228}Ra, ^{228}Th, ^{230}Th, 2^{32}Th) and fallout (^{137}Cs, ^{210}Pb) isotopes were employed in conjunction with sedimentological methods to determine rates of sedimentation in the Nueces Delta and Nueces-Corpus Christi Estuary and to assess the relative importance of marine versus terrestrial sediment sources to the estuary [141]. The results showed that:

- The sediments from Nueces and Corpus Christi Bays exhibit signatures similar to terrestrial components, implying they are exclusively composed of sediment originating from terrestrial sources, differing significantly from marine sediment sources. The GoM and GIWW sediments are mostly sands. This suggest that nearshore oceanic sands largely originating from longshore transport near barrier islands. The GIWW sands likely come from both longshore transport and storm-driven wash over barrier islands due to high-energy storms and waves.
- Sediments from the Nueces River and its eastern tributaries provide sand and fines to the Nueces Delta and Bay, retaining coarser fractions effectively in these areas. Flashy river flow and the shallow depth of Nueces Bay, typically < 6.5 ft (2 m), sustain this scenario. Corpus Christi Bay, which is deeper (10-16.5 ft (3-5 m)), primarily accumulates fine-grained sediments, mainly clay. Suspended sediments that remain in suspension in Corpus Christi Bay move towards the shelf. The data indicates that marine sediment sources from the Gulf of Mexico or GIWW make a negligible contribution due to minimal tidal variation and the presence of barrier islands protecting the estuary.
- Sediment deposition rates exhibit a consistent decrease within the initial 12.4 miles (20 km) from the Nueces River and become constant beyond that, indicating the river's primary role

as the significant sediment source to the estuary. The average sedimentation rates in the river delta and Nueces Bay are reported as 0.001-0.0075 lb/in^2/yr (0.09-0.53 g/cm^2/yr) and 0.004-0.0074 lb/in^2/yr (0.3-0.52 g/cm^2/yr), respectively, whereas the rates in Corpus Christi are notably lower, averaging between 0.003-0.0034 lb/in^2/yr (0.18-0.24 g/cm^2/yr).

Oso Creek serves as another freshwater and sediment source for Corpus Christi Bay. Situated in southern Nueces County, the Oso Creek watershed originates near Robstown and travels through Corpus Christi, eventually emptying into Oso Bay. A pilot study, utilizing the Soil and Water Assessment Tool (SWAT) and the Hydrologic Simulation Program-FORTRAN (HSPF) model, estimated the total suspended loads for the area. As per the model's results, the total suspended solids (TSS) loading to Oso Creek were reported as follows: 1,738 tons in 1989, 4,140 tons in 1990, 10,979 tons in 1991, 1,100 tons in 1992, and 10,050 tons in 1993 [142].

Sediment data were collected from Oso Creek and Oso Bay between 1999 and 2000 [149]. In Oso Creek, the mean TSS values varied from 23 to 137 mg/L, with monthly values ranging from 8 to 552 mg/L. Within Oso Bay, TSS ranged from 82.4 to 144.6 mg/L, while monthly values varied from 11 to 706 mg/L over the same period. The results indicated that mean TSS values were higher in the estuarine waters of Oso Bay.

Also, limited TSS data is available from the USGS station in Oso Creek near Corpus Christi Bay for the period of 2006-2008. The average suspended sediment concentration and load was reported as 390.2 mg/L and 17.3 tones/day, respectively [150]. The limited sediment data from Oso Creek make it challenging to precisely estimate its annual sediment contribution to Corpus Christi Bay. However, due to the significantly smaller watershed of Oso Creek (262 mile^2 (600 km^2) [149] in comparison to the Nueces River (16,800 mi^2 (43,500 km^2) [139]), its sediment impact on Corpus Christi appears to be insignificant.

Shoreline erosion may contribute to the sediment in Corpus Christi Bay. Changes in the position and stability of shorelines in Corpus Christi, Nueces, and Oso Bays since the late 1800s were documented using historical data [151]. The accretion and erosion rates in ft/yr (m/yr) in these bays between 1934 and 1982 are as follows: Northern Corpus Christi Bay: +2/–2 (+0.6/–0.6), Southern Corpus Christi Bay: +10/–5 (+3/–1.5), Eastern Corpus Christi Bay: +8/–50 (+2.4/–15.2); Nueces Bay: +94/–5 (+28.7/–1.5); and Oso Bay: +84/–1(+25.5/–0.3). The shorelines of these bays are mostly in either equilibrium or accretion stages, with erosion being more pronounced in the eastern part of Corpus Christi Bay. Human modifications, such as the placement of dredged materials and artificial land creation, account for significant increases in accreting shoreline values. Conversely, single events such as hurricanes or dredging, are responsible for notable shoreline erosion during this period. While an exact estimate of the sediment entering the bays from the shorelines is not available, studies on the textural characteristics of benthic sediment have revealed the presence of shore materials within these areas. It has been observed that the interiors of Corpus Christi, Nueces, and Oso Bays serve as depocenters for mud (silt and clay) influx from the Nueces River and Oso Creek, as well as for mud eroded from the bays' shorelines. Conversely,

the peripheral sandy sediments appear to mainly consist of residual lag deposits resulting from shoreline erosion [152].

3.9.3 Sediment Delivery from Corpus Christi Bay to Gulf of Mexico

Corpus Christi Bay is connected directly to the Gulf of Mexico through the Aransas Pass. The bay is also connected to the Gulf of Mexico through several smaller natural and constructed channels, such as Fish Pass, Packery Channel, and Wilson Cut. Due to small size of these passes and channels, the water and sediment exchange between the bay and GoM is very limited, except for during flooding and storm event. As discussed in **Section 3.9.2.2**, during large storm events, such as Hurricane Harvey, deposited sediment in Aransas Pass and the Lydia Ann Channel would be carried to the Gulf of Mexico. Under typical conditions, the bay does not discharge sediment into the Gulf of Mexico. Radiochemical techniques applied to sediment samples from Nueces and Corpus Christi Bays showed a minimal inflow of sediment from the GoM to the bay [153]. The study pointed out that the Nueces-Corpus Christi Estuary, characterized as micro-tidal with an extensive barrier island system, limits communication with the GoM and is minimally impacted by shelf or open ocean currents. Considering these factors, the evidence indicates that marine sediment sources to Corpus Christi Bay are negligible.

Shoreline erosion serves as a potential source of sediment transport to the GoM. Both major and minor factors influencing shoreline alterations encompass climate, storm patterns, sea-level changes (local and global), sediment budget, and human interventions. On the Texas Coast, including Mustang and north Padre Island, key factors impacting shoreline changes involve sea-level conditions, subsidence, and sediment supply alterations. The movement of the vegetation line is mainly linked to storm activity. Alterations in the shoreline and vegetation on these islands predominantly stem from natural processes, potentially accelerated by human activities [154]. The long-term net shoreline recession rates have been calculated for the central Texas Gulf shoreline between Pass Cavallo and the Packery Channel area (**Figure 3.32**). Net shoreline changes rates calculated from the 1930s to 2019 averaged retreat at 1.0 ft/yr (0.30 m/yr) in Mustang Island, with an estimated annual land loss rate of 2.1 acres/yr (0.0085 km^2/yr) [27].

There is limited data regarding sediment pathways and the sediment budget in this region. As a result, the rate of sediment delivery from shoreline erosion or the Corpus Christi Bay system to the Gulf of Mexico remains unavailable.

3.10 Baffin Bay System

3.10.1 Baffin Bay System Watershed Characteristics

The Baffin Bay system is located in southern Texas, bordered by Kleberg County to the north and Kennedy County to the south. It encompasses Baffin Bay and its three branches: Cayo del Grullo, Alazan Bay, and Laguna Salada, as well as several ephemeral creeks, including San Fernando, Petronia, and Los Olmos, along with other minor creeks. Baffin Bay is isolated from the Gulf of Mexico by Padre Island and further insulated from the contiguous Laguna Madre system by shallow reefs at the mouth of the bay [155] (**Figure 3.36**). The bay watershed is located in the

semiarid area of South Texas, characterized by high evaporation rates that exceed precipitation. The average annual precipitation in the area is 27.8 inches/yr (700 mm/yr). The area experiences long, hot summers with average high temperatures of 92 °F (33 °C) and short, mild winters with average low temperatures around 47.0 °F (8.3 °C) [156].

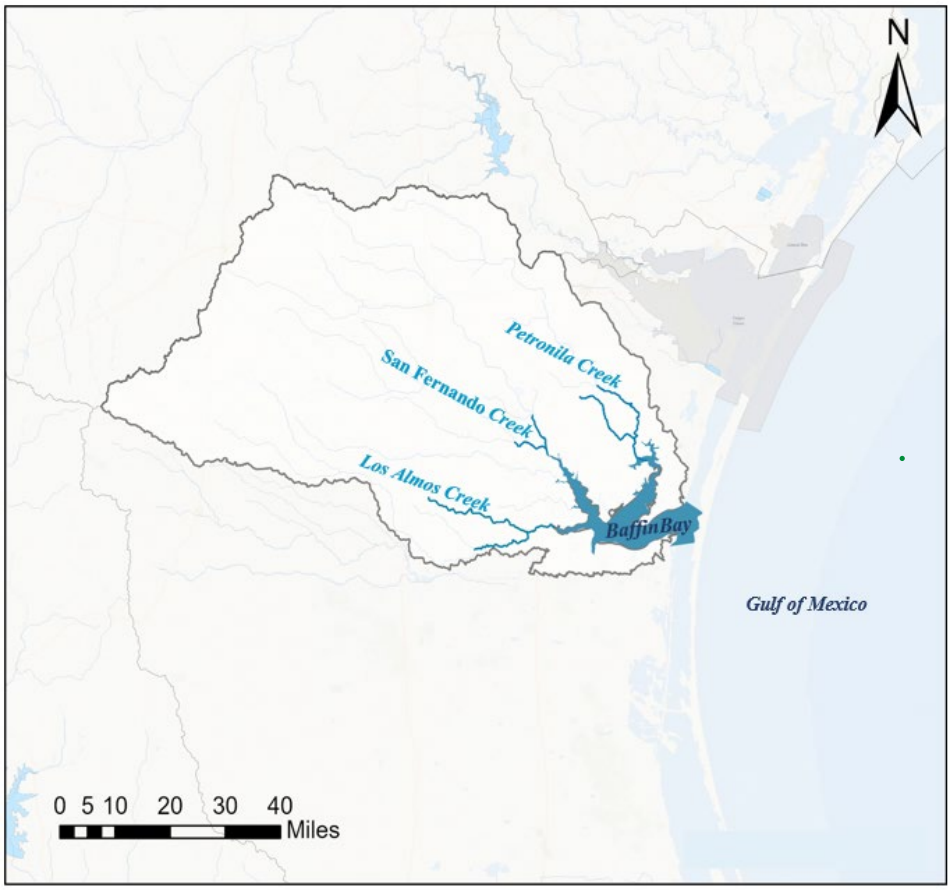

Figure 3.36 Baffin Bay Watershed and USGS Monitoring Station

3.10.1.1 Creeks Flowing to Baffin Bay

Three creeks discharge into Baffin Bay: San Fernando, which flows into Cayo del Grullo; Petronila, which flows into Alazan Bay; and Los Olmos, which flows into Laguna Salada Creeks (**Figure 3.36**).

San Fernando Creek

San Fernando Creek begins at the confluence of San Diego and Chiltipin Creeks in Jim Wells County, northeast of Alice. From there, it flows approximately 44 miles (71 km) downstream to Cayo del Grullo, southeast of Kingsville. Its watershed covers approximately 1,270 mi^2 (3290 km^2) of largely rural land but does include the cities of Alice and Kingsville [157].

Streamflow data for this creek has been collected since 1965 at the USGS-08211900 station in Alice, located 37 miles (60 km) inland from Baffin Bay (**Figure 3.36**). For this period, the daily average flow is reported as 18 ft^3/s (0.51 m^3/s), with a minimum and maximum range of 1.6 to 499 ft^3/s (0.05 to 14 m^3/s) (**Table 3.23**).

Petronila Creek

Petronila Creek originates in western Nueces County, winding its way for approximately 44 miles (71 km) until it converges with Tunas Creek in eastern Kleberg County. From there, it continues its course into Cayo Del Mazón before ultimately emptying into Alvazan Bay. The watershed of Petronila Creek spans across portions of Jim Wells, Nueces, and Kleberg counties, covering an area of 675 mi^2 (1750 km^2), predominantly characterized by rural landscapes with several towns scattered throughout. While Petronila Creek begins as a freshwater stream in its upper stretches, the influence of tides gradually turns it brackish as it nears Baffin Bay [157]. Streamflow data for this creek has been collected since 2018 at the USGS-08212820 station near Driscoll, located 37 miles (60 km) inland from Baffin Bay (**Figure 3.36**). For this period, the daily average flow is reported as 162 ft^3/s (4.6 m^3/s), with a minimum and maximum range of 0.22 to 1,250 ft^3/s (0.006 to 35.4 m^3/s) (**Table 3.23**).

Los Olmos Creek

Los Olmos Creek originates from the merging of Agua Poquita and Concepcion Creeks, located 8 miles (13 km) south of Benavides in southern Duval County. It runs southeast for 71 miles (114 km), passing through Jim Wells and Brooks counties. It delineates the boundary between Kleberg and Kenedy counties before merging into Laguna Salado, an inlet of Baffin Bay. The Los Olmos Creek watershed covers approximately 2,202 mi^2 (5,700 km^2) of primarily rural land to the south of the San Fernando Creek watershed. It is the third largest tributary into Baffin Bay volumetrically; however, its watershed area is larger than the combined watershed area of San Fernando and Petronila Creeks [157]. Streamflow data for this creek has been collected since 1967 at the USGS 08212400 near Falfurrias, located 25 miles (40 km) inland from Baffin Bay (**Figure 3.36**). For this period, the daily average flow is reported as 4.5 ft^3/s (0.13 m^3/s), with a minimum and maximum range of 0.3 to 106 ft^3/s (0.008 to 3 m^3/s) (**Table 3.23**).

In the lower Baffin Bay basin, an assessment conducted in 1979 estimated an annual sediment yield of 0.18 tons/acre (40.4 tonnes/km^2) [10].

Table 3.23 San Fernando, Petronila, and Los Almos Creeks Daily Discharges at USGS Stations

Station	Drainage Area, mi² (km²)	Period	Discharge, cfs (m³/s)		
			Max	Average	Min
San Fernando at Alice[1] (USGS-08211900)	507 (1,313)	1965 - 2023	499 (14)	18 (0.51)	1.6 (0.05)
Petronila at Driscoll[2] (USGS-08212820)	390 (1,010)	2018 - 2023	1,250 (35.4)	162 (4.6)	0.22 (0.006)
Los Almos at Falfurrias[3] (USGS-08212400)	480 (1,243)	1967 - 2023	106 (3)	4.5 (0.13)	0.3 (0.008)

[1] https://waterdata.usgs.gov/nwis/inventory/?site_no=08211900&agency_cd=USGS
[2] https://waterdata.usgs.gov/nwis/inventory/?site_no=08212820&agency_cd=USGS
[3] https://waterdata.usgs.gov/nwis/inventory/?site_no=08212400&agency_cd=USGS

3.10.1.2 Baffin Bay

Baffin Bay, an inlet of the Upper Laguna Madre, is secluded from the Gulf of Mexico by Padre Island, and it is further isolated from the continuous Laguna Madre system by shallow reefs at the bay's entrance [155]. The nearest inlets for exchange between Baffin Bay and the Gulf of Mexico are Packery Channel and Aransas Pass, approximately 25.4 and 43.5 miles (41 and 70 km) north of Baffin Bay, as well as Port Mansfield, around 50 mile (80 km) to the south [158]. Streamflow discharge into Baffin Bay from its tributaries are limited. The bay receives freshwater contributions from Los Olmos, San Fernando, Petronila Creeks, and several minor streams. The bay is a shallow estuary with an average depth of 6.6 ft (2 m) and maximum depth of 10 ft (3 m). It encounters only small astronomical tides (<0.33 ft (0.1 m)) [152]. The bay serves as a crucial habitat for various commercially and recreationally significant marine species. The largely undeveloped land surrounding Baffin Bay contributes to maintaining conditions that are comparatively more pristine than those found in the Nueces Estuary system.

3.10.2 Baffin Bay Sediment Budget

The sediment sources to Baffin Bay primarily come from various natural and anthropogenic origins within its watershed. The primary sources of sediment include fluvial inputs, shoreline erosion, agricultural and urban runoff, tidal action, and human activities. Sediment from fluvial sources can be carried into Baffin Bay by various creeks that drain into the bay. Creeks like San Fernando, Petronila, Los Olmos, and others contribute sediment from the surrounding land.

3.10.2.1 Los Olmos, San Fernando, and Petronila Creeks Sediment Load

There are three major creeks that flow into Baffin Bay: Los Olmos Creek, San Fernando Creek, and Petronila Creek. These creeks drain a total area of 4,324 mi² (11,200 km²). They deliver variable amounts of water and sediment to the bay. The modern drainage of these creeks, especially to the south of Baffin Bay, is disrupted by aeolian dunes. As a result, the delivery of sediment to Baffin Bay from these creeks is sporadic and limited to intense rain events. [155]. Limited

sediment data is available for these creeks from the TCEQ stations. Total suspended solids (TSS) concentrations were collected from San Fernando, Petronila, and Los Olmos Creeks. The locations of stations on these creeks are shown in **Figure 3.37**, and **Table 3.24** presents a summary of sediment data collected at these locations.

Figure 3.37 TCEQ Water Quality Stations on Los Olmos, San Fernando, and Petronila Creeks

Table 3.24 San Fernando, Petronila, and Los Almos Creeks Total Suspended Solids (TSS) Concentration at TCEQ Stations

Station	Period	Total Suspended Sediment Solid, TSS (mg/L)		
		Max	Average	Min
San Fernando Creek[1] (TCEQMAIN-13033)	2005 – 2022	203	65	14
Petronila Creek[2] (TCEQMAIN-13090)	2005 – 2011	436	116	13
Los Olmos Creek[3] (TCEQMAIN-13034)	2018 – 2022	1,168	200	20

[1] https://mywaterway.epa.gov/monitoring-report/STORET/TCEQMAIN/TCEQMAIN-13033/
[2] https://mywaterway.epa.gov/monitoring-report/STORET/TCEQMAIN/TCEQMAIN-13090/
[3] https://mywaterway.epa.gov/monitoring-report/STORET/TCEQMAIN/TCEQMAIN-13034/

3.10.2.2 Sediment Delivery to Baffin Bay

Sediment may enter Baffin Bay from various sources including fluvial inputs by creek and surface runoff, shoreline erosion, coastal and marine sediment delivered by tidal action and overwash. An estimate of sediment load entering Baffin Bay from fluvial sources is not available. In absence of such information the sediment delivery to the bay can be estimated from sediment yield rate of the basin or from the daily average TSS concentration and flow of creeks discharging to the bay.

The annual sediment yield of the Baffin Bay watershed is estimated at 0.18 tons/acre (40.4 tonnes/ km^2) (see **Section 3.10.1.1**), and the total area of the bay's watershed is 4,324 mi^2 (11,200 km^2) (see **Section 3.10.2.1**). Consequently, the annual sediment load to the bay can be calculated as 498,200 tons/yr (451,960 tonnes/yr) or 1,365 tons/day (1,240 tonnes/day).The presented estimates seem exceedingly unrealistic, particularly when considering the relatively small size of the watershed and the limited freshwater inflows into the bay. Multiple studies support this perspective highlighting that Baffin Bay currently receives minimal freshwater and nearly no land-based sediment. This circumstance, along with its placement in a semi-arid region of the western Gulf, leads to Baffin Bay being highly saline [120]. Another source further emphasizes that Baffin Bay is extremely shallow and experiences almost no fluvial and marine input of runoff or sediment [159]. Also, a study on depositional environments in Baffin Bay found a well-developed bayhead delta, indicating that the sediment supplied by the three major creeks flowing into Baffin Bay was greater in the past than it is today. However, no bayhead delta has extended into modern Baffin Bay. Instead of fluvial dominated bayhead deltas, the upper reaches of Baffin Bay are now filling with mudflats due to a significant reduction in fluvial sediment input to the bay. Presently, the modern drainage of the creeks flowing into Baffin Bay, especially to the south of the bay, is disrupted by aeolian dunes. Consequently, the delivery of sediment to Baffin Bay from these creeks occurs sporadically and is limited to intense rain events [155].

The estimation of sediment load carried by creeks to the bay cannot be determined using the flow and suspended sediment concentrations data presented in previous sections (**Table 3.23** and **Table 3.24**). This limitation arises from the disparity in the locations and times at which the flow and sediment data were measured.

Moreover, a comprehensive study to estimate the contribution of sediment load to Baffin Bay due to shoreline erosion is not available. However, it is reported that the Baffin Bay shoreline is not eroding at high rates primarily because of the presence of cemented sediments and the occurrence of beach rock formation in various areas along the bay shoreline [160]. Despite these factors and the characterization of Baffin Bay by its low-energy wave environment [161], tidal movement has still caused significant erosion at a rate of about 1.1 ft/yr (0.34 m/yr) before 2003 along the Loyola Beach shoreline, located southwest of Cayo del Grullo [162].

3.10.3 Sediment Delivery from Baffin Bay to Gulf of Mexico

Baffin Bay is often classified as a reverse estuary, meaning it is more saline than the bay it drains into. This is primarily due to limited freshwater inflows from surface runoff, high rates of

evaporation, and its restricted connection with the Gulf of Mexico. These factors result in extended residence times, exceeding one year, and extremely high salinities [158,163,164]. Similarly, sediment transported into the bay from creeks may predominantly deposit in the secondary bays such as Alazan, Cayo del Grullo, Salada, and Baffin Bay itself, rather than contributing to the Upper Laguna Madre. It was estimated that only 10% of sediment entering Baffin Bay leave the system and enters the Upper Laguna Madre [165]. Analysis of sediment cores indicated highly variable deposition in the creek bays, attributable to the shallow waters and fluvial/terrestrial influences [166]. Additionally, this study showed that sediment deposition rates in Baffin Bay were more than twice the rate calculated for Alazan Bay and over five times larger than the rate observed for Cayo del Grullo.

Even if sediment reaches Laguna Madre, it might not progress to the Gulf of Mexico due to the geographical limitations. The nearest inlets facilitating the exchange between Baffin Bay and the Gulf of Mexico are Packery Channel and Aransas Pass, approximately 25 and 43 miles (41 and 70 km) north of Baffin Bay, respectively, and Port Mansfield 50 miles (80 km) south [158].

3.11 Laguna Madre System

3.11.1 Laguna Madre System Watershed Characteristics

The Laguna Madre is the longest and most expansive among estuarine systems within Texas. It is naturally divided by a coastal land mass known as Saltillo Flats (aka Land Cut) into two sections within the state: the Upper Laguna Madre (ULM) and the Lower Laguna Madre (LLM). The ULM is isolated from the Gulf of Mexico by Padre Island, stretching for 64 miles (101 km) from the southern tip of Corpus Christi Bay to the Saltillo Flats. It connects to Baffin Bay on its eastern side and links to the Gulf of Mexico solely through Packery Channel, which allows the inflow of water from the Gulf of Mexico. The LLM, extending from the Saltillo Flats into Mexico, connects directly with the Gulf of Mexico through Port Mansfield Channel and Brazos-Santiago Pass (**Figure 3.38**) [156].

The watershed of the Laguna Madre system comprises both gauged basins and ungauged sections of small coastal basins. The gauged streams contributing to the Laguna Madre system include San Fernando, Los Olmos, and Petronila Creeks (discharging into the ULM through Baffin Bay as discussed in **Section 3.10.1.1**), as well as Arroyo Colorado in the LLM. Twelve ungauged watersheds contribute to Baffin Bay and the ULM, and nine ungauged watersheds contribute to the LLM (**Figure 3.38**).

The Laguna Madre watershed is classified as a sub-humid, semi-arid, subtropical climate that typically experiences long, hot summers with average high temperature of 92 °F (33.3 °C), and short and mild winters with average low temperatures around 47 °F (8.3 °C). The annul precipitation varies between 18 to 28 inches (457 to 711 mm) [156,167].

Figure 3.38 Laguna Madre System Watershed

3.11.1.1 Arroyo Colorado

The Arroyo Colorado is the primary freshwater source for the Lower Laguna Madre. Its watershed is situated in the Lower Rio Grande Valley of South Texas, extending from near Mission City, Texas, eastward until it eventually flows into the Lower Laguna Madre (**Figure 3.38**). As part of the Nueces-Rio Grande Coastal basin, it specifically represents the Lower Laguna Madre watershed. Stretching across 90 miles (145 km), it encompasses a watershed of approximately 706 mi^2 (1,828 km^2) [168]. The upper drainage area comprises fertile farmland, citrus orchards, and incorporates the cities of Harlingen and Rio Hondo. As the Arroyo progresses downward, it navigates through an expanse featuring farms, ranches, and coastal playas [169].

The Arroyo Colorado watershed experiences warm temperatures and high humidity, representing a semi-arid and subtropical climate. This region typically receives an average annual precipitation from 21 to 26 inches (533 to 660 mm) and maintains a mean temperature of 72 °F (22 °C) with mean monthly temperatures ranging from 58 °F (14.5 °C) in January to 84 °F (28.9 °C) in July [170,171].

The minimum, average, and maximum instantaneous discharge of the Arroyo Colorado at the Harlingen station (**Figure 3.39**) are summarized in **Table 3.25**.

The sediment yield for the Arroyo Colorado was estimated as 0.38 tons/acre (0.34 tonnes/acre) [10], or 172,000 tons/yr (156,000 tonnes/yr).

Figure 3.39 Arroyo Colorado Watershed and USGS and TCEQ Monitoring Stations

Table 3.25 Arroyo Colorado Annual Instantaneous Discharges at USGS Station

Station	Drainage Area, mi^2 (km^2)	Period	Discharge, cfs (m^3/s)		
			Max	Average	Min
Harlingen[1] (USGS- 08470400)		1986 - 2007	1,550 (44)	235.2 (6.6)	63 (1.8)

[1] https://mywaterway.epa.gov/monitoring-report/NWIS/USGS-TX/USGS-08470400/

3.11.1.2 Laguna Madre

The Laguna Madre extends along the lower coast of Texas, reaching from the southern edge of Corpus Christi Bay in the north to the Texas-Mexico border in the south. It covers a surface area of 280,910 acres (1,137 km^2) and maintains an average depth of 4.5 ft (1.37 m). Saltillo Flats divide it into upper and lower bays. The major streams contributing to the Laguna Madre (Upper and Lower) include San Fernando Creek through Baffin Bay in the Upper Laguna Madre and the Arroyo Colorado in the Lower Laguna Madre, in addition to inputs from surrounding coastal

watersheds [172]. For the period of 1941 to 2010, gauged streams accounted for approximately 45% of surface inflows, while ungauged flows constituted 51%, and net diversions made up 4%. The average annual surface inflow to the Laguna Madre for this period was estimated at 743,000 acre-ft (9.16×10^8 m^3), varying from a minimum of 123,000 acre-ft (1.52×10^8 m^3) in 1952 to 3,428,875 acre-ft (42.3×10^8 m^3) in 2010. Over the same period, the average surface inflow to the Lower Laguna Madre was approximately 523,602 acre-ft/yr ft (6.5×10^8 m^3 /yr), ranging from a minimum of 234,158 acre-ft (2.9×10^8 m^3) in 1990 to 2,726,325 acre-ft (34×10^8 m^3) in 2010 [173].

3.11.2 Laguna Madre Sediment Budget

The sediment budget for Laguna Madre reveals the complex relationship of various natural processes, external terrigenous sources, and human activities. While the lagoon collects sediments from aeolian, fluvial, tidal, and overwash processes, the bulk of sediment originates from dredging in the Gulf Intracoastal Waterway (GIWW). The pattern of sediment changing within the lagoon is primarily driven by erosion along the margins and resuspension caused by wave and current action, which significantly contributes to shoaling in the GIWW's Laguna Madre section. The estimated sedimentation rate in Laguna Madre is notably slower than in neighboring Texas bays to the north, highlighting the unique dynamics of this coastal ecosystem.

The fluvial sediment may enter Laguna Madre system by San Fernando, Los Olmos, and Petronila Creeks through Baffin Bay in the Upper Laguna Madre and the Arroyo Colorado in the Lower Laguna Madre. However as discussed in **Section 3.10.3**, sediment transported into Baffin Bay from these creeks may predominantly deposit in the secondary bays such as Alazan, Cayo del Grullo, Salada, and Baffin Bay itself, rather than contributing to the Upper Laguna Madre. Therefore, in the following section, the discussion focuses on the inflow of fluvial sediment from the Arroyo Colorado into the Lower Laguna Madre.

3.11.2.1 Arroyo Colorado Sediment Load

The primary freshwater source for Lower Laguna Madre is the Arroyo Colorado as there are no other streams with substantial drainage basins to provide significant freshwater input to the lagoon. The majority of sediment loads in the Arroyo Colorado stem from nonpoint sources, primarily agricultural and urban runoff. Nevertheless, during dry weather, suspended sediment loads increase significantly due to the substantial sediment contribution from municipal and industrial point-source discharges [174].

Suspended sediment concentration and load are measured between 1986 to 2007 for Arroyo Colorado at Harlingen station (USGS-08470400) located 32 mile (51 km) from its mouth in LLM. For this period, the minimum, average, and maximum daily suspended sediment concentrations are reported as 21, 277, and 1,100 mg/L. The corresponding daily average suspended sediment load is 182 tons/day (165 tonnes/day), with the minimum of 18 tons/day (16 tonnes/day) and maximum of 1,960 tons/day (1768 tonnes/day) (**Table 3.26**). The average annual sediment load at this station may be calculated as 66,430 tons/yr (60,264 tonnes/yr).

Table 3.26 Arroyo Colorado Suspended Sediment Concentration and Load at USGS Station

Station	Period	Suspended Sediment Concentration, mg/L (Suspended Sediment Load, tons/day)		
		Max	Average	Min
Harlingen[1] (USGS- 08470400)	1986 - 2007	1,100 (1,960)	277 (182)	21 (18)

[1] https://mywaterway.epa.gov/monitoring-report/NWIS/USGS-TX/USGS-08470400/

The TCEQ also collected total suspended solids (TSS) from 1996 to 2006 at two stations on the Arroyo Colorado: Station 13074 at Cemetary Road (located upstream of tidal/non-tidal boundary), and Station 1307 at FM 106 Bridge, Rio Hondo located downstream of tidal/non-tidal boundary) [175] (**Figure 3.40**). The TCEQ Station 13074 has the same coordinates as the USGS-08470400 station. For this period, the average TSS at the downstream end of the non-tidal portion of the Arroyo Colorado (just upstream of the Zone of Impairment) was 147 mg/L. The average TSS concentration at the station located in the tidal portion of the Arroyo Colorado (at the Zone of Impairment) was 27 mg/L. Typically, the TSS concentrations were higher at the upstream station. Nevertheless, as depicted in **Figure 3.40**, there is no discernible trend in the TSS data concerning time or the season of the year. While occasionally reaching high levels (80-90 mg/L), TSS in the tidal segment of the Arroyo Colorado were typically considerably lower compared to the above tidal segment. This disparity was attributed to the reduction in stream velocity at the tidal boundary. When the freshwater from the Arroyo Colorado above tidal segment enters the Port of Harlingen, its speed decreases, resulting in the sediment settling out of suspension. The majority of the sediment lost at the onset of the tidal segment can be attributed to be sediment deposition at or in close proximity to the Port of Harlingen [175].

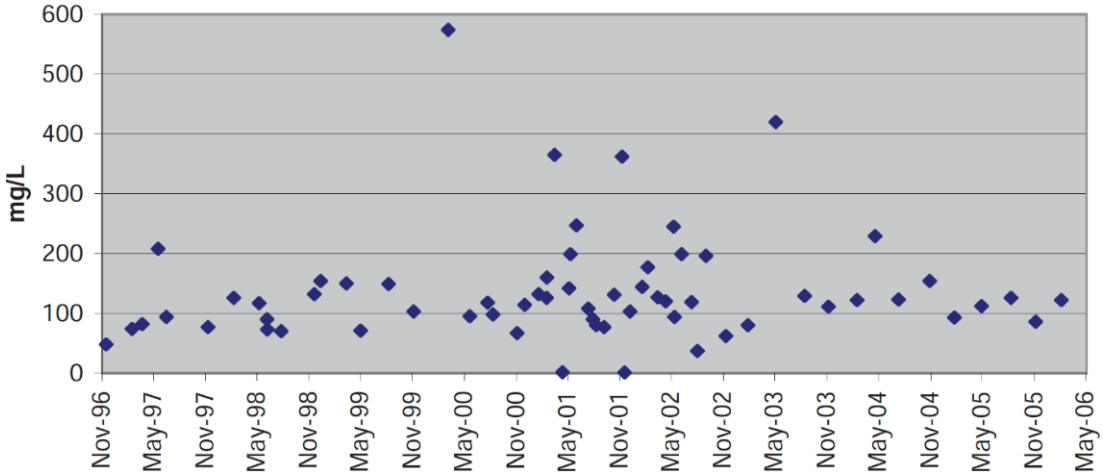

(a)

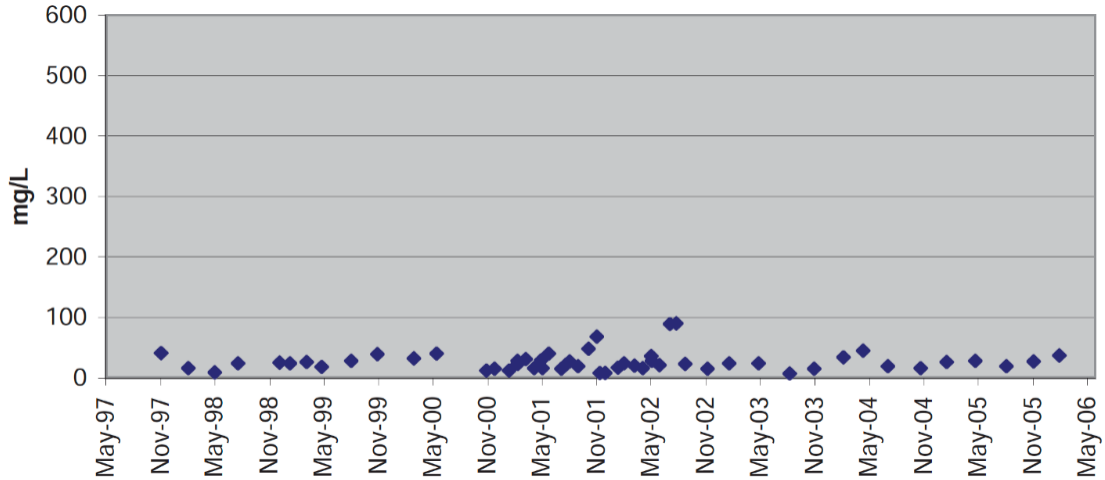

(b)

Figure 3.40 Total Suspended Solids (TSS) concentrations at TCEQ Stations Located (a) Upstream (TCEQMAIN-13074) and (b) Downstream (TCEQMAIN-13072) on the Arroyo Colorado Tidal Segment Boundary [175]

The monthly sediment load carried by the Arroyo Colorado was estimated using the Soil and Water Assessment Tool (SWAT) model. The Arroyo Colorado watershed model was developed to simulate flow and selected water quality parameters, including suspended sediment load. The model was calibrated and tested for suspended sediment using data from 2000-2009. The observed and estimated (predicted) monthly sediment load for Arroyo Colorado near Harlingen (TCEQMAIN-13074/USGS-08470400) were compared. For this period, the model-predicted values were good when compared to observations except for a couple of over-estimated peak sediment discharges [170]. From this study, the observed and simulated mean monthly suspended sediment loads are 5,956 and 8,434 tons (5,403 and 7,651 tonnes), respectively, or an annual total of 71,472 and 101,208 tons/yr (64,838 and 91,814 tonnes/yr) (**Figure 3.41**).

It should be noted that the TCEQ-13074/USGS-08470400 are the closest stations to the Laguna Madre that are not within the tidal zone and do not experience any influence on flow and sediment regime due to tidal activity. However, the contributing drainage area at this location is 381 mi^2 (987 km^2), which accounts for 54% of the total watershed area. The remaining areas of the watershed either contribute to the tidal segment of the river or are ungauged.

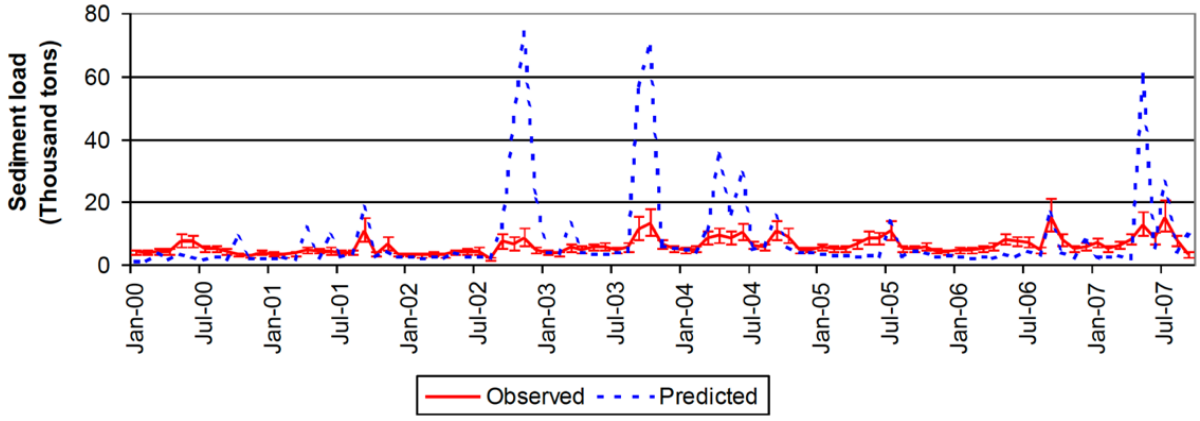

Figure 3.41 Monthly Sediment Load for Arroyo Colorado near Harlingen (TCEQMAIN-13074/USGS-08470400) [170]

3.11.2.2 Sediment Delivery to Laguna Madre Bay

Laguna Madre receives sediment primarily from onshore eolian transport, flood-tidal currents, storm washover, and upland runoff [165]. As discussed earlier, fluvial sediments entering Baffin Bay do not contribute to the sediment load in the Upper Laguna Madre (ULM), and contributions from runoff in the surrounding bay areas are also insignificant. The annual sediment yield of the ULM is estimated at 0.1 tons/acre (22 tonnes/km^2) or 7,467 tons /yr (1,673,879 tonnes/yr) [10].

The annual sediment load carried by the Arroyo Colorado at Harlingen was estimated to range between 66,430 and 84,340 tons/yr (60,264 -76,512 tonnes/yr) (see **Section 3.11.2.1**). Considering that the contributing drainage area at this location represents 54% of the watershed, the annual sediment load of the Arroyo Colorado at its mouth can be estimated to range between 123,000 and 156,000 tons/yr (111,583-141,520 tonnes/yr). This estimate aligns closely with the annual sediment yield for the Lower Laguna Madre based on overland erosion, which is estimated at 0.07 tons/acre (15.7 tonnes/km^2) [10] or 139,279 tons/yr (126,352 tonnes/yr). However, the majority of sediment transported by floodwaters and upland runoff is deposited in the upstream reaches of the Arroyo Colorado and does not reach Laguna Madre. It is estimated that only 10% of the sediment is flushed through the river channel and deposited either on the margins of Laguna Madre or within the Gulf Intracoastal Waterway (GIWW) [165].

The analysis of sediment supply rates from different sources to Laguna Madre revealed that, on an average annual basis, approximately 1.3 $\times 10^6$ cu yd/yr (1 $\times 10^6$ m^3/yr) of sediments are introduced into the lagoon. Eolian transport, tidal exchange, storm washover, mainland runoff, interior shore

erosion, and authigenic mineral production contribute 43%, 38%, 8%, 5%, 2%, and 4%, respectively, to this sediment input. Based on the transport process, sediment deposition in Laguna Madre is localized, leading to highly variable rates of sediment accumulation in the open lagoon and surrounding flats, ranging from 0.004 to 0.05 inches/yr (0.1 to 1.2 mm/yr) [165].

3.11.3 Sediment Delivery from Laguna Madre to Gulf of Mexico

Laguna Madre is connected to the Gulf of Mexico through Port Mansfield Channel and Brazos Santiago Pass. The exchange of sediment through these inlets remains largely undocumented, as very few studies have specifically addressed the sediment budget of Laguna Madre.

A conceptual sediment budget for the southern part of Lower Laguna Madre was prepared using historical data, including dredging records, measurements of shoreline changes, bathymetric data, estimations of sediment transport rates, and insights into engineering activities. The sediment budget covers the period from 1980 to 2008 and is illustrated in **Figure 3.42**. In this figure, arrows represent the annual net sediment transport quantities and directions. The findings indicate that, overall, alongshore transport is directed northward on both the southern and northern sides of the Brazos Santiago Pass. Sediment moving northward toward this inlet has the potential to be transported into the inlet. According to this study, only 50,000 cu yd/yr (38,228 m^3/yr) of sediment exit Laguna Madre into the Gulf of Mexico [176].

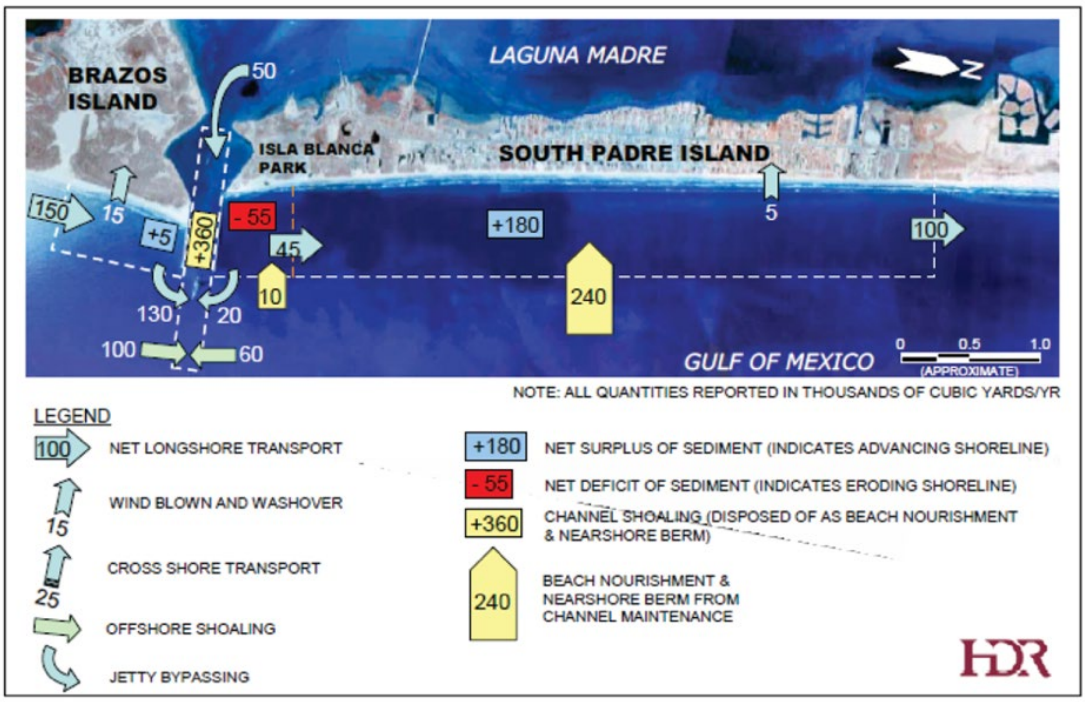

Figure 3.42 Conceptual Sediment Budget for the Southern Part of the Lower Laguna Madre for the Period of 1980-2008 [176]

Sediment contributions to the Gulf of Mexico from shoreline erosion are discussed sporadically in a few studies. In a comprehensive study, long-term net shoreline recession rates were estimated for the central Texas Gulf shoreline, spanning from Packery Channel to the mouth of the Rio

Grande (**Figure 3.43**) [27]. The net longshore drift exhibits a northward direction on the southern part of Padre Island and a southward direction on the northern part of the island. Despite the advantageous location of much of Padre Island in a longshore drift convergence zone, the shoreline exhibited retreat at 85% of the measurement sites during the assessment period from the 1930s to 2019. Net change rates varied from a retreat at 23.6 ft/yr (7.2 m/yr) to an advance at 9.1 ft/yr (2.8 m/yr). The average long-term net shoreline movement rates indicate a retreat at 2.5 ft/yr (0.77 m/yr) on northern Padre Island (Mansfield Channel to Packery Channel), 8.1 ft/yr (2.46 m/yr) on southern Padre Island (Mansfield Channel to Brazos Santiago Pass), and 5.2 ft/yr (1.57 m/yr) on Brazos Island. The estimated net land loss since 1930 is 2,026 acres (8.2 km^2) along northern Padre Island, 3,032 acres (12.3 km^2) along southern Padre Island, and 1405 acres (1.6 km^2) along Brazos Island.

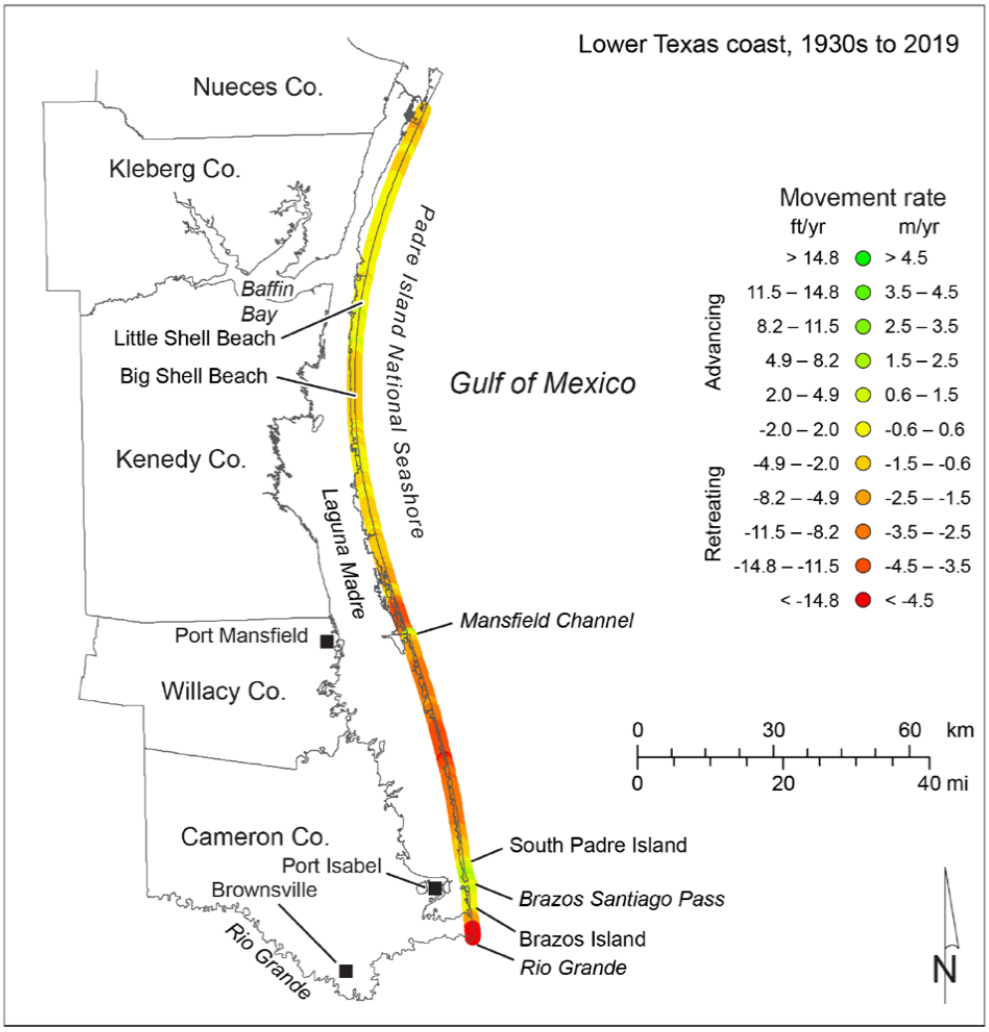

Figure 3.43 Net Rates of Long-term Movement for the Lower Texas Gulf Shoreline Between Packery Channel and the Rio Grande (Padre Island and Brazos Island) Calculated from Shoreline Positions from the 1930s to 2019 [27]

The most extensive sediment budget study for the region was conducted by HR Wallingford [177] as part of the Texas Coastal Resiliency Master Plan-Region 4, developed by the Texas General Land Office (GLO). The methodology employed in this study significantly deviated from previous approaches used to assess sediment budgets in the Texas Coastal areas. Earlier investigations have employed historical beach profiles, dredging data, and quantities associated with beach nourishment to assess volume changes over time. These changes were subsequently utilized to formulate assumptions about the specific sediment fluxes entering or leaving a designated sediment budget cell. In contrast, in this study, sediment fluxes and transport pathways utilized in the sediment budget were directly extracted from the regional sediment transport numerical models.

In this study the sediment budget comprised of 59 cells including 54 open coast cells and 5 inlet cells (**Figure 3.44** to **Figure 3.47**). The open coast cells include: 27 cells (Coastal Cells A) running along the coastline representing the littoral drift spanning the beach front from the shoreline to the *littoral drift depth of closur*e which is different for each cell and has depths ranging approximately between 15 and 35 ft (4.6 to 10.7 m); and 27 cells (Coastal Cells B) adjacent to Cells A, spanning from the *littoral drift depth of closur*e to a cut-off depth of 48 ft (14.6 m) which represent the transport induced by the waves and currents combined. The inlet cells consist of 3 cells representing the inlets on the Laguna Madre side (Mansfield Pass, Brazos Santiago Pass, Rio Grande), and 2 cells representing the inlets in the model. These latter cells are adjacent to the former ones and extend up to a depth of 48 ft (14.6 m) to connect with Coastal Cells B.

It is important to note that the sediment budget was conducted solely for the sand component of the sediment transport, covering a range from very fine sand with an average grain size of 0.125 mm to medium sand with an average grain size of 0.5 mm. The results of the sediment budget for the sand component are presented in **Figure 3.44** to **Figure 3.47** which show the sediment budget cells and the net annual sediment fluxes between them. The following passages are extracted from the results of the regional sediment transport model related do the sediment exchange between the Laguna Madre system with GoM [177].

- The net sediment transport direction at the northernmost cells of the study area is northward in Cell 1A and southward in Cell 1B. The littoral drift transport approximately 59,300 cu yd/yr (45,338 m^3/yr) into Cell 1A from the south and approximately 65,600 cu yd/yr (50,154 m^3/yr) out of the cell to the north. In Cell 1B, approximately 3,000 cu yd/yr (2,293 m^3/yr) enters the cell from the north and approximately 7,800 cu yd/yr (5,963 m^3/yr) leaves the cell at the southern end, driven by the combination of waves and currents. In total, the model predicted an annual loss of 11,100 cu yd/yr (8,486 m^3/yr) of sand for this coastal segment. Assuming the 4 cy/yard/yr of onshore aeolian transport, about 17,100 cu yd/yr (13,073 m^3/yr) of sand is lost from the beach into the dunes within this cell.
- The total net transport entering Cell 15a (Mansfield Pass) from the north is 105,000 cu yd/yr (80,278 m^3/yr). The net transport leaving the cell to the south is 87,600 cu yd/yr (66,795

m^3/yr). According to the model predictions, this cell receives 84,000 cu yd/yr (64,222 m^3/yr) of sand from Mansfield Pass. In total the model predicts that this cell gains 101,400 cu yd/yr (77,525 m^3/yr), which mainly deposits in the navigation channel. The alongshore wind-blown transport removes about 18,900 cu yd/yr (14,450 m^3/yr) of sand from the beach to the jetties area of Mansfield Pass Channel, of which 13,300 cu yd/yr (10,168 m^3/yr) from South Padre Island and 5,600 cu yd/yr (4,281 m^3/yr) from Padre Island.

- The alongshore wind-blown sand transport removes about 8,700 cu yd/yr (6,651 m^3/yr) of sand from the beach to the jetties area of Mansfield Pass Channel, of which 3,900 cu yd/yr (2,982 m^3/yr) from South Padre Island and 4,800 cu yd/yr (3,670 m^3/yr) from Brazos Island. For the Brazos Santiago Pass (Cell 25a), regional sediment model predicts that the total net transport entering the cell from the north is 184,500 cu yd/yr (141,060 m^3/yr). The net transport leaving the cell to the south is 6,700 cu yd/yr (5,122 m^3/yr). According to the model predictions, this cell loses 10,200 cu yd/yr (7,798 m^3/yr) of sand from Brazos Santiago Pass. In addition, 1,000 cu yd (764 m^3) is moved offshore. In total the model predicts that this cell gains 166,600 cu yd (127,374 m^3) of sand per year, which mainly deposits in the navigation channel.
- Cells 25bA and 25bB form the southernmost boundary of the Laguna Madre system. According to the results of the regional sediment transport model, Cell 25bA is a divergence point for the littoral drift. The littoral drift transports approximately 97,700 cy/yr (74,697 m^3/yr) out of cell 25bA to the north and approximately 1,000 cu yd/yr (764 m^3/yr) to the south. The net sediment transport at both ends of cell 25bB is towards the south. Approximately 104,400 cu yd/yr (79,820 m^3/yr) enters the cell from the north and approximately 82,500 cu yd/yr (63,076 m^3/yr) leaves the cell at the southern end, driven by the combination of waves and currents. In total the model predicts this part of the coast to lose 76,600 cu yd (58,564 m^3) of sand per year. Assuming 4 cu yd/yard/yr (3.34 m^3/m/yr) of onshore aeolian transport, about 7,200 cu yd/yr (5,505m^3/yr) of sand is lost from the beach into the dunes within this cell.

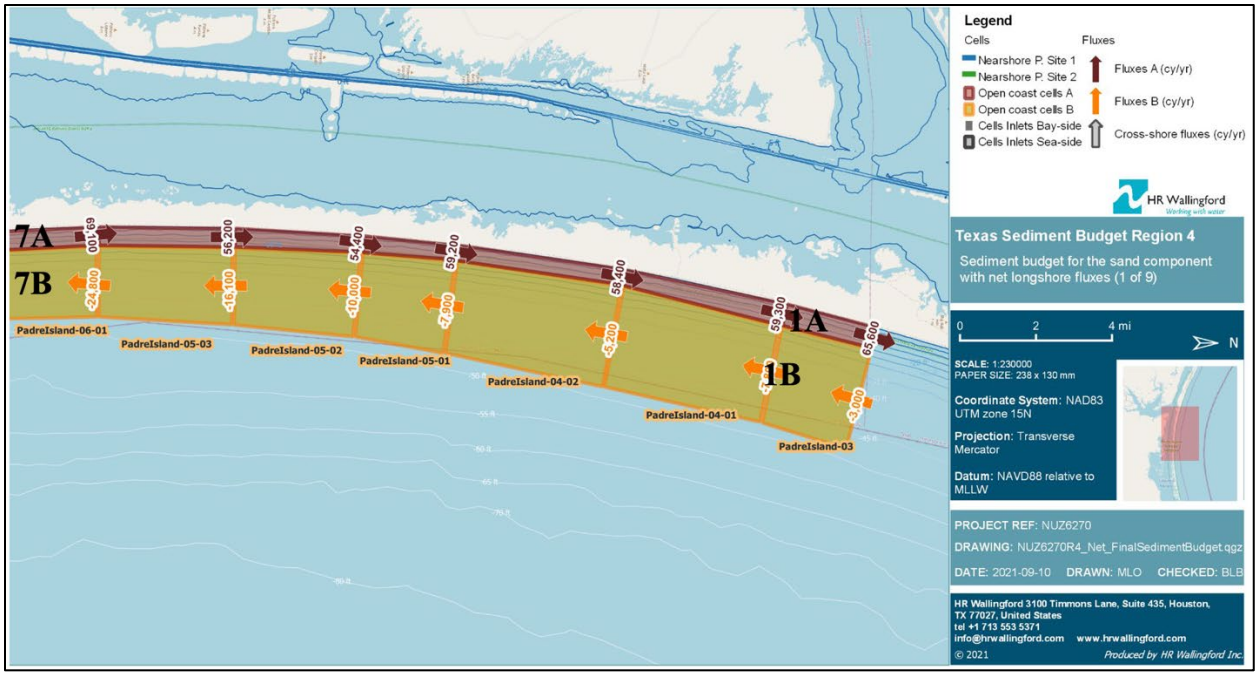

Figure 3.44 Sediment Budget of Laguna Madre System (Cells 1 to 7) in Ref. [177]

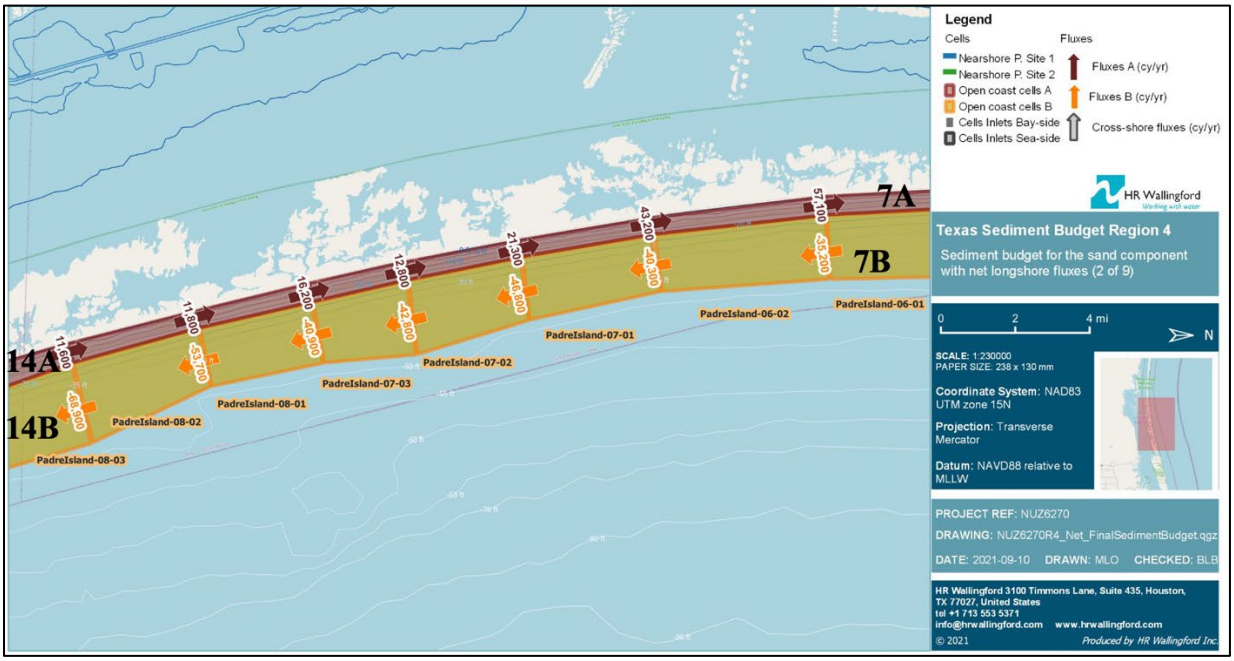

Figure 3.45 Sediment Budget of Laguna Madre System (Cells 7 to 14) in Ref. [177]

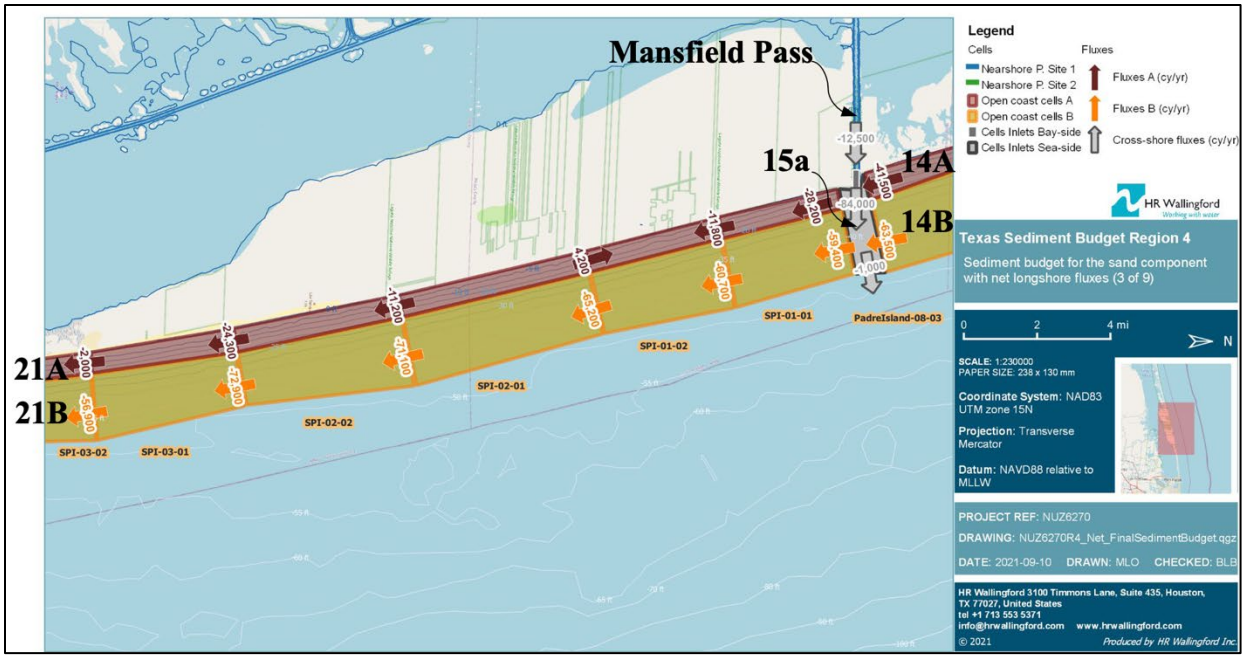

Figure 3.46 Sediment Budget of Laguna Madre System (Cells 14 to 21) in Ref. [177]

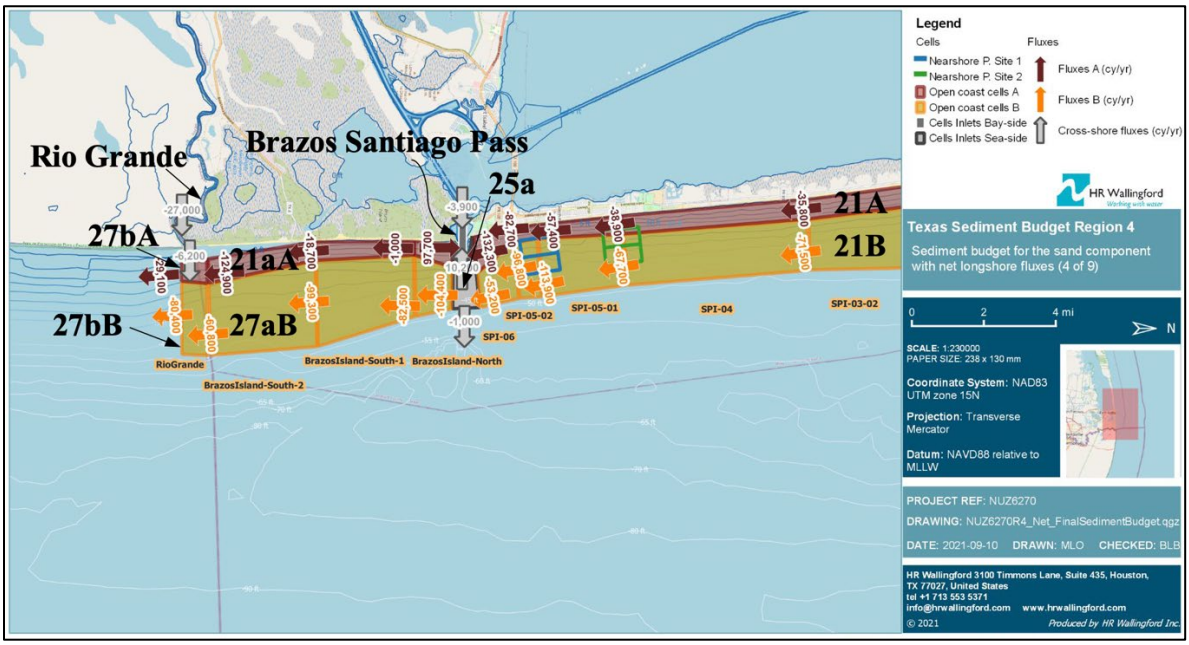

Figure 3.47 Sediment Budget of Laguna Madre System (Cells 21 to 27) in Ref. [177]

3.12 Rio Grande System

3.12.1 Rio Grande System Watershed Characteristics

The Rio Grande stands as one of the key rivers in the southwestern United States and northern Mexico. It ranks as the fourth longest river in both the United States and North America when considering its main stem. Originating in south-central Colorado, the Rio Grande meanders through Texas before finally reaching the Gulf of Mexico (**Figure 3.48**). The Rio Grande drainage basin covers an area of 182,215 mi^2 (472,000 km^2), of which 49,387 mi^2 (127,912 km^2) lies within the state of Texas [178]. However, the inclusion of adjacent endorheic basins within the broader Rio Grande drainage basin expands the total area to 336,000 mi^2 (870,000 km^2) [179]. The Rio Grande, known by its fertile valley and tributaries, serves as a crucial water source for seven U.S. and Mexican states, traversing predominantly through arid and semi-arid regions. However, since the mid-twentieth century, a notable development has occurred: the introduction of several reservoirs, diversion channels, and irrigation canals into the river system. This alteration has led to a situation where only 20% of the Rio Grande's water now makes its way to the Gulf of Mexico [180].

Figure 3.**48** Rio Grande River Watershed and USGS Monitoring Stations

3.12.1.1 Rio Grande River

The Rio Grande River spans a length of 1,896 miles (3,051 km), originating in the San Juan Mountains of southern Colorado and flowing south through New Mexico to Texas, where it serves as the international boundary between the United States and Mexico for 1,250 river miles (2,012 km) [178,180]. The Rio Grande consists of three distinct regions: the Upper Rio Grande, Middle Rio Grande, and Lower Rio Grande. The climate within the Rio Grande watershed undergoes significant changes from upstream to downstream.

In the Upper Rio Grande, mean annual temperatures range from 45 to 55 °F (7.2 to 12.8 °C), with lower temperatures prevailing at mid to high elevations. Precipitation in this region is highly variable, presenting as winter snow and summer rain, influenced by the monsoonal weather pattern. Annual precipitation averages more than 40 inches (1,016 mm) in mountainous areas and drops to about 10 inches (254 mm) in the Rio Grande valley. Moving to the Middle Rio Grande region, the mean annual temperature ranges from approximately 50 to 55 °F (10 to 13 °C), and the mean annual precipitation ranges from 8 inches (203 mm) in the valley to about 30 inches (762 mm) at higher elevations. In the Lower Rio Grande region, mean annual temperatures fluctuate between 50 to 75 °F (10 to 24 °C), and summer temperatures can surpass 100 °F (38 °C) at lower elevations. Mean annual precipitation varies from about 8 to 18 inches (203 to 457 mm), with the majority of precipitation occurring at higher elevations [181].

The USGS operates several streamflow gauging stations on the Rio Grande (**Figure 3.48**). Two of these stations are located downstream in the lower reach of the river: USGS-08473700 (Rio Grande near San Benito) and USGS-08475000 (Rio Grande near Brownsville). **Table 3.27** provides discharge data for these two lowermost USGS stations on the Rio Grande.

The annual sediment yield for the Rio Grande basin varies from 0.03 to 0.73 tons/acre (6.7 to 164 tonnes/km^2) with the annual sediment yield of 0.21 tons/acre (47 tonnes/km^2] in Lower Rio Grande) [10].

Table 3.27 Rio Grande Annual Daily Discharges at USGS Stations

Station	Drainage Area, mi^2 (km^2)	Period	Discharge, cfs (m^3/s)		
			Max	Average	Min
San Benito[1] (USGS-08473700)	176,304 (456,625)	1954 -1983	25,000 (708)	9,247 (262)	1,610 (46)
Brownsville[2] (USGS-08475000)	176,333 (456,700)	1935- 1977	31,700 (898)	14,864 (421)	606 (17)

[1] https://waterdata.usgs.gov/nwis/inventory/?site_no=08473700&agency_cd=USGS
[2] https://waterdata.usgs.gov/nwis/inventory/?site_no=08475000&agency_cd=USGS

3.12.1.2 Reservoirs

The Rio Grande basin features several dams and reservoirs. Some of the notable ones include Rio Grande Dam in Colorado, Elephant Butte and Caballo Dams and Reservoirs, and Jemez Canyon Dam in New Mexico. Additionally, there are Falcon Dam and Reservoir in Texas/Mexico, as well as Amistad and Imperial Dams and Reservoirs, along with other lakes and reservoirs in Texas. Information on some of these dams and reservoirs located in Texas is presented below [182].

- *Amistad Dam and Reservoir (Texas):* Built for flood control and water conservation, this dam is situated on the Rio Grande, forming the Amistad Reservoir. It is shared between the United States and Mexico. The reservoir has a storage capacity of 3,275,532 acre-ft (4.04 $\times 10^9$ m^3), encompassing a surface area of 66,465 acres (269 km^2, at conservation pool elevation, 1,117 ft (340 m) above mean sea level.
- *Falcon Dam and Reservoir (Texas/Mexico):* Falcon Dam creates Falcon Reservoir and is shared between the United States and Mexico. It serves multiple purposes, including flood control and water supply. At conservation pool elevation, 301.2 ft (92 m) above mean sea level, the reservoir has a storage capacity of 2,646,813 acre-ft (3.3 $\times 10^9$ m^3) encompassing a surface area of 85,195 acres (345 km^2).
- *Imperial Reservoir*: Owned and operated by Pecos County Water Improvement District No. 2, the reservoir primarily functions for irrigation and recreation The lake has a capacity of 6,000 acre-ft (7.4 $\times 10^6$ m^3) encompassing a surface area of about 1,530 acres (6.2 km^2) at a designed elevation.

3.12.1.3 Rio Grande Estuary

The Rio Grande Estuary is located at the southern tip of Texas, near the border with Mexico. It encompasses a coastal area that extends into the Gulf of Mexico. Forming a natural border between the United States and Mexico, it is a riverine estuary that flows directly into the Gulf of Mexico with no associated bay system. The estuarine environment is rich in biodiversity, supporting a mix of marine, freshwater, and brackish water species. The marshes and tidal flats in the estuary are crucial for various stages of the life cycle of many aquatic organisms. Like many estuaries worldwide, the Rio Grande Estuary faces challenges such as habitat loss, pollution, altered freshwater flow due to the construction of dams and reservoirs on the river, and changes in sedimentation patterns. These factors can impact the health and functionality of the estuarine ecosystem. The annual average inflow from the Rio Grande is 370,722 acre-ft /yr (4.6 $\times 10^8$ m^3/yr), but it can range widely due to extreme hydrological conditions [183].

3.12.2 Rio Grande Estuary Sediment Budget

The Rio Grande River is vital for supplying sediment to the coast. However, the specific contributions and impact of dam construction on sediment sources are becoming evident. This emphasizes the critical need for a sedimentation budget analysis, requiring detailed data on sediment inflow into the Rio Grande River and subsequent transport from the river to the Gulf of Mexico.

3.12.2.1 Rio Grande Sediment Load

The sediment dynamics in the Lower Rio Grande region of Texas pose a critical environmental challenge, impacting both the river's reservoir system and the Gulf of Mexico. Soil erosion, exacerbated by factors like extended droughts and intensified rainfall events, threatens the storage capacity of the reservoirs and the overall ecological balance of the river estuary. This issue is further compounded by changes in sediment supply patterns, marked by short-duration flash floods and dam releases, which directly affect the Rio Grande's channel conditions and sediment accumulations. Moreover, the construction of reservoirs upstream, such as the Amistad International Reservoir, has profound consequences on sedimentation rates, resulting in complex interactions between river systems and their evolving environments.

The increase in in-channel sediment supply mainly results from short-duration flash floods from tributaries entering the Rio Grande. These floods deposit a significant amount of sediment within the mainstem river, leading to finer channel beds and expanded fine sediment areas. In contrast, moderate-magnitude, long-duration releases from upstream dams lead to minimal fine sediment accumulation or even erosion. The most efficient erosion in the Rio Grande occurs when a moderate dam releases numerous flash floods and substantial fine sediment input into the channel [184]. The reservoir system's storage capacity is anticipated to diminish over time due to sedimentation. This decrease is exacerbated by potential future conditions such as prolonged drought and more intense rainfall events, which could lead to a higher influx of sediment into the reservoirs [185].

Falcon Lake, the lowermost reservoir along the Rio Grande River basin area, is located 283 miles (457 km) upstream of the Gulf of Mexico [186,187]. At this reservoir, the sedimentation rate decreased by approximately 75% after the construction of the Amistad International Reservoir upstream. Between 1969 and 1994, sedimentation rates averaged 17.8 inches/yr (450 mm/yr), resulting in a total deposition of 472 inches (12,000 mm) of sediment in the lower section of the Amistad Reservoir's Rio Grande channel [187].

Sediment data in the Rio Grande at Brownsville have been collected by the USGS since 1966. The suspended concentration and load at this station are summarized in **Table 3.28**. According to this table, the suspended sediment concentration averaged 242 mg/L, with a recorded minimum of 1 mg/L and a maximum of 7000 mg/L between 1966 and 2021. During this period, the suspended sediment load averaged 4,315 tons/day (3,892 tonnes/day), with minimum and maximum values of 0.08 and 139,000 tons/day (0.07 and 126,098 tonnes/day), respectively.

Table 3.28 Rio Grande Suspended Sediment Concentration and Load at USGS Station

Station	Period	Suspended Sediment Concentration, mg/L (Suspended Sediment Load, tons/day)		
		Max	Average	Min
Brownville[1] (USGS-08475000)	1966 - 2021	7,000 (139,000)	242 (4,315)	1 (0.08)

[1] https://mywaterway.epa.gov/monitoring-report/NWIS/USGS-TX/USGS-08475000/

Despite its size, the Rio Grande basin experiences highly localized and notably dynamic discharge and suspended sediment fluxes due to the prevailing arid conditions. The localized nature of this pattern is further influenced by the presence of Amistad and Falcon Reservoirs, which mitigate downstream effects [187]. For example, for the period 1996-1998, the annual suspended sediment flux in Brownsville was estimated at 10,582 tons/yr (9,600 tonnes/yr), equivalent to slightly over 1% of the annual long-term average of 771,620 tons/yr (700,000 tonnes/yr) for the period 1965-1984 [188].

As discussed, the construction of reservoirs upstream of the estuary has significantly impacted sediment load carried by the Rio Grande. **Figure 3.49** show the reduction in suspended sediment concentration (SSC) in Rio Grande at Brownsville due to dam construction [189].

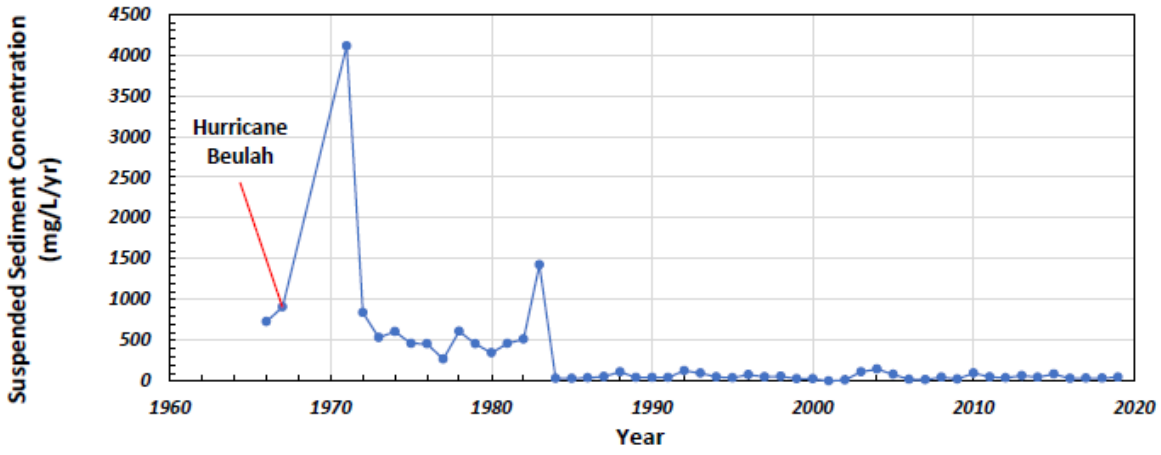

Figure 3.49 Suspended Sediment Concentration in Rio Grande at Brownsville (1966-2019) [189]

Total suspended solids (TSS) concentrations have been collected sporadically by TCEQ in the Lower Rio Grande. The locations of these stations are shown in **Figure 3.50**. The TCEQMAIN-20449 station is the most upstream among the others, and TCEQMAIN-13176 is the closest station to the estuary, located in the tidal zone of the river. No conclusions can be made about the trend in the change of TSS concentration along the river since these stations do not share the same sampling periods. In general, the TSS values at these sites (summarized in **Table 3.29**) are within the

observed suspended sediment concentrations recorded at USGS-08475000 station located in the Lower Rio Grande after 1985 (**Figure 3.49**).

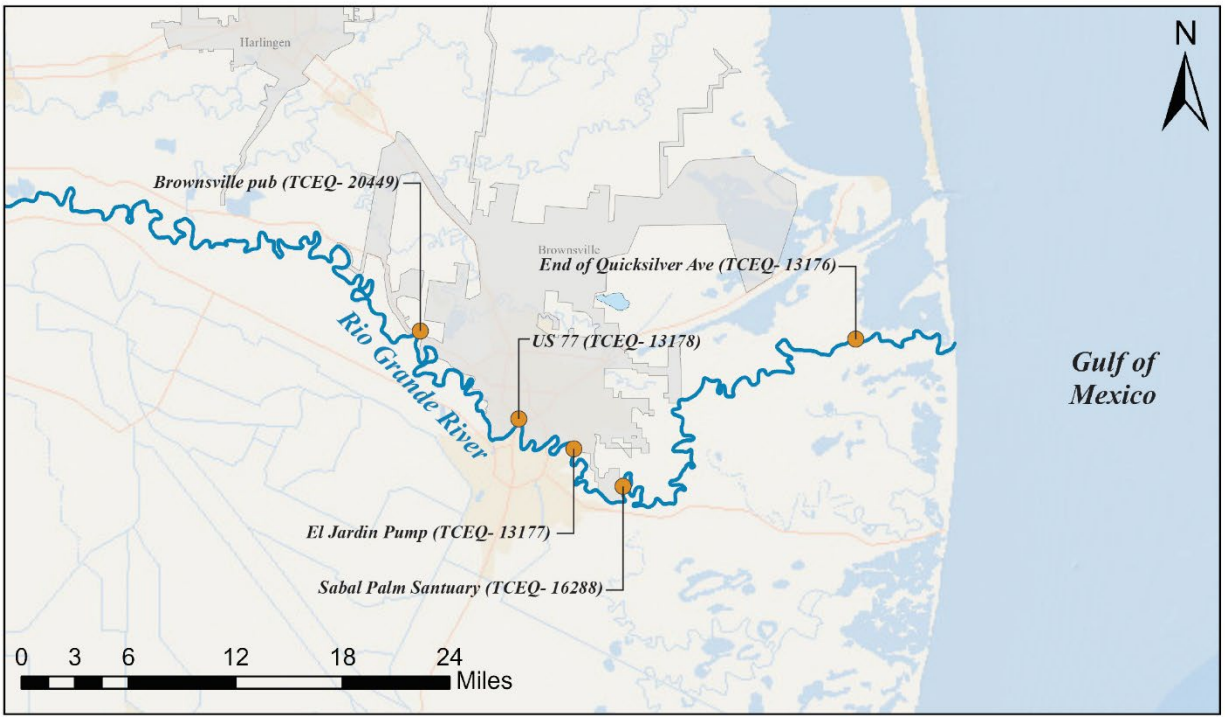

Figure 3.50 TCEQ Monitoring Stations on the Lower Rio Grande

Table 3.29 Rio Grande River Total Suspended Solids (TSS) Concentration at TCEQ Stations

Station	Period	Total Suspended Solids (TSS), mg/L		
		Max	Average	Min
Quicksilver Ave[1] (TCEQ-13176)	2005 - 2022	354	76	4
Sabal Palm Sanctuary[2] (TCEQ-16288)	2003 - 2019	330	91	10
El Jardin Pump Station[3] (TCEQ-13177)	2005 - 2022	200	39	2.8
International Bridge on US 77[4] (TCEQ-13178)	1981 - 2016	216	74	20
Brownsville[5] (TCEQ-20449)	2009 - 2022	243	47	2.5

[1] https://mywaterway.epa.gov/monitoring-report/STORET/TCEQMAIN/TCEQMAIN-13176/
[2] https://mywaterway.epa.gov/monitoring-report/STORET/TCEQMAIN/TCEQMAIN-16288/
[3] https://mywaterway.epa.gov/monitoring-report/STORET/TCEQMAIN/TCEQMAIN-13177/
[4] https://mywaterway.epa.gov/monitoring-report/STORET/TCEQMAIN/TCEQMAIN-13178/
[5] https://mywaterway.epa.gov/monitoring-report/STORET/TCEQMAIN/TCEQMAIN-20449/

3.12.2.2 Sediment Delivery to Rio Grande Estuary

The Rio Grande is a riverine estuary that spans 48 river miles (77 km) from its mouth at the Gulf. The flow of water into the estuary is predominantly regulated by releases from Falcon Dam situated on the river and diversions carried out by water users from both Mexico and the United States. The estuary system has undergone a century of dam construction, withdrawal of water for irrigation and municipal purposes, and alterations in land use that have significantly diminished its sediment load. Based on the average suspended sediment load measured at the Brownsville station (USGS-08475000) from 1966 to 2023, the river transports 4,315 tons (3,914 tonnes) of sediment per day or approximately 1.6×10^6 tons/yr (1.5×10^6 tonnes/yr) (refer to **Table 3.28**). This estimate is more than double the suspended sediment load recorded as 771,620 tons/yr (700,000 tonnes/yr) during the period from 1965 to 1984 [188].

3.12.3 Sediment Delivery from Rio Grande Estuary to Gulf of Mexico

The sediment delivery from the Rio Grande to the Gulf of Mexico is a complex process influenced by multiple factors. The quantity of sediment delivered from the Rio Grande River to the Gulf remains uncertain. Decreased flow in the river, due to dam construction combined with extensive irrigation use of river water on the coastal plain, has reduced the sediment delivered to the coast and led to the buildup of sediment at the river's mouth, hindering its passage into the Gulf of Mexico and presenting a significant challenge. This situation has caused extensive flooding [190], and the lack of regular flushing raises the concern that the tidal segment of the Lower Rio Grande could transform into a closed, hypersaline lagoon system, posing a threat to post-larval and juvenile marine species [191]. A study was conducted on sediment erosion and transport at the mouth of the Rio Grande to assess the potential of the sediments causing the obstruction [190]. The study involved determining erosion rates and sediment grain size distributions by analyzing core samples collected within and around the obstruction. Subsequently, these findings were employed to characterize the erosion potential of the sediments under investigation. The study findings can be summarized as follows:

- Sediment observed within the surf zone, extending from the shore through the Rio Grande delta and at least 246 ft (75 m) into the Rio Grande Channel, exhibited similar erosional properties and mean particle sizes. These sediments primarily consisted of homogeneous mixtures of sand, and all analyzed sediments were transported exclusively as bedload.
- Finer-grained sediments (including sand, silt, clay, and organic material) identified in cores obtained approximately 1,640 ft (500 m) upstream in the Rio Grande Channel proved to be significantly more resistant to erosion compared to the coarser-grained sediments (sand) found closer to the shore. This result was expected, given that the near-shore current is too forceful to accumulate cohesive clay and organic deposits.
- All analyzed sediments were projected to undergo erosion and northward transportation by the Gulf's longshore current. The mean longshore velocities, ranging between 0.7 and 1 ft/s (0.2 and 0.3 m/s), ensured 100% bedload transport, with none of the material carried offshore in the overlying water.

- If the velocities of the Rio Grande discharge do not surpass the Gulf's longshore current speeds (> 1 ft/s (0.3 m/s) on average and > 1.4 ft/s (0.43 m/s) at peak), the effects of longshore transport have the potential to introduce sufficient coarse material into the Rio Grande delta region. This influx could lead to the blockage of the Rio Grande Channel, prompting the river to breach its banks and inundate the adjacent floodplain.

This study highlights that sediment delivery from Rio Grande is minimal unless river flow exceeds certain values to overcome Gulf's longshore current speeds to push the sediment offshore, otherwise sediments brought by the river deposit in the delta area.

A study evaluating the impacts of dam construction and longshore transport on the sedimentation within the Rio Grande delta showed that construction of dams has sufficiently limited delivery of upstream sediment promoting shoreline erosion in the delta area. The study also found no compelling evidence that northward longshore transfer sediment from south as far south as the Vera Cruz coast of southern Mexico [192].

In a comprehensive study, long-term net shoreline recession rates were estimated for the central Texas Gulf shoreline, spanning from Packery Channel to the mouth of the Rio Grande (**Figure 3.43**) [27]. For the period from the 1930s to 2019, the shorelines near the Rio Grande exhibit one of the highest rates of net retreat, i.e., >14.8 ft/yr (4.5 m/y).

The sediment budget analysis for the Rio Grande delta area was undertaken as part of the Texas Coastal Resiliency Master Plan-Region 4, as detailed in **Section 3.11.3**. Cell 27bA and 27bB, representing the Rio Grande delta area, are illustrated in **Figure 3.51**. According to the findings from the regional sediment transport model, there is a southward direction of net sediment transport at both ends of Cell 27bA and in Cell 27bB. This result aligns with the aforementioned study (Ref. [192], which found no evidence supporting a northward longshore transfer of sediment from south of the Rio Grande delta. The following conclusions are drawn from the results of the regional sediment transport model regarding the sand exchange between the Rio Grande Estuary System and the Gulf of Mexico [177].

- In Cell 27bA, approximately 124,900 cu yd/yr (95,492 m^3/yr) of littoral drift moves into the cell from the north, while around 29,100 cu yd/yr (22,248 m^3/yr) exits the cell to the south.
- In Cell 27bB, approximately 60,800 cu yd/yr (46,484 m^3/yr) enter the cell from the north, and about 80,400 cu yd/yr (61,470 m^3/yr) leave the cell at the southern end, driven by a combination of waves and currents.
- The Rio Grande delivers approximately 8,200 cu yd/yr (6,269 m^3/yr) of sand. Overall, the model predicts an annual gain of 82,400 cu yd (62,999 m^3) of sand for this section of the coast. The model's bathymetry for cell 27aA includes a bar at the southern end of the cell, just above the mouth of the Rio Grande, that no longer exists. This suggests that either this bar should not be in the bathymetry, or it has disappeared since the bathymetry survey was conducted. It was concluded that in either case, the model correctly predicts the rapid erosion

of this bar, aligning with the general pattern of erosion shown in shoreline change rates between 2000 and 2019 [27].

The study concluded that due to the dynamic nature of the shoreline at the mouth of the Rio Grande, there exists a higher level of uncertainty in the sediment budget at this specific location. This uncertainty is attributed to the accuracy of the bathymetry used in the regional model and, consequently, impacts the estimation of the sediment supply rate to Cell 27bA.

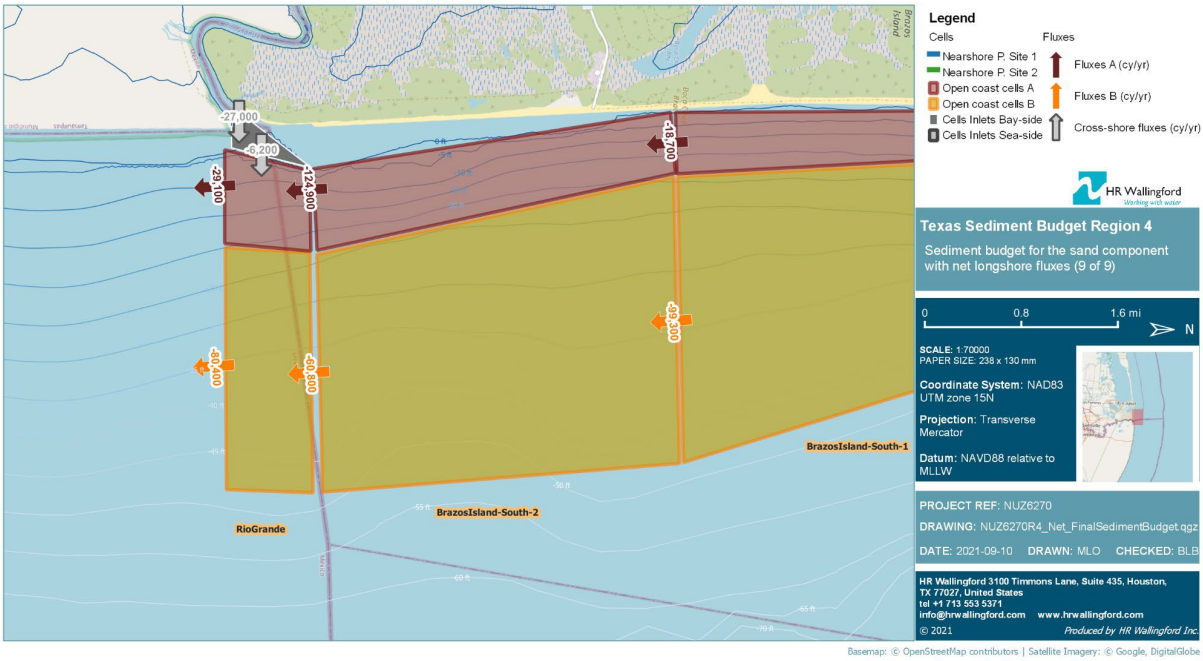

Figure 3.51 Sediment Budget for Rio Grande Estuary System (Cell 27b A and B) [177]

4. SUMMARY, GAP ANALYSIS, AND RECOMMENDATIONS

The Texas coastline faces ongoing challenges related to coastal erosion, a process influenced by factors such as storm events, sea-level rise, and human activities such as coastal development. Hurricanes and tropical storms contribute significantly to erosion, causing the gradual wearing away of land. Rising sea levels, associated with climate change, exacerbate erosion by increasing the frequency and severity of flooding events. Human interventions, including infrastructure projects and navigation channels, can alter natural sediment dynamics, impacting erosion rates.

The primary objective of this study was to conduct a thorough literature review focusing on recent studies documenting sediment budgets along the Texas Coast. The goals included analyzing documented assessments of major waterbodies, river mouths, and both natural and constructed exchange passes. Additionally, the study aimed to review the methodologies, associated assumptions, input datasets, and modeling tools utilized in each of these studies. The overarching aim was to compile a detailed summary of the outcomes, with a specific focus on identifying potential gaps in the existing research on sediment budgets in the Texas Coast.

4.1 Methodologies, Associated Assumptions, Input Datasets, and Modeling Tools Involved in Sediment Budget Analysis Studies for Texas Coast

In this literature review, three distinct approaches to sediment budget analysis along the Texas coast were identified: 1) Quantitative Methods (Mass Balance), 2) Geomorphological Models, and 3) Field Surveys and Sampling. The specific methods employed for each of the 11 selected waterbodies in this project are outlined in **Table 4.1**. It is important to highlight that the use of a particular method for an area does not necessarily imply a comprehensive sediment analysis for the entire study area. The subsequent sections will discuss the three aforementioned approaches, examining the associated assumptions and input data used in the analysis.

4.1.1 Quantitative Methods (Mass Balance)

As outlined in Section 2.3, this approach characterizes a sediment budget as the equilibrium between sediment gain (sources) and sediment loss (sinks) within a designated control volume, cell, or a series of interconnected cells. The Sediment Budget Analysis System (SBAS), developed by the USACE, is built upon the principles of this method. This approach has been utilized for the sediment budget analysis of the East Texas Coast from Sabine Pass to San Luis Pass (**Figure 4.1**), as well as coastal areas between Freeport Entrance and Matagorda Ship Channel (**Figure 3.18**). However, for other parts of the Texas Coast, such analysis has not been conducted.

In this method, sediment sources encompass fluvial inputs from major rivers and creeks discharging into the waterbody, as well as runoff from smaller local tributaries exhibiting local overland erosion. Shoreline erosion is identified as another major sediment source. Conversely, navigational channels that undergo active dredging are designated as the primary sediment sinks.

Quantification of sediment sources from rivers and creeks relied on data from previous studies conducted by or for the USGS and the Texas Water Development Board (TWDB). Shoreline erosion rates were derived from both earlier studies and the Texas Shoreline Changes Project, compiled by the Bureau of Economic Geology. The volumes of sediment sinks are calculated based on historical dredging records provided by USACE.

Table 4.1 Summary of the Sediment Budget Analysis Method Employed in Waterbody Systems Along Texas Coast

Waterbody System	Sediment Budget Analysis Method		
	Quantitative Models	Hydro-geomorphological Models	Field Surveys and Sampling
Sabine Lake	×		×
Galveston Bay	×		×
Brazos-San Bernard Estuary	×	×	×
East Matagorda Bay	×		×
Matagorda Bay	×		×
San Antonio Bay			×
Aransas Bay			×
Corpus Christi Bay			×
Baffin Bay			×
Laguna Madre	×	×	×
Rio Grande Estuary		×	×

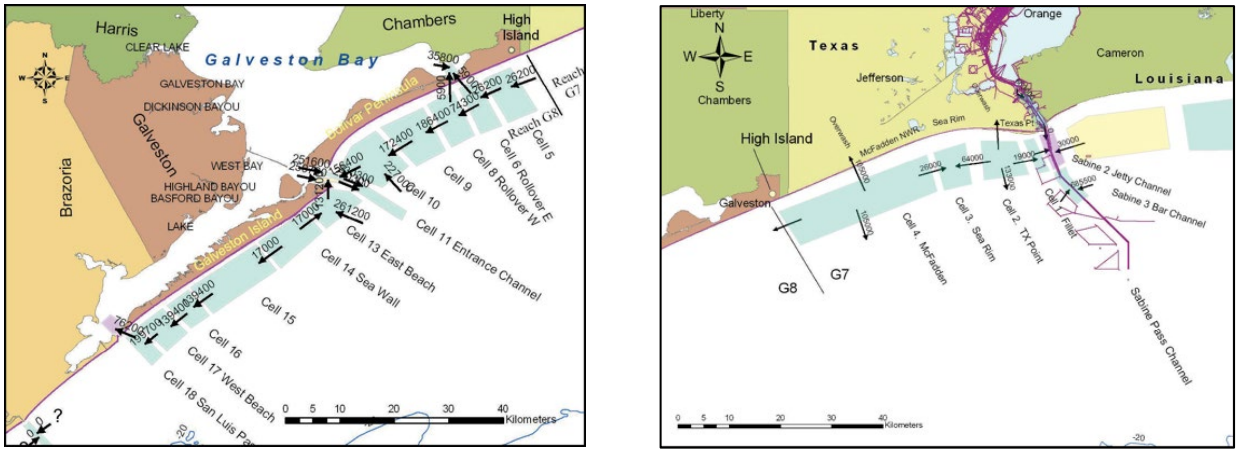

Figure 4.1 East Texas Coast Sediment Budget from Sabine Pass to High Island (Right) and from Bolivar Peninsula and Galveston Island

4.1.2 Hydro-geomorphological Models

Limited studies have employed numerical models to simulate geomorphological processes in Texas coastal areas. As indicated in **Table 4.1**, within the study area of this literature review,

numerical modeling was specifically applied to conduct sediment budget analysis for the Brazos River Estuary, Laguna Madre system, and Rio Grande Estuary.

Brazos River Estuary Model

A study conducted by Matt MacDonald for the Texas Department of Transportation (TxDOT) simulated the integrated effects of tidal circulation and river hydraulics to assess the impact of tidal currents and discharges from the Brazos and San Bernard Rivers on flow velocities, salinity, sedimentation, and water surface elevations in the Brazos River Floodgates area [67]. Although the primary focus of this study was not on sediment budget analysis, its findings provided valuable insights into understanding sediment dynamics in the Brazos River estuary.

Adaptive Hydraulics (ADH) was utilized in this study. The ADH is a modular, parallel, adaptive finite-element model designed for one-, two-, and three-dimensional flow and transport. ADH incorporates various integrated modules to enhance its capabilities. These include SEDLIB, a library for multiple grain sizes of mixed sediment, and a sediment transport module that dynamically couples sediment transport with hydrodynamics, augmenting the shallow water wave module [67].

Publicly accessible data from the USGS stream gauging stations for the Brazos River and San Bernard River served as the basis for inflow information. Bathymetric and topographic datasets were utilized to construct the bathymetric surface essential for wave and current modeling. Tidal elevations, wind, and wave data were acquired from the nearest station to the project site, with considerations for potential impacts due to sea level rise and climate change.

To assess the potential impacts of the Brazos River Flood Gate (BRFG) on sedimentation patterns and volumes in the Gulf Intracoastal Waterway (GIWW), a comprehensive sedimentation study was conducted. This involved a review of available surveys and dredge records, analysis of sediment grab samples, creation of suspended sediment rating curves from measured data, and development of a calibrated sedimentation model.

The sedimentation model employed the same mesh and hydrodynamic forcing conditions as the hydrodynamic and salinity models. Sediment boundary conditions were determined using sediment rating curves, assuming a sediment class distribution of 50% silt and 50% clay. Sand was excluded from the sedimentation model due to high uncertainty in the boundary sand load, and because it was justified that sand would not penetrate the GIWW. However, a sensitivity analysis was carried out to assess the impact of this assumption on the model results.

The findings related to the sediment dynamics and budget of the Brazos River estuary, as determined by the ADH model, are outlined in **Section 3.4.3** and visually represented in **Figure 3.15**. As discussed, the model-derived sediment depositional rate is notably higher than the rates obtained from sediment cores obtained from the estuary area.

Laguna Madre and Rio Grande Estuary Model

As detailed in **Section 3.11.3**, the only extensive sediment budget study employing a geomorphological model in the Texas coastal area was carried out for the Laguna Madre and Rio Grande Estuary by HR Wallingford [177]. The study employs various modeling tools to comprehensively analyze sediment transport along the open Gulf coast. These tools include:

- *TELEMAC for coastal area modeling*: Fully coupled modules of the TELEMAC modeling system was utilized to capture the impacts of wind, waves, and currents on sediment transport. The model assessed transport pathways, fluxes, erosion, and accretion.
- *DRCALC for littoral drift rate calculations*: The point model DRCALC was employed to calculate wave-driven longshore sediment transport potential, providing insights into littoral drift rates.
- *COSMOS for cross-shore distribution modeling*: The 2DV profile model COSMOS was utilized to analyze the cross-shore distribution of wave-driven longshore sediment transport potential, offering a comprehensive perspective on sediment movement.
- *XBeach for extreme events modeling*: XBeach was employed for detailed modeling of the effects of extreme events on specific, representative sections of the study area. This approach enabled a thorough examination of the impacts of such events on sediment dynamics.

The modeling activities in this study encompass wave and flow modeling, as well as sediment transport modeling. Two key modules from the TELEMAC suite were employed for wave and flow modeling: TOMAWAC, the wave model, and TELEMAC, the hydrodynamic module. Large-scale sediment transport pathways throughout the study area were delineated using a model composed of three fully coupled modules that interact during simulation. These modules include:

- TOMAWAC model: Utilized to transform offshore waves into the area of interest.
- TELEMAC-2D (two-dimensional depth-averaged module): Employed to simulate currents and water levels, providing a comprehensive understanding of hydrodynamics.
- SISYPHE model: This module was employed to predict sediment transport under specific hydrodynamic and wave conditions, contributing to the characterization of sediment pathways in the study area.

The models' inputs include waves, winds, ocean currents, river discharges, bathymetry, and bed composition. The models' outputs pertinent to the sediment budget include sediment fluxes, long-shore transport, and current-driven patterns of transport around entrances (passes).

The model covered about 203 miles (327 km) of the Texas coast, from San Jose Island at the northern end to El Mezquital in Mexico at the southern end to eliminate model errors due to boundary effects. The model did not include morphological changes because of cross-shore processes. Furthermore, aeolian sediment transport was not incorporated into the model.

It is important to highlight the exclusion of cohesive sediment in this study. However, unlike other sediment transport models that rely on d_{50}, this model integrated five distinct sediment particle

sizes, spanning from medium silt to medium sand. Notably, it took into account areas with immobile beds and considered spatial variations in grain size. Consequently, the analysis computed actual sediment transport rather than potential values.

Although the decision to present the sediment budget results only for the sand component was directed by the client (Texas General Land Office), it is necessary to acknowledge the study's limitations. The model, while comprehensive, might not present a holistic view of sediment dynamics and the budget in the study area. This limitation stems from the absence of consideration for the interaction between cohesive and non-cohesive sediment in this study. Additionally, the influence of waves and current forces on cohesive beds was not taken into account.

4.1.3 Field Surveys and Sampling Approaches

Numerous studies have employed sediment sampling and bathymetry surveys to investigate sediment dynamics in Texas coastal areas. Sediment sampling may include collecting grab samples and sediment cores. The samples collected from different locations within the coastal area may be used to analyze their characteristics, including grain size, composition, organic content, depositional rate, and sediment origin. The bathymetric surveys methods involve measuring and mapping the underwater topography of the seabed to understand changes in sediment distribution and rate of deposition. Examples of such studies in the Texas coast areas are summarized in **Table 4.2**. In this table, the areas where these methods have been employed, the objectives of the study, and the methods/approaches are presented. As can be observed, not all studies were necessarily conducted with the specific aim of a sediment budget; however, the results could be contributors to the sediment budget of the study area.

Table 4.2 Samples Studies that Utilized Field Surveys and Sampling Approaches to Assess Sediment Budget in Waterbodies Along Texas Coast

Study Area	Study Objectives	Method/Approach	Reference
Sabine Lake System	Estimate sediment accumulation rate in the Sabine-Neches estuary near Beaumon, Texas	Sediment cores were collected, and ^{210}Pb and $^{239, 240}$Pu radioisotopes analyses were conducted to estimate sediment accumulation rates.	[23]
Galveston Bay System	Develop an estimated budget of sediment inputs to Galveston Bay	Sediment inputs from fluvial and other sources into Galveston Bay were estimated. Sediment samples from Trinity River delta were collected and examined to determine sand fraction, texture, grain coatings, rounding/angularity, and color (to discern whether alluvial deposits represented "new" sediment from uplands or reworked deltaic material). The sediment amount in the Trinity River bayhead delta was estimated by measuring the total surface area from maps and determining mean thickness from facies maps.	[44]
Galveston Bay System	Assess the effects of Hurricane Harvey on the hydrodynamic and sediment process in Galveston Bay	Multiple sediment cores were collected before and after Harvey throughout Galveston Bay. The thicknesses of the Harvey flood layer were visually determined from the X-radiographs based on textural variations in the strata. The flood layer thicknesses for individual cores were mapped and contoured using ArcGIS, and a sediment volume was determined for the flood layer based on the contoured data. Using the storm layer deposit volume, a mass of the storm layer was determined using the density of quartz and the water content of the sediment.	[51]
Brazos-San Bernard Estuary	To understand the mechanisms influencing the flux of sediment from the Brazos River to the GoM and evolution of the system	High-resolution geophysical data, sediment cores, water column data, and historic shoreline data were utilized to investigate the mechanisms in which sediment is transported to the coastal ocean, the fate of that sediment as it becomes preserved in the modem geological record, and the evolution of a modem delta. The sediment budget was derived using ^{137}Cs sedimentation rates, indicative of sediment accumulation over approximately the past 50 years.	[66]

Table 4.2 Cont.

Study Area	Study Objectives	Method/Approach	Reference
Galveston, East Matagorda, Matagorda, San Antonio, Aransas, and Corpus Christi Bays	Determine long-term sedimentation rates in Texas coastal bays and lagoons	Detailed unpublished soundings of Texas bays made by the United States Coast and Geodetic Survey since 1887 were compared with the 1953 surveys to estimate the long-term sediment accumulation rates	[45]
Aransas Bay System	Examine the role of climate and sea-level changes in the evolution of the Copano Bay, Texas	123 km of high-resolution 2-D seismic lines and 6 sediment cores up to 16 m in length were collected from Copano Bay. X-rays were taken of selected core segments to help identify sedimentary structures. Radiocarbon Accelerator Mass Spectrometry (AMS) ages from mollusks were obtained to bracket the age of major stratigraphic surfaces and to establish a chronostratigraphic framework for the deposits within Copano Bay. Grain-size analysis was conducted on a 16 m core that contained a record of middle-bay deposits over the last 8.2 ky.	[137]
Baffin Bay System	Reconstruct a detailed history of water quality and sedimentation changes over the last ~150 years in Baffin Bay	Sediment cores were collected from different parts of Baffin Bay. To establish a chronological framework, $^{137}Cs/^{210}Pb$ radioisotope analysis was employed in sediment cores. Radioisotope analyses were supplemented with proxy analyses to further refine the chronological understanding. Grain size analysis was also performed to determine sediment texture and fraction and establish sediment deposition trend within the bay.	[166]
Laguna Madre System	To evaluate the importance of sediment transport into Laguna Madre by wind, runoff, washover, and waves and currents and the effects of different climate zone on these processes within the lagoon	The sediment influx of Laguna Madre was determined by evaluating the individual contributions of each sediment source rather than relying on an aggregated estimator, such as accumulation rate. The rates of lagoon sediment accumulation in Laguna Madre were obtained from previous studies which used bathymetric maps surveyed in 1887 and 1954 and using a radiocarbon date of 3910 year BP for material at a depth of about 4m in a core from northern Laguna Madre.	[165]

4.2 Potential Gaps in the Existing Studies on Sediment Budgets in the Texas Coast

Irrespective of the methods employed for sediment budget analysis, having accurate estimates of sediment sources and sinks is crucial to ensure accuracy in the analysis. Typically, sediment inputs from fluvial sources and shoreline erosion constitute the primary sources of sediment in waterbodies. Other sources of sediment include longshore sediment transport into the study area and beach fill and dredged material placement from navigation channel maintenance. Meanwhile, sediment losses resulting from dredging or longshore transport out of the study area are regarded as sediment sinks. Accretion of the beach and relative sea level rise are other examples of sediment budget sinks [4].

Errors in estimating sediment sources and sinks can lead to an inaccurate sediment budget. The subsequent sections address the sources that can be used to collect sediment data for conducting a sediment budget analysis for the Texas coast and highlight the gaps identified through this literature review.

4.2.1 Potential Gaps in Sediment Sources

4.2.2 Sediment Inputs from Fluvial Sources

The sediment inputs from fluvial sources to the Gulf of Mexico (either directly or through coastal bays and lagoons) can be estimated from historical sediment data collected at gauge stations (e.g., USGS) or by utilizing empirical formulas for calculating overland erosion and sediment yield for a given point in a watershed. These two methods of quantifying fluvial sediment are summarized in the following sections, and the gaps in the sediment data are identified.

4.2.2.1 Estimating Sediment Load from Historical Data

The available historical sediment data for rivers flowing through the 11 selected watersheds in the current literature review, discharging directly or indirectly into the Gulf of Mexico, is summarized in **Table 4.3**. The table lists the foremost downstream USGS station on each river, along with the period for which sediment data are available. Additionally, it provides the distance between the station and the river mouth, where it discharges into a bay or the Gulf of Mexico. Furthermore, the table includes the percentage of the total watershed area located downstream of the station, designating ungauged watershed, and the annual sediment load carried by the river estimated at this station. The following is a summary of the information presented in **Table 4.3**:

- Except for Caney Creek, the remaining rivers and creeks are considered gauged streams. However, sediment data from Los Olmos, San Fernando, and Petronila Creeks have been collected by TCEQ. Unlike USGS stations, where sediment and flow data are routinely collected, these specific stations lack consistent data collection. Consequently, the sediment load carried by Los Olmos, San Fernando, and Petronila Creeks cannot be estimated.

- The period for which sediment data is available varies among the rivers, averaging 34 years. The minimum period is 5 years (Nueces River at Bluntzer), while the maximum is 61 years (Neches River at Evadale and Trinity River at Romayor).
- The distance between the foremost downstream station and the river mouth, where it empties into a bay or the Gulf of Mexico (GoM), varies from 1 mile (Guadalupe River at Tivoli) to 78 miles (Trinity River at Romayor). Although the percentage of the ungauged area of the Guadalupe River at Tivoli is nearly zero, only five years of sediment data are available at this point. In contrast, the Trinity River at Romayor has 61 years of sediment data, but 4.5% of the watershed is located downstream of this station (ungauged area).
- The San Jacinto, Lavaca, and Aransas Rivers show the most extensive ungauged watersheds, comprising 83.7%, 64.6%, and 70.7% ungauged areas, respectively.
- The total annual suspended sediment load discharged into the Texas coast's bays and lagoons, and the Gulf of Mexico (GoM) is estimated at approximately 15.4×10^6 tons/year. The largest contributor, the Brazos River, accounts for around 50% of this load and directly discharges into the GoM. Following, the Colorado River is the second-largest contributor, discharging an annual load of 1.63×10^6 tons into Matagorda Bay, while the Rio Grande ranks third, contributing an annual load of 1.58×10^6 tons directly to the GoM. The Mission River, discharging into Aransas Bay, has the lowest annual suspended sediment load of 10,220 tons/yr.

Limited sediment data and ungauged watershed areas introduce uncertainties into sediment inputs, which are necessary for an accurate sediment budget. Moreover, at the majority of stations, only suspended load is measured and reported, leaving the contribution of bedload to the total load unknown. Bedload and sand transport has been evaluated in very few rivers in the study area. For instance, in the Colorado River, it was estimated that the sand load constitutes 18% of the total sediment load entering Matagorda Bay (**Section 3.6.2.3**). Additionally, in the Brazos River, a ratio of 11 to 1 between suspended sediment and bedload transport is reported (refer to **Section 3.4.2.1**).

The sediment data obtained from USGS gauges requires processing to estimate the annual sediment load transported by a stream through the development of sediment load rating curves. Utilizing the average daily load reported for a station to calculate annual sediment loads may introduce significant errors in load calculations. In **Figure 4.2**, a comparison is made between the annual suspended sediment loads of the Brazos River at Rosharon and Richmond stations, estimated from both the daily average suspended sediment load and suspended sediment load rating curves [40, 65] (**Section 3.4.1**). The sediment load estimates for the Richmond and Rosharon stations derived from the daily average load exceed those obtained from the rating curves by 75% and 86%, respectively. It is important to highlight that the development of a reliable sediment load rating curve requires a long-term sediment dataset that encompasses a broad spectrum of flow and sediment discharge conditions. Unfortunately, such comprehensive information may be lacking for numerous stations. Among the 20 stations listed in **Table 4.3**, only 10 stations have sediment data for more than 30 years.

Table 4.3 Summary of Available Sediment Data for Streams Discharging into the Gulf of Mexico

Watershed	Stream/Creek	Most Downstream Station with Sediment Data	Period	Dist. from Station to Stream Mouth	Total Ungauged Area (%)	Annual Suspended Sediment Load (tons/yr)
Sabine Lake System	Sabine River	Ruliff (USGS-08030500)	1974-1995 (21 yrs)	29 miles (Figure 3.3)	4.4	285,430
	Neches River	Evadale (USGS-08041000)	1960-2021 (61 yrs)	50 miles (Figure 3.4)	20	298,205
Galveston Bay	Trinity River	Romayor (USGS-08066500	1960-2021 (61 yrs)	78 miles (Figure 3.9)	4.5	2,072,105
	San Jacinto River	Conroe (USGS-08068000)	1965-2011 (46 yrs)	41 miles (Figure 3.10)	83.7	104,390
Brazos-San Bernard Estuary	Brazos River	Rosharon (USGS-08116650)	1973-2023 (50 yrs)	35 miles (Figure 3.12)	0.6	8,053,360
	San Bernard River	Boling (USGS-08117500)	1978-2021 (43 yrs)	42 miles (Figure 3.16)	2.4	57,305
East Matagorda	Caney Creek	-	-	-	100	-
Matagorda Bay	Colorado River	Wharton (USGS- 0816200)	1974-2021 (47 yrs)	44 miles (Figure 3.24)	0.7	1,626,440
	Lavaca River	Edna (USGS- 08164000)	1977-2020 (43 yrs)	20 miles (Figure 3.25)	64.6	69,350
San Antonio Bay	Guadalupe River	Victoria (USGS-08176500)	1973-2020 (47 yrs)	28 miles (Figure 3.30)	49	515,745
		Tivoli (USGS-08188810)	2013-18 (5 yrs)	1 mile (Figure 3.30)	0	678,900
	San Antonio River	Goliad (USGS-08188500)	1974-2021 (47 yrs)	35 miles (Figure 3.31)	6.2	542,390
Aransas Bay System	Mission River	Refugio (USGS-08189500)	1973-1993 (20 yrs)	14 miles (Figure 3.33)	32.9	10,220
	Aransas River	Skidmore (USGS-08189700)	1966-1975 (9 yrs)	29 miles (Figure 3.33)	70.7	274,480

Table 4.3 Cont.

Watershed	Stream/Creek	Most Downstream Station with Sediment Data	Observation Period	Dist. from Station to Stream Mouth	Total Ungauged Area (%)	Annual Suspended Sediment Load (tons/yr)
Corpus Christi Bay System	Nueces River	Bluntzer (USGS-08211200)	2006-2010 (4 yrs)	26 miles (Figure 3.35)	0.7	332,515
Baffin Bay System	Los Olmos	Los Olmos Creek (TCEQMAIN-13034)	2005-22 (15 yrs)	27 miles (Figure 3.37)	62.2	-
	San Fernando	San Fernando Creek (TCEQMAIN-13033)	2005-11 (6 yrs)	35 miles (Figure 3.37)	24.9	-
	Petronila Creek	Petronila Creek (TCEQMAIN-13090)	2018-22 (5 yrs)	24 miles (Figure 3.37)	82.3	-
Laguna Madre System	Arroyo Colorado	Harlingen (USGS 08470400)	1986-2007 (21 yrs)	25 miles (Figure 3.39)	46	66,430
Rio Grande System	Rio Grande River	Brownville (USGS-08475000)	1966-2021 (55 yrs)	20 miles (Figure 3.48)	3.2	1,574,975

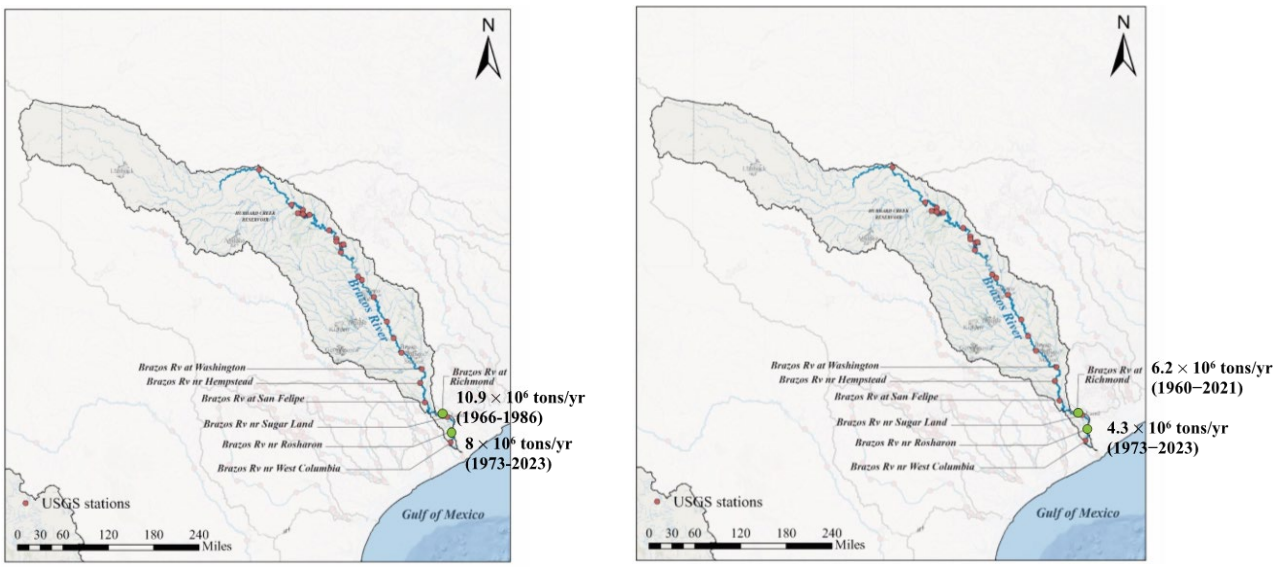

Figure 4.2 Annal Sediment Load of the Brazos River at Richmond and Rosharon Stations Estimated Based on (a) Daily Average Sediment Load, and (b) Sediment Load Rating Curves (**Section 3.4.2.1**)

4.2.2.2 Estimating Sediment Load from Sediment Yield Empirical Formulas

Sediment yield can be calculated using empirical formulas that relate sediment transport to various watershed and climatic factors. One commonly used empirical formula is the Universal Soil Loss Equation (USLE) and its Revised Universal Soil Loss Equation (RUSLE). The USLE and RUSLE provide estimates of soil erosion, and sediment yield can be derived from these estimates.

For the State of Texas, the most comprehensive study was conducted in 1979, titled "*Erosion and Sedimentation by Water in Texas*", and it was published in 1982 [10]. This publication replaced the report published in 1957. The study encompasses the entire State of Texas, including all or parts of the drainage areas of 23 rivers and coastal basins, along with 20 land-resource areas within the study region. The report presents estimates of annual sediment yields at various locations within each watershed.

While this study is comprehensive, it is important to note that it is more than four decades old, and various factors influencing soil erosion may have changed since its completion. These factors include alterations in rainfall intensity and patterns, changes in land use/land cover –particularly in urban and built-up areas– and shifts in land management practices. Additionally, the inherent uncertainty of soil erosion empirical formulas, coupled with the lack of a comprehensive examination of the accuracy of their results through field observations, contributes to the uncertainty surrounding sediment yield estimates.

In **Figure 4.3**, a comparison is presented for the annual sediment load to Sabine Lake using three different methods. These estimates are based on:

a) Sediment load measured at USGS stations on Sabine River and Neches River: The total annual sediment load is estimated as 0.49 $\times 10^6$ tons/yr (**Sections 3.2.2.1** and **3.2.2.2**).
b) Sediment yield empirical formulas: The total annual sediment load is estimated as 2 $\times 10^6$ tons/yr (Sections **3.2.1.1** and **3.2.1.2**).
c) Field survey of sediment deposition rate in Sabine Lake: The total annual sediment load is estimated as 0.64 $\times 10^6$ tons/yr (Section **3.2.2.3**).

Annual sediment loads estimated using USGS data and the field survey of sediment deposition rate in Sabine Lake are comparable despite a 23% difference. However, the estimate from the sediment yield empirical formula is as much as 3-4 times higher than the other two estimates.

Figure 4.4 presents another example with a significant difference between sediment load estimated using USGS data and from sediment yield empirical equation. The annual sediment load from Brazos River to GoM using these two methods are estimated as 8 $\times 10^6$ tons/yr (**Section 3.4.2.1**) and 25 $\times 10^6$ tons/yr (**Section 3.4.1**), respectively.

4.2.3 Sediment Inputs from Coastal Shorelines Erosion

The estimation of sediment inputs resulting from coastal shoreline erosion depends on tracking changes in the shoreline's position. Calculating the volume of sediment released due to shore erosion involves estimating the average rate of shore retreat and the depth of erosion. The composition of the eroded sediments plays a crucial role in determining the degree of subsequent reworking and the potential for transport into other parts of the system. These changes in the shoreline position are determined by compiling data on shoreline and vegetation line positions obtained from various sources, including topographic maps, high-resolution aerial and satellite images, coastal charts, ground GPS surveys, and airborne lidar surveys spanning different time periods.

Numerous studies have investigated the long-term movement of the Texas Gulf shoreline, with references to some of these studies provided in previous sections. The results of the most recent and comprehensive study are summarized in a report titled "*Shoreline Movement Along the Texas Gulf Coast, 1930s to 2019*" [27]. According to the findings, the net rates of long-term movement along the Texas Gulf shoreline facing the Gulf of Mexico average 4.2 ft/yr (1.27 m/yr) of retreat. Approximately 80% of the Texas Gulf shoreline experienced net retreat, leading to an estimated net land loss of 16,375 acres (6,627 ha) since 1930, occurring at an average rate of 184 acres/yr (74 ha/yr). The upper Texas coast exhibited more pronounced recessional rates (net retreat at 5.6 ft/yr (1.71 m/yr) from Sabine Pass to the Colorado River compared to the middle and lower coast (net retreat at 3.2 ft/yr (0.97 m/y) from the Colorado River to the Rio Grande. The net rates of long-term movement of the Texas Gulf shoreline between Sabine Pass and the Rio Grande calculated for the period of the 1930s-2019 are depicted in **Figure 4.5.**

The specifics regarding shoreline erosion rates for each of the 11 selected systems in this literature review are presented in **Chapter 3**.

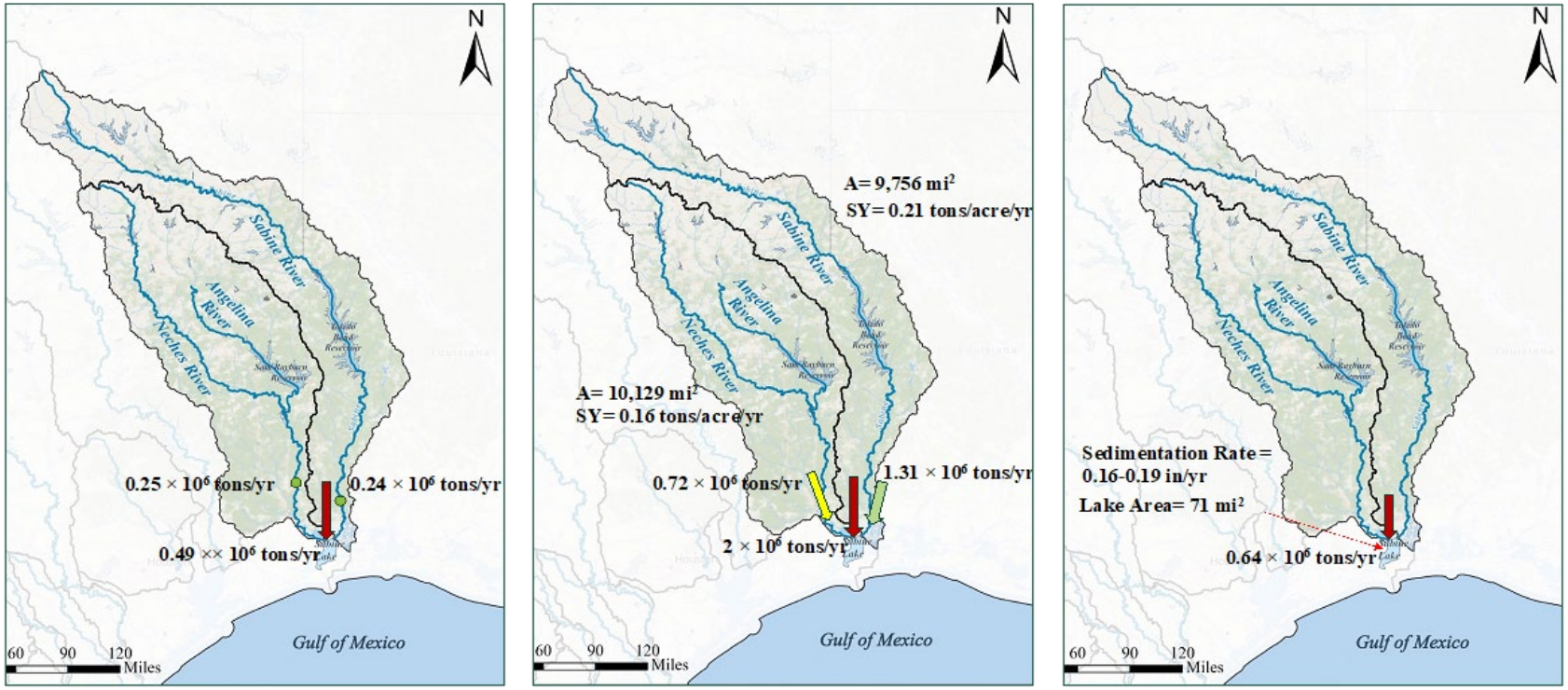

(a) (b) (c)

Figure 4.3 Annal Sediment Load to Sabine Lake Estimated Based on (a) Sediment Load Measured at USGS Stations, (b) Sediment Yield Empirical Formulas, and (c) Field Study of Sediment Deposition Rate in Sabine Lak (**Section 3.2**)

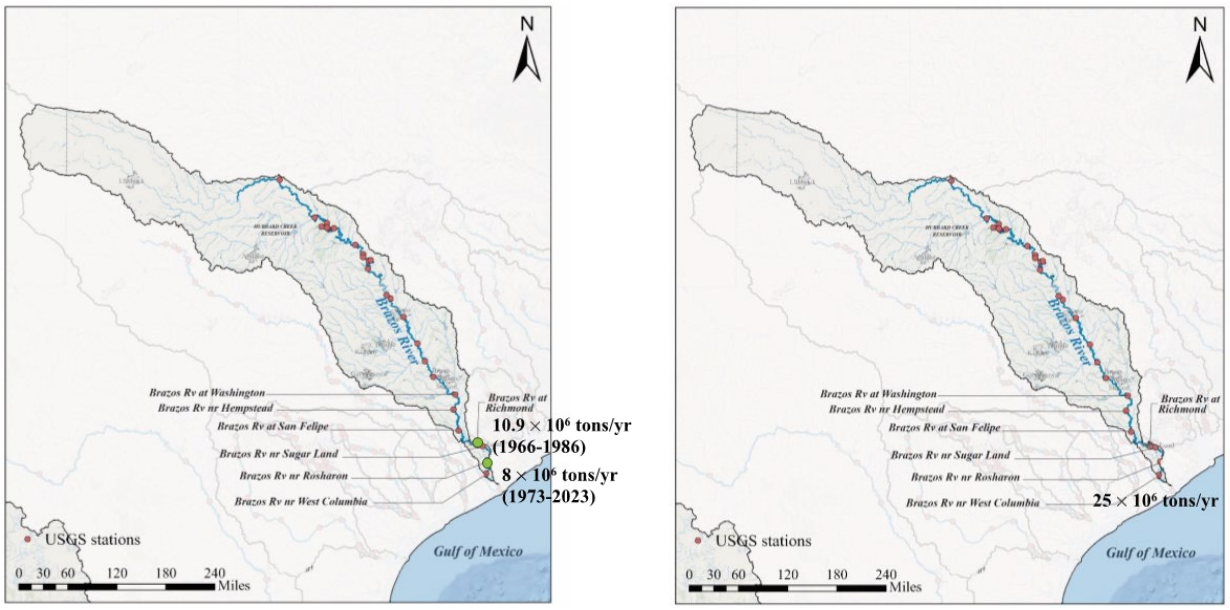

(a) (b)

Figure 4.4 Annal Sediment Load from Brazos River to Gulf of Mexico Estimated Based on (a) Sediment Load Measured at USGS Stations, and (b) Sediment Yield Empirical Formulas (**Section 3.4**)

Estimating coastal shoreline erosion from aerial photos and other sources is subject to various types of error. Challenges include scale and resolution variations, complex topography, temporal factors like time lag and seasonal changes, vegetation and land cover influence, weather conditions, anthropogenic alterations, surveying techniques, data integration inconsistencies, sensor calibration issues, potential human errors in interpretation, and the dynamic nature of coastal processes. These factors collectively contribute to uncertainties in shoreline measurements, highlighting the importance of careful consideration, quality control, and validation with ground-truth data to enhance the accuracy and reliability of the estimation process. Even though the accuracy of determining shoreline positions has improved with advances in technology, due to limitations in the current technique employed, rates of change should be considered secondary to the overall trends or direction of change.

The shoreline changes of different areas along Texas coast between the 1930s and 2019 are summarized in **Table 4.4**. In this table, the annual net rates and the ranges of change in each area are presented. Also, the annual and cumulative land loss are calculated and shown in this table. In this table also the standard divination of net shoreline erosion in each area is presented. This statistical parameter can be interpreted as a measure of inaccuracy in estimating shoreline erosion. The higher this parameter is in comparison to the net erosion rate, the less accurate the shoreline erosion rate is. Therefore, long-term net change values should be considered in context, as short-term changes may exhibit a greater magnitude with higher degree of uncertainty, especially in areas experiencing both accretion and erosion.

The more details of such information for each of the 11 systems selected for this literature review are presented **Chapter 3** and summarized in **Table 4.5**.

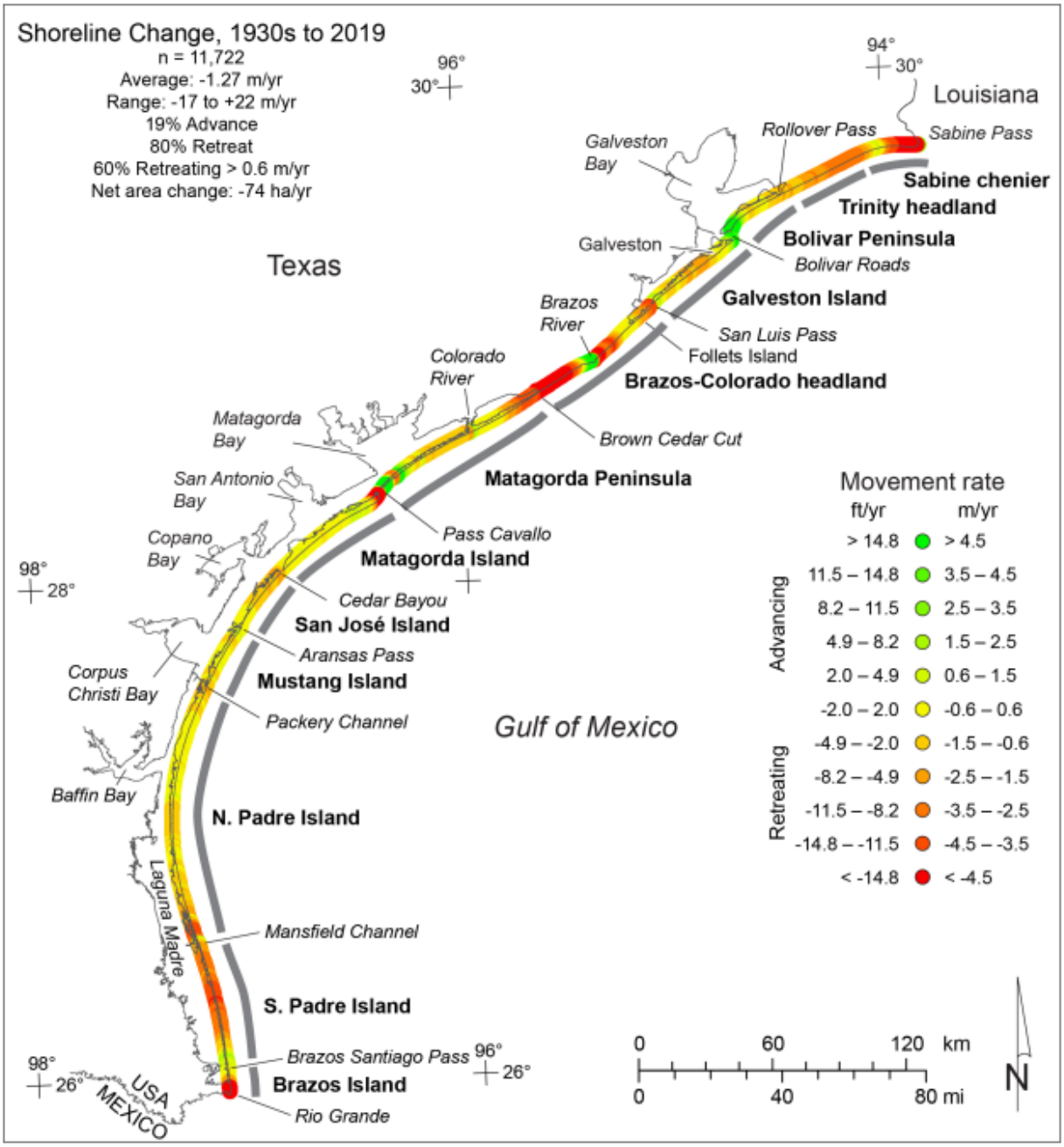

Figure 4.5 Net Rates of Long-term Movement for the Texas Gulf Shoreline Between Sabine Pass and the Rio Grande Calculated from Shoreline Positions from the 1930s to 2019 [27]

Table 4.4 Net Shoreline and Land-area Loss between the 1930s and 2019 for the Texas Gulf Shoreline and Major Geomorphic Areas (**Figure 4.5**) with Shoreline on the Gulf of Mexico [27]

Area	No.	Net rate (m/yr)	Std. dev. (m/yr)	Range (m/yr)	Area change rate (ha/yr)	Area change (ha)
All Texas sites	11,722	-1.27	2.77	-16.5 to +22.0	-74.5	-6,627
Geomorphic Areas						
Sabine Pass to Rollover Pass	1,345	-3.03	2.64	-11.6 to +10.6	-20.4	-1,814
Bolivar Peninsula	542	+0.28	2.60	-1.9 to +14.2	+0.75	+67
Galveston Island (all)	932	-0.21	1.76	-2.5 to +5.9	-0.98	-87
Galv. Is. (no seawall)	704	-0.22	1.99	-2.5 to +5.9	-0.78	-70
Galv. Is. (East Beach)	108	+3.66	1.38	+1.6 to +5.9	+2.0	+176
Galv. Is. (West Beach)	596	-0.93	1.06	-2.5 to +3.8	-2.8	-246
Brazos–Colorado headland	1,244	-2.16	4.79	-13.2 to +18.1	-13.4	-1,194
Matagorda Peninsula	1,589	-0.89	2.84	-12.2 to +22.0	-7.1	-631
Matagorda Island	1,116	-0.91	3.70	-16.5 to +14.4	-5.1	-452
San José Island	622	-0.84	0.67	-1.9 to +0.8	-2.6	-231
Mustang Island	574	-0.29	0.52	-1.4 to +1.7	-0.83	-74
N. Padre Island	2,403	-0.77	0.93	-4.4 to +1.0	-9.2	-820
S. Padre Island	1,120	-2.46	1.51	-4.7 to +2.8	-13.8	-1,227
Brazos Island	235	-1.57	2.60	-7.2 to +2.3	-1.8	-164

Table 4.5 Net Shoreline and land-area change between the 1930s and 2019 for the 11 Waterbody System Along Texas Gulf Shoreline (**Figure 3.1**) [27]

Waterbody System	Net Rate ft/yr (m/yr)	Range ft/yr (m/yr)	Total Land Loss, acres (km^2)	Land Loss Rate, acres/yr (km^2/yr)
Sabine Lake	9.9 (3.03)	–11.6 to +10.6 (–34.05 to +34.8)	4,482 (18.1)	50.4 (0.204)
Galveston Bay	0.7 (0.21)	–2.5 to +5.9 (–8.2 to +19.35)	215 (0.87)	2.42 (0.01)
Brazos-San Bernard	7.1 (2.16)	–13.2 to +18.1 (–34.05 to +59.4)	2,950 (12)	33.1 (0.13)
East Matagorda Bay	5.6 (1.70)	–3.54 to 29.62 (–11.6 to +97.2)	2,594 (10.5)	29.1 (0.12)
Matagorda Bay	1.05 (0.32)	–5.55 to 80.94 (–18.2 to +265.5)	2,706 (10.9)	30.4 (0.12)
San Antonio Bay	1.83 (0.56)	–5.67 to 3.06 (–18.6 to +10.04)	1,011 (4.1)	11.4 (0.05)
Aransas Bay	1.41 (0.43)	–2.62 to 0.57 (–7.4 to +1.87)	550 (2.2)	6.1 (0.03)
Corpus Christi Bay	0.95 (0.29)	–1.4 to +1.7 (–4.6 to +5.6)	183 (0.74)	2.1 (0.0085)
Baffin Bay	2.52 (0.77)	–4.4 to +1.0 (–14.4 to +3.28)	2,026 (8.2)	22.7 (0.92)
Laguna Madre	8.1 (2.46)	–4.7 to +2.8 (–15.4 to +9.2)	2,789 (11.2)	34.1 (0.02)
Rio Grande	5.2 (1.57)	–7.2 to +2.3 (–23.6 to +7.54)	405 (1.64)	4.4 (0.87)

4.2.4 Potential Gaps in Sediment Sinks

Within the Texas coast, the navigational channels undergo active dredging that is designated as the primary sediment sinks. Additionally, sediment may be transported away from the area through wave-driven longshore sediment transport and various other coastal processes.

4.2.4.1 Sediment Loss Due to Dredging

The accurate estimation of dredged material volume is crucial for the sediment budget of any coastal area, including the Texas Coast. The U.S. Army Corps of Engineers (USACE) is responsible for many dredging projects in navigational channels and waterways. The USACE Navigation Data Center Database [193] provided detailed information regarding past USACE dredging projects along the Texas Coast. This information includes the year of the dredging event, the specific name and location of the project, precise latitude and longitude coordinates, and the quantity of dredged materials. For the USACE Galveston District, the database contained 418 dredge projects. **Figure 4.6** shows the annual average of dredged material for each river system along the Texas Coast [52].

Estimating the volume of dredged material involves various challenges, and errors can arise from different sources. Some common sources of error in estimating the volume of dredged material include:

- *Measurement Techniques*: The methods used to measure the volume of dredged material can introduce errors. Inaccuracies may arise from the equipment used for surveys, such as echo sounders or sonar devices, leading to underestimation or overestimation of volumes.
- *Sediment Characteristics*: The nature of the sediment being dredged, including its density and composition, can influence volume estimates. Variability in sediment characteristics may not be fully accounted for in estimations, leading to inaccuracies.
- *Dredging Equipment Performance*: The efficiency and accuracy of dredging equipment play a significant role in volume estimation. Mechanical issues, variations in dredging techniques, or changes in equipment performance during operations can introduce errors.
- *Environmental Conditions*: Factors such as tides, currents, and weather conditions can impact dredging operations and affect volume estimates. Unpredictable environmental changes may not be adequately considered, leading to errors in the estimation process.
- *Survey Frequency and Timing*: The frequency and timing of surveys can influence the accuracy of volume estimates. Infrequent or poorly timed surveys may miss changes in the dredged area, leading to discrepancies in volume calculations.
- *Data Processing and Analysis*: Errors may occur during the processing and analysis of survey data. Inaccurate data interpretation, improper data filtering, or errors in computational methods can contribute to discrepancies in volume estimates.

- *Documentation and Reporting*: Incomplete or inaccurate documentation of dredging activities, including the failure to account for all relevant parameters, can lead to errors in volume estimation.
- *Natural Sediment Redistribution*: The natural redistribution of sediment within the water body after dredging may not be fully accounted for, leading to errors in estimating the long-term effects of dredging activities.

The primary sources of volumetric uncertainty in dredging within the Gulf Intracoastal Waterway (GIWW) are discussed in literature. For example, it was stated that, depending on the method of estimating the quantity of dredged material, the uncertainty of the estimate might vary from 10% to 100% [4]. Also, it is shown that directly comparing hydraulically dredged and deposited sediment volumes is inherently inaccurate due to changes in geotechnical properties influenced by dredging, channel shoaling, and sediment compaction. Hydraulic dredging introduces water, increasing water content and void ratios, while time-dependent processes like sediment compaction and dewatering decrease volume by reducing water content and void ratio, highlighting the complexity of assessing sediment volumes in hydraulic dredging [194]. Moreover, it was reported that out of the 418 dredge projects found in the USACE Galveston District database, 282 projects (67%) did not contain latitude and longitude coordinates [52].

4.2.4.2 Sediment Loss Due to Longshore Sediment Transport

Longshore processes may transport sediment into or out from the study area. The rates of longshore transport may be estimated by considering local knowledge of the site, the history of engineering activities, and the subsequent beach response, such as impoundment at a groin or jetty. Additionally, the calculation of the longshore energy flux due to the site's wave climate is a crucial factor. Defining sediment transport fluxes at inlets, even in a relative sense, is challenging. Factors such as flood and ebb currents, combined waves and currents, wave refraction and diffraction over complex bathymetry, and engineering activities further complicate the determination of transport rate directions and may either increase or decrease their magnitudes [4]. Geomorphological models can be utilized to determine sediment fluxes and transport pathways necessary for a sediment budget analysis. In the case of the Texas coast, such modeling is conducted exclusively for the Laguna Madre and Rio Grande Estuary areas, as well as the Brazos-San Bernard Estuary area, as outline in **Table 4.1**.

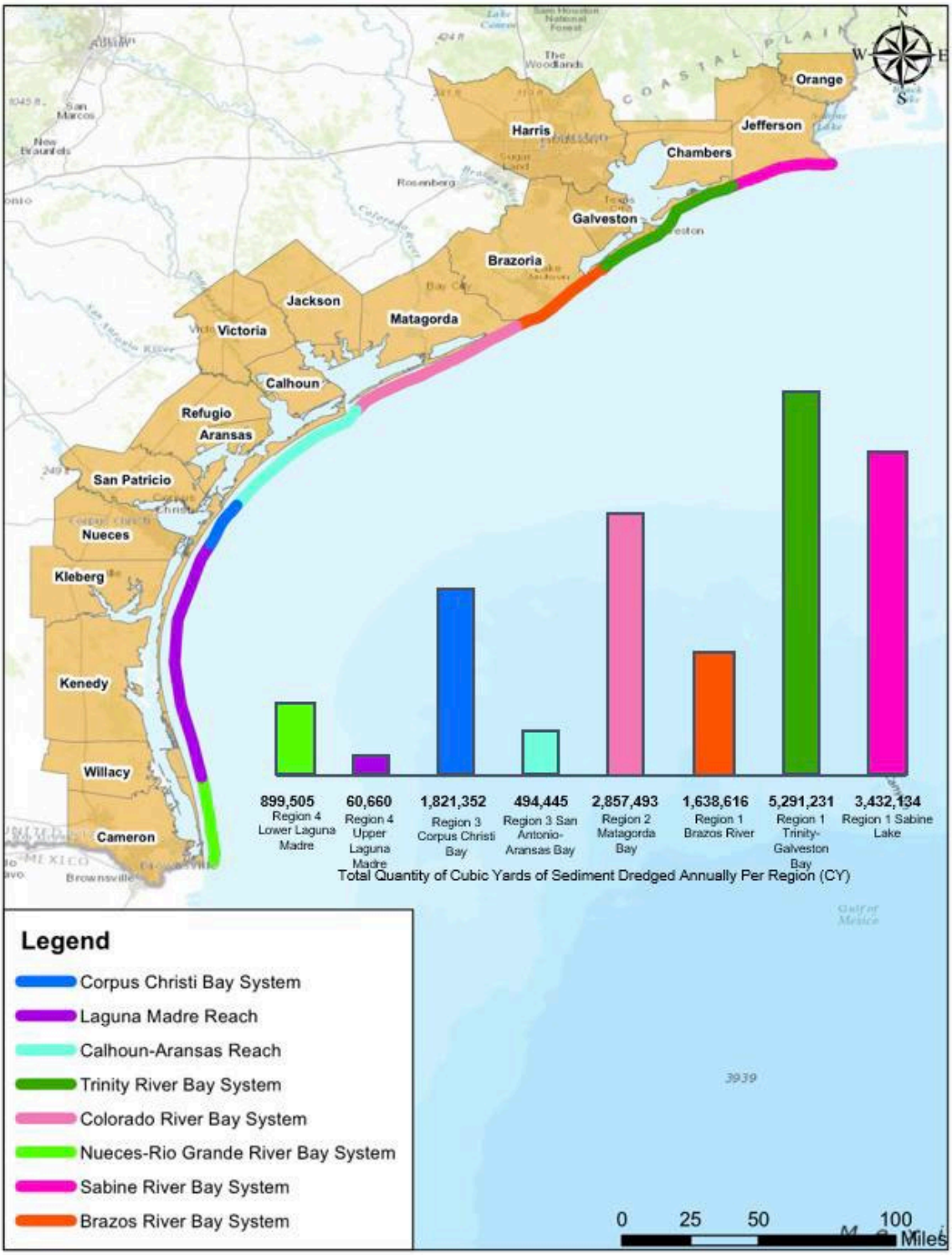

Figure 4.6 USACE Galveston District Annual Average Dredged Material by River System (1991-2015) [52]

4.3 Key Findings and Recommendations for Future Studies

The Texas coastline faces persistent challenges attributed to coastal erosion, influenced by factors such as storm events, sea-level rise, and anthropogenic activities. Hurricanes and tropical storms, in particular, significantly contribute to erosion, causing gradual land loss. Rising sea levels, a consequence of climate change, further intensify erosion by increasing the frequency and severity of flooding events. Human interventions, including coastal development and navigation channels, can alter natural sediment dynamics, impacting erosion rates.

This study's primary objective was to conduct a comprehensive literature review focusing on recent sediment budget research along the Texas Coast. The analysis targeted major waterbodies, river mouths, and both natural and constructed exchange passes. The methodologies, assumptions, input datasets, and modeling tools utilized in these studies were critically examined to compile a detailed summary, emphasizing potential gaps in existing research on sediment budgets in the Texas Coast.

Based on this literature review the following gaps were identified in the sediment budget analysis of the Texas Coast:

- *Limited Coverage of Sediment Budget Analysis*: While three main approaches–quantitative methods, hydro-geomorphological models, and field surveys–have been utilized, there are significant gaps in coverage. Hydro-geomorphological models, the most accurate approach, have only been applied to specific areas like the Brazos River Estuary, Laguna Madre system, and Rio Grande Estuary, leaving other parts of the Texas Coast unexamined.
- *Uncertainties in Sediment Inputs*: Sediment inputs from fluvial sources are estimated using historical data from gauge stations and empirical formulas. However, limited historical sediment data, ungauged watersheds, and uncertainties in estimating sediment load introduce inaccuracies. Another gap exists in the quantification of sediment load entering Texas Coast during extreme hydrological events. Additionally, uncertainties exist in estimating sediment yield from empirical formulas due to changes in factors influencing soil erosion and lack of comprehensive accuracy examination through field observations.
- *Uncertainties in Shoreline Erosion Estimates*: Estimating sediment inputs from coastal shoreline erosion involves tracking shoreline movement, but uncertainties arise from factors like scale and resolution of images and dynamic coastal processes. Shoreline erosion rates are lacking for many bays, further adding to uncertainties in the sediment budget analysis.
- *Incomplete Understanding of Sediment Outputs*: Sediment loss due to dredging and longshore sediment transport is not thoroughly investigated along the Texas Coast. Uncertainties in dredged material volume estimation, sediment characteristics, and incomplete documentation of dredging activities contribute to inaccuracies. Longshore sediment transport analysis is conducted only in specific areas, leaving gaps in understanding sediment fluxes and pathways.

While substantial progress has been made in understanding sediment dynamics along the Texas Coast, this study underscores the need for enhanced methodologies, data integration, and collaborative efforts to fill existing gaps. Accurate sediment budgeting is essential for informed coastal management strategies, particularly in the face of ongoing environmental changes and anthropogenic activities impacting the Texas coastline. Based on the gaps identified in this study, the following recommendations for future work are proposed:

- Conduct sediment budget analysis using hydro-geomorphological models for areas along the Texas Coast where such analyses have not been undertaken to provide a comprehensive understanding of sediment dynamics.
- Improve estimation of sediment inputs by collecting more recent sediment data from gauge stations and installing new gauges closer to the mouth of rivers to reduce the area of ungauged watershed area. Due to the tidal effects in these areas, more advanced technology such as ADCP should be utilized.
- Perform geomorphological studies in downstream reaches of the rivers discharging to the Texas Coast to better estimate the total sediment load.
- Expand monitoring of shoreline erosion rates to cover all bays along the Texas Coast using consistent methods and improve accuracy by addressing factors contributing to uncertainties in shoreline measurements.
- Conduct detailed studies to accurately estimate sediment loss due to dredging activities, focusing on improving methods for estimating dredged material volume and characterizing sediment properties. Field sampling and surveying may be conducted to improve the accuracy of the sediment budget analysis.

REFERENCES

1. Gellis, A. C., Fitzpatrick, F. A., & Schubauer-Berigan, J. (2016). A manual to identify sources of fluvial sediment (No. EPA/600/R-16/210). US Environmental Protection Agency.
2. List, J.H. (2005). Sediment Budget. In: Schwartz, M.L. (eds) Encyclopedia *of* Coastal Science. Encyclopedia of Earth Science Series. Springer, Dordrecht. https://doi.org/10.1007/1-4020-3880-1_277.
3. Komar, P. D., (1996). The budget of littoral sediments – concepts and applications. Shore and Beach 64, 18-26.
4. Rosati, J. D. (2005). Concepts in sediment budgets. *Journal of Coastal Research*, *21*(2), 307-322.
5. Morang, A. (2006). North Texas sediment budget; Sabine Pass to San Luis Pass.
6. Rosati, J. D., & Kraus, N. C. (2003). Sediment budget analysis system (SBAS): Upgrade for regional applications.
7. Dopsovic, R., Hardegree, L., & Rosati, J. D. (2003). Sediment budget analysis system-A: SBAS-A for Arcview© application.
8. Rosati, J. D., Sumner, C. A., & Wilson, D. A. (2013). The Sediment Budget Calculator: a webtool to develop a family of viable inlet and adjacent beach sediment budget solutions.
9. Phillips, J. D., & Slattery, M. C. (2007). Geomorphic processes, controls, and transition zones in the lower Sabine River. Texas Christian University, Department of Environmental Studies.
10. Greiner, J. H. (1982). Erosion and sedimentation by water in Texas: Average annual rates estimated in 1979. Texas Department of Water Resources.
11. Integrated Flood Risk Management(nFRM) (2022). Watershed Hydrology Assessment for the Neches River Basin. *https://webapps.usgs.gov/infrm/pubs/Neches%20InFRM%20WHA%2001%20MainReport_Jan2022.pdf* . Accessed May 27, 2023
12. National Centers for Environmental Information (NCEI) (2017). State Climates Summaries. Texas, https://statesummaries.ncics.org/chapter/tx/. Accessed May 27, 2023
13. Texas Water Development Board (TWDB) (2012). Chapter 4: Climate of Texas, Water for Texas 2012 State Water Plan.
14. United States Geological Survey (USGS). USGS 08041780 Neches River Saltwater Barrier at Beaumont, Tx. https://waterdata.usgs.gov/nwis/dv/?referred_module=sw&site_no=08041780. Accessed May 27, 2023.
15. Blackburn, W.H., Knight, R.W., Wood, J.C., Pearson, H.A. (1990). Stormflow and sediment loss from intensively managed forest watersheds in east Texas. Water Resources Bulletin 26, 465- 477.
16. Blackburn, W.H., Wood, J.C., DeHaven, M.G. (1986). *Stormflow and sediment losses from site-prepared forestland in east Texas.* Water Resources Research 22, 776 – 784.
17. Texas Water Development Board (TWDB). Sabine-Neches Estuary. https://www.twdb.texas.gov/surfacewater/bays/major_estuaries/sabine_neches/index.asp Accessed May 27, 2023.
18. Phillips, J. D. (2003). Toledo Bend Reservoir and geomorphic response in the lower Sabine River. *River Research and Applications*, *19*(2), 137-159.
19. Rosen, T. (2013). *Long-term total suspended sediment yield of coastal Louisiana rivers with spatiotemporal analysis of the Atchafalaya River Basin and Delta Complex*. M.Sc. Thesis, Louisiana State University and Agricultural & Mechanical College.

20. Nimer, H. F. (2020). Effects of Extreme Rainfall Events on Sediment and Contaminants Transport. Doctoral dissertation, Northeastern University.
21. U.S. Congress. (1974). *Toledo Bend Dam and Reservoir Exemption*. Hearing before the Subcommittee on Forest of the Committee on Agriculture, House of Representatives. Ninety-third Congress, Second session on H.E. 15320, October 9, Serial No. 93-PPP, Washington D.C.
22. Lee, L. T. (2001). *Geotechnical Properties and Sediment Characterization for Dredged Material Models* (ERDC TN-DOER-N13). U.S. Army Engineer Research and Development Center, Vicksburg, MS.
23. Ravichandran, M., Baskaran, M., Santschi, P. H., & Bianchi, T. S. (1995). Geochronology of sediments in the Sabine-Neches estuary, Texas, USA. *Chemical Geology*, *125*(3-4), 291-306.
24. Phillips, J. D., & Slattery, M. C. (2006). Sediment storage, sea level, and sediment delivery to the ocean by coastal plain rivers. *Progress in Physical Geography*, *30*(4), 513-530.
25. Morang, A. (2006). *North Texas sediment budget; Sabine Pass to San Luis Pass* (ERDC/CHL TR-06-17). U.S. Army Engineer Research and Development Center, Vicksburg, MS.
26. Willey, S., Campbell, T., Lambert, S., Morang, A., King, D., & Thomas, R. (2013). Identification of Regional Sediment Management (RSM) Opportunities along the Upper Texas Coast Through Sediment Budget Analysis (ERDC/CHL CHETN-XIV-27). U.S. Army Engineer Research and Development Center, Vicksburg, MS.
27. Paine, J. G., and Caudle, T. (2020). Shoreline Movement along the Texas Gulf Coast, 1930 to 2019. Final Report, Bureau of Economic Geology.
28. Texas Commission on Environmental Quality (TCEQ). (2015). Galveston Bay Estuary Program; Lower Galveston Bay Watershed. https://gbep.texas.gov/wp-content/uploads/2018/08/About-the-Estuary-Program-Page.pdf. Accessed July 4, 2023.
29. Lucena, Z., & Lee, M. T. (2017). *Characterization of streamflow, suspended sediment, and nutrients entering Galveston Bay from the Trinity River, Texas, May 2014–December 2015* (No. 2016-5177). US Geological Survey.
30. Wurbs, R. A., & Yang, M. Y. (2022). Statistical Assessments of River Flow Alterations and Environmental Flow Standards. *Journal of Water Management Modeling*, *30*, 481.
31. Phillips, J. D., & Slattery, M. C. (2007). Downstream trends in discharge, slope, and stream power in a lower coastal plain river. *Journal of Hydrology*, *334*(1-2), 290-303.
32. Lucena, Z., & Lee, M. T. (2022). *Distribution of streamflow, sediment, and nutrients entering Galveston Bay from the Trinity River, Texas, 2016–19* (No. 2022-5015). US Geological Survey.
33. Phillips, J. D., Slattery, M. C., & Musselman, Z. A. (2004). Dam-to-delta sediment inputs and storage in the lower Trinity River, Texas. *Geomorphology*, *62*(1-2), 17-3.
34. Freese and Nichols, Halff Associates, Hollaway Environmental, and Communications Services (2021). *2023 Regional Flood Plan Report: Technical Memorandum, Region 6, San Jacinto (Draft).* Prepared for Texas Water Development Board (TWDB) on behalf of Region 6 San Jacinto Regional Flood Planning Group. https://sanjacintofloodplanning.org/wp-content/uploads/2022/09/06_RFP_Draft_Plan_V1.pdf. Accessed July 4, 2023.
35. Texas Water Development Board (TWDB). GIS Data. http://www.twdb.texas.gov/mapping/gisdata.asp Accessed Nov. 5, 2023.
36. United States Geological Survey (USGS). Water data San Jacinto River nr Conroe. https://waterdata.usgs.gov/monitoring-location/08068000/ Accessed Nov. 5, 2023.

37. Texas Water Development Board (TWDB). Texas Lakes & Reservoirs. https://www.twdb.texas.gov/surfacewater/rivers/river_basins/index.asp Accessed November 5, 2023. (View all Texas River basins)
38. Texas Water Development Board (TWDB). San Jacinto River Basin: Lakes in San Jacinto River Basin. https://www.twdb.texas.gov/surfacewater/rivers/river_basins/sanjacinto/index.asp. Accessed July 5, 2023.
39. Longley, W. L. (ed.) (1994). *Freshwater inflows to Texas bays and estuaries: ecological relationships and methods for determination of needs*. Texas Water Development Board and Texas Parks and Wildlife Department, Austin, TX.
40. Yao, Q., Joshi, S., Liu, K. B., Rodrigues, E., & Yin, D. (2022). A multi-decadal analysis of river discharge and suspended sediment load in three Texas coastal rivers in relation to hurricanes, seasonal rainfall, and ENSO. *Frontiers in Earth Science*, *10*, 886614.
41. Lee, M. T. (2010). A preliminary evaluation of Trinity River sediment and nutrient loads into Galveston Bay, Texas, during two periods of high flow. In *Joint Federal Interagency Conference 2010*.
42. Bodkin, L. J., & Oden, J. H. (2010). Streamflow and Water-quality Properties in the West Fork San Jacinto River Basin and Regression Models to Estimate Real-time Suspended-sediment and Total Suspended-solids Concentrations and Loads in the West Fork San Jacinto River and in the Vicinity of Conroe, Texas, July 2008-August 2009. US Department of the Interior, US Geological Survey.
43. Moffatt & Nichol (2010). *Galveston Bay Regional Sediment Management. Galveston, Texas*. Prepared for U.S. Army Corps of Engineers. https://reduceflooding.com/wp-content/uploads/2018/07/Galveston-Bay-Programmatic-RSM-Plan-Rev-1.pdf Accessed July 15, 2023.
44. Phillips, J. D. (2004). A sediment budget for Galveston Bay. Kentucky: Department of Geography, University of Kentucky.
45. Shepard, F. P. (1953). Sedimentation rates in Texas estuaries and lagoons. AAPG Bulletin, 37(8), 1919-1934.
46. Morton, R. A., & McGowen, J. H. (1980). Modern depositional environments of the Texas coast. University of Texas at Austin, Bureau of Economic Geology.
47. White, W. A., Calnan, T. R., Morton, R. A., Kimble, R. S., Littleton, T. G., McGowen, J. H., Nance, H.S. & Schmedes, K. E. (1985). Submerged lands of Texas, Galveston-Houston area: sediments, geochemistry, benthic macroinvertebrates, and associated wetlands. University of Texas at Austin, Bureau of Economic Geology.
48. U.S. Army Corps of Engineers. (1981). Wallisville Lake, Texas, post authorization change report. Main report and final environmental impact statement. Galveston District Galveston, TX. 526 pp.
49. White, W.A., and TR. Calnan. (1990). Sedimentation in fluvial-deltaic wetlands and estuarine areas, Texas Gulf coast: literature synthesis. Report to Texas Parks and Wildlife Department, by Bureau of Economic Geology, University of Texas at Austin, Austin, TX.
50. Slattery, M. C., Todd, L. M., Phillips, J. D., & Breyer, J. A. (2010). Holocene sediment accretion in the Trinity River delta, Texas, in relation to modern fluvial input. Journal of Soils and Sediments, 10, 640-651.

51. Du, J., Park, K., Dellapenna, T. M., & Clay, J. M. (2019). Dramatic hydrodynamic and sedimentary responses in Galveston Bay and adjacent inner shelf to Hurricane Harvey. Science of the Total Environment, 653, 554-564.
52. Freese and Nichols & Coast and Harbor Engineering (2016). Texas Coastal Sediment Sources, General Evaluation Study. Prepared for Texas General Land Office. https://glo.texas.gov/coastal-grants/_documents/grant-project/13-333-sediment-study.pdf (Accessed July 4, 2023).
53. Dunn, D. D., & Raines, T. H. (2001). *Indications and potential sources of change in sand transport in the Brazos River, Texas* (No. 2001-4057). US Department of the Interior, US Geological Survey.
54. Phillips, J. D. (2015). Hydrologic and geomorphic flow thresholds in the Lower Brazos River, Texas, USA. *Hydrological sciences journal*, *60*(9), 1631-1648.
55. Curtis, W. F., Culbertson, J. K., & Chase, E. B. (1973). *Fluvial-sediment discharge to the oceans from the conterminous United States* (Vol. 670). US Geological Survey.
56. Wurbs, R. A., Bergman, C. E., Carriere, P. E., & Walls, W. B. (1988). Hydrologic and institutional water availability in the Brazos River Basin. Texas Water Resources Institute.
57. Malito, J., & Mohrig, D. (2023). Intended vs unintended consequences of modifying coastal river channels. Authorea Preprints.
58. Fraticelli, C. M. (2006). Climate forcing in a wave-dominated delta: The effects of drought–flood cycles on delta progradation. Journal of Sedimentary Research, 76(9), 1067-1076.
59. Carlin, J. A., Dellapenna, T. M., Strom, K., & Noll IV, C. J. (2015). The influence of a salt wedge intrusion on fluvial suspended sediment and the implications for sediment transport to the adjacent coastal ocean: a study of the lower Brazos River TX, USA. Marine Geology, 359, 134-147.
60. Carlin, J. A., & Dellapenna, T. M. (2014). Event-driven deltaic sedimentation on a low-gradient, low-energy shelf: The Brazos River subaqueous delta, northwestern Gulf of Mexico. Marine Geology, 353, 21-30.
61. McGowen, J. H., L. E. Gamer, B. H. Wilkinson, and Bureau of Economic Geology. (1977). The Gulf Shoreline of Texas: Processes, Characteristics, and Factors in Use. Geological Circulars. Geological Circulars. University of Texas at Austin, Bureau of Economic Geology.
62. Chin, A., Harris, D.L., Trice, T.H., Given, J.L. (2002). Adjustment of stream channel capacity following dam closure, Yegua Creek, Texas. Journal of the American Water Resources Association 38, 1521-1531.
63. Andrews, F. L. (1989). Monthly and annual suspended-sediment loads in the Brazos River at Richmond, Texas, 1966-86 water years, Water-Resources Investigations Report. USGS Numbered Series. Austin, TX: U.S. Geological Survey
64. Paine, J. G., & Morton, R. A. (1989). Shoreline and vegetation-line movement, Texas Gulf Coast, 1974-1982.
65. Strom, K. (2013). Suspended sediment sampling and annual sediment yield on the lower brazos river. Department of Civil and Environmental Engineering, University of Houston
66. Carlin, J. A. (2013). *Sedimentation of the Brazos River System: Storage in the Lower River, Transport to Shelf and the Evolution of a Modern Subaqueous Delta* (Doctoral dissertation), Texas A&M University.
67. USACE. (2019). *Gulf Intracoastal Waterway, Brazos River Floodgates and Colorado River Locks, Texas*. Final Integrated Feasibility Report and Environmental Impact Statement. U.S. Army Corps of Engineers Galveston District Southwestern Division.

68. Texas Stream Team (2020). San Bernard Watershed Data Report. The Meadows Center for Water and the Environment, Texas State University.
69. Norris, C. W., Moulton, D. W., El-Hage, A., & Bradsby, D. (2005). Ecologically significant river and stream segments for Region H Water Resources Technical Series-WRTS-2005-01.
70. Kraus, N. C., & Lin, L. H. (2002). Coastal Processes Study of San Bernard River Mouth, Texas: Stability and Maintenance of Mouth (Vol. 2). US Army Corps of Engineers, Engineer Research and Development Center, Coastal and Hydraulics Laboratory.
71. Texas State Historical Association (TSHA). https://www.tshaonline.org/handbook/entries/san-bernard-river Accessed Nov 23, 2023.
72. Texas Water Development Board (TWDB). San Bernard River and Cedar Lakes Estuary. https://www.twdb.texas.gov/surfacewater/bays/minor_estuaries/san_bernard/index.asp. Accessed Sep. 20, 2023.
73. Sanchez, J. A., & Parchure, T. M. (2001). Study of complex flows in the lower San Bernard River, Texas.
74. Thomas, R., & Dunkin, L. (2012). E*rosion control and environment restoration plan development, Matagorda County*, Texas; Phase 1: Preliminary investigation. ERDC/CHL TR-12-11, Coastal and Hydraulics Laboratory, U.S. Army Engineer Research and Development Center, 3909 Halls Ferry Road, Vicksburg, MS 39180-6199.
75. Rosati III, J., Frey, A. E., & Thomas, R. C. (2013). *Erosion Control and Environment Restoration Plan Development: Matagorda County, Texas. Phase 2: Preliminary Design*. ERDC/CHL TR-12-11, Coastal and Hydraulics Laboratory, U.S. Army Engineer Researchand Development Center, 3909 Halls Ferry Road, Vicksburg, MS 39180-6199.
76. Neupane, R., Schoenbaechler, C. (2013). Coastal Hydrology for East Matagorda Bay. Texas Water Development Board. https://www.twdb.texas.gov/surfacewater/bays/minor_estuaries/east_matagorda/doc/TWDB_Hydrology_EastMatagorda_20230413.pdf
77. Gulf of Mexico and Adjacent Watersheds: East Matagorda Bay https://storymaps.arcgis.com/stories/6a5431bf3b504f82bc41c1f57fd9a339. Accessed Oct. 4, 2023
78. US Climate Data. Climate Matagorda Texas. https://www.usclimatedata.com/climate/matagorda/texas/united-states/ustx0844. Accessed Oct 4. 2023.
79. Austin, B., Kennedy, A., Osting, T., & Walker, C. (2015). Evaluation of Freshwater Delivery Alternatives to East Matagorda Bay.
80. Handbook of Texas Online. (2010). Texas State Historical Association (TSHA) web resource: https://www.tshaonline.org/handbook/entries/caney-creek-wharton-county. Accessed Nov. 23, 2023.
81. US Army Corps of Engineers. (2006). Lower Colorado River Basin Interim Feasibility Report and Phase I, Texas Integrated Environmental Assessment, Appendix F-Recreation.
82. Texas Commission on Environmental Quality (TCEQ). (2010). Central and Southeast Texas Recreational Use Attainability Analyses Project Caney Creek Above Tidal. https://wayback.archive-it.org/414/20190907211405/https://www.tceq.texas.gov/assets/public/waterquality/standards/ruaa/caney/CaneyCreekCompRUAAFinalReport.pdf . Accessed Nov 6, 2023
83. Johnston, S., Hoffman, W., Ranatunga, T. (2019). Technical Support Document for Two Total Maximum Daily Loads for Indicator Bacteria in the Caney Creek Watershed, Prepared

for Total Maximum Daily Load Program Texas Commission on Environmental Quality MC–203 P.O. Box 13087 Austin, Texas 78711-3087. https://www.tceq.texas.gov/downloads/water-quality/tmdl/caney-creek-linnville-bayou-recreational-115/115-caney-creek-tsd-2020-04.pdf. Accessed Nov 6, 2023.
84. Hamilton, P. B., Lin, L., & Jones, S. W. (2021). Investigation for Shoaling Reduction along the Gulf Intracoastal Waterway (GIWW) at Caney Creek, Sargent, Texas, ERDC/TN RSM-21-1.
85. McGowen, J. H. (1979). Geochemistry of bottom sediments--Matagorda Bay system, Texas. *Virtual Landscapes of Texas*.
86. Olariu, C., Liu, Z., Bailey, W., Jiang, X., Lu, K. (2023). Microplastic concentration in sediments and waters of Matagorda and San Antonio Bays: Initial assessment and mitigation plans. Activity Report on the Project-Period April 1st, 2023, to June 30th, 2023. https://mbmtrust.com/media/nckj0s3w/mbmt-ut-010-report-8-23.pdf. Accessed Oct. 4, 2023
87. Pollack, J. B., Palmer, T. A., & Montagna, P. A. (2011). Long-term trends in the response of benthic macrofauna to climate variability in the Lavaca-Colorado Estuary, Texas. Marine Ecology Progress Series, 436, 67-80.
88. Lee, T., Srinivasan, R., Moon, J., & Omani, N. (2011). Estimation of freshwater inflow to bays from gaged and ungaged watersheds. Applied engineering in agriculture, 27(6), 917-923.
89. Kammerer, J. C. (1990). Largest Rivers in the United States. United States Geological Survey. https://mbmtrust.com/media/nckj0s3w/mbmt-ut-010-report-8-23.pdf. Accessed Oct. 5, 2023
90. Tillman, F. D., Gangopadhyay, S., & Pruitt, T. (2020). *Trends in recent historical and projected climate data for the Colorado River Basin and potential effects on groundwater availability* (No. 2020-5107). US Geological Survey.
91. Texas Water Development Board (TWDB). River Basin. https://www.twdb.texas.gov/surfacewater/rivers/river_basins/index.asp Accessed Nov 08, 2023.
92. National Oceanic and Atmospheric Administration (NOAA). Climate Data Online. https://www.ncdc.noaa.gov/cdo-web/search. Accessed on 07 Dec 2023.
93. Texas Water Development Board (TWDB). Colorado River Basin. https://www.twdb.texas.gov/surfacewater/rivers/river_basins/colorado/index.asp Accessed Nov 08, 2023.
94. Texas Water Development Board (TWDB). Lavaca River Basin. https://www.twdb.texas.gov/surfacewater/rivers/river_basins/lavaca/index.asp Accessed Nov 08, 2023.
95. Texas Water Development Board (TWDB). Colorado-Lavaca Estuary (Matagorda Bay) https://www.twdb.texas.gov/surfacewater/rivers/river_basins/lavaca/index.asp. Accessed Nov 08, 2023.
96. Hydrology Report: Schoenbaechler, C., C. G. Guthrie, and Q. Lu. (2011) Coastal Hydrology for the Lavaca-Colorado Estuary, February 11, 2011, Texas Water Development Board, Austin, Texas. 18 pp.
97. McGowen, J. H., & Brewton, J. L. (1975). Historical changes and related coastal processes, gulf and mainland shorelines, Matagorda Bay area, Texas.
98. Morton, R. A., Pieper, M. J., & McGowen, J. H. (1976). Shoreline changes on Matagorda Peninsula (Brown Cedar Cut to Pass Cavallo): an analysis of historical changes of the Texas Gulf shoreline. *Geological Circulars*.

99. Bouma, A. H., and W. R. Bryant. (1969). *Rapid Delta Growth in Matagorda Bay, Texas, Lagunas Costeros Un Sinposio,* Nov., 171-189.
100. United States Geological Survey (USGS). USGS 08162000 Colorado Rv at Wharton, TX https://waterdata.usgs.gov/nwis/inventory/?site_no=08162000. Accessed 9 November 2023.
101. Buzan, D., Cook, B. P., Fontenot, M. M., Hardy, T., Hoffpauir, R. J., Kennedy, K., & Watters, S. P. (2011). Colorado and Lavaca Rivers and Matagorda and Lavaca Bays Basin and Bay Expert Science Team. Environmental Flow Regime Recommendations Report.
102. Wadsworth Jr, A. H. (1966). Historical deltation of the Colorado River, Texas.
103. White, W. A., and T. R. Calnan. (1987). *Colorado River diversion project reconnaissance work to establish monitoring stations in Matagorda BJY near the mouth of the Colorado River*. 10. draft report to Texas Parks and Wildlife Department.
104. Lambert, S. S., Willey, S. S., Campbell, T., Thomas, R. C., Li, H., Lin, L., & Welp, T. L. (2013). Regional sediment management studies of Matagorda Ship Channel and Matagorda Bay System, Texas.
105. Wilkinson, B. H., & Byrne, J. R. (1977). Lavaca Bay—transgressive deltaic sedimentation in central Texas estuary. *AAPG Bulletin*, *61*(4), 527-545.
106. BEG, Shoreline Movement in the Copano, San Antonio, and Matagorda Bay Systems, Central Texas Coast, 1930s to 2010s. https://www.beg.utexas.edu/research/programs/coastal/measurement-and-characterization-of-bay-shoreline-change. Accessed on 9 November 2023.
107. Moffat and Nichol. (2007). *Matagorda Ship Channel Improvement Project Point Comfort, Texas Sediment Study*. M&N Project No. 5669.
108. Agnew, M. (2018). Hydrodynamic evaluation of proposed navigation improvements at the Colorado River intersection with the Gulf Intra-Coastal Waterway. USACE New Orleans District.
109. San Antonio Bay, Handbook of Texas Online https://www.tshaonline.org/handbook/entries/san-antonio-bay. Accessed October 07, 2023.
110. Ockerman, D. J., & Slattery, R. N. (2008). Streamflow conditions in the Guadalupe River Basin, south-central Texas, water years 1987-2006—An assessment of streamflow gains and losses and relative contribution of major springs to streamflow (No. 2008-5165). US Geological Survey
111. Leitch, M. B. (2011). *Oxbow Lake sedimentation along the lower Guadalupe River, Texas* (Doctoral dissertation). The University of Texas at Austin
112. San Antonio River Authority. San Antonio River Basin. https://www.sariverauthority.org/education/san-antonio-river-basin. Accessed Nov 10, 2023.
113. J. Phillips. (2011). Channel Change Caused by Water and Sediment Distribution in the San Antonio River Deltaic Plain. *FINAL REPORT*, 2011.
114. Texas Water Development Board (TWDB). Guadalupe River Basin https://www.twdb.texas.gov/surfacewater/rivers/river_basins/guadalupe/index.asp. Accessed Nov 10, 2023.
115. Texas State Historical Association (TSHA). San Antonio River. https://www.tshaonline.org/handbook/entries/san-antonio-river. Accessed Nov 10, 2023.

116. Texas Water Development Board (TWDB). San Antonio River Basin https://www.tshaonline.org/handbook/entries/san-antonio-river. Accessed Nov 10, 2023
117. Armstrong, N. E. (1987). *The ecology of open-bay bottoms of Texas: A community profile*. US Department of the Interior, Fish and Wildlife Service, Research and Development, National Wetlands Research Center.
118. Britton, J.C. and B. Morton. (1989). Shore Ecology of the Gulf of Mexico. University of Texas Press, Austin. 387 pp.
119. Texas Water Development Board (TWDB). Guadalupe Estuary (San Antonio Bay) https://www.tshaonline.org/handbook/entries/san-antonio-river Accessed Nov 10, 2023.
120. Davis, R. A. (2017). Sediments of the Gulf of Mexico. *Habitats and Biota of the Gulf of Mexico: Before the Deepwater Horizon Oil Spill: Volume 1: Water Quality, Sediments, Sediment Contaminants, Oil and Gas Seeps, Coastal Habitats, Offshore Plankton and Benthos, and Shellfish*, 165-215.
121. Ward, G.H. (2012). Ecological Study of San Antonio Bay. The University of Texas at Austin. Prepared for Texas Water Development Board. https://www.twdb.texas.gov/publications/reports/contracted_reports/doc/0900010973_SanAntonioBay.pdf Accessed Dec 19, 2023.
122. Holley, E. R. (1992). *Sediment transport in the lower Guadalupe and San Antonio Rivers*. Texas Water Resources Institute.
123. Crow, C. L., Banta, J. R., & Opsahl, S. P. (2014). *Sediment characteristics in the San Antonio River Basin downstream from San Antonio, Texas, and at a site on the Guadalupe River downstream from the San Antonio River Basin, 1966-2013* (No. 2014-5048). US Geological Survey.
124. Ockerman, D. J., Banta, J. R., Crow, C. L., & Opsahl, S. P. (2015). Sediment Conditions in the San Antonio River Basin Downstream from San Antonio, Texas, 2000-13. US Department of the Interior, US Geological Survey.
125. Donaldson, A. C., Martin, R. H., & Kanes, W. H. (1970). Holocene Guadalupe delta of Texas gulf coast.
126. White, W. A., & Morton, R. A. (1987). Historical shoreline changes in San Antonio. Espiritu Santo, and Mesquite Bays: The University of Texas at Austin, Bureau of Economic Geology, Geological Circular, 87-1.
127. Chen, G. F. (2010). Freshwater inflow recommendation for the Mission-Aransas estuarine system. Texas Parks and Wildlife Department, Austin, TX, 120.
128. Evans, A., Madden, K., & Palmer, S. (2012). The ecology and sociology of the Mission-Aransas estuary: an estuarine and watershed profile.
129. Texas Water Resources Institute (2019). Mission and Aransas River Watersheds Protection Plan
130. Texas State Historical Association (TSHA). Aransas River. https://www.tshaonline.org/handbook/entries/aransas-river. Accessed Nov 10, 2023.
131. Chandler, C., Knox, J., Byrd, L. (Eds.). (1981). Nueces and Mission-Aransas Estuaries: A Study of the Influence of Freshwater Inflows. Limited Publication 108. Texas Department of Water Resources, Austin, 362 pp.
132. Smith, E. H., and S. J. Dilworth. (1999). Mission/Aransas Watershed Wetland Conservation Plan. Texas General Land Office.

133. Ward, G.H., and N.E. Armstrong. (1997). Ambient water, sediment, and tissue quality of the Corpus Christi Bay National Estuary Program Area, present status and historical trends. CCBNEP-23. Texas Natural Resource Conservation Commission, Austin, Texas.
134. Welborn, C.T. and R.B. Bezent. (1978). Sediment Yields for Selected Streams in Texas. U.S. Geological Open-File Report 78-83
135. Texas Department of Water Resources. (1982). Nueces and Mission-Aransas Estuaries: An Analysis of Bay Segment Boundaries, Physical Characteristics, and Nutrient Processes. LP-83. Texas Department of Water Resources, Austin, TX
136. Paine, J. G. (1993). *Historical Shoreline Changes in Copano, Aransas, and Redfish Bays, Texas Gulf Coast* (Vol. 93, No. 1). Bureau of Economic Geology, the University of Texas at Austin.
137. Troiani, B. T., Simms, A. R., Dellapenna, T., Piper, E., & Yokoyama, Y. (2011). The importance of sea-level and climate change, including changing wind energy, on the evolution of a coastal estuary: Copano Bay, Texas. Marine Geology, 280(1-4), 1-19.
138. Goff, J. A., Swartz, J. M., Gulick, S. P., Dawson, C. N., & de Alegria-Arzaburu, A. R. (2019). An outflow event on the left side of Hurricane Harvey: Erosion of barrier sand and seaward transport through Aransas Pass, Texas. Geomorphology, 334, 44-57.
139. Robert S. Weddle, "Nueces River," Handbook of Texas Online. https://www.tshaonline.org/handbook/entries/nueces-river. Accessed October 27, 2023
140. Texas Water Development Board (TWDB). Nueces River Basin. https://www.twdb.texas.gov/surfacewater/rivers/river_basins/nueces/index.asp. Accessed Nov 17, 2023.
141. Yeager, K. M., Santschi, P. H., Schindler, K. J., Andres, M. J., & Weaver, E. A. (2006). The relative importance of terrestrial versus marine sediment sources to the Nueces-Corpus Christi Estuary, Texas: An isotopic approach. *Estuaries and coasts*, *29*, 443-454.
142. Baird, C., Jennings, M., Ockerman, D., & Dybala, T. (1996). Characterization of nonpoint sources and loadings to the Corpus Christi Bay National Estuary Program study area. Final report (No. PB-96-196845/XAB). Natural Resources Conservation Service, Washington, DC (United States).
143. Corpus Christi Bay. GulfBase. Resource Database for Gulf of Mexico Research. Texas A&M University-Corpus Christi: Harte Research Institute for Gulf of Mexico Studies. (https://web.archive.org/web/20100924182710/http://gulfbase.org/bay/view.php?bid=ccb. Accessed Oct. 26, 2023.
144. Texas Water Development Board (TWDB). Nueces Estuary (Corpus Christi Bay). https://www.twdb.texas.gov/surfacewater/bays/major_estuaries/nueces/index.asp. Accessed November 17, 2023.
145. Leibbrand, N. F. (1987). Estimated sediment deposition in Lake Corpus Christi, Texas, 1977-1985. US Geological Survey Open File Report, 87-239.
146. Texas Commission on Environmental Quality (TCEQ). (2023). "Water Quality Portal Data Sites for TCEQMAIN." https://www.waterqualitydata.us/provider/STORET/TCEQMAIN/. Accessed August 25, 2023.
147. Ockerman, D. J., Heitmuller, F. T., & Wehmeyer, L. L. (2013). Sources of suspended-sediment loads in the lower Nueces River watershed, downstream from Lake Corpus Christi to the Nueces Estuary, south Texas, 1958–2010 (No. 2013-5059). US Geological Survey.
148. Paudel, B. (2014). "Interaction between suspended sediment, nutrients and freshwater inflow in Texas estuaries." *Ecological Informatics*.

149. Nicolau, B. A. (2001). "Water Quality and Biological Characterization of Oso Creek & Oso Bay, Corpus Christi, Texas." *Center for Coastal Studies, Texas A&M University Corpus Christi*.
150. EPA, U. (2023). "How's My Waterway? Corpus Christi Oso Creek." Data and Tools. https://mywaterway.epa.gov/monitoring-report/NWIS/USGS-TX/USGS-08211525/. Accessed September 24, 2023.
151. Morton, R. A., Paine, J. G., & Robinson, D. E. (1983). *Historical Monitoring of Shoreline Changes in Corpus Christi, Nueces, and Oso Bays*. Bureau of Economic Geology, University of Texas at Austin
152. Shideler, G. L., Stelting, C. E., & McGowen, J. H. (1981). Maps showing textural characteristics of benthic sediments in the Corpus Christi Bay estuarine system, south Texas: US Geological Survey Misc. *Field Studies Map MF-1275*.
153. Santschi, P. H., & Yeager, K. M. (2004). *Quantification of Terrestrial and Marine Sediment Sources to a Managed Fluvial, Deltaic and Estuarine System: The Nueces-Corpus Christi Estuary, Texas*. Lab. for Oceanographic and Environmental Research, Department of Marine Science, Texas A & M University at Galveston.
154. Morton, R. A., and Pieper, M. J. (1977). Shoreline Changes on Mustang Island and North Padre Island (Aransas Pass to Yarborough Pass): An Analysis of Historical Changes of the Texas Gulf Shoreline: The University of Texas at Austin, Bureau of Economic Geology, Geological CIrcular 77-1, 45 p. doi.org/10.23867/gc7701D
155. Simms, A.R., Aryal, N., Miller, L., Yokoyama, Y. (2010) The incised valley of Baffin Bay, Texas: a tale of two climates. Sedimentology 57, 642-669.
156. TPWD, Texas Parks and Wildlife Department. Upper Laguna Madre. https://tpwd.texas.gov/landwater/water/habitats/bays/ulm/ulm_index.phtml. Accessed November 18, 2023.
157. Gregory, L., Escamilla, C, Rios, E (2022). San Fernando and Petronila Creeks Watershed Protection Plan, Texas Water Resources Institute Technical Report – 541June 2022College Station, Texas
158. Wetz, M.S., Cira, E.K., Sterba-Boatwright, B., Montagna, P.A., Palmer, T.A., Hayes, K.C. (2017) Exceptionally high organic nitrogen concentrations in a semi-arid South Texas estuary susceptible to brown tide blooms. Estuarine, Coastal and Shelf Science 188, 27-37.
159. White WA, Calnan TR, Morton RA, Kimble RS, Littleton TG, McGowen JH, Nance HS (1989) Submerged lands of Texas: Kingsville area: Sediments, geochemistry, benthic macroinvertebrates, and associated wetlands. Bureau of Economic Geology, Austin, TX, USA
160. Aryal, N. (2007). *Depositional History of Upper Baffin Bay, Texas* (Doctoral dissertation, Oklahoma State University).
161. Shrestna, A. (2000). *Development of a two-dimensional hydrodynamic model of Baffin Bay, Texas*. Texas A&M University-Kingsville.
162. Jones, K., Pan, X., Garza, A., & Lloyd-Reilley, J. (2010). Multi-level assessment of ecological coastal restoration in South Texas. Ecological Engineering, 36(4), 435-440.
163. Behrens, E. W., and L. S. Land. (1972). "Subtidal Holocene dolomite, Baffin Bay, Texas." *Journal of Sedimentary Research*, 42 (1): 155–161. https://doi.org/10.1306/74D724C3-2B21-11D7-8648000102C1865D

164. Folk, R.L., Siedlecka, A. (1974) The "schizohaline" environment: its sedimentary and diagenetic fabrics as exemplified by Late Paleozoic rocks of Bear Island, Svalbard. Sedimentary Geology 11, 1-15.
165. Morton, R. A., Ward, G. H., & White, W. A. (2000). Rates of sediment supply and sea-level rise in a large coastal lagoon. Marine Geology, 167(3-4), 261-284.
166. Besonen, M., E. M. Hill, and C.-P. Investigator. (2016). "Baffin Bay Sediment Core Profiling for Historical Water Quality
167. Lower Rio Grande Basin Study Under the Authority of the SECURE Water Act (Public Law 111-11) Great Plains Region, Oklahoma-Texas Area Office. https://www.usbr.gov/watersmart/bsp/docs/finalreport/LowerRioGrande/LowerRioGrandeBasinStudy.pdf. Accessed November 18, 2023.
168. Arroyo Colorado Watershed. https://arroyocolorado.org/about/watershed/. Accessed November 18, 2023.
169. Whorter, Mac William (1952). Texas State Historical Association (TSHA). Arroyo Colorado. https://www.tshaonline.org/handbook/entries/arroyo-colorado. Accessed on 19 November 2023
170. Kannan, N. (2012). SWAT modeling of the Arroyo Colorado Watershed. Texas Water Resources Institute.
171. Flores, J., Benavides, J. A., & Cawthon, T. (2017). Update to the Arroyo Colorado watershed protection plan. *Texas Water Resources Institute Technical Report—504*, 3-152.
172. Texas Water Development Board (TWDB). Laguna Madre Estuary. https://www.twdb.texas.gov/surfacewater/bays/major_estuaries/laguna_madre/index.asp. Accessed November 07, 2023.
173. Schoenbaechler, C., Guthrie, C. G., & Lu, Q. (2011). Coastal hydrology for the Laguna Madre Estuary, with emphasis on the upper Laguna Madre. Texas Water Development Board, Austin, Texas, 28.
174. Alan Plummer Associates, Inc. (APAI)(2006). *Feasibility Study for Habitat Restoration/Modifi cation to Improve Water Quality in the Arroyo Colorado: Strategies to Enhance Both Water Quality and Habitat*, prepared in association with CRESPO Consulting Services, Inc. Final Report for Texas Parks and Wildlife Department Project No. 101732, Contract No. 153411. January 18, 2006. https://arroyocolorado.org/media/vlqbpw0v/habitatfeasibilitystudy-finaltechnicalreport.pdf. Accessed Dec 10, 2023.
175. Texas Commission on Environmental Quality (TCEQ), (2007). A Watershed Protection Plan for the Arroyo Colorado Phase I. https://www.tceq.texas.gov/downloads/water-quality/tmdl/arroyo-colorado-watershed-plan-13/13-arroyo-wpp.pdf. Accessed on Dec 06, 2023
176. Henningson, Durham, and Richardson (HDR). (2009). *Desktop Evaluation of Shoaling: Federal Feasibility Study to Deepen and Widen the Brownsville Ship Channel.* Corpus Christi, TX. Report prepared for Port of Brownsville, TX. Corpus Christi, TX: HDR.
177. Freese and Nichols, F., and N. (2021). Sediment Budget Analysis and Modeling of the Texas Coast. Task 2D.1b - Region 4 Sediment Budget. Prepared for *Texas General Land Office*.
178. Texas Water Development Board (TWDB). River Basins. https://www.twdb.texas.gov/surfacewater/rivers/river_basins/index.asp. Accessed November 12, 2023.

179. Benke, Arthur C.; Cushing, Colbert E. (2005). Rivers of North America. Academic Press. pp. 186–192. ISBN 978-0120882533.
180. Metz, C. Leon (1952). Texas State Historical Association (TSHA). Rio Grande. https://www.tshaonline.org/handbook/entries/rio-grande. Accessed on 19 November 2023.
181. Moeser, C. D., Chavarria, S. B., & Wootten, A. M. (2021). Streamflow response to potential changes in climate in the upper Rio Grande basin. US Department of the Interior, US Geological Survey.
182. Texas Water Development Board (TWDB). Texas Lakes and Reservoir. https://www.twdb.texas.gov/surfacewater/rivers/reservoirs/. Accessed November 13, 2023.
183. Texas Water Development Board (TWDB). Rio Grande Estuary. https://www.twdb.texas.gov/surfacewater/bays/minor_estuaries/rio_grande/index.asp. Accessed November 13,2023.
184. USGS. (2016). Suspended-Sediment Transport Dynamics of the Rio Grande/Rio Bravo, U.S. Geological Survey. https://www.usgs.gov/centers/southwest-biological-science-center/science/suspended-sediment-transport-dynamics-rio. Accessed September 26, 2023.
185. Reclamation. (2021). *Rio Grande Basin SECURE Water Act Section 9503(c) Report to Congress*. United States Congress, U.S. Bureau of Reclamation.
186. Myers, R., and M. Nisbet. (2022). *Falcon Lake Water Levels and Recreational Fisheries*. Texas Parks and Wildlife Department.
187. Metre, P. C. V., B. J. Mahler, and E. C. Callender. (1997). *Water-quality trends in the Rio Grande/Rio Bravo Basin using sediment cores from reservoirs*. *Fact Sheet*. U.S. Geological Survey
188. Horowitz, A. J., Elrick, K. A., & Smith, J. J. (2001). Annual suspended sediment and trace element fluxes in the Mississippi, Columbia, Colorado, and Rio Grande drainage basins. *Hydrological Processes*, *15*(7), 1169-1207.
189. Davila, E. (2021). Assessing the Anthropogenic Footprint on the Channel Sinuosity of the Rio Grande the Delta.
190. Jepsen, R., Langford, R., Neu, R., Chapin, D. M., & Buhalts, R. (2001). Sediment Erosion and Transport at the Rio Grande Mouth.
191. Ernest, A., Bokhim, B., Chang, N. B., & Huang, I. J. (2007). Fluvial Geomorphologic and Hydrodynamic Assessment in the Tidal Portion of the Lower Rio Grande River, US-Mexico Borderland. Journal of Environmental Informatics, 10(1), 10.
192. Moore, S., Heise, E. A., Grove, M., Reisinger, A., & Benavides, J. A. (2021). Evaluating the impacts of dam construction and longshore transport upon modern sedimentation within the Rio Grande Delta (Texas, USA). *Journal of Coastal Research*, *37*(1), 26-40.
193. USACE. 2016. USACE Galveston District Navigation Data Center Database. http://www.navigationdatacenter.us/data/data1.htm. Accessed Dec 10, 2023.
194. Morton, R. A., Nava, R. C., & Arhelger, M. (2001). Factors controlling navigation-channel shoaling in Laguna Madre, Texas. *Journal of waterway, port, coastal, and ocean engineering*, *127*(2),

UNIVERSITY OF TEXAS ARLINGTON

COASTAL MANAGEMENT PROGRAM – CYCLE 26

BEST PRACTICES IN MODELING SEDIMENT TRANSPORT AND BUDGET ALONG THE TEXAS COAST

Task 2: Review of State-of-the-Art Morphodynamical Modeling Practices

(CONTRACT NO. 23-020-018-D867)

Prepared for:

Texas General Land Office

1700 N. Congress Avenue, Mail Code 158

Austin, TX 78701

Submitted by:

Habib Ahmari, Ph.D., P.E.

Nabila Khandaker, M.Sc.

Yu Zhang, Ph.D., P.E.

Behzad Nazari, Ph.D., P.E.

The University of Texas at Arlington, Arlington, Texas, USA

May 2024

EXECUTIVE SUMMARY

The Texas coastline faces persistent challenges related to coastal erosion, influenced by storm events, sea-level rise, and human activities such as coastal development. Hurricanes and tropical storms significantly contribute to erosion, gradually wearing away the land. Rising sea levels, driven by climate change, exacerbate erosion by increasing the frequency and severity of flooding events. Human interventions, including infrastructure projects and navigation channels, can alter natural sediment dynamics and impact erosion rates.

Sediment dynamics in coastal zones are inherently challenging to quantify or predict due to the complexity of processes governing erosion on land and sediment transport along channels, in estuaries, and offshore waters. This complexity leads to significant uncertainties in sediment budget estimates, stemming from mechanistic deficiencies in transport models and a lack of accurate sediment supply information. Sediment budget analysis is often conducted using quantitative methods and hydro-geomorphological models.

This study aimed to conduct a thorough literature review on the current state of practice in sediment dynamics modeling in coastal areas. The objectives included examining approaches for modeling sediment dynamics in coastal rivers and estuaries, identifying the advantages and shortcomings of widely used hydro-morphodynamic models, and exploring the uncertainties and errors in current sediment transport modeling practices.

Quantitative sediment budget models are simple, efficient, and cost-effective, integrating various data sources to provide a comprehensive overview of sediment dynamics over large scales. However, their simplicity results in limited detail and accuracy, high uncertainty, and a static nature that fails to capture dynamic processes effectively. In contrast, hydro-geomorphological models offer detailed process representation and predictive capabilities, making them valuable for scenario testing and planning. They simulate interactions between hydrodynamics, sediment transport, and morphological changes accurately, but are complex, resource-intensive, and require extensive data and user expertise.

The report provides a comprehensive review of nine widely-used hydro-geomorphological models, emphasizing their application in coastal settings. The models evaluated include Delft3D, TELEMAC, MIKE 21, ADCIRC, XBeach, LITPAK, CoSMoS, GENESIS, and SBEACH. The assessment focused on each model's ability to reproduce the complex relationships between hydrodynamics, sediment transport, and morphological changes.

This review highlights the importance of selecting the appropriate model based on project requirements and environmental conditions. For optimal results, the model's setup, input requirements, and output capabilities must align with the project's objectives. The comparison study not only clarifies the capabilities of these models but also identifies potential areas for future improvement.

TABLE OF CONTENTS

EXECUTIVE SUMMARY **1**

TABLE OF CONTENTS **2**

1. INTRODUCTION **6**

1.1 Objectives 6
1.2 Significance of the Study 6
1.3 Structure of the Report 7

2. SEDIMENT BUDGET QUANTITATIVE MODELS **8**

2.1 Sediment Budget Analysis System (SBAS) 8
2.1.1 SBAS/SBAS-A Inputs and Outputs 9
2.1.2 SBAS/SBAS-A Pros and Cons 10
2.2 Sediment Budget Calculator (SBC) 10
2.2.1 SBC Inputs and Outputs 10
2.2.2 SBC's Pros and Cons 11
2.3 Example Studies 11

3. HYDRO-GEOMORPHOLOGICAL MODELS **18**

3.1 Delft3D 20
3.2 TELEMAC 22
3.3 MIKE 21 26
3.4 ADCIRC 29
3.5 XBeach 32
3.6 LITPACK 35
3.7 CoSMoS 38
3.8 GENESIS 40
3.9 SBEACH 43
3.10 Examples of Morphodynamical Modeling in Coastal Areas 47
3.11 Applications of Remote Sensing in Study of Sediment Dynamics in Coastal Areas 49

4. SUMMARY AND CONCLUSIONS **50**

4.1 Summary of Evaluating Hydro-geomorphological Models for Coastal Applications 50
4.2 Conclusions 53

REFERENCES **54**

LIST OF FIGURES

Figure 2.1 SBAS Toolbars and Button Functions [1]. 9

Figure 2.2 Screenshot of the SBAS setup in ArcGIS tracking the sediment budget in Chandeleur Islands to Breton Island study area for the 2007–2015 period. The polygons represent the accretion (green) and erosion (red) cells and are attributed with the net volume change (ΔV) [4]. 12

Figure 2.3 Map of littoral cells in the Chandeleur Islands to Breton Island study area for the period of 2007-2015. The net volume change (ΔV) is positive (green) or negative (red). Blue arrows represent sediment flux direction from sediment sources (Q_{source}) sediment sinks (Q_{sink}) [4]. 13

Figure 2.4 Kahului Region sediment budget developed using SBAS for ArcGIS-10 [6]..... 14

Figure 2.5 Kihei Region sediment budget developed using SBAS for ArcGIS-10 [6]. 15

Figure 2.6 Masonboro Inlet, North Carolina sediment budget analysis cells and the rate of sediment fluxes between the cells [7]. 16

Figure 2.7 Volume change in sediment budget cells for Pinellas counties beaches [8]. 17

Figure 3.1 (a) System architecture of Delft3D [10], and (b) Dynamic exchange of data among the modules [13]. 20

Figure 3.2 Delf3D outputs showing total sediment transport (TST) in the delta area of the Rhone River in the Mediterranean Sea [22]. 22

Figure 3.3 An Example of interaction among several TELEMAC modules including Waves (TOMAWAC), Flow (TELEMAC-2D), and Sediment Transport (SISPHE) [30]. 23

Figure 3.4 Output of TELEMAC showing sediment transport along the Texas Coast (Cameron, Kenedy, and Willacy counties). Blue indicates negligible transport, while vectors show the transport direction. The scale bar colors denote the sediment transport rate or the amount that would be trapped in the unit area ($ft^3/s/ft$) [30]. 25

Figure 3.5 Interaction among MIKE 21 wave (SW), hydrodynamics (HD), and sand transport (ST) modules [42]. 27

Figure 3.6 Output of the MIKE 21 model presenting morphological bed evolution of the Port of Rethymno in Greece over 7 days, resulting in the east to west sediment transport and accretive patterns on the beach face [47]. 28

Figure 3.7 Flow diagram of the coupled ADCIRC-2D hydrodynamic and SWAN wave models [53]. 30

Figure 3.8 Sediment deposition in the James River, Virginia after dredging the navigation channel and placement of dredged materials in the designated site. The simulation conducted

using ADCIRC for the period of Jan 14-Feb 14, 2000 showed that most placement sediments stayed in the designated site, with some accumulating on nearby shoals and downstream [56]. 31

Figure 3.9 XBeach model architecture and interconnection among different modules (Arrows indicate connectivity, and terms in italics show relevant output parameters) [59]. 33

Figure 3.10 Bed Elevation of Maengbang beach, South Korea: (a) Before the storms (white dash line: position of the crescentic bar), (b) After the storms (white dash line: position of the longshore bar), and (c) Elevation difference and closure depth of sediment transport between before and after the storms (red dash line: depth of closure with little sediment transport). These bed elevation data were used to model erosion and morphological changes in the surf zone due to four consecutive typhoons using XBeach [64] 34

Figure 3.11 Accumulation and retreat areas along the shoreline of the Gulf of Manfredonia, Italy simulated using LITPACK. Shoreline accretion is evident in Cell I near the Port of Margherita di Savoia and in Cell III near the Port of Barletta. In contrast, significant erosion occurred in Cell II, near the Ofanto River [75]. 37

Figure 3.12 CoSMoS simulation results for long-term projected cliff retreat and sandy beach shoreline change under various sea level rise scenarios at seaward lagoon entrance of Del Mar, California [84]. 39

Figure 3.13 Relation between GENESIS and RCPWAVE in the overall calculation flow [87]. 41

Figure 3.14 Rate of shoreline change of Tanjung Motong Coast simulated using GENESIS. After processing 1990 and 2014 Landsat data, the digitized shorelines were overlaid to identify changes over 24 years, revealing erosion and sedimentation areas. The shoreline change rate at the coast was analyzed across 72 stations at 100-meter intervals [85]. 42

Figure 3.15 Schematic diagram of the four sediment transport regions determined by cross-shore wave height profile [98]. 45

Figure 3.16 SBEACH analysis reaches along Bogue Banks of Carteret County in North Carolina. The limits of each SBEACH analysis reach and the adjusted long-term erosion rates, along with survey transects from the Bogue Banks Beach and Nearshore Mapping Program (BBBNMP). Representative profiles for each reach were created using BMAP (Beach Morphology Analysis Package) within CEDAS [101]. 46

LIST OF TABLES

Table 3.1 General information and main features of several hydro-geomorphological models utilized in coastal areas. 19

Table 4.1 Capabilities of several hydro-geomorphological models in simulating sediment dynamics in coastal area. 52

1. INTRODUCTION

Coastal regions serve as dynamic interfaces where land and sea converge, shaping unique ecosystems vital for diverse flora and fauna. At the center of this dynamic equilibrium lies the perpetual movement and interaction of sediments along the coastline. The continuous processes of erosion, sediment transport, and deposition, driven by waves, tides, and currents influenced by meteorological and oceanographic forces, continually reshape coastlines. Understanding these processes is not only essential for comprehending the evolving physical characteristics of coastal areas but also for elucidating their broader ecological and societal implications.

The Texas Coast, characterized by diverse landforms, climates, and drainage systems, exhibits correspondingly varied coastal sediment processes. Excessive sediment deposition and shoreline erosion pose significant challenges to the economic vitality of coastal communities. Moreover, human-induced disturbances such as damming and land development further complicate these processes, impacting the delicate balance of sedimentation. In response to these challenges, the Texas General Land Office (TGLO) is leading efforts to develop a coordinated plan for sedimentation management along the Texas Coast. A critical step in this process is a thorough review of the state of practice of morphodynamic modeling in coastal areas. To address this need, a comprehensive review of widely-used software was conducted and presented in this report.

1.1 Objectives

The primary objective of this study was to conduct a comprehensive literature review, examining modeling-based investigations undertaken over the past decade related to hydro-morphodynamic processes in coastal zones worldwide that resemble the Texas Coast. By conducting this review, our aim was to achieve the following key goals:

- Examining the approaches for modeling sediment dynamics in coastal rivers and estuaries.
- Identifying the pros and cons of widely-used hydro-morphodynamic models.
- Exploring the uncertainties and errors of current sediment transport modeling practices and offering recommendations for best practices to inform the Texas General Land Office (TGLO) Texas Sediment Management Plan.

1.2 Significance of the Study

Several numerical models have been developed for sediment budget analysis in coastal areas. These models simulate the processes of sediment transport, erosion, and deposition along coastlines. When conducting sediment budget analysis, the choice of model depends on the specific characteristics and processes of the coastal area under study. It is important to note that model selection should align with the goals and scope of the analysis, considering factors such as the scale of the study area, data availability, and sedimentation processes.

Hydro-geomorphological models are considered the most accurate approach to sediment budgeting in coastal areas. Unlike quantitative sediment budget models, these models offer a

comprehensive understanding of sediment dynamics by estimating sediment quantities and providing additional information such as sediment fluxes and transport pathways. This comprehensive report serves as a guide to the capabilities of the hydro-geomorphological models commonly used for simulating sediment dynamics in coastal areas. It offers insights into the required input data for these models, examines the advantages and disadvantages of each, and outlines the specific outputs they generate. By examining these aspects, stakeholders and practitioners gain a comprehensive understanding of the strengths and limitations of different models, enabling them to make informed decisions in coastal management and conservation efforts.

1.3 Structure of the Report

Chapter 1 serves as an introductory section to this report. Chapter 2 provides a brief overview of sediment budget quantitative models for coastal regions. Chapter 3 presents an in-depth review of nine widely-utilized hydro-morphodynamic models employed in coastal areas, with a particular emphasis on their capabilities, model architecture, advantages and disadvantages, input and output, and examples of applications in coastal areas. Chapter 4 consolidates the findings of this review and highlights the most recent advances in numerical models that can be adopted for sediment modeling of Texas Coast areas.

2. SEDIMENT BUDGET QUANTITATIVE MODELS

A sediment budget is a record of sediment sources and sinks within a defined area or a series of interconnected areas over a given time period. Sediment budget calculation entails balancing the incoming and exiting sediment in each location, and thus for the overall system, in order to match the rate of sediment volume change in the study region. Sediment budget tools are essential for understanding the generation, distribution and movement of sediments in environments such as rivers and coastal areas. There are several sediment budget tools available, each designed for a particular environment. Tools developed for coastal locations help to understand the distribution of sediment specific to these places, while those developed for riverine regions address issues related to river sedimentation. In colder climates, where specific factors such as ice cover and permafrost affect sedimentation processes, there are also tools designed specifically for these locations.

The Sediment Budget Analysis System (SBAS), Sediment Budget Analysis System for Arc GIS (SBAS-A), and Sediment Budget Calculator (SBC) are some of the tools developed for sediment budget analysis in coastal areas that are developed by the U.S. Corps of Engineers. The details of these models and their applications in coastal area sediment budget analysis are presented in the following sections.

2.1 Sediment Budget Analysis System (SBAS)

The SBAS is a tool that allows local (project-level) sediment budget to be characterized within one or more regional sediment budgets. Features of SBAS have been designed to facilitate creation and display of both the local and regional sediment budgets. SBAS is available in two versions: SBAS for ArcGIS (SBAS-A) and SBAS Standalone. The SBAS Standalone is designed for PC application with the option to use non-georeferenced images as a background for local and regional sediment budgets. SBAS-A was developed to provide the sediment budget capability within the ArcGIS environment. The SBAS can be utilized to design sediment budget cells, sources, and sinks using a graphical interface. After defining a sediment budget alternative and creating sediment budget cells with sources and sinks, values can be assigned to the various components of the sediment budget topology. The SBAS can also import geo-referenced photos. It translates the coordinate system of the map to the project coordinate system. In the sediment budget, many pictures (maps, aerial shots, contour maps, etc.) can be stacked. The SBAS supports 55 different map coordinate systems. **Figure 2.1** shows the SBAS Toolbars and button functions [1].

Sediment Budget Analysis System for Arc GIS (SBAS-A)

The SBAS-A was developed specifically for use with ESRI's ArcMap environment. The SBAS-A enables users to use the standard spatial tools included in the ArcView environment. If a sediment budget is created in stand-alone version of SBAS then it can be exported as ArcMap-ready shapefiles and sediment budgets created with SBAS-A can also be displayed in SBAS-

Stand-Alone [2]. The main difference between the older and the latest version of SBAS, which was developed in 2020, is a custom toolbar for ArcGIS 10 and later versions and ArcGIS Pro. The latest version allows the user to import existing GIS files or data from GenCade, a shoreline change model, as input for the sediment budget. It can export the sediment budget data as CSV files or share them online using ArcGIS Online or Portal for ArcGIS. It has a more user-friendly interface and workflow, with fewer steps and dialogs to create and edit a sediment budget [3].

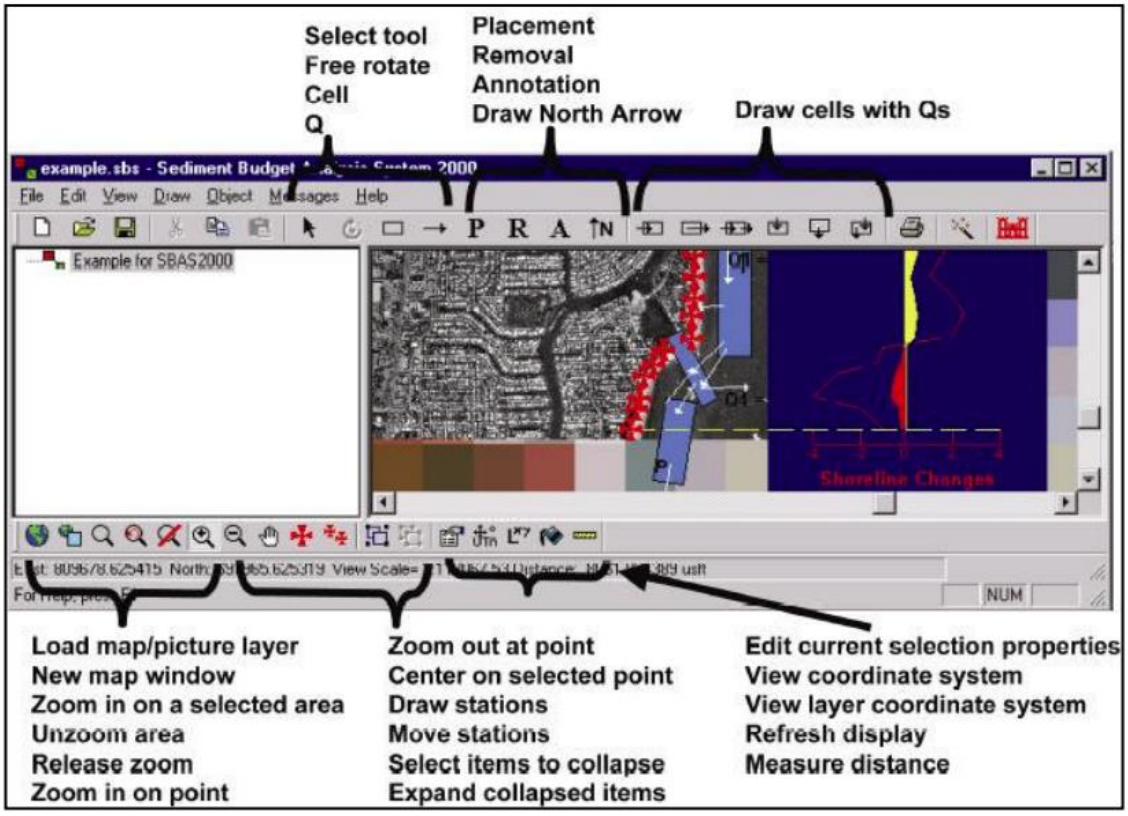

Figure 2.1 SBAS Toolbars and Button Functions [1].

2.1.1 SBAS/SBAS-A Inputs and Outputs

The input data for SBAS-A can be any geospatial datasets that ArcMap can translate, such as georeferenced aerial photography, beach profile surveys, shoreline position data, dredging history, coastal process, and bathymetry surveys. The output data can be viewed spatially in the data frame, and its attributes can be viewed in the associated database file [2]. The output data for SBAS standalone version can be any image files that SBAS can import, such as .bmp, .jpg, .png, or .tif. The output data can be exported as .csv files that contain the sediment budget values and uncertainties [1].

2.1.2 SBAS/SBAS-A Pros and Cons

SBAS is a free, open-source toolset compatible with ArcGIS, offering extensive capabilities in coastal sediment analysis. It supports a diverse range of data types, including geospatial datasets, images, GenCade models, CSV files, and online platform data. A key feature in ArcView is its ability to overlay littoral cells and sediment pathways onto aerial images, enhancing the understanding of nearshore sediment dynamics and cell interactions. The SBAS's ability to create irregular polygons for representing littoral cells makes it particularly effective for analyzing shorelines with complex geomorphological characteristics.

In coastal regions characterized by a seasonal wave climate with significant variations in wave energy, amplitude, and direction, calculating field data using SBAS can be challenging. Factors such as bi-directional sediment transport and changes in annual gross transport direction due to storm strength and climatic conditions complicate this process. Additionally, the coastline's numerous bays and variations in orientation over short distances (tens of miles) can dramatically alter regional longshore transport rates and directions. Furthermore, cross-shore sediment transport, especially during large storms or hurricanes, becomes a significant factor in these areas, particularly where wide, fringing reefs are present, adding to the complexity of accurately assessing sediment transport patterns [4].

2.2 Sediment Budget Calculator (SBC)

The Sediment Budget Calculator (SBC) is an online tool developed by the U.S. Corps of Engineers that calculates viable solutions for an inlet and adjacent beach sediment budget. The SBC applies the Bodge Method to determine sediment budget solutions. The Bodge Method examines all viable solutions based on user-defined constraints and known site conditions. The method uses sediment transport pathways to analyze an idealized inlet. It considers sediment transport pathways, including longshore sand transport rates, inlet processes, bypassing, jetty performance, and volume change rates from adjacent beaches, engineering activities, river influx, and gross change in the inlet system. These solutions provide a range of sediment budget scenarios or can be used to present a solution with uncertainty values to account for the variability in coastal processes and volume changes within the littoral system [5].

2.2.1 SBC Inputs and Outputs

By introducing site-specific parameters and known volume change rates, the SBC applies the Bodge Method to calculate the sediment budget solutions. The tool generates plots and data that show the fluxes and volume changes associated with the selected solution. It requires specific data inputs such as sand transport rates, inlet processes, and volume change rates. It also allows users to formulate traditional sediment budgets and consider different scenarios by selecting different data points. The outputs of the SBC include a family of viable sediment budget solutions for an inlet and adjacent beach. These outputs help in understanding the variability in coastal processes and the resulting volume changes within the littoral system [5].

2.2.2 SBC's Pros and Cons

The SBC is easy to use and does not require any software installation or GIS skills. It applies the Bodge Method, which is a widely accepted and robust method for sediment budget analysis. It also allows the user to explore different scenarios and uncertainties by varying the input parameters and ranges and provides graphical and tabular outputs that can be downloaded and shared. The SBC is limited by the availability and quality of the input data, which may be scarce, outdated, or inaccurate. It does not account for some complex processes such as tidal asymmetry, wave refraction, or sediment sorting and may not be applicable to some types of inlets, such as mixed-energy or multiple-inlet systems [5].

2.3 Example Studies

The SBAS has been utilized in several sediment budget studies. Some of these studies are briefly discussed in the following sections:

- ***Chandeleur Islands to Breton Island Bathymetric and Topographic Datasets and Operational Sediment Budget Development***

The SBAS was utilized in the Chandeleur and Breton Islands, Louisiana, which are part of the barrier island arc in the northern Gulf of Mexico Breton National Wildlife Refuge. This area also encompasses Curlew and Grand Gosier Shoals. In this study, topographic and bathymetric data were utilized to generate digital elevation models (DEMs) and assess elevation change and sediment budgets for the barrier island system across three different time frames. The SBAS was used for various calculations and some of the results are provided in **Figures 2.2** and **2.3**. **Figure 2.2** displays a screenshot of the SBAS setup in ArcGIS tracking the sediment budget in Chandeleur Islands to Breton Island area. **Figure 2.3** shows the net volume change (ΔV) in each cell (positive: green and negative: red) and the sediment flux between cell from sources (Q_{source}) to sinks (Q_{sink}) the cell. In this study the impact of major hurricanes (such as Camille, Ivan, and Katrina) on sediment displacement were assessed [4].

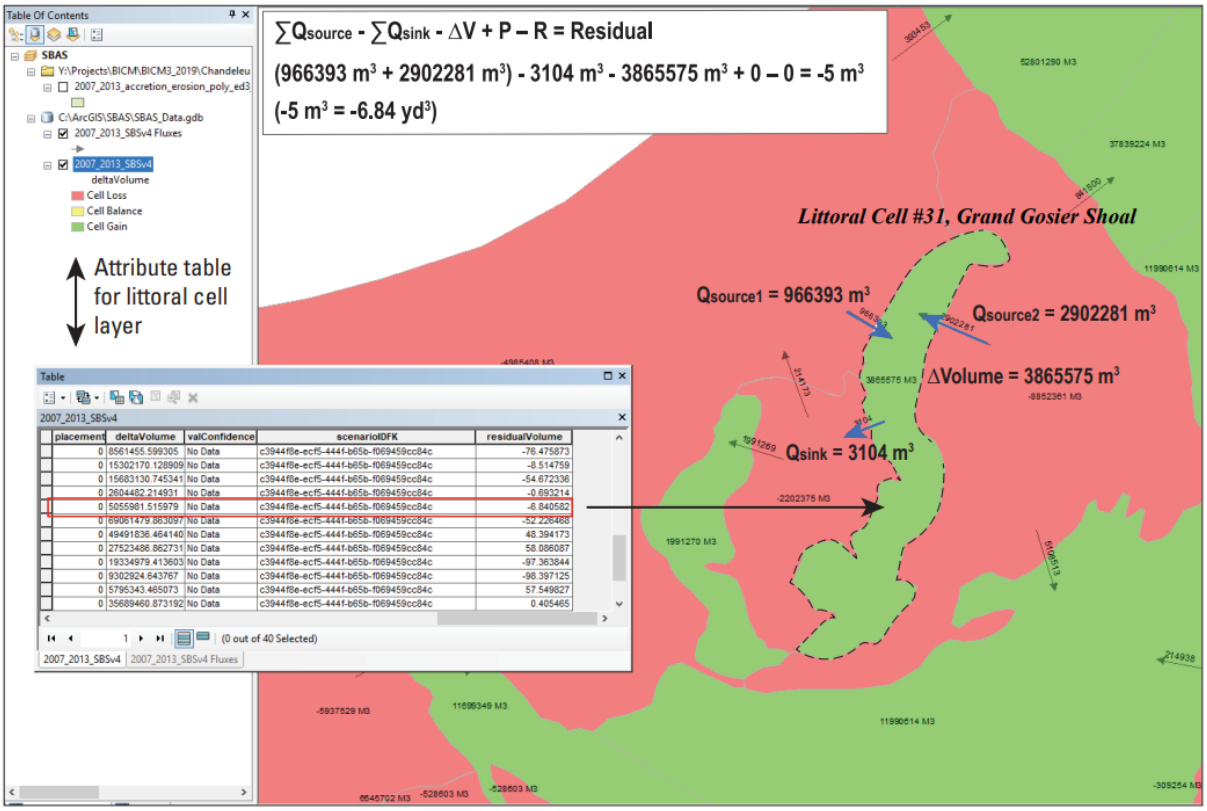

Figure 2.2 Screenshot of the SBAS setup in ArcGIS tracking the sediment budget in Chandeleur Islands to Breton Island study area for the 2007–2015 period. The polygons represent the accretion (green) and erosion (red) cells and are attributed with the net volume change (ΔV) [4].

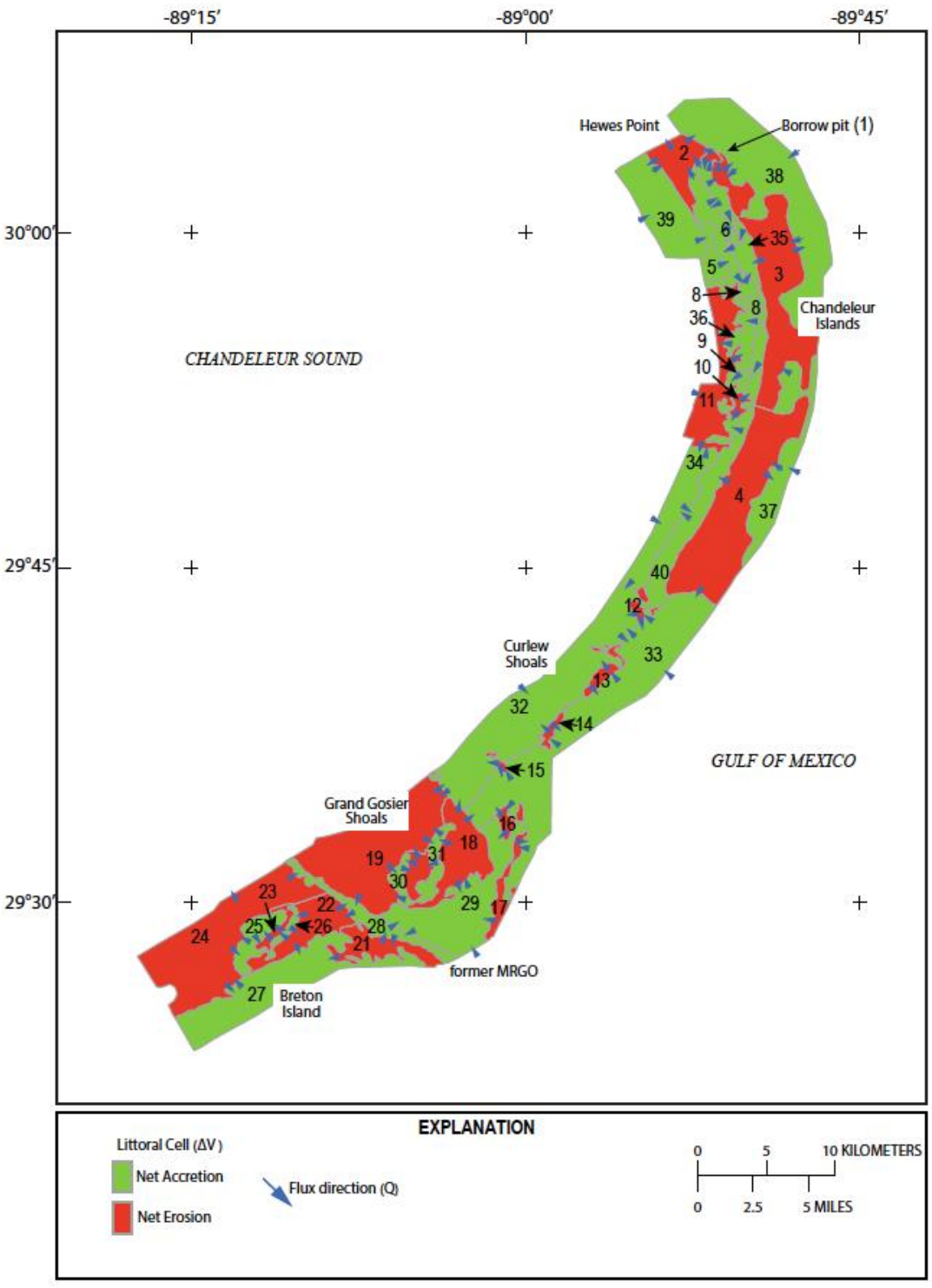

Figure 2.3 Map of littoral cells in the Chandeleur Islands to Breton Island study area for the period of 2007-2015. The net volume change (ΔV) is positive (green) or negative (red). Blue arrows represent sediment flux direction from sediment sources (Q_{source}) sediment sinks (Q_{sink}) [4].

- ***Application of SBAS for ArcGIS© 10 to Develop Regional Sediment Budgets for the Island of Maui, HI***

The SBAS and ArcGIS 10 were used to calculate sediment budget for the Kahului Region and Kihei Region on the Island of Maui in Hawaii. **Figures 2.4** and **2.5** show these two study areas that were divided into several polygons and the net accretion and deposition in each polygon. The study highlighted some of the challenges and uncertainties in developing a balanced sediment budget along the shorelines in these two regions. These challenges and uncertainties include [6]:

- In these regions, sediment quantities are relatively small due to mainly calcareous sediment sources. The limited quantities pose challenges in measuring volume changes and sediment transport, leading to an empirical sediment transport coefficient that is unrealistically small.
- Hawaii experiences a seasonal wave climate, with varying wave energy magnitude and direction throughout the year. This leads to bi-directional sediment transport and changing annual gross transport direction based on storm strength and climatic tradewind conditions.
- The coastline morphology includes numerous bays and orientation changes over short distances (~10s of miles), causing dramatic shifts in longshore transport rates and directions. Intermediate littoral barriers like headlands and complex nearshore features such as coral reefs create sub-cells within each littoral cell, limiting the applicability of accepted longshore sediment transport equations.
- During large Kona storms or hurricanes, cross-shore sediment transport may significantly impact sediment transport patterns, especially in areas with wide, fringing reefs. However, there is limited data and empirical methods to quantify this component's significance.

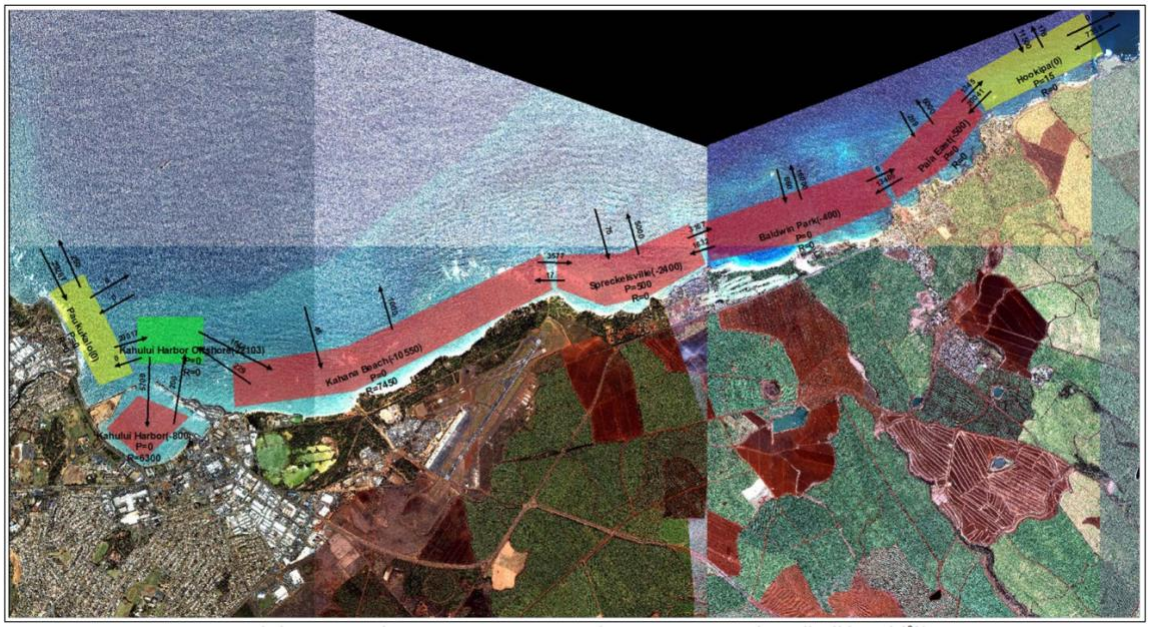

Figure 2.4 Kahului Region sediment budget developed using SBAS for ArcGIS-10 [6].

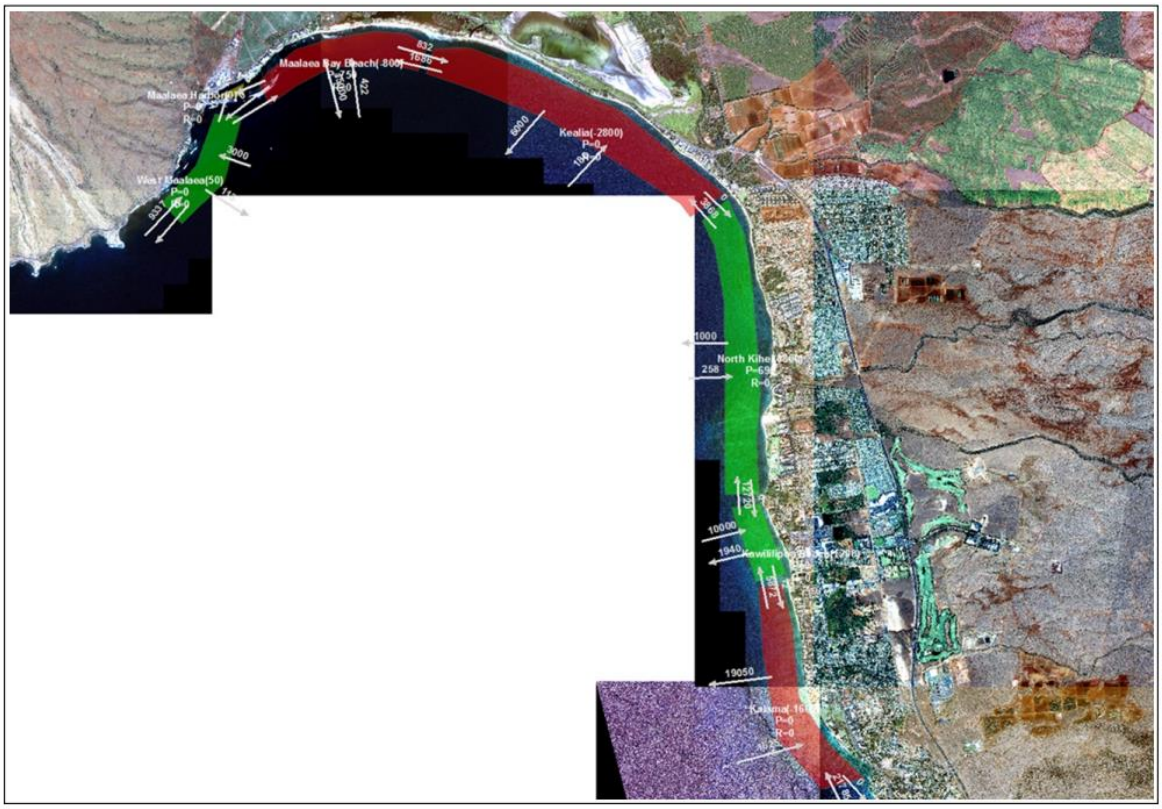

Figure 2.5 Kihei Region sediment budget developed using SBAS for ArcGIS-10 [6].

- ***Sediment Budget Analysis: Masonboro Inlet, North Carolina***

SBAS was also employed at Masonboro Inlet on North Carolina's southeast coast. The study examined a sediment budget to understand how beaches and the associated inlet complex respond to the dredging of Masonboro Inlet and the placement of dredged material along Masonboro Island's beaches (south side of the inlet) and Wrightsville Beach (north side of the inlet). For Wrightsville Beach, there were four sediment placements totaling over 2.9 million cubic yards over the study period, resulting in a placement rate of 181,000 cubic yards per year. However, a net loss was observed, indicating a need for additional sediment to achieve equilibrium. In contrast, a total of 1.1 million cubic yards material was placed along the beaches of Masonboro Island over several years, but these area still experienced significant losses, particularly at the southern end, requiring a substantial increase in sediment placement to balance out erosion [7]. **Figure 2.6** shows the budget analysis cells and the rate of sediment fluxes between the cells in Masonboro Inlet, North Carolina.

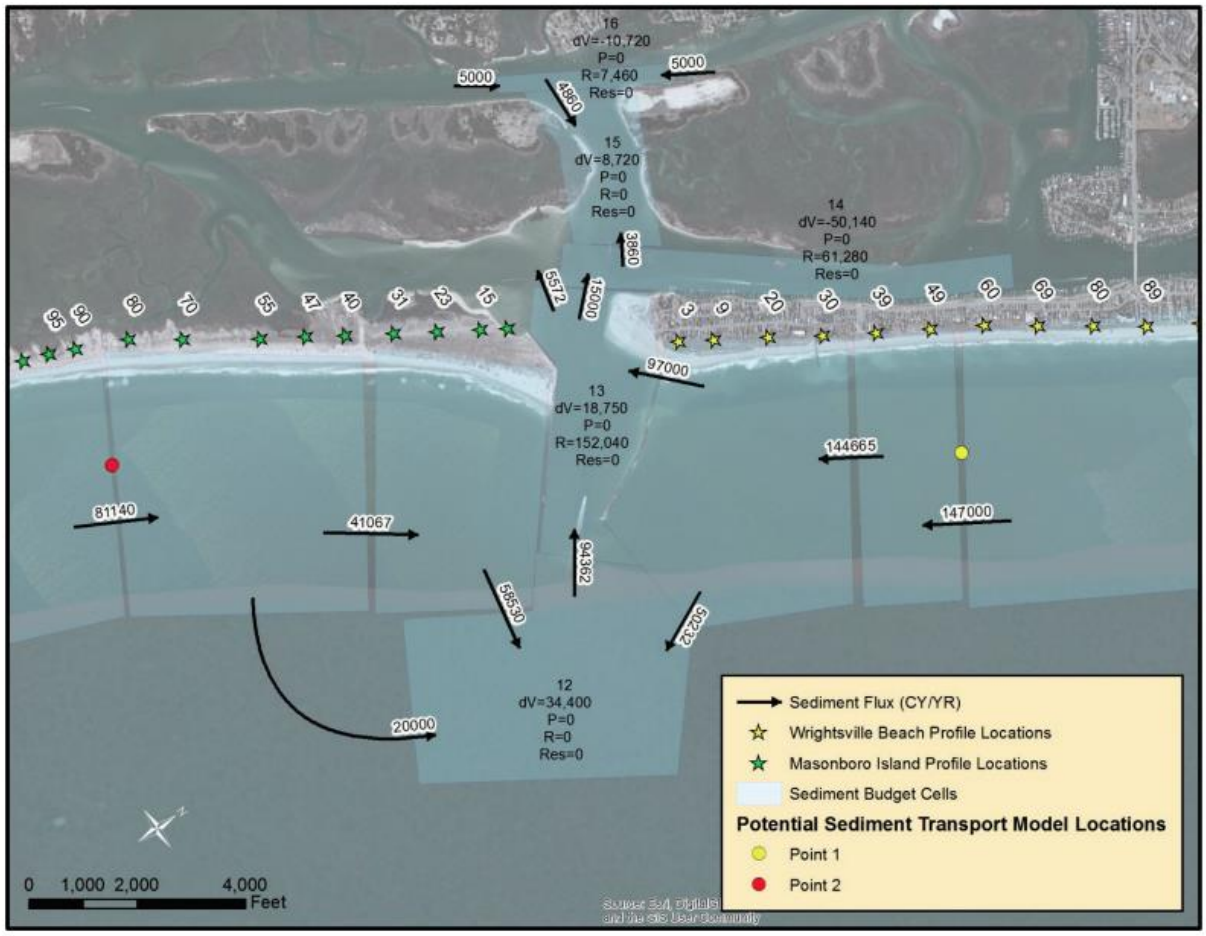

Figure 2.6 Masonboro Inlet, North Carolina sediment budget analysis cells and the rate of sediment fluxes between the cells [7].

- ***Pinellas, Manatee, and Sarasota Counties, Florida; Regional Sediment Budget***

The SBAS was utilized to develop a regional sediment budget in the southwest Gulf Coast of Florida. The aim of this study was to improve navigation and to provide storm damage reduction along the shoreline beaches. The objective of the study was to create a sediment budget for the entire 70-mile region of shoreline from synoptic lidar measurements. The study area includes several federal and local projects aimed at improving navigation and providing storm damage reduction along the shoreline beaches. The study's objective was to develop a regional sediment management approach, determining the best sediment management practices and examining the system holistically. As an example, the results from the SBAS with regards to sediment budget in Pinellas County are shown in **Figure 2.7**. In this figure, green cells indicate volume gains and red cells show volume losses. This assessment showed significant overall volume gain in Pinellas County beaches, primarily attributed to beach nourishment, despite losses in some cells. In

contrast, Manatee County experienced a net volume loss, while Sarasota County gained sediment primarily through nourishment activities in specific cells [8].

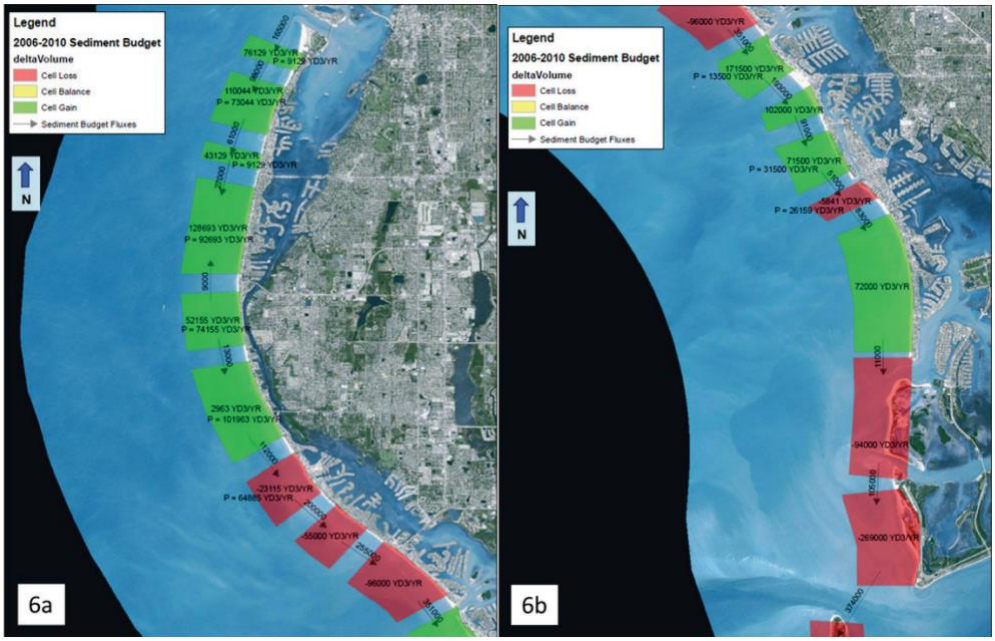

Figure 2.7 Volume change in sediment budget cells for Pinellas counties beaches [8].

3. HYDRO-GEOMORPHOLOGICAL MODELS

Over the past few decades, several hydrodynamic and sediment transport models have been developed to estimate the movement and evolution of sediment in coastal areas in response to natural and anthropogenic changes. These models vary in their applications (e.g., suspended load vs. bedload, cohesive vs. noncohesive sediment) and formulation in spatial and temporal schemes (e.g., two- vs. or three-dimensional, and steady vs. unsteady). Several criteria, including problem complexity, model capabilities, data availability for calibration and verification, and time and budget constraints, influence the choice of model for a given situation. These models all have different advantages and disadvantages and are equipped with tools suitable for modeling the complicated interactions between water, sediment, and morphology in coastal areas. This review evaluates the performance of these models in various circumstances and emphasizes their importance in developing successful coastal management plans. Nine widely-used hydro-geomorphological models selected for this review include Delf3D, TELEMAC, ADCIRC, MIKE 21, XBeach, LITPACK, CosMoS, GENESIS, and SBEACH.

Features of these models are obtained from their user manuals, reference manuals, and published scientific journals. The main features are groups as operating system and programming, hydrodynamic model configuration, and sediment dynamics modeling components. These features and general information about each model are summarized in **Table 3.1**.

Table 3.1 General information and main features of several hydro-geomorphological models utilized in coastal areas.

	Features	Hydro-geomorphology Model								
		Delft 3D	**TELEMAC**	**MIKE21**	**ADCIRC**	**XBeach**	**LITPACK**	**CoSMoS**	**GENESIS**	**SBEACH**
Operating System and Programming	Model Availability	Public	Public	Commercial	Public	Public	Commercial	Public	Public	Public
	Version and Last Update	flow2d3d, version 6.04.02.142586 and 23 Feb 2023	TELEMAC v8p4, 12 Jan 2023	MIKE2024, Nov2023	ADCIRC v55, 23 Feb 2021	XBeach_v1.24	LITPACK 2024	CoSMoS Southern California v3.0 Phase 2, Oct 2021	CEDAS 4.03, Jan 2009 (Genesis is a Module of CEDAS	CEDAS 4.03, Jan 2009 (SBeach is a Module of CEDAS
	Graphic Interface	Included and restricted	Partially included	Included Commercial	Partially included commercial	Available through OpenEarth toolbox	Included Commercial	-	-	-
	Source code[1]	Limited distribution	Proprietary	Proprietary	Copyrighted and limited distribution	Open Source	Proprietary	Open Source	Proprietary	Proprietary
	Language	Fortran	Fortran	Fortran	Fortran	Primary in Fortran	Fortran	Fortran	-	Fortran
	Open Source	Yes	Yes	No	Yes	Yes	No	Yes	Yes	Yes
	Fully Documented	Yes	Yes	Yes	Partially Included	Yes	Yes	Yes	Yes	Yes
	Operating System and Programing	Windows and Linux	Windows and Linux	Windows	Windows	Windows and Linux	Windows	Windows and Linux	Windows	Windows
Hydrodynamic Model Configuration	Type of Computational Grid	Structured and non-structured	Structured and Non-structured	Structured and Non-Structured	Structured and Non-Structured	Structured and Non-Structured	Structured	Depends on integrated model	Structured	Structured
	Grid Construction	Structured with domain decomposition and unstructured flexible mesh	Flexible Mesh	Unstructured Flexible Mesh	Unstructured Flexible Mesh	Structured with domain decomposition	Structured grid linear feature	Depends on integrated model	uniform grids at arbitrary orientation	Variable grids one-dimensional
	Flow Type Simulation	Unsteady	Unsteady	Unsteady	Unsteady	Unsteady	Unsteady	Unsteady	Unsteady	Unsteady
	Numerical Scheme	Finite Difference	Finite Elements	Finite Difference and Element	Finite Difference	Finite Difference	Finite Difference	Depends on integrated model	Finite Difference	Finite Difference
	Coord. Horizontal Plane	Cartesian and Curve	Cartesian and Spherical	Cartesian and Spherical	Cartesian	Cartesian	Cartesian	Cartesian and Curve	Cartesian and Curve	Cartesian
	Coord. Vertical Plane	Z Coordinate	Z Coordinate and Hybrid: Z Sigma coordinate[2]	Hybrid, Sigma, General Sigma coordinate[2]	Sigma coordinate[2]	Sigma coordinate[2]	Z coordinate	Z coordinate	1-D, No Z axis	Z Coordinate
	Non-hydrostatic Approach	Yes	Yes	Yes	No	Yes	No	Yes	-	Yes
	Temperature Transport Equation	Yes	Yes	Yes	No	No	No	No	No	No
	Heat Fluxes Equations	Yes	No	Yes	No	No	No	No	No	Yes
Sediment Dynamics Modeling	Vertical Mixing Model	No	No	NO	No	-	-	-	-	-
	Sediment Transport Mod	Yes	Yes	Yes	Yes	Yes	Yes	No	No, simulates only shoreline change based on sediment volume	Calculates by Wave model and Storm-induced beach change numerical model
	Type of Sediment Load	Suspended Load and Bed Load	Suspended Load and Bed Load	Suspended Load and Bed Load	Suspended Load	Suspended Load and Bed Load	Suspended Load and Bed Load	-	-	Suspended Load and Bed Load
	Sediment Mixtures[3]	No	No	No	No	No	No	-	-	-
	Sediment Types	ohesive and Non-cohesi	Non-Cohesive and Sediment Distribution[4]	hesive and Non-Cohes	Cohesive	Non-Cohesive	Non-cohesive	-	-	Cohesive and Non-Cohesive
	Sediment Exchange Processes	Entrainment and deposition[6]	Entrainment and deposition[6]	Entrainment and deposition[6]	Advection-Diffusion[6]	Entrainment and deposition[6]	Entrainment and deposition[6]	-	-	-
	Real Time Control[5]	Yes	No	Yes	-	No	No	-	-	-
	Morphologic Evolution	Yes	Yes	Yes	No	Yes	Yes	Yes	Yes	Yes

Note:

1. Source code- Limited distribution: Restricts the distribution of the source code of a software program to a specific group of individuals or organizations, Proprietary: Refers to the legal rights and ownership associated with the software, including the right to control its distribution and use.
2. The Sigma coordinate system uses a dimensionless coordinate (σ) normalized by the total water depth. In regions with sloping topography, z-coordinates can lead to unrealistic vertical velocities near the bottom due to intersecting grid levels. Sigma (σ)-coordinates follow the bathymetry, maintaining a consistent number of vertical grid points across the domain regardless of water depth. This approach helps avoid grid-level intersections and improves accuracy, especially in areas with varying topography. A hybrid z-sigma coordinate system combines the strengths of z-coordinates and sigma coordinates to provide an effective and versatile vertical coordinate system for numerical modeling of oceanographic and hydrodynamic processes. For the generalized sigma grid, it is dominated by z coordinates in the deep ocean, but follows the topography like sigma coordinates. (https://www.oc.nps.edu/nom/modeling/vertical_grids.html, https://www.researchgate.net/publication/4010298_Finite_volume_ocean_circulation_model, https://link.springer.com/chapter/10.1007/978-3-662-22648-3_4)
3. Sediment Mixture: Predicts the gradation of sediment mixtures; whereas the other models apply to uniform sediment only.
4. Sediment distribution: Refers to the spatial arrangement or pattern of sediment particles within a given area.
5. Real-time control module: Permits change in the gate height during the simulating period.
6. Advection-diffusion describes lateral and vertical spreading of sediment within the flow, while entrainment-deposition describes the lifting and transport of sediment from the bed into the water column, followed by its settling and accumulation back onto the bed.

3.1 Delft3D

Delft3D, developed by Deltares, is a comprehensive modeling software with a primary focus on applications within free surface water environments. This integrated modeling suite offers simulations in two-dimensional (either horizontal or vertical planes) and three-dimensional scenarios, encompassing flow, sediment transport, morphology, waves, water quality, and ecology, with the capability to handle interactions between these processes. Delft3D enables the simulation of flow, sediment, ecology, and water quality interactions over time and space. Widely applied in modeling natural environments such as coastal, river, and estuarine areas, it is equally suitable for artificial settings such as harbors and locks [9].

System Architecture

Delft3D comprises multiple modules, each targeting specific areas such as flow, water quality, waves, morphology, and sediment transport, with pre-processing and post-processing functionalities (**Figure 3.1a**) [10]. The sediment transport module, Delft3D-SED, is a sub-module of the water quality module that mainly focuses on cohesive and non-cohesive sediment transport. Along with the Delft3D-SED, the following modules are used for modeling sediment transport: FLOW for hydrodynamic computations, WAVE for wave transformations using the SWAN model [11], and MOR that is integrated into FLOW for simulating morphology changes [12]. These modules dynamically exchange data and results are generated based on the assigned formulas according to the process requirements. (**Figure 3.1b**). Delft3D-FLOW and MOR handle 2D and 3D hydrodynamics, salinity, temperature, transport, and morphological development in sediment transport. Delft3D-SED focuses on cohesive and non-cohesive sediment transport, allowing studies on dredged material spreading, sedimentation/erosion patterns, water quality, and ecology. Additionally, this module simulates sediment transport for various applications by integrating waves, currents, and morphological effects [10].

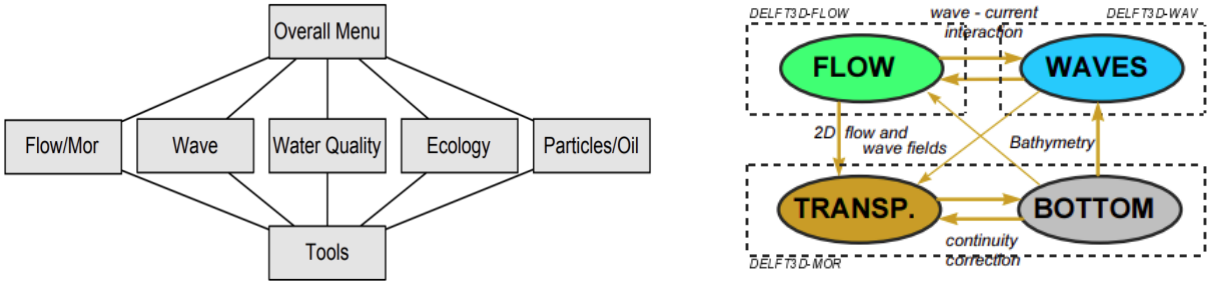

(a) (b)

Figure 3.1 (a) System architecture of Delft3D [10], and (b) Dynamic exchange of data among the modules [13].

The FLOW module solves the Navier-Stokes equations to model incompressible fluid flow, incorporating both shallow water and Boussinesq assumptions. The system of equations includes momentum equations, continuity equations, transport equations, and a turbulence closure model.

The vertical momentum equation is simplified to the hydrostatic pressure relation, making the Delft3D-FLOW adept at predicting flow in shallow seas, coastal areas, estuaries, lagoons, rivers, and lakes, particularly for scenarios where horizontal length and time scales significantly exceed vertical scales [14]. Sediment transport, influenced by combined waves and currents, is computed using an advection-diffusion equation while morphology updates can be accelerated using a morphological acceleration factor [12]. In terms of formulation, the sediment transport and morphology module accommodates bedload and suspended load transport for non-cohesive sediments, along with suspended load transport for cohesive sediments [15].

Inputs and Outputs

Modeling coastal sediment transport using Delft3D involves several inputs and outputs. The FLOW module's water level and currents prediction data are used as input to compute sediment transport and bathymetry update [16]. As input, it also needs the initial conditions for variables such as salinity, and temperature and boundary conditions including flow and transport boundary conditions. Moreover, the consideration of "*Physical Parameters*" is crucial for modeling the physical conditions of the system. For sediment and morphology processing, this section covers parameters such as sediment characteristics (cohesive, non-cohesive, shear stress, density, settling velocity) and bathymetry for morphological considerations [15].

The output of Delft3D sediment transport modeling represents the direction and magnitude of overall sediment movement and sediment parameters over the study period, which includes sediment concentration profiles, dynamic updates of bathymetry changes, sediment transport rates, sediment deposition, erosion, and flow pattern [13]. The outputs of the model can be compared with observational data to assess model capabilities and limitations [17]. As an example of model outputs, the information about the wave climate and the quantification of sediment transport rates along a coast can be extracted as output which helps to design coastal structures [18].

Examples of Model Applications

The Delft3D has been utilized in several studies for morphodynamical modeling and assessing sediment transport in coastal areas. Examples of some recent applications of Delft3D to understand the morphological behavior of coastal areas are Ibajay- Philippines [19], Dauphin Island- Alabama, U.S. [20], Kenitra Coast on Northern-Western of Morocco [18], the shoreline of Santa Barbara and Ventura County in California, U.S. [21], and the delta of the Rhone River in the Mediterranean Sea [22] (**Figure 3.2).**

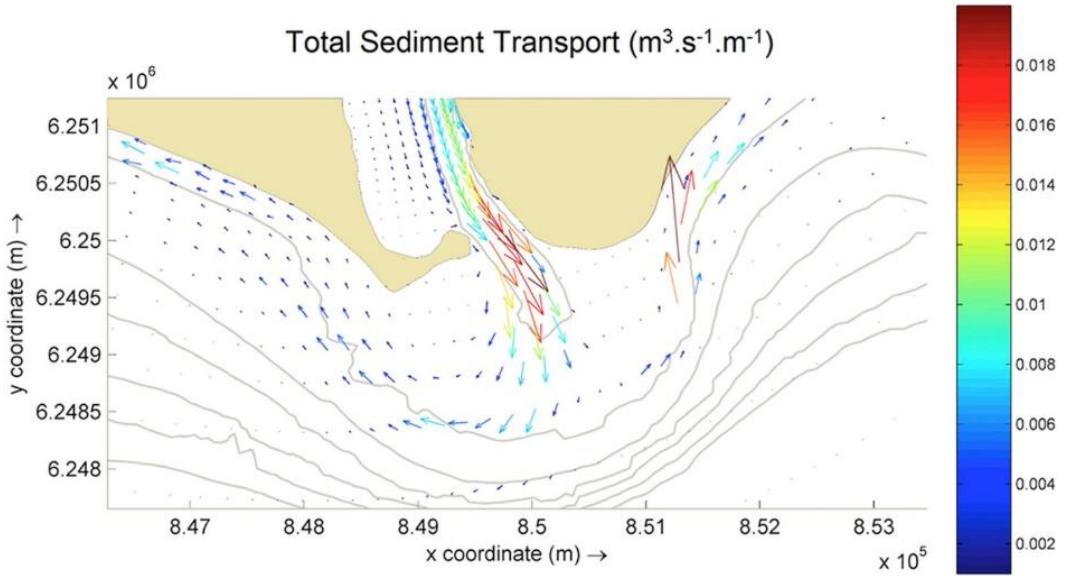

Figure 3.2 Delf3D outputs showing total sediment transport (TST) in the delta area of the Rhone River in the Mediterranean Sea [22].

Pros and Cons

Delft3D software is used to model sediment transport in coastal regions. It has the advantage of being able to simulate sedimentation processes and the movement of sediments along the coast [18] [23]. The model can be used to simulated the effectiveness of permeable structures in protecting coastal areas from erosion and aiding in their recovery [24]. It can also help in understanding wave climate and quantifying sediment transport rates, which are important for designing coastal structures [18]. However, there are limitations to the software. It does not predict suspended sediment transport under breaking wave conditions accurately and overestimates the offshore-directed suspended sediment transport in certain conditions [25]. Since Delft 3D does not have the option to consider variation in grain size, it needs to incorporate another model (Van Rijn model, which considers both the single-fraction and multi-fraction approach model of sediment transport rates [26]) for considering the graded sediment approach over the uniform sediment approach [27].

3.2 TELEMAC

TELEMAC-2D is a computational model that solves depth-averaged equations for free surface flows. It is primarily utilized for maritime and river hydraulics by incorporating features such as wave-induced currents and sediment transport. The model can be coupled with the sediment transport modules (SISYPHE) and the wave module (TOMAWAC) to simulate changes in the seabed over time [28]. In the TELEMAC system, the SISYPHE module calculates sediment movement based on water flow and sediment properties along with updating the seabed by using hydrodynamic and sediment transport equations. Moreover, long-term shoreline changes in large areas can be simulated by SISYPHE along with other TELEMAC modules. The model has been

available for free download since 2010 on the TELEMAC website, where users can also get help and share their feedback [29].

System Architecture

SISYPHE interacts closely with TELEMAC-2D for currents and water levels, as well as with the wave module, i.e., TOMAWAC [30]. These three modules interact dynamically during runtime to simulate the morphodynamic response across the study area. The interaction among these modules is depicted in **Figure 3.3**.

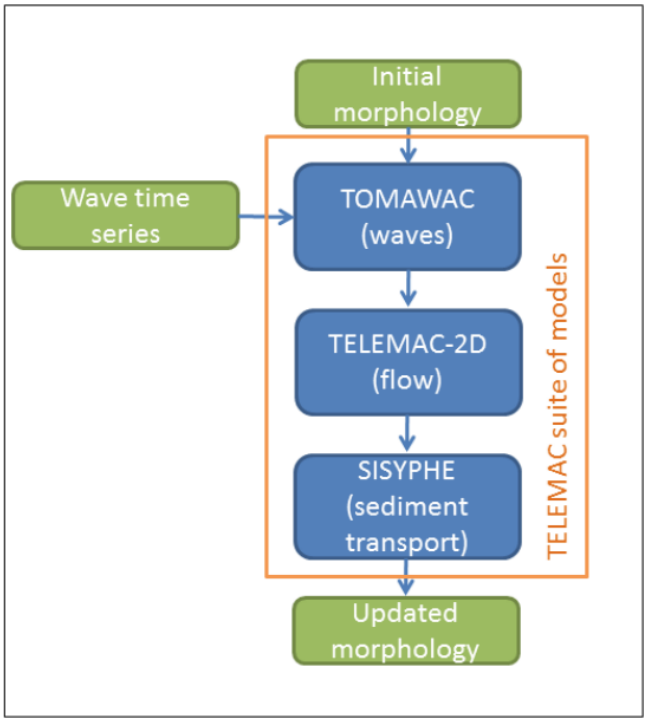

Figure 3.3 An Example of interaction among several TELEMAC modules including Waves (TOMAWAC), Flow (TELEMAC-2D), and Sediment Transport (SISPHE) [30].

For non-equilibrium flow conditions, where dynamic changes are dominant, separate treatment is necessary for both bedload and suspended load sediment transport. SISYPHE accommodates this requirement by offering distinct approaches for modeling each type of sediment transport. For calculating bedload transport rates, SISYPHE provides various options based on numerous semi-empirical formulas from the available literature. Among the choices, there are some well-known formulas such as Meyer-Peter and Müller, Engelund-Hansen, and Einstein-Brown , which offer flexibility in modeling sediment transport under different conditions. Additionally, for suspended sediment transport, SISYPHE employs a 2D transport advection-diffusion equation to determine the depth-averaged mean concentration by integrating concentration over depth. This comprehensive approach allows SISYPHE to accurately simulate sediment transport processes in diverse hydraulic environments [29].

Inputs and Outputs

The input parameters for SISYPHE include different initial conditions and computational settings like duration and time step. Physical parameters are also needed to define along with input data files such as the geometry and boundary condition files. The geometry file describes the unstructured triangular grid, while the boundary condition file sets conditions for the grid. Some optional files like previous sedimentological computations or references for validation can be considered as input. Moreover, settings can be specified in a steering or Fortran file, including: i) the name of input/output files, ii) sediment parameters (sand diameter, cohesive or non-cohesive, settling velocity), iii) selected transport processes (skin friction, bedload, suspended load, transport formulas), and iv) numerical options (finite elements or finite volumes). Additionally, hydrodynamic conditions as well as wave data can be provided as input. The hydrodynamic condition contains the hydrodynamic results of a previous hydrodynamic computation (TELEMAC-2D or 3D). Similarly, the wave file is used as input also contains the results from a previous wave computation (TOMAWAC) [29].

The SISYPHE model outputs contain water depth and velocity at each node, along with bedload transport rates for the chosen formula. It also provides suspended sediment concentrations and transport rates. Detailed listings of output show computation inputs, geometry file data, and previous computations. Furthermore, it can provide maximum and minimum values, cumulative evolution integrals, and values for the selected variables at each grid points [29].

Examples of Model Applications

To explore the sediment transport phenomena across a range of diverse aquatic environments, there are many studies, which have utilized different configurations of the TELEMAC. Some of these studies cover the following locations: the Têt River in Italy [31], Sea Scheldt at the Dutch and Belgian border [32], Cameron, Kenedy, and Willacy counties along the Texas Coast [30] (Figure **3.4**), the lower Rhine River, Gironde Estuary, and the tidal mouth of the Gironde Estuary [33].

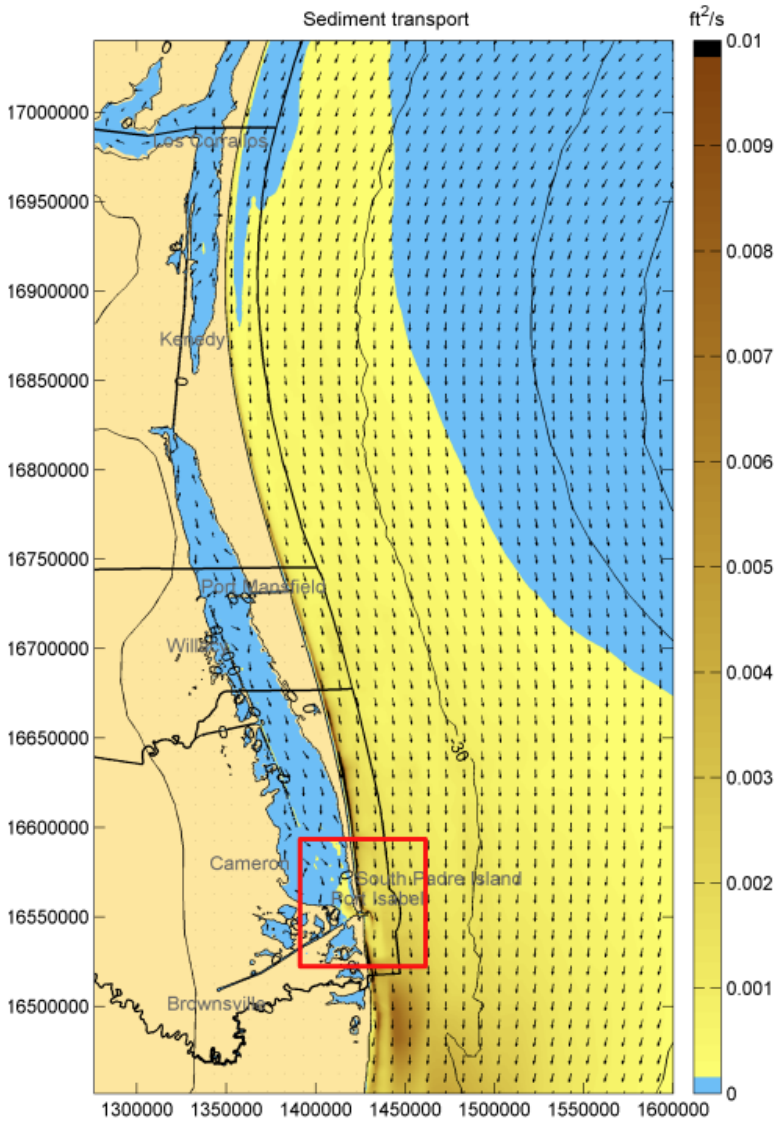

Figure 3.4 Output of TELEMAC showing sediment transport along the Texas Coast (Cameron, Kenedy, and Willacy counties). Blue indicates negligible transport, while vectors show the transport direction. The scale bar colors denote the sediment transport rate or the amount that would be trapped in the unit area ($ft^3/s/ft$) [30].

Pros and Cons

TELEMAC is a comprehensive hydraulic modeling software that offers detailed capabilities in simulating hydrodynamic and sediment transport phenomena, particularly valued for its accuracy and ability to handle various sediment types and transport modes. The system's use of an unstructured finite element grid allows for flexible meshing to accurately represent complex waterbody geometries, making it ideal for a wide range of environmental and engineering applications. Accurate modeling and uncertainty quantification are achieved by improving model state accuracy through variational data assimilation [34]. Moreover, the model's proficiency in

simulating long wavelength phenomena in shallow waters, and its effectiveness in capturing wave propagation, diffraction, and refraction are notable strengths [35]. However, TELEMAC also presents certain limitations that may restrict its utility in specific scenarios. The model demands significant computational resources, which can become a barrier in projects with limited access to computing power, leading to longer processing times. This can be particularly challenging when handling large-scale or highly detailed simulations, which are necessary for accurate modeling but computationally intensive. Additionally, while TELEMAC provides comprehensive tools for uncertainty quantification and the construction of metamodels, these processes themselves can be complex and require a sophisticated understanding of the model's workings [36]. There are also inherent challenges with the numerical schemes used for vertical sediment transport, which can introduce substantial numerical diffusion, necessitating the use of more complex hybrid schemes to achieve accurate results [37]. These computational demands highlight the need for further optimization to enhance efficiency without compromising the detailed insights TELEMAC offers.

3.3 MIKE 21

MIKE21, developed by the Danish Hydraulic Institute (DHI), is a comprehensive modeling tool that utilizes spectral waves and radiation stress to drive sediment transport in its two-dimensional model. This model encompasses various coastal processes such as waves, winds, currents, water levels, and sediment transport. However, it requires extensive computing time due to their complexity and non-open-source code restrictions. MIKE 21 consists of modules for wave transformation, hydrodynamics, and sediment transport. For data visualization and analysis, this model provides capabilities for calculating current fields, water levels, temperature, and salinity [38]. Additionally, MIKE 21 offers modules like LITPACK for coastline evolution, Mud Transport for siltation impact assessment, Shoreline Morphology for long-term shoreline modeling, and Sand Transport for infrastructure vulnerability assessment against erosion and sedimentation [39].

System Architecture

In MIKE 21, the hydrodynamic module (HD) can be coupled with sediment modules to study sediment transport patterns for both cohesive and non-cohesive sediment separately. The choice between 2D and 3D models depends on factors, like water depth and mixing conditions. Data gathering involves collecting wind, wave, water surface elevation, and hydrographic points.

It uses a flexible mesh approach to study sediment patterns in coastal areas and river deltas by integrating hydrodynamic module (HD), Spectral Wave (SW), and Sand Transport (ST) modules. The SW module output feeds into the HD module, which in turn provides initial inputs for the ST module (Figure **3.5**) [40].

The modeling system relies on solving the two or three-dimensional incompressible Reynolds-averaged Navier-Stokes equations, incorporating the Boussinesq assumptions and hydrostatic pressure considerations. Therefore, the model includes continuity, momentum, temperature,

salinity, and density equations, closed by a turbulence closure scheme. In MIKE 3, the 3-D model incorporates the free surface by employing either a sigma-coordinate transformation approach or a combination of sigma and z-level coordinate systems. [41]. The flowchart in Figure **3.5** shows how different modules interact with each other to calculate sediment transport.

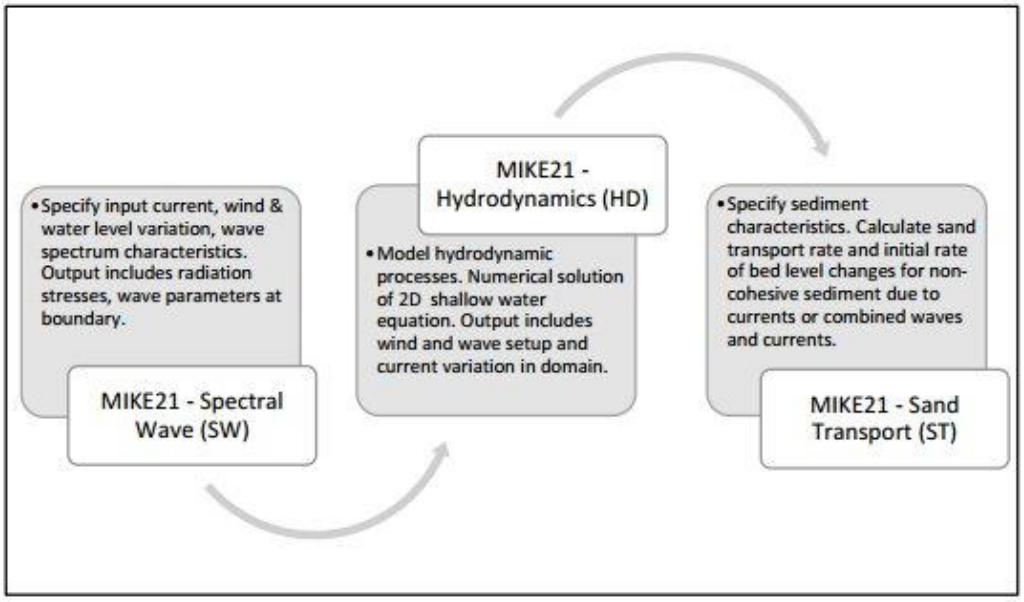

Figure 3.5 Interaction among MIKE 21 wave (SW), hydrodynamics (HD), and sand transport (ST) modules [42].

Inputs and Outputs

Essential input for developing a sediment transport model includes bathymetric maps, wave and wind statistics, water level data, and bed material gradation. For the Sand Transport (ST) module, a sand transport table with rates for combined wave and current scenarios is required, along with sediment properties and morphology parameters. For the Mud Transport (MT) module, input parameters contain settling velocity, critical shear stress, erosion coefficients, suspended sediment concentration, and dispersion coefficients [43] [44].

The outputs of the Spectral Wave (SW) can be incorporated into the HD module, which then serves as input for the sediment transport modules. Output from the MT module includes suspended sediment concentration, sediment in bed layers as mass or thickness, sediment rates, bed shear stresses, settling velocities, and updated bathymetry. For the ST module, output data consists of sediment transport rates and results of morphological changes, which can be in various formats like points, lines, or areas. Basic output variables for both ST and MT include suspended sediment concentration, bed load, suspended load, total load in x- and y-direction, and bed level changes. Additional output variables provide transport magnitudes and directions, along with accumulated values and hydrodynamic and wave variables [43] [44].

Examples of Model Applications

The MIKE 21 has been employed in several studies to determine sediment transport in coastal environments. These studies encompass locations such as the Port of Rethymno in Greece (Figure **3.6**); the Australian East Coast [45]; New York [46]; Puerto Rico [46]; Southern California [46]; Baydara Bay in Russia [42]; and the southeast of the Caspian Sea [40].

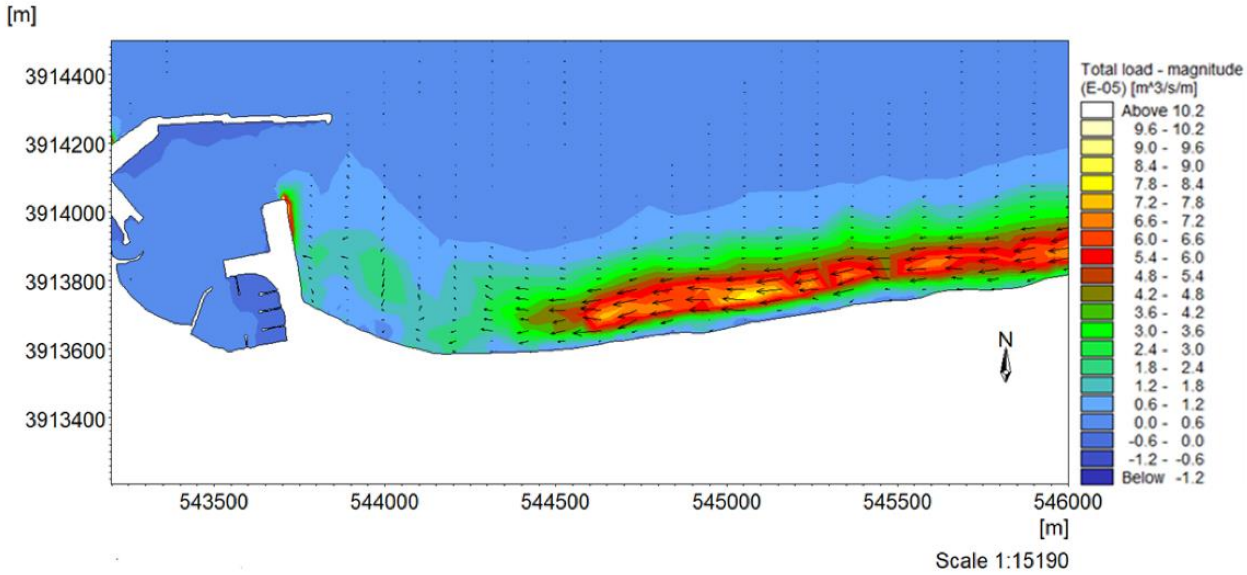

Figure 3.6 Output of the MIKE 21 model presenting morphological bed evolution of the Port of Rethymno in Greece over 7 days, resulting in the east to west sediment transport and accretive patterns on the beach face [47].

Pros and Cons

The morphologic changes in the MIKE 21 model are adaptable, and the model is able to handle features such as islands, bays, and inlets. MIKE 21 is also capable of dealing with suspended sediment, which makes it a widely used and tested method. Additionally, it offers an optional unstructured finite element mesh, allowing increased resolution where needed. The MIKE21 SW wave model boasts a fast and efficient solution scheme. [38]. The has limitations that could affect its utility depending on the specific requirements of a project. It is not open source, which limits its accessibility and flexibility for customization. Users might find the licensing cost and the closed nature of its development a barrier, especially in academic or research settings where open-source tools are preferred for their adaptability and community support. Furthermore, the software traditionally supports simulations for relatively short durations due to limitations in sequential wave forcing, which might not be ideal for long-term coastal evolution studies. Another potential drawback is the computational intensity required for running high-resolution models, especially on standard CPUs, though this is somewhat mitigated by compatibility with GPU acceleration. This feature, however, demands additional hardware investments [38].

3.4 ADCIRC

Advanced Three-Dimensional Circulation (ADCIRC) model is designed to solve time-dependent, free-surface circulation and transport problems in both two and three dimensions. Initially, it was intended to generate a database of harmonic constituents for tidal elevation and current along the coasts of the United States, including the east, west, and Gulf of Mexico Coasts [48]. Currently, two main versions of the model is available: ADCIRC-2DDI, a two-dimensional depth-integrated hydrodynamic model; and ADCIRC-3D, a three-dimensional model that couples external and internal solutions. The model can simulate hydrodynamic circulation in shelves, coasts, and estuaries by offering a high computational efficiency for long simulations over large domains [49]. The sediment transport modeling capabilities were incorporated in ADCIRC to extend its functionality for studying erosion, deposition, and suspension processes of both cohesive and non-cohesive sediments. ADCIRC is widely used for accurately and efficiently modeling storm tides and circulation patterns in various marine environments [50].

System Architecture

ADCIRC is a sophisticated computer program designed for modeling fluid dynamics by using hydrostatic pressure and Boussinesq approximations. It employs the finite element method for spatial discretization and the finite difference method for temporal discretization. The program calculates water elevation using a depth-integrated continuity equation and velocity from nonlinear two-dimensional or three-dimensional momentum equations. It supports both Cartesian and spherical coordinate systems and offers various options for solving the generalized wave-continuity equation (GWCE), including different mass matrix forms and time-stepping schemes. In its 3D mode, ADCIRC handles vertical diffusion with an implicit approach and manages complex matrix problems vertically at each horizontal node. Additionally, it includes optimized computing techniques and supports efficient parallel processing by achieving high performance across different computing architectures [51].

ADCIRC adopts a probabilistic approach that accounts for both bed and suspended load, which are influenced by currents and waves. Moreover, the incorporation of a baroclinic module has enhanced its capabilities to consider salinity, temperature, and sediment concentration changes [49] [50]. In version 55, spherical coordinates were integrated, enabling the simulation of larger domains with a global scope [52]. Moreover, sediment resuspension in shallow bay areas is mainly due to wind-generated waves. The SWAN model, capable of predicting time-varying wave climates in coastal regions and estuaries, is governed by factors like wind, sea surface elevation, depth, and current conditions. SWAN considers various wave generation mechanisms such as wind, shoaling, and refraction due to currents and non-uniform depths. A flow diagram In Figure **3.7** illustrates the coupled ADCIRC-2DTR and SWAN model, where output from ADCIRC-2DTR is transformed into input files for SWAN, requiring data on wind velocity, direction, water depth, surface elevation, and current vectors, often obtained from meteorological stations and the ADCIRC-2DTR model output [53].

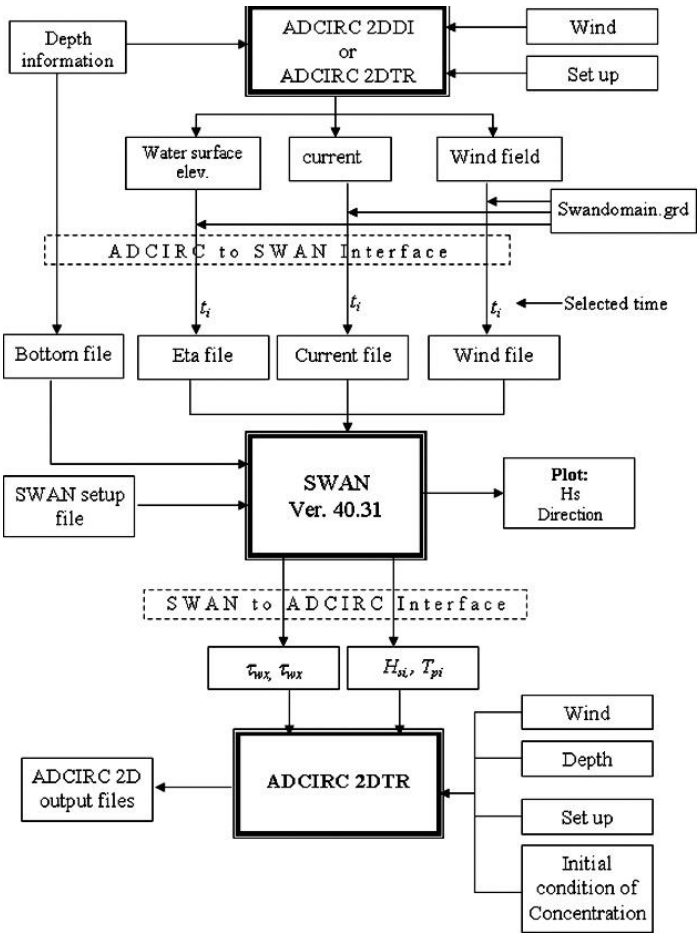

Figure 3.7 Flow diagram of the coupled ADCIRC-2D hydrodynamic and SWAN wave models [53].

Inputs and Outputs

ADCIRC utilizes a range of inputs to model water dynamics effectively. These include detailed topographic and bathymetric data to define the physical terrain along with meteorological conditions such as wave, depth, wind, and atmospheric pressure. Boundary conditions set the initial environmental states, and an unstructured grid allows for targeted resolution enhancements in critical areas. Moreover, inputs include detailed data on sediment type, grain size, and sediment concentration for functioning sediment transport, and hydrodynamic interactions accurately. Physical parameters like surface roughness and wind-wave interactions are also integrated to consider the hydrodynamic conditions efficiently [50] [51] [53] [54].

ADCIRC produces a comprehensive set of outputs for understanding the flow dynamics in modeled environments. These include detailed predictions of water level and velocity across the model's domain. If wave models are coupled, the outputs also include significant wave characteristics such as height, period, and direction. In scenarios where ADCIRC is integrated with sediment transport models, it provides detailed profiles of sediment concentration over time,

which helps to understand sediment suspension, transport, and settling phases within the waterbody. Furthermore, the model outputs contain salinity and temperature profiles, which are particularly important for ecological studies and managing estuarine environments [50] [54].

Examples of Model Applications

ADCIRC integrated with sediment transport module has been used to sediment dynamics in several coastal areas such as Southeast Oahu in Hawaii [54], from the mouth of the Mississippi River along the north shore of the Gulf of Mexico towards and along the Texas Coast [50], Matagorda Bay in Texas [53] and Long Island in New York [55], and the James River in Virginia (**Figure 3.8**) [56].

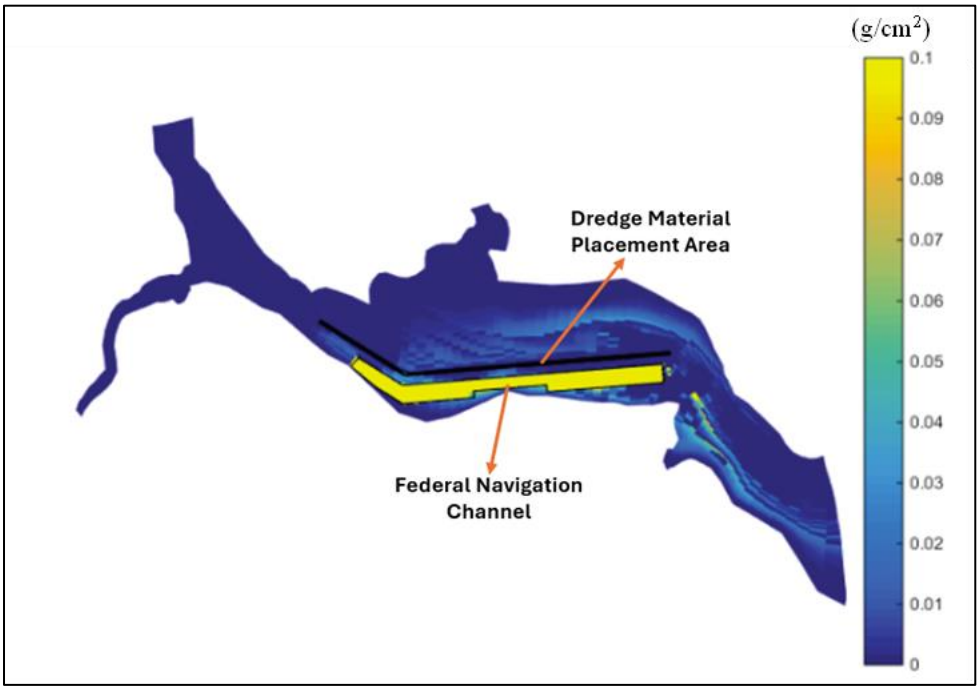

Figure 3.8 Sediment deposition in the James River, Virginia after dredging the navigation channel and placement of dredged materials in the designated site. The simulation conducted using ADCIRC for the period of Jan 14-Feb 14, 2000 showed that most placement sediments stayed in the designated site, with some accumulating on nearby shoals and downstream [56].

Pros and Cons

ADCIRC is a robust modeling tool recognized for its critical inputs from authoritative sources like the US Army Corps of Engineers (USACE), ensuring reliability and precision in its simulations. It is particularly adept at handling mixed sediment systems, including both cohesive and non-cohesive, which allows for a comprehensive understanding of sediment dynamics in diverse coastal environments. The model is well-equipped to handle complex coastal processes, which is essential for predicting phenomena such as overtopping, longshore transport, and associated losses. A notable feature is its adaptive mesh technology, which significantly improves

computational efficiency by focusing resources on areas of the grid where more detail is necessary [38] [54]. However, ADCIRC also has its limitations. Although it can estimate suspended sediment load, it cannot calculate bedload and suspended load separately within its core functionality. The model's focus on short-term simulations (typically 1-2 years) restricts its utility for long-term environmental impact assessments, posing challenges in strategic coastal planning. Furthermore, although it is open source, facilitating broad accessibility and customization, this aspect requires users to possess a considerable degree of technical expertise to deploy and modify the model for specific applications effectively. This could be a barrier for users without extensive modeling experience or those lacking technical resources [38] [54].

3.5 XBeach

XBeach is a complete numerical model designed to simulate nearshore processes during storms, including dune erosion, overwash, and breaching. Hydrodynamic processes in XBeach involve the transformation of short and long waves, the generation of wave-induced setup, and the dynamics of unsteady currents. The morphodynamic processes in the model include the movement of sediment, occurrences of dune face avalanches, and adjustments to the seabed. XBeach has undergone comprehensive validation through various analytical, laboratory, and field test situations. It supports both hydrostatic and non-hydrostatic modes by giving computational flexibility and precision. The original application, funded by the U.S. Corps of Engineers under the Morphos project and the U.S. Geological Survey, aimed to assess hurricane impacts on sandy beaches. Over time, it has broadened its scope to include a variety of coastal settings and applications, such as sandy beaches, urbanized coasts, coral reefs, and gravel beaches [57] [58].

System Architecture

XBeach's architecture consists of multiple interconnected modules, including wave, hydrodynamic, sediment transport, and morphological components. The wave module has a complex wave action balance solver that simulates wave propagation, refraction, and dissipation. Furthermore, the hydrodynamic module employs depth-averaged shallow flow equations using the Generalized Lagrangian Mean (GLM) technique to improve the representation of undertow and sediment transport implications. Moreover, the sediment transport module calculates sediment movement using the Soulsby-Van Rijn transport formulas and advection-diffusion equations. It covers processes for cohesive and non-cohesive sediments and considers numerous sediment components. The morphological module additionally addresses morphological changes caused by sediment movement, using a strong avalanching process that simulates slumping in dunes and bathymetric updates [57] [58]. Figure **3.9** illustrates how these four major modules are interconnected, with output from one module frequently functioning as input for another.

The model's design allows it to dynamically incorporate various processes, resulting in a comprehensive tool for forecasting coastal reactions to extreme weather. The system is designed

to be flexible and durable in a variety of computing contexts since it supports both independent and integrated system applications [57] [58].

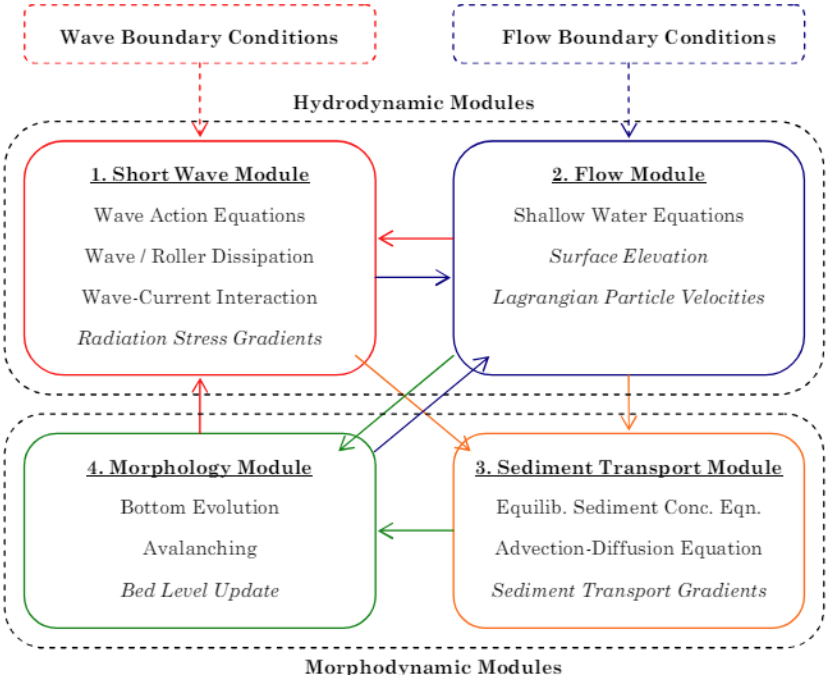

Figure 3.9 XBeach model architecture and interconnection among different modules (Arrows indicate connectivity, and terms in italics show relevant output parameters) [59].

Inputs and Outputs

The model input and output parameters are quite extensive and critical for simulating coastal processes accurately. The input parameters include: i) grid and bathymetry information, which describe the underwater topography, ii) wave and flow conditions to specify the hydrodynamic conditions including wave spectra, water levels, and current velocities, iii) sediment properties by providing the sediment type, size distribution, and other physical properties relevant to transport processes, iv) morphological settings to controls the simulation of morphological changes, v) operational settings, which includes simulation time frame, timestep settings, and specific model functionalities. The Xbeach model provides the details of state of model at specific time steps across the entire model domain as output, such as water depth, bed elevation, and hydrodynamic variables. The model also generates averaged values of variables over specified periods. Moreover, it provides time series data for specific locations within the model domain, which are useful for detailed analysis at points of interest such as inlet channels or near structures. These input and output settings allow XBeach to perform detailed simulations of coastal dynamics under various environmental conditions [57] [58].

Examples of Model Applications

Many studies have developed to understand the morphodynamic and sediment transport pattern by using XBeach. Some of these studies covered the following area: Galveston Bay on the Texas Coast [60], long sandy beaches on the Croatia's Adriatic Coast [61], Maengbang Beach located in Samcheok in South Korea (Figure **3.10**), an open coast of the capital of Aotearoa New Zealand, Wellington [62], Haikou Bay sandy beach in China [63].

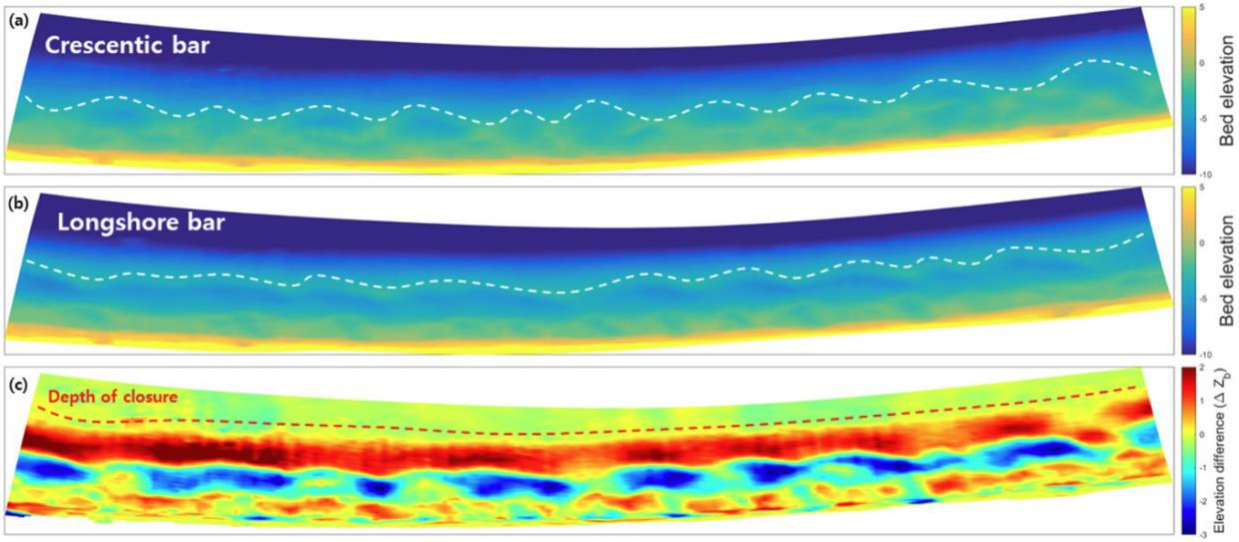

Figure 3.10 Bed Elevation of Maengbang beach, South Korea: (a) Before the storms (white dash line: position of the crescentic bar), (b) After the storms (white dash line: position of the longshore bar), and (c) Elevation difference and closure depth of sediment transport between before and after the storms (red dash line: depth of closure with little sediment transport). These bed elevation data were used to model erosion and morphological changes in the surf zone due to four consecutive typhoons using XBeach [64] .

Pros and Cons

A significant benefit of XBeach is its adeptness at simulating both hydrodynamics and morphodynamics in coastal zones, which is essential for assessing storm impacts on beaches. XBeach advantage lies in its ability to simulate the hydrodynamic and morphodynamic effects of adding a sand cover to hard coastal structures under extreme storm conditions by aiding in the assessment of hybrid coastal protection measures [60]. Moreover, it is a versatile numerical model capable of simulating sediment transport and morphological changes on gravel beaches with low-energetic wave conditions [61]. Additionally, it can handle complex coastal environments with multiple physical processes, such as embayments and different substrate types, while providing high spatial resolution results [62]. Furthermore, XBeach simulations can predict erosion spots under various wave events, aiding in the design of artificial beaches for stability and protection against wave action [63]. However, XBeach has limitations that should

be considered. Its one-dimensionality restricts wave event selection, particularly reduced longshore transport area by limiting its ability to accurately represent sediment changes on gravel beaches [61]. The model also faces challenges in accurately representing erosion and accretion patterns in the surf zone and shoreline, although efforts were applied to optimize parameter ranges through calibration methods [64]. In addition, there is limited validation of sediment transport formulations for the XBeach's morphological response for sandy beaches, despite its capacity to model wave-resolving dynamics in the swash zone [65]. Additionally, while XBeach offers advanced morphological change predictions, its accuracy can be contingent on the precise calibration of model parameters, which may pose a challenge without extensive validation data. Furthermore, the model primarily functions in a 2D vertical plane for most simulations, which might not capture the three-dimensional complexities of some coastal processes, particularly in varied and structurally complex coastal environments.

3.6 LITPACK

LITPACK, developed by the Danish Hydraulic Institute (DHI), is a comprehensive numerical modeling system designed specifically for analyzing littoral processes and coastline kinetics. Its development stems from the need to address complex coastal engineering challenges, such as shoreline erosion, sediment transport, and coastal zone management. One of the key features of LITPACK is its integration of several proven numerical models for simulating distinct littoral processes. This integration allows the system to handle complex interactions between hydrodynamics, sediment transport, and morphological changes, which are crucial for accurate coastal management and planning. LITPACK operates as a 'stand-alone' system, meaning it can function independently of other models by providing a complete solution within one package. LITPACK modules employ a fully deterministic approach, enabling the consideration of numerous factors that may not be accessible to semi-empirical formulations. This approach allows for precise control over all variables and conditions within the simulations, leading to more accurate and reliable outcomes. The model is designed to be versatile, and suitable for a wide range of coastal engineering applications from basic research to practical implementation in coastal protection projects [66] [67].

System Architecture

The system architecture of LITPACK integrates several modules, each dedicated to simulating particular coastal processes and linking among modules. This setup facilitates rapid simulation of complex coastal problems without compromising the detail in individual process simulations. LITPACK consists of the following modules:

- Sediment Transport Processes (STP): This module calculates non-cohesive sediment transport in combined waves and currents. STP solves the vertical sediment diffusion equation on an intra-wave period grid by offering a detailed description of non-cohesive sediment transport for both breaking and non-breaking waves, as well as current.

- LITDRIFT: This module focuses on littoral drift along a uniform beach with an arbitrary coastal profile.
- LITLINE: This module simulates coastline development due to changes in transport capacity.
- LITTREN: This module addresses channel backfilling due to non-equilibrium sediment transport mechanisms.
- LIRPROF: This module develops the cross-shore profile due to transport processes.

The hydrodynamic processes are modeled using fundamental hydrodynamic equations adjusted for littoral contexts by incorporating interactions between wave and current dynamics [66] [67]. The STP module employs Fredsøe's model for turbulent wave-current boundary layers by dividing the boundary layer into regions [68]. Besides, for bedload transport, it uses Engelund and Fredsøe's formula, which is calculated as a function of the dimensionless bed shear stress [69]. It uses Bagnold's dynamic considerations for suspended load transport by incorporating sediment concentration near the bed [70].

Inputs and Outputs

The model inputs include: i) hydrodynamic inputs: water depth, wave properties (height, period, angle), current velocity, and direction; ii) sediment characteristics: sediment properties such as size, gradation, and fall velocity; and iii) coastal profile information: bed slope and coastal geometry. The outputs from LITPACK include time-averaged and time-varying profiles of eddy viscosity, and sediment concentration, velocity, water level, sediment transport in two directions (cross-shore and long-shore), total bedload, and suspended load.

Examples of Model Applications

LITPACK has been used to determine shoreline changes and sediment dynamics in several coastal areas including: Gulf of Manfredonia in Southern Italy [71], West Coast of India [72], the Southeastern Coast of the Apulian region (Italy) along the Adriatic Sea, namely in the Gulf of Manfredonia (Figure **3.11**), the Midia-Mangalia region in Romania [73] and Cat Hai Island in Hai Phong City, Vietnam [74].

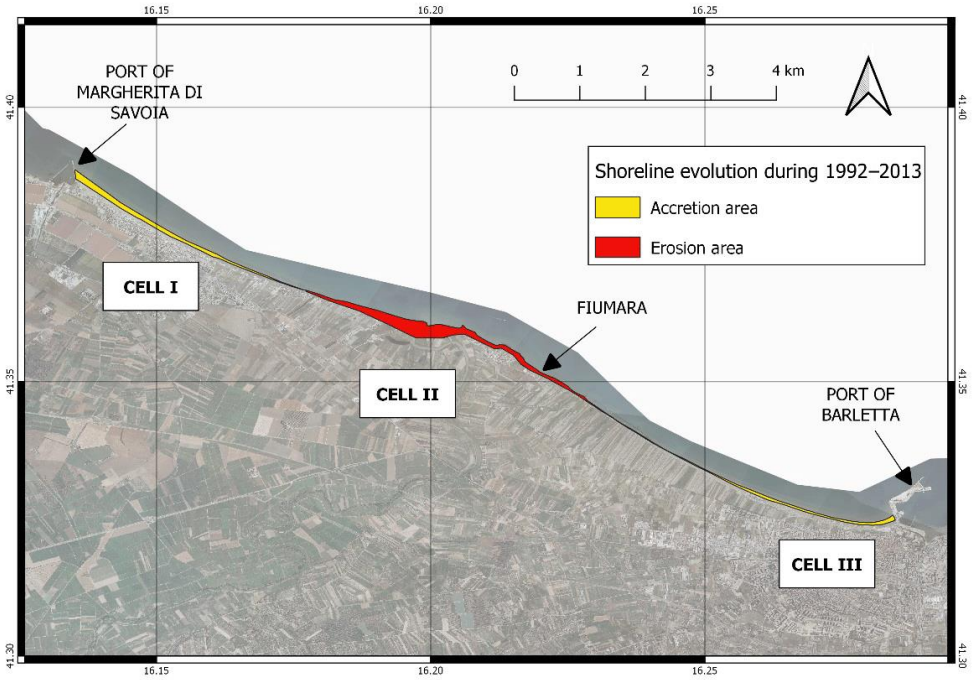

Figure 3.11 Accumulation and retreat areas along the shoreline of the Gulf of Manfredonia, Italy simulated using LITPACK. Shoreline accretion is evident in Cell I near the Port of Margherita di Savoia and in Cell III near the Port of Barletta. In contrast, significant erosion occurred in Cell II, near the Ofanto River [75].

Pros and Cons

LITPACK demonstrates significant strengths in sediment transport modeling, particularly in managing both long-term and short-term coastal evolution processes. The software excels in detailed sediment transport analysis, which allows it to predict erosion and accretion patterns accurately over various temporal scales. The model offers a widely used and tested methodology for handling suspended sediment, characterized by its relatively simple coding approach. It is recognized for its efficiency in modeling coastal processes and has been rigorously validated in various engineering projects. It can simulate coastline evolution, profile development, non-cohesive sediment transport, long-shore currents, and littoral drift along beaches. LITPACK has been widely used in the study of shoreline changes in various areas. [73] [74]. However, LITPACK is not open source, limiting customization and broader accessibility. It is primarily designed for non-cohesive sediment transport modeling. The model operates primarily on a one-line basis, which restricts its ability to perform detailed acreage calculations or evaluate the benefits of overwash. Additionally, the software's performance in long-term simulations remains unclear, particularly in handling complex scenarios such as overwash and dune lowering [38].

3.7 CoSMoS

The Coastal Storm Modeling System (CoSMoS) is an advanced dynamic modeling framework developed by the United States Geological Survey (USGS). CoSMoS is designed to address the impacts of climate change-driven sea-level rise and coastal storms by providing detailed predictions of coastal flooding and shoreline changes such as beach erosion and cliff retreat. CoSMoS operates on multiple spatial and temporal scales, from local to national, integrating oceanographic and terrestrial processes to model coastal changes dynamically. One of its unique approaches is the incorporation of data assimilation to refine largescale modeling with site-specific characteristics and behaviors. Enhancements to the model include the integration of weekly satellite-derived shoreline observations, which significantly increases the volume of data assimilated and improves the accuracy of model predictions [76] [77].

System Architecture

The CoSMoS model is a 2DV coastal profile model designed for simulating nearshore hydrodynamics and sediment transport. Its architecture includes wave transformation processes such as refraction, shoaling, Doppler shifting, bottom friction, and wave breaking. Hydrodynamics are modeled through wave set-up from radiation stress gradients, longshore currents driven by wave-induced and tidal forces, and a three-layer model for the cross-shore undertow. Sediment transport rates are calculated using Baillard's energetics approach, and seabed level changes are simulated based on these transport processes. The model uses offshore wave height, period, direction data, and water levels from fixed poles to drive its simulations. Bathymetric updates are made using longshore-averaged profiles and time series data of wave heights and longshore currents over specified periods (pre-storm, storm, post-storm). CoSMoS employs various statistical measures, such as the Brier Skill Score, Root-Mean-Square Error (RMSE), Mean Absolute Error (MAE), and Willmott's indices of agreement, to evaluate the accuracy and skill of its predictions. The model is efficient and straightforward to set up, making it suitable for modeling coastal processes along straight coastlines with parallel depth contours [78] [79].

CoSMoS has been validated against a broad spectrum of field and experimental data, confirming its predictive accuracy for coastal erosion and accretion. The model's comprehensive treatment of wave transformations, such as shoaling, refraction, and breaking, alongside its ability to model wave setup and longshore currents, provides a robust framework for understanding and predicting coastal dynamics. This capability is enhanced by the model's programming in FORTRAN and its structured modular design, which supports detailed scenario analysis for both cross-shore and longshore transport processes [80].

Inputs and Outputs

Inputs to the CoSMoS model include data on bathymetry, wave and water levels, sediment grain size, and nearshore wave hindcasts [80]. These inputs feed into models that simulate the detailed hydrodynamics and sediment transport dynamics of coastal regions [81]. Outputs from CoSMoS

include detailed flood projections, erosion and sedimentation patterns, and changes in shoreline positions. These outputs are used to inform regional sediment transport predictions and assist in coastal management and planning efforts. Outputs are typically provided as GIS shapefiles along with extensive metadata, facilitating their use in ecological, land use, and infrastructure planning [76] [81].

Examples of Model Applications

CoSMoS has been used in coastal areas such as the Corpus Christi Ship Channel in Texas that connect the Port of Corpus Christi to the Gulf of Mexico [82], at Poole Bay in the UK [80], in the La Jolla region of California [83], Texas Coastal Region 4 covering Cameron, Kenedy, and Willacy Counties in the waters of the Gulf of Mexico [81], at Seaward Lagoon Entrance of Del Mar, California (**Figure 3.12**) [84].

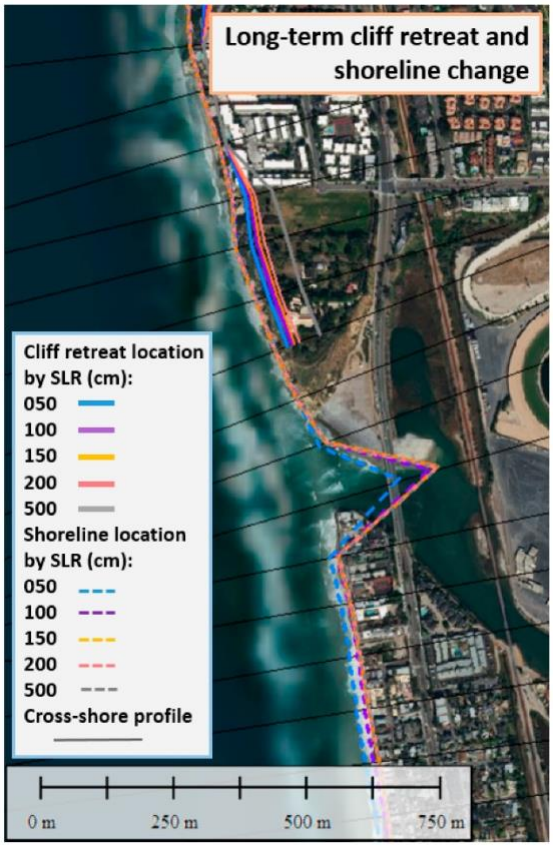

Figure 3.12 CoSMoS simulation results for long-term projected cliff retreat and sandy beach shoreline change under various sea level rise scenarios at seaward lagoon entrance of Del Mar, California [84].

Pros and Cons

CoSMoS offers significant advantages in coastal hazard prediction by providing detailed and scalable simulations that inform a wide range of planning and emergency response activities. A

major advantage of CoSMoS is its integrated approach that combines global, regional, and local modeling scales to assess the impacts of sea-level rise, storm surges, and climate change (summary table). Its ability to simulate a variety of storm conditions and sea-level rise scenarios helps communities understand potential future changes and plan accordingly [76]. However, the model's complexity and computational demands limit its ability to run continuous long-term simulations, which can be a drawback for ongoing monitoring needs [80]. Additionally, while CoSMoS incorporates a vast array of data, the integration and interpretation of these data require significant expertise, which may not be readily available in all regions or organizations [80]. Since it mainly predicts long-term beach changes and coastal cliff retreat, it does not have the option to consider cohesive and non-cohesive soil separately.

3.8 GENESIS

The GENESIS (GENEralized model for SImulating Shoreline change) is a comprehensive numerical modeling system developed to simulate long-term shoreline change in response to various coastal engineering projects. It is a linear shoreline evolution model developed by the U.S. Army Engineer Research and Development Center (ERDC) that uses a mass-balance routine to predict future shoreline positions [85]. GENESIS is particularly adept at predicting shoreline changes due to modifications in longshore sand transport caused by installations such as groins, jetties, detached breakwaters, and other coastal structures. It allows the simulation of nearly any configuration of coastal protection structures, adjusting for a wide range of input variables such as wave conditions, beach configurations, and sediment transport dynamics. Additionally, the model supports the integration of user-defined parameters through a structured, user-friendly interface, allowing for the simulation of diverse scenarios without the need to investigate the complexities of the underlying code. The model assumes that cross-shore transport processes average over the modeling period, focusing instead on the effects of longitudinal transport changes. It is particularly effective for projects aiming to achieve equilibrium between newly installed structures and natural sand transport processes to provide valuable predictions that can guide the design and implementation of coastal protection and rehabilitation projects [86] [87].

System Architecture

The system architecture of GENESIS is a comprehensive framework designed to model coastal processes such as wave transformation, sediment transport, and shoreline change. It consists of several interconnected computer programs that work together to simulate these processes effectively. The Regional Coastal Processes WAVE (RCPWAVE) model, used with GENESIS, directly solves for wave height and angle on a grid. At the core of GENESIS, the system relies on two primary submodels. The first submodel calculates the longshore sand transport rate and shoreline change. This is crucial for understanding how sand moves along the shore due to wave action and how this movement affects the shoreline over time. The second submodel focuses on breaking wave height and angle along the shore, determined from wave information provided at

a reference depth offshore. Additionally, there is an option to use an external wave transformation model, which can provide nearshore wave information to GENESIS. The system operates under several key assumptions typical in shoreline change modeling. These assumptions include a constant beach profile shape, fixed shoreward and seaward profile limits, sand being transported alongshore primarily by breaking waves, the detailed structure of nearshore circulation being negligible, and a long-term trend in shoreline evolution. The governing equation for shoreline change in GENESIS is based on the conservation of sand volume, reflecting these assumptions [87] [88]. Figure **3.13** illustrates the interaction between GENESIS and RCPWAVE within the overall calculation flow of the shoreline response model. GENESIS, which simulates shoreline changes, relies on accurate wave data to predict sediment transport and shoreline evolution.

The architecture of GENESIS ensures that data and results are dynamically exchanged between the submodels. The process begins with the generation of a computational mesh, which represents the study area's bathymetry and topography. This mesh interacts with the hydrodynamic and sediment transport modules to simulate currents and sediment transport. These simulations help generate insights into coastal dynamics, aiding in the prediction and management of shoreline changes [87] [88].

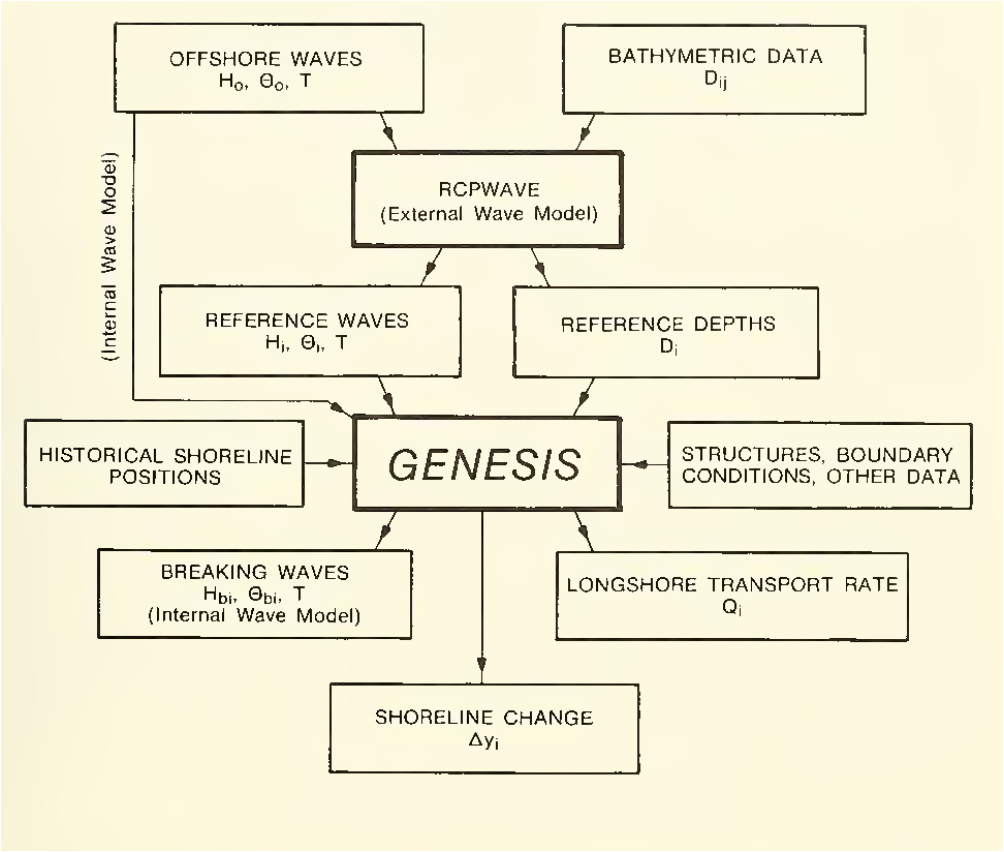

Figure 3.13 Relation between GENESIS and RCPWAVE in the overall calculation flow [87].

Inputs and Outputs

GENESIS requires several key input files and physical parameters for accurate simulations. The mandatory input files for running the model are START, WAVES, SHORL, and SHORM. The START file contains the instructions controlling the simulation, SHORL contains initial shoreline positions, SHORM holds measured shoreline positions for comparison, and WAVES provides wave information needed for calculating sand transport rates. Additional files such as SEAWL, NSWAV, and DEPTH are required only if specified by the project. SEAWL includes seawall positions, NSWAV contains nearshore wave height and direction data, and DEPTH provides water depths necessary for wave propagation [87] [88].

The model outputs are stored in three files: SETUP.DAT, OUTPT.DAT, and SHORC.DAT. SETUP.DAT contains basic information, instructions, and error messages, helping the modeler review parameters and identify errors quickly. OUTPT.DAT includes major calculation results, such as shoreline positions, sand transport volumes, and breaking wave data, while SHORC.DAT holds the final calculated shoreline position, useful for subsequent simulation stages and compared with measured data [88].

Examples of Model Applications

GENESIS has been used to predict shoreline changes in in several coastal areas including Rangsang Island, Riau province, Indonesia (**Figure 3.14**), at Milford-on-Sea; in the county of Hampshire on the Southern coast of the United Kingdom [89], Grays Harbor, Washington [90], and Sarasota County, Florida [91].

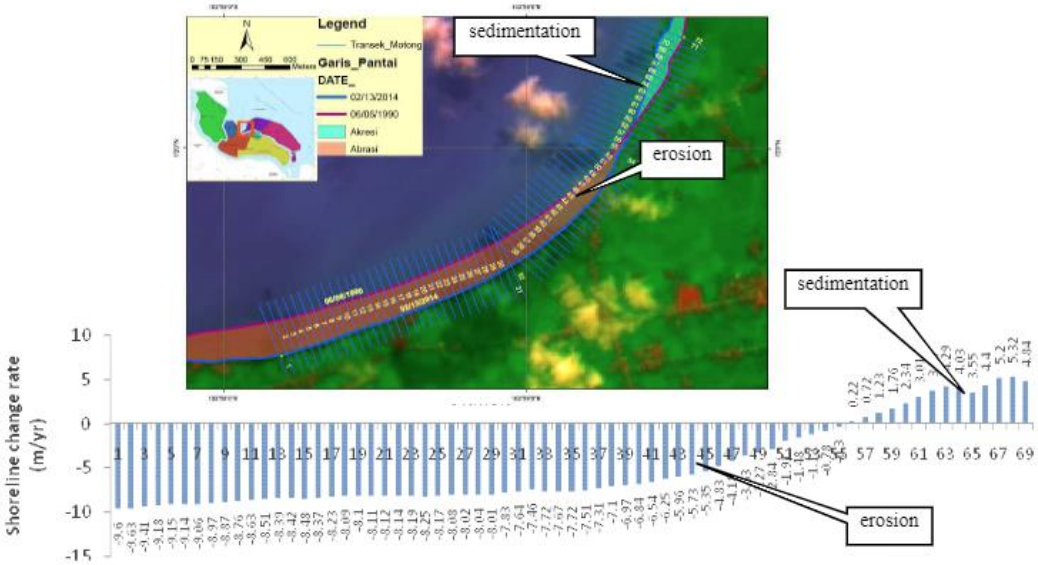

Figure 3.14 Rate of shoreline change of Tanjung Motong Coast simulated using GENESIS. After processing 1990 and 2014 Landsat data, the digitized shorelines were overlaid to identify changes over 24 years, revealing erosion and sedimentation areas. The shoreline change rate at the coast was analyzed across 72 stations at 100-meter intervals [85].

Pros and Cons

GENESIS is typically used to calculate shoreline response to engineered or natural perturbations, such as constructing a breakwater, placing beach fill, or sand discharge from a river. The model can handle numerous combinations of coastal structures, sand bypassing, diffraction at structures, wide spatial coverage, arbitrary offshore wave inputs, multiple wave trains, sand transport due to oblique waves, and longshore wave height gradients [87] [88]. The GENESIS shoreline response model was enhanced with automated time-dependent calculations of the wave transmission coefficient using published empirical formulas, improving its predictive capability for shoreline response [92]. It is a widely used tool for predicting shoreline behavior in response to various coastal engineering activities [93]. However, the model is not suitable for simulating randomly fluctuating beach systems without evident shoreline trends. It cannot accurately model shoreline changes due to beach changes inside inlets, areas dominated by tidal flow, wind-generated currents, storm-induced beach erosion, or scour at structures. The model limitations include no wave reflection from structures, no tombolo development, minor restrictions on structures' placement, and no direct provision for changing tide levels. [87] [88]. Moreover, the model's assumptions and oversimplifications, hindering its effectiveness as a predictive tool [94]

3.9 SBEACH

The SBEACH (Storm-induced BEAch CHange) model, developed the U.S. Army Corps of Engineers, calculates beach and dune erosion under storm conditions. SBEACH is part of the CEDAS (Coastal Engineering Design & Analysis System) package and is designed to predict beach changes near coastal projects. The model focuses on macroscale sediment transport over meters and hours, excluding longshore transport gradients and assuming that sediment transport rates from large wave tank experiments apply to field conditions. Initial field tests required scaling adjustments, after which the model showed favorable agreement with measured post-storm profiles on U.S. coasts [95] [96].

Several reports were published from 1989 to 1998 detailing updates to the SBEACH model. The first report (1989) details the large wave tank experiments and the data analysis techniques used to derive the fundamental equations for the numerical model [97]. The second report (1990) provides an in-depth description of the model development and the numerical scheme [98]. The third report (1993) offers hands-on guidance for implementing SBEACH via a user interface available for personal computers [99]. The fourth report (1996), presents verification tests and the development of an optional randomized wave model that can be used within the SBEACH program [100]. In Report 5 (1998), a hard bottom (HB) is defined as a non-erodible bottom feature that can be located anywhere on the subaerial and subaqueous beach. This report focuses on modifying SBEACH to account for non-erodible (hard) bottoms in the calculations of dune and beach erosion [97].

System Architecture

The SBEACH model consists of several components, each addressing different aspects of coastal erosion dynamics [95]:

- *Wave Height Module:* This module calculates wave height across the profile considering wave breaking and reformation. It uses various equations to manage wave transformations as they approach the shore, including energy flux calculations and adjustments based on seabed contours. Wave height determines where and how waves break and reform, which is critical for understanding the impact of wave energy on sediment transport and beach profile changes.
- *Sediment Transport Module:* Sediment transport is calculated based on the energy dissipation of breaking waves. This module uses empirically derived formulas to estimate sediment movement, considering different zones along the shore. Four distinct transport zones are defined based on nearshore wave dynamics and sediment transport characteristics (**Figure 3.15**): Zone I extends from the seaward depth of effective sand transport to the break point, known as the pre-breaking zone, Zone II spans from the break point to the plunge point, referred to as the breaker transition zone, Zone III covers the area from the plunge point to the point of wave reformation or the swash zone, known as the broken wave zone, and Zone IV ranges from the shoreward boundary of the surf zone to the shoreward limit of run-up, termed the swash zone. This is crucial for predicting how materials move along the shore during storm events, influencing erosion and deposition patterns [98].
- *Profile Change Module:* This module applies the sediment transport calculations to predict changes in the beach profile. It uses the concept of conservation of mass to adjust the profile based on predicted sediment transport by addressing the changes in the beach's physical shape due to erosion and deposition.

These components work together within the SBEACH model to provide a comprehensive tool for simulating and understanding the dynamics of coastal erosion [95].

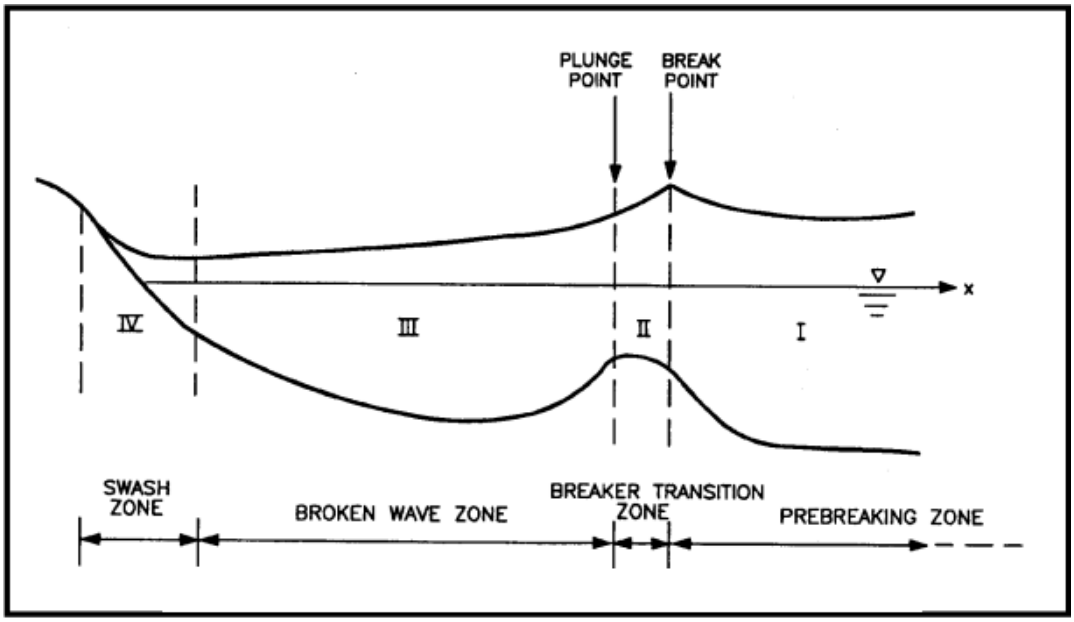

Figure 3.15 Schematic diagram of the four sediment transport regions determined by cross-shore wave height profile [98].

Inputs and Outputs

To run the SBEACH model, five types of input data are required: i) initial beach profile (a two-dimensional shoreline description), ii) median grain size, iii) water level time series, iv) wave height and period time series, and v) model parameters. The beach characteristics and sediment transport parameters are also needed for model calibration. There is the option for incorporating shoreward boundary conditions, wave direction time series, and wind speed or direction time series [99] [100] [101].

The SBEACH model outputs four files. At first, "*data_set.PRC*" contains simulated profiles at intermediate time steps and the final calculated profile. Secondly, "*data_set.XVR*" provides a cross-shore variation of wave height and water elevation. Thirdly, "*data_set.LOG*" records coastal processes such as accretion and erosion. Lastly, "*data_set.RPT*" reports input data and beach profile changes, including berm erosion and bar formation. These files collectively capture key beach profile changes during and after the simulation [95] [99].

Examples of Model Applications

SBEACH has been employed in several coastal areas to calculate the shoreline changes. Examples include Assateague Island of Maryland and Virginia coastline [95], Hatteras Island on the North Carolina coastline [95], Bogue Banks of Carteret County in North Carolina (**Figure 3.16**), Broward County for Hurricane Irma (2017) in Florida [102], and Sabine Pass to Galveston Bay, Texas [103].

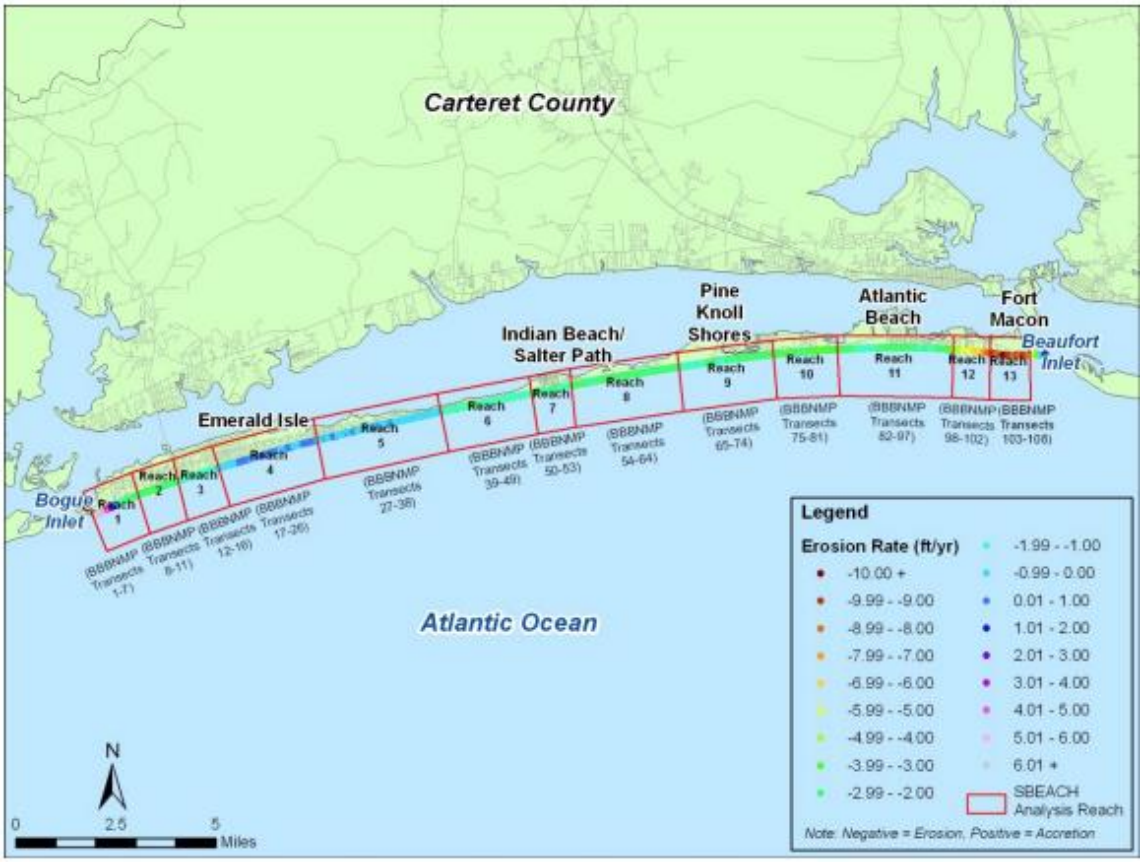

Figure 3.16 SBEACH analysis reaches along Bogue Banks of Carteret County in North Carolina. The limits of each SBEACH analysis reach and the adjusted long-term erosion rates, along with survey transects from the Bogue Banks Beach and Nearshore Mapping Program (BBBNMP). Representative profiles for each reach were created using BMAP (Beach Morphology Analysis Package) within CEDAS [101].

Pros and Cons

SBEACH, a geomorphic-based model, specializes in assessing storm-induced erosion, making it ideal for short-term analyses. By prioritizing breaking waves and fluctuating water levels, it offers insights into beach dynamics, especially in sandy environments with uniform grain sizes. Its adaptability to varying water levels, wave characteristics, and shoreline conditions. Notably, it excels in simulating breakpoint bar formation and beach recovery and analyzing cross-shore sand transport rates for its advanced wave modeling capabilities. The effectiveness of SBEACH in the short-term prediction of beach profile response to storm events makes it particularly useful for emergency response planning and coastal engineering applications. However, SBEACH is not without limitations. Its effectiveness diminishes when faced with non-uniform grain sizes or underlying clay or rock layers. SBEACH is primarily designed for storm-induced changes over shorter periods, which may not accurately reflect long-term coastal evolution and sediment dynamics. Historically, its approach to overwash was simplistic, resulting in inaccuracies due to data constraints, particularly regarding dune overwash. Additionally, its focus primarily on the

dune, beach face, and surf zone dynamics excludes detailed predictions of sediment movement offshore or under non-breaking waves. The hard-bottom capability limitations further restrict its applicability in certain scenarios, making it less suitable for comprehensive long-term coastal assessments [98] [99] [100].

3.10 Examples of Morphodynamical Modeling in Coastal Areas

Among the morphodynamical modeling studies conducted in coastal areas, three were selected that utilized Delft3D, TELEMAC, and MIKE 21. These studies were briefly presented in the previous sections; however, additional information on these studies, including the modeling approach and findings, is provided in the following sections.

Case Study #1: Dynamic Sediment Modeling in the Rhone Delta, Italy Using Delft3D [22]

Using Delft3D's high-resolution modeling capabilities, the study investigated sediment flow in the Rhone delta in the Mediterranean Sea, specifically during storm and flood events. This study highlighted how storm occurrences are the main causes of morphological changes in the Rhone delta, an area where it is difficult to detect changes in-situ because of environmental factors. In order to quantify the impact of storm and flood events on sediment transport, the modeling efforts considered a variety of hydrodynamical and morphological observations and included scenarios that represent varied wave and flow conditions. For instance, it highlighted storms, which accounted for a significant proportion of events between 1979 and 2010, often preceded floods by a few days. These observations were utilized to adjust the Delft3D simulations under specific conditions. The results of the simulations showed patterns in the transport of bedload sediment that correspond with bathymetric data that has been obtained. In particular, the study found that total sediment transport at the Rhone's outlet is predominantly influenced by river flow, while sediment transport at the mouth-bar relied on a balance between the impacts of floods and storms events. A 10-year flood with 5-meter waves was one of the scenarios used to compute the total sediment transportation, and the results showed that a maximum of 0.02 m^3/s was moved both landward and seaward (**Figure 3.2**).

The study emphasized the significance of temporal succession in sediment dynamics, pointing out that sediment transport can be significantly influenced by even short intervals, such as two or three days, between storm and flood peak. Overall, the study shows how utilizing geomorphological models such as Delft3D may improve our understanding of sediment transport patterns, particularly in dynamic and complicated settings such as river deltas.

Case Study # 2: Sediment Transport Modeling along Region 4 of Texas Gulf Coast Using TELEMAC [30]

The TELEMAC modeling system was utilized in to examine the dynamics of regional sand movement in Texas Gulf Coast. The main object of the study was to enhance understanding of the pathways and fluxes of sand transport in this area by incorporating several modeling techniques into the TELEMAC system. TELEMAC-2D was used in the study to simulate water

levels and currents throughout the Region 4 (**Figure 3.4**). An adaptive unstructured mesh was incorporated into the model design to improve accuracy and computational efficiency in the areas of interest. By solving equations for bedload and suspended load for a range of sediment sizes, the SISYPHE module was used to describe the movement of sediment. This model is particularly adept at handling mixed sediment systems, which was essential for the diverse sediment profiles along the Texas coast.

In order to address the transformation of wave energy throughout the coastal area, including processes such wave shoaling, refraction, and breaking, TELEMAC was additionally combined with the wave model TOMAWAC. The findings provided insight into the complex interactions between sediment transport and wave-induced currents, helping to explain how regional sediment dynamics affect coastal accretion and erosion patterns. At the regional level, ocean currents cause sediment pathways to move across the continental shelf to the south (Figure **3.4**). The intensity of southward transport increases towards the south, with higher rates off the coast of Cameron County compared to Kenedy and Willacy Counties. By incorporating littoral drift rates from historical and recent studies as well as sedimentation rates in navigation channels, the model outputs were verified against observable data. A multi-dimensional analysis of sediment transport was made possible by the integration of different TELEMAC modules, which provides a foundation for future coastal management and environmental conservation initiatives along the Texas Gulf Coast.

Case Study #3: Modeling Sediment Dynamics in the Rethymno Coastline, Greece Using MIKE 21 [47]

The objective of the study was to develop and assess a novel input-reduction method for simulating long-term morphological bed evolution by focusing on the initiation of sediment motion. The methodology involved comparing the newly developed pick-up rate method with the widely used energy-flux wave schematization method. The study utilized the MIKE21 Coupled Model FM, known for its robust and detailed simulation capabilities in wave propagation, hydrodynamic circulation, sediment transport, and morphology. This model's strength lies in its ability to accurately simulate complex coastal processes over large areas and extended periods. Data sets of 7, 20, and 365 days were used to evaluate the model's performance. This approach was applied to the coastline near the port of Rethymno, Greece, and validated against observed data. The results demonstrated that the pick-up rate method significantly reduced computational time while maintaining high accuracy. For example, in a year-long simulation, the pick-up rate method reduced the data set by 57.17%, cutting the model run-time by 56.80%, compared to the energy-flux method's run-time reduction. **Figure 3.6** illustrates the model performance by comparing the observed and simulated shoreline changes over different periods, showing that the pick-up rate method closely matches the observed data. The study concludes that the pick-up rate method can effectively predict long-term bed evolution with reduced computational effort by leveraging the strengths of the MIKE21 model and offering a valuable tool for engineers and scientists involved in coastal morphological simulations.

3.11 Applications of Remote Sensing in Study of Sediment Dynamics in Coastal Areas

Utilizing numerical models is essential for understanding sediment dynamics in coastal areas. The performance of these models depends on accurate calibration and validation using field sediment data. Traditionally, measuring suspended sediment involves collecting field samples, which is time-consuming and dangerous, especially during severe storms. Additionally, these samples provide only point values at the time of collection. Less labor-intensive methods, such as satellite imagery, specifically surface reflectance data, may be used to estimate suspended sediment concentration (SSC) in coastal areas. Satellite imagery offers spatial and temporal measures of suspended sediment that field data cannot easily achieve.

Remote sensing data have been used to develop new models by correlating reflectance values with field sediment values. This method provides high-resolution, real-time monitoring and forecasting of SSC dynamics. For example, in the Gulf of Bohai, remote sensing data were used to assess the accuracy and applicability of several retrieval models, including statistical regression, principal component analysis, neural networks, and semi-analytical models. Results of this assessment supported further studies of marine sediment migration and served as a reference for selecting SSC models in similar regions [104]. In large-scale basins, remote sensing data such as surface spectral reflectance improved sediment transport model evaluations by offering better spatial and temporal coverage than traditional SSC measurements. This was particularly beneficial for poorly gauged or ungauged basins, enhancing the analysis of simulated SSC dynamics [105]. Sediment data obtained from remote sensing methods have been employed in several coastal studies to enhance the accuracy and reliability of numerical models. For example, the MEdium Resolution Imaging Spectrometer (MERIS) was used to validate and enhance the Delft3D-WAQ model for the Southern North Sea along the Dutch coast [106]. Similarly, in the Jiaojiang Estuary, the MIKE 3D model integrated data from the Geostationary Ocean Color Imager (GOCI), achieving a 72% correlation between remotely sensed and simulated SSC [107].

Remote sensing techniques provide a transformative approach to sediment modeling by enabling more precise, extensive, and timely data collection. These advancements can improve model validation, calibration, and accuracy, leading to a more comprehensive understanding of sediment dynamics in coastal areas.

4. SUMMARY AND CONCLUSIONS

The Texas coastline faces ongoing challenges from coastal erosion due to storms, sea-level rise, and human activities like coastal development. Quantifying or predicting sediment dynamics in coastal areas is complex because of the varied processes influencing erosion and sediment transport. Sediment budget analysis employs quantitative methods and hydro-geomorphological models, which simulate sediment transport, erosion, and deposition. The choice of model depends on the study area's characteristics and available data. Hydro-geomorphological models are particularly accurate, providing detailed insights into sediment quantities, fluxes, and transport pathways.

The primary objective of this study was to conduct a thorough literature review on the state of practice in sediment dynamics modeling of coastal areas. The goals included examining approaches for modeling sediment dynamics in coastal rivers and estuaries, identifying the advantages and shortcomings of widely used hydro-morphodynamic models, and exploring the uncertainties and errors in current sediment transport modeling practices. This report guides the use of these models for simulating coastal sediment dynamics.

4.1 Summary of Evaluating Hydro-geomorphological Models for Coastal Applications

The report provides a comprehensive review of nine widely-used hydro-geomorphological models, emphasizing their application in coastal settings. The ability of various models, including Delft3D, TELEMAC, MIKE 21, ADCIRC, XBeach, LITPAK, CoSMoS, GENESIS, and SBEACH to reproduce the complex relationships between hydrodynamics, sediment transport, and morphological changes was assessed. Several of these models simulate wave propagation, currents, and tidal movements, which are essential for analyzing coastal dynamics. Detailed sediment transport simulations, handling both bedload and suspended load, are offered by Delft3D, TELEMAC, MIKE 21, and XBeach. LITPACK, SBEACH, and GENESIS primarily focus on longshore and cross-shore sediment transport, while CoSMoS specializes in coastal hazard simulations, including morphodynamic changes. Table 4.1 provides a summary of each model's capabilities, including their morphological features and additional functionalities. Table 4.1 provides a summary of each model's capabilities, including their morphological features and additional functionalities.

Each model presents unique characteristics and capabilities in simulating sediment dynamics in coastal settings and estuaries. For example, Delft3D stands out for its ability to simulate detailed morphodynamics, making it ideal for settings where the interaction of many physical processes is important. TELEMAC is an excellent tool for managing huge datasets and provides reliable hydrodynamic modeling, which is critical for large-scale coastal studies.

The review also highlights the challenges associated with each model. For instance, MIKE 21 is recognized for its user-friendly design and wide range of modeling possibilities, but its high computing demands may limit its use in projects with limited resources. Additionally, certain

models, such as MIKE 21, are not open source, which limits their adaptability and accessibility, a significant consideration for the scientific community.

ADCIRC, XBeach, LITPAK, CoSMoS, GENESIS, and SBEACH each offer specific advantages for particular applications. ADCIRC is noted for its capability in simulating storm surge and tidal effects. Xbeach demonstrates unique capabilities in modeling coastal processes during extreme storm events. LITPAK is useful for long-term shoreline evolution studies. CoSMoS provides detailed sediment transport and coastal morphodynamic predictions. GENESIS is effective in simulating longshore sediment transport and shoreline change. SBEACH is particularly valuable for predicting beach profile changes under storm conditions, making it a crucial tool for understanding and mitigating coastal erosion during extreme weather events.

Delft3D, MIKE 21, and TELEMAC handle large spatial scales and long-term simulations, making them suitable for extensive environmental studies. In contrast, SBEACH and GENESIS are more suitable for short-term event-based simulations.Delft3D, MIKE 21, and TELEMAC are versatile for various environments, including rivers, estuaries, and coasts, whereas GENESIS and SBEACH are specialized for coastal processes.

TELEMAC, XBeach, and ADCIRC are open source, facilitating customization and broad use, while MIKE 21 and LITPACK are commercial, limiting accessibility. SBEACH and GENESIS are user-friendly and less complex, whereas Delft3D and TELEMAC require advanced user expertise.

Commonalities among these models include their ability to simulate essential hydrodynamic processes and incorporate sediment transport mechanisms. Many models, such as Delft3D, TELEMAC, and MIKE 21, also provide detailed morphodynamic simulations. However, there are notable differences in computational demands and application specificity. TELEMAC, MIKE 21, and ADCIRC are more resource-intensive, while GENESIS and SBEACH focus on shoreline changes and are less demanding computationally.

Accessibility also varies, with open-source models offering more customization options compared to commercial models. XBeach is particularly useful for simulating storm impacts on coastal morphology, dune erosion, and overwash. LITPACK is effective for analyzing longshore sediment transport, coastal profile development, and shoreline evolution. CoSMoS is valuable for predicting coastal hazards and long-term shoreline changes due to sea-level rise. GENESIS and SBEACH are suitable for projects focused on short-term shoreline changes, sediment transport by wave action, and the impact of coastal structure.

Table 4.1 Capabilities of several hydro-geomorphological models in simulating sediment dynamics in coastal area.

Software	Basic Capabilities				Morphological Capabilities			Other Capabilities			General Notes	Reference No.
	Bed Load and Suspended Load Calculations	Meshing	Governing Equations	Grain Size (Bed Material and Sediment Flux)	Shoreline	Bed Change/ Bathymetry	Bank Accretion/Erosion Rate	Wind	Wave	Cohesive and Non-Cohesive Sediment Modeling		
Delft3D	Sediment transport and morphology module supports both bedload and suspended load transport separately.	Grid refinement both in the horizontal and vertical directions.	The equation system includes momentum equations, continuity equations, transport equations, and a turbulence closure model. Sediment transport, influenced by combined waves and currents, is computed using an advection-diffusion equation. The FLOW module solves the Navier–Stokes equations to model incompressible fluid flow, incorporating both shallow water and Boussinesq assumptions.	Grain size can be specified for bed material and sediment flux separately.	It can determine shoreline accretion/ erosion rate.	During the suspended sediments and bedload transport modeling, the software updates the bathymetry during the FLOW simulation.	For cohesive sediment, it uses Partheniades-Krone formulations, and for non-cohesive sediment in 2D and 3D; it calculates based on the transfer of sediment between the bed and the flow.	The FLOW module's current/wind prediction data are used as input to compute sediment transport.	WAVE module is used for modeling sediment transport for wave transformations using SWAN model. Although the information about wave climate can be extracted as output, it does not predict suspended sediment transport under breaking wave conditions accurately.	Delft3D-SED is a sub-module of the water quality module, that mainly focuses on cohesive and non-cohesive sediment transport. It accommodates bedload and suspended load transport for non-cohesive sediments, along with suspended load transport for cohesive sediments.	Delft3D-SED sub-module mainly focuses on sediment transport, FLOW for hydrodynamic computations, WAVE for wave transformations, and morphology (MOR) integrated into FLOW and interact with SED and WAVE.	[9] [15][14]
TELEMAC	SYSPHE, the sediment transport module uses various sediment transport formulas to calculate both bedload and suspended load within its sediment transport modules.	It employs an unstructured finite element grid that allows flexible meshing, which is suitable for complex geometries.	The software solves the shallow water Saint-Venant equations for hydrodynamics and uses advection-diffusion equations for sediment transport.	It allows for the specification of different grain sizes, which affect bed material and sediment flux calculations.	It observes shoreline changes over time.	It can model bed level changes over time, along with updating bathymetry based on sediment transport.	The system can assess and predict the rates of erosion or accretion along coastal lines impacted by currents and sediment dynamics.	It considers the wind influence on water surfaces to simulate sediment transport.	Wave propagation simulations, along with wave-induced currents and longshore sediment transport, are conducted by using a 2D sediment and hydrodynamic model.	It handles both cohesive and non-cohesive types of sediments within its sediment transport module, SYSPHE for allowing diverse applications.	It provides comprehensive interaction modeling between hydrodynamic, sediment transport, and morphodynamic processes for an analysis.	[28] [29] [27]
ADCIRC	It is capable of calculating suspended load but does not calculate bed load and suspended load separately within its core functionality.	It uses a flexible, unstructured grid that allows for refinement in areas of interest.	Governing equations for sediment concentration is advection-diffusion quasi 3D equation. For ADCIRC v55, the governing equation was corrected by incorporating spherical coordinates, which enables simulations of larger global domains.	The model accommodates multiple grain sizes in a simulation. It sequentially processes suspended distribution for each size, which is corresponding to depth change.	It can predict changes in shoreline features.	The bathymetric change is calculated by weighted inverse-distance interpolation method, which consider the bed change rate and existing water column concentration.	The model output is utilized to estimate spatial and temporal advection, dispersion, and bottom shear stress by addressing erosion, suspension, deposition, and transport processes.	It can model the effects of wind on water surface elevations and currents.	It often couples with wave models like SWAN to simulate wave dynamics.	The sediment transport module covers both cohesive and non-cohesive types of sediments independently.	It has the capability to interact among wind-driven wave generation, wave-induced current and seabed shear stress to model hydrodynamics and sediment transport processes.	[49] [51]
MIKE21	Sediment Transport module calculates bed load and suspended load separately.	A flexible mesh approach in horizontal direction only, high-resolution in areas of interest, coarser elsewhere, for computational efficiency.	The hydrodynamic module uses the shallow water equations. The sediment transport integrates these equations with the advection-diffusion equation for sediment continuity. It uses empirical formulas like the Engelund-Hansen for bed load and the Van Rijn formula for suspended load, depending on the module configuration.	It supports multiple grain sizes and enabling the user to define specific sediment classes.	It integrates 1D shoreline morphology with 2D wave, current, and sediment transport from MIKE 21 Sediment Transport module.	The Hydrodynamic and Sediment Transport modules collectively predict bed level changes using sediment continuity equations.	Simulation of bank changes by using the hydrodynamic and sediment transport data can be inferred as erosion or accretion.	It incorporates wind effects on wave generation, water levels, and sediment dynamics. That is how it enables accurate simulation of sediment resuspension and transport processes.	It can compare wave, current, and sediment transport patterns by selecting between interpolation-based or Bijker's method for sediment transport calculation in MIKE 21 sand transport simulations.	It has Sand Transport Module for non-cohesive and Mud Transport Module for cohesive sediment transport modelling.	It has an integrated approach, where sediment transport interacts with hydrodynamics, wave transformations, and morphological changes. This approach ensures a comprehensive environmental simulation.	[42] [43]
XBeach	Both bed load and suspended load account sediment movement along the bed and within the water column, respectively.	It can make structured and non-structured grid, which must be curvilinear.	The sediment transport module uses coupled equations for bed load and suspended load transport, influenced by currents and waves. For bed load, it typically employs empirical formulas like the Meyer-Peter & Müller formula, while suspended load is often calculated using advection-diffusion equations.	Although XBeach is primarily focused on non-cohesive sediments, it can account for different grain sizes in its sediment transport calculations, which impacts the bed material and sediment flux modeling.	It utilizes cross-shore and longshore transport equations to simulate shoreline changes.	It applies the gradients of sediment transport, which is integrated with hydrodynamic calculations to simulate bed level changes.	Generally, it relies on the same morphodynamic principles and sediment transport equations to develop shoreline and bed change simulations	It accounts for wind-induced effects on wave generation, which impacting sediment transport through wave-driven currents and shear stress mechanisms.	It simulates wave processes (long wave and turbulence-induced short wave separately), which directly influence sediment resuspension, transport, and deposition.	It is primarily designed for non-cohesive sediment modeling.	It can interact among wave, current, mean flow and sediment characteristics to determine how sediment is eroded, transported, and deposited along the coast.	[56] [57]
LITPACK	It can consider both bed load and suspended load sediment transport, which are calculated separately.	It can calculate long shore and cross shore sediment transportation by one-dimensional grids.	Bed load transport follows Engelund and Fredsoe's 1976 model, while suspended load transport is determined by the vertical turbulent diffusion equation.	The model allows the specification of different grain sizes for both the bed material and the sediment in transport, which can be defined by either uniform or graded grain descriptions.	It can simulate shoreline evolution including accretion and erosion dynamics, which are influenced by waves, currents, and sediment availability.	The model can update the bathymetry changes as a result of sediment transport processes for both short-term events and long-term developments.	It can calculate beach accretion and erosion close to shoreline.	It can account for the impact of wind on wave generation, which indirectly affects sediment transport.	It simulates wave-induced currents and their effect on sediment movement along with beach profile development.	It is primarily designed for non-cohesive sediment transport modeling.	It integrates the effects of hydrodynamics, sediment transport, and morphological change. That is how this comprehensive approach is essential to coastal process simulation.	[65] [66] [42]
CoSMoS	It can calculate both bed load and suspended sediment load, but not separately.	It has flexible meshing capabilities, which can incorporate wave or hydrodynamic model grid size.	The model balances sediment gains and losses to ensure that sediment volume remains constant by using energetics approach and the continuity equation.	Sediment size of 0.25 and 0.28 mm are incorporated in version 1.0 and 2.0, respectively. One constant mean grain size is used for an specific area.	For predicting shoreline evolution, the drifts calculated by CoSMoS are to be applied for further calculations in others software like BEACHPLAN of XBeach.	In Morphological module, bathymetry updates corresponding to hydrodynamic module. The Lax-Wendroff scheme is employed to simulate seabed level changes caused by cross-shore sediment transport.	It can evaluate and predict locations and magnitudes of erosional hot spots during storms. Coastal erosion and shoreline retreat can be measured within CoSMoS by simulating in another software like XBeach or BEACHPLAN.	It can estimate the surge to downscale wind data obtained from Global Climate Models (GCM).	It is used to measure wave transformations and beach responses.	Since it mainly predict long-term beach changes and coastal cliff retreat, it does not have the option to consider cohesive and non-cohesive soil separately.	It interacts with other models, which facilitates the consideration of various coastal variables such as wind, waves, discharge, and sediment transportation.	[77] [78] [79] [81]
GENESIS	It does not calculate bed load and suspended load. It calculates the volume of sediment to measure shoreline changes.	It uses a one-dimensional grid along the shoreline to simulate changes over time.	The governing equation for shoreline change is formulated by conservation of sand volume.	It determines effective median grain size to represent the profile shape of beach grain size.	It is mainly a model to calculate the shoreline change by spatial and temporal differences along the longshore.	Hydrographic charts are utilized for digitizing bathymetry onto the numerical grid.	It can identify the location of erosion and accretion based on bathymetry data.	It can consider the effects of daily and seasonal trends in wind speed, gustiness, and direction to determine the shoreline	It allows simulation of a wide variety of user-specified offshore wave inputs.	Since it only determines the effect of shoreline change based on sediment volume, it does not consider cohesive and non-cohesive sediment	The interaction between wave action and sediment availability is developed to determine the affect of shoreline evolution.	[85]
SBEACH	It models cross-shore sediment transport primarily due to storm surge and wave action, but not specifically calculate bed load and suspended load.	It develops a cross-shore and one-dimensional grid system to simulate changes in beach profiles.	The wave transformation, net cross-shore transport rate, and beach change are calculated based on empirical relationships and conservation of energy flux.	It can calculate for an arbitrary initial beach profile shape and a specified grain size in the sand range.	It can predict short-term erosion and accretion of the shoreline due to storm impacts, but not long-term evolution.	It sequentially compute wave height, cross-shore sand transport, and profile change, which update the bathymetry iteratively to measure morphological evolution over the simulation period.	It focuses on forecasting profile change during erosional and accretionary occurrences, particularly for storm events.	It can specify wind speed and direction to calculate beach profile and sediment transport.	It is primarily focused on wave action. It simulates the impact of breaking waves on the beach profile during storm events.	It is developed for sandy, non-cohesive beaches.	It considers the interaction between wave action and sediment transport in its simulations.	[93] [94] [95]

4.2 Conclusions

Sediment dynamics in coastal zones are challenging to quantify due to the complexity of processes governing erosion and sediment transport. This leads to significant uncertainties in sediment budget estimates, which arise from deficiencies in transport models and lack of accurate sediment supply information. Currently, sediment budget analysis is often conducted using quantitative models (discussed in **Chapter 2**) and hydro-geomorphological models (discussed in **Chapter 3**).

Quantitative sediment budget models are simple, efficient, and cost-effective, integrating various data sources to provide a comprehensive overview of sediment dynamics over large scales. However, their simplicity results in limited detail and accuracy, high uncertainty, and a static nature that fails to capture dynamic processes effectively. In contrast, hydro-geomorphological models offer detailed process representation and predictive capabilities, making them valuable for scenario testing and planning. They simulate interactions between hydrodynamics, sediment transport, and morphological changes accurately. However, these models are complex, resource-intensive, and require extensive data and user expertise. This complexity can be a barrier for smaller projects or organizations with limited resources.

This review highlights the importance of selecting the appropriate model based on project requirements and environmental conditions. For optimal results, the model's setup, input requirements, and output capabilities must align with the project's objectives. The comparison study not only clarifies the capabilities of these models but also identifies potential areas for future improvement.

REFERENCES

[1] Rosati, J. D., and Kraus, N. C., 2003, Sediment Budget Analysis System (SBAS) : Upgrade for Regional Applications, Coastal and Hydraulics Laboratory (U.S.).

[2] Dopsovic, R., Hardegree, L., and Rosati, J. D., 2003, Sediment Budget Analysis System-A : SBAS-A for ArcView© Application, Coastal and Hydraulics Laboratory (U.S.).

[3] McGill, S. P., Eisemann, E. R., and Dopsovic, R., 2022, Sediment Budget Analysis System (SBAS) 2020 User's Guide : Version 1.0, Engineer Research and Development Center (U.S.).

[4] Flocks, J. G., Forde, A. S., and Bernier, J., 2022, Chandeleur Islands to Breton Island Bathymetric and Topographic Datasets and Operational Sediment Budget Development: Methodology and Analysis Report, 2022–1020, U.S. Geological Survey.

[5] Rosati, J. D., Sumner, C. A., and Wilson, D. A., 2013, The Sediment Budget Calculator : A Webtool to Develop a Family of Viable Inlet and Adjacent Beach Sediment Budget Solutions, Engineer Research and Development Center (U.S.).

[6] Podoski, J. H., 2013, Hawaii Regional Sediment Management : Application of SBAS for ArcGIS© 10 to Develop Regional Sediment Budgets for the Island of Maui, HI, Coastal and Hydraulics Laboratory (U.S.).

[7] Conner, K. B., and Lillycrop, L. S., 2017, Sediment Budget Analysis : Masonboro Inlet, North Carolina, Coastal and Hydraulics Laboratory (U.S.).

[8] Legault, K. R., and Frey, A. E., 2017, Pinellas, Manatee, and Sarasota Counties, Florida; Regional Sediment Budget, Coastal and Hydraulics Laboratory (U.S.).

[9] Deltares, "Delft3D 4 Suite | Deltares" [Online]. Available: https://www.deltares.nl/en/software-and-data/products/delft3d-4-suite. [Accessed: 05-Feb-2024].

[10] Deltars, 2024, "Delft3D Functional Specifications."

[11] Booij, N., Ris, R., and Holthuijsen, L., 1999, "A Third-Generation Wave Model for Coastal Regions, Part I, Model Description and Validation," J. Geophys. Res., 104, pp. 7649–7656.

[12] Trouw, K. J. M., Zimmermann, N., Mathys, M., Delgado, R., and Roelvink, D., 2012, "Numerical Modelling of Hydrodynamics and Sediment Transport in the Surf Zone: A Sensitivity Study with Different Types of Numerical Models," Coastal Engineering Proceedings, (33), pp. 23–23.

[13] Lesser, G., Kester, J., and Roelvink, J., 2000, "On-Line Sediment Transport within Delft3D-FLOW."

[14] Van Rijn, L. C., and Walstra, D. J. R., 2003, "Modelling of Sand Transport in DELFT3D," WL| Delft Hydr. Re, 3624.

[15] Manual, 2024, "Delft3D-FLOW User Manual."

[16] Chu, P. C., Pessanha, V. S., Fan, C., and Calantoni, J., 2021, "Coupled Delft3D-Object Model to Predict Mobility of Munition on Sandy Seafloor," Fluids, 6(9), p. 330.

[17] Huff, T. P., Feagin, R. A., and Figlus, J., 2022, “Delft3D as a Tool for Living Shoreline Design Selection by Coastal Managers,” Frontiers in Built Environment, 8.

[18] Azidane, H., Boko, M., and El Bouhaddioui, M., 2020, “Delf3D Morphological Modelling of Wave Climate and Sediment Transport in Kenitra Coast (Morocco),” Proceedings of the 4th Edition of International Conference on Geo-IT and Water Resources 2020, Geo-IT and Water Resources 2020, Association for Computing Machinery, New York, NY, USA, pp. 1–5.

[19] Bautista, D., Herrera, E., Hernandez, B., Yoshikai, M., Nakamura, T., and Nadaoka, K., 2020, “Numerical Investigation of Coastal Sediment Transport for Assessment of Coastal Erosion of a Philippine Coastline Using a 3D Hydrodynamic Model,” IOP Conference Series: Materials Science and Engineering, 849, p. 012091.

[20] Iii, R. L. J., Long, J. W., Dalyander, P. S., Thompson, D. M., and Mickey, R. C., 2020, Development of a Process-Based Littoral Sediment Transport Model for Dauphin Island, Alabama, 2020–1011, U.S. Geological Survey.

[21] Elias, E., Barnard, P., and Brocatus, J., 2009, “Littoral Transport Rates in the Santa Barbara Littoral Cell: A Process- Based Model Analysis,” Journal of Coastal Research.

[22] Boudet, L., Sabatier, F., and Radakovitch, O., 2017, “Modelling of Sediment Transport Pattern in the Mouth of the Rhone Delta: Role of Storm and Flood Events,” Estuarine, Coastal and Shelf Science, 198, pp. 568–582.

[23] Pinho, J., Coelho, J., Venâncio, S., Vieira, L., Vieira, B., and Vieira, J., 2018, “Application of Delft3d for Designing and Assessing New Solutions to Improve Sediment Input to an Erosion Prone Coast,” pp. 1664–1655.

[24] Iqbal, M., Widyaningtias, Wiyono, A., Adityawan, M. B., Sukarno, I., and Bumi, I. S., 2021, “Effect of Permeable Structure on Coastal Sediment Transport in Demak Regency, Central Java, Indonesia Model by Using Delft3D Software,” IOP Conf. Ser.: Earth Environ. Sci., 698(1), p. 012040.

[25] He, M., 2017, “Improving Suspended Sediment Transport Models for Breaking Wave Conditions,” University of Twente.

[26] Rijn, V., and C, L., 2007, “Unified View of Sediment Transport by Currents and Waves. III: Graded Beds,” Journal of Hydraulic Engineering, 133(7), pp. 761–775.

[27] Wardt, W. V. D., 2018, “Modelling Cross-Shore Transport of Graded Sediments under Waves.”

[28] Riadh, A., Cédric, G., and Hervouet, J. M., 2014, TELEMAC User Manual.

[29] C Villaret, 2010, SYSPHE 6.0 User Manual.

[30] Besley, J., 2021, “Task 2B.6 Regional Sand Transport Modeling and Verification - Region 4.”

[31] Pinel, S., Cherif, F., Meslard, F., Labrousse, C., and Bourirn, F., 2020, “Development of a Hydro-Morphodynamic Model for Simulation of Bed Load and Morphological Changes of Flash-Floods (Têt River, France).”

[32] Bi, Q., Shen, X., Lee, B. J., and Toorman, E., 2020, “Investigation on Estuarine Turbidity Maximum Response to the Change of Boundary Forcing Using 3CPBE Flocculation Model.”

[33] Tassi, P., Benson, T., Delinares, M., Fontaine, J., Huybrechts, N., Kopmann, R., Pavan, S., Pham, C.-T., Taccone, F., and Walther, R., 2023, “GAIA - a Unified Framework for Sediment Transport and Bed Evolution in Rivers, Coastal Seas and Transitional Waters in the TELEMAC-MASCARET Modelling System,” Environmental Modelling & Software, 159, p. 105544.

[34] Ricci, S., Piacentini, A., Weaver, A., Ata, R., and Goutal, N., 2015, “Variational Data Assimilation with TELEMAC. Proof of Concept for Model State Correction on the Berre Lagoon 3D-Model,” Engineering Geology for Society and Territory - Volume 5, G. Lollino, A. Manconi, F. Guzzetti, M. Culshaw, P. Bobrowsky, and F. Luino, eds., Springer International Publishing, Cham, pp. 633–637.

[35] Cooper, A., Cuomo, G., Bourban, S., Turnbull, M., and Roscoe, D., 2012, “Testing TELEMAC-2D Suitability for Tsunami Propagation from Source to near Shore,” Oxford, pp. 89–92.

[36] Zaoui, F., Goeury, C., and Audouin, Y., 2019, “A Metamodel of the Telemac Errors.”

[37] Wolf, T., Breugem, W. A., Chu, K., Decrop, B., Van Holland, G., Plancke, Y., and Stark, J., 2021, “Sediment Transport Modelling (TELEMAC-3D + GAIA) Case Study: Sand Disposals in the Western Scheldt.”

[38] Michael, P., Ioannis, G., Mark, K., Mark, L., Gordon, T., and Walstra, D. J., 2015, 2017 Coastal Master Plan Attachment C3-4: Barrier Island Model Development (BIMODE).

[39] DHI, 2024, “MIKE 21/3” [Online]. Available: https://www.mikepoweredbydhi.com/products/mike-21-3/. [Accessed: 11-Apr-2024].

[40] Sakhaee, F., and Niksokhan, M. H., 2021, “Investigation of Sedimentation Patterns of Amirabad Port (Caspian Sea) Using a Coupled Hydrodynamic and Sediment Transport Model,” Trends in Techinal & Scientific Research.

[41] DHI, 2017, MIKE 21 and MIKE 3 Flow Model FM Hydrodynamic Module.

[42] Kulkarni, R. R., 2013, “Numerical Modelling of Coastal Erosion Using MIKE21,” NORWEGIAN UNIVERSITY OF SCIENCE AND TECHNOLOGY.

[43] DHI, “MIKE 21 Flow Model FM. Mud Transport Module. User Guide” [Online]. Available: https://manuals.mikepoweredbydhi.help/latest/Coast_and_Sea/MIKE_FM_MT_2D.pdf.

[44] DHI, 2024, “MIKE 21 Flow Model FM Sand Transport Module, Incl. Shoreline Morphology User Guide” [Online]. Available: https://manuals.mikepoweredbydhi.help/latest/Coast_and_Sea/MIKE_FM_ST_2D.pdf.

[45] Mortlock, T., Goodwin, I., McAneney, J., and Roche, K., 2017, “The June 2016 Australian East Coast Low: Importance of Wave Direction for Coastal Erosion Assessment,” Water, 9(2), p. 121.

[46] Seenath, A., 2022, "On Simulating Shoreline Evolution Using a Hybrid 2D/One-Line Model," Coastal Engineering, 178, p. 104216.

[47] Papadimitriou, A., Panagopoulos, L., Chondros, M., and Tsoukala, V., 2020, "A Wave Input-Reduction Method Incorporating Initiation of Sediment Motion," JMSE, 8(8), p. 597.

[48] Blain, C. A., Westerink, J. J., Luettich, R. A. (Richard A., and Scheffner, N. W., 1994, ADCIRC : An Advanced Three-Dimensional Circulation Model for Shelves, Coasts, and Estuaries. Report 4, Hurricane Storm Surge Modeling Using Large Domains, Coastal Engineering Research Center (U.S.).

[49] Luettich, R. A. (Richard A., Westerink, J. J., and Scheffner, N. W., 1992, ADCIRC : An Advanced Three-Dimensional Circulation Model for Shelves, Coasts, and Estuaries. Report 1, Theory and Methodology of ADCIRC-2DD1 and ADCIRC-3DL, Coastal Engineering Research Center (U.S.).

[50] Pandoe, W. W., 2004, "Extended Three-Dimensional ADCIRC Hydrodynamic Model to Include Baroclinic Flow and Sediment Transport," Book, Texas A&M University.

[51] ERDC, E. R. and D. C. W., 2024, "Introduction to the Interim Draft of the National Ordinary High Water Mark (OHWM) Manual," Engineer Research and Development Center [Online]. Available: https://www.erdc.usace.army.mil/Media/Fact-Sheets/Fact-Sheet-Article-View/Article/476698/advanced-circulation-model/https%3A%2F%2Fwww.erdc.usace.army.mil%2FMedia%2FFact-Sheets%2FFact-Sheet-Article-View%2FArticle%2F476698%2Fadvanced-circulation-model%2F. [Accessed: 16-Apr-2024].

[52] Pringle, W. J., Wirasaet, D., Roberts, K. J., and Westerink, J. J., 2021, "Global Storm Tide Modeling with ADCIRC V55: Unstructured Mesh Design and Performance," Geoscientific Model Development, 14(2), pp. 1125–1145.

[53] Pandoe, W. W., and Edge, B. L., 2008, "Case Study for a Cohesive Sediment Transport Model for Matagorda Bay, Texas, with Coupled ADCIRC 2D-Transport and SWAN Wave Models," Journal of Hydraulic Engineering, 134(3), pp. 303–314.

[54] Cialone, M. A., Brown, M. E., Smith, J. M., and Hathaway, K. K., 2008, Southeast Oahu Coastal Hydrodynamic Modeling with ADCIRC and STWAVE, Coastal and Hydraulics Laboratory (U.S.).

[55] Hodge, M., and LLC, Hodge. W., 2022, Suspended Sediment Transport Modeling Study Offshore Submarine Cable Installation Juno Power Express Project, Hodge Water Resource.

[56] Lackey, T. C., Bailey, S. E., Gailani, J. Z., Kim, S.-C., and Schroeder, P. R. (Paul R.), 2020, Hydrodynamic and Sediment Transport Modeling for James River Dredged Material Management, Coastal and Hydraulics Laboratory (U.S.).

[57] Quataert, E., de Bakker, A., de Ridder, M., de Goede, R., de Vet, L., and van der Lugt, M., 2022, "XBeach Documentation."

[58] Roelvink, D., Reniers, A., Ap van Dongeren, J. V. T., de Vries, J. L., and McCall, R., 2010, "XBeach Model Description and Manual. Unesco-IHE Institute for Water Education, Deltares and Delft University of Tecnhology."

[59] Daly, C. J., 2009, "Low Frequency Waves in the Shoaling and Nearshore Zone."

[60] Muller, J. R. M., Figlus, J., and De Vries, S., 2018, "XBeach Simulation of Hybrid Coastal Protection: A Galveston Seawall Test Case," Int. Conf. Coastal. Eng., (36), p. 100.

[61] Bogovac, T., Carević, D., Bujak, D., and Miličević, H., 2023, "Application of the XBeach-Gravel Model for the Case of East Adriatic Sea-Wave Conditions," JMSE, 11(3), p. 680.

[62] Rautenbach, C., Trenham, C., Benn, D., Hoeke, R., and Bosserelle, C., 2022, "Computing Efficiency of XBeach Hydro- and Wave Dynamics on Graphics Processing Units (GPUs)," Environmental Modelling & Software, 157, p. 105532.

[63] Zhou, Y., Feng, X., Liu, M., and Wang, W., 2023, "Influence of Beach Erosion during Wave Action in Designed Artificial Sandy Beach Using XBeach Model: Profiles and Shoreline," JMSE, 11(5), p. 984.

[64] Bae, H., Do, K., Kim, I., and Chang, S., 2022, "Proposal of Parameter Range That Offered Optimal Performance in the Coastal Morphodynamic Model (XBeach) Through GLUE," J. Ocean Eng. Technol., 36(4), pp. 251–269.

[65] Mancini, G., Briganti, R., Ruffini, G., McCall, R., Dodd, N., and Zhu, F., 2020, "Analysis of the Performance of Different Sediment Transport Formulations in Non-Hydrostatic XBeach," Int. Conf. Coastal. Eng., (36v), p. 35.

[66] "Litpack an Integrated Modelling System for Modeling System and Coastaline Kinetics."

[67] MIKE website, "LITPACK" [Online]. Available: https://www.mikepoweredbydhi.com/products/litpack. [Accessed: 26-Apr-2024].

[68] Fredsøe, J., 1984, "Turbulent Boundary Layer in Wave-current Motion," Journal of Hydraulic Engineering, 110(8), pp. 1103–1120.

[69] Engelund, F., and Fredsøe, J., 1976, "A Sediment Transport Model for Straight Alluvial Channels," Hydrology Research, 7(5), pp. 293–306.

[70] Bagnold, R. A., 1997, "Experiments on a Gravity-Free Dispersion of Large Solid Spheres in a Newtonian Fluid under Shear," Proceedings of the Royal Society of London. Series A. Mathematical and Physical Sciences, 225(1160), pp. 49–63.

[71] Armenio, E., De Serio, F., Mossa, M., Nobile, B., and Petrillo, A. F., 2017, "Investigation on Coastline Evolution Using Long-Term Observations and Numerical Modelling," OnePetro.

[72] Varangalil, N., and Kankara, R. S., 2018, Shoreline Prediction Using A Numerical Model Along Rathnagiri Coast, West Coast of India.

[73] Anton, I. A., Panaitescu, M., and Panaitescu, F. V., 2017, "Optimizing Romanian Maritime Coastline Using Mathematical Model Litpack," IOP Conf. Ser.: Mater. Sci. Eng., 227(1), p. 012009.

[74] Nguyen, N., Truc, N. N., and Luong, P., 2007, "Studying Shoreline Change by Using LITPACK Mathematical Model (Case Study in Cat Hai Island, Hai Phong City, Vietnam)," VNU J. Sci. Earth Sci., 23.

[75] Armenio, E., De Serio, F., Mossa, M., and Petrillo, A. F., 2019, "Coastline Evolution Based on Statistical Analysis and Modeling," Natural Hazards and Earth System Sciences, 19(9), pp. 1937–1953.

[76] Our Coast Our Future, O. C. O. F., 2024, "USGS Coastal Storm Modeling System Southern California Region (CoSMoS 3.0) Frequently Asked Questions."

[77] Pacific Coastal and Marine Science Center, 2021, "Coastal Storm Modeling System (CoSMoS)" [Online]. Available: https://www.usgs.gov/centers/pcmsc/science/coastal-storm-modeling-system-cosmos.

[78] HR Wallingford, 2003, Overstrand to Walcott Littoral Sediment Processes Part II: Technical Support Information.

[79] Sutherland, J., and Brady, A., 2001, COSMOS Modelling of COAST3D Egmond Main Experiment.

[80] Zhou, Z., 2011, "Feasibility Study of a Coupled Numerical Model for Longshore Sediment Transport and Beach Response."

[81] HR Wallingford, 2021, Sediment Budget Analysis and Modeling of the Texas Coast. Task 2D1b. Region Sediment Budget – Report RT022.

[82] Quan, R., Dibajnia, M., Wise, L., and Das, H. S., 2022, "BENEFICIAL USE OF DREDGED MATERIAL AND FATE OF PLACED SAND USING A HYBRID COSMOS-XBEACH SEDIMENT BUDGET MODEL," Coastal Engineering Proceedings, (37), pp. 37–37.

[83] Barnard, P. L., Van Ormondt, M., Erikson, L. H., Eshleman, J., Hapke, C., Ruggiero, P., Adams, P. N., and Foxgrover, A. C., 2014, "Development of the Coastal Storm Modeling System (CoSMoS) for Predicting the Impact of Storms on High-Energy, Active-Margin Coasts," Nat Hazards, 74(2), pp. 1095–1125.

[84] O'Neill, A., Erikson, L., Barnard, P., Limber, P., Vitousek, S., Warrick, J., Foxgrover, A., and Lovering, J., 2018, "Projected 21st Century Coastal Flooding in the Southern California Bight. Part 1: Development of the Third Generation CoSMoS Model," JMSE, 6(2), p. 59.

[85] Sutikno, S., Murakami, K., Handoyo, D. P., and Fauzi, M., 2015, "Calibration of Numerical Model for Shoreline Change Prediction Using Satellite Imagery Data," MST, 19(3), p. 113.

[86] Gravens, M. B., 1992, User's Guide to the Shoreline Modeling System (SMS), Coastal Engineering Research Center (U.S.).

[87] Gravens, M. B., Hanson, H., and Kraus, N. C., 1991, GENESIS: Generalized Model for Simulating Shoreline Change. Report 2: Workbook and System User's Manual, US Army Corps of Engineers Waterways Experiment Station.

[88] Hanson, H., 1989, "Genesis: A Generalized Shoreline Change Numerical Model," Journal of Coastal Research, 5(1), pp. 1–27.

[89] Tomasicchio, G. R., Francone, A., Simmonds, D. J., D'Alessandro, F., and Frega, F., 2020, "Prediction of Shoreline Evolution. Reliability of a General Model for the Mixed Beach Case," Journal of Marine Science and Engineering, 8(5), p. 361.

[90] Wamsley, T. V., Hanson, H., and Kraus, N. C., 2002, Wave Transmission at Detached Breakwaters for Shoreline Response Modeling, Engineer Research and Development Center (U.S.).

[91] ATKINS, 2015, Peer Review of the Lido Key Federal Shore Protection Project Sarasota County, Environmental Planning Department.

[92] Wamsley, T., Kraus, N. C., and Hanson, H., 2003, Shoreline Response to Breakwaters with Time-Dependent Wave-Transmission., International Conference on Coastal Sediments.

[93] Buccino, M., Ciccaglione, M. C., and Paola, G. D., 2020, "The Use Of One-Line Model and Littoral Drift Rose Concept in Predicting Long Term Evolution of the Molise Coast," Int. Conf. Coastal. Eng., (36v), p. 44.

[94] Young, R. S., Pilkey, O. H., Bush, D. M., and Thieler, E. R., 1995, "A Discussion of the Generalized Model for Simulating Shoreline Change (GENESIS)," Journal of Coastal Research, 11(3), pp. 875–886.

[95] Fauver, L., 2005, "Toward Predicting Barrier Island Vulnerability: Simple Models for Dune Erosion," USF Tampa Graduate Theses and Dissertations.

[96] Lee, F. C., Lin, W. H., and Hsu, J. R.-C., 2010, "STORM BEACH BUFFER REQUIREMENT FOR STORM WAVES FROM A TROPICAL CYCLONE," Coastal Engineering Proceedings, (32), pp. 46–46.

[97] Larson, Magnus., and Kraus, N. C., 1998, SBEACH: Numerical Model for Simulating Storm-Induced Beach Change. Report 5: Representation of Nonerodible (Hard) Bottoms.

[98] Larson, Magnus., Byrnes, M. R., and Kraus, N. C., 1990, SBEACH: Numerical Model for Simulating Storm-Induced Beach Change. Report 2, Numerical Formulation and Model Tests., U.S. Army Engineer Waterways Experiment Station, Vicksburg, Miss.

[99] Rosati, J. D., Wise, R. A., Kraus, N. C., and Larson, Magnus., 1993, SBEACH: Numerical Model for Simulating Storm-Induced Beach Change. Report 3—User's Manual.

[100] Wise, R. A., Smith, S. J., and Larson, Magnus., 1996, SBEACH: Numerical Model for Simulating Storm-Induced Beach Change. Report 4. Cross-Shore Transport under Random Waves and Model Validation with SUPERTANK and Field Data., CERC-89-9., Coastal Engineering Technical Report.

[101] Matthews, J., 2013, "Final Integrated Feasibility Report and Environmental Impact Statement Coastal Storm Damage Reduction Bogue Banks, Carteret County North Carolina."

[102] Bacopoulos, P., 2020, Storm-Induced Beach Change (SBEACH) High-Frequency Storm Erosion Model Study for Broward County.

[103] King, D. B. (David B., 2007, Wave and Beach Processes Modeling for Sabine Pass to Galveston Bay, Texas Shoreline Erosion Feasibility Study, Coastal and Hydraulics Laboratory (U.S.).

[104] Kong, J., Shan, Z., Chen, Y., Yang, J., Hu, Y., and Wang, L., 2019, "Assessment of Remote-Sensing Retrieval Models for Suspended Sediment Concentration in the Gulf of Bohai," International Journal of Remote Sensing, 40(5–6), pp. 2324–2342.

[105] 2020, "Sediment Modeling of a Large-Scale Basin Supported by Remote Sensing and in-Situ Observations," CATENA, 190, p. 104535.

[106] Kamel, A. M. Y., El Serafy, G. Y., Bhattacharya, B., van Kessel, T., and Solomatine, D. P., 2013, "Using Remote Sensing to Enhance Modelling of Fine Sediment Dynamics in the Dutch Coastal Zone," Journal of Hydroinformatics, 16(2), pp. 458–476.

[107] Lu, C., Li, H., Dai, W., Tao, J., Xu, F., Cybele, S., Zhang, X., and Guo, H., 2018, "3-D Simulation of the Suspended Sediment Transport in the Jiao Jiang Estuary: Based on Validating by Remote Sensing Retrieval," coast, 85(sp1), pp. 116–120.

UNIVERSITY OF TEXAS ARLINGTON

COASTAL MANAGEMENT PROGRAM – CYCLE 26

BEST PRACTICES IN MODELING SEDIMENT TRANSPORT AND BUDGET ALONG THE TEXAS COAST

Task 3: Morphodynamical Scenario Analyses for the Brazos River and the Colorado River (CONTRACT NO. 23-020-018-D867)

Prepared for:

Texas General Land Office

1700 N. Congress Avenue, Mail Code 158

Austin, TX 78701

Submitted by:

Behzad Nazari, Ph.D., P.E.

Yu Zhang, Ph.D., P.E.

Habib Ahmari, Ph.D., P.E.

The University of Texas at Arlington, Arlington, Texas, USA

August 2024

EXECUTIVE SUMMARY

This report documents the findings from Task 3 of the Texas General Land Office (GLO) project 'Best Practices in Modeling Sediment Transport and Budget Along the Texas Coast'. Task 3 focuses on Morphodynamical Scenario Analyses for the Brazos River and the Colorado River. This study investigates the complexities of sediment transport modeling in coastal areas, focusing on the Brazos-San Bernard region and the Colorado River in Texas. Using advanced numerical modeling techniques, namely the Delft3D Flexible Mesh software, the analyses conducted explore various scenarios to highlight uncertainties and potential inaccuracies in current sediment transport modeling practices. This research contributes to the GLO Sediment Management Program.

This report provides an overview of the fundamentals of sediment transport modeling to make the advanced topics more accessible to a broader audience, including stakeholders and coastal managers who may not have specialized knowledge in this field.

Elaborating on significant challenges in accurately representing sediment transport regimes and long-term morphological changes especially in coastal regions, this study demonstrates that factors such as morphological acceleration, selection of representative flow for analyzing long term sediment regime, considering the type of sediments for example mud versus sand, and the conventional modeling practice of using lumped versus spatially variable sediment influx have substantial, often non-linear impacts on sediment transport patterns.

The research includes scenario analyses looking into altered regimes due to gradual stressors or floods. It shows that current morphodynamical models have come a long way and can model complex phenomena such as the opening of a river mouth during a hurricane, yet still a lot of challenges remain. Notably, the study finds that considering cohesive sediment significantly increases simulated sediment transport rates.

The study also highlights the limitations of current approaches to determining representative flows for sediment transport modeling. It proposes using median flow values to be used with morphological acceleration as a potentially more robust method for long-term simulations. Importantly, the research underscores the need for caution when interpreting results from morphologically accelerated models. While these techniques allow for simulation of long-term trends, they also propagate uncertainties and may not accurately capture the impacts of extreme events or highly variable oscillatory boundary conditions such as tides.

These findings contribute to the body of knowledge on sediment transport modeling practice for coastal management and engineering practices in the Gulf of Mexico region.

The study recommends more comprehensive data collection efforts, particularly for sediment composition and distributed sediment inputs along river reaches. It also emphasizes the importance of considering a range of scenarios and sediment types in future modeling efforts to better account for the complexities of coastal sediment dynamics.

The research also addresses challenges related to the non-stationarity of sediment discharge regimes and highlights differences observed between the Brazos and Colorado River systems in terms of sediment yield and response to factors like sea level rise.

By highlighting these challenges and uncertainties, this research provides insights to inform future studies and improve decision-making processes for coastal management projects in Texas and similar coastal environments.

Table of Contents

EXECUTIVE SUMMARY 2

1. Introduction 9

2. Objectives and Scope 10

3. Theoretical Overview of Key Concepts in Sediment Transport Modeling 12

3.1 Exploring the Idealized Equilibrium Principle 13

3.2 Practical limitation and Time to Reach Equilibrium 15

4. A Brief Introduction to Computational Sediment Transport Modeling 18

4.1 Erosion, Transportation, and Deposition 18

4.2 Modes of transport: bed load and suspended load 20

4.3 Sediment transport rate 21

4.4 Sediment-Discharge Formulas 21

4.5 Bagnold's equation 22

4.6 Computing bed level changes 24

4.7 Morphological Acceleration 26

5. Study Area 28

5.1 Brazos River 29

5.2 San Bernard River 30

5.3 Colorado River 32

6. Morphodynamical Scenario Analyses 33

6.1 Overarching goal 33

I. Long-term Sediment Regime under Prescribed LDCs and Morphological Acceleration Factors 33

II. Alteration of Long-term Sediment Regime due to Gradual Stressors 34

III. Alteration of Sediment Regime due to Spatially Varied Sediment Supply LDCs 35

IV. Disturbances Caused by Floods and Droughts 35

V. Treatment of Sediment Types (Cohesive vs. Non-cohesive) 36
6.2 Determining Representative Flows for Sediment Transport Modeling 37
6.3 Nonstationary of Sediment Discharge Regime 43
6.4 Hydro-Morphological Model Development 44
6.4.1. Introduction to Delft3D-FM: 45
6.4.2. Model Configuration 45
6.4.3. Brazos -San Bernard Study Area 47
6.4.4. Colorado River Study Area 51
6.5 Representative Simulation Results 53
I. Hurricane Harvey 53
II. Long-Term Trends and Morphological Acceleration 56
III. Sea Level Rise 57
IV. Spatially Varied Sediment Influx 58
V. Cohesive vs. Noncohesive Sediment 58
VI. Flooding in Colorado River 58
7. Conclusions and Key Insights 60
References 63
APPENDIX A: NAMING CONVENTION FOR SCENARIO ANALYSIS 65
APPENDIX B: THE EFFECT OF MORPHOLOGICAL ACCELERATION IN BRAZOS DOMAIN 67
APPENDIX C: THE EFFECT OF MORPHOLOGICAL ACCELERATION IN COLORADO DOMAIN 93
APPENDIX D: EROSION/SEDIMENTATION OF BRAZOS WITH MORFAC=365 101
APPENDIX E: EROSION/SEDIMENTATION OF COLORAD WITH MORFAC=365 (MUD) 118
APPENDIX F: THE EFFECT OF SEA LEVEL RISE IN BRAZOS DOMAIN 127
APPENDIX G: THE EFFECT OF SEA LEVEL RISE IN COLORADO DOMAIN 129

APPENDIX H: THE EFFECT OF SPATIALLY VARIABLE LDC 137

APPENDIX I: THE EFFECT OF COHESIVE VS. NON-COHESIVE SEDIMENT IN BRAZOS DOMAIN 154

APPENDIX J: THE EFFECT OF COHESIVE VS. NON-COHESIVE SEDIMENT IN COLORADO DOMAIN 180

APPENDIX K: THE EFFECT OF SEDIMENT INFLUX FROM UPSTREAM VS. NO SEDIMENT INFLUX 192

APPENDIX L: THE EFFECT OF FLOODS IN COLORADO DOMAIN 208

Table of Figures

Figure 1 Lane's Balance for idealized sediment regime [14] 15
Figure 2 General trend of variables along a stream [14] 16
Figure 3 Typical complexities of flow and sediment dynamics in coastal areas. (a) An estuarine system; (b) Deltaic or open coast system [5] 17
Figure 4 Modified Shields Diagram [5] also known as Hjulström-Sundborg diagram with Wentworth-Krumbein grade scale. 19
Figure 5 Texas Gulf of Mexico shoreline taken from [1] 28
Figure 6 Brazos River watershed adapted from Texas parks and Wildlife's Texas Watershed Viewer [18] 30
Figure 7 San Bernard River watershed adapted from Texas parks and Wildlife's Texas Watershed Viewer [18] 31
Figure 8 Colorado River watershed adapted from Texas parks and Wildlife's Texas Watershed Viewer [18] 32
Figure 9 Inundation of 0.6m sea level rise, a value in between the two scenarios investigated in this study, taken from NOAA Sea Level Rise Viewer [20] 34
Figure 10 Schematics of calculating effective discharge by traditional method 38
Figure 11 Examples of different effective discharges obtained for Brazos at Rosharon Station, using various number of bins 40
Figure 12 Examples of different effective discharges obtained for Brazos at Rosharon Station, using various number of bins and using only the 90% lower values 41
Figure 13 Nonstationary of sediment rating curve at Rosharon Station can be seen by separating the data collected before and after 2015 44
Figure 14 The Brazos- San Benrad Study area; The region's complexity arises from its highly interconnected and continuously evolving flowpaths. 48
Figure 15 Historical flow data at USGS Brazos Station at Rosharon 48
Figure 16 Model domain and computational mesh for the Brazos-San Bernard Study area 49
Figure 17 Range of elevations in Brazos - San Bernard study area 50
Figure 18 Computational domain and elevations of Colorado River model 51
Figure 19 Baseline boundary conditions ontained from LCRA station at Matagorda 52
Figure 20 LCRA dam south of Bay City (Source: Google Earth) 52
Figure 21 Colorado River near Wadsworth, TX 53

Figure 22 The San Bernard River mouth was closed as shown in the image from Aug 12, 2017 54
Figure 23 The San Bernard River mouth was closed as shown in the image from Sep 13, 2017 54
Figure 24 Evolution of simulated bed level elevations during Hurricane Harvey shows the morphodynamic model successfully replicating opening ane Harvey of San Bernard mouth 55
Figure 25 Observed meander migration of Brazos extracted from surface water extent 57
Figure 26 Simulated long-term erosion and sedimentation patters of the location shown in Figure 25..... 57
Figure 27 Examples of different hydraulic conditions resulting from the existing spillway structure at the Lower Colorado River Authority's Bay City Dam..... 59

1. INTRODUCTION

Coastal sediment dynamics represent a complex and challenging area of study in environmental sciences. The intricate interplay of processes governing erosion, sediment transport, and deposition across terrestrial, fluvial, estuarine, and marine environments creates significant challenges in coastal management. These processes prevail across a wide range of spatial and temporal scales, from individual grain movements to large-scale geomorphological changes over decades or centuries. Consequently, sediment budget estimates are often associated with substantial uncertainties, stemming from both mechanistic limitations in transport models and inadequate data on sediment supply.

In coastal systems, the influx of sediment from inland catchments via rivers constitutes a primary source of sediment input. This is particularly true for the Gulf of Mexico, where riverine sediment transport plays a crucial role in coastal sediment budgets. The Gulf Coast, with its extensive network of rivers and estuaries, presents a unique and complex environment for sediment dynamics. Sediment supply to coastal areas is influenced by a multitude of factors [1]:

- Climate and meteorological conditions, including extreme events: Hurricanes, tropical storms, and intense rainfall events can significantly alter sediment transport patterns.
- Freshwater inflow dynamics: Seasonal variations in river discharge affect sediment carrying capacity and transport rates.
- Wave action and tides: Coastal processes that influence sediment movement, deposition, and erosion along shorelines and in shallow waters.
- Land use changes, such as urbanization and deforestation: These alterations can dramatically impact erosion rates and sediment yields from catchments.
- Implementation of conservation practices: Soil conservation measures in agricultural areas can reduce sediment yields.
- Sediment entrapment in artificial water bodies: Dams, reservoirs, and detention ponds interrupt the natural sediment continuum, often leading to sediment deficits downstream.
- Morphological evolution of channels and floodplains: Natural and anthropogenic changes in river morphology can alter sediment transport and deposition patterns.

Current practices in sediment analysis often rely on simplistic assumptions regarding sediment sources, composition, and supply volumes. These assumptions introduce several limitations:

- Direct application of Load Duration Curves (LDCs) from upstream observation stations to downstream inlets, neglecting longitudinal variations: This approach fails to account for spatial variability in sediment inputs and losses along the river course.
- Inadequate accounting for sediment contributions from lateral flow and bank erosion: These sources can significantly contribute to overall sediment budgets, particularly during high-flow events.
- Lack of consideration for hysteresis effects, and reverse flows: The most common approach to use a single sediment-discharge relationship, without consideration of differences between the initial rising state flooding and later recession state. In addition, these simple relationships do not account for the times when there is potential of sediment going upstream in reverse direction.
- Insufficient treatment of supply-limited sediment budget rather than flow-limited: This approach fails to account for the fact that sediment transport is often limited by the availability of sediment rather than the capacity of the flow to transport it, particularly for fine sediments.
- Absence of specific considerations for salinity impacts on cohesive sediment deposition at the estuary-ocean interface: Salinity gradients can significantly influence flocculation and deposition processes of fine sediments.

Additionally, the increasing impacts of climate change and sea-level rise add another layer of complexity to coastal sediment dynamics. Rising sea levels can alter coastal hydrodynamics, potentially leading to increased erosion and changes in sediment transport patterns. Climate change-induced alterations in precipitation patterns and storm intensity may also significantly impact sediment yields and transport regimes.

2. OBJECTIVES AND SCOPE

This study aims to address some of these limitations, contributing to the Texas General Land Office (GLO) Coastal Management Program. By employing advanced numerical modeling techniques and incorporating the latest developments in sediment transport theory and coastal hydrodynamics, this study analyzes the effect of uncertainties and potential inaccuracies in current sediment transport modeling practices, to inform the stakeholders and coastal managers about these issues while planning for future projects.

The study focuses on two study areas among Texas rivers: the lower reaches of Brazos-San Bernard region and the Colorado River. These river systems, with their distinct characteristics

and significant contributions to the Gulf of Mexico's sediment budget. Most rivers in Texas do not drain directly into the Gulf of Mexico without passing through a coastal water body, which complicates the analysis of flow and sediment in estuarine settings. However, the three rivers focused on in this study are among the best candidates, as they allow for a more straightforward analysis of sediment transport within a riverine environment, which is the primary focus of this research.

It's important to recognize that each of these limitations represents an active area of research with ongoing challenges. The complexities inherent in sediment transport processes continue to pose significant challenges for researchers and coastal managers. This study, therefore, focuses on addressing select scenarios to demonstrate the impact of several of these factors on model outputs. By doing so, we aim to highlight the challenges and uncertainties in sediment transport modeling, providing insights for future research and management strategies.

The scenarios herein focus on long-term sediment regimes under baseline conditions and their alterations due to various factors. These include gradual environmental stressors such as sea level rise and urbanization, spatially varied sediment supply, and extreme hydrological events like floods and droughts. Additionally, the study considers the differential behavior of cohesive and non-cohesive sediments, a critical aspect often oversimplified in current models.

By employing advanced numerical modeling techniques and incorporating recent developments in sediment transport theory and coastal hydrodynamics, this study analyzes the effect of uncertainties and potential errors in current sediment transport modeling practices. The goal is to inform stakeholders and coastal managers about these issues, enhancing their ability to make informed decisions when planning future projects.

The study focuses on two key areas among Texas rivers: the lower reaches of the Brazos-San Bernard region and the Colorado River. These river systems, with their distinct characteristics, contribute significantly to the Gulf of Mexico's sediment budget. Unlike most Texas rivers that pass through coastal water bodies before reaching the Gulf, complicating flow and sediment analysis in estuarine settings, these rivers offer a more direct path to the Gulf. This characteristic allows for a more straightforward analysis of sediment transport within a riverine environment, aligning with the primary focus of this research.

3. THEORETICAL OVERVIEW OF KEY CONCEPTS IN SEDIMENT TRANSPORT MODELING

Sediment transport encompasses the process by which sediment, composed of particles from rocks or biological materials, moves within a waterbody [2]. These particles may either be suspended in the water column or settle on the bed, depending on various hydrodynamic conditions and the sediment's properties. The process begins with erosion, where the shear stress exerted by the flow exceeds a critical threshold, causing sediment to be lifted from the bed. As the water carries the sediment, it eventually reaches a point where its capacity to transport the particles is exceeded, leading to deposition. Therefore, the patterns of erosion and deposition within waterbodies can be achieved by examining the **net sediment balance**. When the sediment balance is positive—meaning that more sediment is entering a region of a waterbody than leaving—deposition is likely to occur. Conversely, a negative sediment balance, where more sediment is exiting the region than entering, typically leads to erosion [5]. This sediment balance can be evaluated by the application of the sediment continuity equation, which provides a quantitative measure of these processes. This framework is essential for analyzing and predicting how sediment dynamics will influence the morphology and stability of various aquatic environments.

The movement of sediment is governed by several primary processes: entrainment and resuspension of particles from the bed, transport as suspended load or bed load, settling of suspended particles, and depositions and consolidation of the bed material.

These processes are influenced by the flow's hydrodynamic conditions and the physical properties of the sediment, such as particle size, shape, density, and composition. Additionally, the exchange of sediment between the bed and the water column, through deposition and resuspension, is a complex interaction that depends not only on the flow conditions but also on the characteristics of the sediment within the bed. High sediment concentrations can also affect the flow, altering water density and reducing turbulence, which influences the transport and deposition of sediment within the system.

Rivers play a crucial role in the continuous transport of sediment from land to the ocean, shaping the dynamic nature of coastlines. The interaction between rivers and the coastal water bodies is a key factor in predicting changes in coastline morphology. Following the general **net sediment balance** concept discussed before, when a river supplies sediment to a delta faster than tidal and wave forces can redistribute it, a prominent delta can form. Conversely, if the forces of tides and

waves disperse sediments more rapidly than the river can replenish them, the balance between deposition and erosion is disturbed, leading to coastal erosion and the inland retreat of the coastline [3]. This dynamic is particularly evident in deltaic regions, where the stability and shape of the delta are directly influenced by the interplay of riverine sediment supply and marine dispersal processes.

This underscores the importance of accounting for the continuum of sediment transport from rivers, through coastal zones, and into the ocean is essential for effective coastal management. Without considering this upstream contribution, efforts to manage coastal erosion, deposition, and overall shoreline stability may be incomplete or ineffective, potentially leading to unintended consequences along the coast. Any major project affecting coastal environments must consider the entire spectrum of riverine and marine interactions to ensure sustainability and minimize unforeseen impacts. A comprehensive approach that integrates these natural processes is critical to maintaining the balance between sediment deposition and erosion, ultimately shaping the long-term evolution of coastal landscapes. Ignoring these broader influences can lead to significant and potentially irreversible changes in coastline morphology, emphasizing the importance of a holistic perspective in managing coastal regions.

3.1 Exploring the Idealized Equilibrium Principle

Modeling and predicting changes in river systems due to the interactions between water flow and sediment transport are inherently complex. Rivers are dynamic environments where the balance between the forces of water and the movement of sediment plays a crucial role in shaping their channels. Variations in water discharge, sediment load, and channel slope can lead to significant changes in the river’s morphology, potentially causing erosion, deposition, or shifts in the riverbed. To better comprehend these processes, one must consider the principles that govern how rivers maintain a state of balance between the forces at play. A key concept in this regard is Lane's equilibrium, which offers insight into how rivers naturally adjust their channels to maintain stability in response to changes in flow and sediment conditions. This equilibrium model serves as a foundational tool for understanding the dynamic interplay between sediment load, particle size, water discharge, and channel slope, and how these factors collectively influence the behavior and evolution of river systems.

Lane's equilibrium is a concept in fluvial geomorphology that describes the balance between the sediment transport capacity of a river and the actual sediment load being carried. It is often represented by a simple equation or relationship that helps to explain how rivers adjust their

channel characteristics-such as slope, width, and depth-in response to changes in water flow (discharge) and sediment load.

The concept is typically expressed as follows:

$Q_s \cdot D \propto Q_w \cdot S$

Where:

- Q_s represents the sediment load (the quantity of sediment being transported by the river),
- D represents the sediment particle size (typically the median grain size),
- Q_w represents the water discharge (the volume of water flowing through the river),
- S represents the channel slope (the steepness of the riverbed).

This relationship implies that there is a balance (or equilibrium) between the stream's ability to transport sediment and the amount of sediment available. If the balance is disrupted, the river will adjust its slope, depth, or other characteristics to restore equilibrium.

A few examples of application of lane's equilibrium in river dynamics include:

- Increase in Water Discharge or Slope: If the water discharge increases, or if the slope becomes steeper, the river's capacity to transport sediment increases. If the sediment load and sediment size remain constant, the river may start eroding its bed or banks to pick up more sediment, leading to degradation.
- Increase in Sediment Load or Size: Conversely, if the sediment load or the sediment particle size increases, without a corresponding increase in discharge or slope, the river may not be able to transport all the sediment. This can lead to sediment deposition, causing the riverbed to aggrade (build up).
- Restoring Equilibrium: Rivers naturally adjust their channel characteristics over time to maintain or restore this equilibrium. For example, if too much sediment is being deposited, the river might increase its slope by deepening or widening its channel, thereby increasing its capacity to transport sediment.

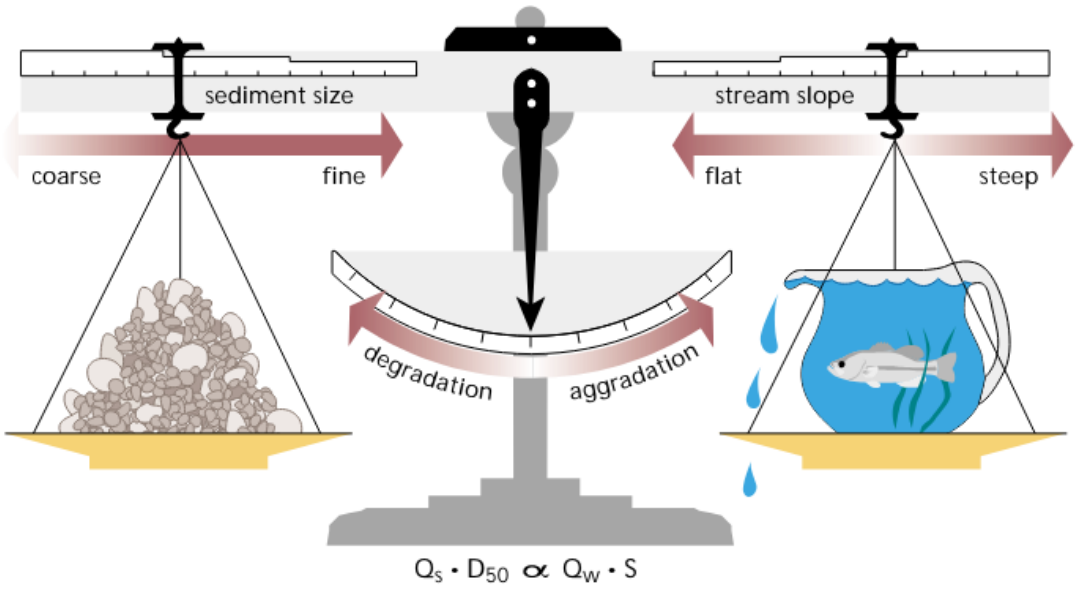

Figure 1 Lane's Balance for idealized sediment regime [14]

3.2 Practical limitation and Time to Reach Equilibrium

The concept of equilibrium in sedimentary environments is inherently abstract and often difficult to define with precision. Many of these environments exist in a state of continuous change, driven by both natural and human-induced factors, and may not exhibit clear signs of reaching equilibrium. This is particularly true because the timescales over which significant morphological changes occur often exceed the periods during which these stressors act.

When a system is disturbed, the time it takes to return to equilibrium is known as its relaxation time, which reflects the system's inertia [5]. Generally, the larger and more complex the system, the longer the relaxation time required. In coastal environments, relaxation time is influenced by several key factors.

Firstly, energy levels play a significant role; higher energy conditions, such as those caused by large storms, result in larger sediment transport rates and shorter relaxation times, meaning the system responds more quickly. In contrast, lower energy conditions, such as during post-storm recovery, lead to slower morphological changes.

Secondly, sediment mobility affects relaxation time. Systems with low sediment mobility, such as structural man-made adaptation strategies such as reservoirs, jetties, breakwaters etc. have a higher resistance to change and thus exhibit longer relaxation times. In contrast, sandy coastal landforms, where sediment is more easily moved, have shorter relaxation times compared to gravelly ones.

Thirdly, the spatial scale of the landform is directly related to its relaxation time. Larger landforms, such as coastal barriers, have longer relaxation times because they involve the movement of larger volumes of sediment, whereas smaller landforms, like beach cusps, respond more quickly.

However, calculating the relaxation time for coastal systems is challenging due to the constant changes in environmental conditions, which continuously perturb the system. As a result, it is unlikely that a true steady-state equilibrium is ever reached, particularly for large coastal landforms where ongoing environmental changes constantly interrupt the system's ability to fully relax.

Many of coastal areas are in a state of continuous change, driven by both natural and human-induced factors, and may not exhibit any clear signs of reaching equilibrium. This is particularly true given that the time scales over which significant morphological changes occur are often much longer than the periods over which these stressors act. As we move closer to coastal areas, the number and intensity of processes affecting the balance of sediment and flow increase significantly, further complicating the system. The dynamic and complex nature of these interactions is evident even when examining a single stream, as illustrated in Fig. [14]. This complexity grows exponentially when the analysis is expanded to encompass an entire coastal system, where multiple processes interact in a constantly shifting environment.

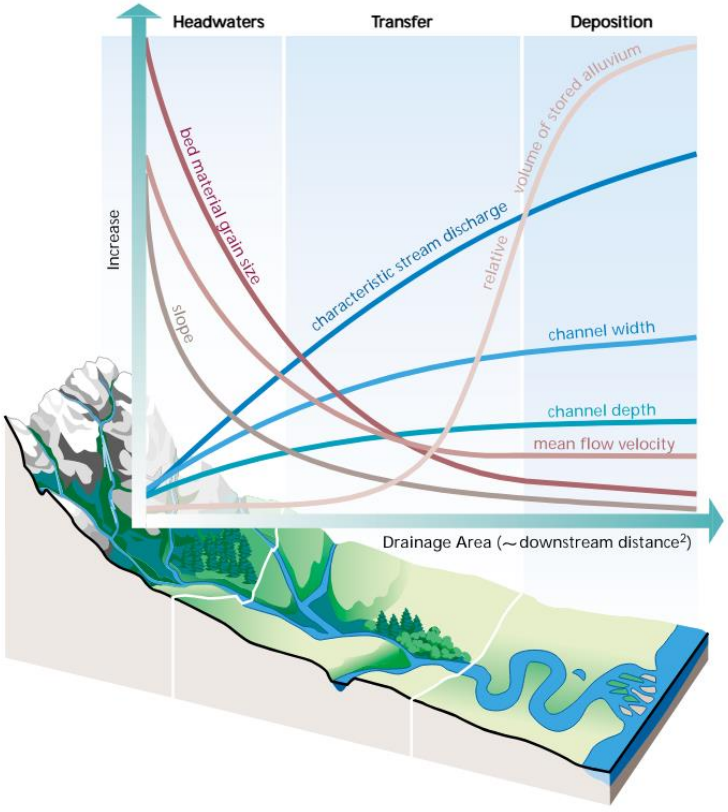

Figure 2 General trend of variables along a stream [14]

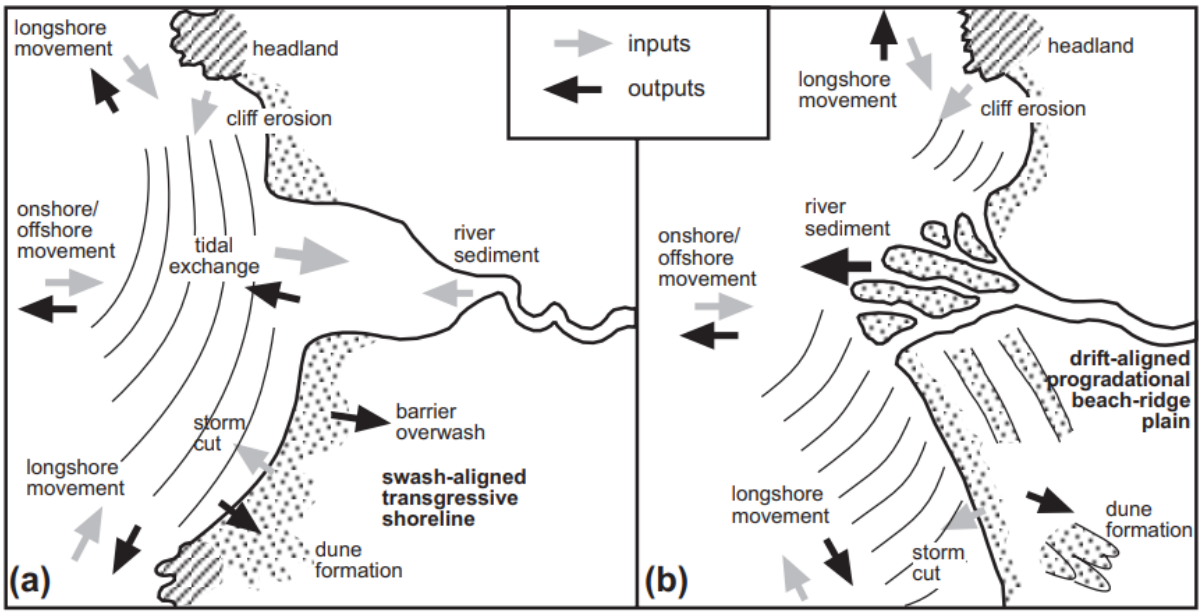

Figure 3 Typical complexities of flow and sediment dynamics in coastal areas. (a) An estuarine system; (b) Deltaic or open coast system [5]

The complexity of sediment and flow interactions quickly becomes apparent, making it clear that qualitative assessments alone cannot fully capture the nuances involved. This complexity necessitates the use of advanced modeling to gain a deeper understanding of how these processes interact and evolve. To demonstrate this, we employ a state-of-the-art model to predict these interactions under various scenarios, highlighting the importance of sophisticated tools for analyzing and interpreting such dynamic systems.

However, simulating these complex processes is challenging and requires the use of mathematical process-based models. Significant advancements in numerical methods for fluid mechanics have greatly enhanced the ability of computational models to simulate the dynamics of flow, sediment transport, and the morphology of rivers, lakes, and coastal zones. In coastal areas, where the interaction between flow and sediment is further complicated by factors like tides and waves, these models are particularly crucial for effective management and planning. Despite these advancements, such modeling efforts still face considerable challenges in practice. These limitations stem from an incomplete understanding of the systems, insufficient data, and the vast scale of interconnected processes influenced by various drivers and stressors. As a result, the models can produce significantly different outcomes depending on the data, parameters, model configurations, and assumptions incorporated into them.

In this study, we conduct a series of sensitivity analyses for two study areas to illustrate these variations and demonstrate how the results can be interpreted in multiple ways. This underscores the need for a careful and thorough analysis of multiple factors to account for a broad range of potential outcomes, particularly when considering changes driven by human activities or natural processes.

4. A BRIEF INTRODUCTION TO COMPUTATIONAL SEDIMENT TRANSPORT MODELING

It is evident that even in abstract sense, understanding the dynamics of sediment transport is complicated. Computation involving these processes is significantly more challenging. Here, we provide a summary on the basics of these computational methods.

4.1 Erosion, Transportation, and Deposition

In summary, computation of sediment transport dynamics involves determining when erosion, transportation, and deposition occur.

The behavior of sediment in a moving fluid is strongly influenced by the size of the sediment grains. For larger grain sizes, individual grain properties, such as size, play a significant role because these grains behave independently. In contrast, for smaller grain sizes, the sediment becomes cohesive due to electrostatic forces, and the behavior of the sediment is more dependent on bulk properties such as floc size and water content.

When it comes to sediment entrainment and deposition, the size and cohesion of the grains are crucial. Non-cohesive grains resting on the bed experience forces such as lift, drag, and weight. For movement to occur, the lift and drag forces must overcome the weight force. The critical conditions required to initiate sediment movement can be predicted using mathematical models, although these forces are challenging to quantify precisely due to variable flow conditions. Instead, experimental data, such as the Shields parameter, is often used to relate bed shear stress to grain size.

The **Shields parameter** is a dimensionless number that represents the ratio between the shear stress acting on the sediment bed and the gravitational force resisting particle movement. It is used to determine the critical shear stress required to initiate sediment motion. The relationship between the Shields parameter and grain size indicates that for smaller grains, especially those less than a certain dimensionless grain diameter (around 10), the bed shear stress required to move the sediment increases as the grain size decreases. This is due to factors such as

compaction of finer grains, which prevents them from protruding through the viscous sublayer and being exposed to turbulent flow, as well as the cohesive forces that bind smaller particles together. For larger grains, which disrupt the viscous sublayer and are less influenced by cohesion, the relationship between critical bed shear stress and grain size is weaker, and the weight of the grains becomes the dominant factor in determining whether they will move.
These concepts have traditionally been summarized into a diagram called the Shields diagram, illustrating the relationship between dimensionless shear stress (Shields parameter) and grain size, which defines the critical conditions necessary for initiating sediment movement.
Figure 4 shows Hjulström-Sundborg diagram [6], a modified version of the Shields diagram and graphically illustrates the physics behind sediment erosion and deposition by water, focusing on the relationship between particle size and current speed. The lower axis shows particle diameter on a logarithmic scale, categorized by grade classes, while the upper axis introduces the φ-scale, a logarithmic transformation of particle size. This diagram, represented by two main curves, explains sediment behavior in a flowing stream. The upper curve (A) represents the critical current speed needed to initiate particle movement (incipient motion) on the riverbed, while the lower curve (B) indicates the speed at which suspended particles begin to settle out of the flow.

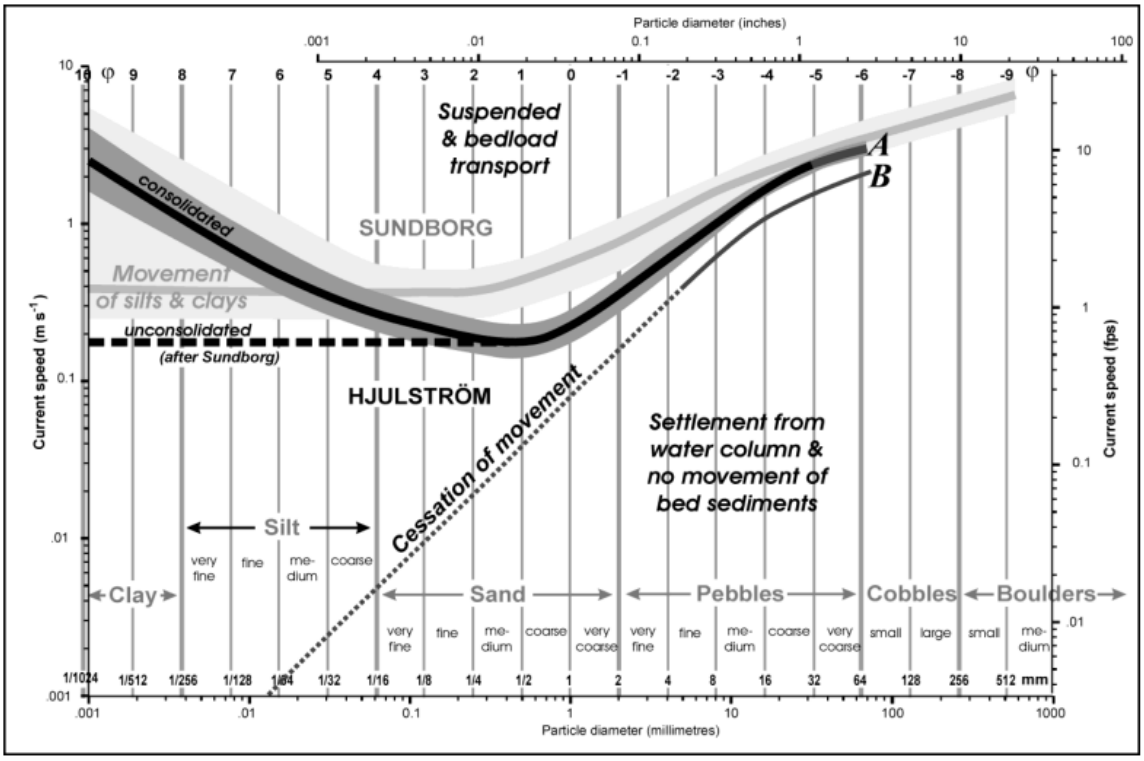

Figure 4 Modified Shields Diagram [5] also known as Hjulström-Sundborg diagram with Wentworth-Krumbein grade scale.

The area between these curves marks a transitional zone where particles may be in different modes of movement, such as sliding, rolling, saltation, or suspension.

4.2 Modes of transport: bed load and suspended load

Once sediment is in motion, the mode of transport is largely determined by grain size and current speed. There are two main modes of sediment transport in water: **bedload** and **suspended load**. Bedload transport occurs when grains are in continuous or intermittent contact with the bed, either sliding or bouncing along it. This mode is typical for sands in weak currents or larger particles like pebbles in stronger currents. Suspended load transport happens when grains are lifted and carried by turbulence within the fluid, common for finer particles like silts in moderate currents or sands in stronger currents.

The **total sediment load** refers to all the sediment being transported by the flow at a given time, including both bed load and suspended load [7]. This can be visualized as the total sediment mass within a block of flow that, if isolated, would reveal the sediment content once the water is removed. Importantly, there is no strict separation between bed load and suspended load [7]; a given particle can transition between these states depending on the flow conditions. For instance, a particle might be traveling as bed load, become suspended, or even temporarily rest on the bed surface.

The bed load consists of particles that remain in close contact with the bed, moving through rolling, sliding, or short hops (saltation). This layer is thin relative to the suspended-load layer, serving as its lower boundary. The sediment concentration in the bed-load layer is generally much higher than in the suspended-load layer. In contrast, the suspended load is composed of particles that are carried within the turbulent flow above the bed, typically moving irregularly due to being buffeted by turbulent eddies. While the bed-load particles are in near-constant contact with the bed, the suspended particles are supported by the turbulence in the water column.

Measuring the sediment transport rate, involves determining how much sediment the flow carries. For practical purposes, the **unit sediment transport rate** (sediment transport per unit width of the flow) is often used. Various methods can be employed to measure this, such as capturing the sediment moving through a vertical slice of the flow or using depth-integrated sampling.

Measuring bed load can be challenging because it involves capturing particles moving near the bed, often using traps that might distort the flow and affect the accuracy of the measurement [7].

Conversely, measuring the suspended load is somewhat simpler, typically involving trapping a portion of the flow at different heights above the bed to assess the sediment concentration and flow velocity at each level. When measurements are taken at multiple heights, the combined data provide a good estimate of the suspended-load transport rate.

The relationship between current velocity and sediment transport mode can be described using the **Transport Stage**, defined as the ratio of shear velocity (which represents the collective forces that drive sediment transport) to grain settling velocity (forces responsible for sediment deposition). As this ratio increases, the amount of sediment transported as suspended load increases, while bedload transport decreases. This transition is gradual, with no clear threshold between bedload and suspended load modes [5].

4.3 Sediment transport rate

The sediment transport rate is defined as the mass of sediment transported per unit of cross-sectional area of flow per unit time. For bedload transport, the transport rate can be calculated by integrating the product of grain velocity and sediment concentration over the height of the bedload layer. Although this method is theoretically valid, it is challenging to measure these parameters directly due to the thinness of the bedload layer, typically only a few centimeters high. As a result, an alternative approach is often used, based on the relationship between sediment transport rate and bed shear stress. Field and laboratory experiments have shown that the bedload transport rate can be estimated as a power of difference between flow induced bed shear stress (flow-related parameters) and the critical shear stress required to initiate sediment movement (sediment-related parameters).

Similar to bedload transport, the suspended load transport rate can be determined using a similar integral over the entire water column height, although typically only the mean current velocity is available for such predictions.

4.4 Sediment-Discharge Formulas

Predicting and modeling sediment transport rates commonly involves using sediment discharge relationships, which are mathematical formulas designed to estimate the rate at which sediment is moved by a flow [7]. These relationships are widely used in both research and practical applications to understand and manage sediment dynamics in various environments.

The first modern sediment discharge formula was developed by DuBoys in 1879, and many others have followed, often associated with key figures like Hans Albert Einstein, Meyer–Peter and Müller, Bagnold, Engelund, and Hansen.

Ancey (2020) provides a modern review of these sediment discharge relationships, offering insights into their development, application, and limitations. Different sediment-discharge formulas also exhibit considerable variability in their accuracy, particularly when applied outside the specific conditions they were designed for, highlighting the importance of using these formulas within their intended context. The complexity of particle transport in turbulent shear flows makes it challenging to develop a universally applicable sediment transport model [7]. As a result, the common practice involves creating equations with adjustable parameters based on a rational dynamical framework and then fitting these equations to data from laboratory or field studies. However, this approach has limitations, as there is no guarantee that the resulting sediment-discharge formulas will work well beyond the specific data sets they were calibrated with. In addition, significant variability and spread exist in the data, often showing an order-of-magnitude difference for a given shear stress. This variability is expected due to factors such as unaccounted particle size distribution, the presence of bed forms, and the inherent difficulties in accurately measuring sediment transport rates.

In a recent study, [10], highlights the persistent challenge in accurately predicting bedload transport rates in rivers, a problem that has remained largely unchanged since the Meyer-Peter and Müller equation was published 70 years ago. The difficulty stems from the significant temporal and spatial variability in transport rates, which are conventionally seen as noise from various processes. However, recent evidence suggests that these fluctuations are intrinsic to sediment transport, indicating that improving predictive models will require a deeper understanding of how these fluctuations arise and influence overall dynamics.

4.5 Bagnold's equation

As previously discussed, many sediment-discharge equations have been proposed in earlier studies. A detailed comparison of these equations falls outside the scope of the present work. Additionally, an effective search for the most applicable sediment discharge formula for a specific study area requires a coordinated field campaign with high-frequency sediment sampling at multiple locations. Readers are referred [8] and [9] for further information regarding these topics. In this study, Bagnold's sediment transport model was chosen due to its simplicity and proven accuracy.

Bagnold's approach to modeling sediment transport conceptualizes the process as analogous to the operation of a machine, where the transporting current functions as the machine, and the movement of sediment represents the work done by that machine. In this perspective, known as the "energetics approach," the work done—reflected as the sediment transport rate—is proportional to the power of the machine, which in this case is the transporting current.

In this approach, the energy provided by the current is used to overcome the forces resisting sediment movement, such as gravity and friction. The more powerful the current, the greater its capacity to transport sediment, and the faster it can move that sediment. This concept provides a framework for understanding how variations in flow energy can lead to changes in sediment transport rates.

A recent study that Ancey and Recking published in 2023 [9], they provided a comprehensive review of sediment discharge relationships and demonstrated the robustness of Bagnold's approach under various conditions.

The study examined the scaling behavior of bedload transport, focusing on whether a power-law relationship between the bedload transport rate and the Shields stress could describe both laboratory and field data. While the study suggested that a universal law for bedload transport might be elusive, Bagnold's model was shown to effectively describe bedload transport rates across two orders of magnitude of the Shields stress, with reasonable prediction skill of transport rates under different regimes: the no-transport regime, the transitional or kinetic regime, and the high-transport or sheetflow regime.

Although Bagnold's model performed well in laboratory flume experiments and was generally accurate for real-world rivers, some limitations are reported, particularly in gravel-bed rivers. Overall, Ancey and Recking [9] concluded that Bagnold's approach remains highly relevant and effective for a wide range of flow conditions, confirming the validity of the core relationship for sediment transport.

Bagnold's equation for bedload transport under this approach can be expressed as [5]:

$$q_b = \frac{\tau_b u e_b}{\tan\phi - \tan\beta}$$

In this equation τ_b represents the bed shear stress, which is the force exerted by the flow on the bed, u is the flow velocity, reflecting the speed of the transporting current, e_b is an efficiency factor that accounts for how effectively the current's energy is used to move sediment, ϕ is the angle of repose of the sediment, indicating the steepest angle at which sediment can remain stable without sliding, β is the bed slope, representing the inclination of the bed surface. Bedload

efficiency is smaller than one because some of the power is converted to frictional dissipation and other losses.

This equation illustrates that the sediment transport rate q_b depends not only on the flow's physical characteristics (such as velocity and shear stress) but also on how efficiently the flow's energy is utilized to transport sediment. The energetics approach, therefore, provides a comprehensive method for analyzing and predicting sediment transport by focusing on the flow's energy as a key driving factor.

Similarly, Bagnold's equation for suspended load transport is:

$$q_s = \frac{\tau_0 u e_s}{(w_s u) - tan\ \beta}$$

Where $\mathbf{w_s}$is sediment settling velocity, and e_s is the suspended load efficiency factor depending on both flow conditions and sediment properties.

4.6 Computing bed level changes

Morphodynamics is a term used for the mutual adjustment of morphology and hydrodynamic processes involving sediment transport [3]. There are many morphodynamical models available, each employing various formulations and mathematical approaches to simulate sediment transport and morphological changes. In this section, a general framework is presented in a simplified form to familiarize readers with the fundamental underlying concepts of typical morphodynamic models to simulate sediment transport and the evolution of bed levels in aquatic environments.

In sediment transport modeling, when horizontal variations in sediment concentration are more critical than vertical differences, a depth-averaged approach is in the form of advection-diffusion equation:

$$\frac{\partial(h\bar{c})}{\partial t} + \bar{u}\frac{\partial(h\bar{c})}{\partial x} + \bar{v}\frac{\partial(h\bar{c})}{\partial y} - \frac{\partial}{\partial x}\left(\varepsilon_h \frac{\partial(h\bar{c})}{\partial x}\right) - \frac{\partial}{\partial y}\left(\varepsilon_h \frac{\partial(h\bar{c})}{\partial y}\right) = S$$

In this equation:

- h represents the water depth, and $\bar{c}$ is the depth-averaged sediment concentration.
- t denotes time.
- $\bar{u}$ and $\bar{v}$ are the depth-averaged velocities in the horizontal x and lateral y directions, respectively.
- ε_h is the horizontal diffusion coefficient, accounting for the mixing of sediment due to turbulence across the horizontal plane.

- S is the source/sink term, representing the exchange of sediment between the water column and the bed, covering processes such as erosion and deposition.

Since spatial and temporal variations of flow variables such as depth and velocity are required, many morphodynamic models incorporate a depth-averaged hydrodynamic solver, either as an internal component or through coupling with an external solver.

The source/sink term S plays a critical role in determining bed level changes over time. As sediment is either eroded from the bed or deposited onto it, the bed level adjusts accordingly. For example, when S is positive, it indicates that more sediment is being deposited than eroded, leading to bed aggradation (a rise in bed level). Conversely, a negative S value implies net erosion, causing the bed level to lower (degradation).

Near a sandy bottom, the sediment concentration reacts quickly to changes in bed shear stress, which is a key factor in driving erosion and deposition. This near-bed concentration, or reference concentration c_{ref}, is typically defined at a certain height above the bed, based on either the sediment grain size or the roughness of the bed surface.

The vertical flux of sediment between the bed and the water column, which directly affects bed level changes, can be modeled using:

$$S_z = -\varepsilon_s \frac{\partial c}{\partial z} - w_s c$$

Here:

S_z represents the vertical sediment flux.

ε_s is the vertical diffusion coefficient, capturing vertical mixing of sediment.

$\frac{\partial c}{\partial z}$ is the vertical concentration gradient, which describes how sediment concentration changes with height above the bed.

w_s is the sediment settling velocity, indicating the rate at which particles settle toward the bed.

c is the local sediment concentration at a specific point within the water column.

The vertical concentration gradient $\frac{\partial c}{\partial z}$ can be approximated as:

$$\frac{\partial c}{\partial z} \approx \frac{c(z_{\text{ref}} + \Delta z) - c_{\text{ref}}}{\Delta z}$$

where:

z_{ref} is the reference height above the bed, and Δz is a small vertical distance used to measure the change in concentration.

When the shear stress exerted by the flow increases, the reference concentration c_{ref} rises, leading to a steeper concentration gradient. This causes sediment to be entrained into the water column from the bed, resulting in erosion and a lowering of the bed level. Conversely, when the shear stress decreases, the sediment settling velocity w_s becomes more significant, leading to sediment deposition onto the bed, thereby increasing the bed level.

The source and sink terms in the horizontal space are connected to bed level changes through the governing equation typically in the following form:

$$(1-\eta)\frac{\partial z_b}{\partial t}+\frac{\partial S_x}{\partial x}+\frac{\partial S_y}{\partial y}=D-E$$

where:

- z_{b} is the bed level.
- η is the porosity of the bed material.
- S_x and S_y are the bed-load transport rates in the x and y directions, respectively. Many existing empirical equations such as previously discussed Bagnold method can be used here.
- D represents the deposition rate of sediment.
- E is the erosion rate of sediment.

This equation is sometimes called **Exner's equation** and accounts for conservation of sediment mass in bed. It describes how sediment transport in the horizontal plane, along with erosion and deposition processes, influences the changes in bed level over time.

Such process-based analysis of bed evolution can be performed by tight coupling hydrodynamic and morphodynamic simulations. This is because the movement of sediment is directly governed by the characteristics of flow, while the accurate simulation of flow characteristics requires continuously updated bathymetry, which is in turn achieved by applying the erosion and deposition results from the morphological component.

4.7 Morphological Acceleration

Modeling of long-term morphodynamical processes is computationally intensive. Even with modern 2D models, simulations can take days to complete. These processes, occurring over large areas over decades, are driven by hydrodynamics and sediment transport at much smaller scales. For instance, basin-scale changes in river profiles, involve sediments moving in subbasin scales. However, the underlying processes happen at much finer scales. This disparity creates a significant challenge in numerical simulation, requiring both large spatial coverage and fine

resolution, which dramatically increases computational demands given that computational time can increase exponentially with the number of cells modeled. Longer-term simulations spanning years become particularly difficult to complete within typical computational resources.

To address this issue, researchers employ a morphological acceleration factor (morfac or Mf). This scalar value is applied to the sediment continuity equation (Exner's equation), based on the assumption that morphodynamic changes that occur more slowly than hydrodynamic processes, can be made more consistent in temporal scales. By assuming a linear relationship between hydrodynamics and morphodynamics, the morfac effectively compresses the simulation time. This allows modelers to conduct long-term simulations within manageable timeframes without compromising result accuracy.

While morphological acceleration is a powerful tool, it comes with important caveats. The technique requires the observed flow hydrograph to be dilated to align timescales, which can unrealistically alter flood wave timing. Moreover, large floods typically exert significant energy, resulting in substantial sediment transport. Applying morfac to accelerate these high sediment transport values could lead to unrealistic overestimations. To address this issue, one can analyze these flow regimes separately: analyzing high-energy flood events without acceleration (morfac=1), while applying higher morfac values to moderate flow conditions. This method aims to balance computational efficiency with accurate representation of extreme events, recognizing that different flow regimes may require distinct modeling strategies to maintain fidelity to real-world processes.

In this section, a brief overview of theoretical backgrounds involved in computational sediment transport modeling was provided. Understanding these concepts and their limitations is essential for developing robust sediment transport models and interpreting their results in the context of coastal management and river system analysis. It is worth mentioning that the overview provided in this section, was a simplified summary, as modern models are highly sophisticated and integrate a wide range of components, such as multiple sediment material groups with grain-size distributions, turbulence models, bank erosion and stability modules, cohesive sediment transport, wave effects, hiding and exposure phenomena, and the impact of sediment on water density and the resulting flow fields.

5. STUDY AREA

This study's scenario analysis concentrates on two Texas regions: the lower reaches of the **Brazos** and **San Bernard** rivers, in addition to the **Colorado River** (in Texas) from Bay City to the Gulf Intercoastal Waterway. As illustrated in the figure below, most rivers in Texas do not drain directly into the Gulf of Mexico without passing through a coastal water body, which complicates the analysis of flow and sediment in estuarine settings. However, the three rivers focused on in this study are among the best candidates, as they allow for a more straightforward analysis of sediment transport within a riverine environment, which is the primary objective of this research.

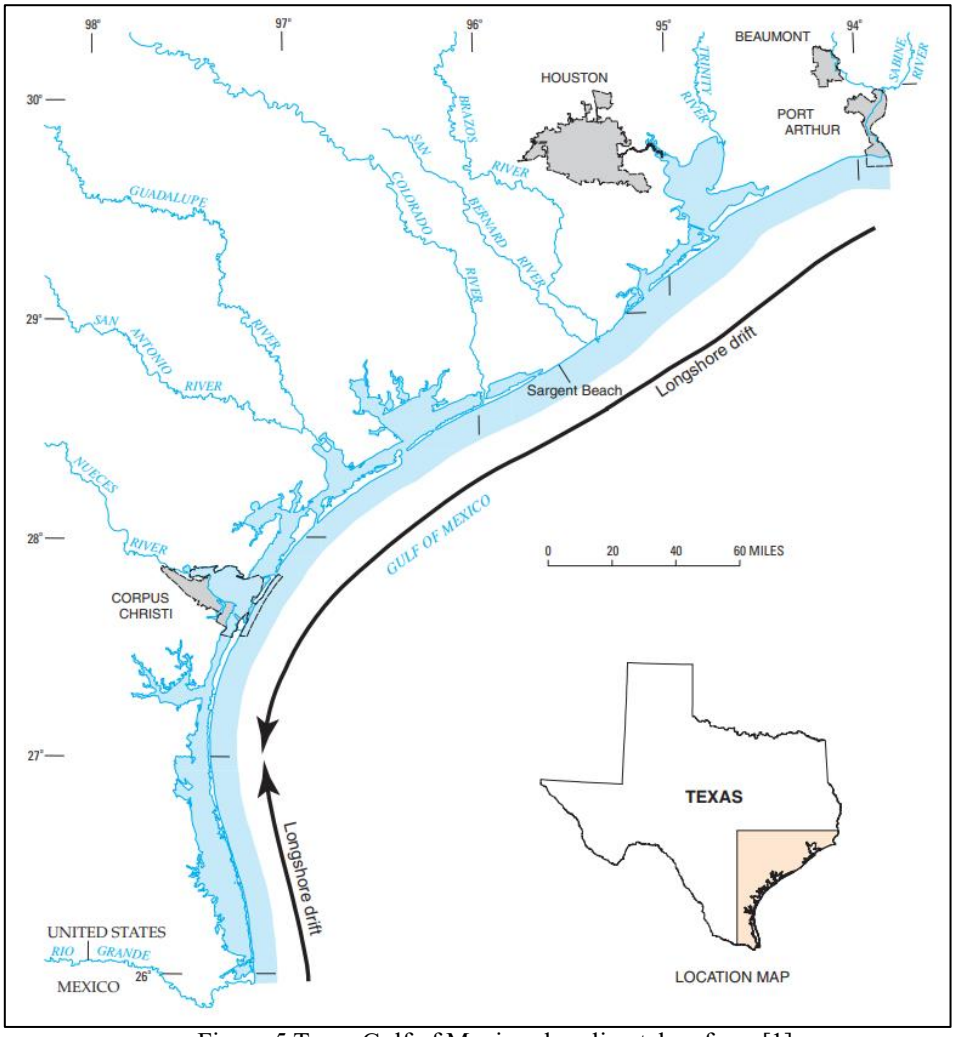

Figure 5 Texas Gulf of Mexico shoreline taken from [1]

5.1 Brazos River

The Brazos River holds the distinction of being the longest river flowing entirely within Texas [16]. However, its watershed extends from New Mexico to the Gulf of Mexico, covering 45,510 square miles. Of this area, 94% lies within Texas, while the remaining 6% is in New Mexico. The river's main stem begins in Stonewall County, where the Salt Fork and Double Mountain Fork converge. As it flows southeastward, it's joined by the Clear Fork above Possum Kingdom Lake in Young County. After traversing much of Texas, the Brazos finally drains into the Gulf of Mexico near Freeport in Brazoria County.

Throughout its ~1000-mile length, the Brazos crosses diverse physiographic regions of Texas, including the High Plains, Blackland Prairie, Edwards Plateau, and Gulf Coast Prairies & Marshes. This variety results in a changing landscape, from canyons in the upper reaches to rolling hills and plains in the central portions, and finally coastal beaches near its mouth. The river's gradient varies from three feet per mile in its upper course to a mere half-foot per mile as it approaches the Gulf.

Brazos River has several major tributaries, including the aforementioned Salt Fork and Double Mountain Fork, as well as the Clear Fork, Yegua Creek, and the Bosque, Little, and Navasota rivers. Within this network are 15 subtributaries, such as the Leon River, which feeds into the Little River.

The Brazos watershed encompasses numerous cities, with Lubbock, Graham, Waco, Temple, Belton, Georgetown, Round Rock, Bryan-College Station, Freeport, and Galveston being the most prominent.

The river basin's climate varies significantly, and this climatic diversity supports a range of natural vegetation, from grasses in drier areas to hardwoods in wetter regions.

Attempts to make the Brazos navigable have been challenging due to its alternating periods of drought and flooding. In 1929, its natural mouth was diverted several miles southwest by the Corps to its current mouth.

Figure 6 Brazos River watershed adapted from Texas parks and Wildlife's Texas Watershed Viewer [18]

Brazos is one of the largest Texas rivers maintaining a consistent discharge into the Gulf. Interestingly, the majority of rainfall in its watershed occurs downstream of the lowest main reservoir [1].

This might be one of the reasons for its high sediment yield. Human intervention has also significantly altered the lower river's regime through channelization and levee construction [1], disrupting natural flooding patterns and trapping most sediment in the lower river instead of dispersing it across the floodplain.

5.2 San Bernard River

Neighboring the Brazos, the smaller San Bernard River flows approximately 120 miles from its origin near New Ulm to its mouth [17]. The river meanders through several Texas counties, including Austin, Colorado, Wharton, Fort Bend, and Brazoria. Its drainage area encompasses two distinct ecological zones: the upper part lies in Bay Prairieland, while the lower section is part of the Gulf Coast Prairies and Marshes. Various creeks and bayous feed into the San

Bernard, including branches of Bernard Creek, as well as Peach, Mound, Coushatta, and Bell creeks, among others.

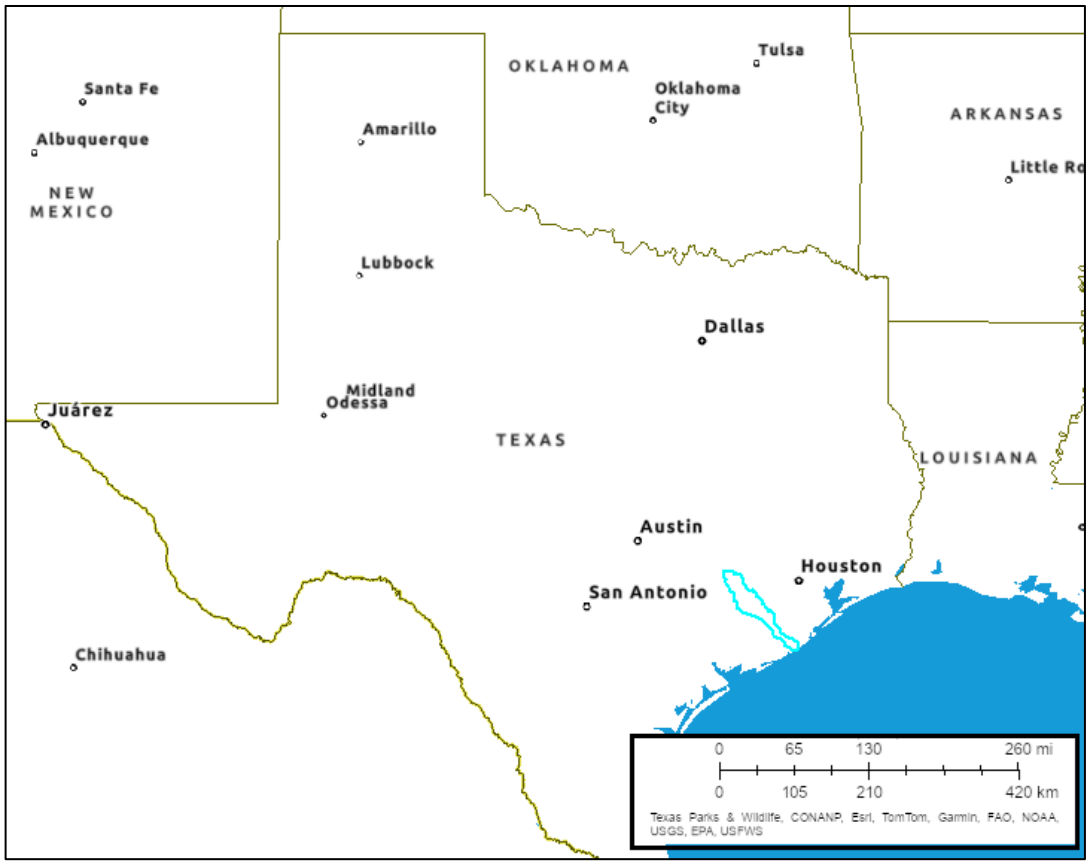

Figure 7 San Bernard River watershed adapted from Texas parks and Wildlife's Texas Watershed Viewer [18]

The San Bernard's surrounding terrain is predominantly level, with elevations barely exceeding 30 feet above sea level. This area experiences gradual water drainage and receives substantial annual rainfall, ranging from 40 to 54 inches. The river's banks showcase a diverse soil composition, featuring sand, gravel, clay, silt, and mud. The watershed primarily supports agricultural activities and grazing, interspersed with small rural communities. Recreational pursuits like boating and fishing are popular along the river.

San Bernard's mouth has experienced frequent closures, which has led to altered flow and sediment dynamics and disrupting local ecosystems and recreational activities. These closures are thought to stem from the Brazos River's high sediment yield, with the intracoastal waterway and coastal currents likely transporting this material to the San Bernard's mouth.

The central Texas coastline near the Brazos outlet has undergone significant transformations, particularly following the relocation of the Brazos inlet and the construction of the Gulf

Intracoastal Waterway. The shifting Brazos Delta is believed to be a key factor in the San Bernard inlet's recurrent closures and increased sedimentation in nearby tidal flats.

5.3 Colorado River

The Colorado River (in Texas) is one of longest waterways in the state [19]. Originating south of Lubbock, its watershed encompasses over 42,000 square miles – about 16% of Texas's total area. As it approaches the Gulf, the Colorado's yearly runoff surpasses 2 million acre-feet, highlighting its importance to the state's water resources.

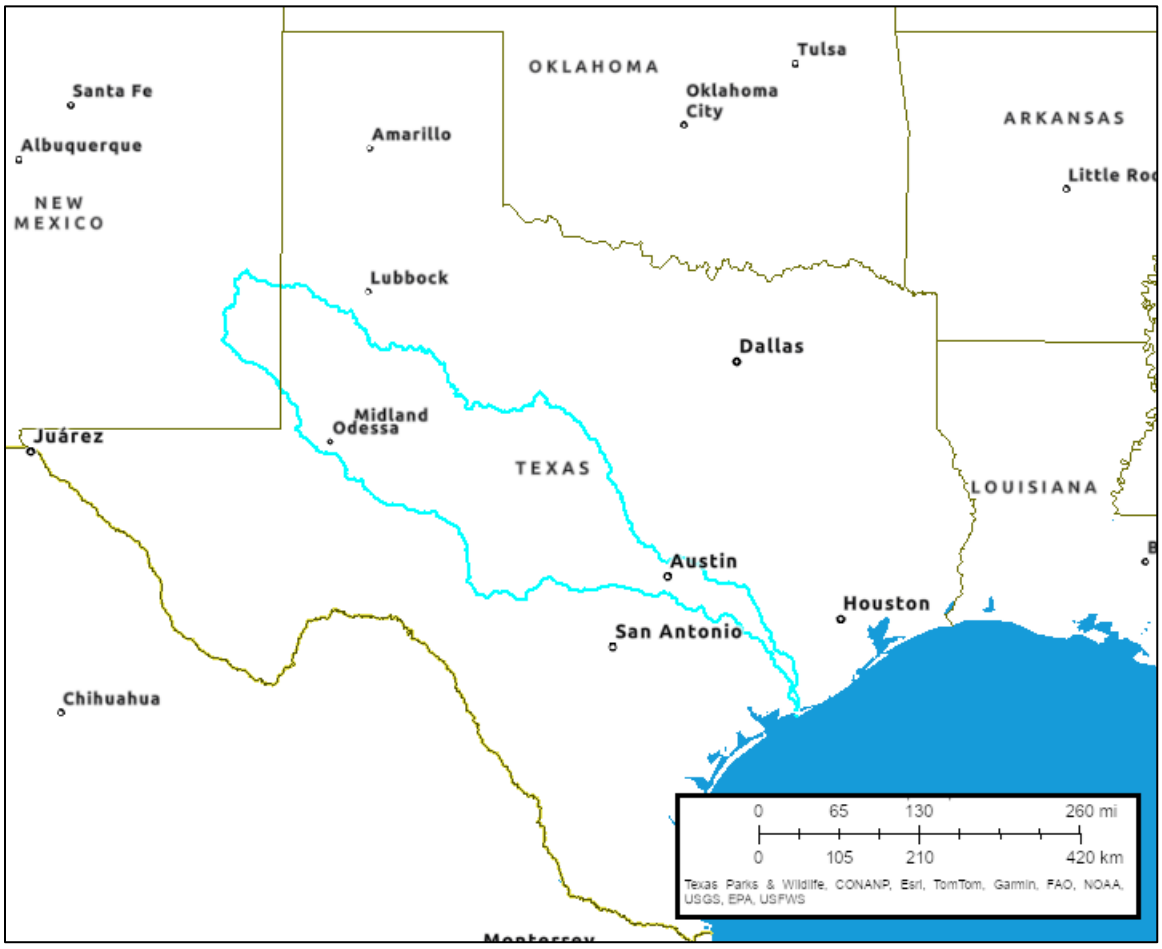

Figure 8 Colorado River watershed adapted from Texas parks and Wildlife's Texas Watershed Viewer [18]

Historically, Colorado River was prone to extreme fluctuations, experiencing severe droughts and catastrophic floods. The construction of several dams in the 1930s and 1940s helped regulate its flow and mitigate these events. However, in the Hill Country region, the river can still dwindle to a trickle during prolonged dry spells while remaining capable of significant flooding during heavy rainfall.

Management of the Colorado is divided among three state-created entities: the Lower, Central, and Upper Colorado River Authorities. These organizations are responsible for regulating river flow, preserving water quality, and overseeing flood control infrastructure, playing a vital role in managing one of Texas's most critical water systems.

6. MORPHODYNAMICAL SCENARIO ANALYSES

Sediment transport analysis is characterized by numerous challenges and complexities. Even with the application of advanced modeling techniques, the results can exhibit significant variability due to the intricate nature of the processes involved, limitations in available data, and inherent simplifications in modeling approaches. These challenges arise from the complex interactions between hydrodynamics, sediment properties, and geomorphological processes, which are often difficult to accurately represent in models. Additionally, the data requirements for comprehensive sediment transport modeling are extensive and not always readily available, potentially leading to inaccuracies in input parameters. This study aims to analyze the effects of these potential uncertainties inherent in current sediment transport modeling practices. By examining various scenarios and their implications, this research seeks to provide insights that can inform more robust management decisions, taking into account the range of possible outcomes rather than relying on a single deterministic result.

6.1 Overarching goal

The general description of the scenarios analyzed in this study is as follows:

I. **Long-term Sediment Regime under Prescribed LDCs and Morphological Acceleration Factors**

This group of scenarios serves as the long term result of baseline conditions for understanding sediment transport under various morphological acceleration factors. Boundary conditions in the form of Load Duration Curves (LDCs) provide a representation of sediment loads across various flow conditions, capturing the variability in upstream influx that occurs over extended periods. The application of different morphological acceleration factors allows for the simulation of long-term morphological changes within computationally feasible timeframes. These factors essentially compress hydrodynamic time scales (or dilate morphological time) in the model, enabling the observation of channel evolution and sediment deposition patterns that would typically occur over weeks or months. For the baseline condition, a 50% exceedance flow and corresponding sediment load were employed as constant boundary conditions for a 24-hour simulation period. Morphological accelerations of 10, 30, 180, 365 were then applied to this

baseline scenario, providing a representative average condition as a proxy for long-term morphological changes over 10 days, 1 month, 6 months, and 1 year.

II. Alteration of Long-term Sediment Regime due to Gradual Stressors

This scenario examines how gradual environmental changes and human interventions affect the long-term sediment regime. Factors such as sea level rise, urbanization, variation land cover including marsh lands, and upstream sediment entrapment can significantly alter sediment dynamics over time.

In this study, tidal downstream boundary conditions were offset by 0.56 meters for “intermediate low”, and, 0.72 meters by “high”. According to NOAA sea level rise projections.

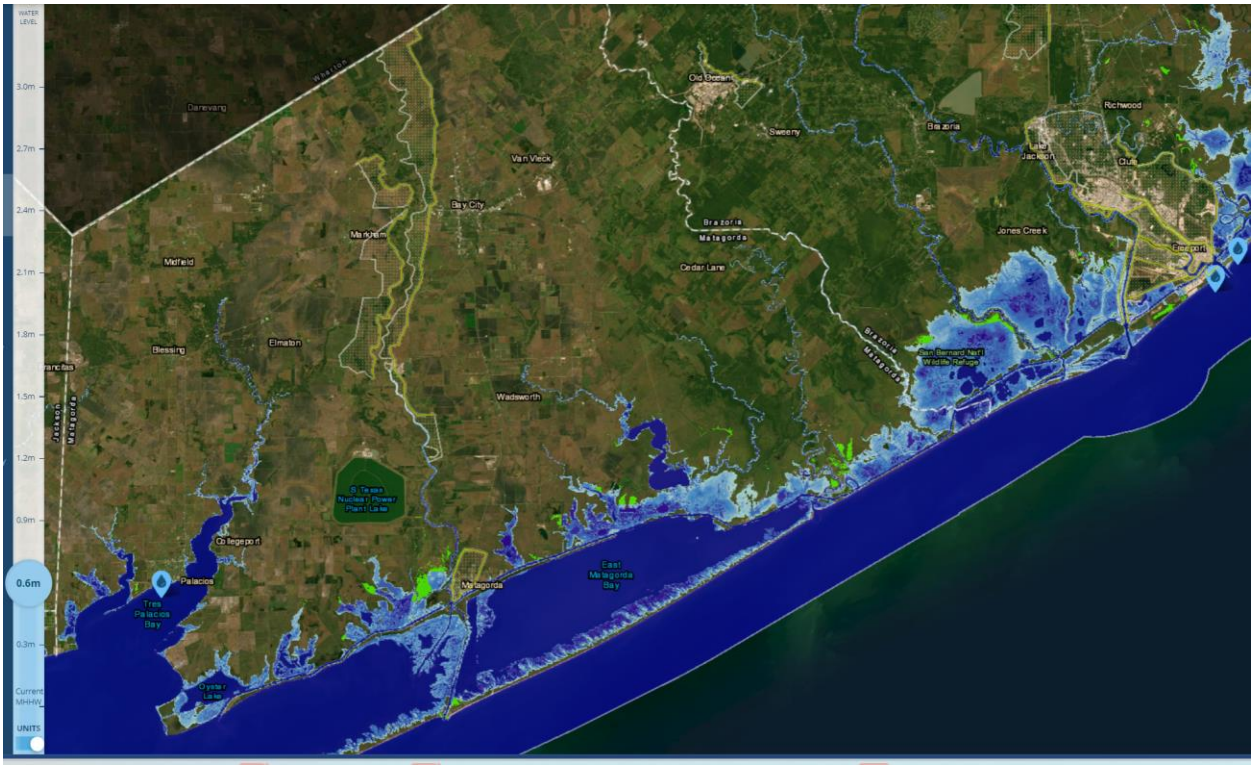

Figure 9 Inundation of 0.6m sea level rise, a value in between the two scenarios investigated in this study, taken from NOAA Sea Level Rise Viewer [20]

Urbanization typically increases impervious surface area within a watershed, leading to flashier hydrographs and potentially higher peak flows.

Urbanization also reduces upstream sediment supply as was documented in a USGS study of Brazos River. Changes in marsh lands can alter the sediment trapping efficiency of coastal areas, while upstream sediment entrapment can significantly reduce sediment supply to downstream reaches. These factors can lead to long-term changes in channel morphology and coastal landforms, potentially causing shifts in the grain size distribution of transported sediments.

Changes in marsh lands are usually modeled by increasing roughness to account for their ability to slow flow and increase sediment deposition. However, in this study, it was found that since the current scenario analysis does not account for out-of-channel rainfall runoff modeling that would require precipitation on wetlands where marshes would be located, these changes do not manifest in the expected manner. Instead, their effect is similar to reduced LDC boundary conditions, analogous to the impacts of urbanization and reservoir construction. Upstream sediment entrapment can significantly reduce sediment supply to downstream reaches. These factors can lead to long-term changes in channel morphology and coastal landforms, potentially causing shifts in the grain size distribution of transported sediments.

III. Alteration of Sediment Regime due to Spatially Varied Sediment Supply LDCs

This scenario considers how variations in sediment supply along the river course affect overall sediment transport dynamics. It recognizes that sediment inputs are not uniform along a river's length and can vary significantly due to tributaries, local geology, and land use patterns. Spatially varied LDCs account for these differences by applying distinct sediment supply characteristics to different river segments. This was modeled by prescribing the same total of sediment influx at multiple locations along the river reaches, as opposed to the common practice of only considering upstream inputs. This approach provides a more realistic representation of sediment inputs and allows for the examination of how these spatial variations influence downstream sediment transport and deposition patterns. It enables the simulation of key sediment source areas and their relative contributions, for example multiple small tributaries, allowing for the assessment of how localized changes in sediment supply propagate downstream.

IV. Disturbances Caused by Floods and Droughts

This scenario focuses on the impacts of varied hydrological regimes. Floods, modeled as event-scale high flows, can cause significant sediment mobilization and transport. Droughts, represented by medium to long-timescale low flows, can lead to sediment deposition and changes in channel characteristics. During flood events, the increased stream power can mobilize and transport large quantities of sediment, including coarser materials that are usually stable under normal flow conditions. Prolonged drought conditions can result in reduced sediment transport capacity, leading to increased deposition in the channel. It's important to note that flood scenarios were modeled separately without morphological acceleration to maintain the realistic temporal scale of these acute events, while drought conditions were modeled by a smaller upstream flow.

V. Treatment of Sediment Types (Cohesive vs. Non-cohesive)

This scenario examines the differences in transport behavior between cohesive (e.g., clays, silts) and non-cohesive (e.g., sands, gravels) sediments. Most of the studies and theoretical background in sediment transport are focused on granular sediment transport, mainly sand. The distinct physical properties of cohesive sediment types lead to significant differences in their erosion, transport, and deposition characteristics. Non-cohesive granular sediments are primarily influenced by particle size and flow velocity, and their transport can often be reasonably well predicted using established sediment transport equations based on shear stress or stream power. Cohesive sediments, on the other hand, are influenced by complex physicochemical interactions and often exhibit a critical shear stress for erosion and can form consolidating deposits that become more resistant to erosion over time. This scenario necessitates different modeling approaches for cohesive and non-cohesive sediments, highlighting the importance of considering sediment composition in transport predictions. In this study, these differences were analyzed by changing the sediment type in the model. Since Delft 3D FM was used for modeling in this study, according to the manual, "mud" (cohesive suspended load transport) was used for the cohesive case versus "sand" (non-cohesive bedload and suspended load transport) for the non-cohesive case.

A comprehensive scenario analysis plan was developed, with the majority of scenarios systematically named and assigned a coded identifier. These scenarios represent various combinations of factors, including flow regimes (median and mean flows), the inclusion or exclusion of suspended sediment influx, morphological acceleration factors (morfac), sea level rise (SLR) scenarios, and spatially varied lateral distribution coefficients (LDC). The naming convention, as detailed in Appendix A, reflects these combinations. Additional isolated scenarios were created by introducing changes to specific parameters within these base configurations. A number of additional scenarios, such as the Hurricane Harvey case study, which do not fit this naming convention, were also analyzed.

For the majority of the modeled scenarios, results were analyzed at specific cross sections placed across the Brazos, San Bernard, and Colorado rivers. These cross sections were located and named using a station numbering convention common in river engineering, where the station number represents the distance in meters from the most downstream point, typically the river mouth.

6.2 Determining Representative Flows for Sediment Transport Modeling

Unlike flood analysis, where return period conventions are well established, determining a characteristic flow for sediment transport analysis is less straightforward and lacks consensus. While flood frequency analysis typically uses statistical methods to associate specific flow magnitudes with return periods (e.g., 100-year flood), sediment transport processes are more complex and occur across a wide range of flow conditions, making it challenging to identify a single representative flow.

In attempts to characterize flows significant for sediment transport, several important concepts have emerged. One such representative flow is **bankfull discharge**, which refers to the flow that just fills the channel to the top of its banks before overflowing onto the floodplain. This concept is based on the idea that it represents a geomorphologically significant flow that shapes the channel over time, often corresponding to a flow with a return period of 1-2 years in many rivers. It's also relatively easy to identify in the field based on physical indicators.

However, the applicability of bankfull discharge for sediment transport analysis can be limited. Not all rivers have well-defined bankfull levels, especially in highly modified or incised channels, and the relationship between bankfull discharge and sediment transport can vary significantly between river systems. Moreover, for the coastal area of the study in question, bankfull discharge is associated with larger than regime flows. Since the analysis is focusing on flooding separate from the normal regime for the baseline scenario, using bankfull discharge with morphological acceleration could result in simulating a continuous 1–2-year return period flood occurring all the time, which is not representative of typical conditions. Additionally, in highly channelized and regulated waterways, bank locations may be determined by factors beyond the natural flow regime for example bridge abutments, levees etc. which further complicates the use of bankfull discharge as a representative measure.

Another representative flow is **effective discharge**, which is the flow that transports the largest fraction of the annual sediment load over the long term. This concept integrates flow frequency and sediment transport rate, often representing a moderate flow that occurs frequently enough to do significant geomorphic work over time. It can be calculated using flow duration curves and sediment rating curves. However, effective discharge also has its challenges. It can be sensitive to the method of calculation and the quality of available data, may not always correspond well to observable geomorphic features, and in some systems, it may not adequately represent the full range of flows important for sediment transport.

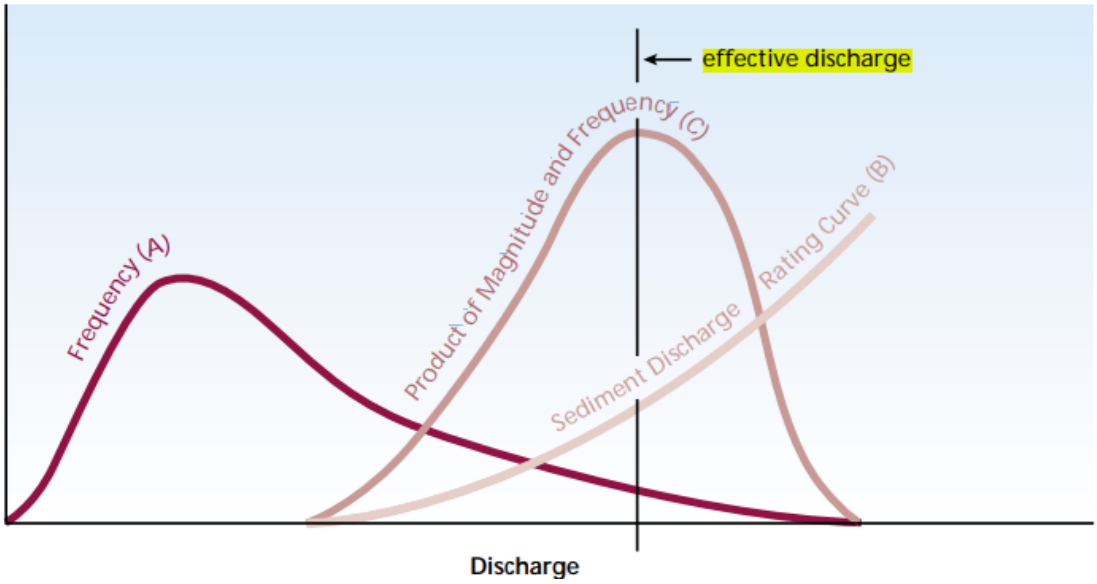

Figure 10 Schematics of calculating effective discharge by traditional method

The calculation of effective discharge is a complex process that integrates flow frequency with sediment transport rates. Typically, it involves dividing the range of observed flows into a number of discrete classes or "bins," calculating the sediment transport rate for each bin, and then multiplying this rate by the frequency of occurrence for flows within that bin. The product of these calculations represents the total sediment load transported by flows in each bin over time. The flow class that produces the highest total sediment load is then identified as the effective discharge.

However, the results of this calculation can be highly sensitive to methodological choices, particularly the number and width of flow bins used. Using too few bins may obscure important variations in sediment transport rates, while using too many can lead to noisy results that are difficult to interpret. Furthermore, the choice of sediment transport equation and the quality of the input data can significantly influence the outcome. These sensitivities mean that different analysts may arrive at different effective discharge values for the same river system, underscoring the need for careful consideration and transparency in the calculation process.

Figures 11 and 12 present the results of analyses conducted to determine effective discharge using two methodologies: the traditional approach utilizing the complete dataset, and a filtered approach considering only flows below the 90th percentile. Additionally, these figures illustrate the impact of varying the number of bins in the creation of histograms for flow duration curves. Examination of these figures reveals substantial variability in the calculated effective discharge values based on the chosen analytical approach. The effective discharge appears to be highly

sensitive to both the data filtering method and the number of histogram bins employed. This sensitivity suggests that the determined effective discharge could easily fluctuate from one analysis to another, depending on the specific methodological choices made by the researcher. The observed variability underscores the importance of careful consideration when selecting analytical parameters for effective discharge calculations. It also highlights the potential limitations of relying on a single effective discharge value for sediment transport studies, particularly in complex river systems where a range of flow conditions may contribute significantly to overall sediment dynamics.

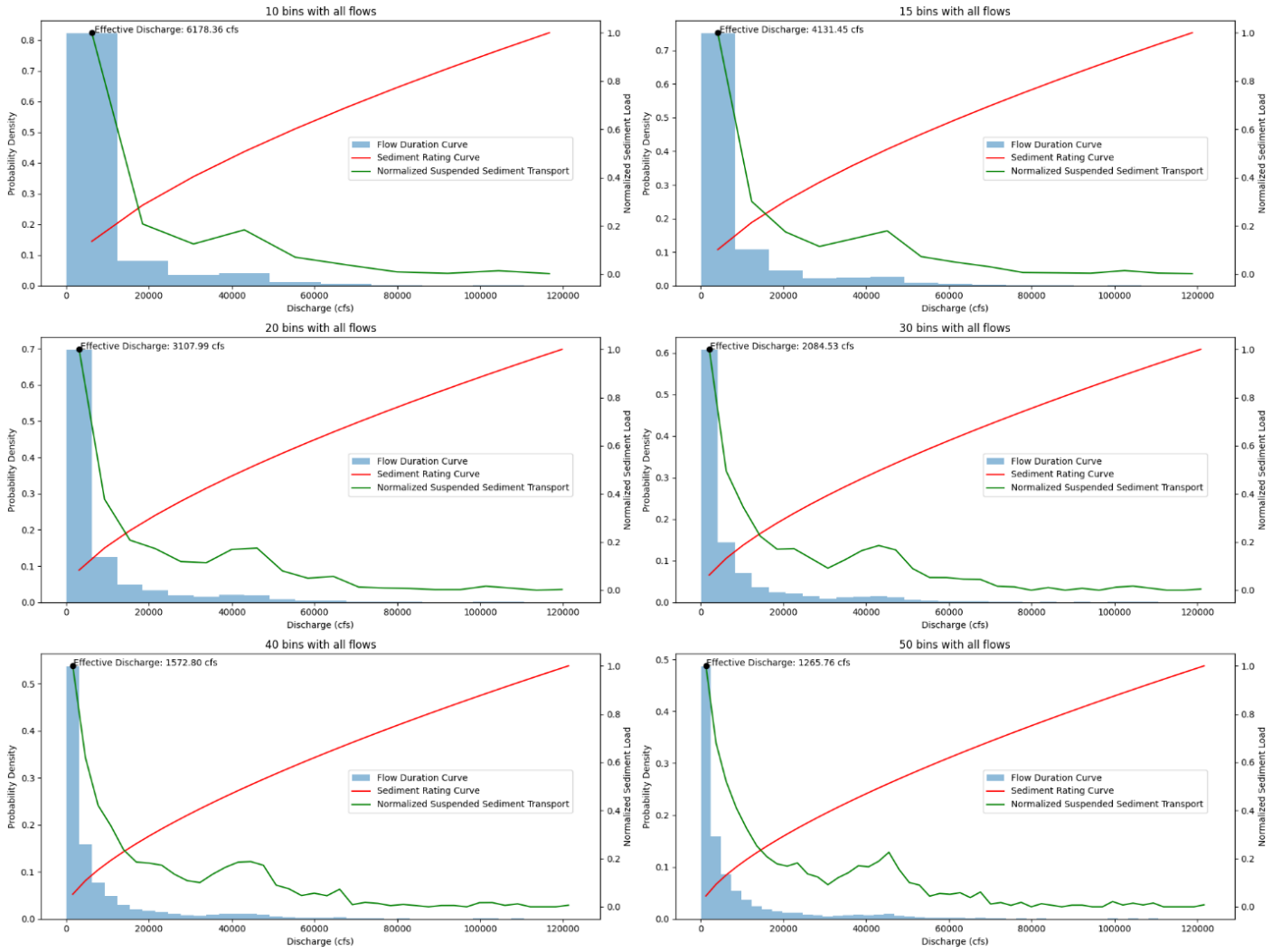

Figure 11 Examples of different effective discharges obtained for Brazos at Rosharon Station, using various number of bins

The analysis presented above exemplifies the case-dependent nature of the relationship between sediment transport magnitude and flow frequency. As demonstrated, this relationship does not always exhibit a clear maximum. In certain cases, it may increase or decrease monotonically with discharge, suggesting that the effective discharge could be either the maximum flood of record or the median value of the lowest flow bin (the smallest representative flow, which is a function of the number of histogram bins - a somewhat arbitrary and non-physical parameter).

These scenarios present several challenges and may reduce the accuracy of sediment transport analyses. It may be more appropriate to consider a range of flow magnitudes, including moderate

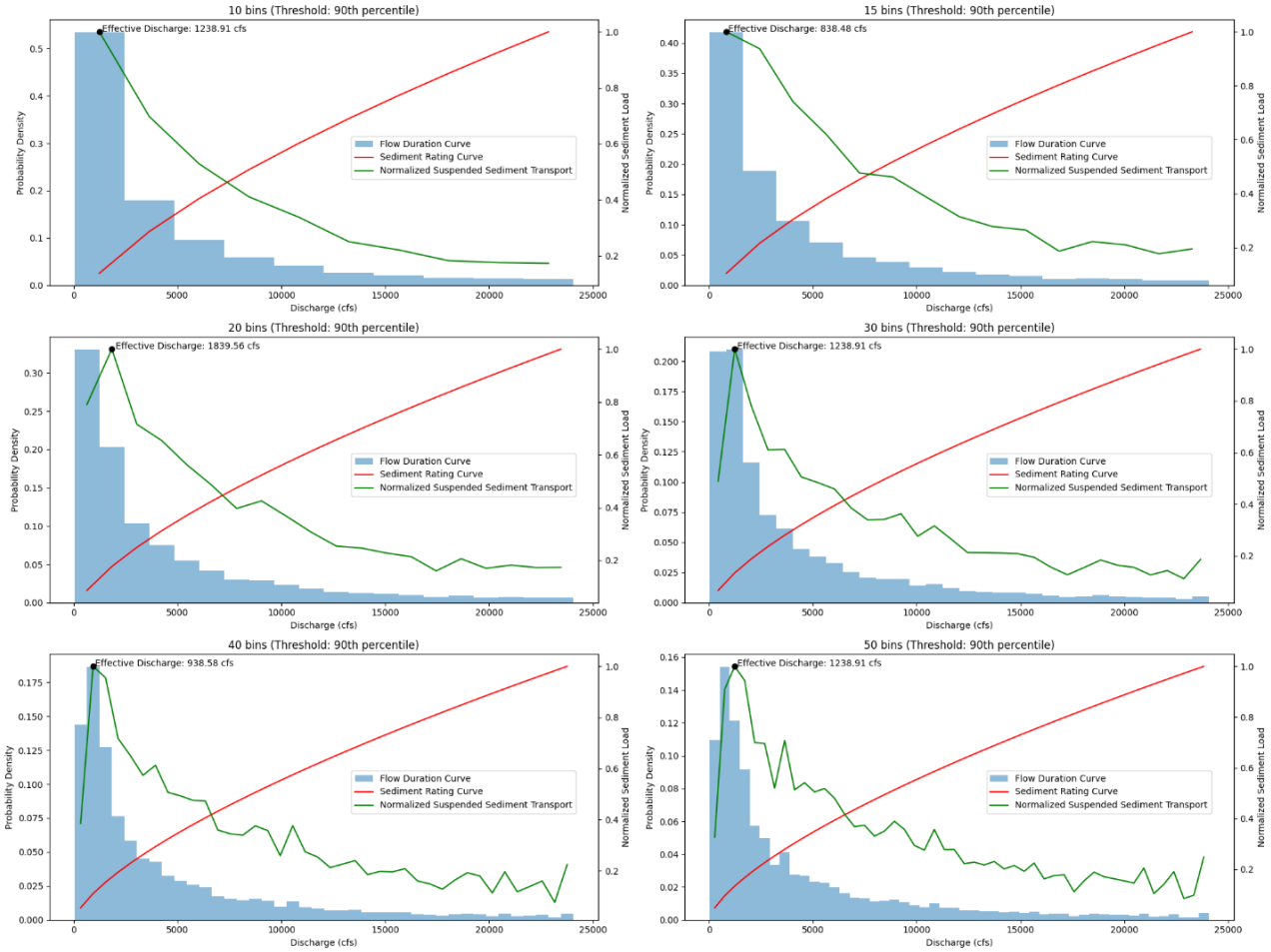

Figure 12 Examples of different effective discharges obtained for Brazos at Rosharon Station, using various number of bins and using only the 90% lower values

flow regimes that could cumulatively contribute significant geomorphic work over time, rather than focusing solely on very high or low-magnitude events at the tails of the distribution. While floods play a crucial role in the sedimentary regime, river morphologies still undergo changes during extended periods without flooding. The approach of concentrating exclusively on large flood events, similar to the bankfull discharge concept, may overlook important sediment movement processes occurring during more frequent, moderate flow conditions.

In addition, in coastal regions with tidally influenced reaches where reverse flows are common, additional uncertainties may arise in these analyses. These uncertainties can manifest in both the regression of sediment discharge rating curves and in the frequency analysis required for duration curves.

To address these issues, one potential approach is to exclude a certain percentage of high flows from the analysis. For instance, excluding the top 10% of flows may be appropriate, particularly when flooding scenarios are being analyzed separately without morphological acceleration.

However, this method introduces its own uncertainties, as the choice of exclusion percentage can significantly affect the resulting effective discharge value, and there is no universally accepted threshold for this exclusion.

Given these uncertainties and the potential for varying results depending on the selection of methods, this study has adopted an alternative strategy. By utilizing the flow with 50% exceedance probability, the analysis aligns more closely with the concept of a sediment load duration curve. This approach offers several potential advantages:

- It is potentially a consistent approach with application of morphological acceleration factor,
- It represents a flow condition that occurs frequently enough to potentially be "effective" in shaping the channel over time,
- It may be less sensitive to extreme events that could skew the analysis,
- It could provide a more robust and reproducible metric across different river systems,
- It may better capture the sediment transport processes occurring during the more moderate flow conditions observed in the study area between major hydrological events.

This method acknowledges that while high-magnitude floods play a significant role in sediment transport and channel morphology, the cumulative effect of more frequent, moderate flows could potentially be significant in determining the overall sediment regime of a river system. By focusing on these more representative flows, the analysis may provide insights that are relevant to long-term sediment management and river system behavior, particularly in coastal areas where the interaction between fluvial and marine processes adds complexity to sediment dynamics. It is important to note that floods are not disregarded in this study; high-magnitude floods, which are essential in shaping banks and eroding floodplains, are analyzed separately. Extreme flood events often differ significantly from one another. Unless a simplified approach, such as empirical synthetic hydrographs, is used, analyzing a historical extreme flood is more of a case study than indicative of long-term trends within the system. Despite differences from one event to another, general trends can still be observed across various floods. Therefore, it is imperative to analyze extreme events separately to gain understanding of the dynamics of flow and sediment regimes in the study area

As an illustrative example, consider the USGS gauge at Rosharon, where a 43 ft elevation is designated as flood stage by the NWS OWP. As of the time of preparation of this report, the most

recent crests recorded were 46.96 ft on 05-13-2024, 45.63 ft on 06-07-2021, and 43.77 ft on 06-06-2019. These data indicate multiple years between bankfull flood events, highlighting the potential importance of considering sediment transport processes during non-flood periods.

The challenges mentioned above highlight the lack of universal approaches and the need for careful consideration of local river characteristics and sediment dynamics. It suggests that using multiple flow regimes in sediment transport modeling may be necessary to capture the full range of possible conditions.

6.3 Nonstationary of Sediment Discharge Regime

The combination of low availability of data and long-term changes in morphological regimes introduces additional uncertainty in sediment transport studies. This combination is particularly challenging because it is not only due to the fact that sediment data are usually sparse, but also potentially altering over time [1]. The scarcity of data leads to gaps in our understanding of sediment dynamics, while the long-term morphological changes can render even the available data inconsistent.

These morphological shifts can be due to various factors such as climate variations or anthropogenic influences including dam construction, land-use changes, or even changes in data collection methodologies or instruments. As a result, the sediment transport characteristics of a river can change notably over decades or even years, making it difficult to establish reliable long-term trends. Sometimes these changes can be identified by examining the dates when sediment sampling was performed.

An example of such effects is evident in the sediment discharge data collected at the USGS station on the Brazos River at Rosharon. Analysis of this dataset reveals a distinctive shift in sediment discharge trends when comparing data from before and after 2015. Figure 13 shows the sediment-discharge trend for this station, with a noticeable change when the data points from before 2015 and after 2015 are analyzed separately.

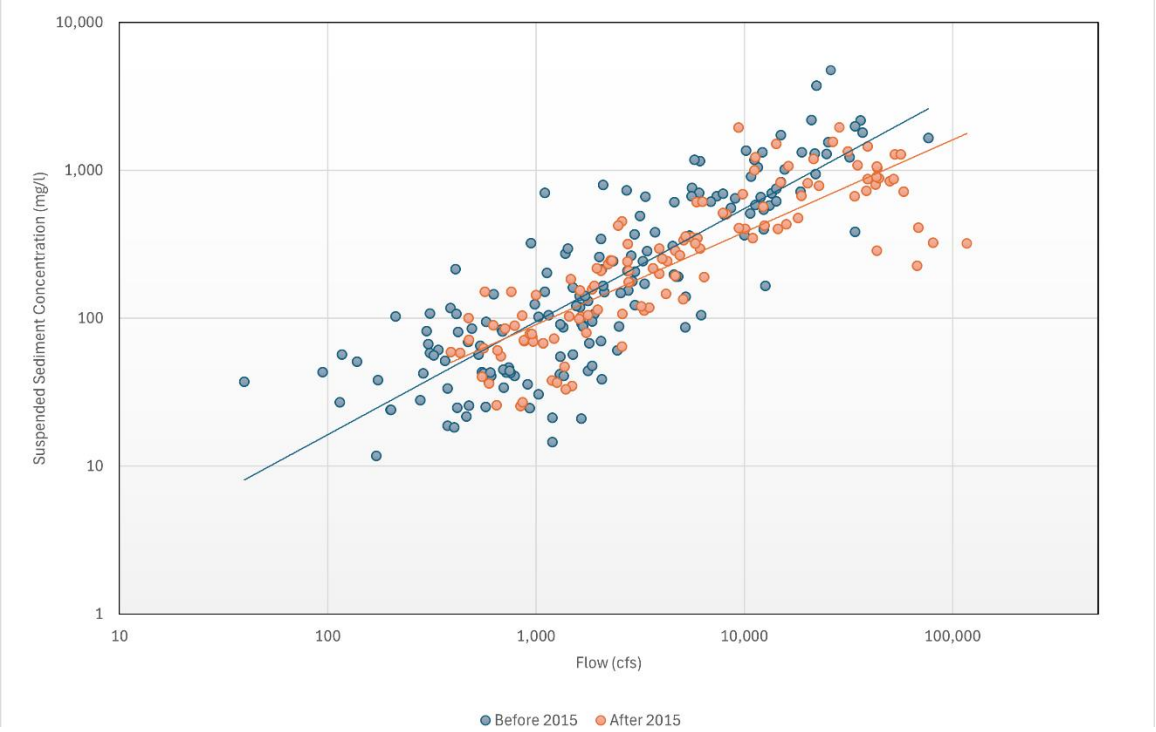

Figure 13 Nonstationary of sediment rating curve at Rosharon Station can be seen by separating the data collected before and after 2015

The changed trends essentially means that for the same flood, lower rates of suspended sediment are being observed in recent years. There may be various reasons for such a change, but other studies have mentioned reduced sediment supply in this watershed. In essence, this makes the high flow regime “supply limited”.

These challenges underline the need for more frequent and comprehensive sediment sampling campaigns, careful examination of historical data with close attention to sampling dates, and consideration of potential regime shifts when interpreting long-term sediment transport data.

6.4 Hydro-Morphological Model Development

To effectively simulate the complex hydrodynamic and morphological processes in the Brazos-San Bernard and Colorado River systems, a robust and versatile modeling tool is required. Delft3D Flexible Mesh (Delft3D-FM) was selected for this study due to its advanced capabilities

in handling multi-scale coastal and riverine environments. The following sections provide an overview of the modeling software and detail the specific model configurations used in this study.

6.4.1. Introduction to Delft3D-FM:

Delft3D Flexible Mesh (Delft3D-FM) is a state-of-the-art hydrodynamic and morphodynamic modeling suite developed by Deltares [15]. It is designed to simulate multi-dimensional (2D and 3D) flow, sediment transport, morphology, and water quality for fluvial, estuarine, and coastal environments. The key features of Delft3D-FM include its flexible mesh, which allows for the use of unstructured grids, enabling high resolution in areas of interest while maintaining computational efficiency. It also offers coupled processes, integrating hydrodynamics, wave, sediment transport, and morphological changes in a single modeling framework. Delft3D-FM is capable of multi-scale modeling, simulating processes from river basin scale down to coastal dynamics. The software has been extensively tested and validated against field and laboratory data for various coastal and riverine applications. For this study, Delft3D-FM was chosen due to its ability to handle the complex geometries and multi-scale processes present in the Brazos -San Bernard and Colorado River systems, as well as its capacity to simulate long-term morphological changes under various scenarios.

6.4.2. Model Configuration

In complex hydrodynamic and sediment transport modeling studies, achieving accurate and physically realistic outcomes often requires fine-tuning configurations and finding optimal settings by iteration. The process is inherently challenging, as it involves balancing various factors to ensure the model reflects natural processes accurately.

For this study, various scenarios were tested to capture the complexities of sediment transport and morphology under different conditions. However, some scenarios encountered issues that prevented the model from converging or producing meaningful results. These issues can usually arise due to several factors:

- **Numerical instability:** The model may reduce sediment transport rates to maintain numerical stability, particularly if sediment concentrations or bed level changes become unrealistically large.
- **Mass conservation issues:** Adjustments to sediment fluxes might occur to ensure that mass is conserved within the system, potentially leading to discrepancies in sediment transport.

- **Unrealistic physics:** Input data such as flows, sediment loads, or bed composition that do not match the natural system being analyzed can cause the model to compensate in ways that lead to unrealistic outcomes. For example, if a bankfull discharge with a 1-2 year return period is used but morphological acceleration is applied, this could simulate a flood that lasts for an unrealistically long time.
- **Grid resolution issues:** Abrupt changes or inadequacies in grid resolution near specific nodes can introduce numerical problems that the model attempts to resolve, potentially affecting the accuracy of the results.
- **Boundary problems:** When a node is near a boundary, challenges can arise in how flow and sediment is entering or leaving the model domain, leading to inconsistencies in sediment transport.

Boundary conditions are of utmost importance in mathematical models. Prescribing boundary conditions for sediment transport studies is particularly challenging for several reasons:

- The model domain may or may not have a boundary at a gaged location with observed data.
- Even when observed data is available, it may not include long-term flow records and/or the specific variables required for the study, such or sediment load or size distribution.
- Using data from a gage outside the domain (upstream) as a boundary condition is sometimes acceptable, but this approach becomes problematic if there is a hydraulic structure between the gage and the study area, as such structures can significantly alter flow and sediment patterns.
- The use of morphological acceleration in the modeling process complicates the application of observed hydrographs. As this technique changes timescales, in order to ensure the model accurately reflects the long-term sediment transport dynamics, it is crucial to use representative values for flows and sediment loads carefully, rather than directly using observed data

In this study, we explored several approaches, with varying degrees of success. The mean flow at a station is often skewed and larger than the median value due to the impact of flood events. Extreme flooding events, which are infrequent but intense, significantly increase the average (mean) flow, causing it to be higher than the median flow, which represents the 50% exceedance probability. This makes the median flow an ideal choice for long-term morphologically accelerated sediment transport modeling, as it reflects the consistent flow conditions that shape

sediment transport over extended periods of low to moderate flow. Conversely, the mean (average) flow, which is skewed by extreme flood influence, can represent higher-flow periods, capturing scenarios where flooding occurs and offering insight into the dynamics of sediment transport processes during wet years, while still being consistent with morphological acceleration.

In practical applications, particularly when a specific scenario is required for a design or another critical project, numerous iterations and adjustments are necessary to achieve a reliable model. Hydrodynamic modeling alone requires careful fine-tuning, and when sediment transport and morphology are included, the complexity—and the need for tweaking—increases substantially.

In this study, our focus was exclusively on sediment mechanisms commonly referred to as **sediment routing**. This term encompasses the processes that occur once sediment has entered a water body—such as a stream, river, ocean, lake, or reservoir. **Sediment production**, which refers to the processes that generate sediment in the watershed before it reaches the water body, is outside the scope of this study.

6.4.3. Brazos -San Bernard Study Area

The region's unique characteristics stem from its intricate flow connectivity including several rivers and estuaries heavily influenced by human-made alterations such as intercoastal navigational canals and coastal jetties, as illustrated in Figure 14.

While existing models were available for this study area, attempts to expand them with river meshes northward resulted in prohibitively long computational times required for long-term morphological assessments, rendering some of the planned scenario analyses unfeasible. To overcome this limitation, a new model was developed with an optimized domain that balances geographical coverage with computational efficiency. The newly developed model domain now extends northward to include critical data collection points, specifically reaching north of the Sweeny USGS station for the San Bernard River and the Rosharon station for Brazos River. The extension of mesh to Rosharon station is of particular importance due to the availability of sediment data at this location. Figure 15 shows the historic flow data for this station.

For the baseline conditions, tidal constituents (Table 1) were obtained from NOAA Tides and Currents Freeport station and used as baseline downstream boundary conditions.

Figure 16 shows the computational domain for this study area and Figure 17 shows the bottom elevations assigned.

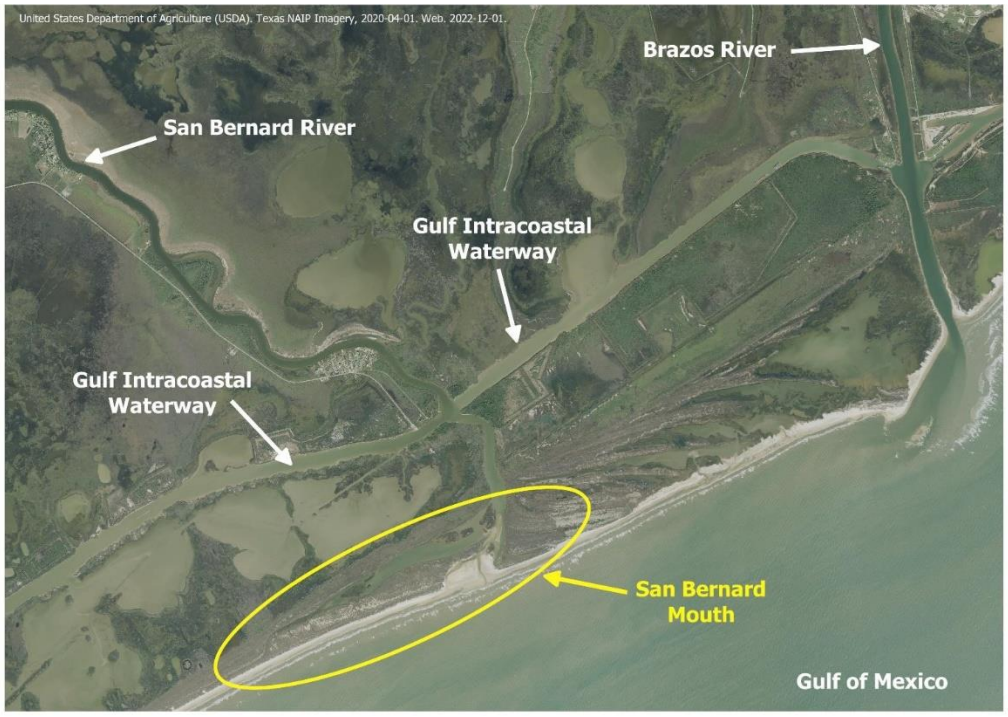

Figure 14 The Brazos- San Benrad Study area; The region's complexity arises from its highly interconnected and continuously evolving flowpaths.

Table 1 Tidal constituents used as baseline downstream boundary conditions

Component [-]	Amplitude [m]	Phase [deg]
O1	0.147	295
K1	0.152	296.3
N2	0.024	82.7
M2	0.096	101.4
S2	0.027	94.6
M4	0.005	177.9

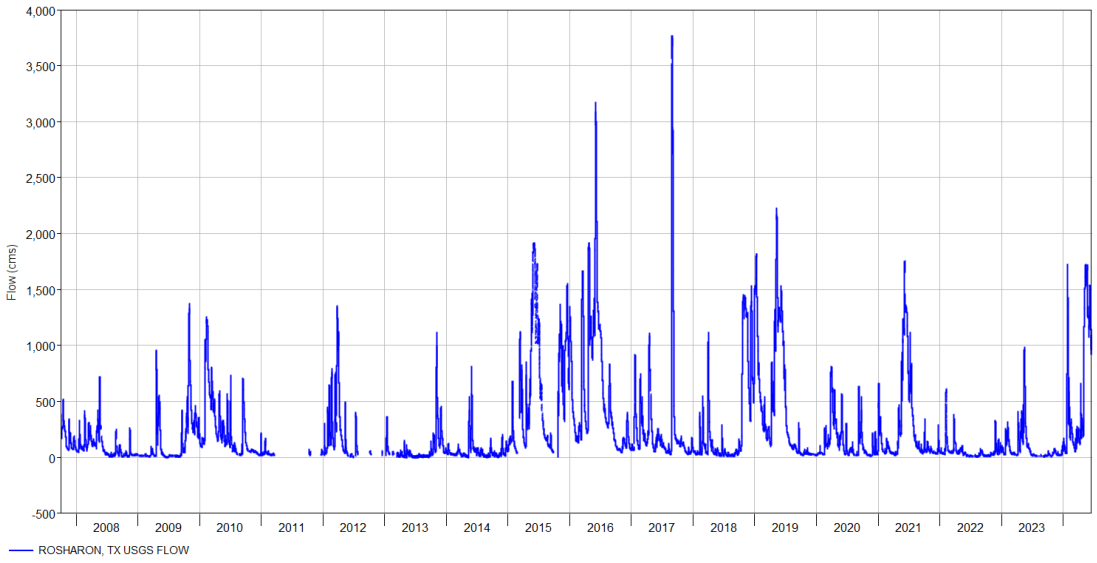

Figure 15 Historical flow data at USGS Brazos Station at Rosharon

Figure 16 Model domain and computational mesh for the Brazos-San Bernard Study area

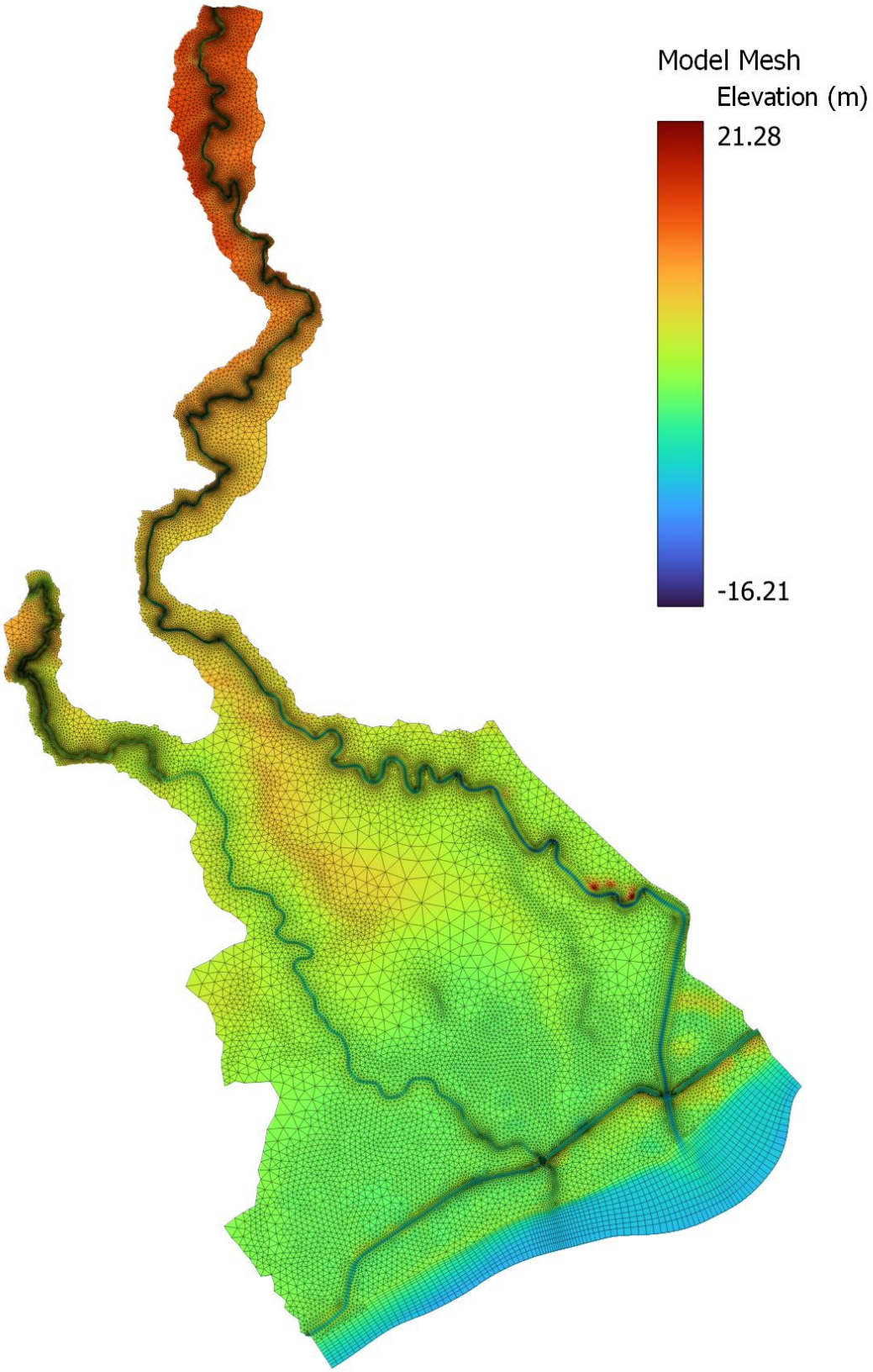

Figure 17 Range of elevations in Brazos - San Bernard study area

6.4.4. Colorado River Study Area

A new hydro-morphological model for the Colorado River from the Bay City to the Gulf Intracoastal Waterway was developed as depicted in Figure 18.

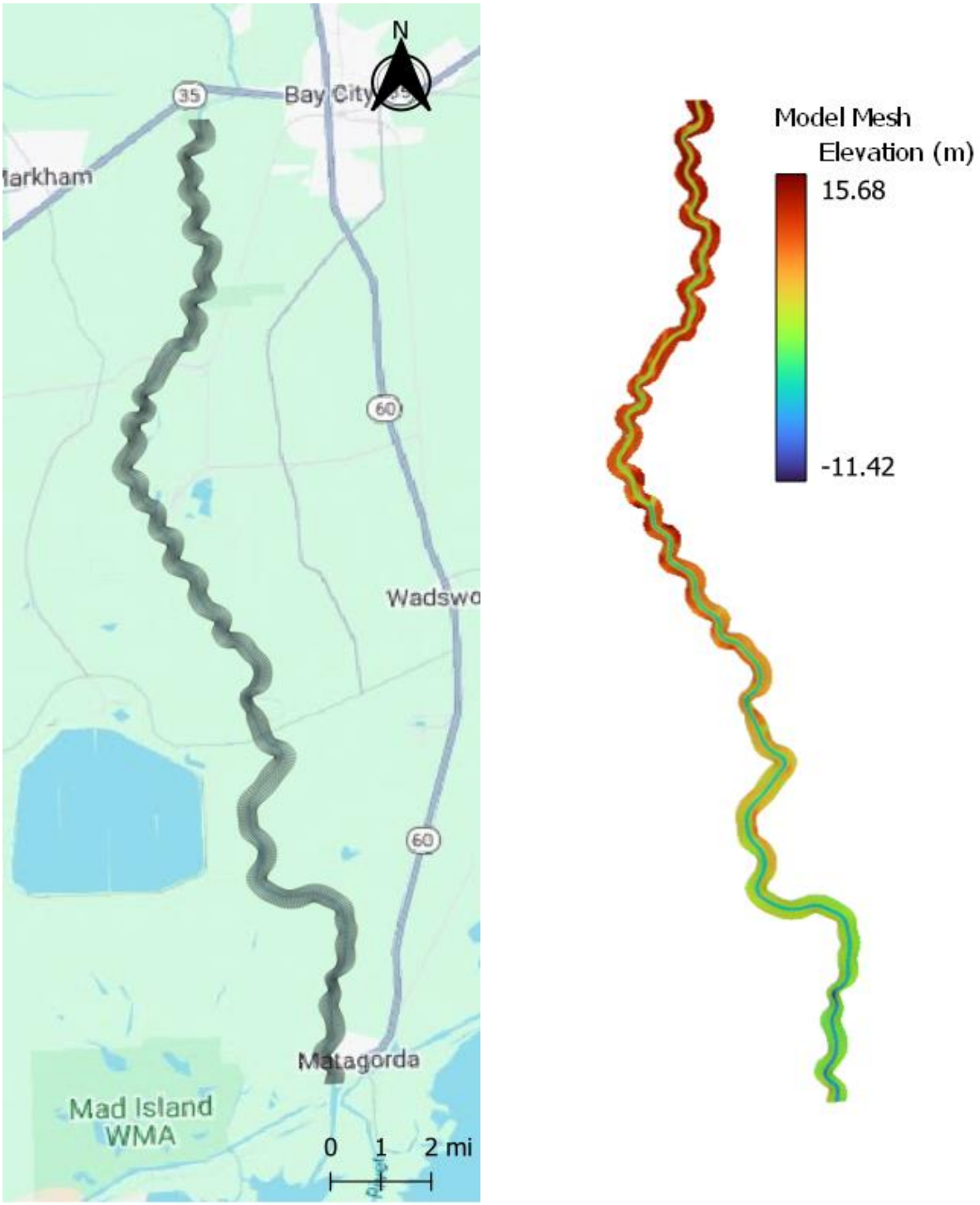

Figure 18 Computational domain and elevations of Colorado River model

Prescribing boundary conditions for this domain proved challenging. On the downstream side, there is an LCRA gauge, but only data from the past six months is available from the public website at any given time. A 4-day average condition period as shown in Figure 19 was used as the baseline.

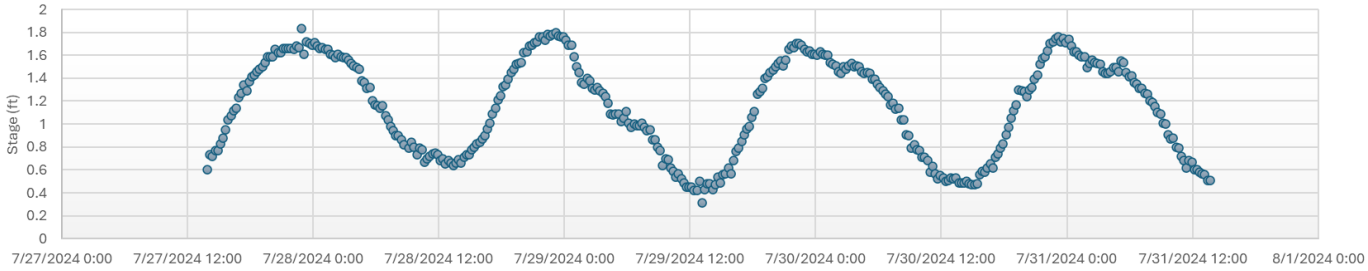

Figure 19 Baseline boundary conditions ontained from LCRA station at Matagorda

Assigning the upstream boundary conditions are notably problematic. South of Bay City, there is an LCRA reservoir, as shown in Figure 20. Therefore, we adjusted the upstream limits of our domain just south of this reservoir. The presence of such a reservoir, combined with the lack of observed data, significantly alters flow and sediment dynamics. A substantial portion of sediments may become trapped in the reservoir, and determining the amount that passes through may require advanced 3D modeling calibrated by collected data. To address this, we used the mean and median flow data from an upstream USGS station at Wadsworth, acknowledging the uncertainties this introduces into our analysis. Figure 21 shows the historical discharge values for this station.

Figure 20 LCRA dam south of Bay City (Source: Google Earth)

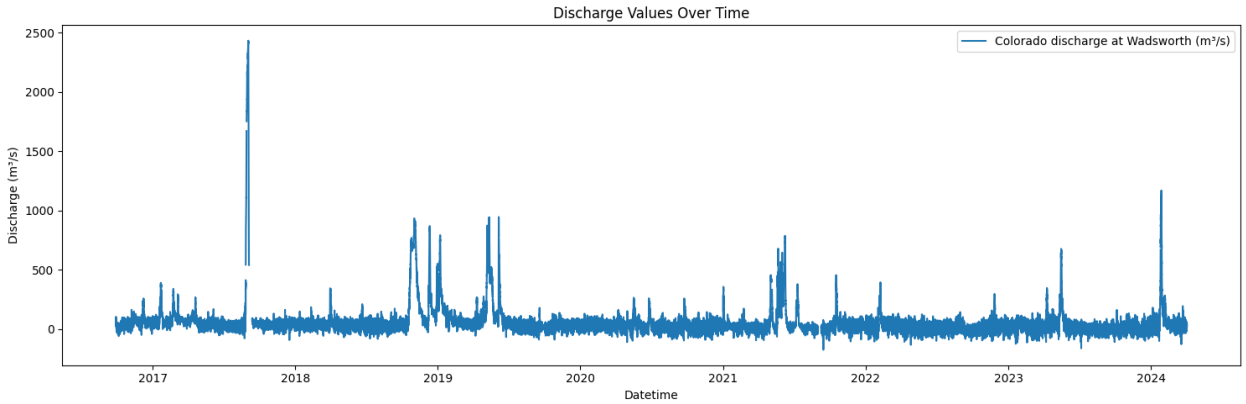

Figure 21 Colorado River near Wadsworth, TX

6.5 Representative Simulation Results

Many scenarios were analyzed, but it was observed that not all combinations of factors led to successful simulations. In some cases, the simulations failed to produce meaningful results, likely due to incompatible physical processes imposed by the morphological acceleration (morfac). It was noted that certain models would fail at specific morfac values while performing successfully at higher or lower morfacs. The following section presents results from some of the more insightful and significant cases.

I. Hurricane Harvey

The first notable result comes from the Hurricane Harvey case study, where the San Bernard River mouth, which was closed prior to the event (Figure 22), reopened during the hurricane (Figure 23). Our simulations demonstrate that a well-developed morphodynamic model successfully captured this complex phenomenon during an extreme event. This result highlights the capability of numerical models to simulate such intricate processes, showcasing their potential for accurately predicting significant geomorphological changes. Figure 24 illustrates the evolution of bed elevations during this simulation scenario, depicting the reopening of the river mouth. The implications of this modeling exercise suggest that state-of-the-art models have the capability to simulate such complex processes, provided that efforts are made to their accurate development and application.

Figure 22 The San Bernard River mouth was closed as shown in the image from Aug 12, 2017

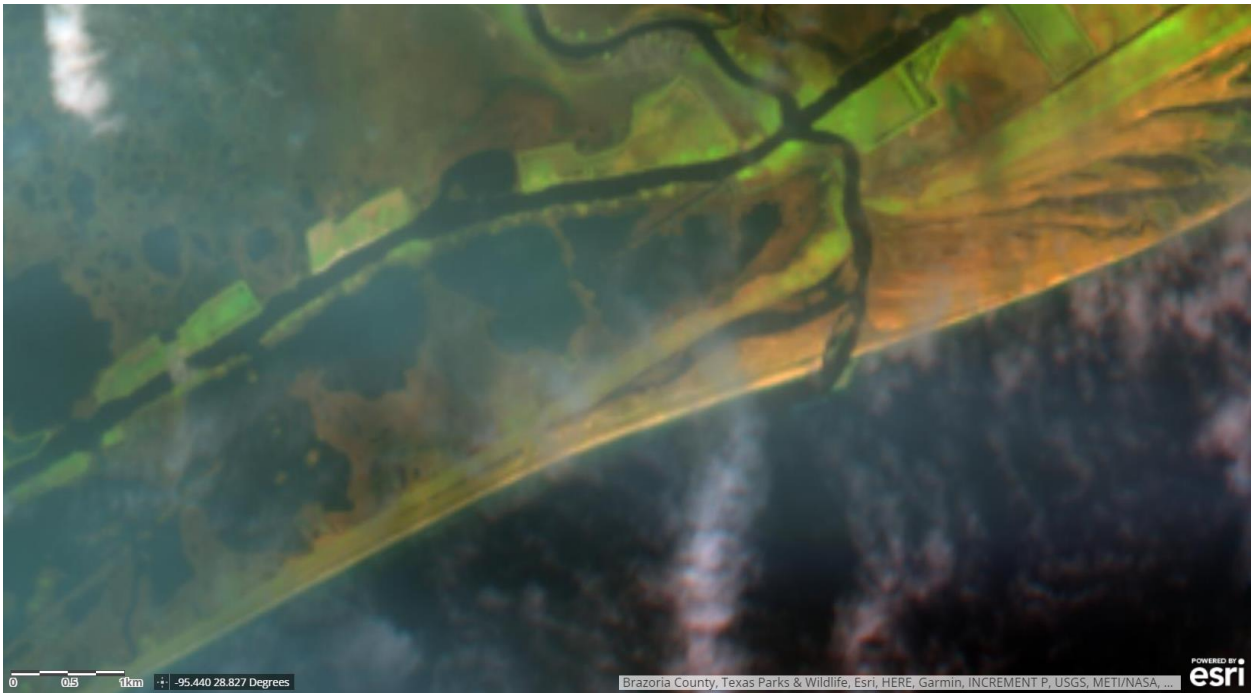

Figure 23 The San Bernard River mouth was closed as shown in the image from Sep 13, 2017

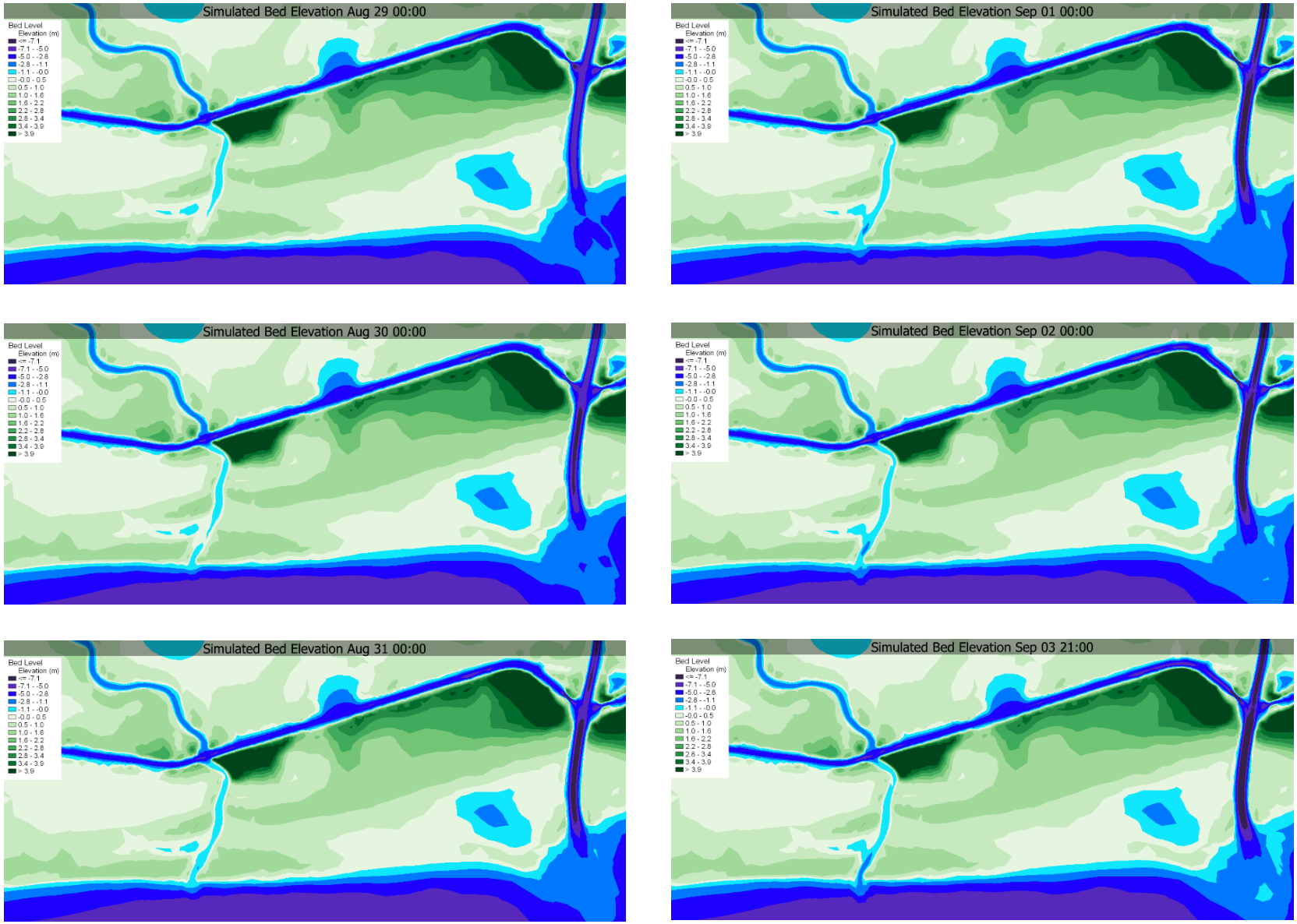

Figure 24 Evolution of simulated bed level elevations during Hurricane Harvey shows the morphodynamic model successfully replicating opening ane Harvey of San Bernard mouth

II. Long-Term Trends and Morphological Acceleration

Morphological acceleration is a useful technique, but its main application might be for estimating long-term trends, rather than very accurate predictive modeling. Given that even normal time-scale morphodynamic modeling still has many uncertainties and is often unable to reproduce observed data, and that perfect calibration of these models is almost impossible, it should be recognized that morphological acceleration will propagate these issues into long-term projections. Therefore, we emphasize the concept of "trend" when discussing the results of morphological acceleration, acknowledging its limitations and forecasting capabilities while still valuing its ability to indicate general directional changes over extended periods. Appendix B shows results of variations in morphological acceleration. It is observed that, despite the underlying assumption of linear acceleration, the final results show significant nonlinearities that would be difficult to predict without the use of a morphodynamic model.

Another noteworthy observation was that for moderate flow events, the channel's properties and geometry (such as meandering or straight configuration, slope, and width) had a greater impact on long-term (morfac=365) erosion and deposition patterns than the influx of sediment. This finding aligns with conventional river engineering principles that local hydrodynamics play a crucial role in channel migration, as exemplified by the discrepancy of evolution of inner and outer bends in meandering rivers.

One approach to evaluating the results of such simulations is to compare them against long-term observed channel migration in highly active and variable areas. The Brazos River, being a high sediment yield channel, is geomorphologically diverse with some very sharp meanders. An analysis of historical surface water changes obtained by processing Landsat satellite imagery dating back to 1985 reveals the migration of the Brazos in one of its high activity areas, as shown in Figure 25.

Simulation results of changes in bed elevation using morphodynamical modeling with a morfac of 365, serving as a proxy for long-term trends, show similar patterns to the observed changes. This similarity is particularly evident in sedimentation areas, which are locations where the main channel used to flow but has since migrated away from.

However, it is crucial to exercise caution when interpreting these results. These comparisons are primarily pattern analyses and not exact reproductions of the processes involved over such long-term simulation periods. The simulations cannot account for the precise boundary conditions, including floods, sediment yield into the channel from upstream and distributed along the

channel reaches, dredging activities, and land use changes that happened through these long times scales. Currently, it is not feasible to simulate all these factors comprehensively due to limitations in data availability, computational power, and our understanding of the underlying physics over periods of years to decades, which is the main reason of attraction for morphological acceleration.

Figure 25 Observed meander migration of Brazos extracted from surface water extent

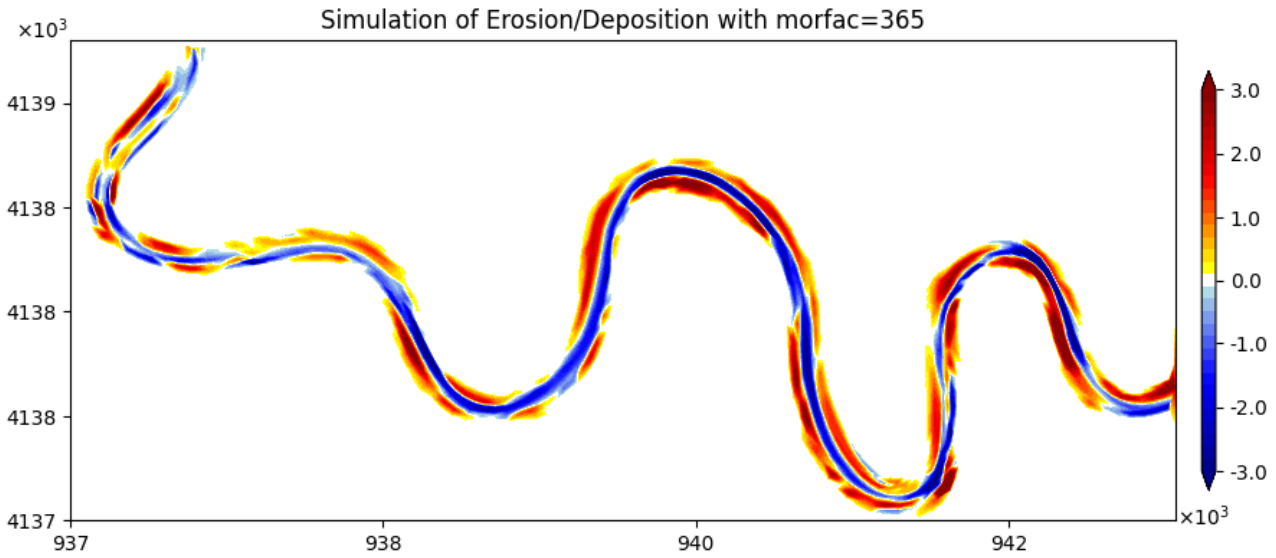

Figure 26 Simulated long-term erosion and sedimentation patters of the location shown in Figure 25

III. Sea Level Rise

Sea level rise, modeled as higher downstream boundary conditions, was shown to have a more pronounced effect in the Brazos domain (Appendix F) compared to the Colorado domain. (Appendix G). The modeled sea level rise scenarios of "intermediate low" and "high" appear to not propagate as far upstream in the Colorado River. However, potential inaccuracies may arise

from simply offsetting a typical stage hydrograph at Matagorda to represent sea level rise. For improved compatibility with morphological acceleration, it is likely worth investigating the use of harmonically analyzed values at this location.

IV. Spatially Varied Sediment Influx

Most modeling efforts assume that all sediment inflow enters the rivers solely from upstream in a lumped form. However, in reality, sediment influx occurs as both point and non-point sources throughout the reach. For this scenario, we divided the total LDC influx into several smaller LDC values and assigned them as point sources at the locations of tributaries.

As demonstrated by the plots in Appendix H, the effects of these distributed inputs on simulated general sediment transport were shown to be quite obvious and complicated to predict. This indicates that more attention is needed to account for the uncertainties inherent in the conventional lumped influx assumption.

V. Cohesive vs. Noncohesive Sediment

Changing model settings to use equations for mud as a cohesive sediment instead of sand resulted in a significant increase in the amount of total sediment transported, as shown in Appendices I and J. Previous studies have reported that even in areas with a majority of sand, using mud equations may reproduce natural patterns more accurately. It is more desirable to include more accurate sediment composition and fractions with their respective properties obtained from field surveys. However, if this is not possible, exploring modeling scenarios that assume more mud in the system might prove beneficial.

VI. Flooding in Colorado River

Accounting for flooding by assigning higher flows in morphologically accelerated simulations results in a combined effect that is highly nonlinear and cannot be predicted by simply scaling the sediment yield of lower flows. As shown in Appendix H for the Colorado River, when the flow almost doubled, the suspended sediment transport usually more than doubled, but the effects are highly variable across the river reach. This underscores the complex relationship between flow increase and sediment transport in river systems. It is imperative to account for the range of regimes dictated by the operation of the inline spillway structure at the LCRA dam south of Bay City as depicted in Figure 27. This makes accurate prediction of how much flow and sediment will be entering this reach significantly more complicated than just assuming upstream values or hydraulic normal discharge. The dam operation adds another layer of complexity to the already intricate process of modeling sediment transport in this river system.

Figure 27 Examples of different hydraulic conditions resulting from the existing spillway structure at the Lower Colorado River Authority's Bay City Dam

7. CONCLUSIONS AND KEY INSIGHTS

Coastal areas represent the buffer region where streams meet the open ocean, characterized by a dynamic interplay of various processes including tides, freshwater inflow, wave action, and sediment transport. The flow and sediment movement in these areas can be complex, often amplified by the diverse processes that are possible in various geographical regions. These complex processes lead to many variations that significantly influence the flow and sediment patterns of incoming streams and receiving large open waters. Wave dynamics also play a crucial role, with energy from waves affecting erosion and deposition patterns along the shorelines. These dynamics are further complicated by periods of floods and droughts, sea level rise, and urbanization. Coastal communities are often densely populated and economically significant, making them highly vulnerable to these complex intertwined processes. Planning sustainable development requires investigating these processes both locally and in adjacent areas, due to the continuum of streams to coast to ocean environment.

The complexity of coastal processes necessitates an integrated modeling framework. Sediment transport is of particular importance, as changes in bed levels used in hydrodynamic models can have significant impacts on flow patterns and flood inundation. Similarly, waves play a critical role, especially during storm events, with longshore transport and littoral drift being among the primary drivers in shaping coastlines. Recent studies have provided insights into long-term morphological modeling techniques, revealing several key challenges and areas where the field is still not mature, and uncertainties persist.

Incorporating certain key factors in sediment transport modeling remains challenging, yet their impact is significant. For example, directly incorporating drought conditions is complicated. Lower flows during droughts lead to smaller velocities, requiring longer simulation periods for sediment pulses to travel from upstream to downstream limits. This can conflict with morphological acceleration techniques, increasing discrepancies between time scales of flow processes and morphological changes. Without validation against observed data, which is often unavailable, the current methodology is not recommended for such scenarios.

Despite these challenges, the study demonstrated the effects of factors like droughts, urbanization, land use changes, and vegetation alterations using proxy methods. For instance, urbanization can be represented through increased flows and decreased sediment influx, while drought conditions can be simulated by reductions in both flow and sediment input. This

approach, although simplified, led to significant differences in the results, emphasizing the critical influence of these factors on sediment behavior.

More targeted studies will require full watershed-scale modeling, demanding considerably more data and computational resources. Nonetheless, by simulating these complex phenomena through alterations in prescribed flow and sediment influx at the model boundaries, the study confirmed that these factors play a crucial role in shaping riverine and coastal systems.

Investigations into morphological modeling techniques, particularly the use of morphological acceleration, have shown that due to changes in temporal timescale, it is preferable to run scenario models with relatively consistent flow and sediment boundary conditions, avoiding time series with significant variations. This limitation poses additional challenges in coastal areas, where downstream values are inherently influenced by tides, longshore transport, and other complex factors. Comparing case studies of the Brazos and Colorado Rivers yielded interesting results. The Brazos River models produced more realistic outcomes, likely due to the absence of reservoirs in the lower reaches and the availability of observed flow and sediment data at upstream gauges. In contrast, the Colorado River study presented greater challenges, primarily due to a lack of essential data and the absence of a tidal gauge in the coastal area.

The study revealed potential differences in sediment yield between the Colorado and Brazos Rivers, attributed to factors such as land use in upstream watersheds, the presence of reservoirs, and geographical location.

The Brazos system showed higher variability in sediment regime compared to the Colorado study area. Interestingly, the effect of sea level rise did not reach far enough upstream in the Colorado River to significantly impact sediment transport scenarios. However, this conclusion requires caution due to the model's limitations in representing the Gulf Intracoastal Waterway and adjacent Matagorda bays.

One key finding of particular importance was that considering cohesive sediment noticeably increased sediment transport rates. In the Colorado River study, incorporating mud equations produced promising outcomes, aligning with a previous observation made in other studies by modelers. It has been suggested to check mud equations in coastal areas as they may better replicate observed phenomena, even when sand constitutes a large portion of the sediment composition. These findings emphasize the need for continued research, data collection efforts, and refinement of modeling techniques to advance the reliability and applicability of long-term

morphological modeling across diverse river systems, particularly in complex coastal environments and when considering various environmental and anthropogenic factors.

REFERENCES

[1] Dunn, David D., and Timothy H. Raines. "Indications and Potential Sources of Change in Sand Transport in the Brazos River, Texas." U.S. Geological Survey Water-Resources Investigations Report 01-4057, 2001.

[2] Ji, Zhen-Gang. Hydrodynamics and water quality: modeling rivers, lakes, and estuaries. John Wiley & Sons, 2017.

[3] Bosboom, Judith, and Marcel JF Stive. "Coastal dynamics." (2021).

[4] Papanicolaou, Athanasios (Thanos) N., et al. "Sediment transport modeling review—current and future developments." *Journal of hydraulic engineering* 134.1 (2008): 1-14.

[5] Masselink, Gerd, Michael Hughes, and Jasper Knight. *Introduction to coastal processes and geomorphology*. Routledge, 2014.

[6] Schmandt, Jurgen, et al., eds. Sustainability of engineered rivers in arid lands: challenge and response. Cambridge University Press, 2021.

[7] Southard, John. Introduction to fluid motions and sediment transport. LibreTexts, 2019.

[8] Ancey, Christophe. "Bedload transport: a walk between randomness and determinism. Part 1. The state of the art." *Journal of Hydraulic Research* 58.1 (2020): 1-17.

[9] Ancey, Christophe, and Alain Recking. "Scaling behavior of bedload transport: what if Bagnold was right?." *Earth-Science Reviews* (2023): 104571.

[10] Ancey, Christophe. "Bedload transport: a walk between randomness and determinism. Part 2. Challenges and prospects." *Journal of Hydraulic Research* 58.1 (2020): 18-33.

[11] Roelvink, Dano. *A guide to modeling coastal morphology*. Vol. 12. world scientific, 2011.

[12] The Meadows Center for Water and the Environment. *San Bernard River Watershed Data Report.* Texas State University, July 2013

[13] Morgan, Jacob A., et al. "The use of a morphological acceleration factor in the simulation of large-scale fluvial morphodynamics." *Geomorphology* 356 (2020): 107088.

[14] FISRWG (10/1998). Stream Corridor Restoration: Principles, Processes, and Practices. By the Federal Interagency Stream Restoration Working Group (FISRWG)(15 Federal agencies of the US gov't). GPO Item No. 0120-A; SuDocs No. A 57.6/2:EN3/PT.653.ISBN-0-934213-59-3.

[15] D-Flow Flexible Mesh. *Computational Cores and User Interface: User Manual*. August 2024.

[16] *About the Brazos River*, Brazos River Authority, https://brazos.org/About-Us/About-the-BRA/About-the-Brazos-River. Accessed 10 Aug. 2024.

[17] "San Bernard River Watershed-Based Plans." *Houston-Galveston Area Council*, https://www.h-gac.com/watershed-based-plans/san-bernard-river. Accessed 10 Aug. 2024.
[18] "Watershed Viewer." *Texas Parks and Wildlife Department*, https://tpwd.texas.gov/education/water-education/Watershed%20Viewer. Accessed 10 Aug. 2024.
[19] Samady, Mohammad Khalid. *Continuous Hydrologic Modeling for Analyzing the Effects of Drought on the Lower Colorado River in Texas*. Master's thesis, Michigan Technological University, 2017.
[20] NOAA Sea Level Rise Viewer. National Oceanic and Atmospheric Administration, https://coast.noaa.gov/slr/#/layer/slr. Accessed 10 Aug. 2024.

APPENDIX A: NAMING CONVENTION FOR SCENARIO ANALYSIS

Model Description	ID
Median Flows and Median suspended sediment with morfac 1	Baseline-LDC-Morpho1-MedFlow-MedSed
Median Flows and Median suspended sediment with morfac 10	Baseline-LDC-Morpho10-MedFlow-MedSed
Median Flows and Median suspended sediment with morfac 30	Baseline-LDC-Morpho30-MedFlow-MedSed
Median Flows and Median suspended sediment with morfac 180	Baseline-LDC-Morpho180-MedFlow-MedSed
Median Flows and Median suspended sediment with morfac 360	Baseline-LDC-Morpho360-MedFlow-MedSed
Mean flow, no suspended sediment with morfac 1	Baseline-LDC-Morpho1-MeanFlow-NoSed
Mean flow, no suspended sediment with morfac 10	Baseline-LDC-Morpho10-MeanFlow-NoSed
Mean flow, no suspended sediment with morfac 30	Baseline-LDC-Morpho30-MeanFlow-NoSed
Mean flow, no suspended sediment with morfac 180	Baseline-LDC-Morpho180-MeanFlow-NoSed
Mean flow, no suspended sediment with morfac 360	Baseline-LDC-Morpho360-MeanFlow-NoSed
Median flow and SLR scenarios of intermediate low with morfac 30	AlteredRegime-Gradual-SLRIntLow-Morpho30-MedFlow
Median flow and SLR scenarios of high with morfac 30	AlteredRegime-Gradual-SLRHigh-Morpho30-MedFlow
Median flow, Spatially varied LDC with morfac 1	AlteredRegime-SpatialLDC-Morpho1-MedFlow
Median flow, Spatially varied LDC with morfac 30	AlteredRegime-SpatialLDC-Morpho30-MedFlow
Median Flows and Median suspended sediment with morfac 365	Baseline-LDC-Morpho365-MedFlow-MedSed
Mean flow, no suspended sediment with morfac 365	Baseline-LDC-Morpho365-MeanFlow-NoSed
Median Flows and no suspended sediment with morfac 365	Baseline-Morpho365-MedFlow-NoSed
Mean flow, no suspended sediment with morfac 30	Baseline-Morpho30-MedFlow-NoSed
Mean flow, no suspended sediment with morfac 180	Mud-Morpho180-MedFlow-NoSed
Median flow, Spatially varied LDC with morfac 180	Mud-AlteredRegime-SpatialLDC-Morpho180-MedFlow
dian Flows and Median suspended sediment with morfac 1	Baseline-LDC-Morpho1-MedFlow-MedSed
Median Flows and Median suspended sediment with morfac 10	Baseline-LDC-Morpho10-MedFlow-MedSed
Median Flows and Median suspended sediment with morfac 30	Baseline-LDC-Morpho30-MedFlow-MedSed
Median Flows and Median suspended sediment with morfac 180	Baseline-LDC-Morpho180-MedFlow-MedSed
Median Flows and Median suspended sediment with morfac 360	Baseline-LDC-Morpho360-MedFlow-MedSed
Mean flow, no suspended sediment with morfac 1	Baseline-LDC-Morpho1-MeanFlow-NoSed
Mean flow, no suspended sediment with morfac 10	Baseline-LDC-Morpho10-MeanFlow-NoSed

APPENDIX B: THE EFFECT OF MORPHOLOGICAL ACCELERATION IN BRAZOS DOMAIN

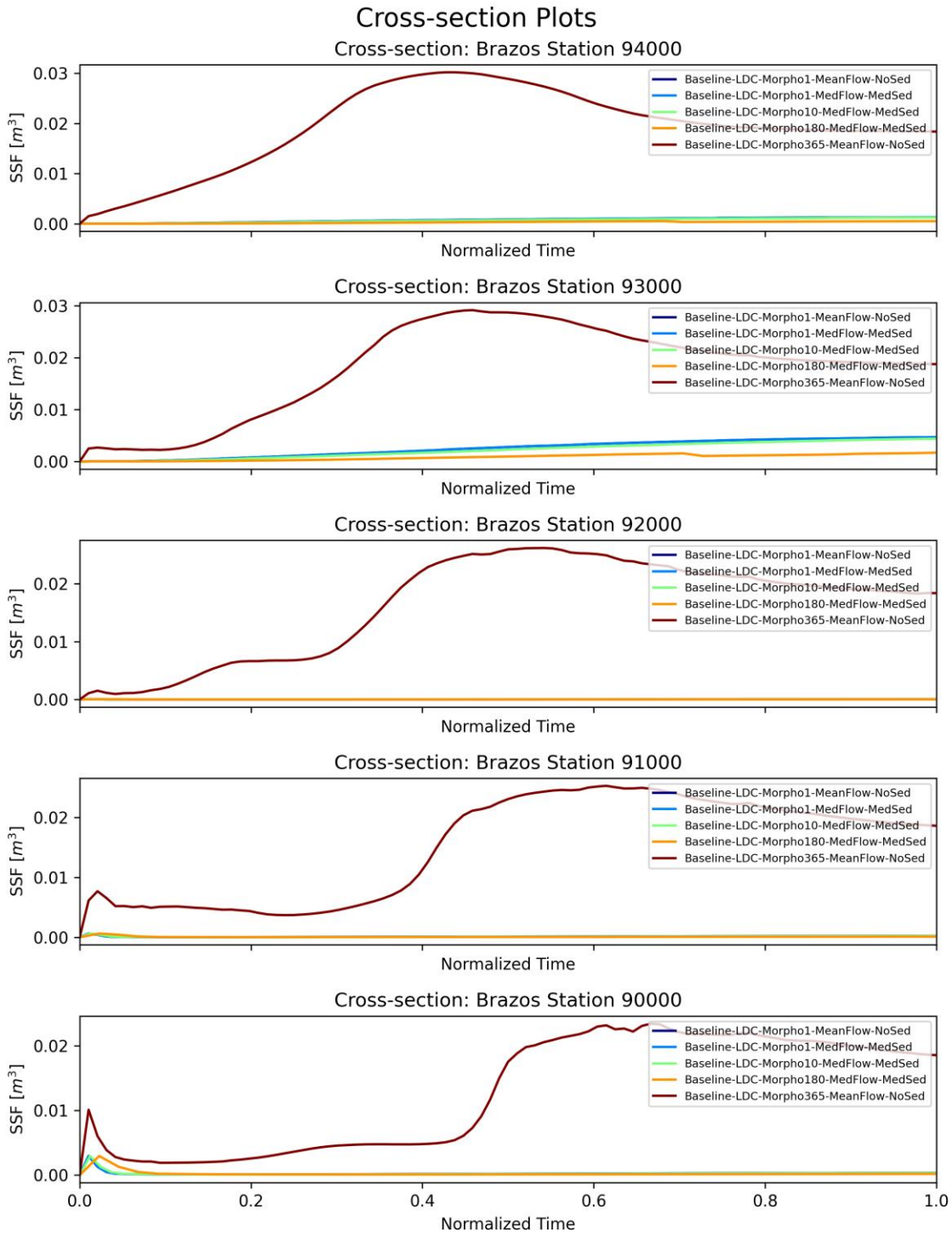
Cross-section Plots
Cross-section: Brazos Station 94000
Cross-section: Brazos Station 93000
Cross-section: Brazos Station 92000
Cross-section: Brazos Station 91000
Cross-section: Brazos Station 90000
SSF [m^3]
Normalized Time
Baseline-LDC-Morpho1-MeanFlow-NoSed
Baseline-LDC-Morpho1-MedFlow-MedSed
Baseline-LDC-Morpho10-MedFlow-MedSed
Baseline-LDC-Morpho180-MedFlow-MedSed
Baseline-LDC-Morpho365-MeanFlow-NoSed

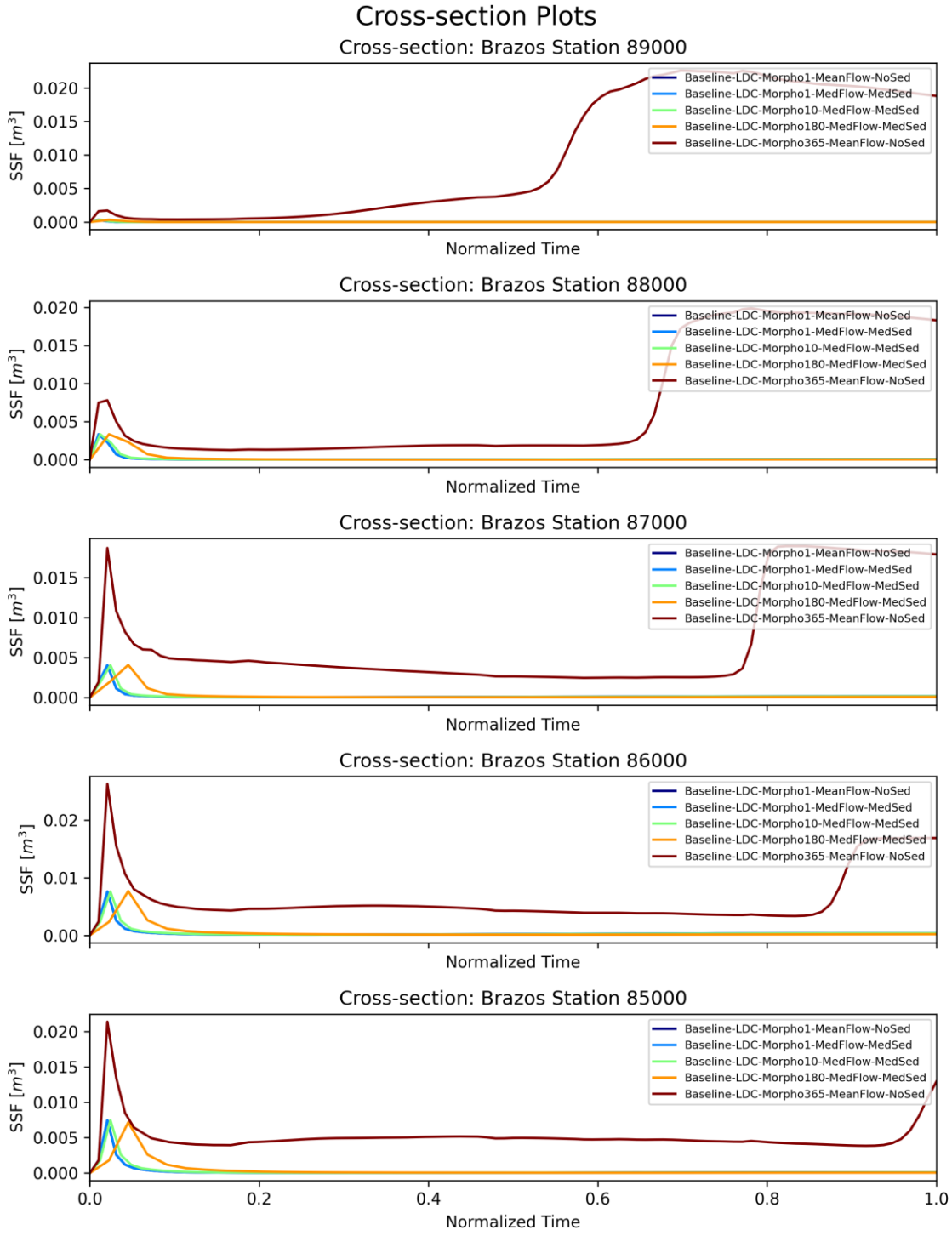
Cross-section Plots
Cross-section: Brazos Station 89000
Cross-section: Brazos Station 88000
Cross-section: Brazos Station 87000
Cross-section: Brazos Station 86000
Cross-section: Brazos Station 85000
SSF [m^3]
Normalized Time
Baseline-LDC-Morpho1-MeanFlow-NoSed
Baseline-LDC-Morpho1-MedFlow-MedSed
Baseline-LDC-Morpho10-MedFlow-MedSed
Baseline-LDC-Morpho180-MedFlow-MedSed
Baseline-LDC-Morpho365-MeanFlow-NoSed

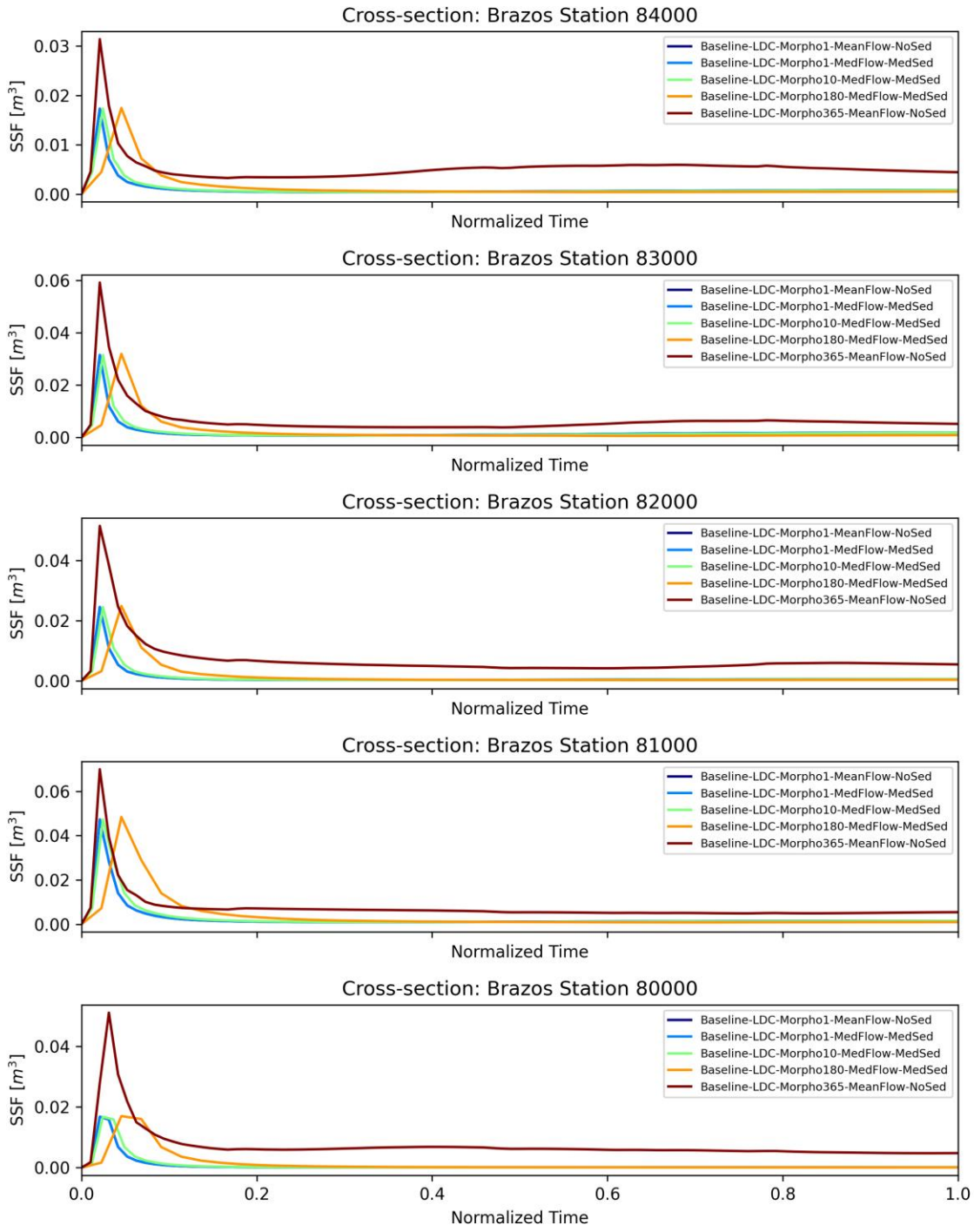
Cross-section Plots
Cross-section: Brazos Station 84000
Cross-section: Brazos Station 83000
Cross-section: Brazos Station 82000
Cross-section: Brazos Station 81000
Cross-section: Brazos Station 80000
SSF [m^3]
Normalized Time
Baseline-LDC-Morpho1-MeanFlow-NoSed
Baseline-LDC-Morpho1-MedFlow-MedSed
Baseline-LDC-Morpho10-MedFlow-MedSed
Baseline-LDC-Morpho180-MedFlow-MedSed
Baseline-LDC-Morpho365-MeanFlow-NoSed

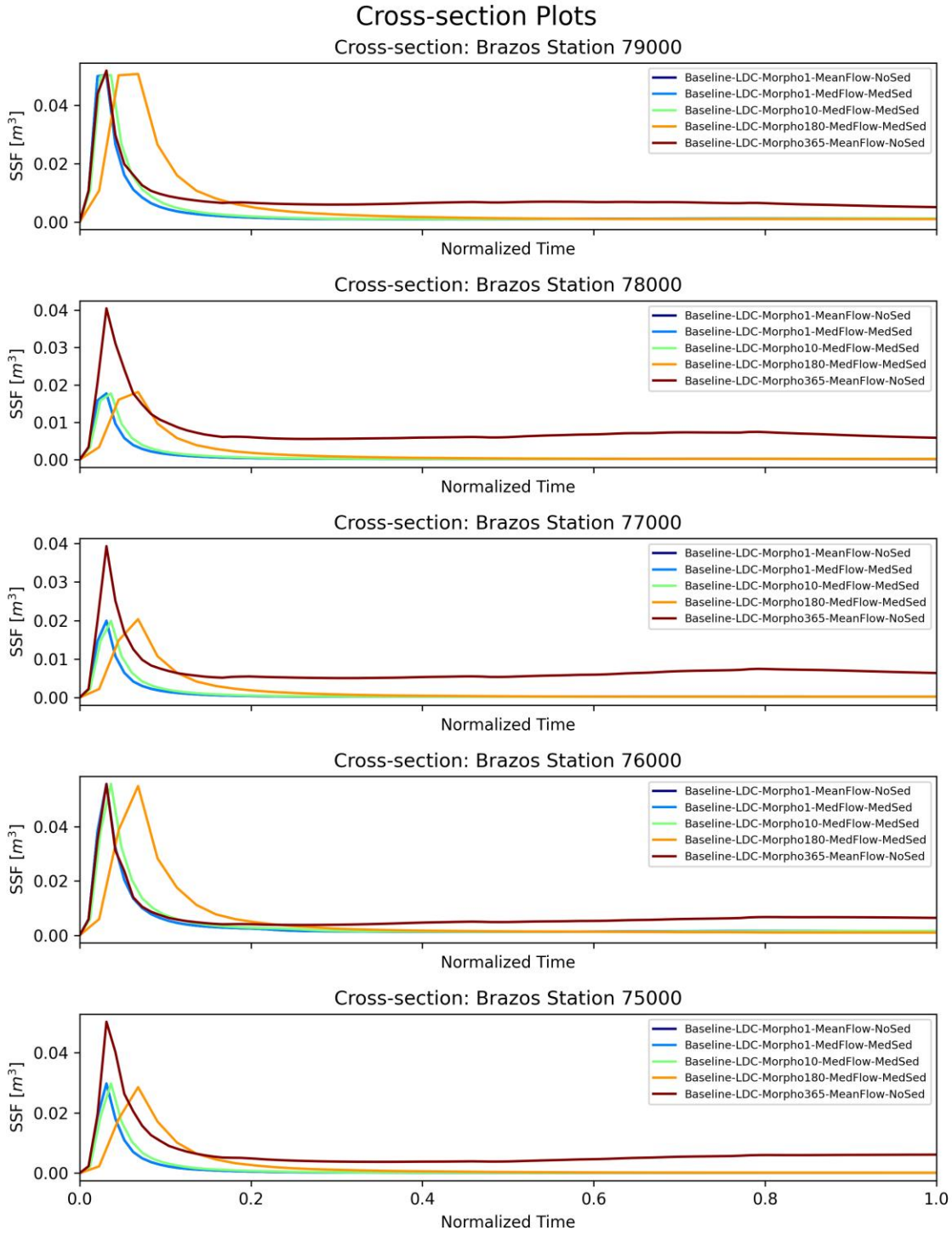
Cross-section Plots
Cross-section: Brazos Station 79000
Cross-section: Brazos Station 78000
Cross-section: Brazos Station 77000
Cross-section: Brazos Station 76000
Cross-section: Brazos Station 75000
SSF [m^3]
Normalized Time
Baseline-LDC-Morpho1-MeanFlow-NoSed
Baseline-LDC-Morpho1-MedFlow-MedSed
Baseline-LDC-Morpho10-MedFlow-MedSed
Baseline-LDC-Morpho180-MedFlow-MedSed
Baseline-LDC-Morpho365-MeanFlow-NoSed

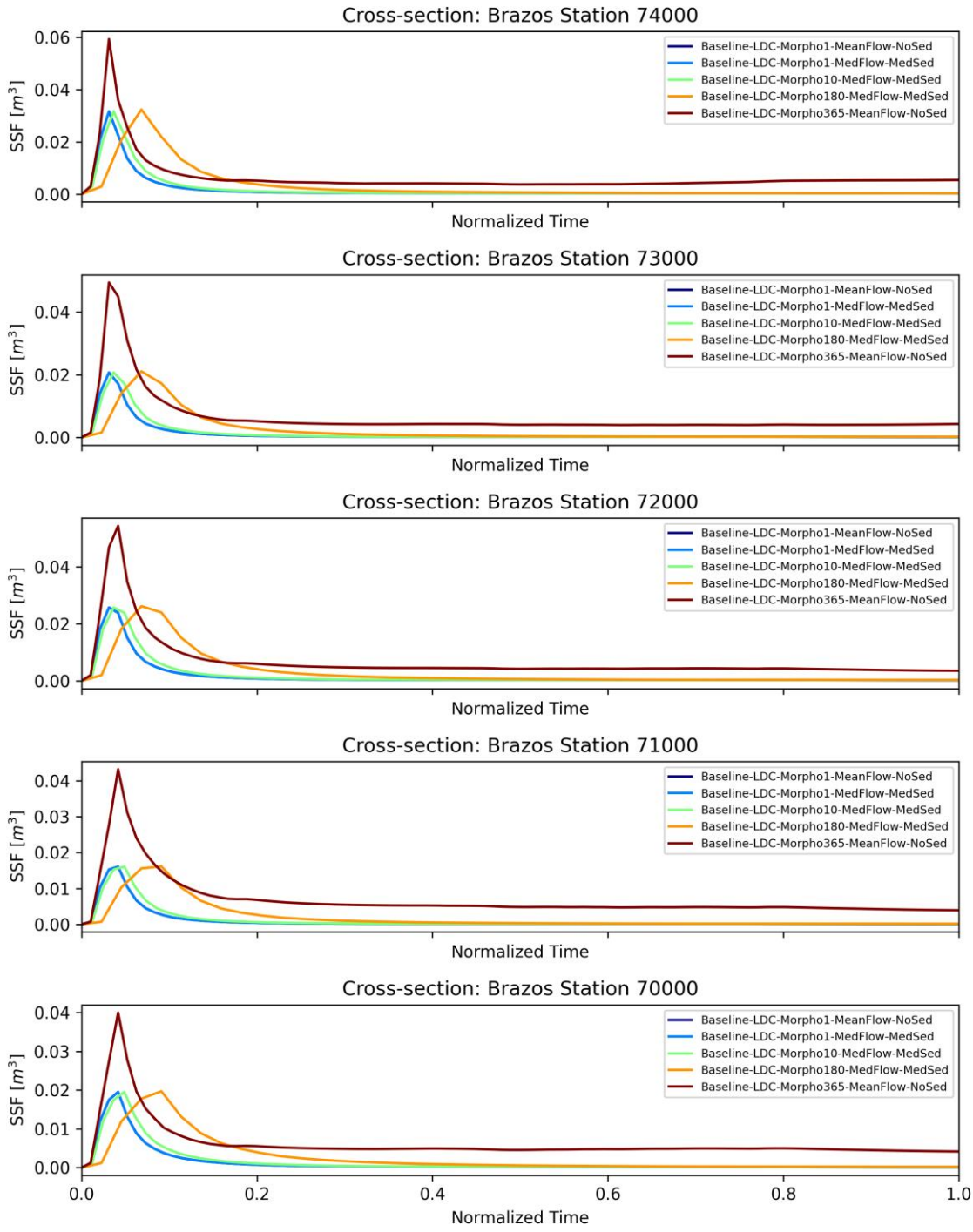
Cross-section Plots
Cross-section: Brazos Station 74000
Cross-section: Brazos Station 73000
Cross-section: Brazos Station 72000
Cross-section: Brazos Station 71000
Cross-section: Brazos Station 70000
SSF [m^3]
Normalized Time
Baseline-LDC-Morpho1-MeanFlow-NoSed
Baseline-LDC-Morpho1-MedFlow-MedSed
Baseline-LDC-Morpho10-MedFlow-MedSed
Baseline-LDC-Morpho180-MedFlow-MedSed
Baseline-LDC-Morpho365-MeanFlow-NoSed

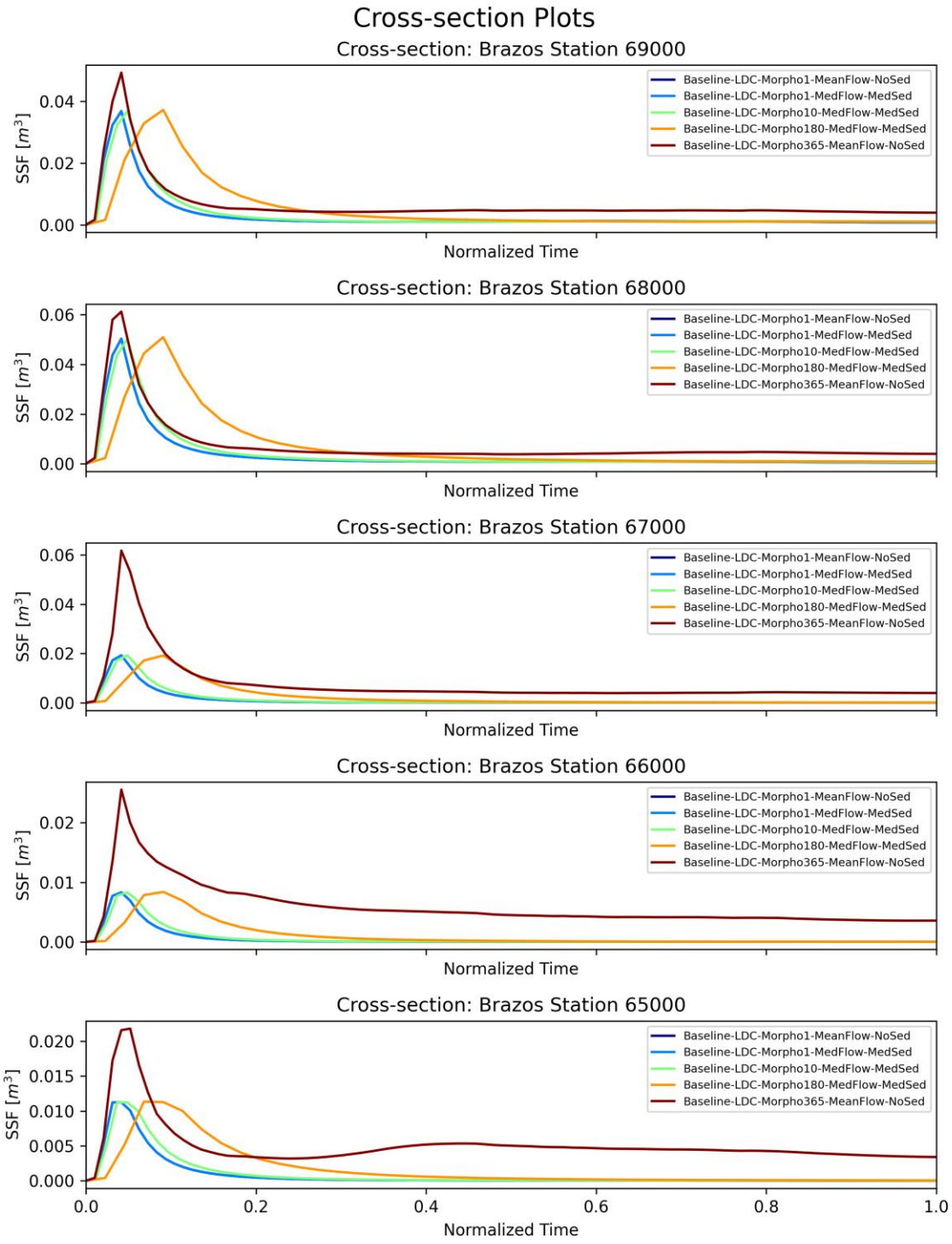
Cross-section Plots
Cross-section: Brazos Station 69000
Cross-section: Brazos Station 68000
Cross-section: Brazos Station 67000
Cross-section: Brazos Station 66000
Cross-section: Brazos Station 65000
SSF [m^3]
Normalized Time
Baseline-LDC-Morpho1-MeanFlow-NoSed
Baseline-LDC-Morpho1-MedFlow-MedSed
Baseline-LDC-Morpho10-MedFlow-MedSed
Baseline-LDC-Morpho180-MedFlow-MedSed
Baseline-LDC-Morpho365-MeanFlow-NoSed

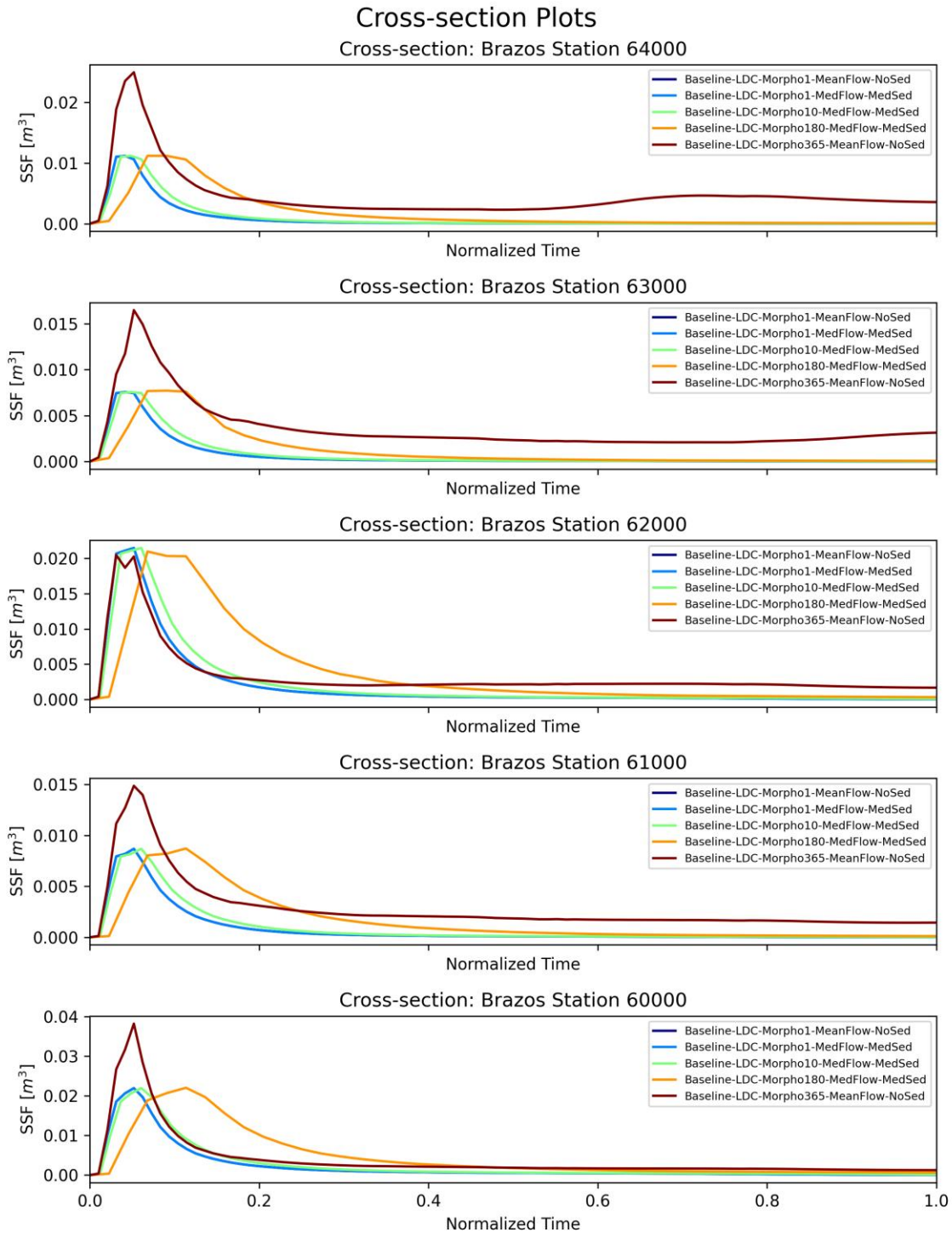
Cross-section Plots
Cross-section: Brazos Station 64000
Cross-section: Brazos Station 63000
Cross-section: Brazos Station 62000
Cross-section: Brazos Station 61000
Cross-section: Brazos Station 60000
SSF [m^3]
Normalized Time
Baseline-LDC-Morpho1-MeanFlow-NoSed
Baseline-LDC-Morpho1-MedFlow-MedSed
Baseline-LDC-Morpho10-MedFlow-MedSed
Baseline-LDC-Morpho180-MedFlow-MedSed
Baseline-LDC-Morpho365-MeanFlow-NoSed

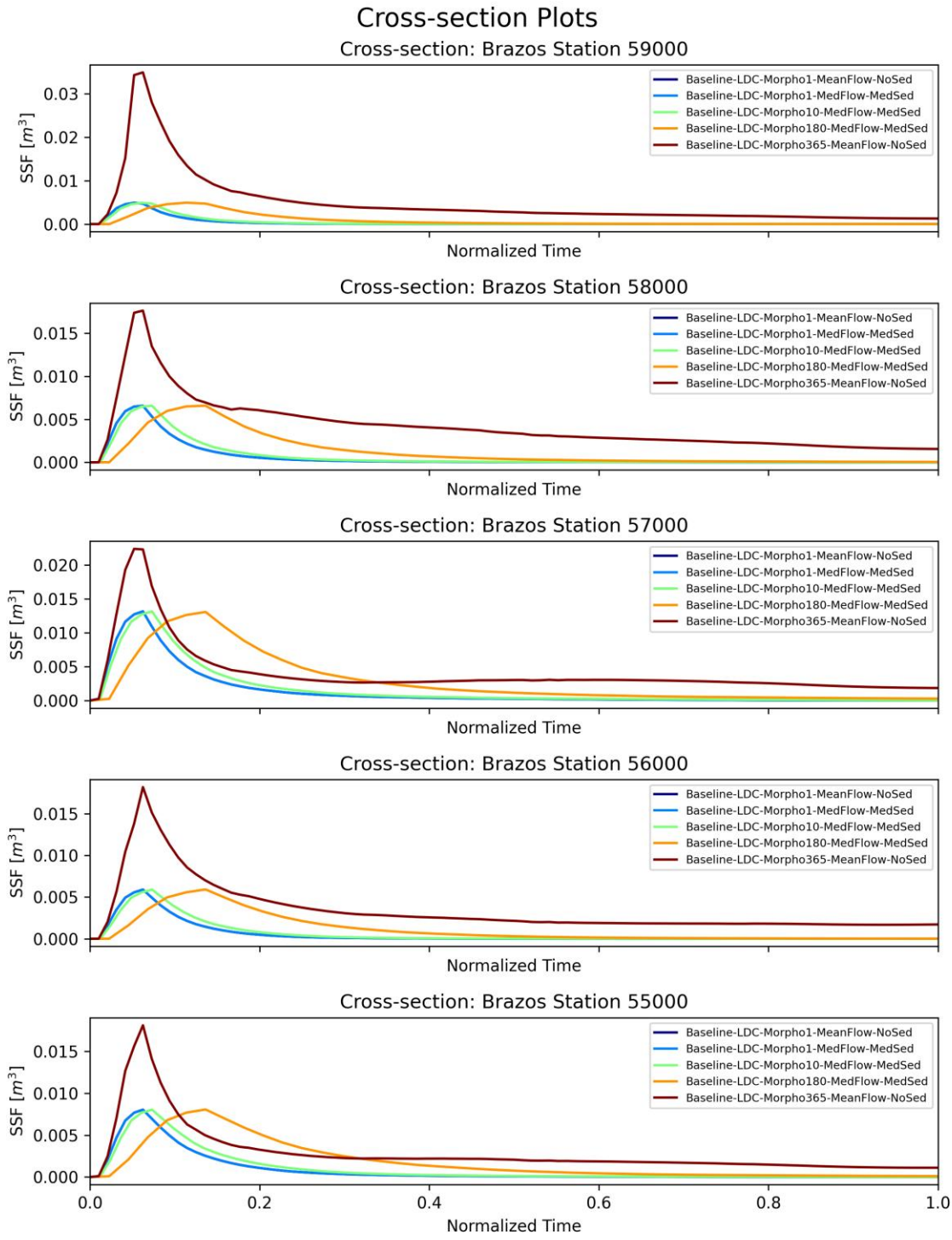
Cross-section Plots
Cross-section: Brazos Station 59000
Cross-section: Brazos Station 58000
Cross-section: Brazos Station 57000
Cross-section: Brazos Station 56000
Cross-section: Brazos Station 55000
SSF [m^3]
Normalized Time
Baseline-LDC-Morpho1-MeanFlow-NoSed
Baseline-LDC-Morpho1-MedFlow-MedSed
Baseline-LDC-Morpho10-MedFlow-MedSed
Baseline-LDC-Morpho180-MedFlow-MedSed
Baseline-LDC-Morpho365-MeanFlow-NoSed

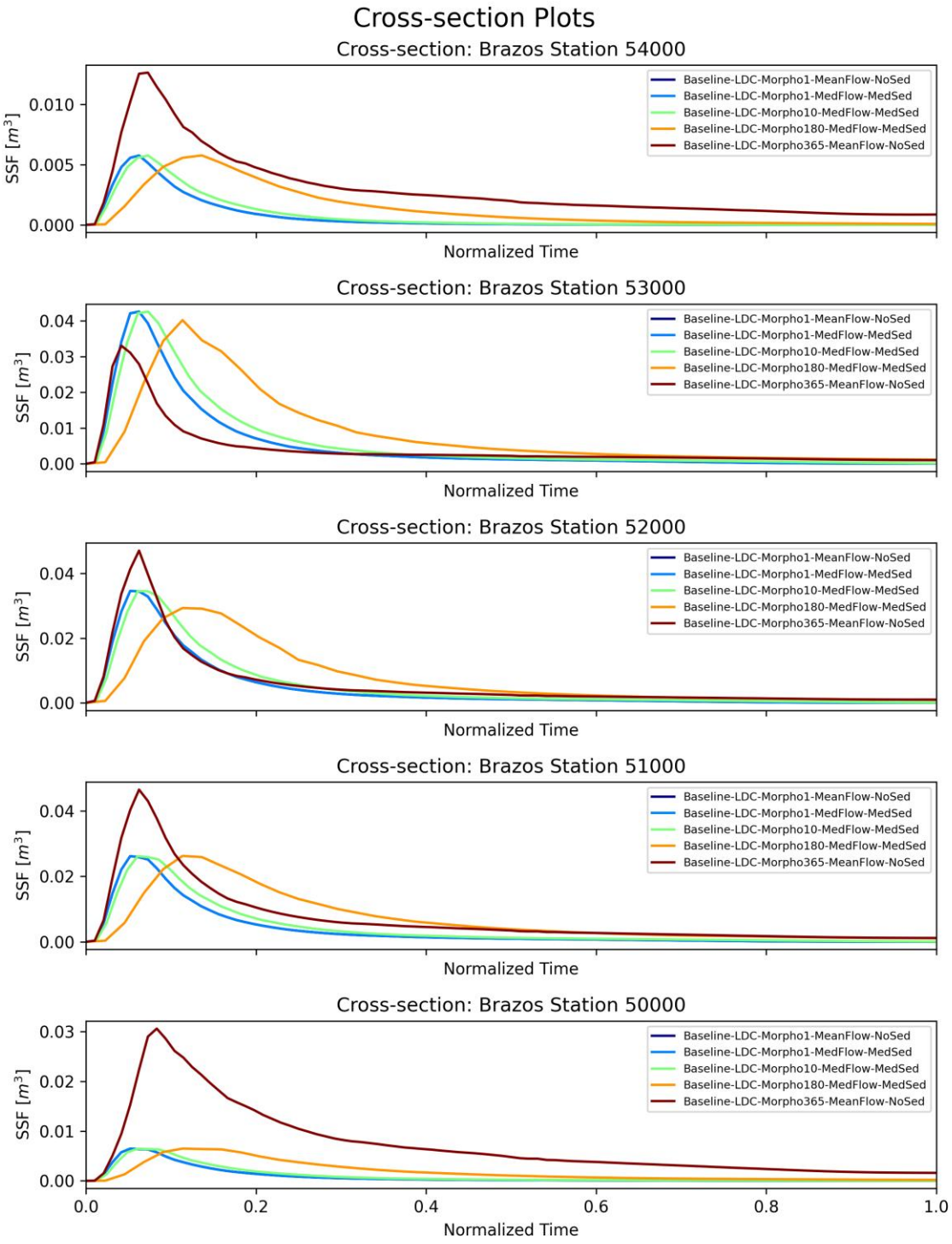
Cross-section Plots
Cross-section: Brazos Station 54000
Cross-section: Brazos Station 53000
Cross-section: Brazos Station 52000
Cross-section: Brazos Station 51000
Cross-section: Brazos Station 50000
SSF [m^3]
Normalized Time
Baseline-LDC-Morpho1-MeanFlow-NoSed
Baseline-LDC-Morpho1-MedFlow-MedSed
Baseline-LDC-Morpho10-MedFlow-MedSed
Baseline-LDC-Morpho180-MedFlow-MedSed
Baseline-LDC-Morpho365-MeanFlow-NoSed

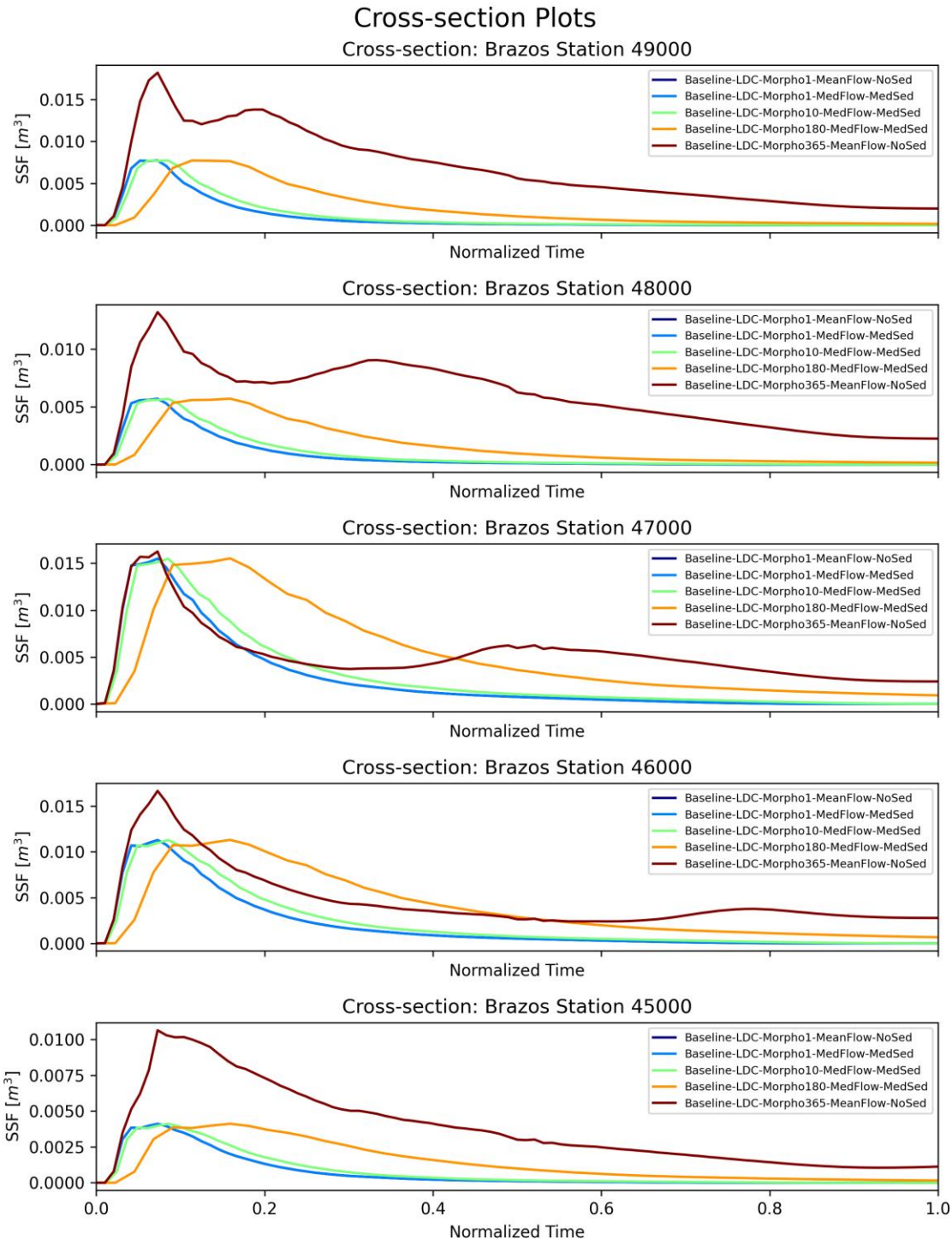
Cross-section Plots
Cross-section: Brazos Station 49000
Cross-section: Brazos Station 48000
Cross-section: Brazos Station 47000
Cross-section: Brazos Station 46000
Cross-section: Brazos Station 45000
SSF [m^3]
Normalized Time
Baseline-LDC-Morpho1-MeanFlow-NoSed
Baseline-LDC-Morpho1-MedFlow-MedSed
Baseline-LDC-Morpho10-MedFlow-MedSed
Baseline-LDC-Morpho180-MedFlow-MedSed
Baseline-LDC-Morpho365-MeanFlow-NoSed

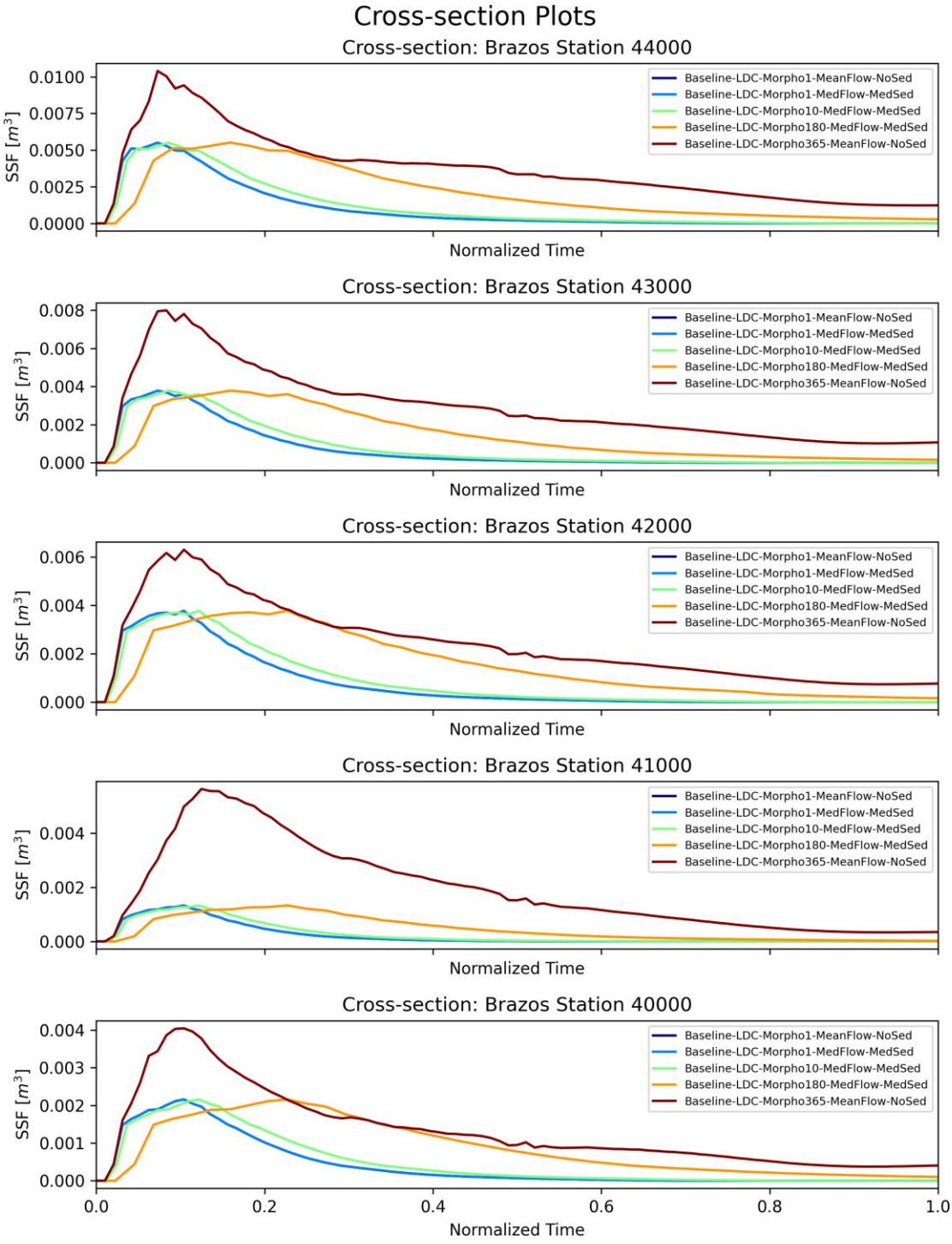
Cross-section Plots
Cross-section: Brazos Station 44000
Cross-section: Brazos Station 43000
Cross-section: Brazos Station 42000
Cross-section: Brazos Station 41000
Cross-section: Brazos Station 40000
SSF [m^3]
Normalized Time
Baseline-LDC-Morpho1-MeanFlow-NoSed
Baseline-LDC-Morpho1-MedFlow-MedSed
Baseline-LDC-Morpho10-MedFlow-MedSed
Baseline-LDC-Morpho180-MedFlow-MedSed
Baseline-LDC-Morpho365-MeanFlow-NoSed

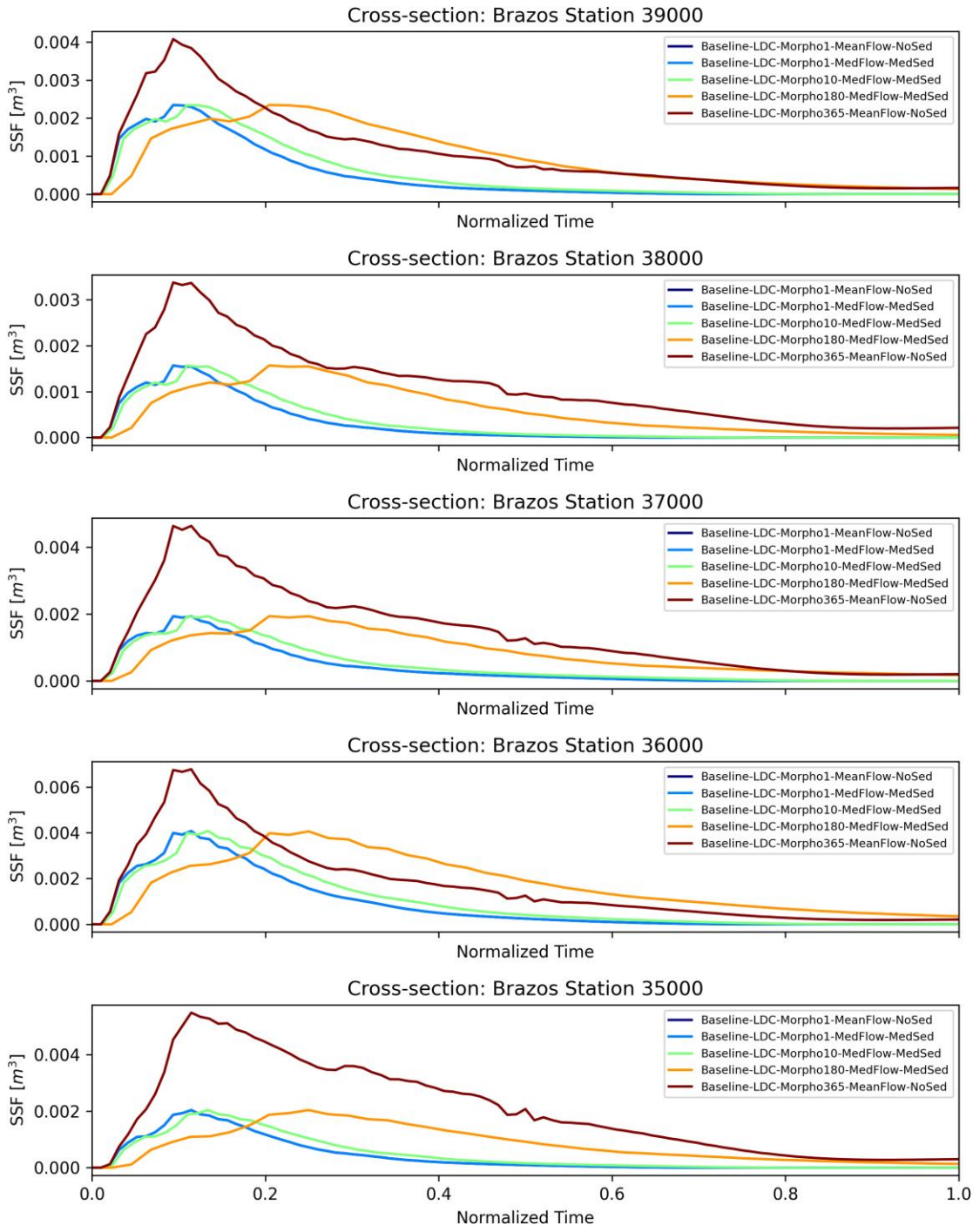
Cross-section Plots
Cross-section: Brazos Station 39000
Cross-section: Brazos Station 38000
Cross-section: Brazos Station 37000
Cross-section: Brazos Station 36000
Cross-section: Brazos Station 35000
SSF [m^3]
Normalized Time
Baseline-LDC-Morpho1-MeanFlow-NoSed
Baseline-LDC-Morpho1-MedFlow-MedSed
Baseline-LDC-Morpho10-MedFlow-MedSed
Baseline-LDC-Morpho180-MedFlow-MedSed
Baseline-LDC-Morpho365-MeanFlow-NoSed

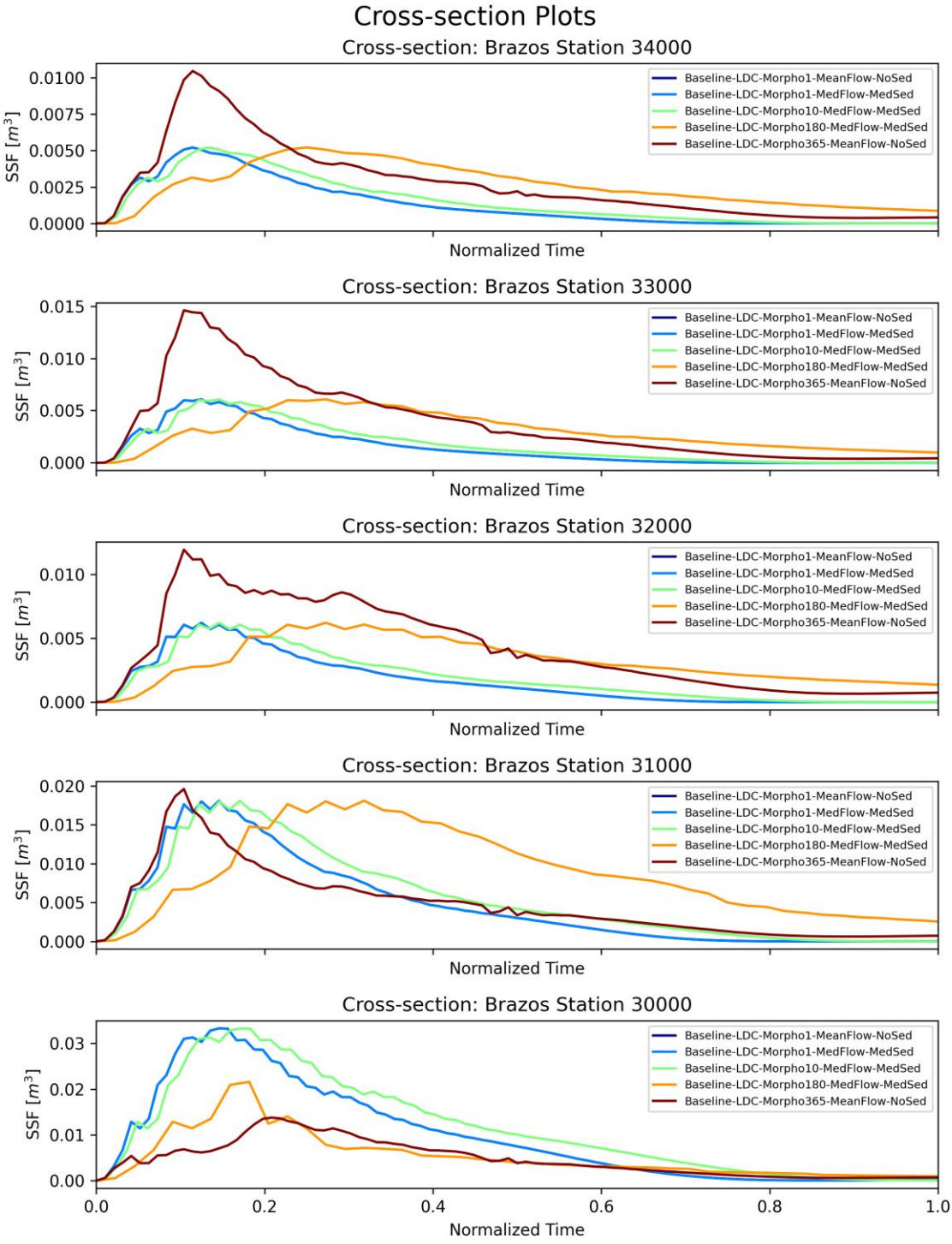
Cross-section Plots
Cross-section: Brazos Station 34000
Cross-section: Brazos Station 33000
Cross-section: Brazos Station 32000
Cross-section: Brazos Station 31000
Cross-section: Brazos Station 30000
SSF [m^3]
Normalized Time
Baseline-LDC-Morpho1-MeanFlow-NoSed
Baseline-LDC-Morpho1-MedFlow-MedSed
Baseline-LDC-Morpho10-MedFlow-MedSed
Baseline-LDC-Morpho180-MedFlow-MedSed
Baseline-LDC-Morpho365-MeanFlow-NoSed

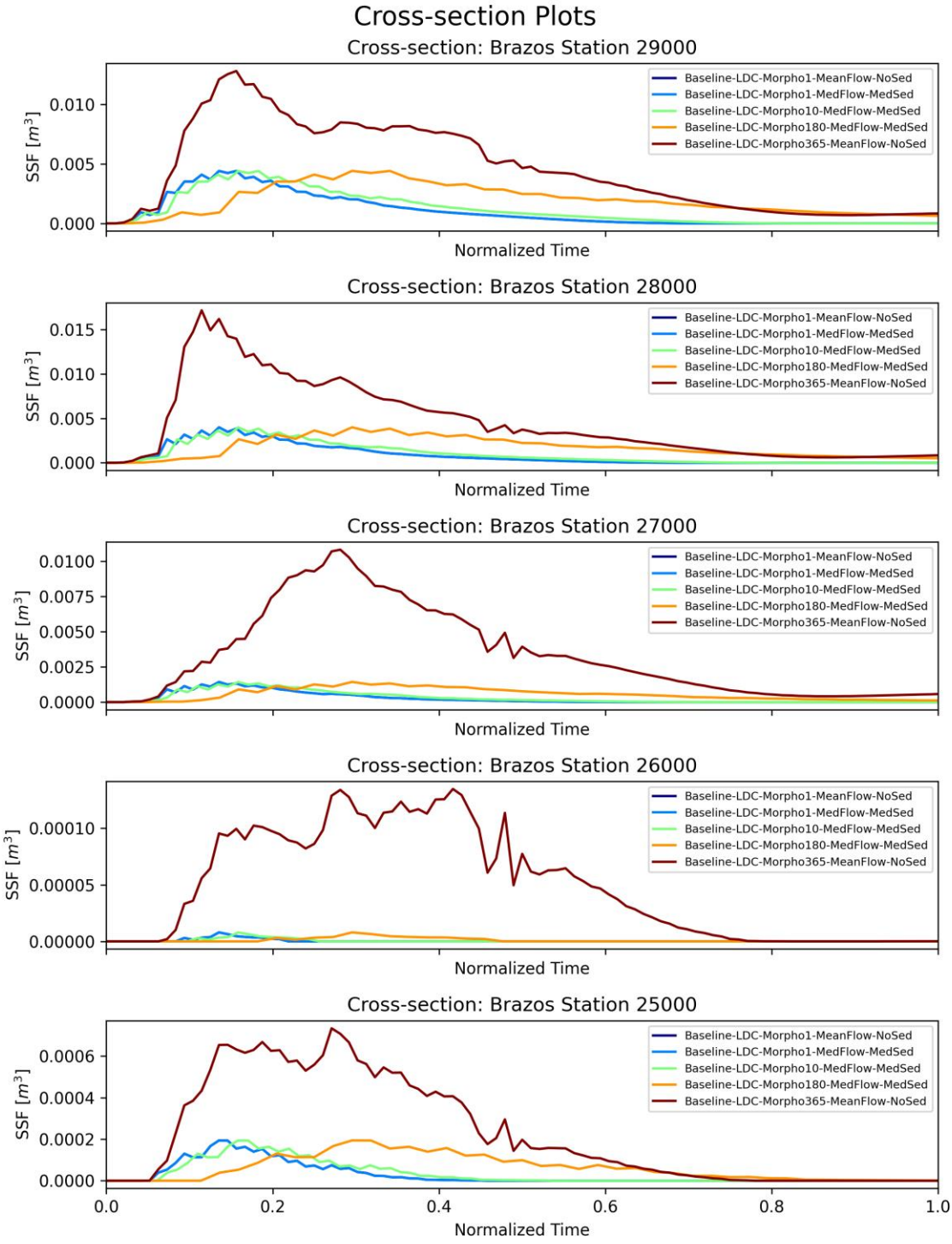
Cross-section Plots
Cross-section: Brazos Station 29000
Cross-section: Brazos Station 28000
Cross-section: Brazos Station 27000
Cross-section: Brazos Station 26000
Cross-section: Brazos Station 25000
SSF [m^3]
Normalized Time
Baseline-LDC-Morpho1-MeanFlow-NoSed
Baseline-LDC-Morpho1-MedFlow-MedSed
Baseline-LDC-Morpho10-MedFlow-MedSed
Baseline-LDC-Morpho180-MedFlow-MedSed
Baseline-LDC-Morpho365-MeanFlow-NoSed

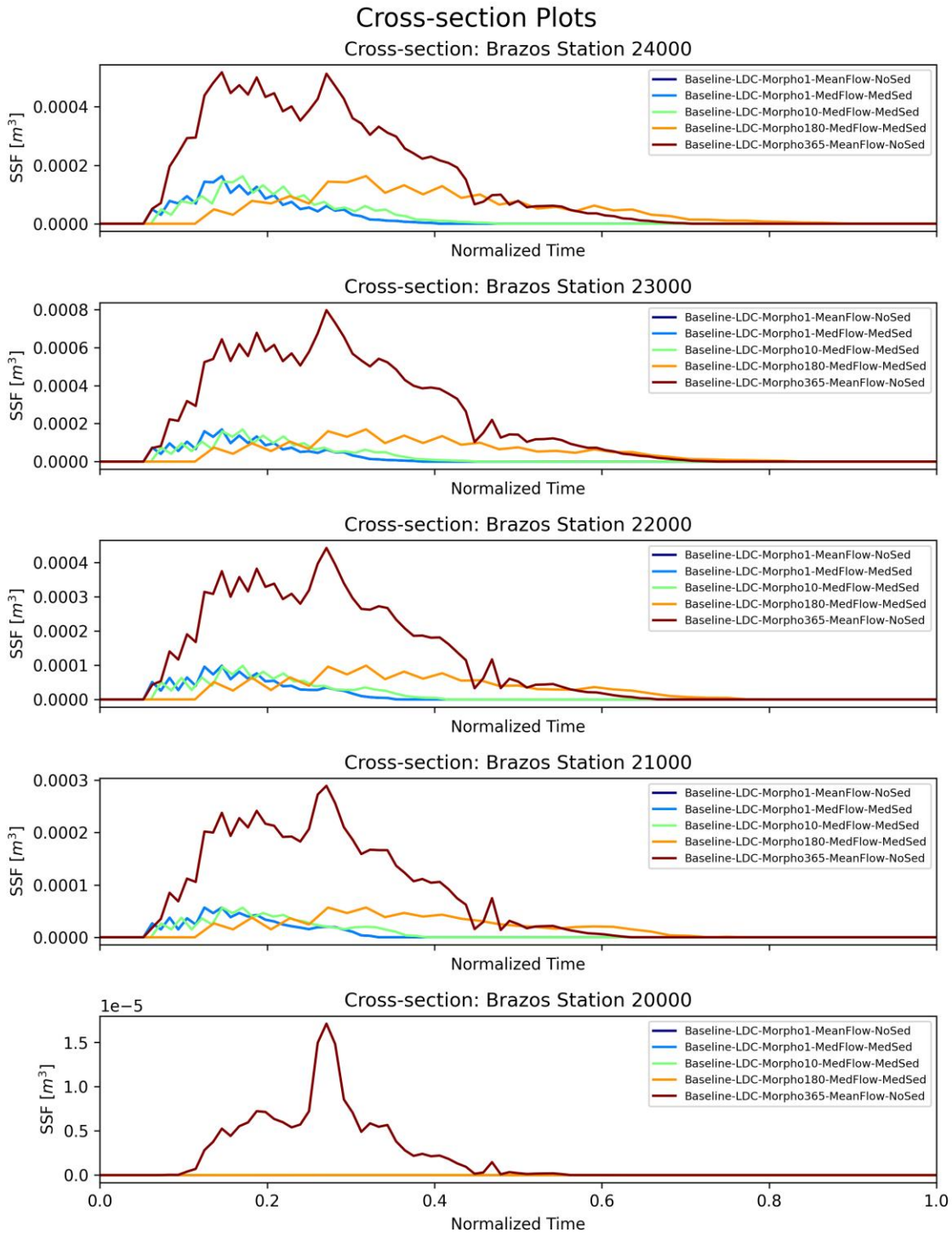
Cross-section Plots
Cross-section: Brazos Station 24000
Cross-section: Brazos Station 23000
Cross-section: Brazos Station 22000
Cross-section: Brazos Station 21000
Cross-section: Brazos Station 20000
SSF [m^3]
Normalized Time
1e−5
Baseline-LDC-Morpho1-MeanFlow-NoSed
Baseline-LDC-Morpho1-MedFlow-MedSed
Baseline-LDC-Morpho10-MedFlow-MedSed
Baseline-LDC-Morpho180-MedFlow-MedSed
Baseline-LDC-Morpho365-MeanFlow-NoSed

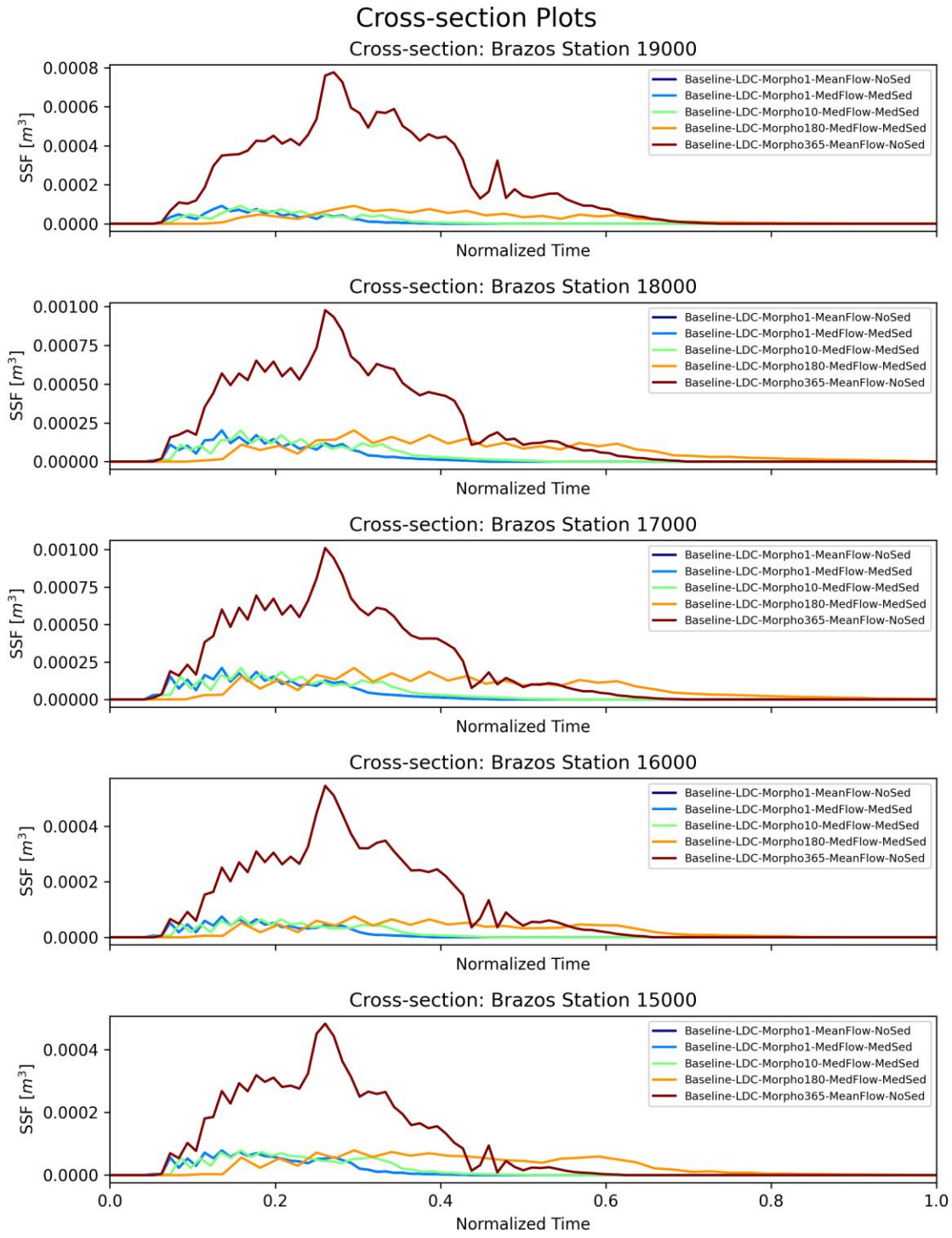
Cross-section Plots
Cross-section: Brazos Station 19000
Cross-section: Brazos Station 18000
Cross-section: Brazos Station 17000
Cross-section: Brazos Station 16000
Cross-section: Brazos Station 15000
SSF [m^3]
Normalized Time
Baseline-LDC-Morpho1-MeanFlow-NoSed
Baseline-LDC-Morpho1-MedFlow-MedSed
Baseline-LDC-Morpho10-MedFlow-MedSed
Baseline-LDC-Morpho180-MedFlow-MedSed
Baseline-LDC-Morpho365-MeanFlow-NoSed

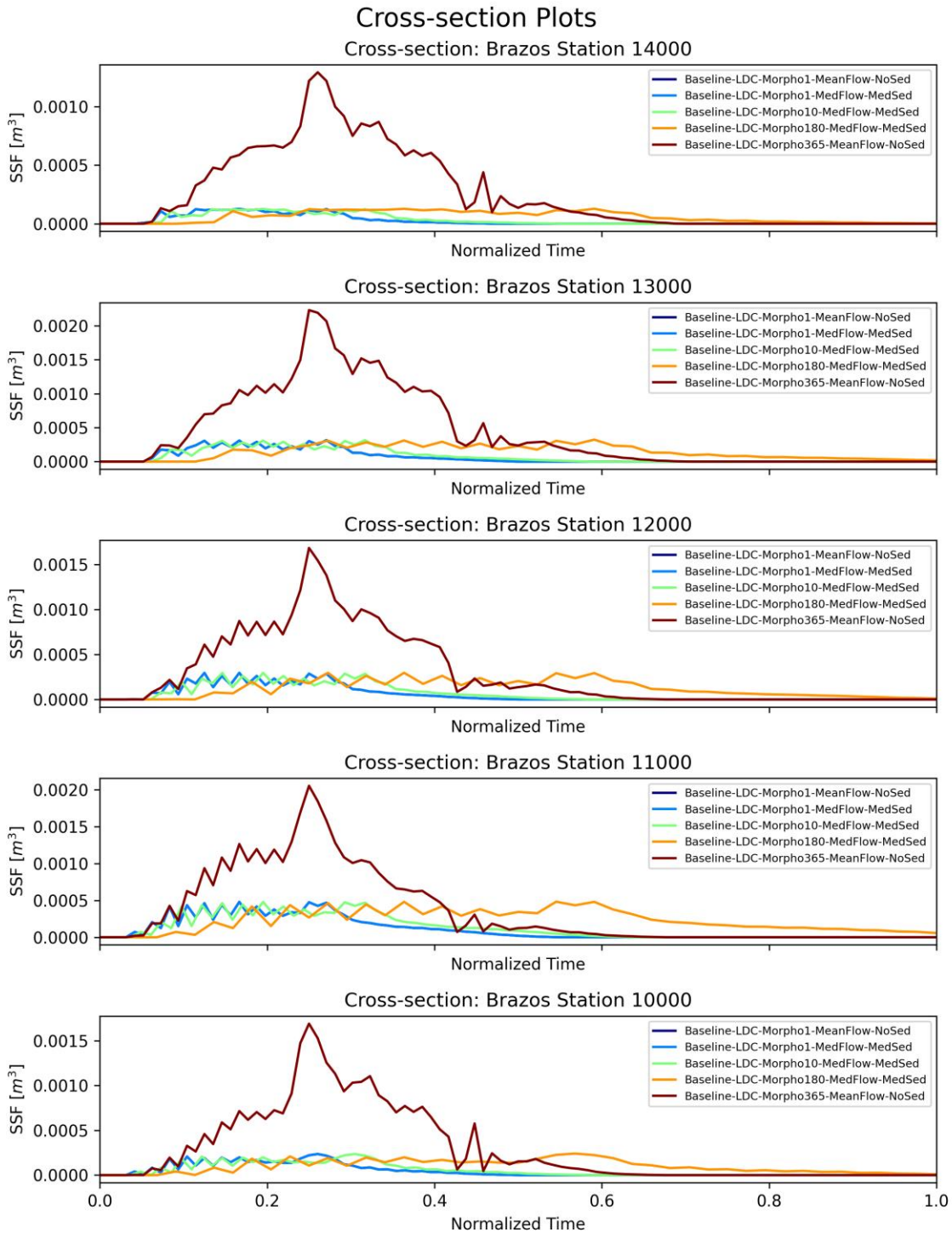
Cross-section Plots
Cross-section: Brazos Station 14000
Cross-section: Brazos Station 13000
Cross-section: Brazos Station 12000
Cross-section: Brazos Station 11000
Cross-section: Brazos Station 10000
SSF [m^3]
Normalized Time
Baseline-LDC-Morpho1-MeanFlow-NoSed
Baseline-LDC-Morpho1-MedFlow-MedSed
Baseline-LDC-Morpho10-MedFlow-MedSed
Baseline-LDC-Morpho180-MedFlow-MedSed
Baseline-LDC-Morpho365-MeanFlow-NoSed

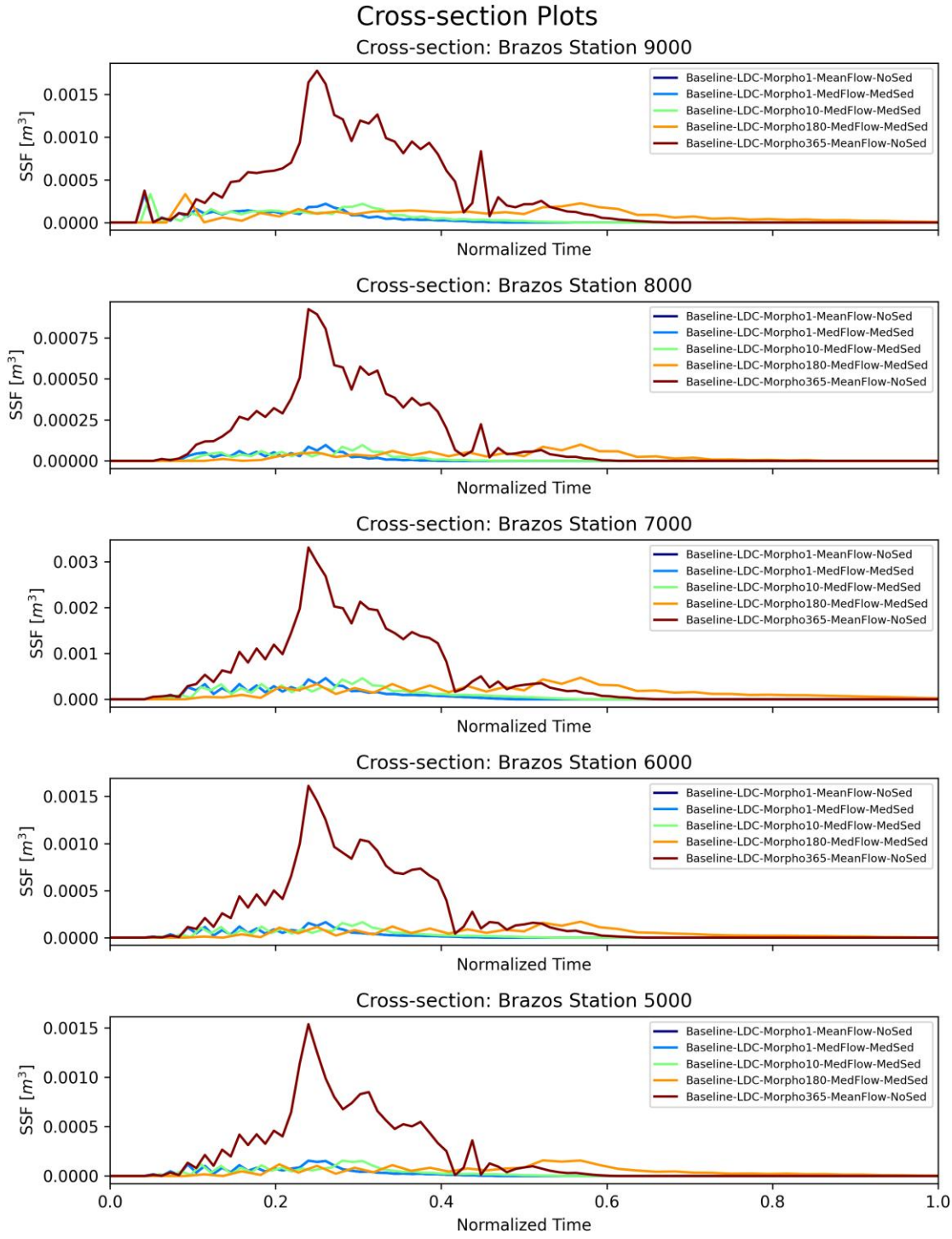
Cross-section Plots
Cross-section: Brazos Station 9000
Cross-section: Brazos Station 8000
Cross-section: Brazos Station 7000
Cross-section: Brazos Station 6000
Cross-section: Brazos Station 5000
SSF [m^3]
Normalized Time
Baseline-LDC-Morpho1-MeanFlow-NoSed
Baseline-LDC-Morpho1-MedFlow-MedSed
Baseline-LDC-Morpho10-MedFlow-MedSed
Baseline-LDC-Morpho180-MedFlow-MedSed
Baseline-LDC-Morpho365-MeanFlow-NoSed

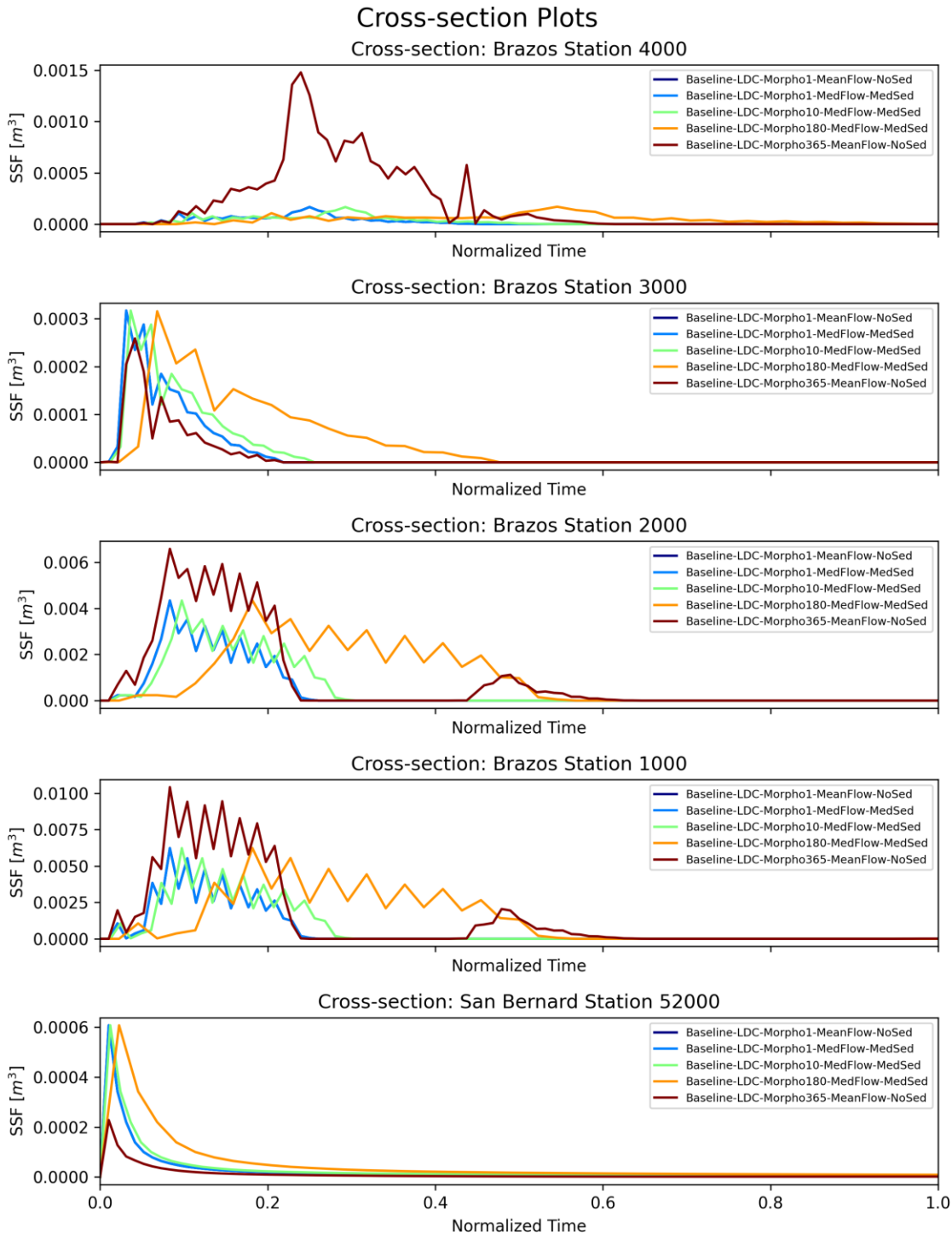
Cross-section Plots
Cross-section: Brazos Station 4000
Cross-section: Brazos Station 3000
Cross-section: Brazos Station 2000
Cross-section: Brazos Station 1000
Cross-section: San Bernard Station 52000
SSF [m^3]
Normalized Time
Baseline-LDC-Morpho1-MeanFlow-NoSed
Baseline-LDC-Morpho1-MedFlow-MedSed
Baseline-LDC-Morpho10-MedFlow-MedSed
Baseline-LDC-Morpho180-MedFlow-MedSed
Baseline-LDC-Morpho365-MeanFlow-NoSed

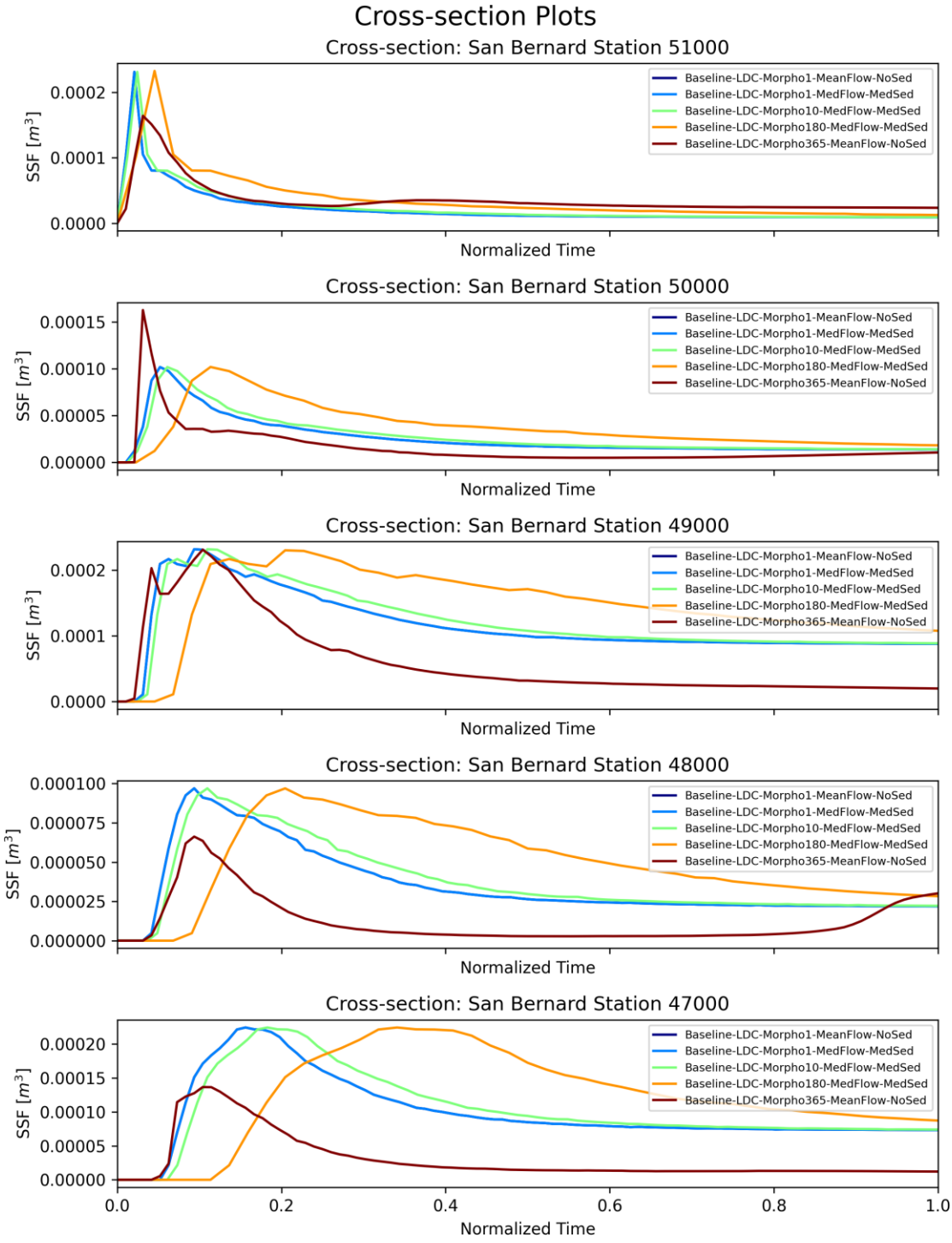
Cross-section Plots
Cross-section: San Bernard Station 51000
Cross-section: San Bernard Station 50000
Cross-section: San Bernard Station 49000
Cross-section: San Bernard Station 48000
Cross-section: San Bernard Station 47000
SSF [m^3]
Normalized Time
Baseline-LDC-Morpho1-MeanFlow-NoSed
Baseline-LDC-Morpho1-MedFlow-MedSed
Baseline-LDC-Morpho10-MedFlow-MedSed
Baseline-LDC-Morpho180-MedFlow-MedSed
Baseline-LDC-Morpho365-MeanFlow-NoSed

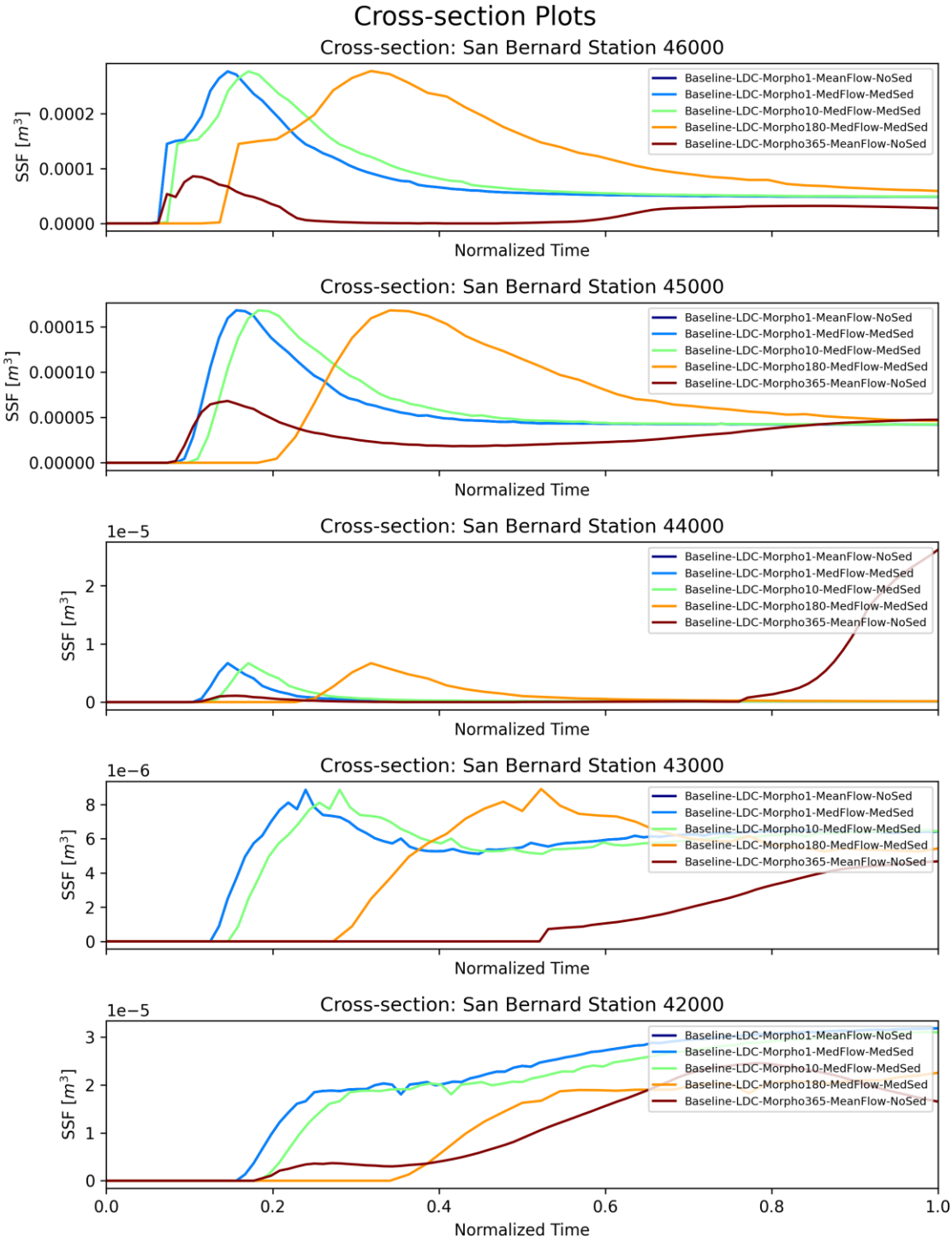
Cross-section Plots
Cross-section: San Bernard Station 46000
Cross-section: San Bernard Station 45000
Cross-section: San Bernard Station 44000
Cross-section: San Bernard Station 43000
Cross-section: San Bernard Station 42000
SSF [m^3]
Normalized Time
1e−5
1e−6
Baseline-LDC-Morpho1-MeanFlow-NoSed
Baseline-LDC-Morpho1-MedFlow-MedSed
Baseline-LDC-Morpho10-MedFlow-MedSed
Baseline-LDC-Morpho180-MedFlow-MedSed
Baseline-LDC-Morpho365-MeanFlow-NoSed

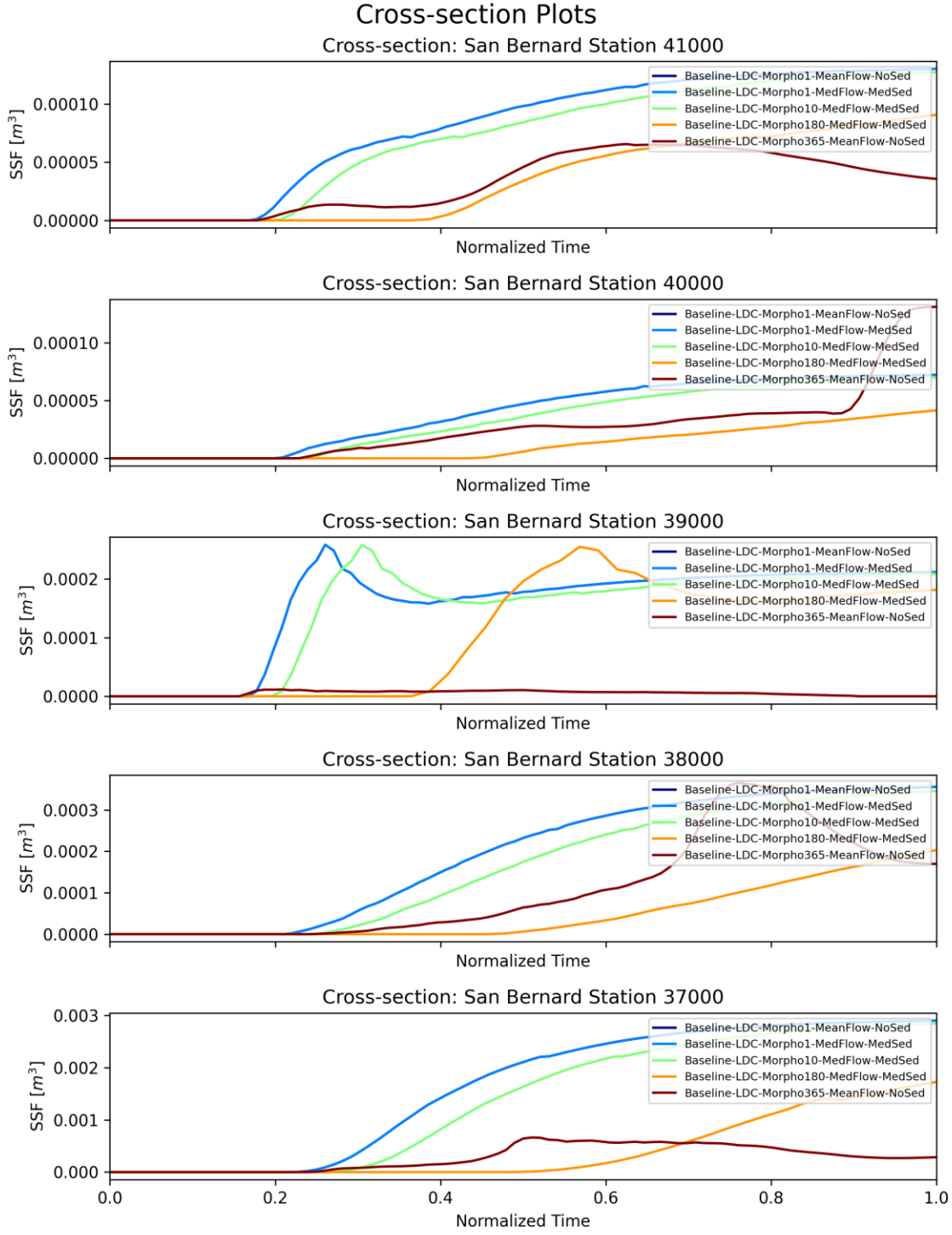
Cross-section Plots
Cross-section: San Bernard Station 41000
Cross-section: San Bernard Station 40000
Cross-section: San Bernard Station 39000
Cross-section: San Bernard Station 38000
Cross-section: San Bernard Station 37000
SSF [m^3]
Normalized Time
Baseline-LDC-Morpho1-MeanFlow-NoSed
Baseline-LDC-Morpho1-MedFlow-MedSed
Baseline-LDC-Morpho10-MedFlow-MedSed
Baseline-LDC-Morpho180-MedFlow-MedSed
Baseline-LDC-Morpho365-MeanFlow-NoSed

APPENDIX C: THE EFFECT OF MORPHOLOGICAL ACCELERATION IN COLORADO DOMAIN

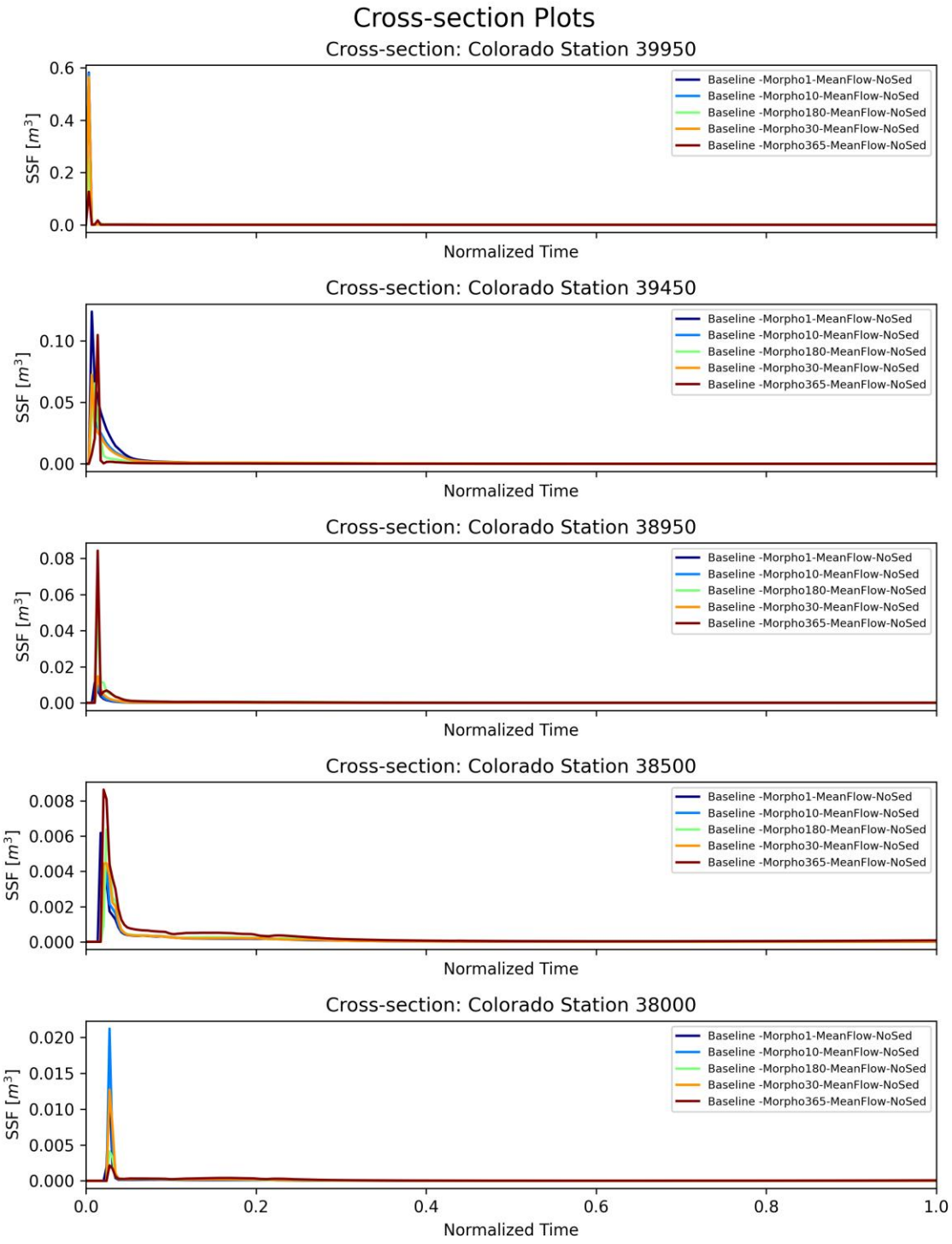
Cross-section Plots
Cross-section: Colorado Station 39950
Cross-section: Colorado Station 39450
Cross-section: Colorado Station 38950
Cross-section: Colorado Station 38500
Cross-section: Colorado Station 38000
SSF [m^3]
Normalized Time
Baseline -Morpho1-MeanFlow-NoSed
Baseline -Morpho10-MeanFlow-NoSed
Baseline -Morpho180-MeanFlow-NoSed
Baseline -Morpho30-MeanFlow-NoSed
Baseline -Morpho365-MeanFlow-NoSed

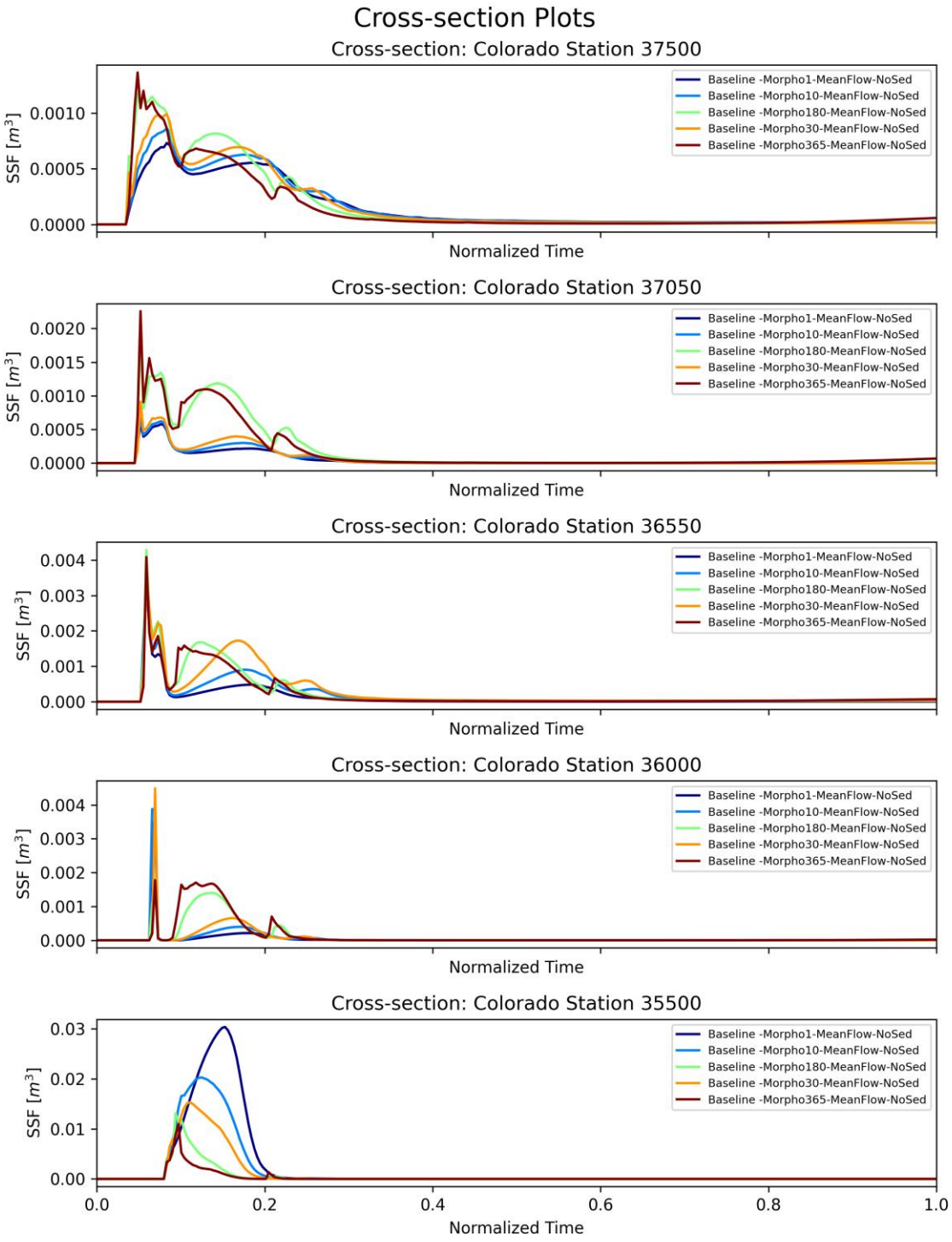
Cross-section Plots
Cross-section: Colorado Station 37500
Cross-section: Colorado Station 37050
Cross-section: Colorado Station 36550
Cross-section: Colorado Station 36000
Cross-section: Colorado Station 35500
SSF [m^3]
Normalized Time
Baseline -Morpho1-MeanFlow-NoSed
Baseline -Morpho10-MeanFlow-NoSed
Baseline -Morpho180-MeanFlow-NoSed
Baseline -Morpho30-MeanFlow-NoSed
Baseline -Morpho365-MeanFlow-NoSed

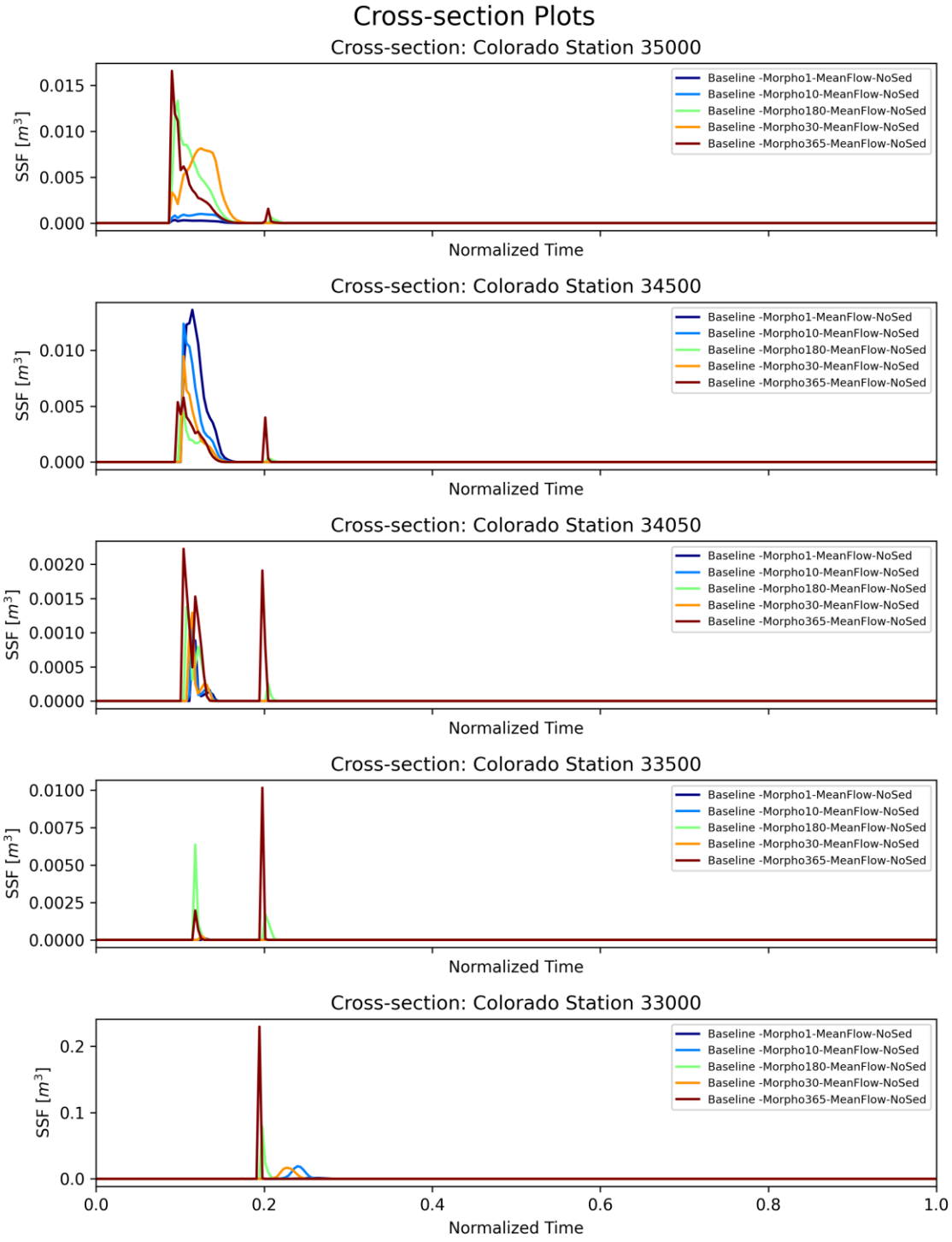
Cross-section Plots
Cross-section: Colorado Station 35000
Cross-section: Colorado Station 34500
Cross-section: Colorado Station 34050
Cross-section: Colorado Station 33500
Cross-section: Colorado Station 33000
SSF [m^3]
Normalized Time
Baseline -Morpho1-MeanFlow-NoSed
Baseline -Morpho10-MeanFlow-NoSed
Baseline -Morpho180-MeanFlow-NoSed
Baseline -Morpho30-MeanFlow-NoSed
Baseline -Morpho365-MeanFlow-NoSed

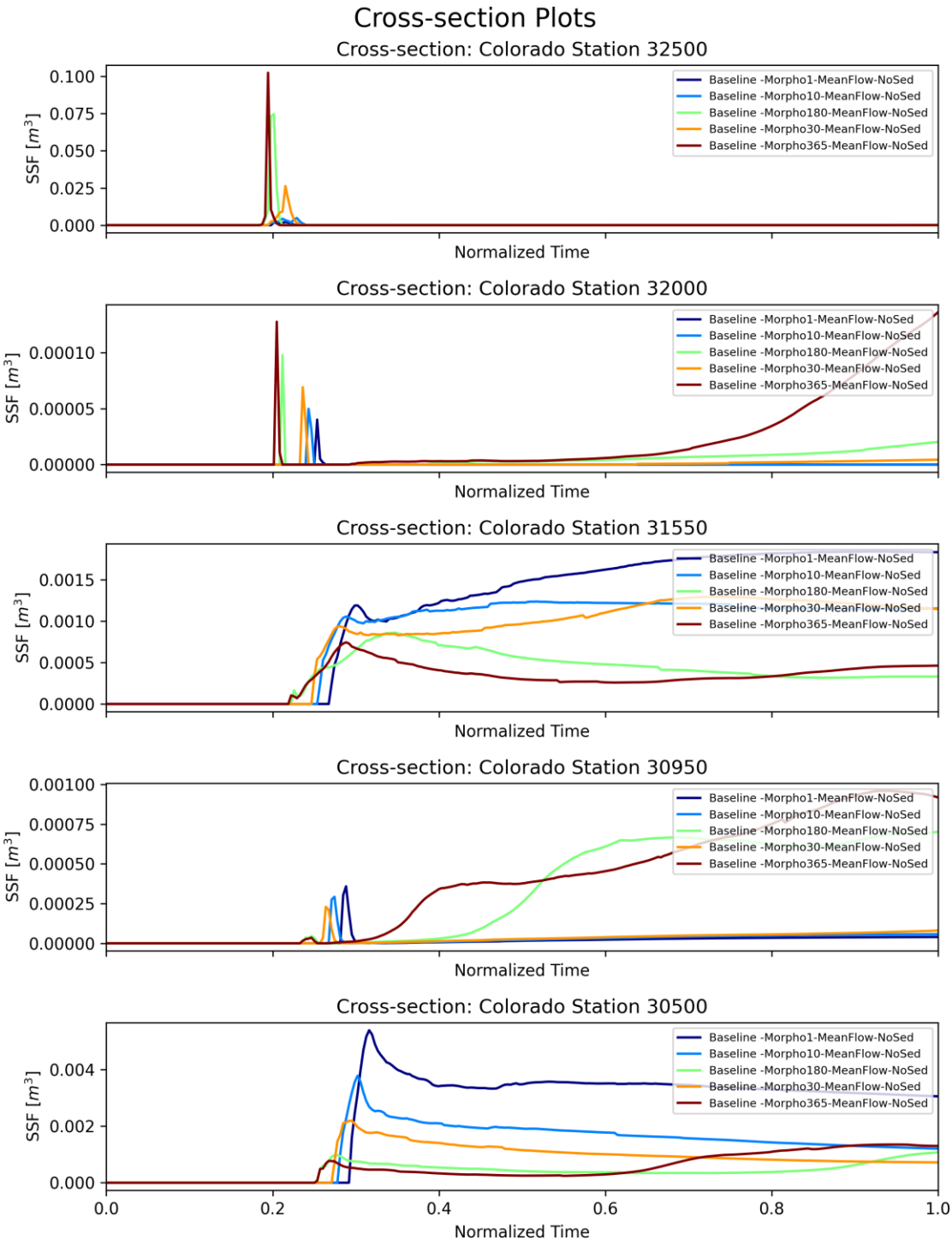
Cross-section Plots
Cross-section: Colorado Station 32500
Cross-section: Colorado Station 32000
Cross-section: Colorado Station 31550
Cross-section: Colorado Station 30950
Cross-section: Colorado Station 30500
SSF [m^3]
Normalized Time
Baseline -Morpho1-MeanFlow-NoSed
Baseline -Morpho10-MeanFlow-NoSed
Baseline -Morpho180-MeanFlow-NoSed
Baseline -Morpho30-MeanFlow-NoSed
Baseline -Morpho365-MeanFlow-NoSed

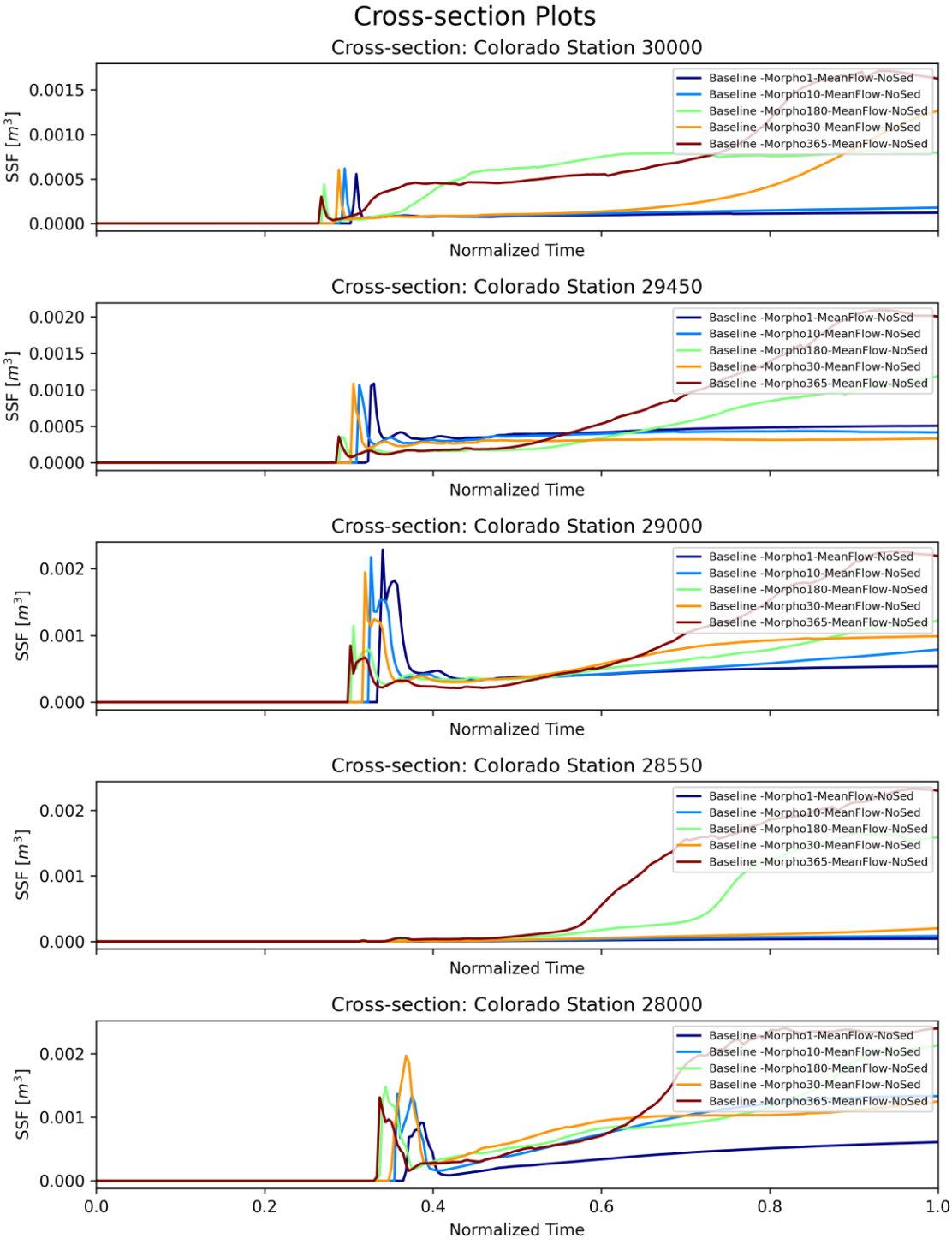
Cross-section Plots
Cross-section: Colorado Station 30000
Cross-section: Colorado Station 29450
Cross-section: Colorado Station 29000
Cross-section: Colorado Station 28550
Cross-section: Colorado Station 28000
SSF [m^3]
Normalized Time
Baseline -Morpho1-MeanFlow-NoSed
Baseline -Morpho10-MeanFlow-NoSed
Baseline -Morpho180-MeanFlow-NoSed
Baseline -Morpho30-MeanFlow-NoSed
Baseline -Morpho365-MeanFlow-NoSed

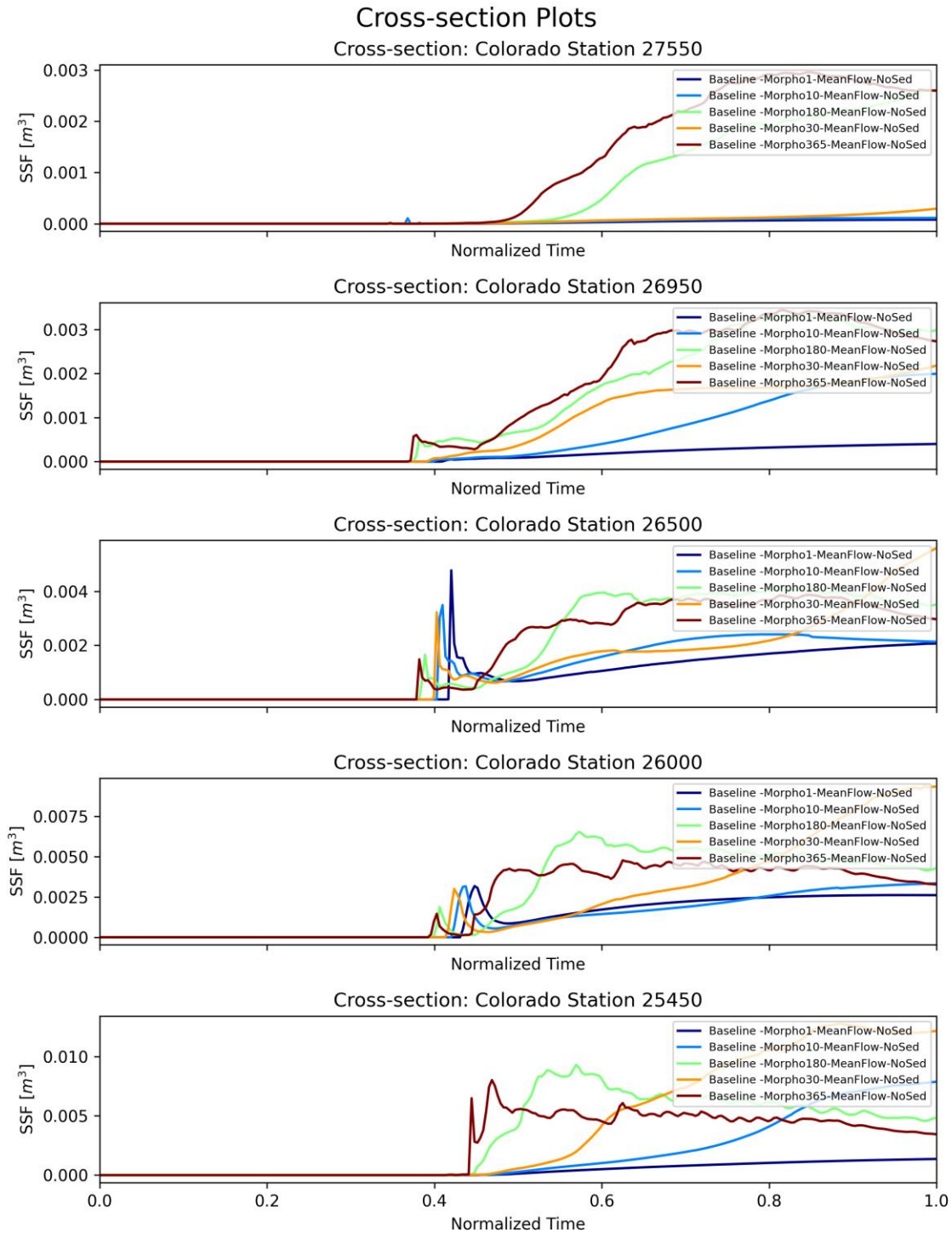
Cross-section Plots
Cross-section: Colorado Station 27550
Cross-section: Colorado Station 26950
Cross-section: Colorado Station 26500
Cross-section: Colorado Station 26000
Cross-section: Colorado Station 25450
SSF [m^3]
Normalized Time
Baseline -Morpho1-MeanFlow-NoSed
Baseline -Morpho10-MeanFlow-NoSed
Baseline -Morpho180-MeanFlow-NoSed
Baseline -Morpho30-MeanFlow-NoSed
Baseline -Morpho365-MeanFlow-NoSed

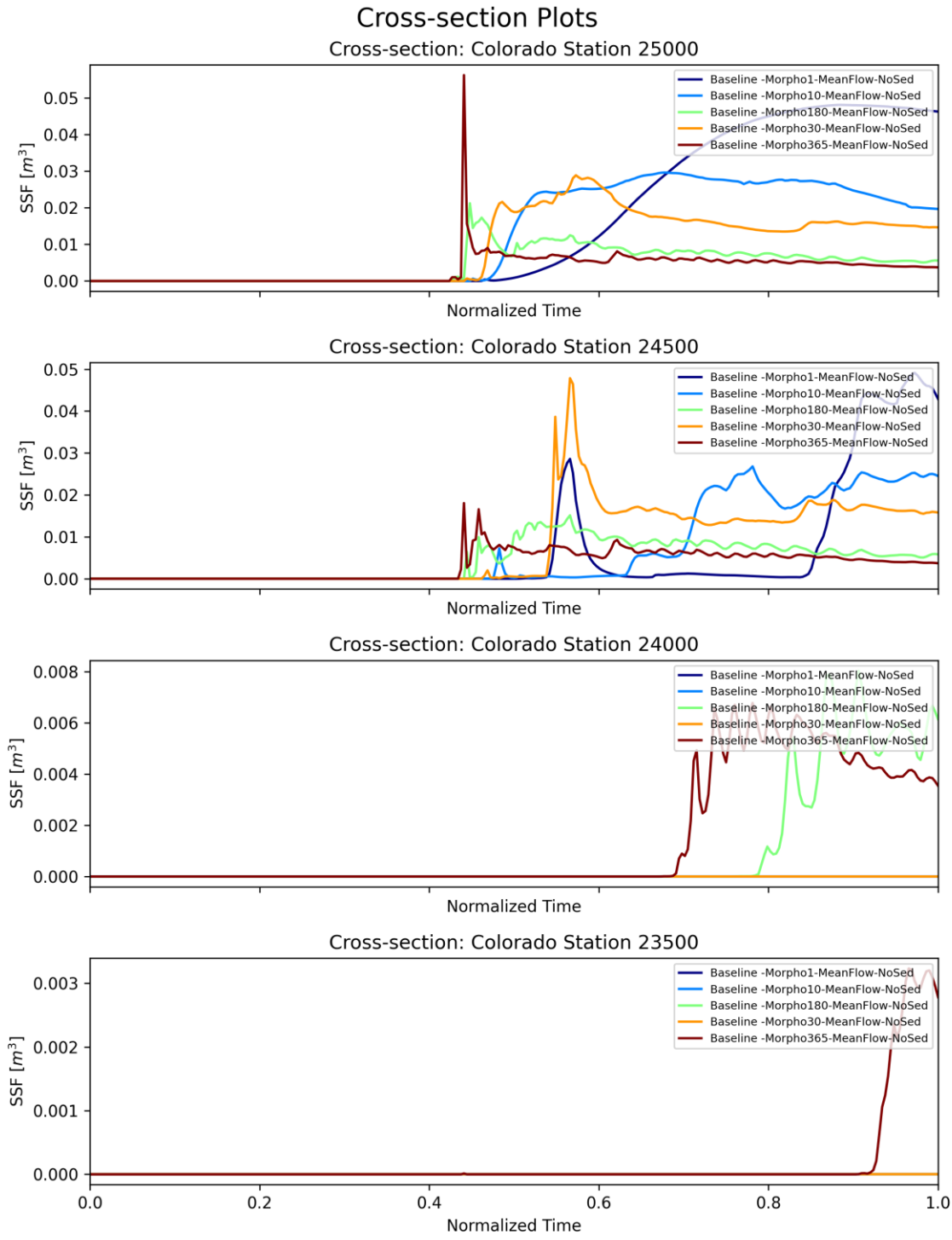
Cross-section Plots
Cross-section: Colorado Station 25000
Cross-section: Colorado Station 24500
Cross-section: Colorado Station 24000
Cross-section: Colorado Station 23500
Baseline -Morpho1-MeanFlow-NoSed
Baseline -Morpho10-MeanFlow-NoSed
Baseline -Morpho180-MeanFlow-NoSed
Baseline -Morpho30-MeanFlow-NoSed
Baseline -Morpho365-MeanFlow-NoSed
SSF [m^3]
Normalized Time

APPENDIX D: EROSION/SEDIMENTATION OF BRAZOS WITH MORFAC=365

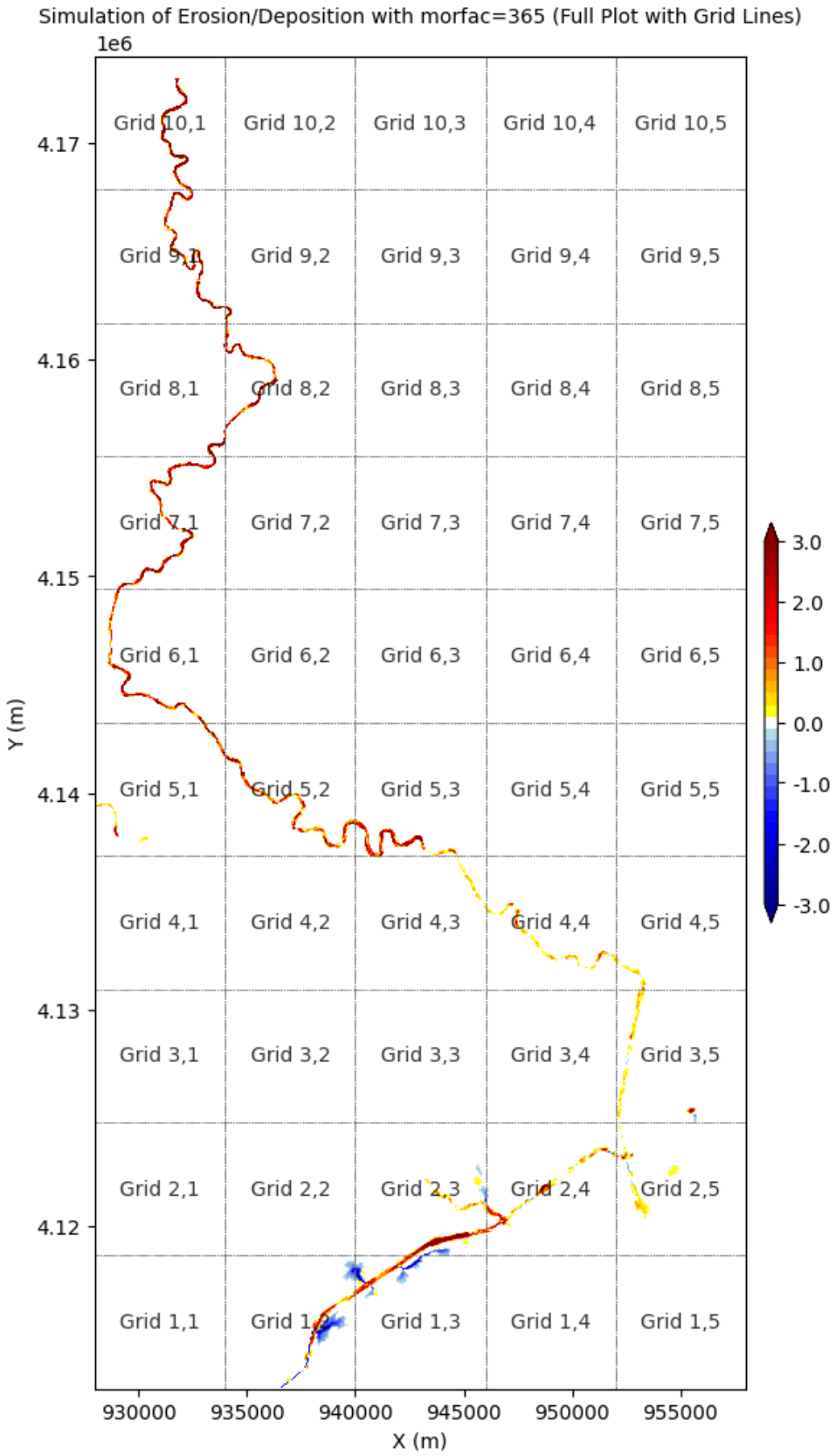

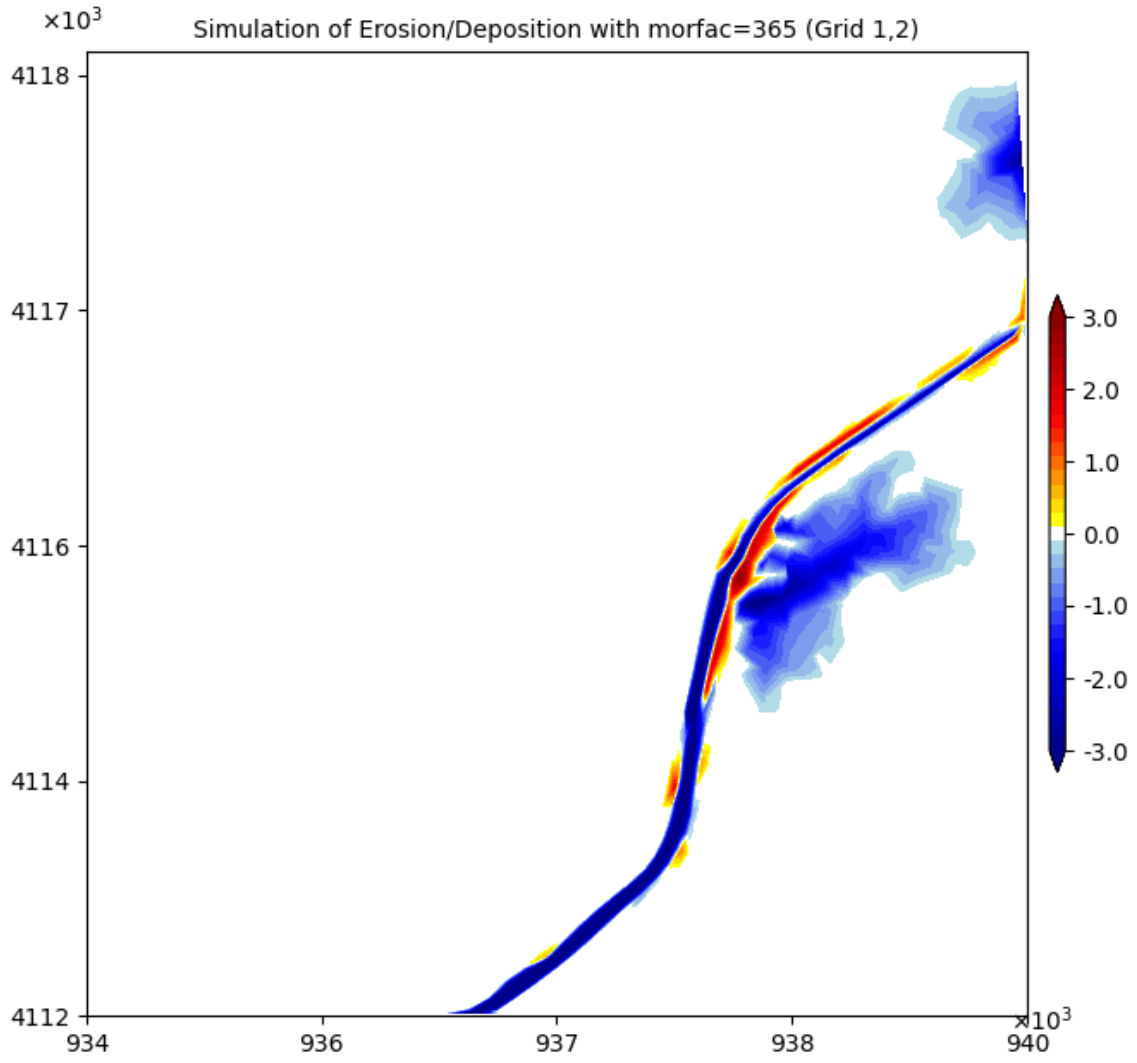
Simulation of Erosion/Deposition with morfac=365 (Grid 1,2)
×10^3
4118
4117
4116
4114
4112
934
936
937
938
940
×10^3
3.0
2.0
1.0
0.0
-1.0
-2.0
-3.0

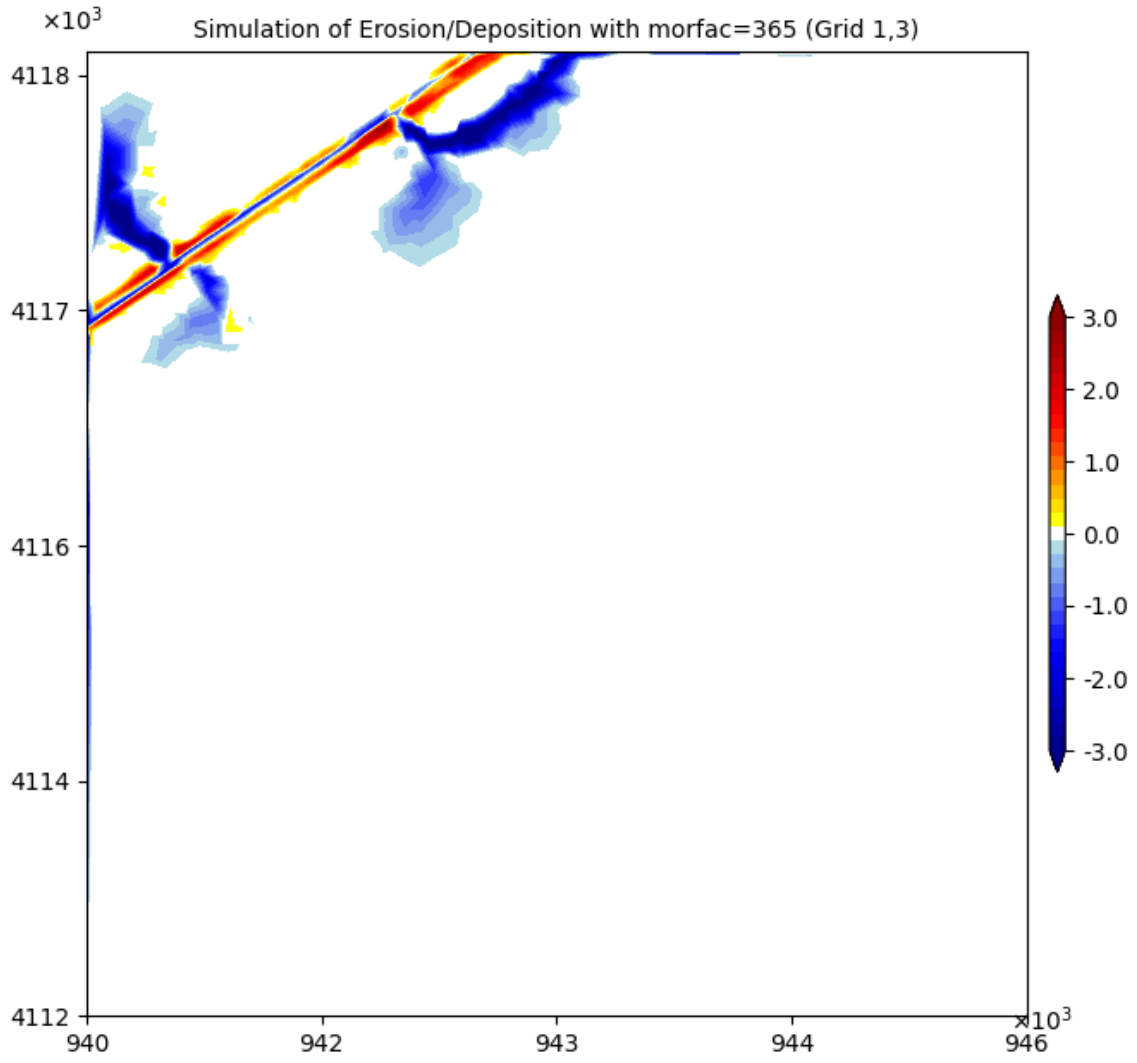
Simulation of Erosion/Deposition with morfac=365 (Grid 1,3)
×10^3
4118
4117
4116
4114
4112
940
942
943
944
946
×10^3
3.0
2.0
1.0
0.0
-1.0
-2.0
-3.0

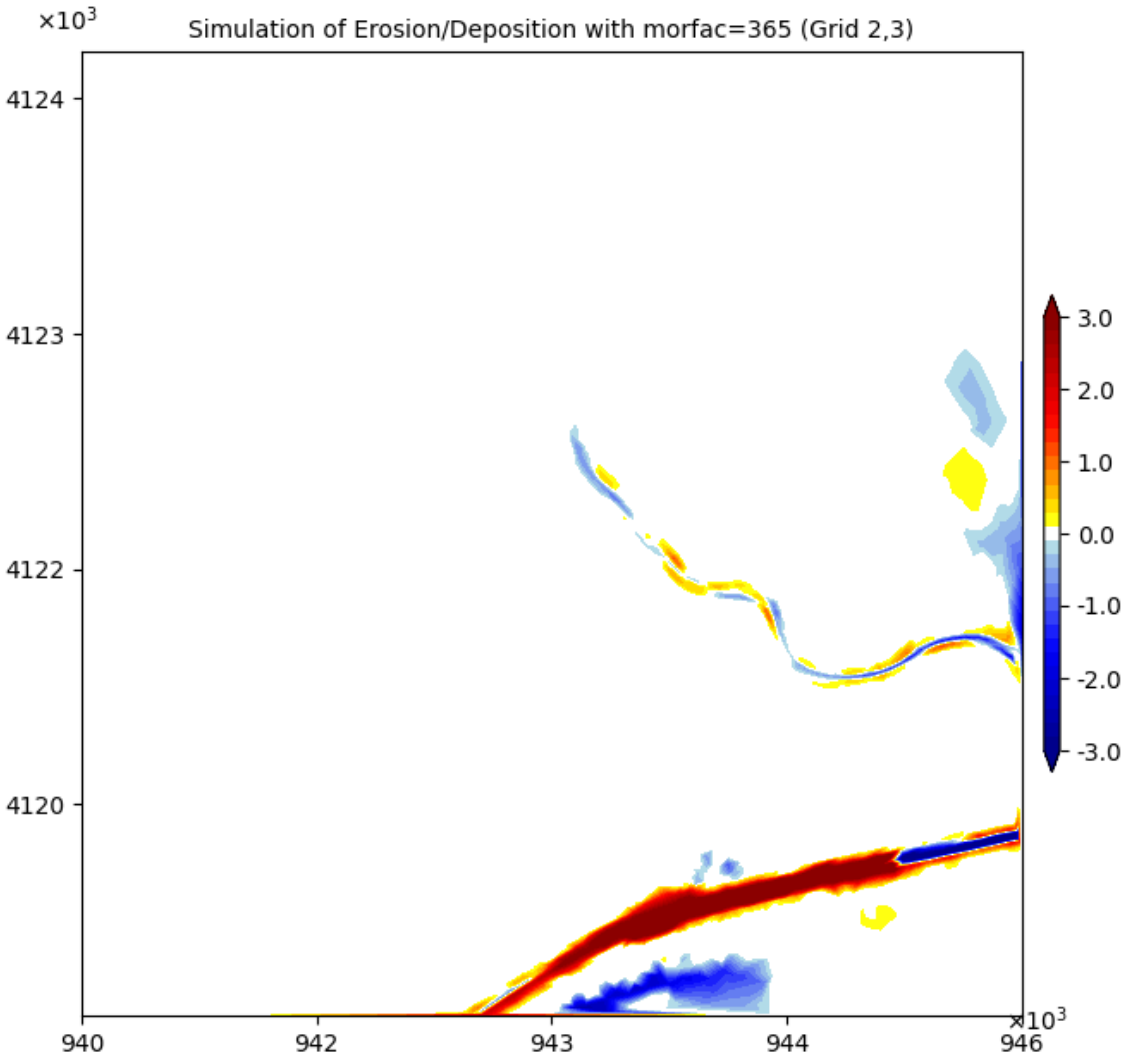
Simulation of Erosion/Deposition with morfac=365 (Grid 2,3)
×10^3
4124
4123
4122
4120
940
942
943
944
946
×10^3
3.0
2.0
1.0
0.0
-1.0
-2.0
-3.0

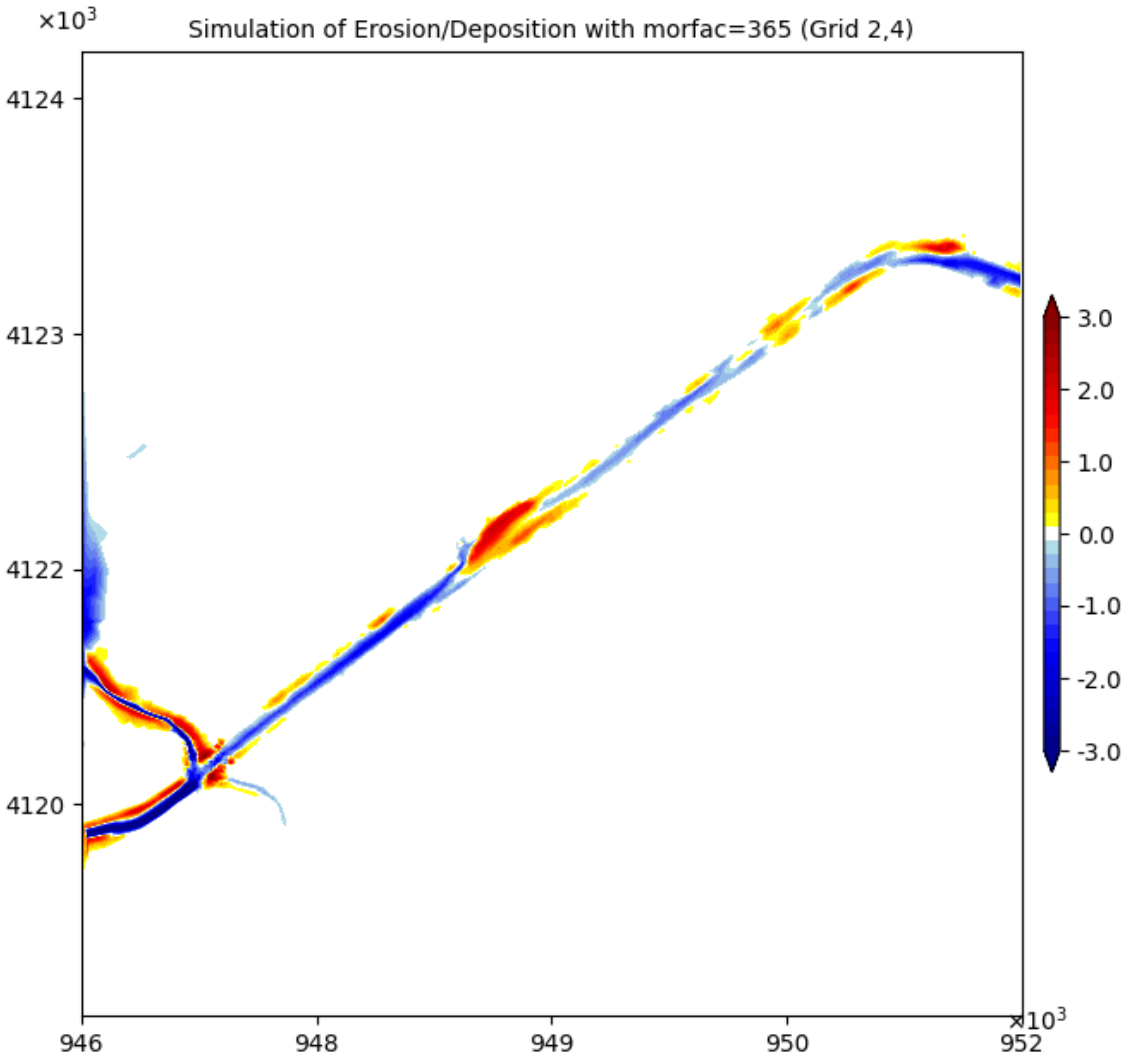
Simulation of Erosion/Deposition with morfac=365 (Grid 2,4)
×10^3
4124
4123
4122
4120
946
948
949
950
952
×10^3
3.0
2.0
1.0
0.0
-1.0
-2.0
-3.0

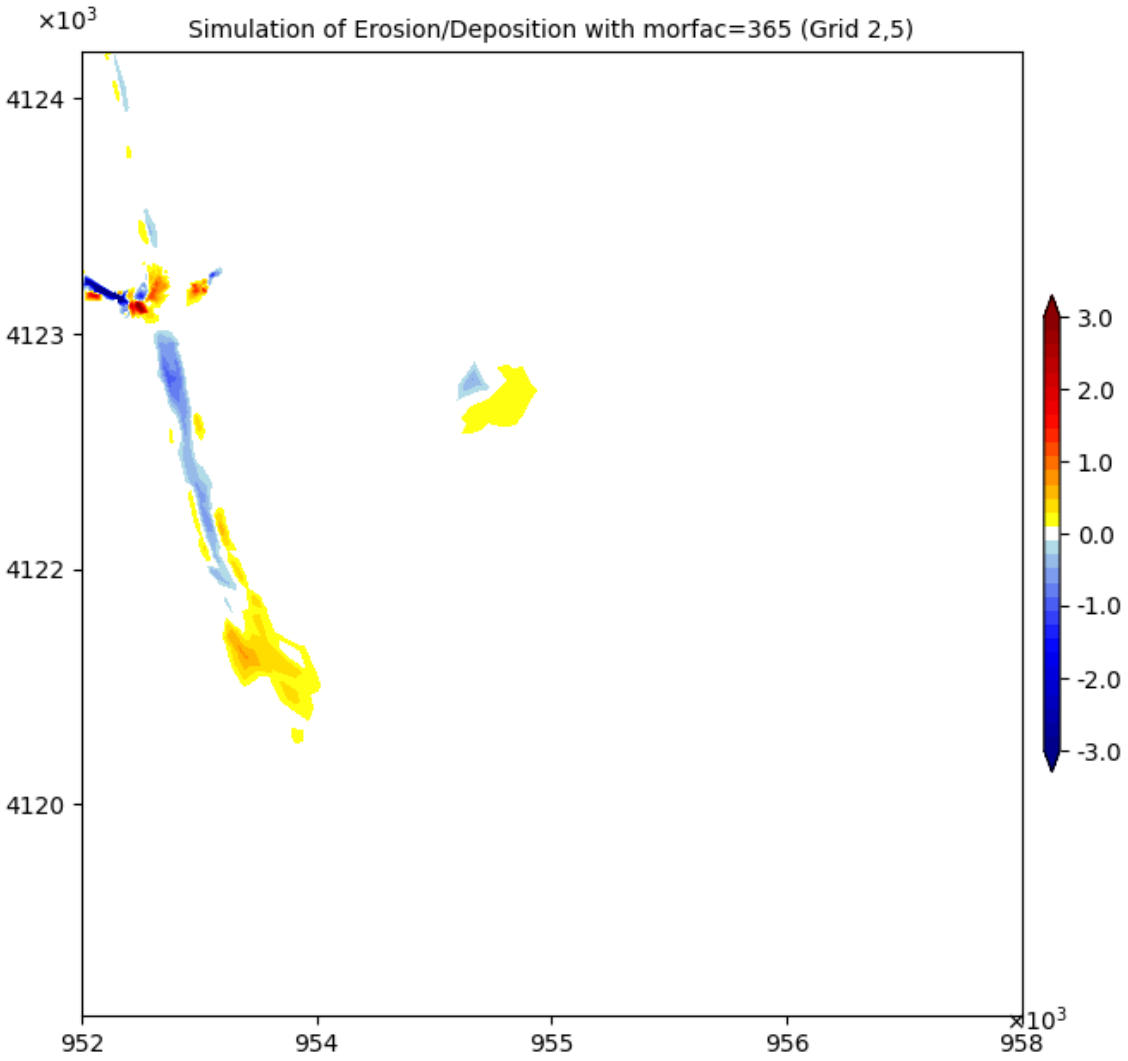
Simulation of Erosion/Deposition with morfac=365 (Grid 2,5)
×10^3
4124
4123
4122
4120
952
954
955
956
958
×10^3
3.0
2.0
1.0
0.0
-1.0
-2.0
-3.0

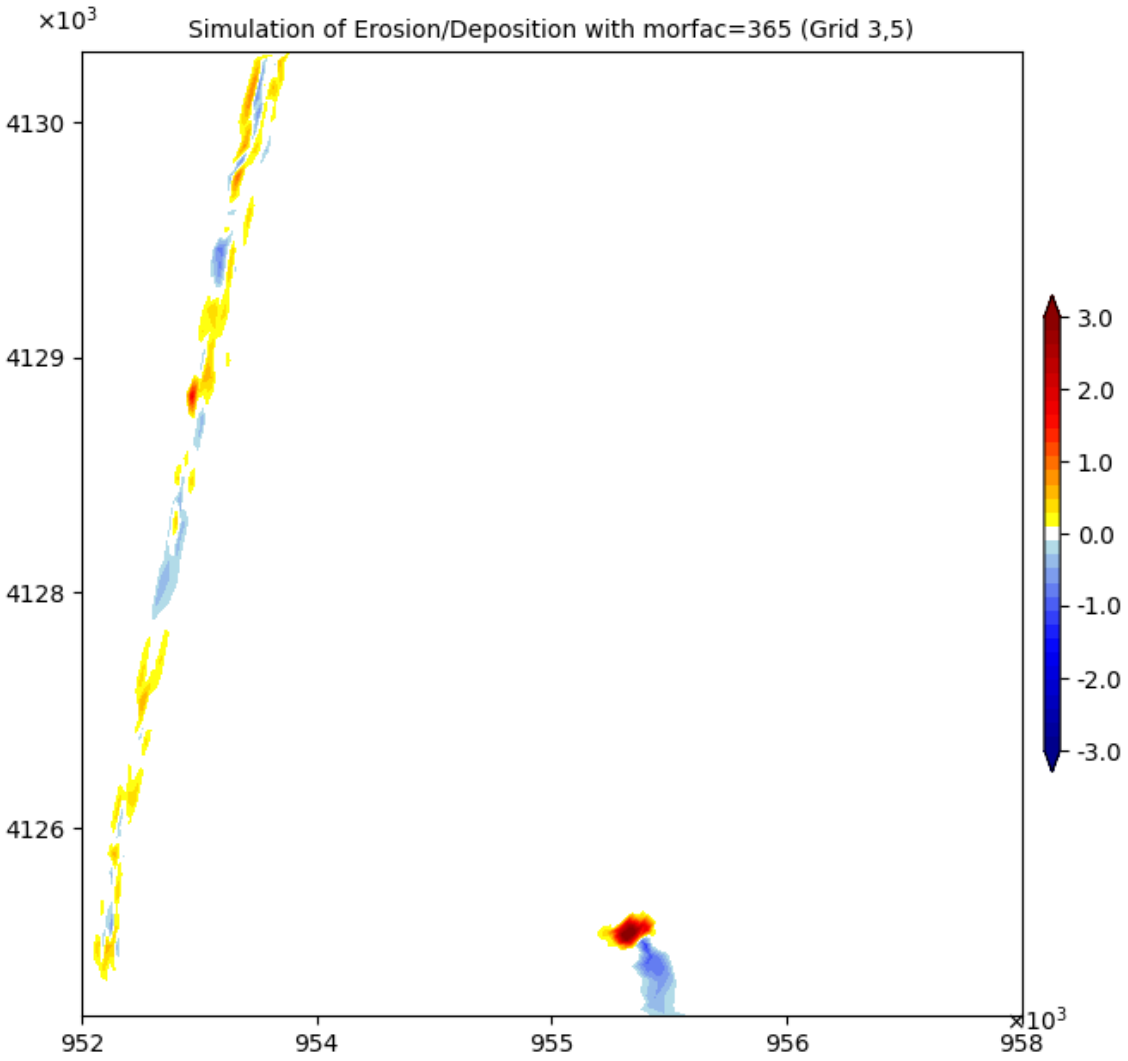
Simulation of Erosion/Deposition with morfac=365 (Grid 3,5)
×10^3
4130
4129
4128
4126
952
954
955
956
958
×10^3
3.0
2.0
1.0
0.0
-1.0
-2.0
-3.0

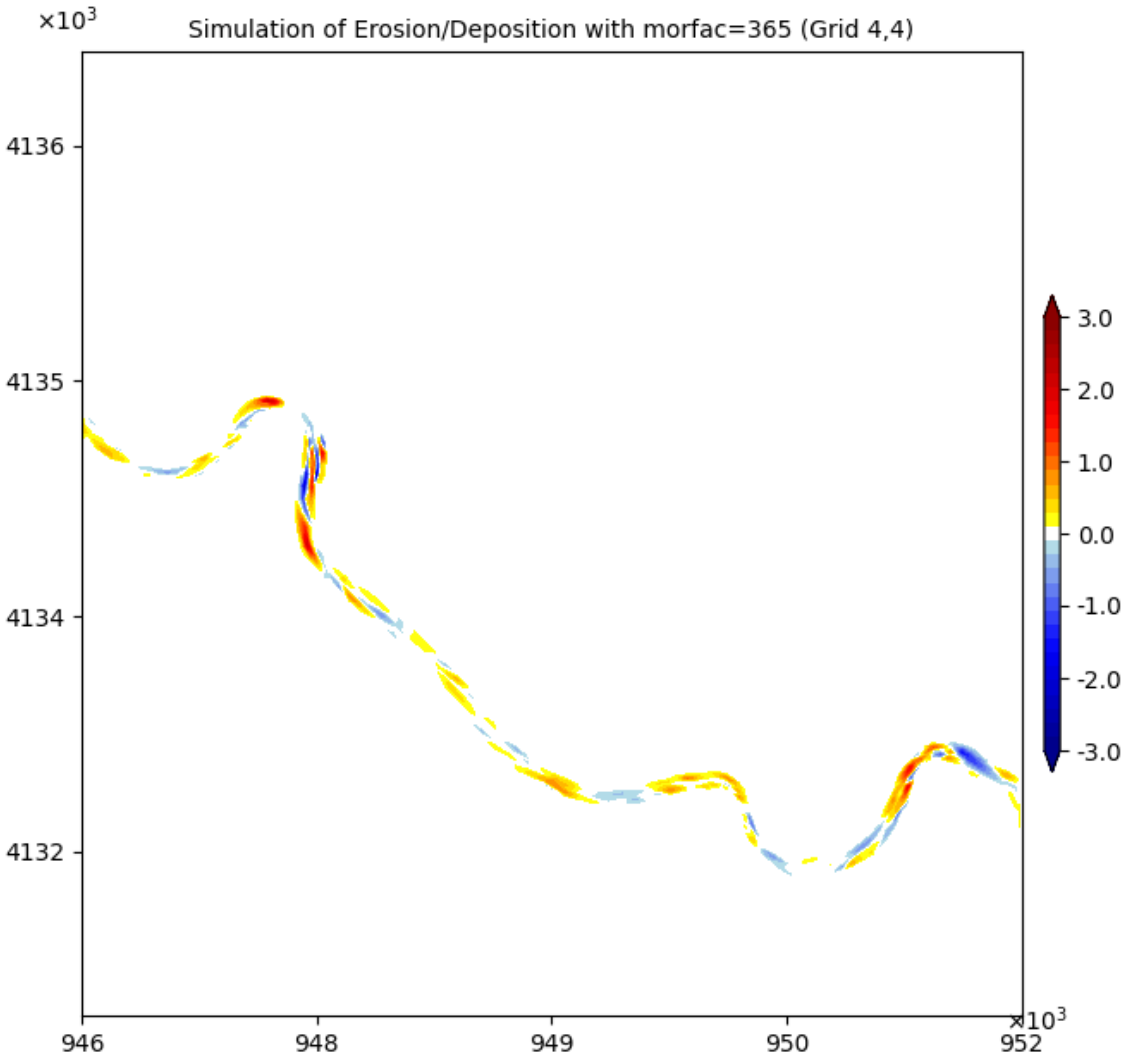
Simulation of Erosion/Deposition with morfac=365 (Grid 4,4)
×10^3
4136
4135
4134
4132
946
948
949
950
952
×10^3
3.0
2.0
1.0
0.0
-1.0
-2.0
-3.0

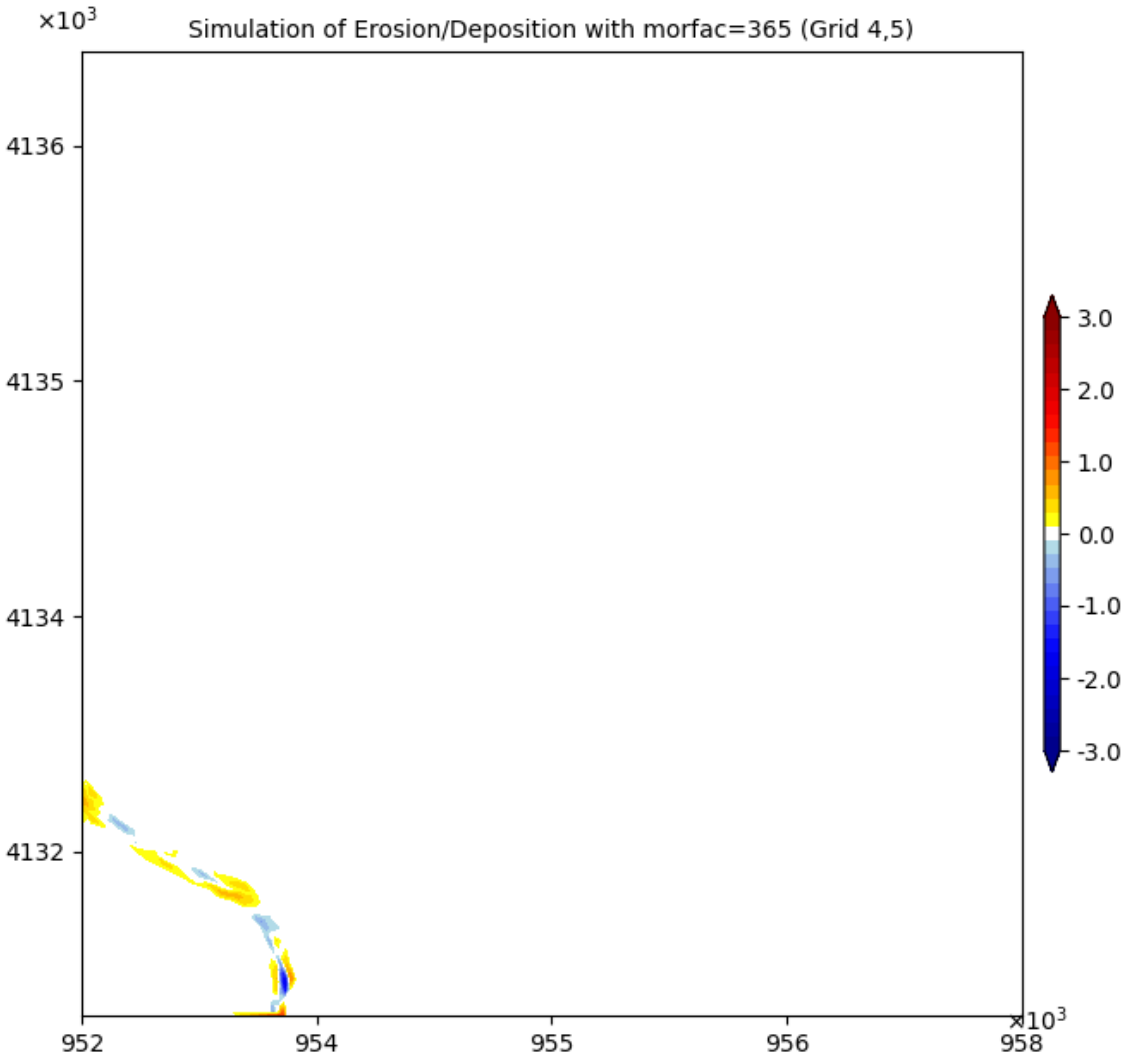
Simulation of Erosion/Deposition with morfac=365 (Grid 4,5)
×10^3
4136
4135
4134
4132
952
954
955
956
958
×10^3
3.0
2.0
1.0
0.0
-1.0
-2.0
-3.0

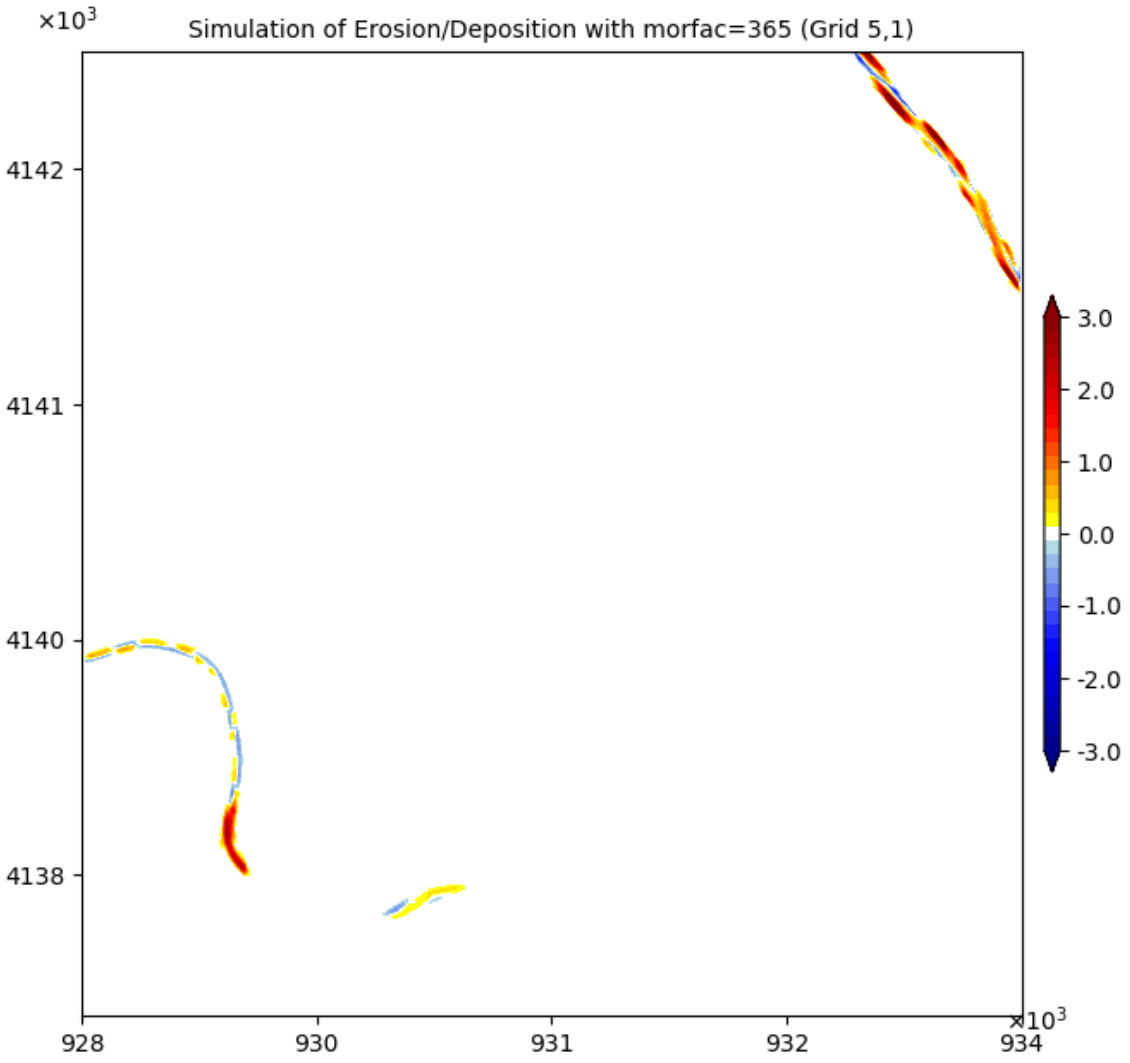
Simulation of Erosion/Deposition with morfac=365 (Grid 5,1)
×10^3
4142
4141
4140
4138
928
930
931
932
934
×10^3
3.0
2.0
1.0
0.0
-1.0
-2.0
-3.0

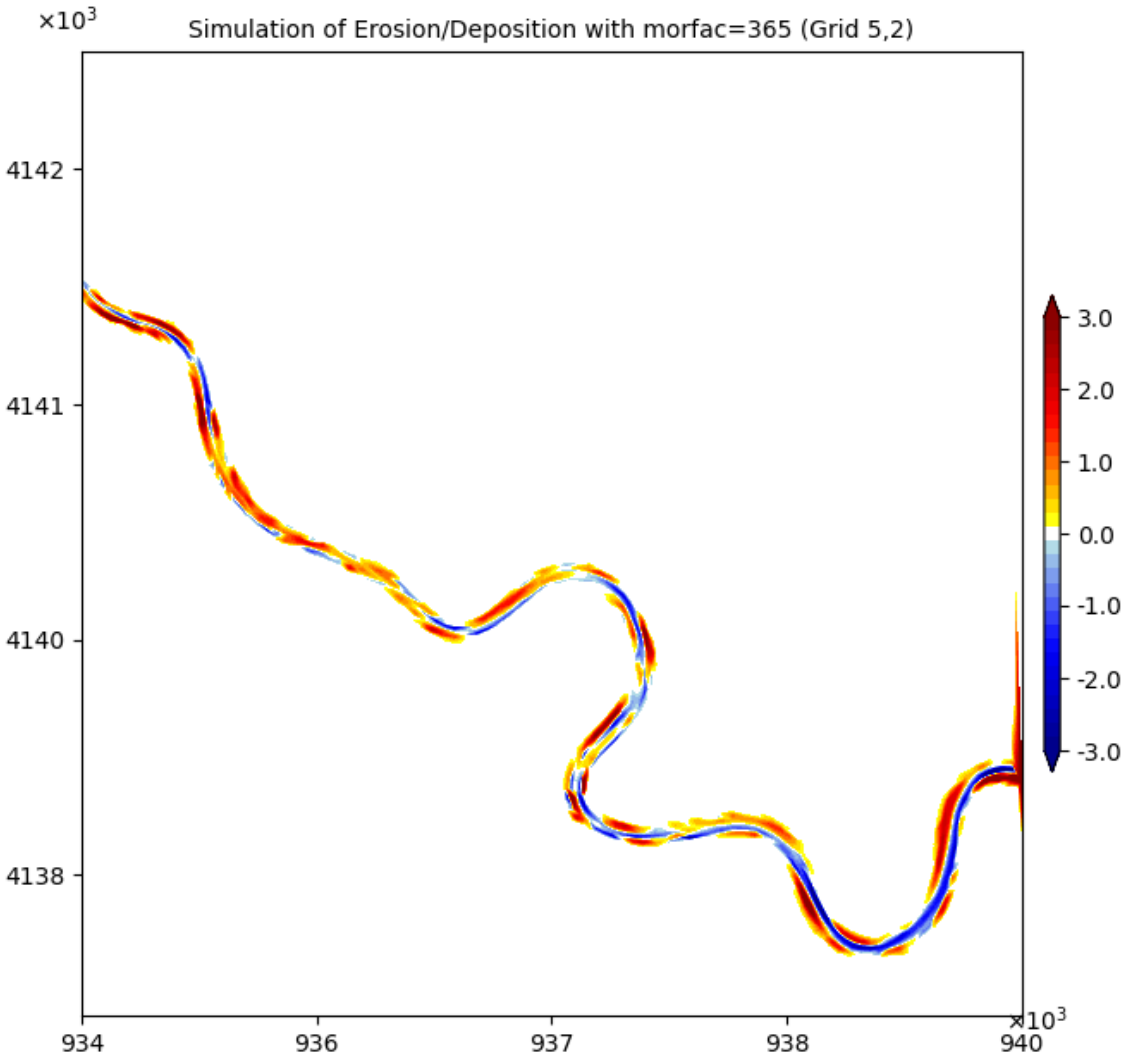
Simulation of Erosion/Deposition with morfac=365 (Grid 5,2)
×10^3
4142
4141
4140
4138
934
936
937
938
940
×10^3
3.0
2.0
1.0
0.0
-1.0
-2.0
-3.0

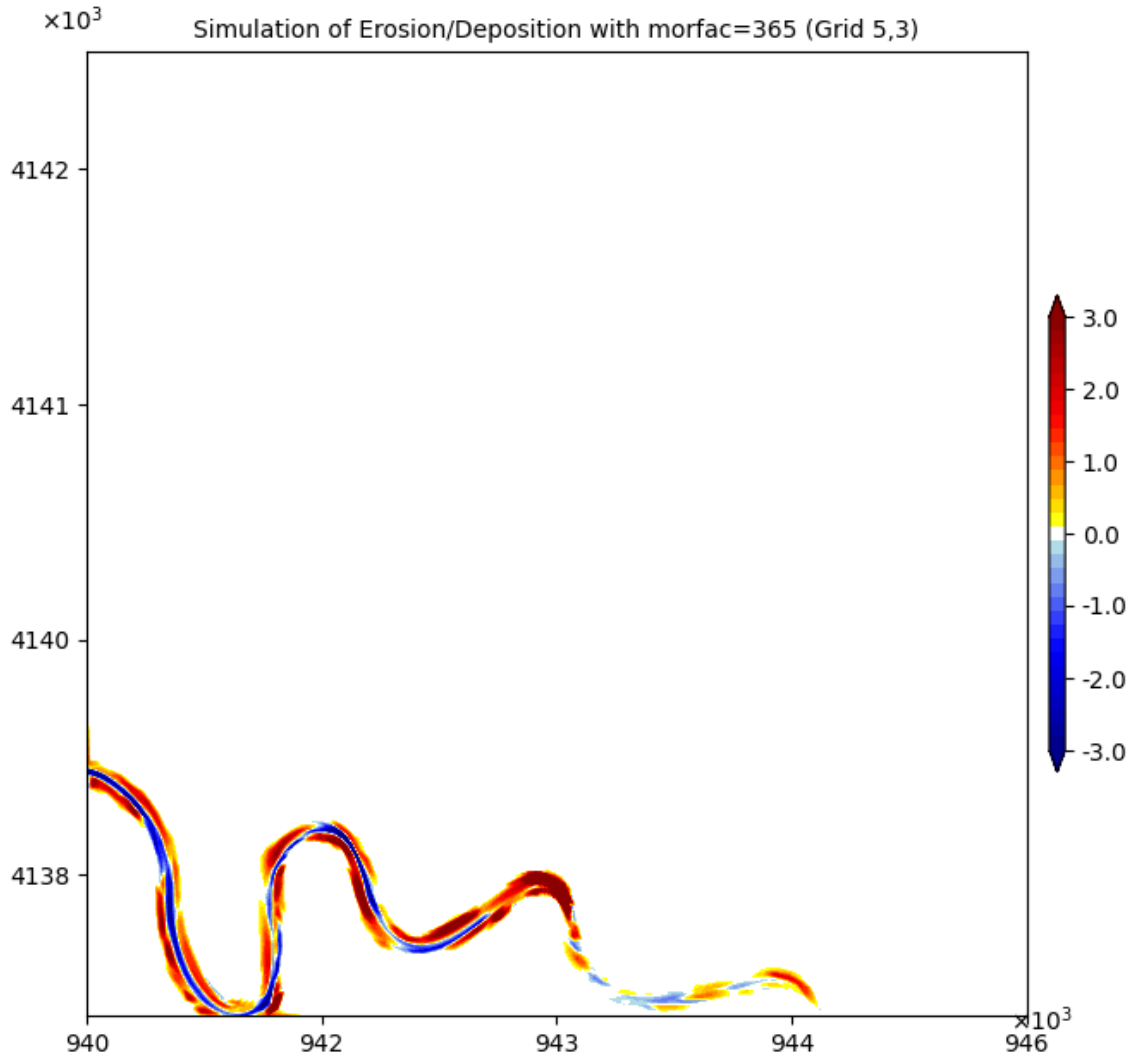
Simulation of Erosion/Deposition with morfac=365 (Grid 5,3)
×10^3
4142
4141
4140
4138
940
942
943
944
946
×10^3
3.0
2.0
1.0
0.0
-1.0
-2.0
-3.0

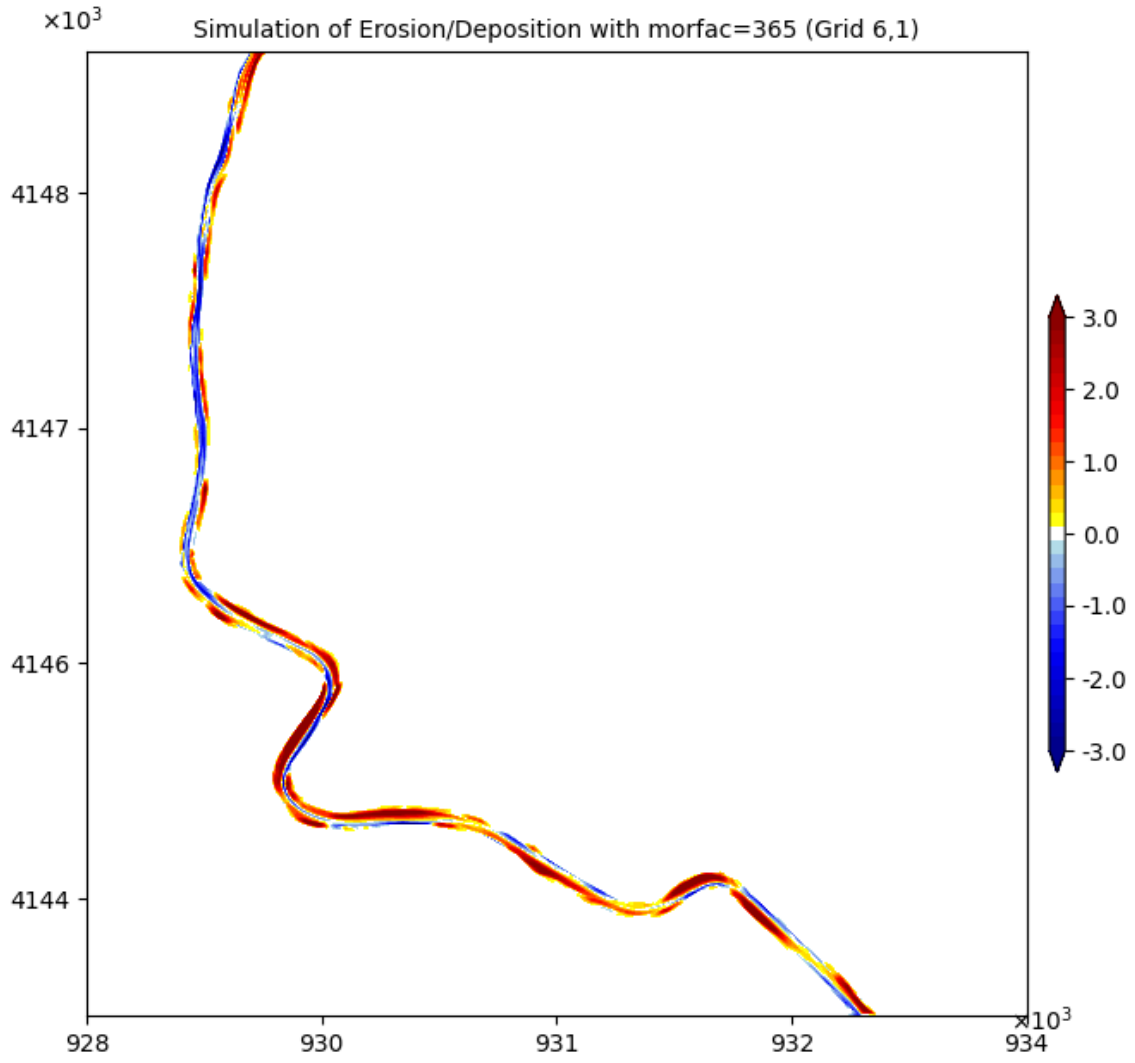
×10^3
Simulation of Erosion/Deposition with morfac=365 (Grid 6,1)
4148
4147
4146
4144
928
930
931
932
934
×10^3
3.0
2.0
1.0
0.0
-1.0
-2.0
-3.0

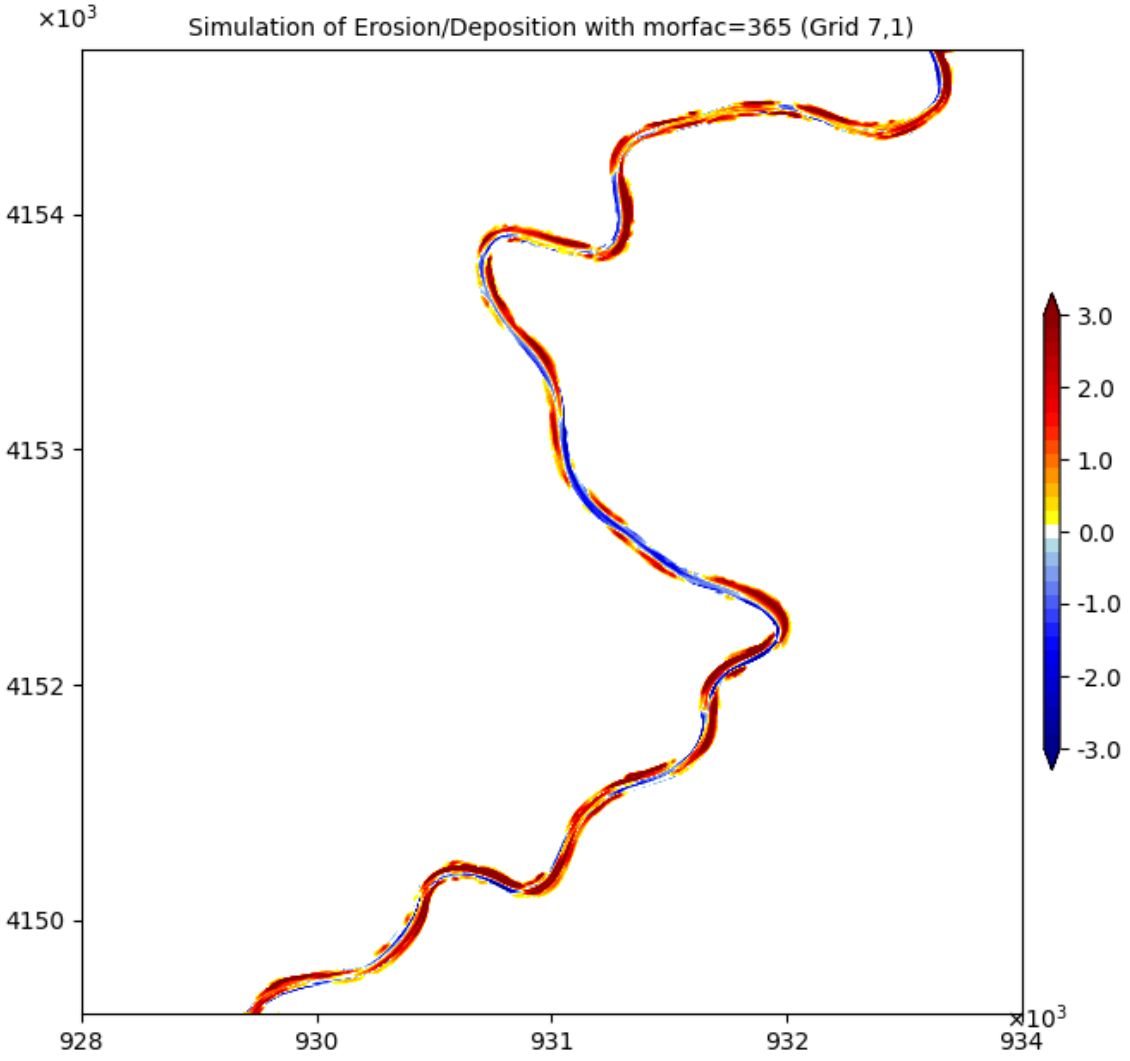
Simulation of Erosion/Deposition with morfac=365 (Grid 7,1)
×10^3
4154
4153
4152
4150
928
930
931
932
934
×10^3
3.0
2.0
1.0
0.0
-1.0
-2.0
-3.0

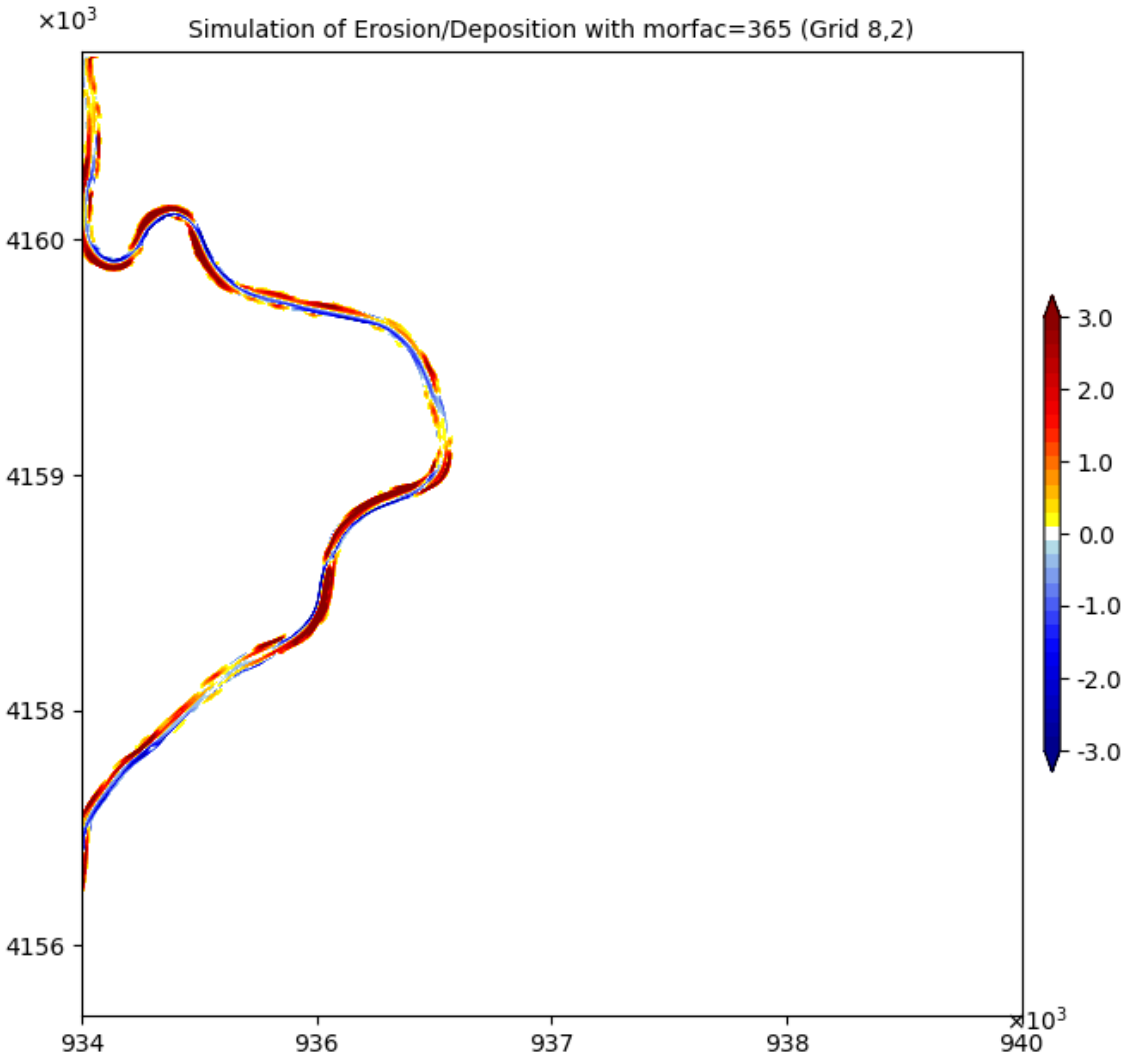
×10^3
Simulation of Erosion/Deposition with morfac=365 (Grid 8,2)
4160
4159
4158
4156
934
936
937
938
940
×10^3
3.0
2.0
1.0
0.0
-1.0
-2.0
-3.0

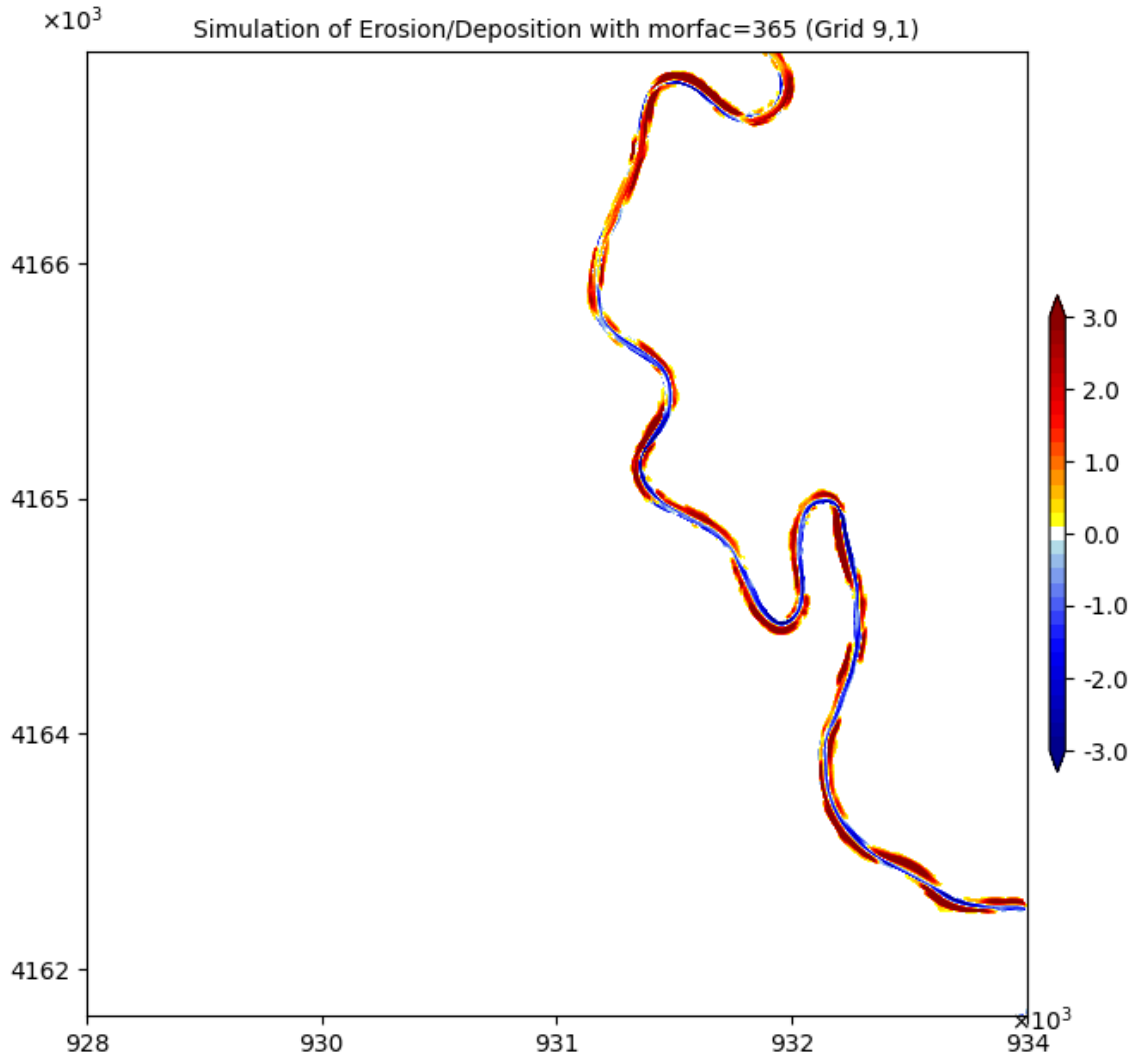
Simulation of Erosion/Deposition with morfac=365 (Grid 9,1)
×10^3
4166
4165
4164
4162
928
930
931
932
934
×10^3
3.0
2.0
1.0
0.0
-1.0
-2.0
-3.0

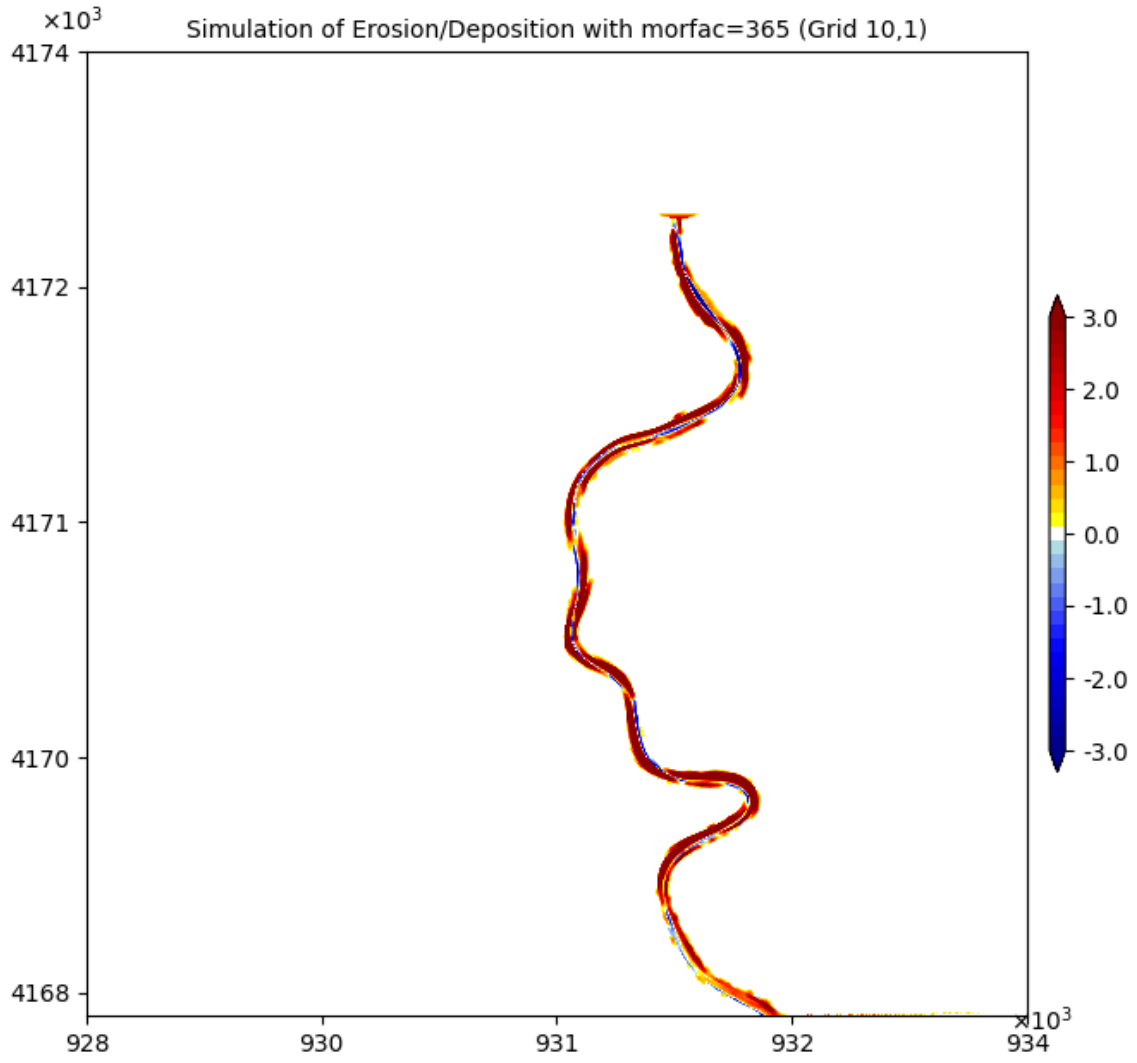
Simulation of Erosion/Deposition with morfac=365 (Grid 10,1)
×10^3
4174
4172
4171
4170
4168
928
930
931
932
934
×10^3
3.0
2.0
1.0
0.0
-1.0
-2.0
-3.0

APPENDIX E: erosion/sedimentation of colorad with morfac=365 (mud)

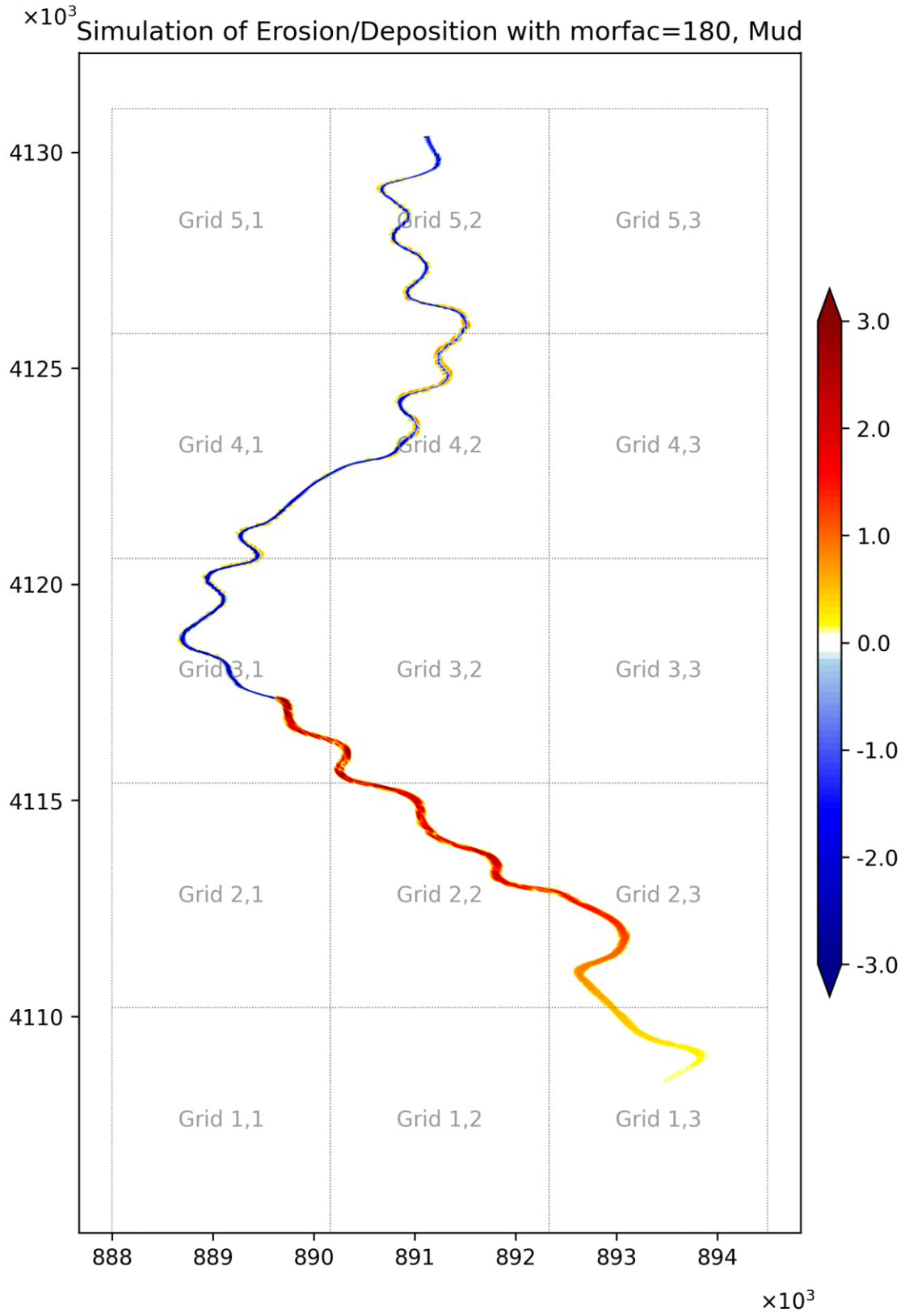

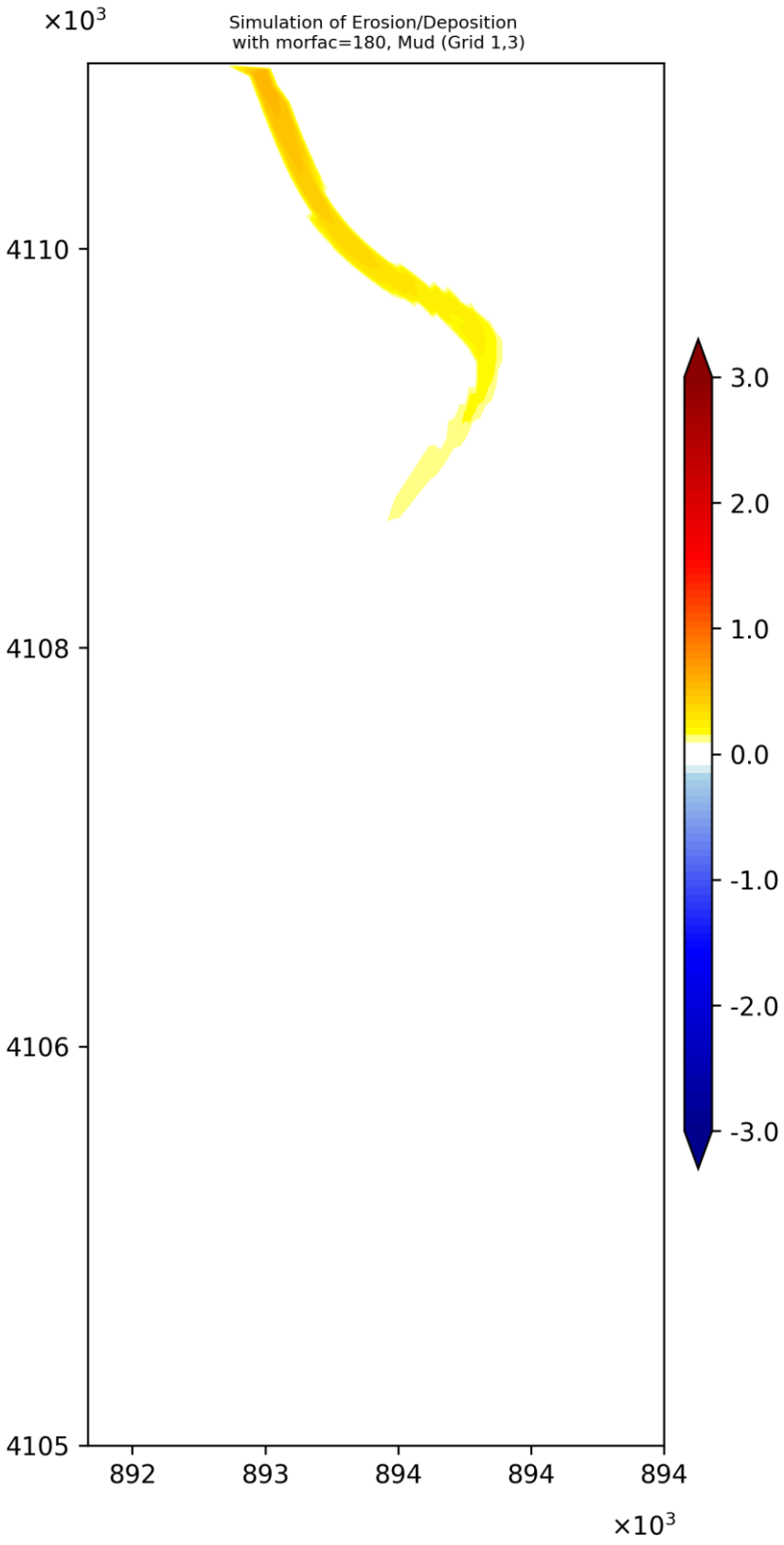
×10^3
Simulation of Erosion/Deposition
with morfac=180, Mud (Grid 1,3)
4110
4108
4106
4105
892
893
894
894
894
×10^3
3.0
2.0
1.0
0.0
-1.0
-2.0
-3.0

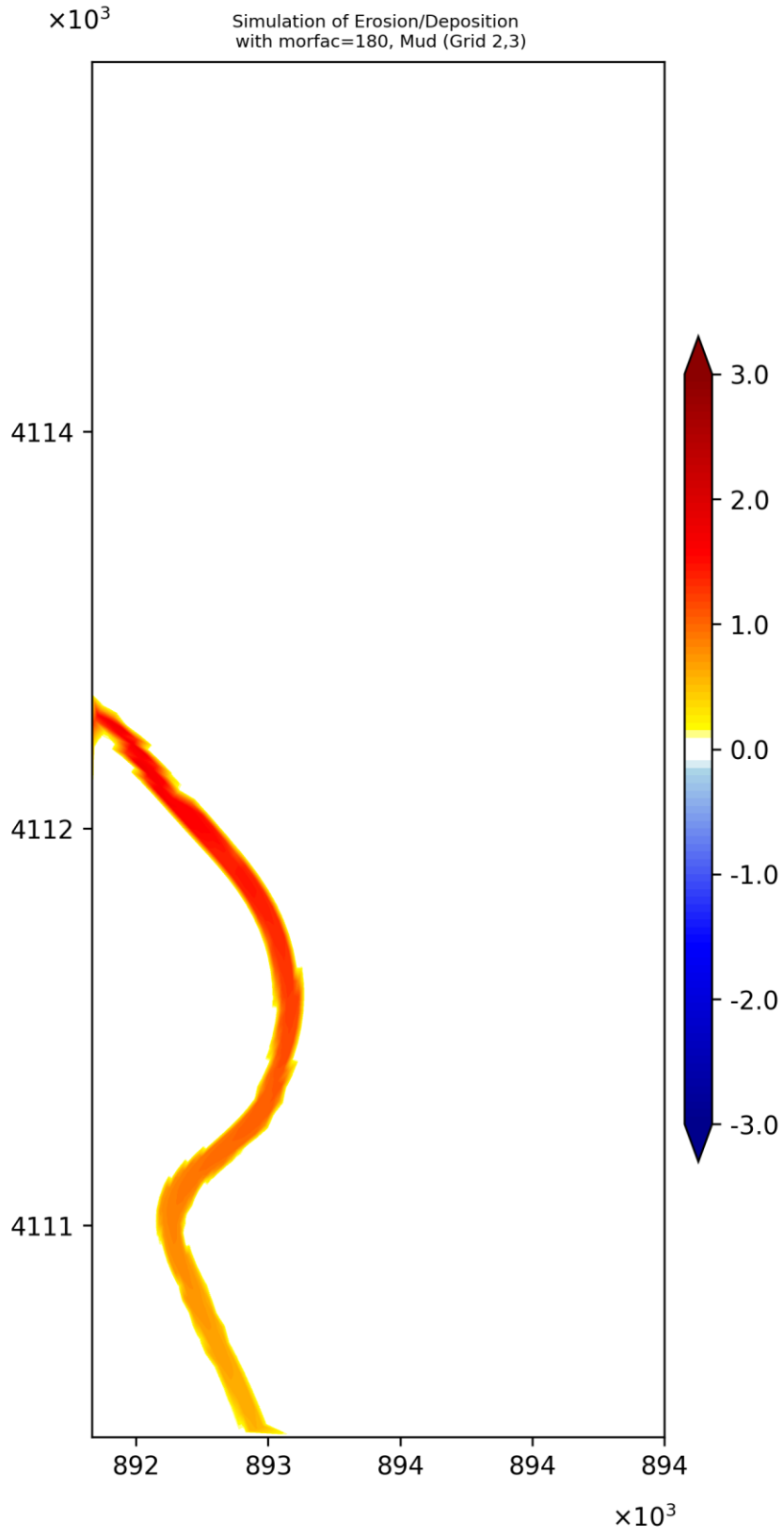
×10^3
Simulation of Erosion/Deposition
with morfac=180, Mud (Grid 2,3)
4114
4112
4111
892
893
894
894
894
×10^3
3.0
2.0
1.0
0.0
-1.0
-2.0
-3.0

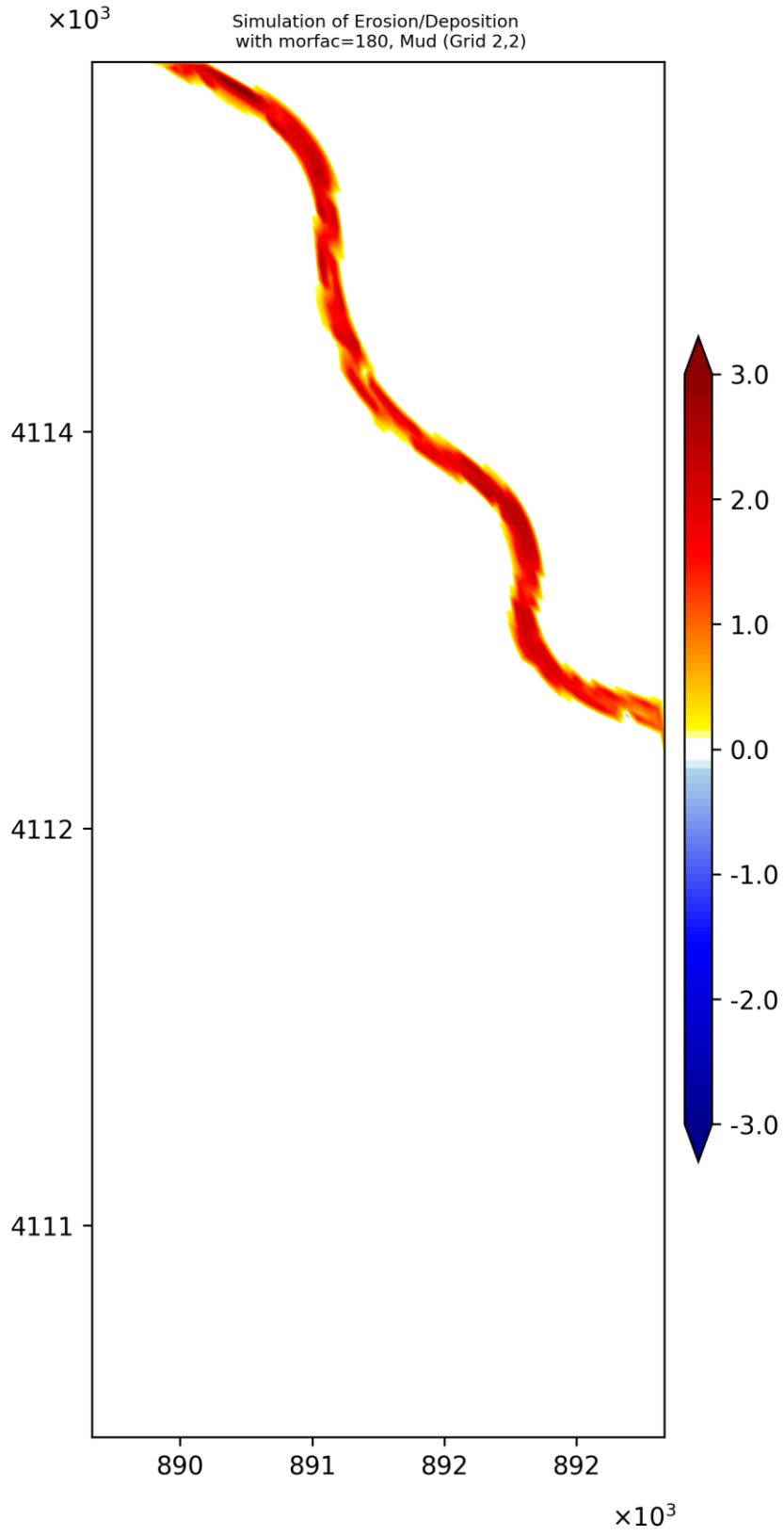
×10^3
Simulation of Erosion/Deposition
with morfac=180, Mud (Grid 2,2)
4114
4112
4111
890
891
892
892
×10^3
3.0
2.0
1.0
0.0
-1.0
-2.0
-3.0

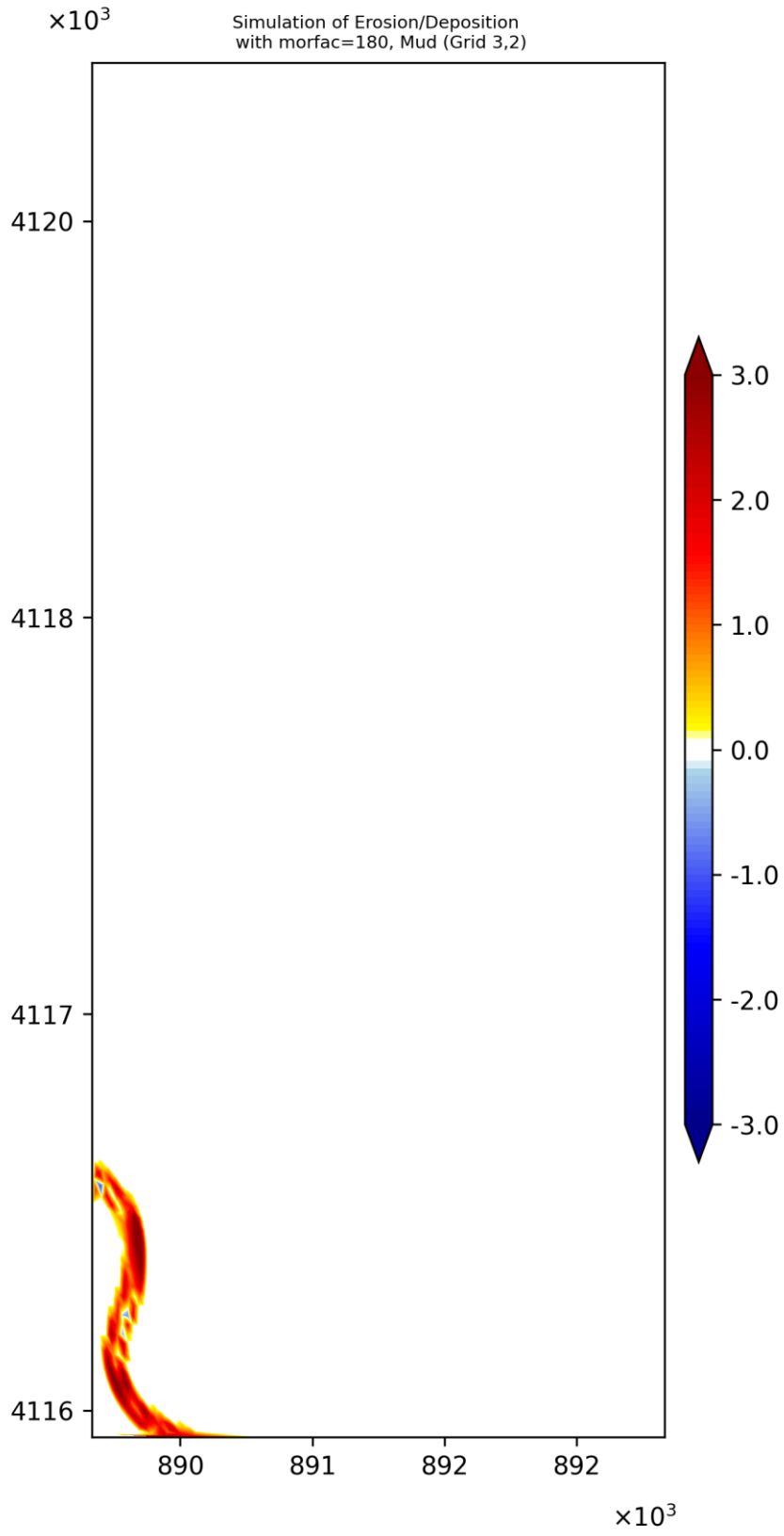
×10^3
Simulation of Erosion/Deposition
with morfac=180, Mud (Grid 3,2)
4120
4118
4117
4116
890
891
892
892
×10^3
3.0
2.0
1.0
0.0
-1.0
-2.0
-3.0

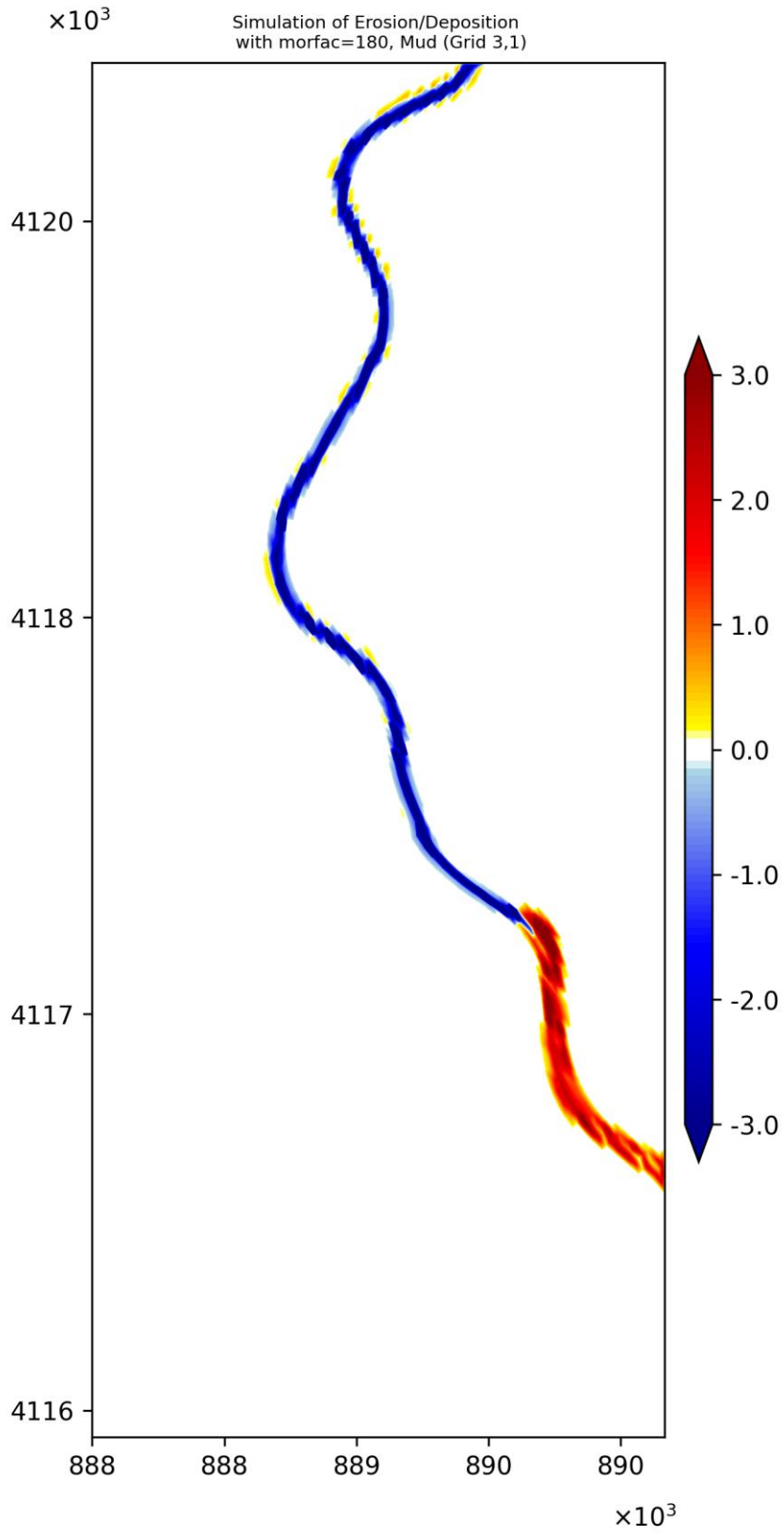
×10^3
Simulation of Erosion/Deposition
with morfac=180, Mud (Grid 3,1)
4120
4118
4117
4116
888
888
889
890
890
×10^3
3.0
2.0
1.0
0.0
-1.0
-2.0
-3.0

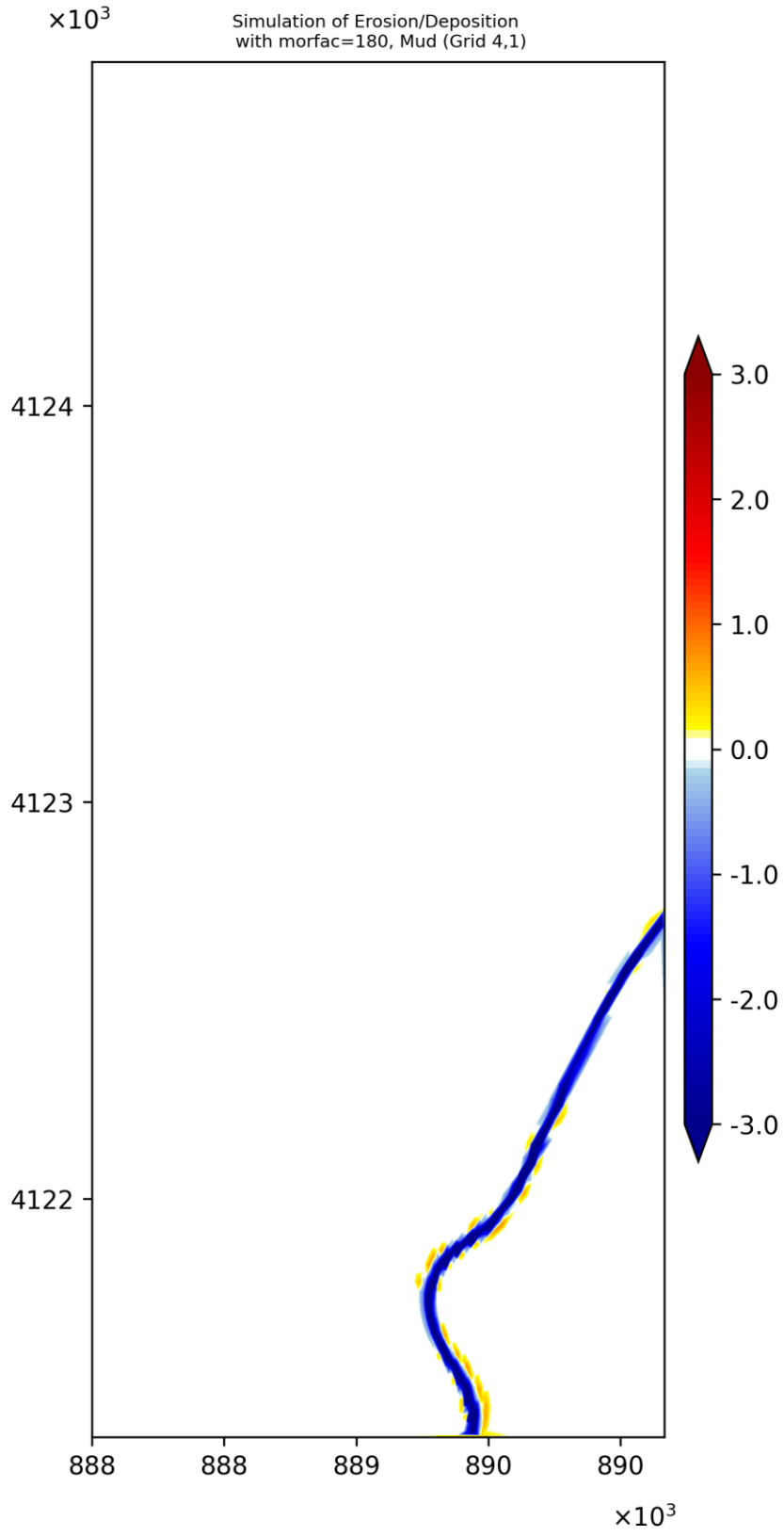
×10^3
Simulation of Erosion/Deposition
with morfac=180, Mud (Grid 4,1)
4124
4123
4122
888
888
889
890
890
×10^3
3.0
2.0
1.0
0.0
-1.0
-2.0
-3.0

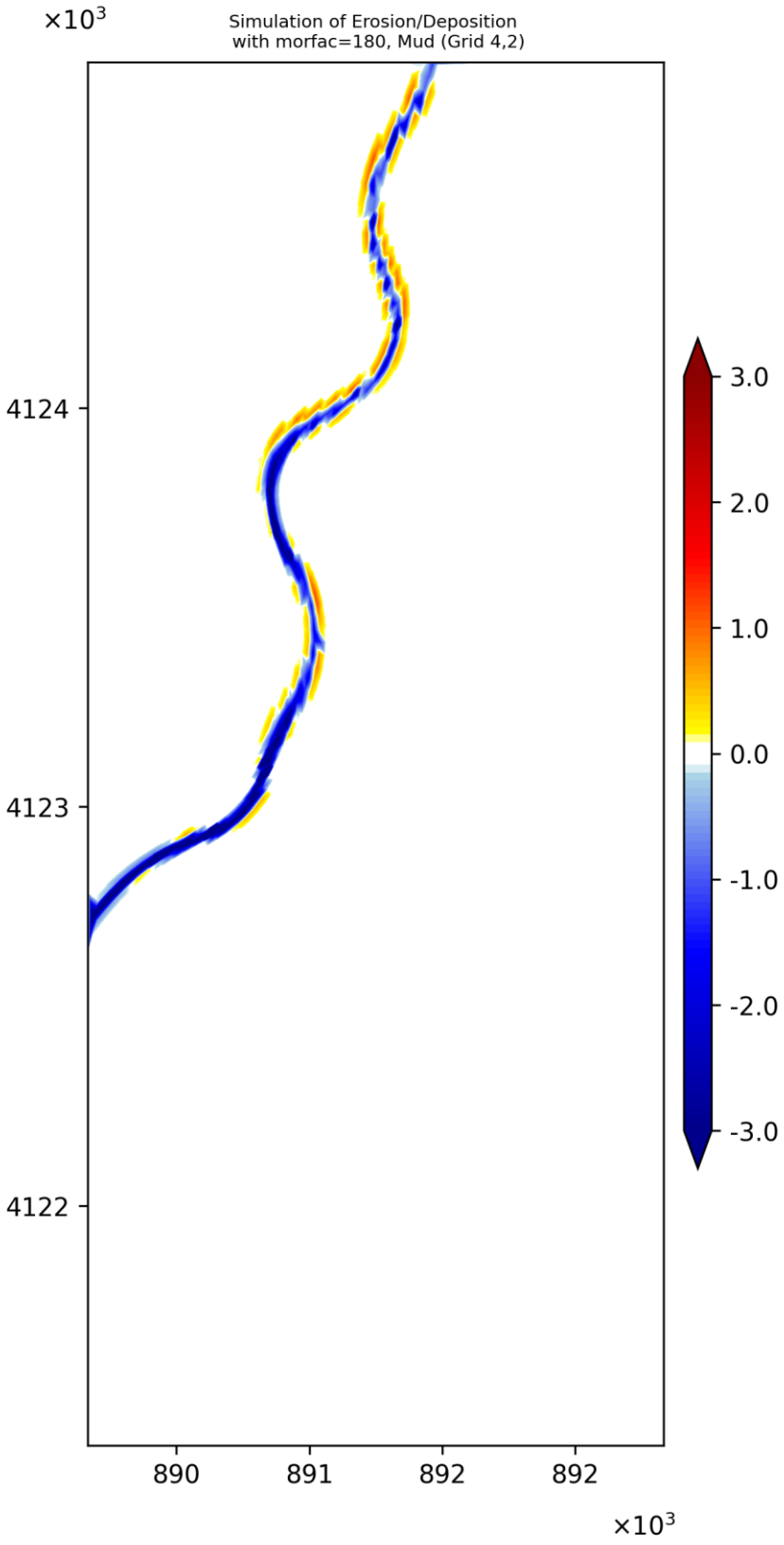
×10^3
Simulation of Erosion/Deposition
with morfac=180, Mud (Grid 4,2)
4124
4123
4122
890
891
892
892
×10^3
3.0
2.0
1.0
0.0
-1.0
-2.0
-3.0

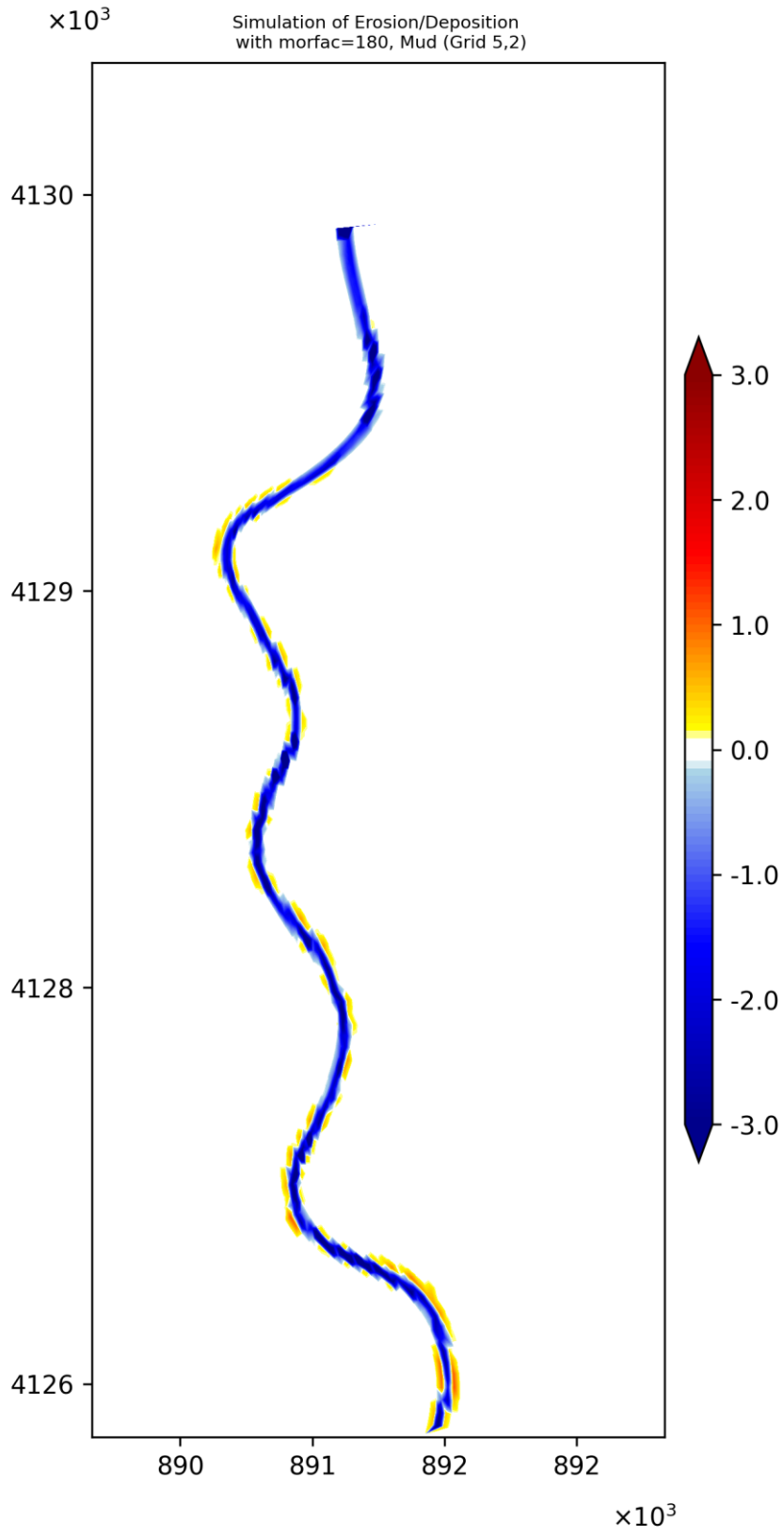
×10^3
Simulation of Erosion/Deposition
with morfac=180, Mud (Grid 5,2)
4130
4129
4128
4126
890
891
892
892
×10^3
3.0
2.0
1.0
0.0
-1.0
-2.0
-3.0

APPENDIX F: THE EFFECT OF SEA LEVEL RISE IN BRAZOS DOMAIN

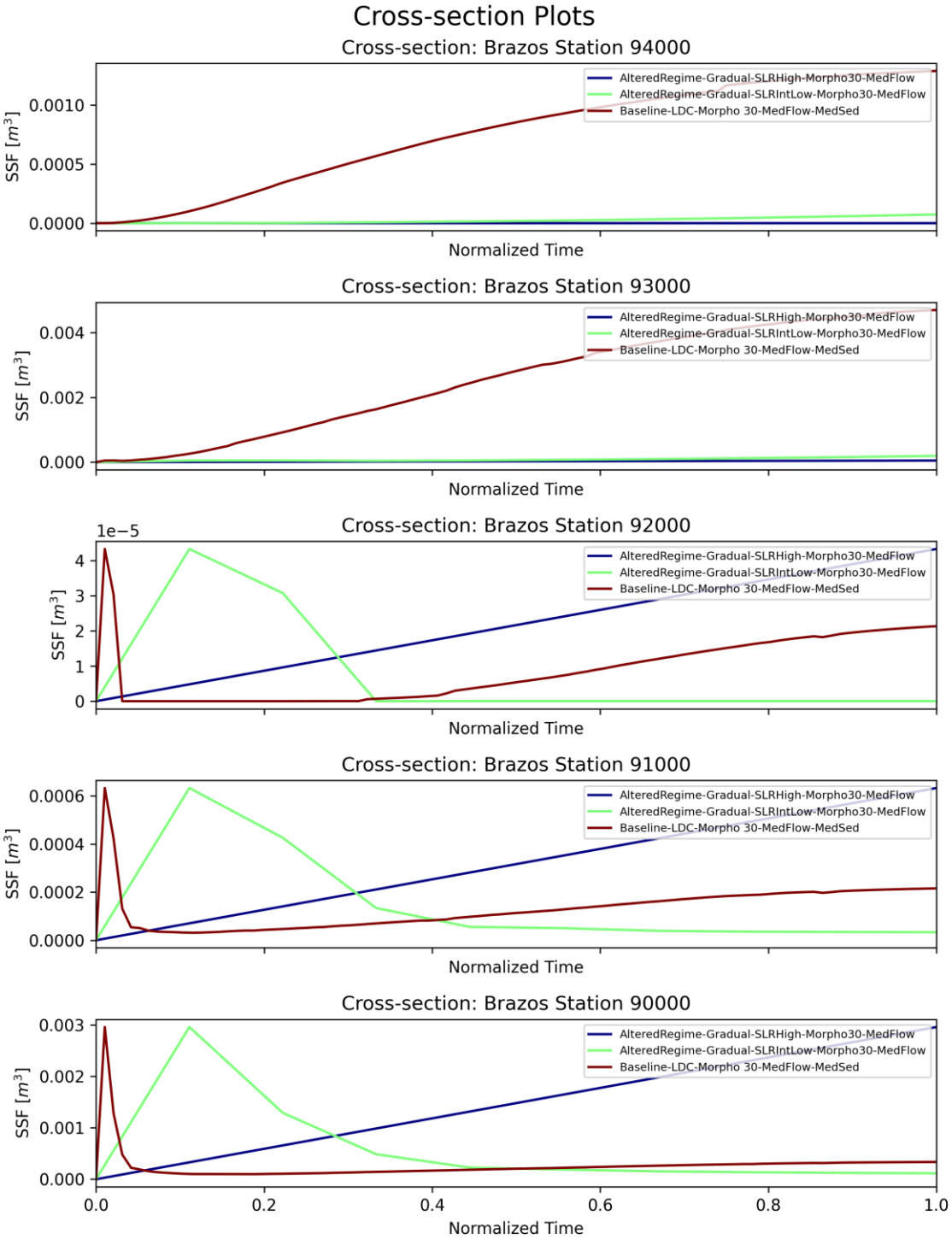
Cross-section Plots
Cross-section: Brazos Station 94000
AlteredRegime-Gradual-SLRHigh-Morpho30-MedFlow
AlteredRegime-Gradual-SLRIntLow-Morpho30-MedFlow
Baseline-LDC-Morpho 30-MedFlow-MedSed
SSF [m^3]
0.0000
0.0005
0.0010
Normalized Time
Cross-section: Brazos Station 93000
AlteredRegime-Gradual-SLRHigh-Morpho30-MedFlow
AlteredRegime-Gradual-SLRIntLow-Morpho30-MedFlow
Baseline-LDC-Morpho 30-MedFlow-MedSed
SSF [m^3]
0.000
0.002
0.004
Normalized Time
Cross-section: Brazos Station 92000
1e−5
AlteredRegime-Gradual-SLRHigh-Morpho30-MedFlow
AlteredRegime-Gradual-SLRIntLow-Morpho30-MedFlow
Baseline-LDC-Morpho 30-MedFlow-MedSed
SSF [m^3]
0
1
2
3
4
Normalized Time
Cross-section: Brazos Station 91000
AlteredRegime-Gradual-SLRHigh-Morpho30-MedFlow
AlteredRegime-Gradual-SLRIntLow-Morpho30-MedFlow
Baseline-LDC-Morpho 30-MedFlow-MedSed
SSF [m^3]
0.0000
0.0002
0.0004
0.0006
Normalized Time
Cross-section: Brazos Station 90000
AlteredRegime-Gradual-SLRHigh-Morpho30-MedFlow
AlteredRegime-Gradual-SLRIntLow-Morpho30-MedFlow
Baseline-LDC-Morpho 30-MedFlow-MedSed
SSF [m^3]
0.000
0.001
0.002
0.003
0.0
0.2
0.4
0.6
0.8
1.0
Normalized Time

APPENDIX G: THE EFFECT OF SEA LEVEL RISE IN COLORADO DOMAIN

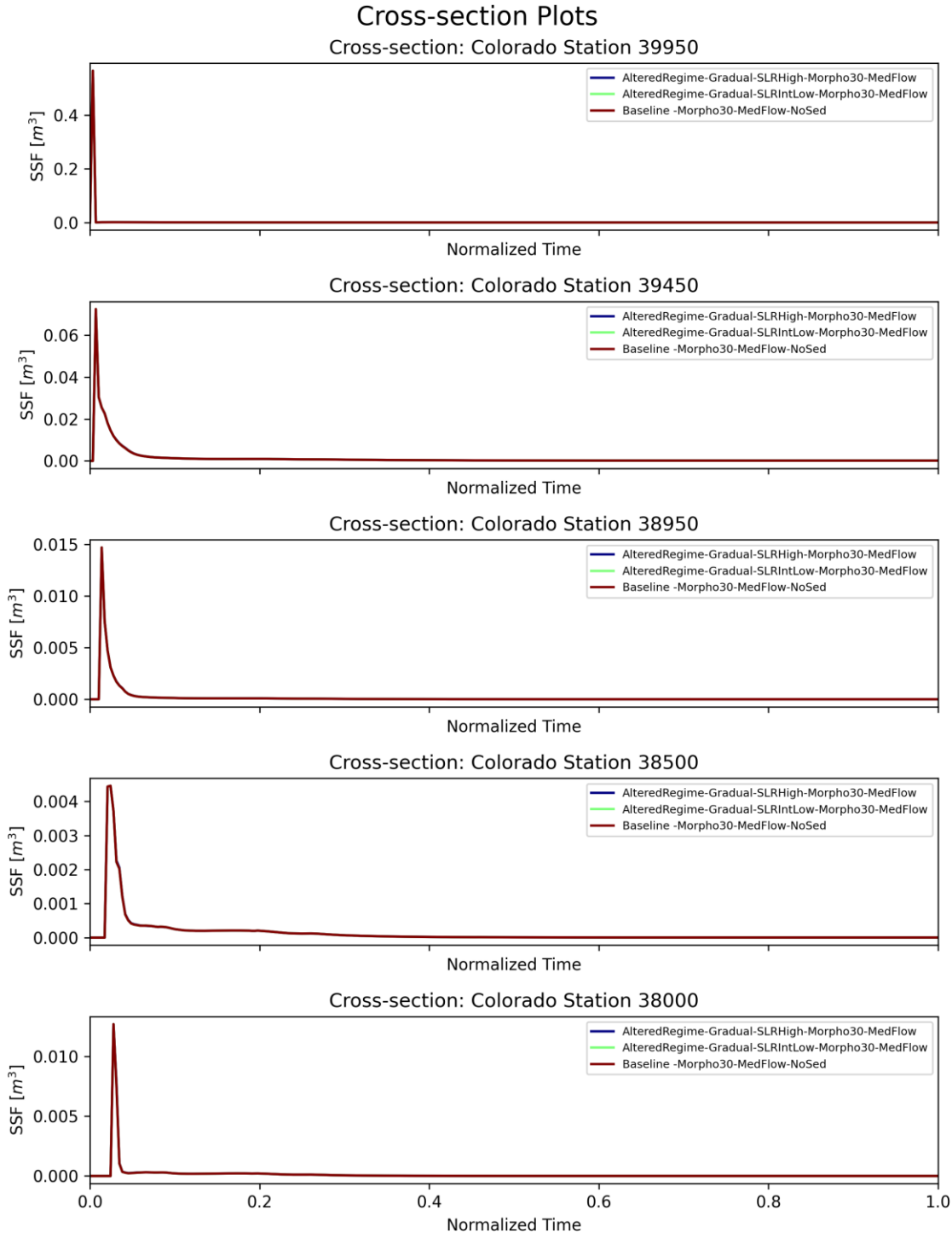
Cross-section Plots
Cross-section: Colorado Station 39950
AlteredRegime-Gradual-SLRHigh-Morpho30-MedFlow
AlteredRegime-Gradual-SLRIntLow-Morpho30-MedFlow
Baseline -Morpho30-MedFlow-NoSed
SSF [m^3]
0.0
0.2
0.4
Normalized Time
Cross-section: Colorado Station 39450
AlteredRegime-Gradual-SLRHigh-Morpho30-MedFlow
AlteredRegime-Gradual-SLRIntLow-Morpho30-MedFlow
Baseline -Morpho30-MedFlow-NoSed
SSF [m^3]
0.00
0.02
0.04
0.06
Normalized Time
Cross-section: Colorado Station 38950
AlteredRegime-Gradual-SLRHigh-Morpho30-MedFlow
AlteredRegime-Gradual-SLRIntLow-Morpho30-MedFlow
Baseline -Morpho30-MedFlow-NoSed
SSF [m^3]
0.000
0.005
0.010
0.015
Normalized Time
Cross-section: Colorado Station 38500
AlteredRegime-Gradual-SLRHigh-Morpho30-MedFlow
AlteredRegime-Gradual-SLRIntLow-Morpho30-MedFlow
Baseline -Morpho30-MedFlow-NoSed
SSF [m^3]
0.000
0.001
0.002
0.003
0.004
Normalized Time
Cross-section: Colorado Station 38000
AlteredRegime-Gradual-SLRHigh-Morpho30-MedFlow
AlteredRegime-Gradual-SLRIntLow-Morpho30-MedFlow
Baseline -Morpho30-MedFlow-NoSed
SSF [m^3]
0.000
0.005
0.010
0.0
0.2
0.4
0.6
0.8
1.0
Normalized Time

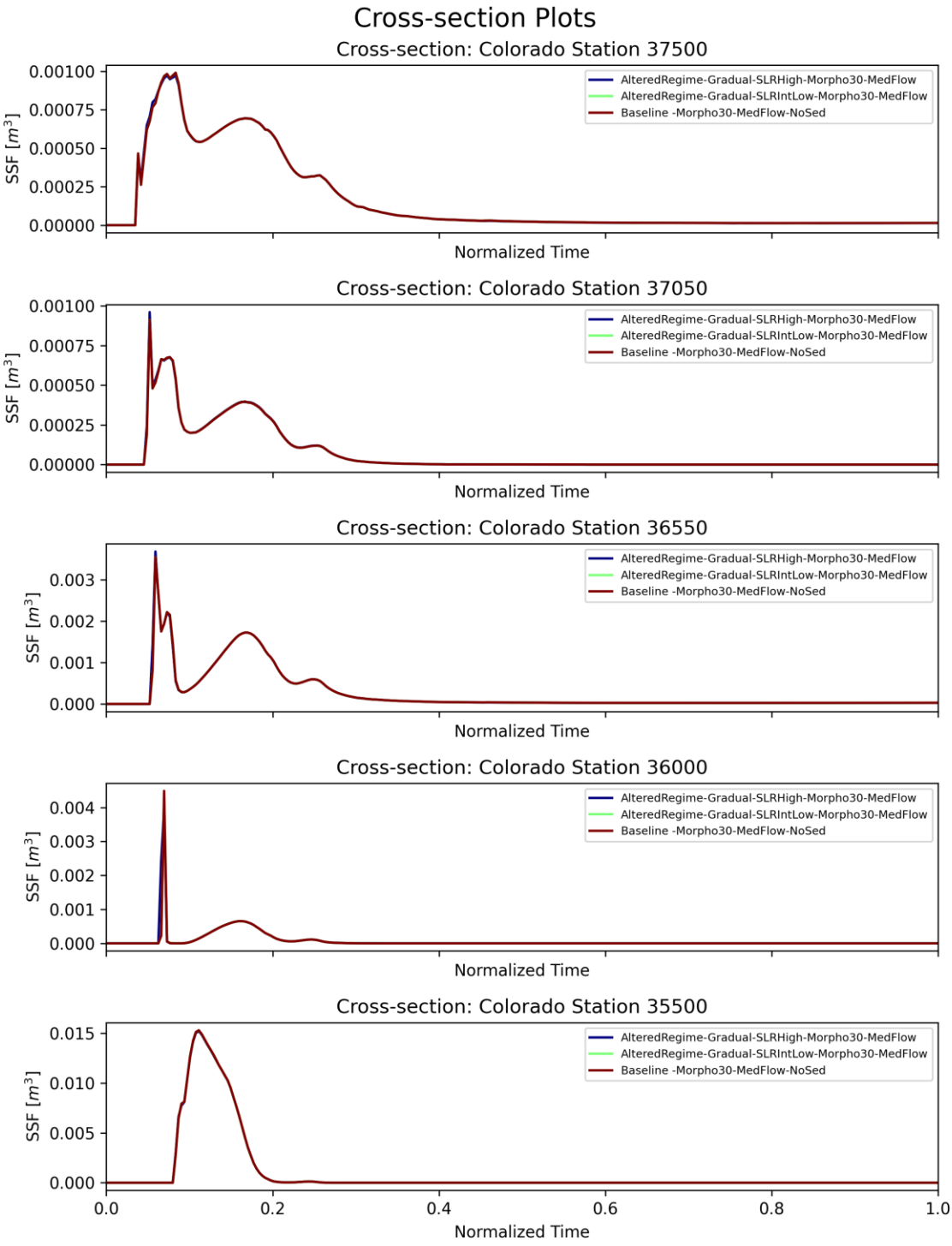
Cross-section Plots
Cross-section: Colorado Station 37500
Cross-section: Colorado Station 37050
Cross-section: Colorado Station 36550
Cross-section: Colorado Station 36000
Cross-section: Colorado Station 35500
AlteredRegime-Gradual-SLRHigh-Morpho30-MedFlow
AlteredRegime-Gradual-SLRIntLow-Morpho30-MedFlow
Baseline -Morpho30-MedFlow-NoSed
SSF [m^3]
Normalized Time

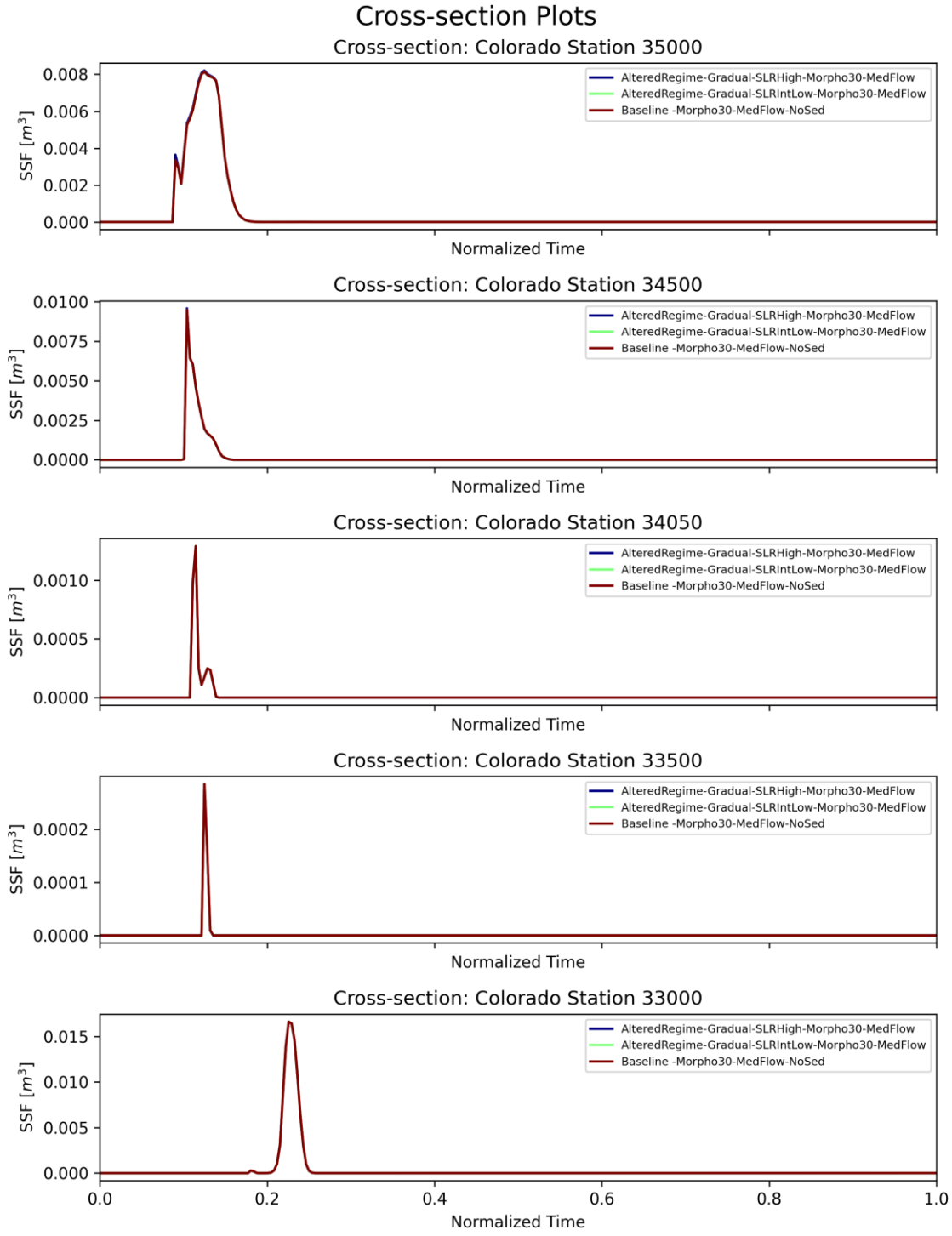
Cross-section Plots
Cross-section: Colorado Station 35000
Cross-section: Colorado Station 34500
Cross-section: Colorado Station 34050
Cross-section: Colorado Station 33500
Cross-section: Colorado Station 33000
AlteredRegime-Gradual-SLRHigh-Morpho30-MedFlow
AlteredRegime-Gradual-SLRIntLow-Morpho30-MedFlow
Baseline -Morpho30-MedFlow-NoSed
SSF [m^3]
Normalized Time

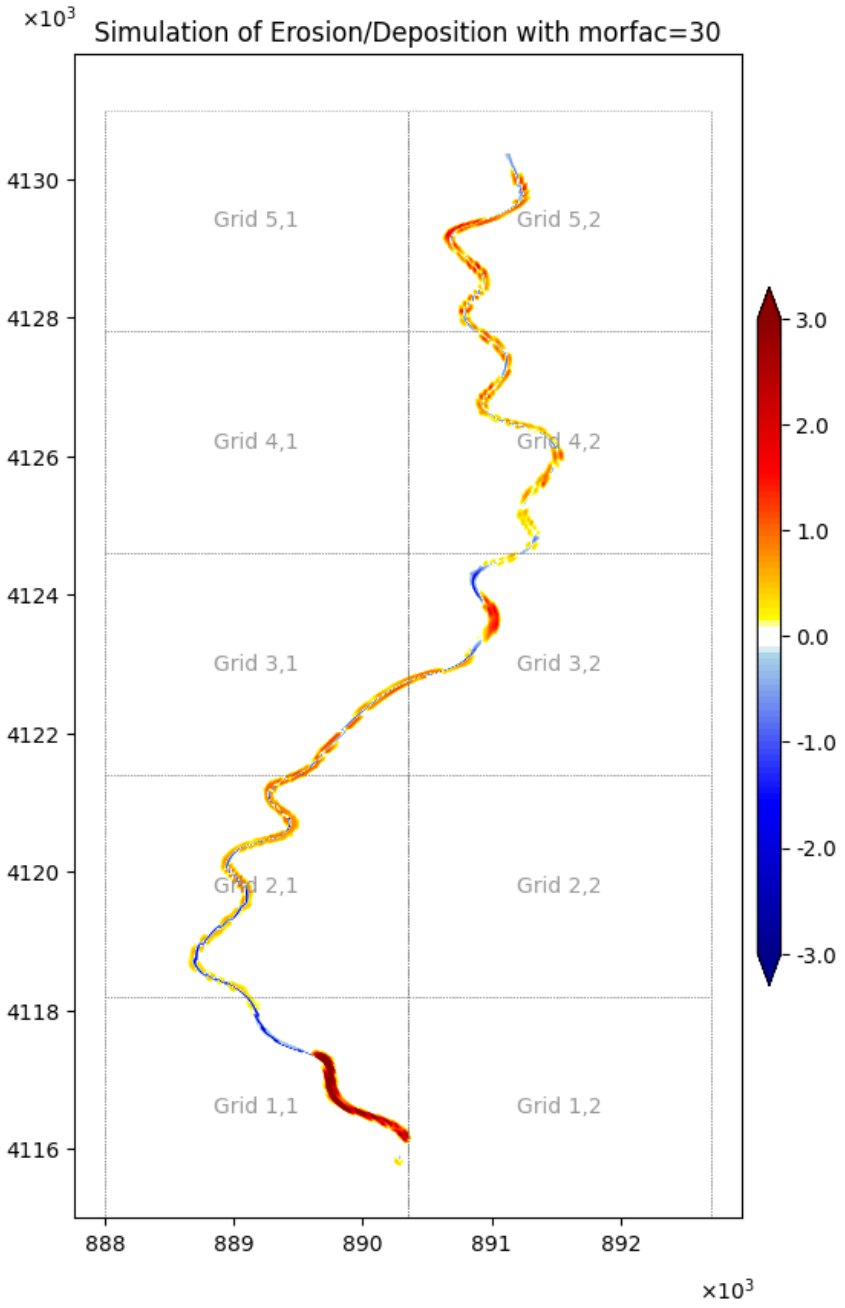
×10^3
Simulation of Erosion/Deposition with morfac=30
4130
4128
4126
4124
4122
4120
4118
4116
Grid 5,1
Grid 5,2
Grid 4,1
Grid 4,2
Grid 3,1
Grid 3,2
Grid 2,1
Grid 2,2
Grid 1,1
Grid 1,2
888
889
890
891
892
×10^3
3.0
2.0
1.0
0.0
-1.0
-2.0
-3.0

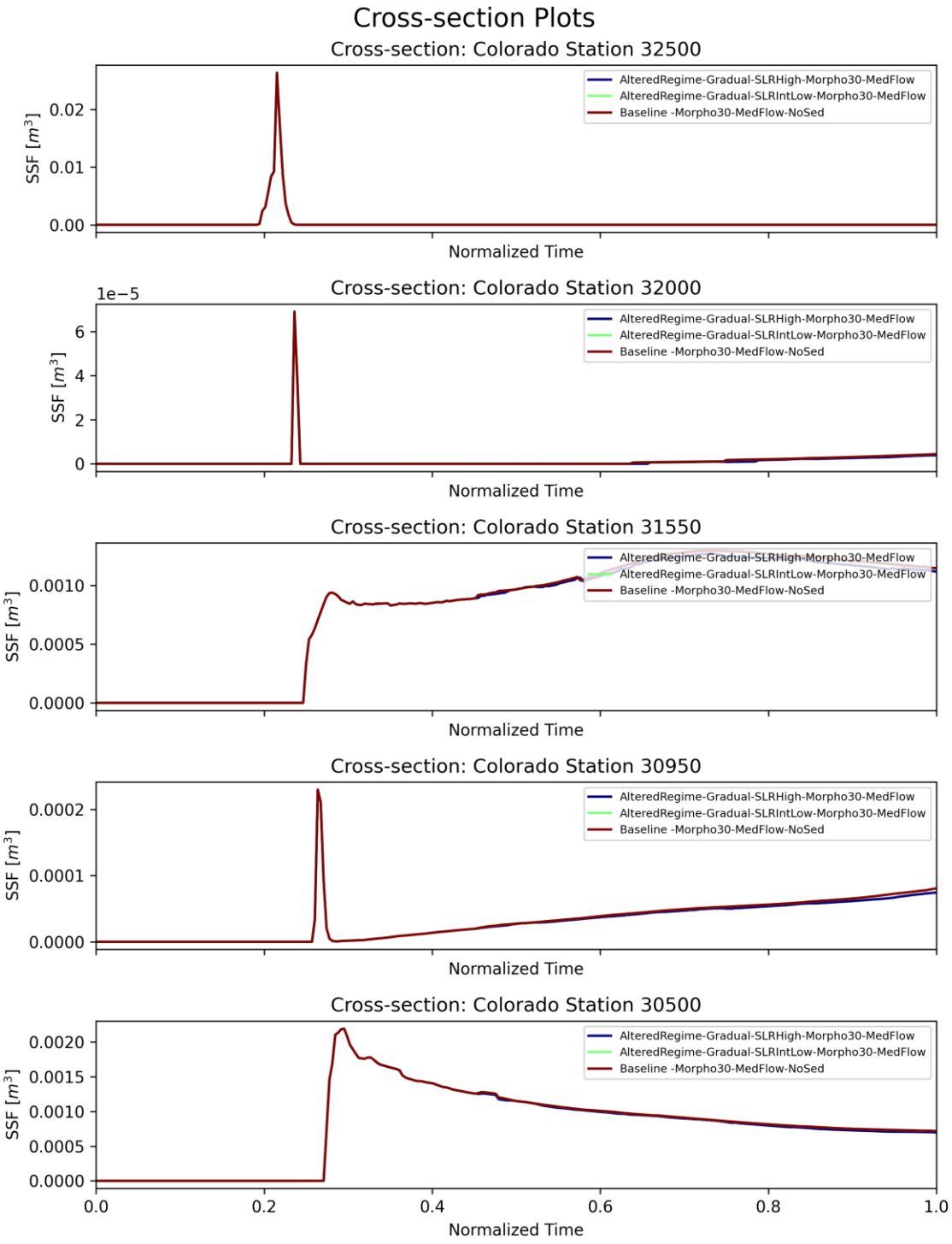
Cross-section Plots
Cross-section: Colorado Station 32500
AlteredRegime-Gradual-SLRHigh-Morpho30-MedFlow
AlteredRegime-Gradual-SLRIntLow-Morpho30-MedFlow
Baseline -Morpho30-MedFlow-NoSed
SSF [m^3]
0.02
0.01
0.00
Normalized Time
Cross-section: Colorado Station 32000
1e−5
6
4
2
0
Normalized Time
Cross-section: Colorado Station 31550
0.0010
0.0005
0.0000
Normalized Time
Cross-section: Colorado Station 30950
0.0002
0.0001
0.0000
Normalized Time
Cross-section: Colorado Station 30500
0.0020
0.0015
0.0010
0.0005
0.0000
0.0
0.2
0.4
0.6
0.8
1.0
Normalized Time

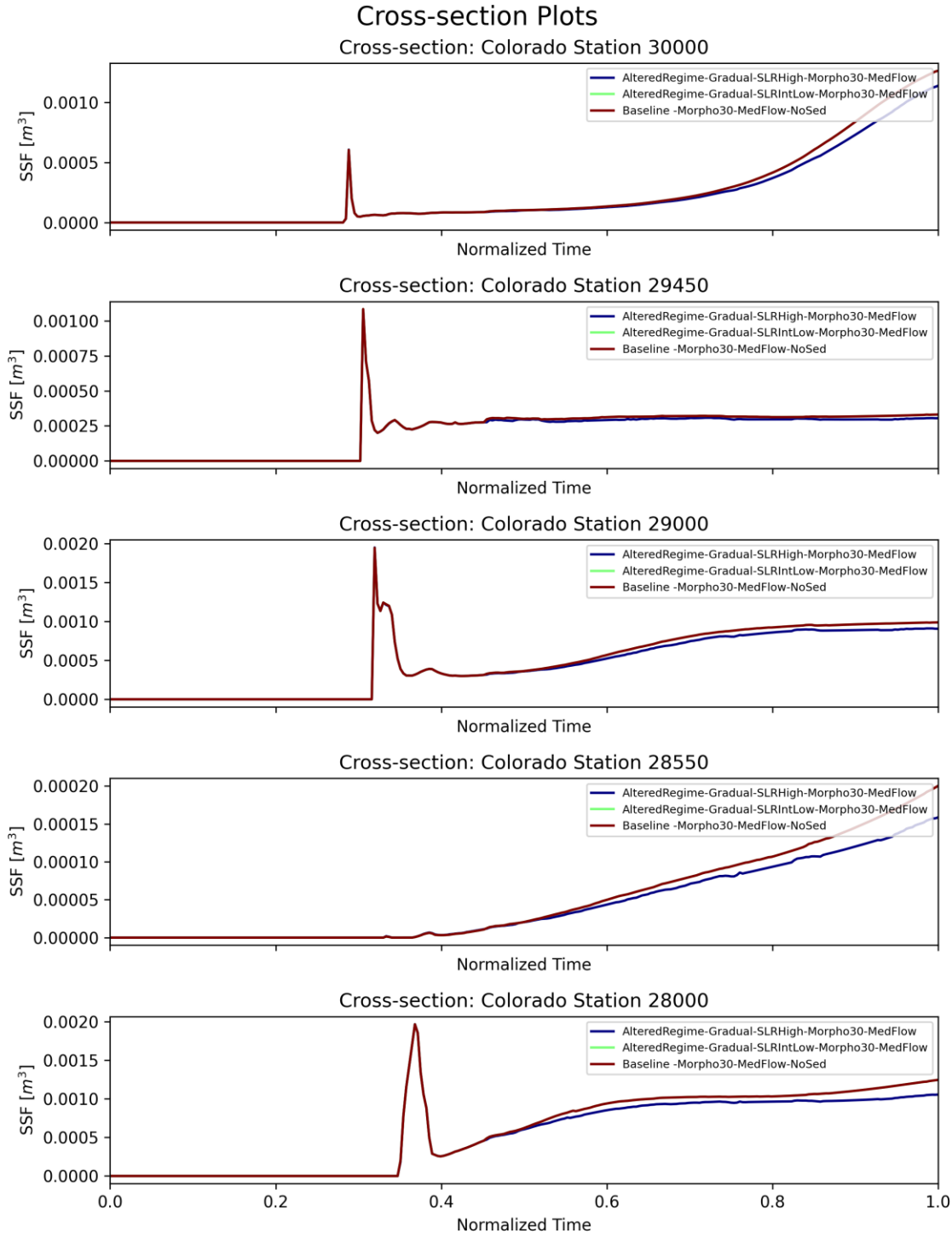
Cross-section Plots
Cross-section: Colorado Station 30000
AlteredRegime-Gradual-SLRHigh-Morpho30-MedFlow
AlteredRegime-Gradual-SLRIntLow-Morpho30-MedFlow
Baseline -Morpho30-MedFlow-NoSed
SSF [m^3]
0.0010
0.0005
0.0000
Normalized Time
Cross-section: Colorado Station 29450
AlteredRegime-Gradual-SLRHigh-Morpho30-MedFlow
AlteredRegime-Gradual-SLRIntLow-Morpho30-MedFlow
Baseline -Morpho30-MedFlow-NoSed
SSF [m^3]
0.00100
0.00075
0.00050
0.00025
0.00000
Normalized Time
Cross-section: Colorado Station 29000
AlteredRegime-Gradual-SLRHigh-Morpho30-MedFlow
AlteredRegime-Gradual-SLRIntLow-Morpho30-MedFlow
Baseline -Morpho30-MedFlow-NoSed
SSF [m^3]
0.0020
0.0015
0.0010
0.0005
0.0000
Normalized Time
Cross-section: Colorado Station 28550
AlteredRegime-Gradual-SLRHigh-Morpho30-MedFlow
AlteredRegime-Gradual-SLRIntLow-Morpho30-MedFlow
Baseline -Morpho30-MedFlow-NoSed
SSF [m^3]
0.00020
0.00015
0.00010
0.00005
0.00000
Normalized Time
Cross-section: Colorado Station 28000
AlteredRegime-Gradual-SLRHigh-Morpho30-MedFlow
AlteredRegime-Gradual-SLRIntLow-Morpho30-MedFlow
Baseline -Morpho30-MedFlow-NoSed
SSF [m^3]
0.0020
0.0015
0.0010
0.0005
0.0000
0.0
0.2
0.4
0.6
0.8
1.0
Normalized Time

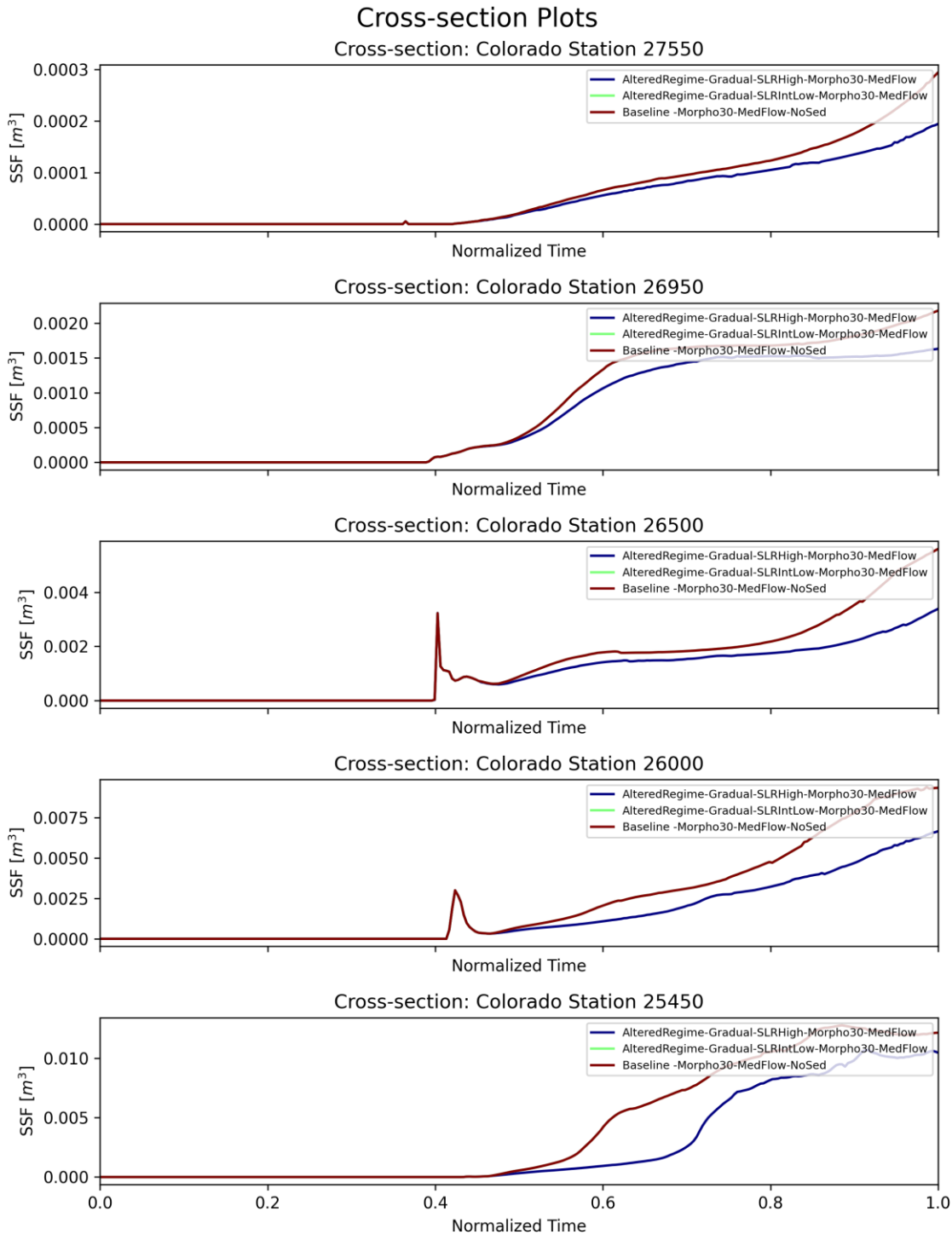
Cross-section Plots
Cross-section: Colorado Station 27550
Cross-section: Colorado Station 26950
Cross-section: Colorado Station 26500
Cross-section: Colorado Station 26000
Cross-section: Colorado Station 25450
AlteredRegime-Gradual-SLRHigh-Morpho30-MedFlow
AlteredRegime-Gradual-SLRIntLow-Morpho30-MedFlow
Baseline -Morpho30-MedFlow-NoSed
SSF [m^3]
Normalized Time

APPENDIX H: THE EFFECT OF SPATIALLY VARIABLE LDC

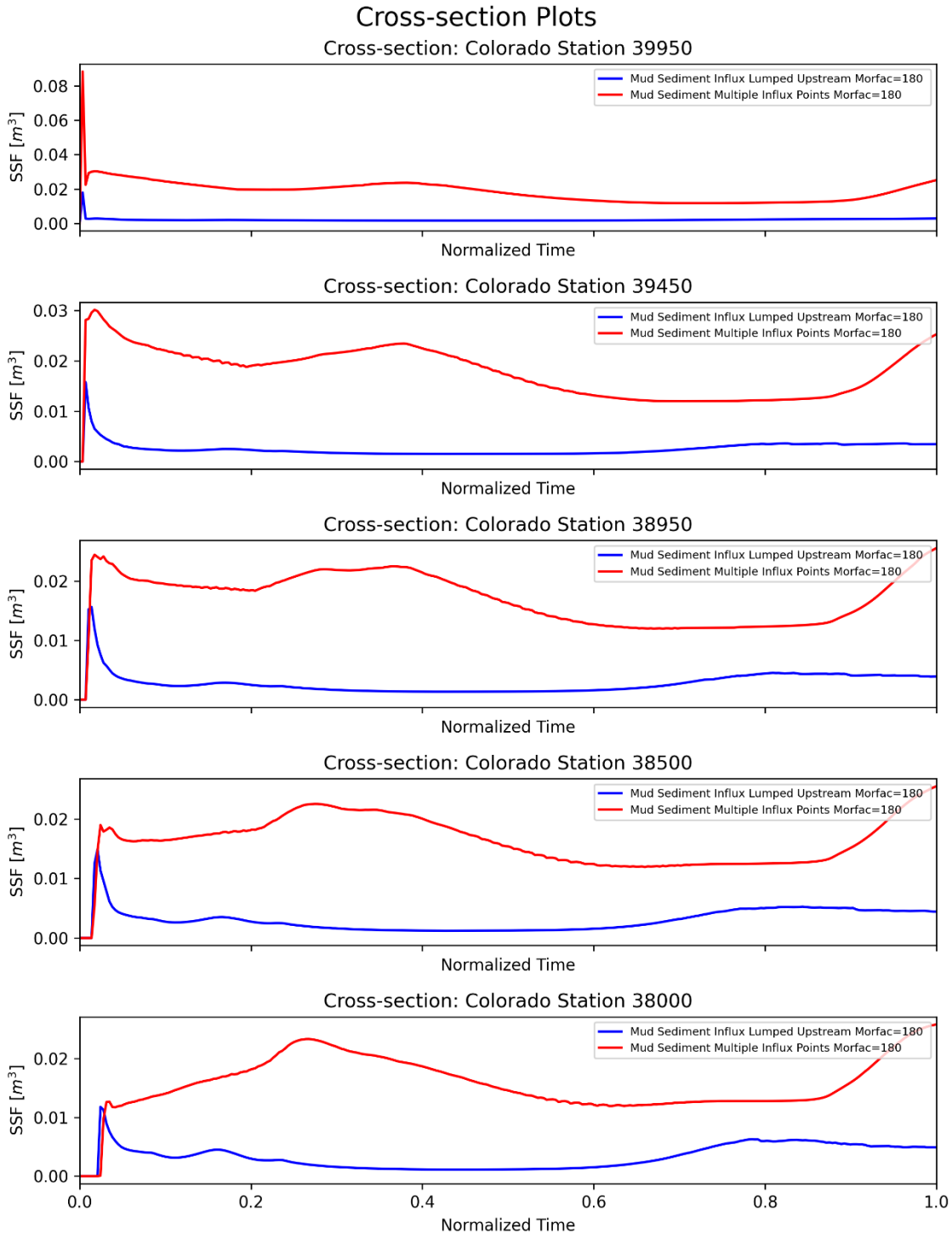
Cross-section Plots
Cross-section: Colorado Station 39950
Mud Sediment Influx Lumped Upstream Morfac=180
Mud Sediment Multiple Influx Points Morfac=180
SSF [m^3]
0.00
0.02
0.04
0.06
0.08
Normalized Time
Cross-section: Colorado Station 39450
Mud Sediment Influx Lumped Upstream Morfac=180
Mud Sediment Multiple Influx Points Morfac=180
SSF [m^3]
0.00
0.01
0.02
0.03
Normalized Time
Cross-section: Colorado Station 38950
Mud Sediment Influx Lumped Upstream Morfac=180
Mud Sediment Multiple Influx Points Morfac=180
SSF [m^3]
0.00
0.01
0.02
Normalized Time
Cross-section: Colorado Station 38500
Mud Sediment Influx Lumped Upstream Morfac=180
Mud Sediment Multiple Influx Points Morfac=180
SSF [m^3]
0.00
0.01
0.02
Normalized Time
Cross-section: Colorado Station 38000
Mud Sediment Influx Lumped Upstream Morfac=180
Mud Sediment Multiple Influx Points Morfac=180
SSF [m^3]
0.00
0.01
0.02
0.0
0.2
0.4
0.6
0.8
1.0
Normalized Time

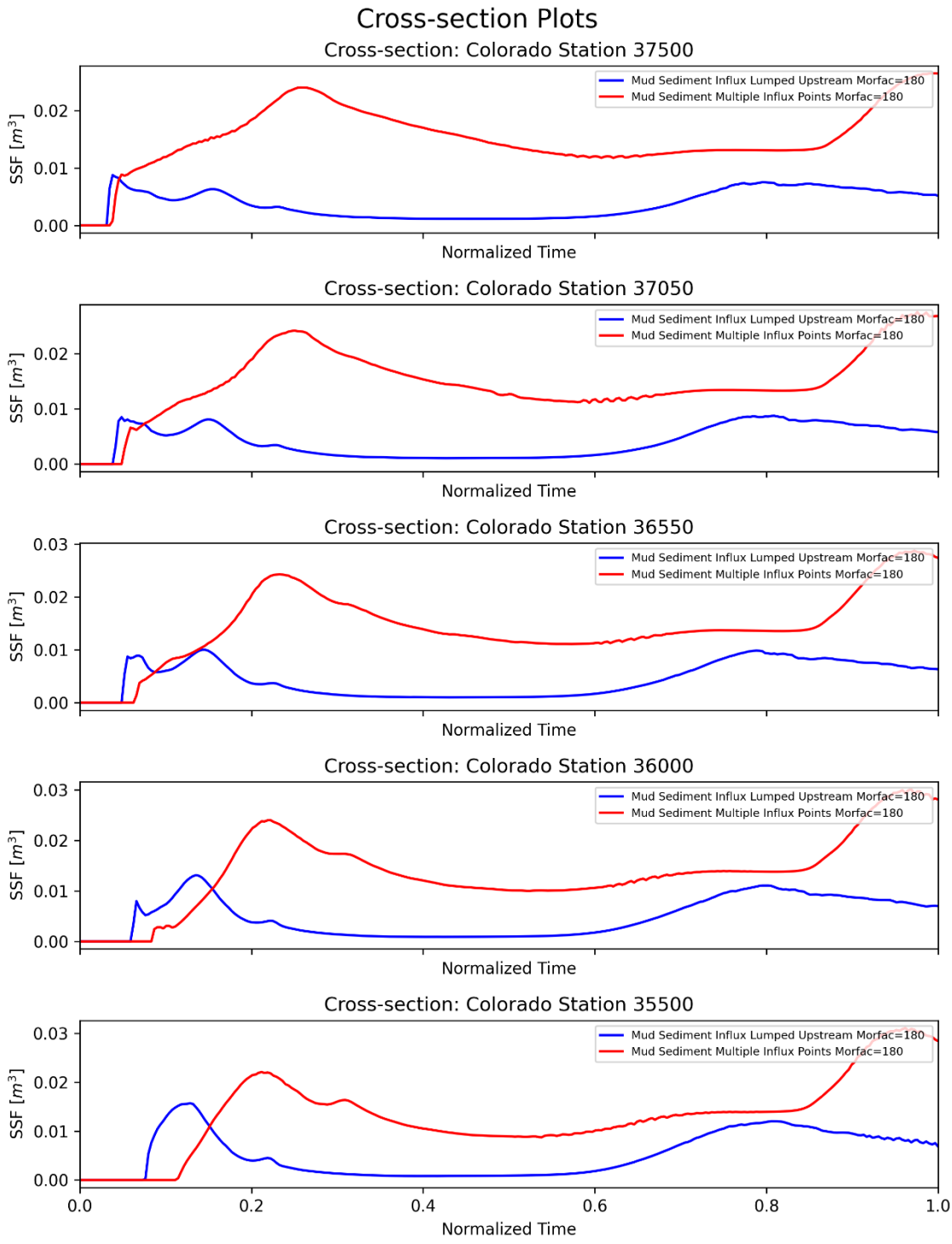
Cross-section Plots
Cross-section: Colorado Station 37500
Cross-section: Colorado Station 37050
Cross-section: Colorado Station 36550
Cross-section: Colorado Station 36000
Cross-section: Colorado Station 35500
Mud Sediment Influx Lumped Upstream Morfac=180
Mud Sediment Multiple Influx Points Morfac=180
SSF [m^3]
Normalized Time
0.00
0.01
0.02
0.03
0.0
0.2
0.4
0.6
0.8
1.0

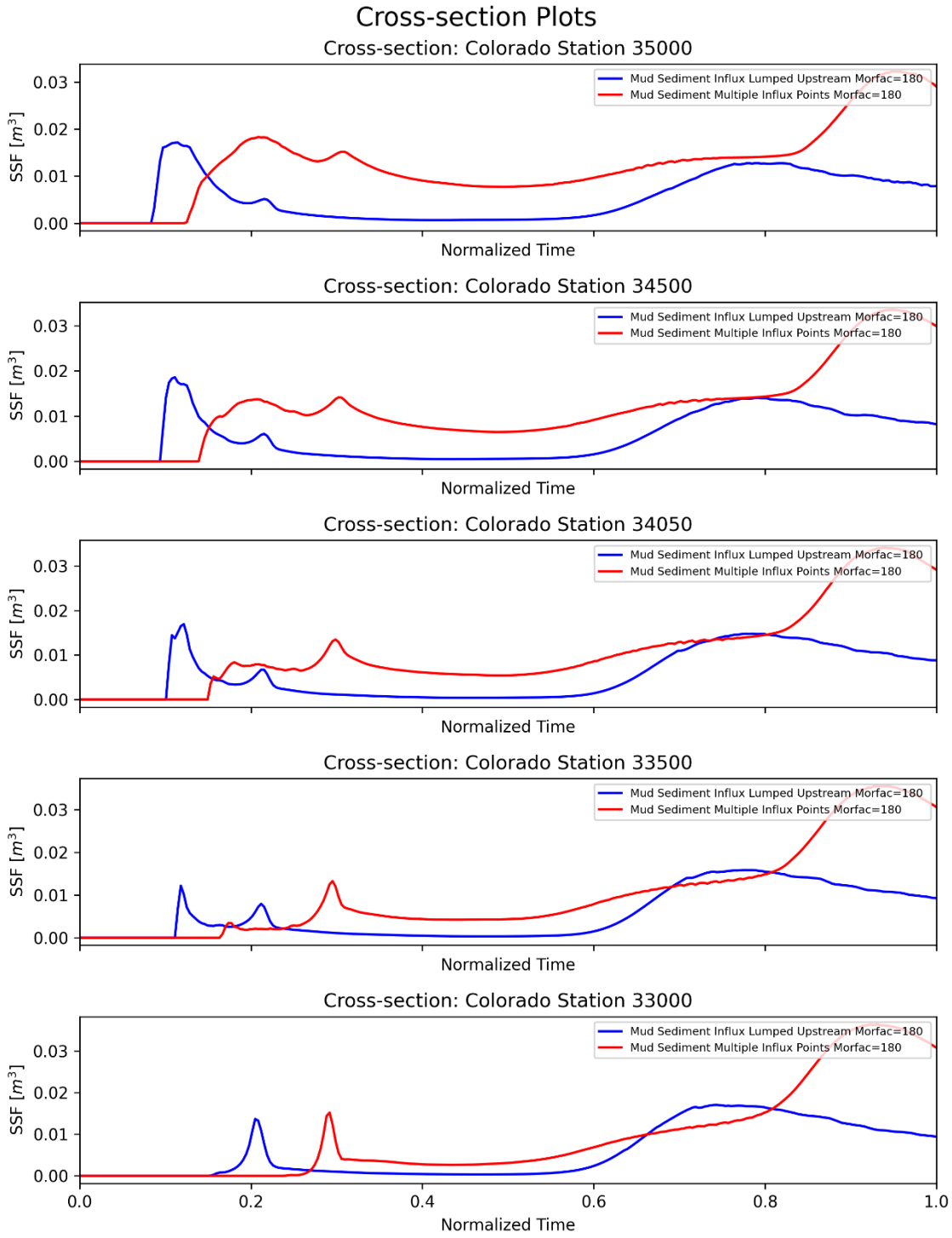
Cross-section Plots
Cross-section: Colorado Station 35000
Cross-section: Colorado Station 34500
Cross-section: Colorado Station 34050
Cross-section: Colorado Station 33500
Cross-section: Colorado Station 33000
Mud Sediment Influx Lumped Upstream Morfac=180
Mud Sediment Multiple Influx Points Morfac=180
SSF [m^3]
0.00
0.01
0.02
0.03
0.0
0.2
0.4
0.6
0.8
1.0
Normalized Time

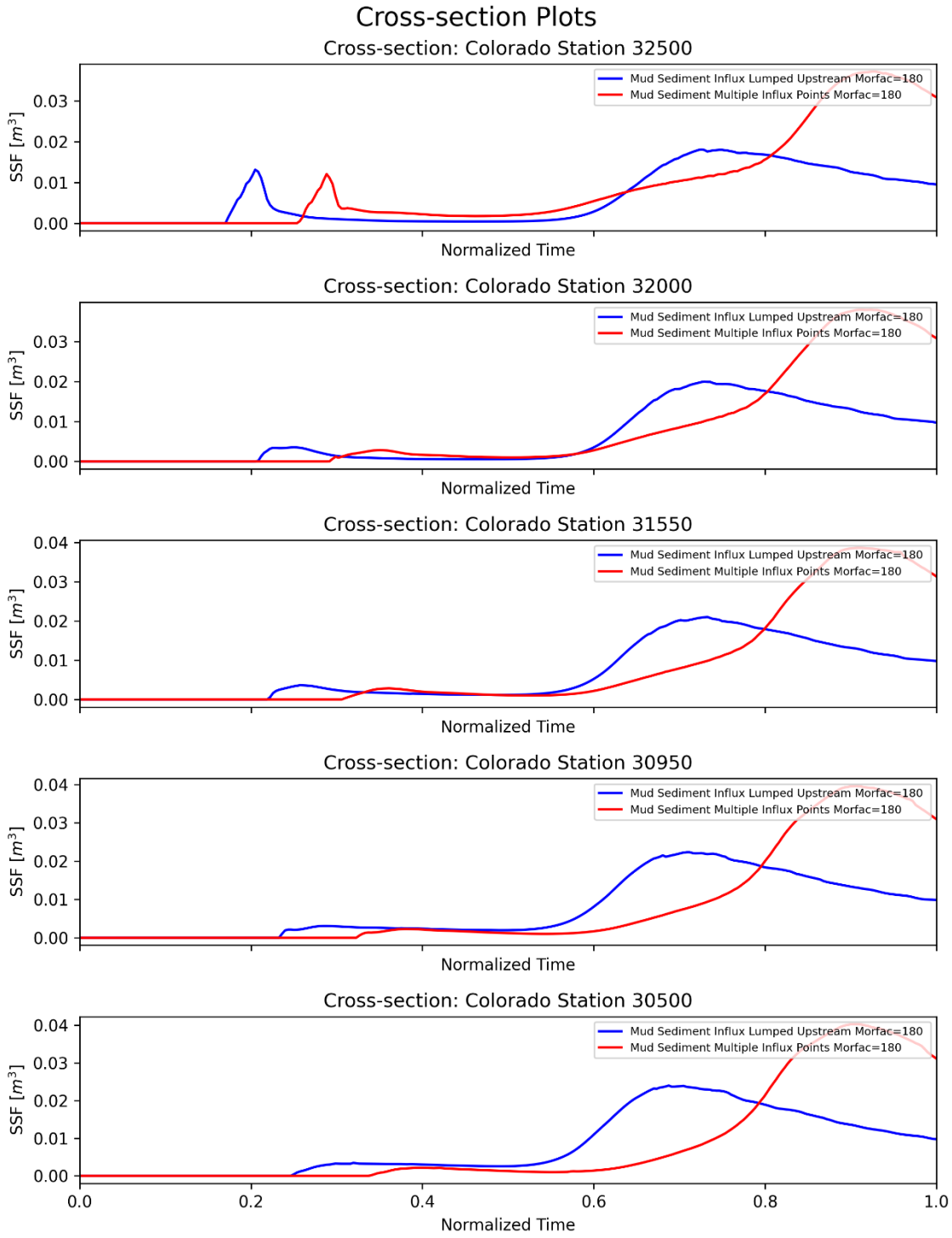
Cross-section Plots
Cross-section: Colorado Station 32500
Cross-section: Colorado Station 32000
Cross-section: Colorado Station 31550
Cross-section: Colorado Station 30950
Cross-section: Colorado Station 30500
Mud Sediment Influx Lumped Upstream Morfac=180
Mud Sediment Multiple Influx Points Morfac=180
SSF [m^3]
Normalized Time
0.00
0.01
0.02
0.03
0.04
0.0
0.2
0.4
0.6
0.8
1.0

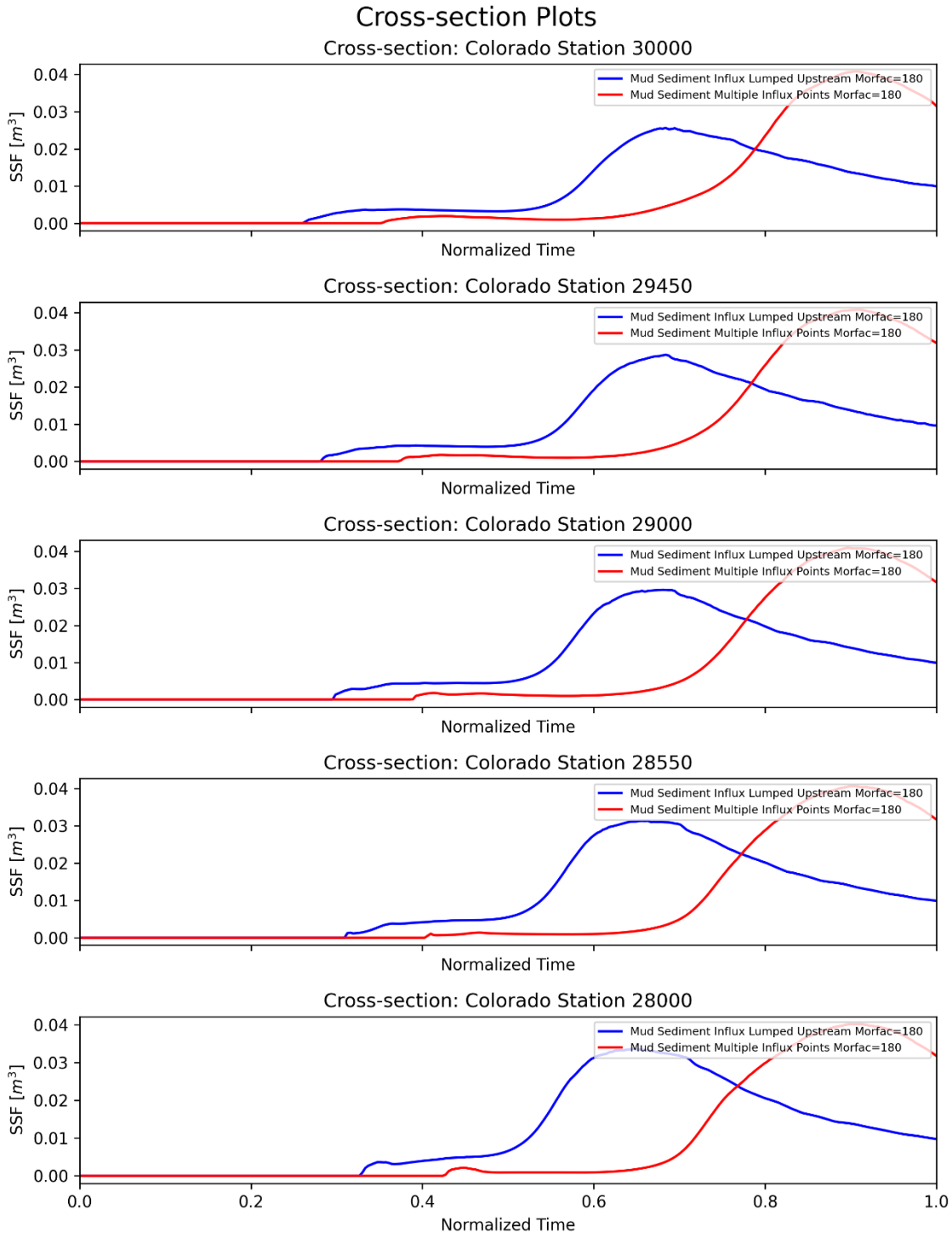
Cross-section Plots
Cross-section: Colorado Station 30000
Cross-section: Colorado Station 29450
Cross-section: Colorado Station 29000
Cross-section: Colorado Station 28550
Cross-section: Colorado Station 28000
Mud Sediment Influx Lumped Upstream Morfac=180
Mud Sediment Multiple Influx Points Morfac=180
SSF [m^3]
0.00
0.01
0.02
0.03
0.04
0.0
0.2
0.4
0.6
0.8
1.0
Normalized Time

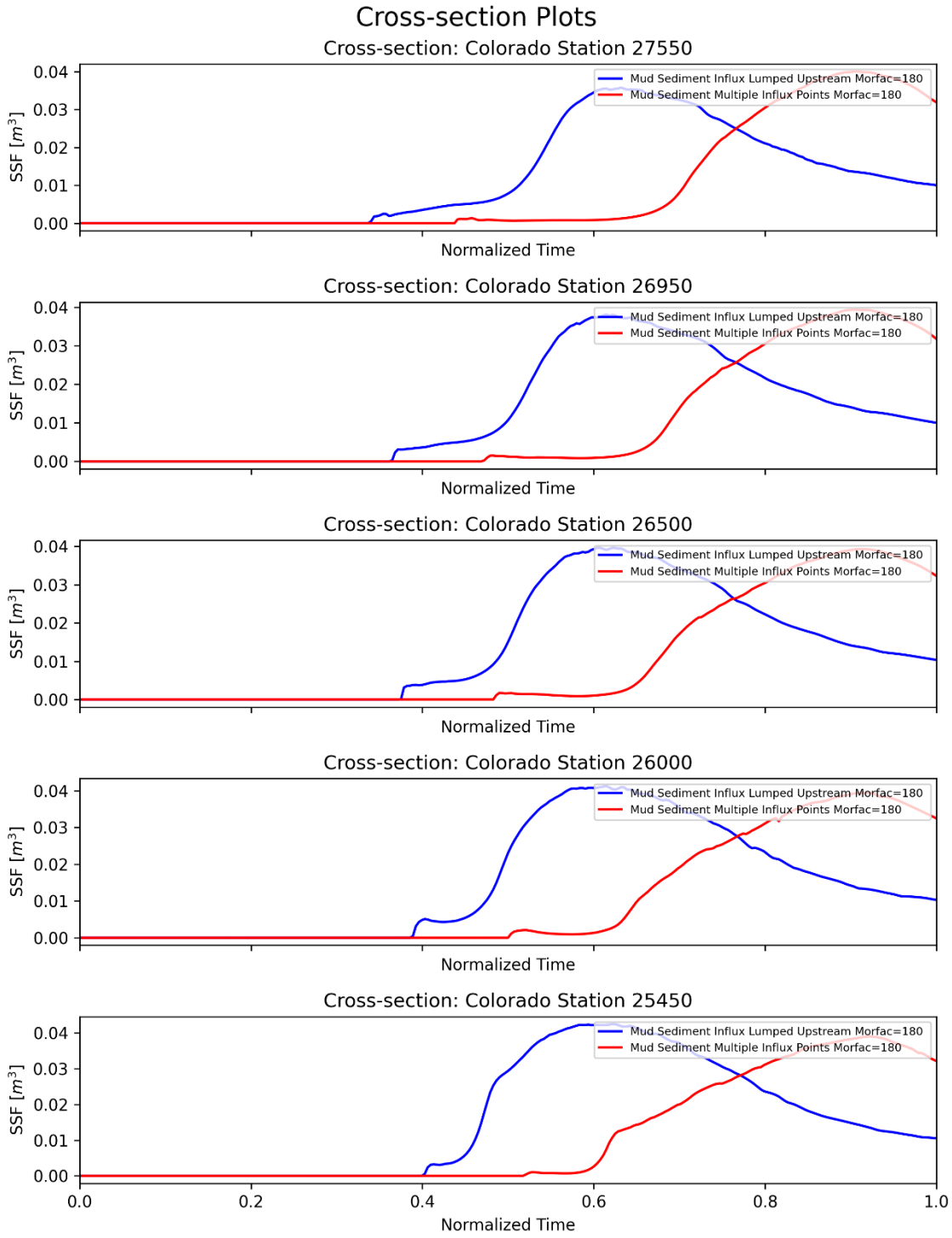
Cross-section Plots
Cross-section: Colorado Station 27550
Cross-section: Colorado Station 26950
Cross-section: Colorado Station 26500
Cross-section: Colorado Station 26000
Cross-section: Colorado Station 25450
Mud Sediment Influx Lumped Upstream Morfac=180
Mud Sediment Multiple Influx Points Morfac=180
SSF [m^3]
0.00
0.01
0.02
0.03
0.04
0.0
0.2
0.4
0.6
0.8
1.0
Normalized Time

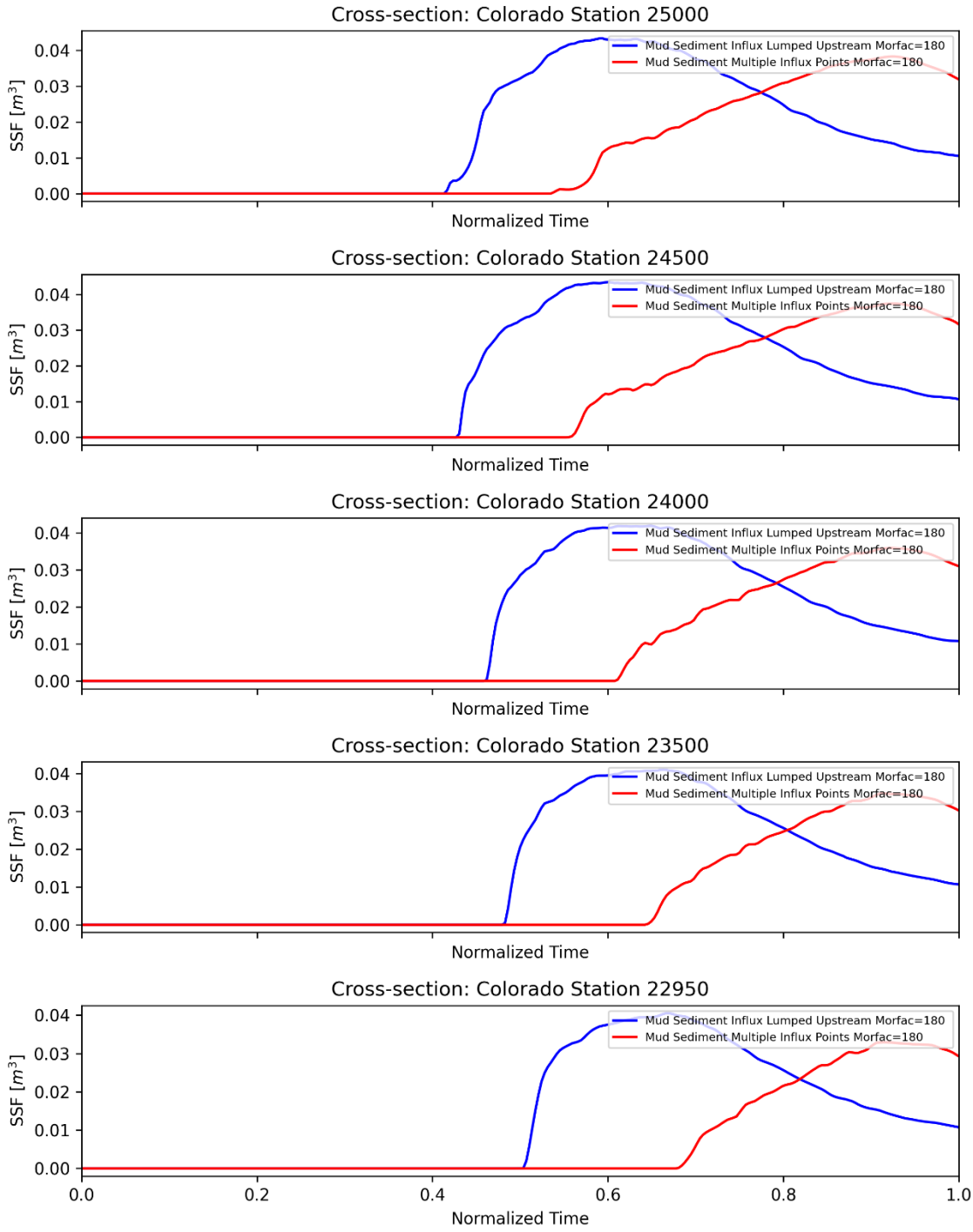
Cross-section Plots
Cross-section: Colorado Station 25000
Cross-section: Colorado Station 24500
Cross-section: Colorado Station 24000
Cross-section: Colorado Station 23500
Cross-section: Colorado Station 22950
Mud Sediment Influx Lumped Upstream Morfac=180
Mud Sediment Multiple Influx Points Morfac=180
SSF [m^3]
0.00
0.01
0.02
0.03
0.04
0.0
0.2
0.4
0.6
0.8
1.0
Normalized Time

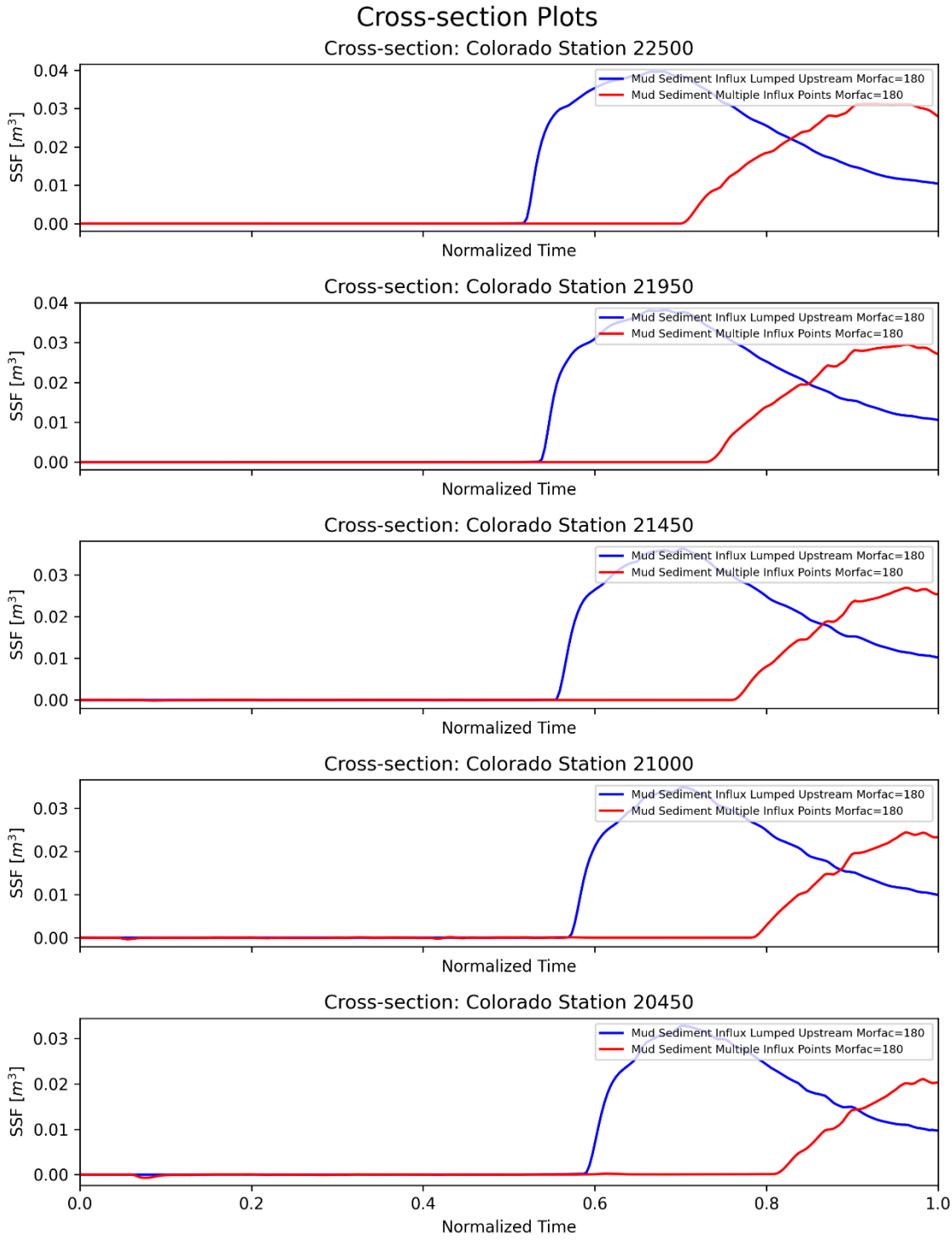
Cross-section Plots
Cross-section: Colorado Station 22500
Cross-section: Colorado Station 21950
Cross-section: Colorado Station 21450
Cross-section: Colorado Station 21000
Cross-section: Colorado Station 20450
Mud Sediment Influx Lumped Upstream Morfac=180
Mud Sediment Multiple Influx Points Morfac=180
SSF [m^3]
Normalized Time
0.00
0.01
0.02
0.03
0.04
0.0
0.2
0.4
0.6
0.8
1.0

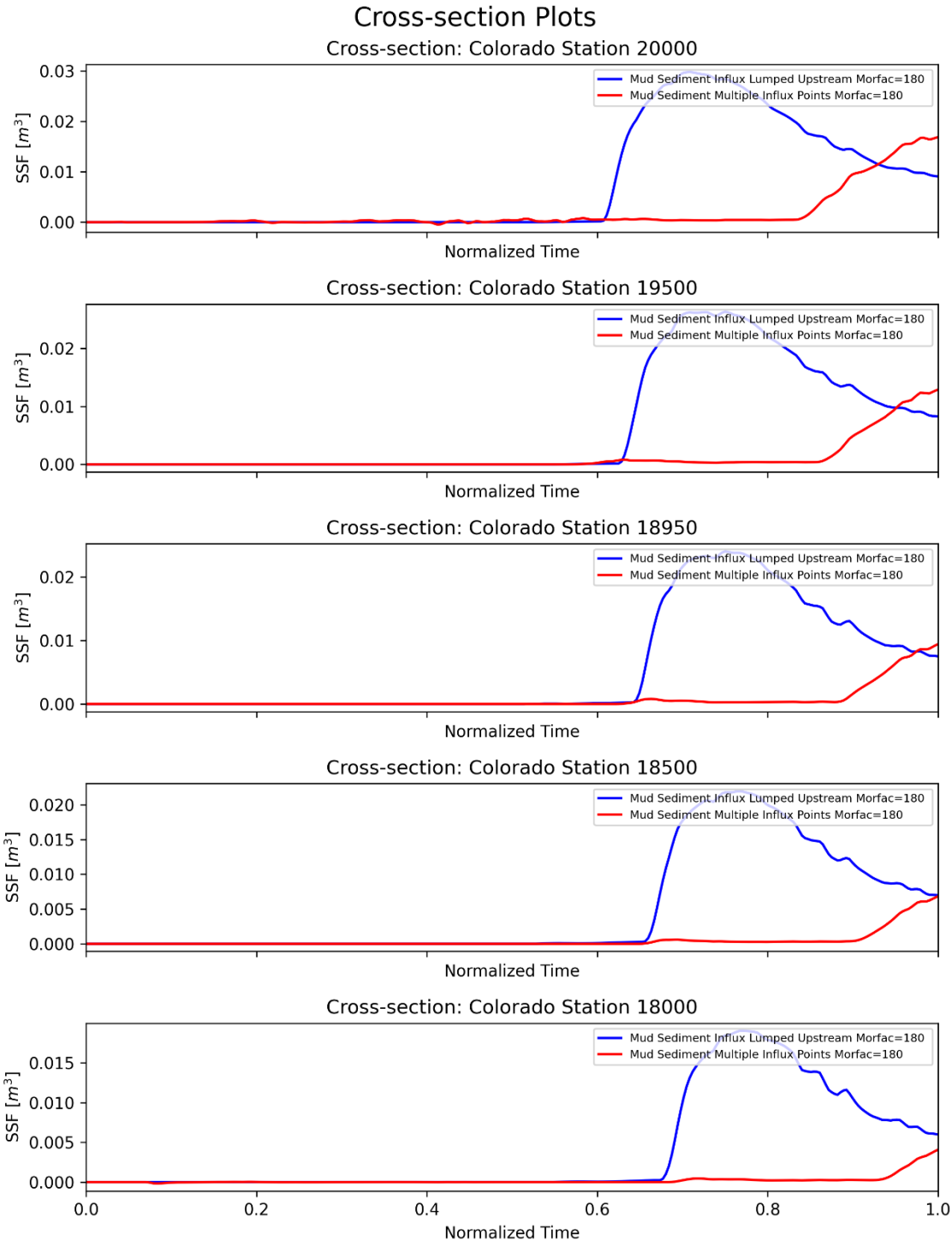
Cross-section Plots
Cross-section: Colorado Station 20000
Mud Sediment Influx Lumped Upstream Morfac=180
Mud Sediment Multiple Influx Points Morfac=180
SSF [m^3]
0.03
0.02
0.01
0.00
Normalized Time
Cross-section: Colorado Station 19500
Mud Sediment Influx Lumped Upstream Morfac=180
Mud Sediment Multiple Influx Points Morfac=180
SSF [m^3]
0.02
0.01
0.00
Normalized Time
Cross-section: Colorado Station 18950
Mud Sediment Influx Lumped Upstream Morfac=180
Mud Sediment Multiple Influx Points Morfac=180
SSF [m^3]
0.02
0.01
0.00
Normalized Time
Cross-section: Colorado Station 18500
Mud Sediment Influx Lumped Upstream Morfac=180
Mud Sediment Multiple Influx Points Morfac=180
SSF [m^3]
0.020
0.015
0.010
0.005
0.000
Normalized Time
Cross-section: Colorado Station 18000
Mud Sediment Influx Lumped Upstream Morfac=180
Mud Sediment Multiple Influx Points Morfac=180
SSF [m^3]
0.015
0.010
0.005
0.000
0.0
0.2
0.4
0.6
0.8
1.0
Normalized Time

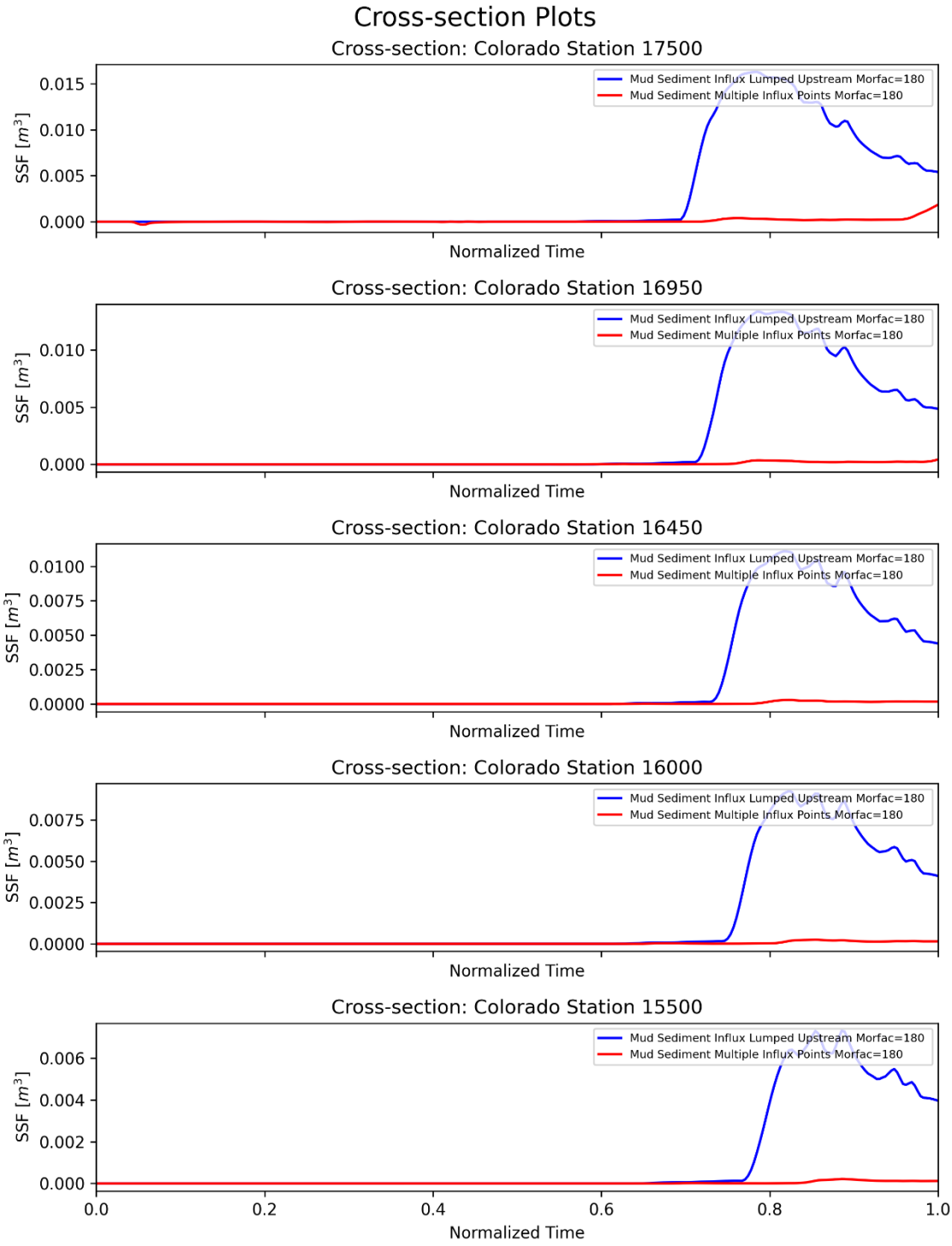
Cross-section Plots
Cross-section: Colorado Station 17500
Mud Sediment Influx Lumped Upstream Morfac=180
Mud Sediment Multiple Influx Points Morfac=180
SSF [m^3]
0.015
0.010
0.005
0.000
Normalized Time
Cross-section: Colorado Station 16950
Mud Sediment Influx Lumped Upstream Morfac=180
Mud Sediment Multiple Influx Points Morfac=180
SSF [m^3]
0.010
0.005
0.000
Normalized Time
Cross-section: Colorado Station 16450
Mud Sediment Influx Lumped Upstream Morfac=180
Mud Sediment Multiple Influx Points Morfac=180
SSF [m^3]
0.0100
0.0075
0.0050
0.0025
0.0000
Normalized Time
Cross-section: Colorado Station 16000
Mud Sediment Influx Lumped Upstream Morfac=180
Mud Sediment Multiple Influx Points Morfac=180
SSF [m^3]
0.0075
0.0050
0.0025
0.0000
Normalized Time
Cross-section: Colorado Station 15500
Mud Sediment Influx Lumped Upstream Morfac=180
Mud Sediment Multiple Influx Points Morfac=180
SSF [m^3]
0.006
0.004
0.002
0.000
0.0
0.2
0.4
0.6
0.8
1.0
Normalized Time

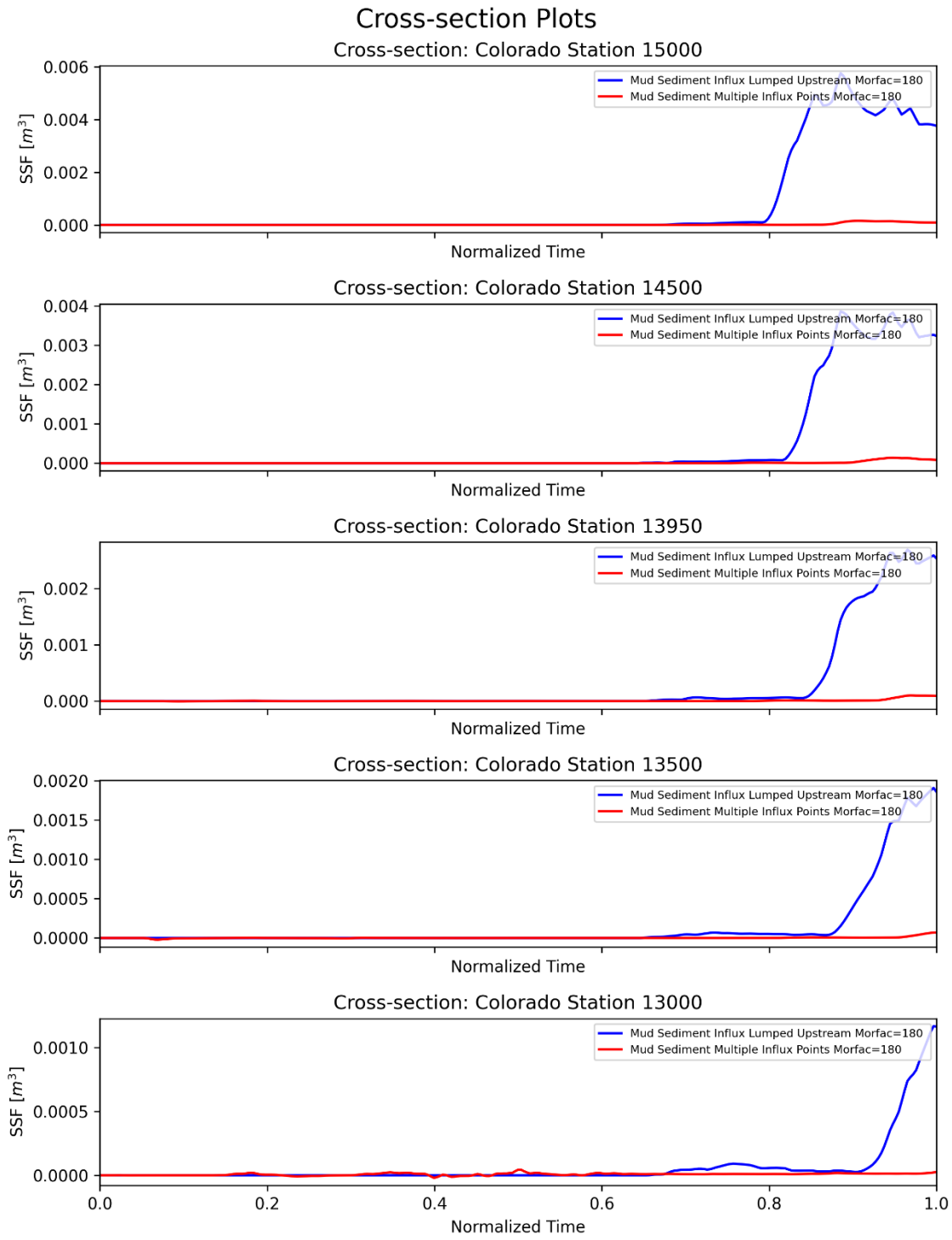
Cross-section Plots
Cross-section: Colorado Station 15000
Mud Sediment Influx Lumped Upstream Morfac=180
Mud Sediment Multiple Influx Points Morfac=180
SSF [m^3]
0.006
0.004
0.002
0.000
Normalized Time
Cross-section: Colorado Station 14500
Mud Sediment Influx Lumped Upstream Morfac=180
Mud Sediment Multiple Influx Points Morfac=180
SSF [m^3]
0.004
0.003
0.002
0.001
0.000
Normalized Time
Cross-section: Colorado Station 13950
Mud Sediment Influx Lumped Upstream Morfac=180
Mud Sediment Multiple Influx Points Morfac=180
SSF [m^3]
0.002
0.001
0.000
Normalized Time
Cross-section: Colorado Station 13500
Mud Sediment Influx Lumped Upstream Morfac=180
Mud Sediment Multiple Influx Points Morfac=180
SSF [m^3]
0.0020
0.0015
0.0010
0.0005
0.0000
Normalized Time
Cross-section: Colorado Station 13000
Mud Sediment Influx Lumped Upstream Morfac=180
Mud Sediment Multiple Influx Points Morfac=180
SSF [m^3]
0.0010
0.0005
0.0000
0.0
0.2
0.4
0.6
0.8
1.0
Normalized Time

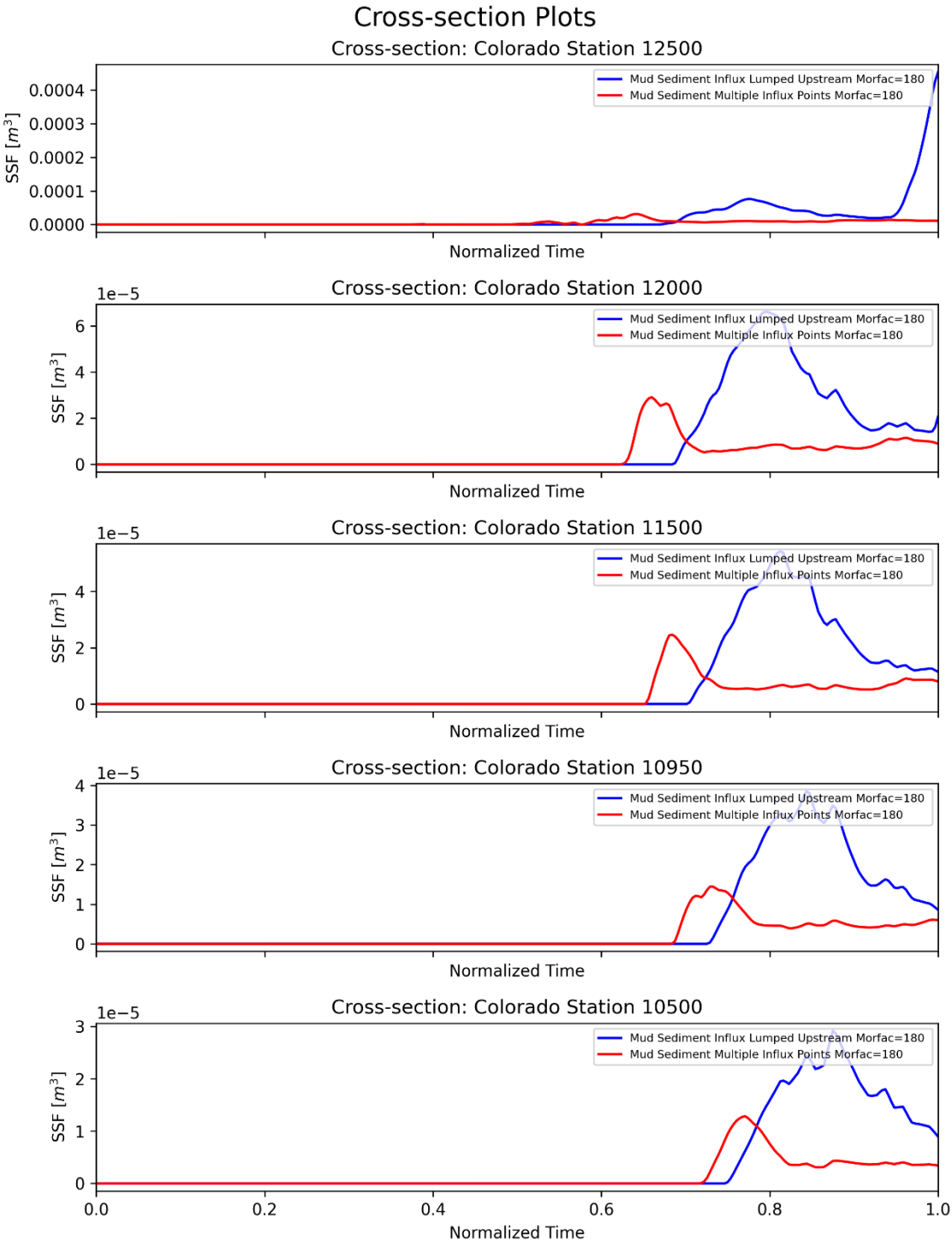
Cross-section Plots
Cross-section: Colorado Station 12500
Mud Sediment Influx Lumped Upstream Morfac=180
Mud Sediment Multiple Influx Points Morfac=180
SSF [m^3]
0.0004
0.0003
0.0002
0.0001
0.0000
Normalized Time
Cross-section: Colorado Station 12000
1e−5
6
4
2
0
Cross-section: Colorado Station 11500
Cross-section: Colorado Station 10950
Cross-section: Colorado Station 10500
0.0
0.2
0.4
0.6
0.8
1.0

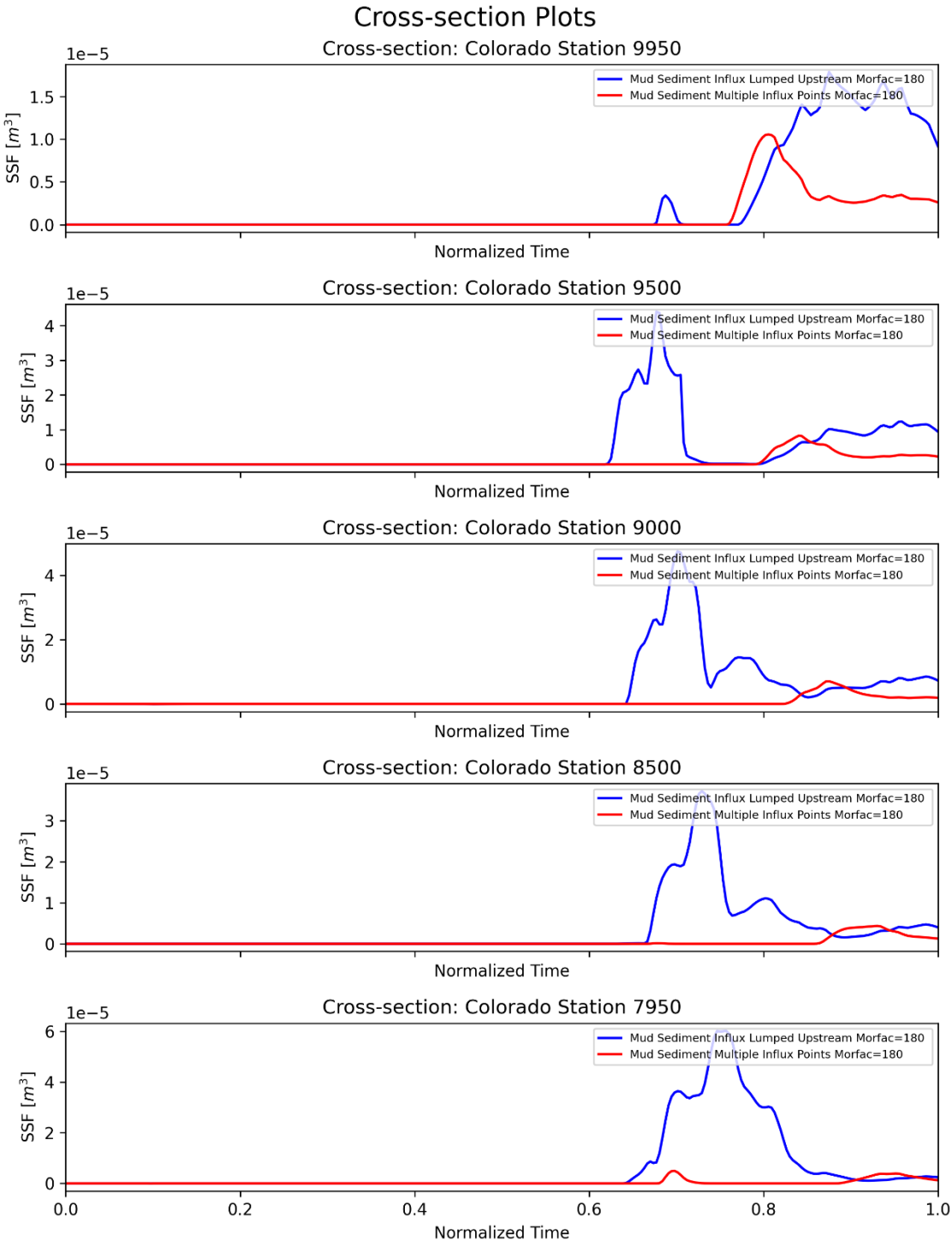
Cross-section Plots
Cross-section: Colorado Station 9950
Cross-section: Colorado Station 9500
Cross-section: Colorado Station 9000
Cross-section: Colorado Station 8500
Cross-section: Colorado Station 7950
Mud Sediment Influx Lumped Upstream Morfac=180
Mud Sediment Multiple Influx Points Morfac=180
SSF [m^3]
1e−5
Normalized Time

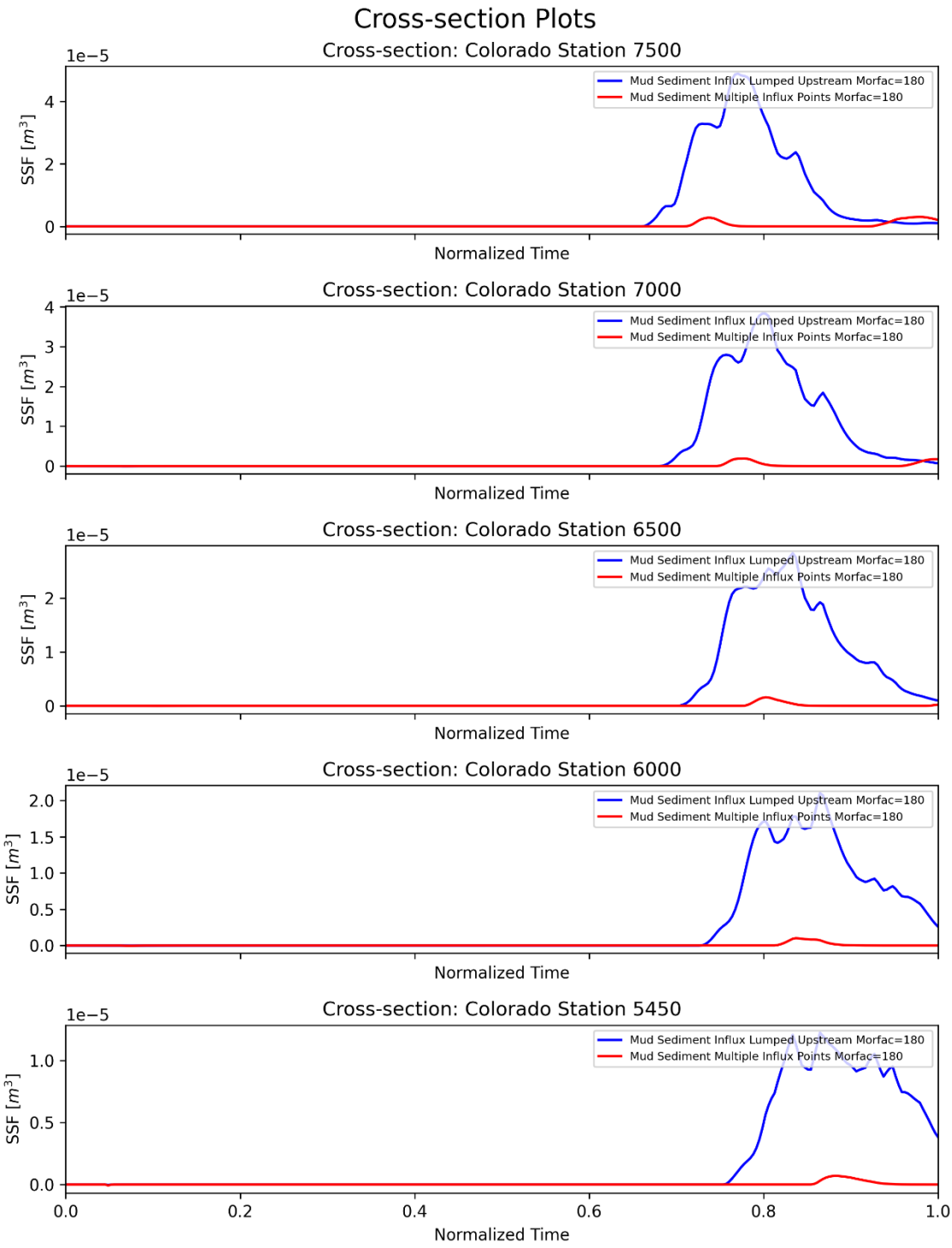
Cross-section Plots
Cross-section: Colorado Station 7500
Cross-section: Colorado Station 7000
Cross-section: Colorado Station 6500
Cross-section: Colorado Station 6000
Cross-section: Colorado Station 5450
Mud Sediment Influx Lumped Upstream Morfac=180
Mud Sediment Multiple Influx Points Morfac=180
SSF [m^3]
1e−5
Normalized Time

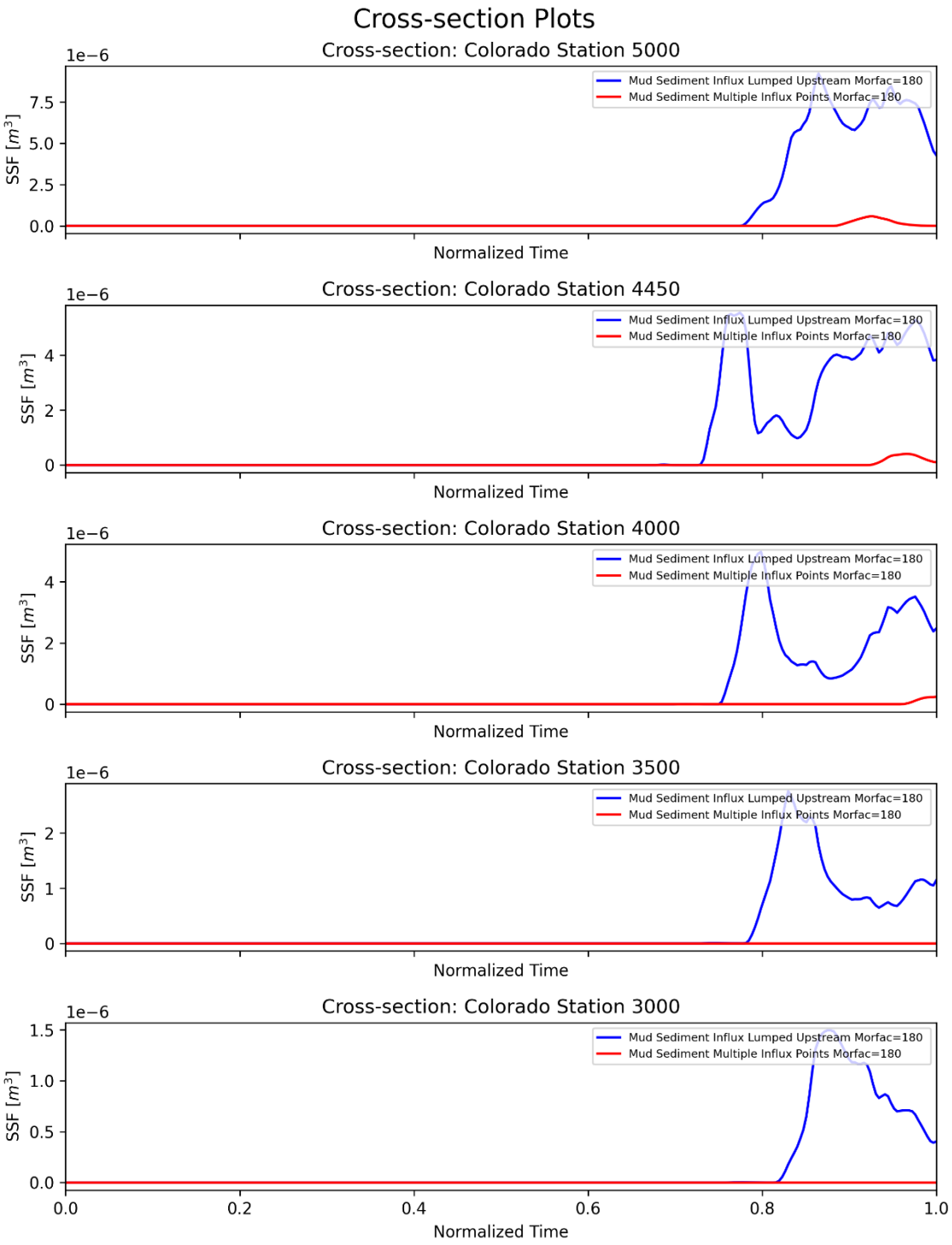
Cross-section Plots
Cross-section: Colorado Station 5000
Cross-section: Colorado Station 4450
Cross-section: Colorado Station 4000
Cross-section: Colorado Station 3500
Cross-section: Colorado Station 3000
Mud Sediment Influx Lumped Upstream Morfac=180
Mud Sediment Multiple Influx Points Morfac=180
1e−6
SSF [m^3]
Normalized Time

APPENDIX I: THE EFFECT OF COHESIVE VS. NON-COHESIVE SEDIMENT IN BRAZOS DOMAIN

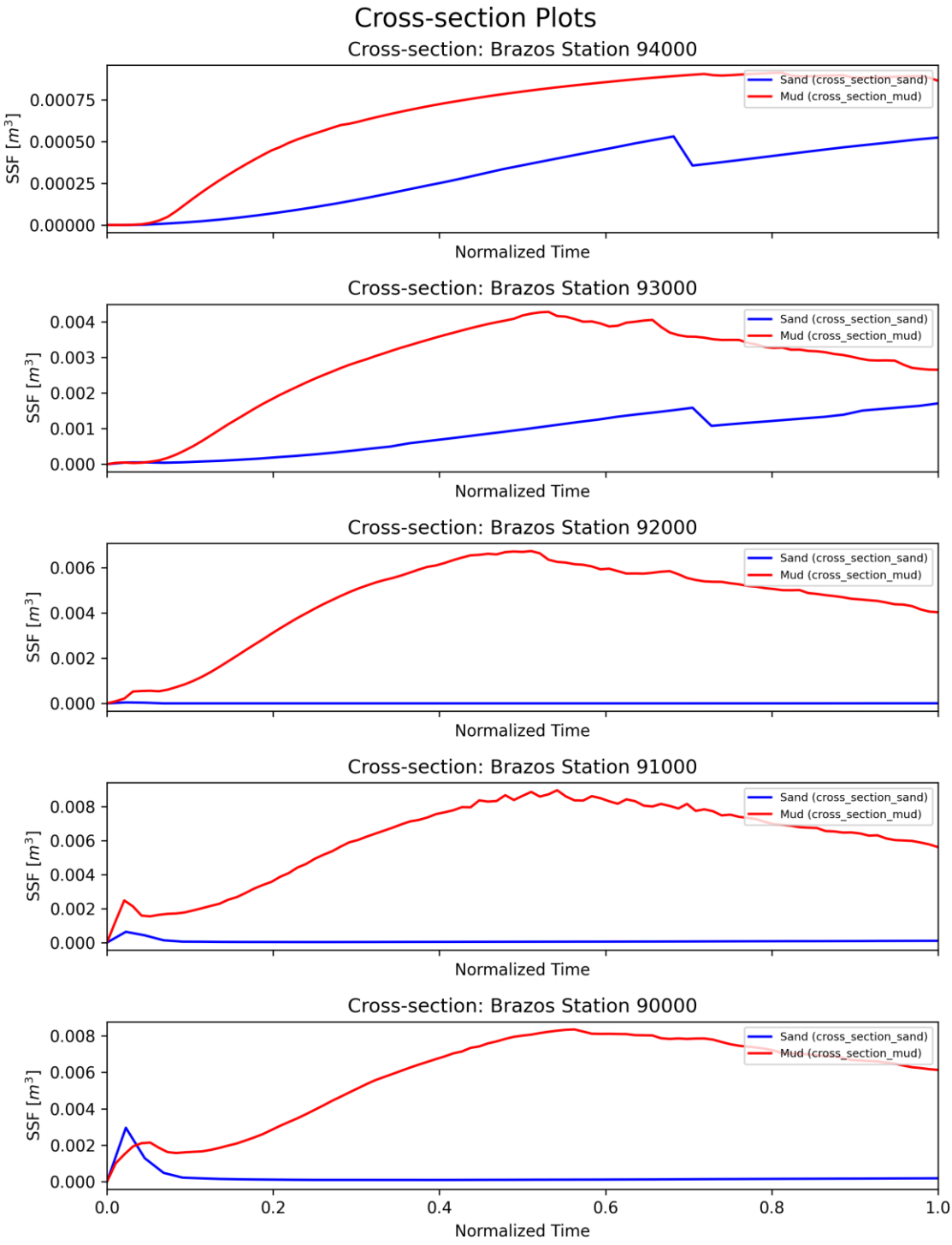
Cross-section Plots
Cross-section: Brazos Station 94000
Cross-section: Brazos Station 93000
Cross-section: Brazos Station 92000
Cross-section: Brazos Station 91000
Cross-section: Brazos Station 90000
Sand (cross_section_sand)
Mud (cross_section_mud)
SSF [m^3]
Normalized Time
0.00000
0.00025
0.00050
0.00075
0.000
0.001
0.002
0.003
0.004
0.006
0.008
0.0
0.2
0.4
0.6
0.8
1.0

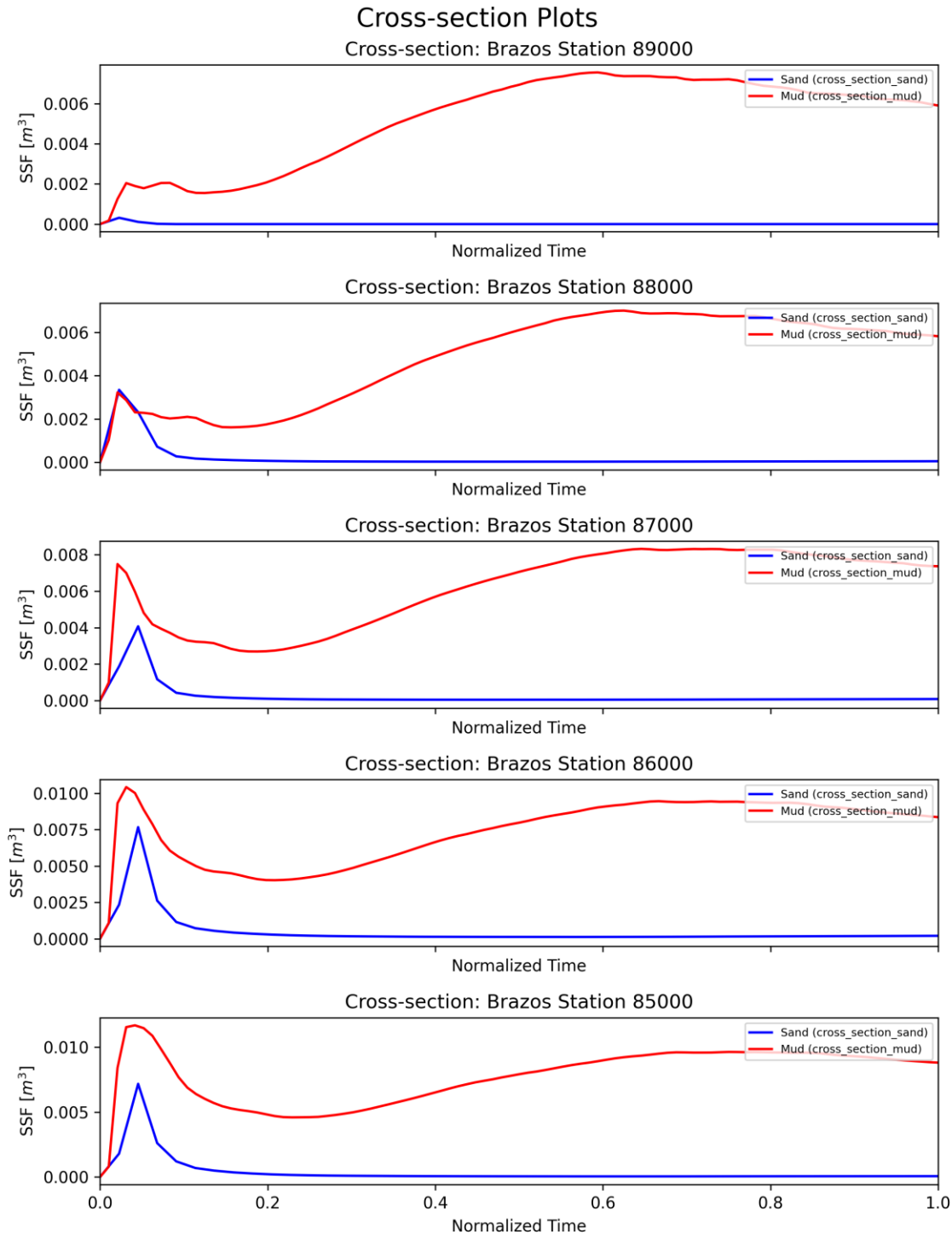
Cross-section Plots
Cross-section: Brazos Station 89000
Cross-section: Brazos Station 88000
Cross-section: Brazos Station 87000
Cross-section: Brazos Station 86000
Cross-section: Brazos Station 85000
Sand (cross_section_sand)
Mud (cross_section_mud)
SSF [m^3]
Normalized Time

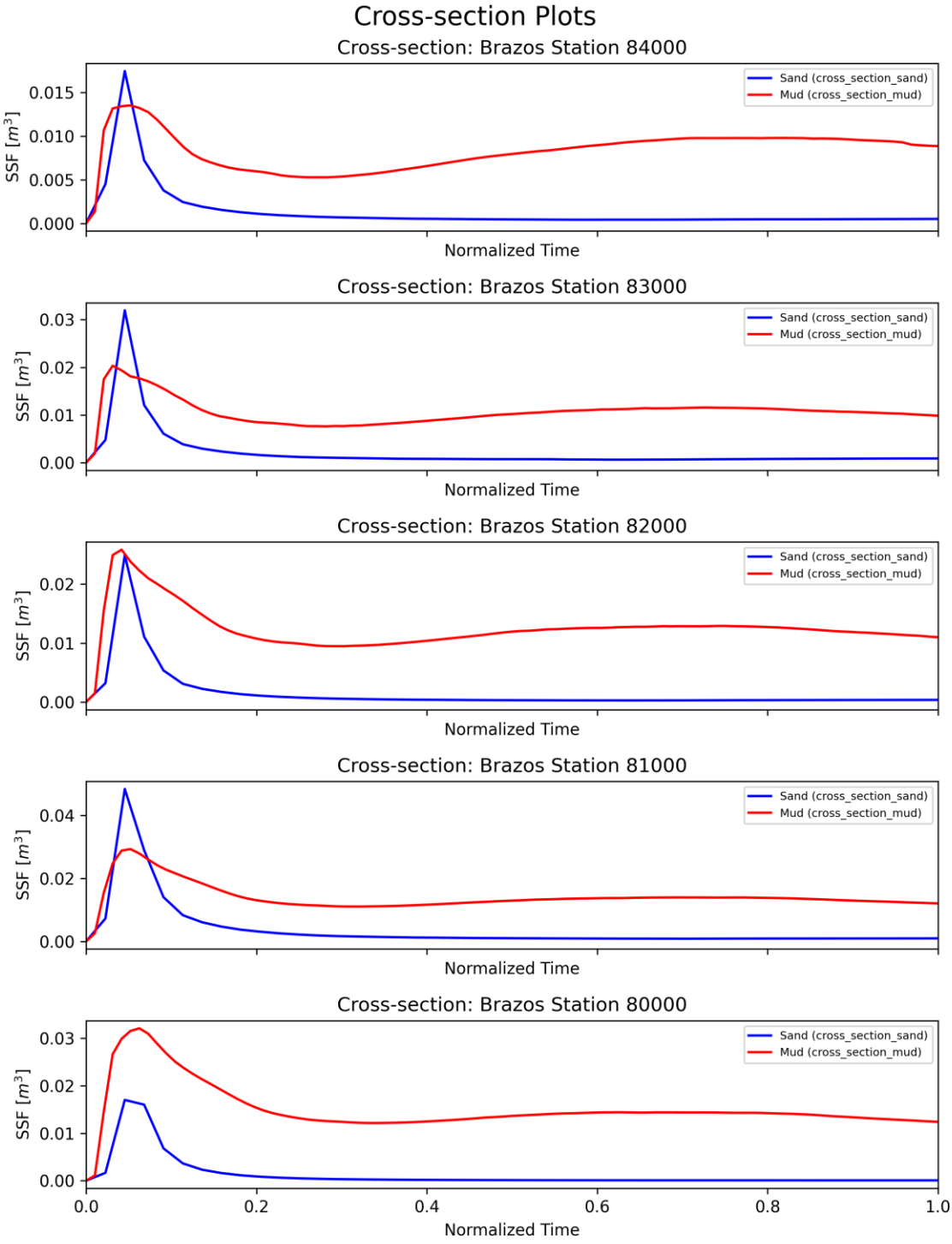
Cross-section Plots
Cross-section: Brazos Station 84000
Sand (cross_section_sand)
Mud (cross_section_mud)
SSF [m^3]
0.015
0.010
0.005
0.000
Normalized Time
Cross-section: Brazos Station 83000
Sand (cross_section_sand)
Mud (cross_section_mud)
SSF [m^3]
0.03
0.02
0.01
0.00
Normalized Time
Cross-section: Brazos Station 82000
Sand (cross_section_sand)
Mud (cross_section_mud)
SSF [m^3]
0.02
0.01
0.00
Normalized Time
Cross-section: Brazos Station 81000
Sand (cross_section_sand)
Mud (cross_section_mud)
SSF [m^3]
0.04
0.02
0.00
Normalized Time
Cross-section: Brazos Station 80000
Sand (cross_section_sand)
Mud (cross_section_mud)
SSF [m^3]
0.03
0.02
0.01
0.00
0.0
0.2
0.4
0.6
0.8
1.0
Normalized Time

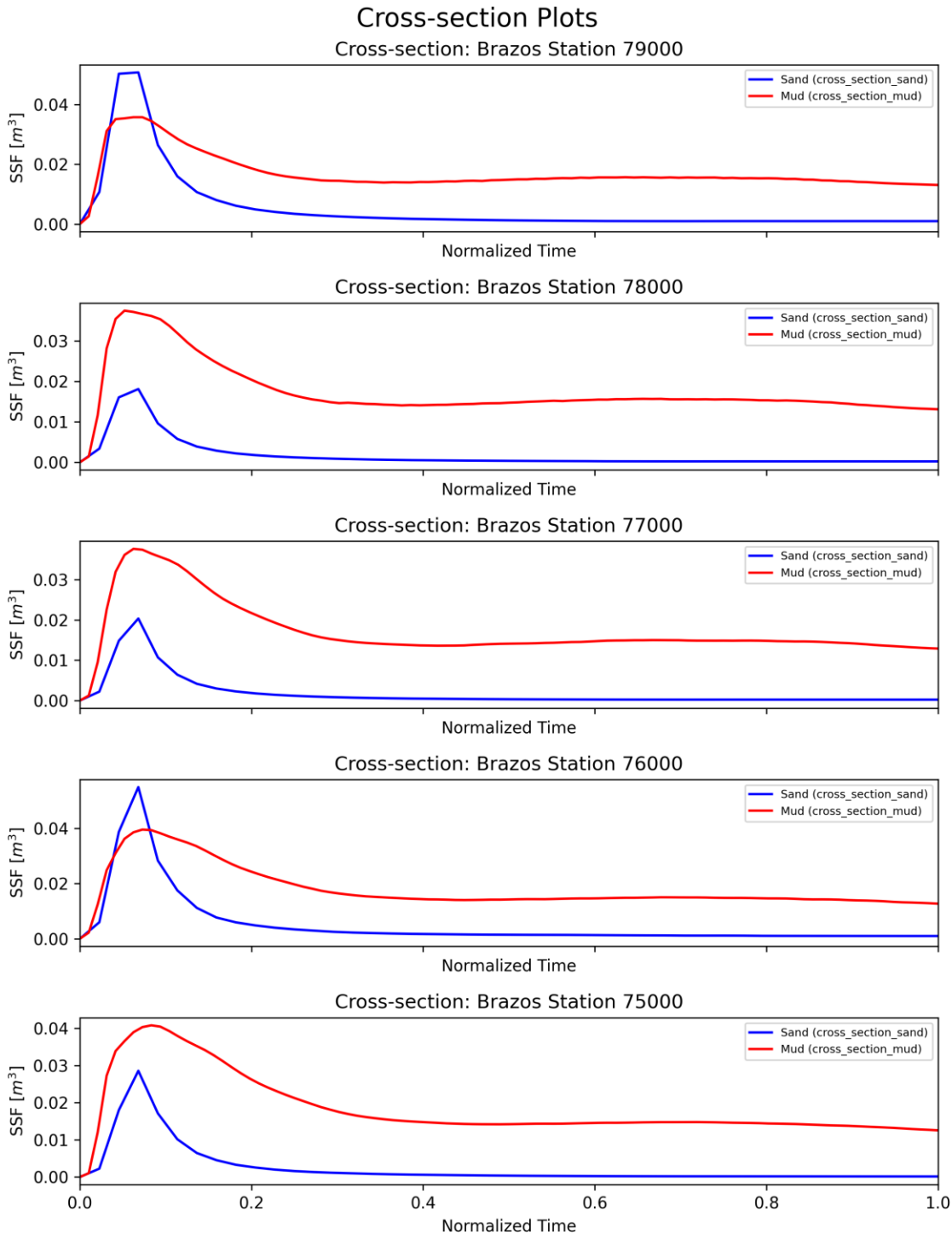
Cross-section Plots
Cross-section: Brazos Station 79000
Cross-section: Brazos Station 78000
Cross-section: Brazos Station 77000
Cross-section: Brazos Station 76000
Cross-section: Brazos Station 75000
Sand (cross_section_sand)
Mud (cross_section_mud)
SSF [m^3]
Normalized Time
0.00
0.01
0.02
0.03
0.04
0.0
0.2
0.4
0.6
0.8
1.0

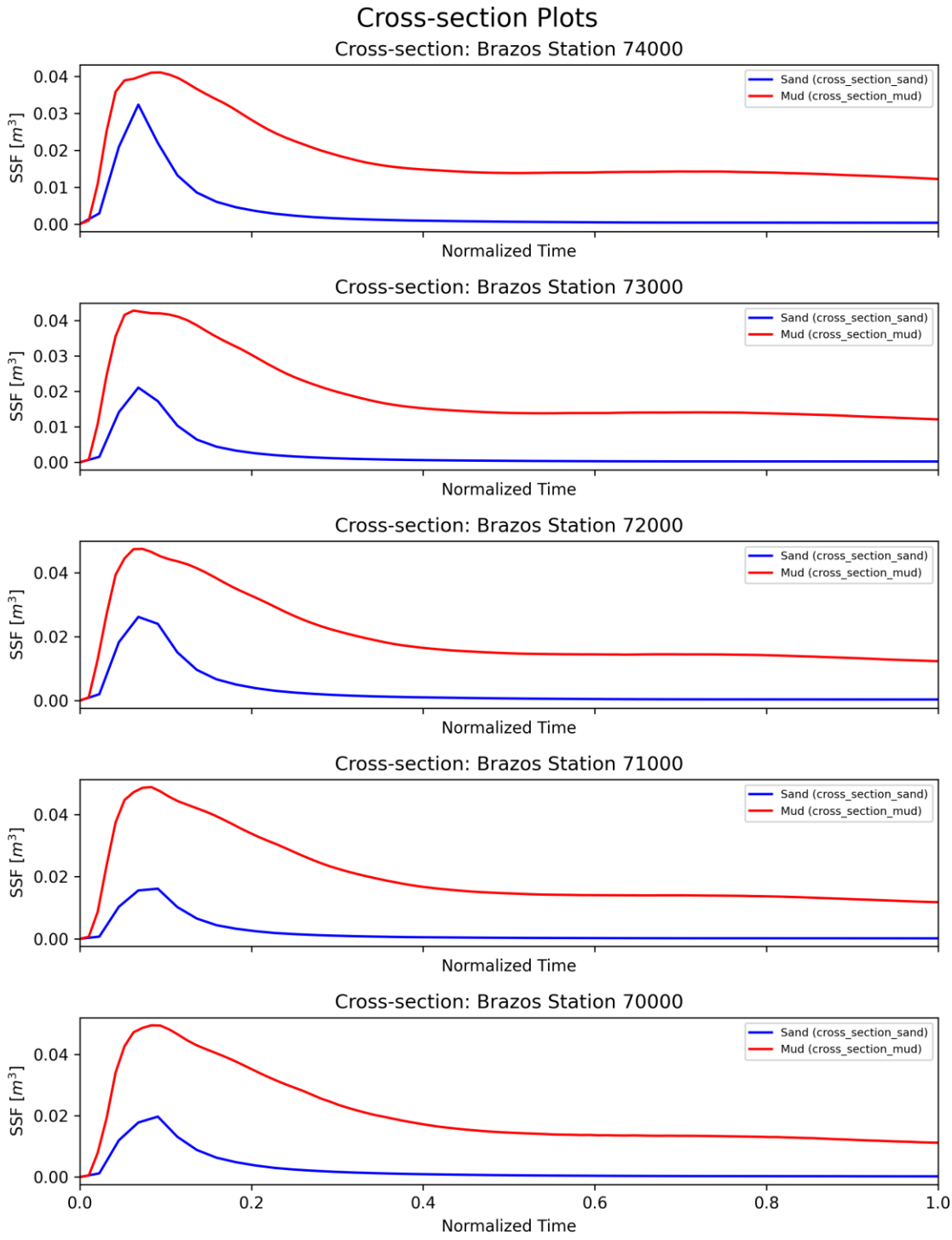
Cross-section Plots
Cross-section: Brazos Station 74000
Cross-section: Brazos Station 73000
Cross-section: Brazos Station 72000
Cross-section: Brazos Station 71000
Cross-section: Brazos Station 70000
Sand (cross_section_sand)
Mud (cross_section_mud)
SSF [m^3]
Normalized Time
0.00
0.01
0.02
0.03
0.04
0.0
0.2
0.4
0.6
0.8
1.0

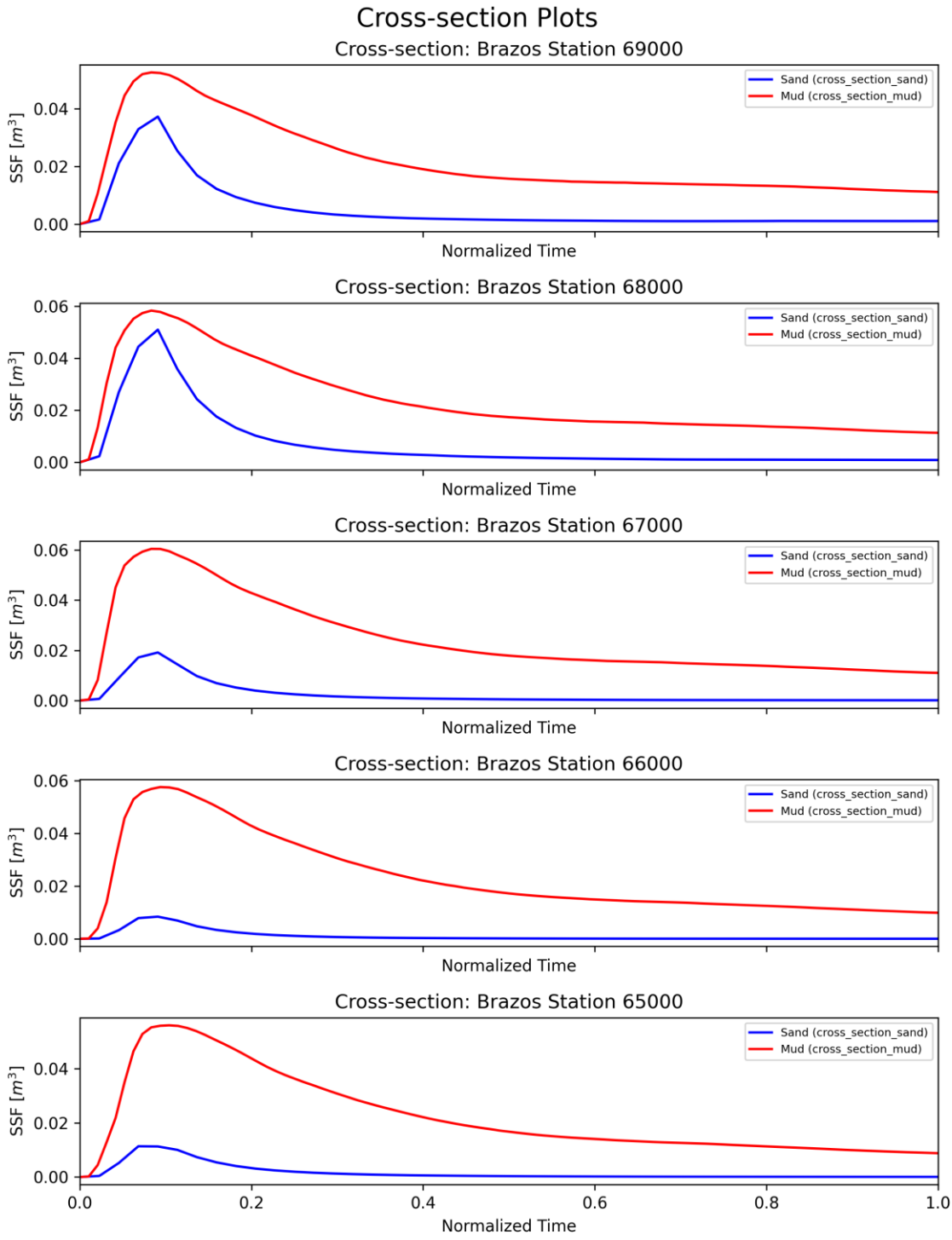
Cross-section Plots
Cross-section: Brazos Station 69000
Cross-section: Brazos Station 68000
Cross-section: Brazos Station 67000
Cross-section: Brazos Station 66000
Cross-section: Brazos Station 65000
Sand (cross_section_sand)
Mud (cross_section_mud)
SSF [m^3]
Normalized Time
0.00
0.02
0.04
0.06
0.0
0.2
0.4
0.6
0.8
1.0

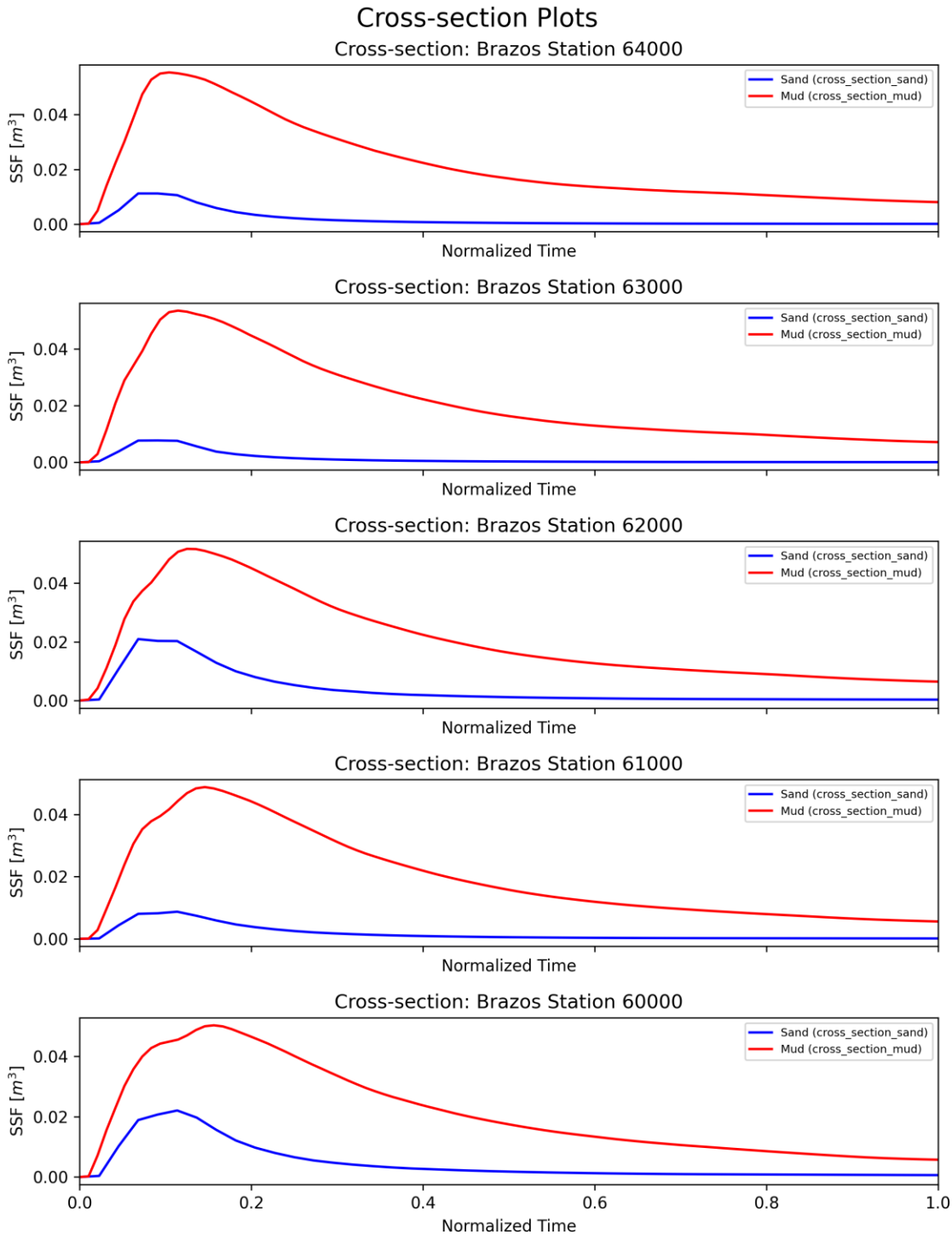
Cross-section Plots
Cross-section: Brazos Station 64000
Cross-section: Brazos Station 63000
Cross-section: Brazos Station 62000
Cross-section: Brazos Station 61000
Cross-section: Brazos Station 60000
Sand (cross_section_sand)
Mud (cross_section_mud)
SSF [m^3]
0.00
0.02
0.04
0.0
0.2
0.4
0.6
0.8
1.0
Normalized Time

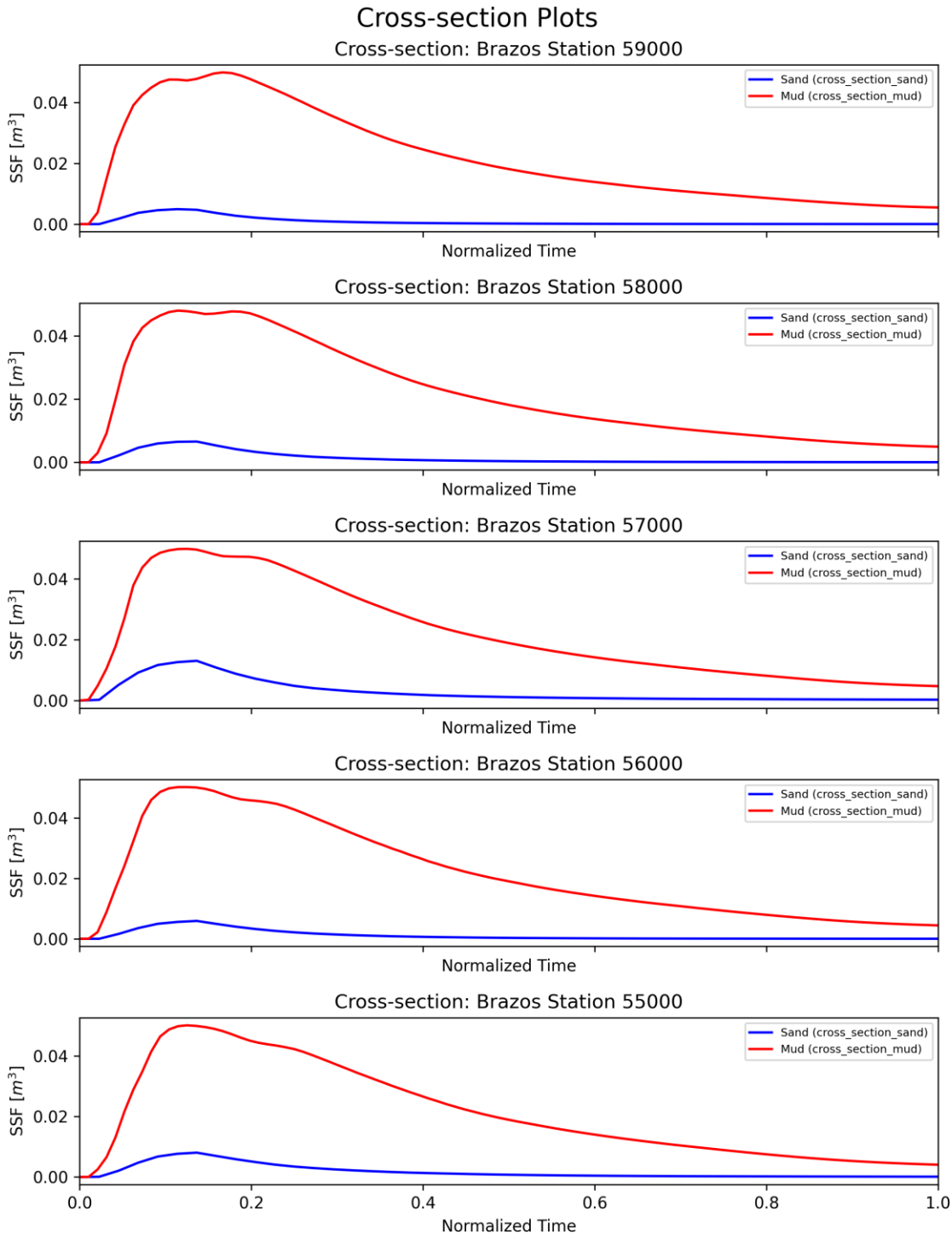
Cross-section Plots
Cross-section: Brazos Station 59000
Cross-section: Brazos Station 58000
Cross-section: Brazos Station 57000
Cross-section: Brazos Station 56000
Cross-section: Brazos Station 55000
Sand (cross_section_sand)
Mud (cross_section_mud)
SSF [m^3]
0.00
0.02
0.04
0.0
0.2
0.4
0.6
0.8
1.0
Normalized Time

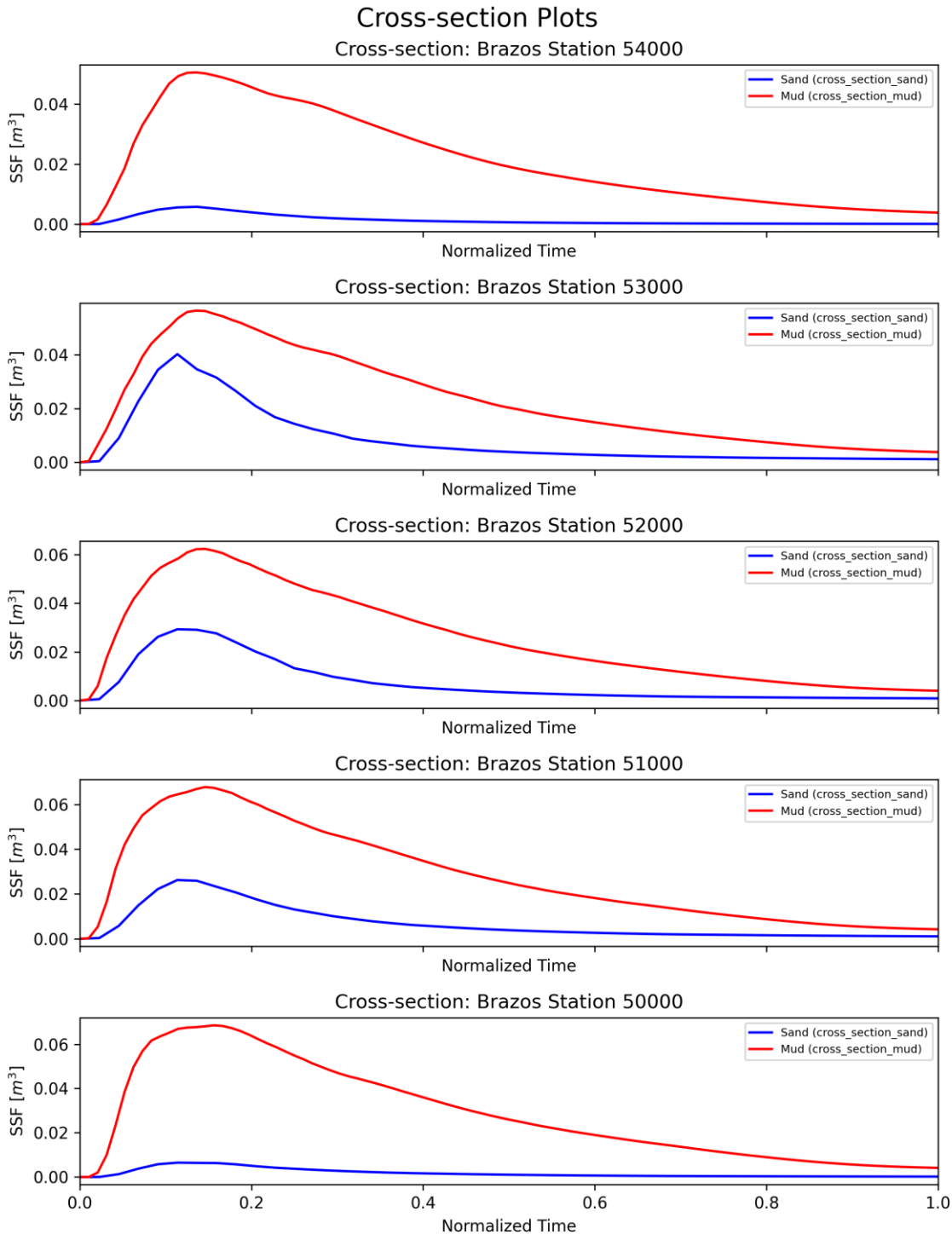
Cross-section Plots
Cross-section: Brazos Station 54000
Cross-section: Brazos Station 53000
Cross-section: Brazos Station 52000
Cross-section: Brazos Station 51000
Cross-section: Brazos Station 50000
Sand (cross_section_sand)
Mud (cross_section_mud)
SSF [m^3]
Normalized Time
0.00
0.02
0.04
0.06
0.0
0.2
0.4
0.6
0.8
1.0

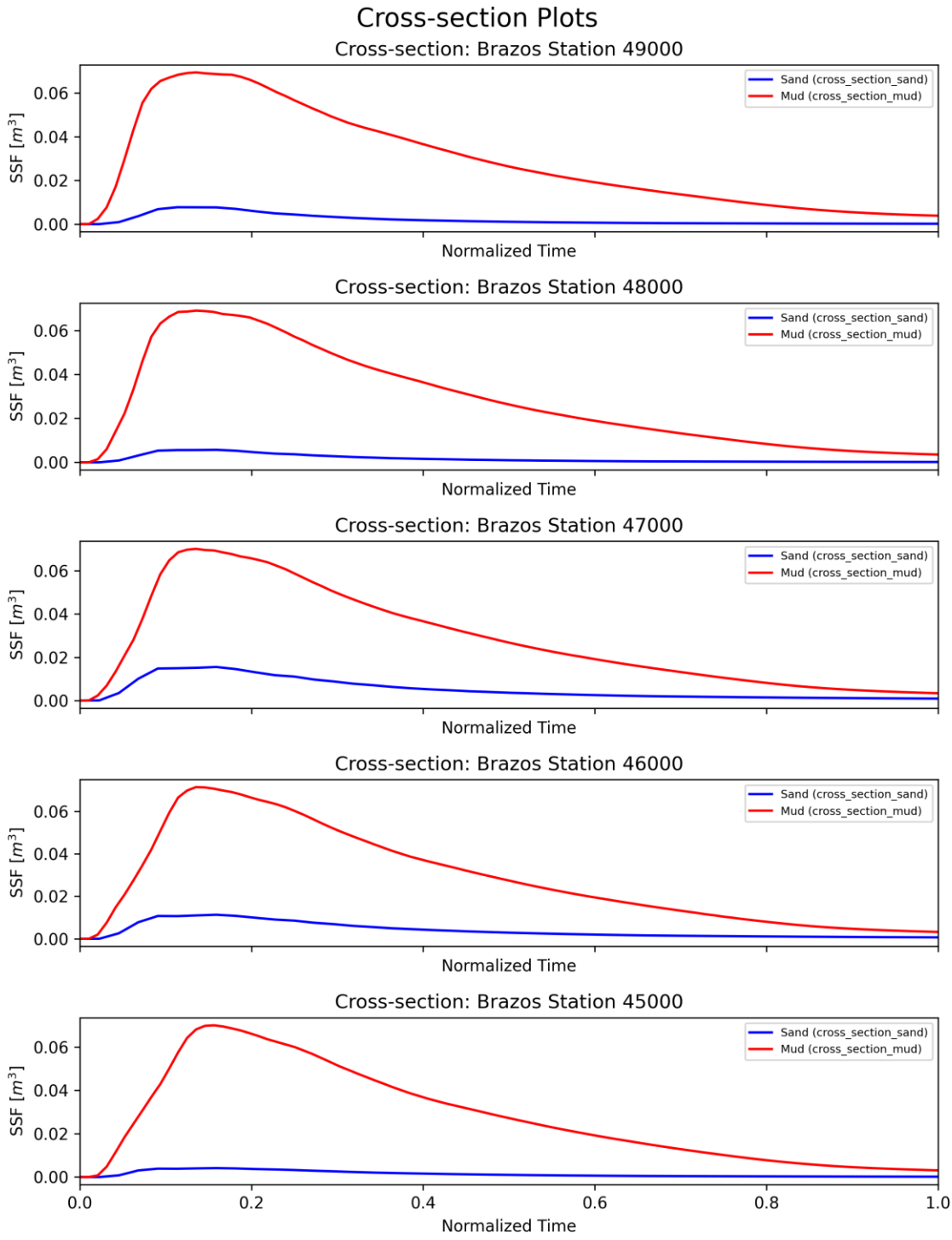
Cross-section Plots
Cross-section: Brazos Station 49000
Cross-section: Brazos Station 48000
Cross-section: Brazos Station 47000
Cross-section: Brazos Station 46000
Cross-section: Brazos Station 45000
Sand (cross_section_sand)
Mud (cross_section_mud)
SSF [m^3]
0.00
0.02
0.04
0.06
0.0
0.2
0.4
0.6
0.8
1.0
Normalized Time

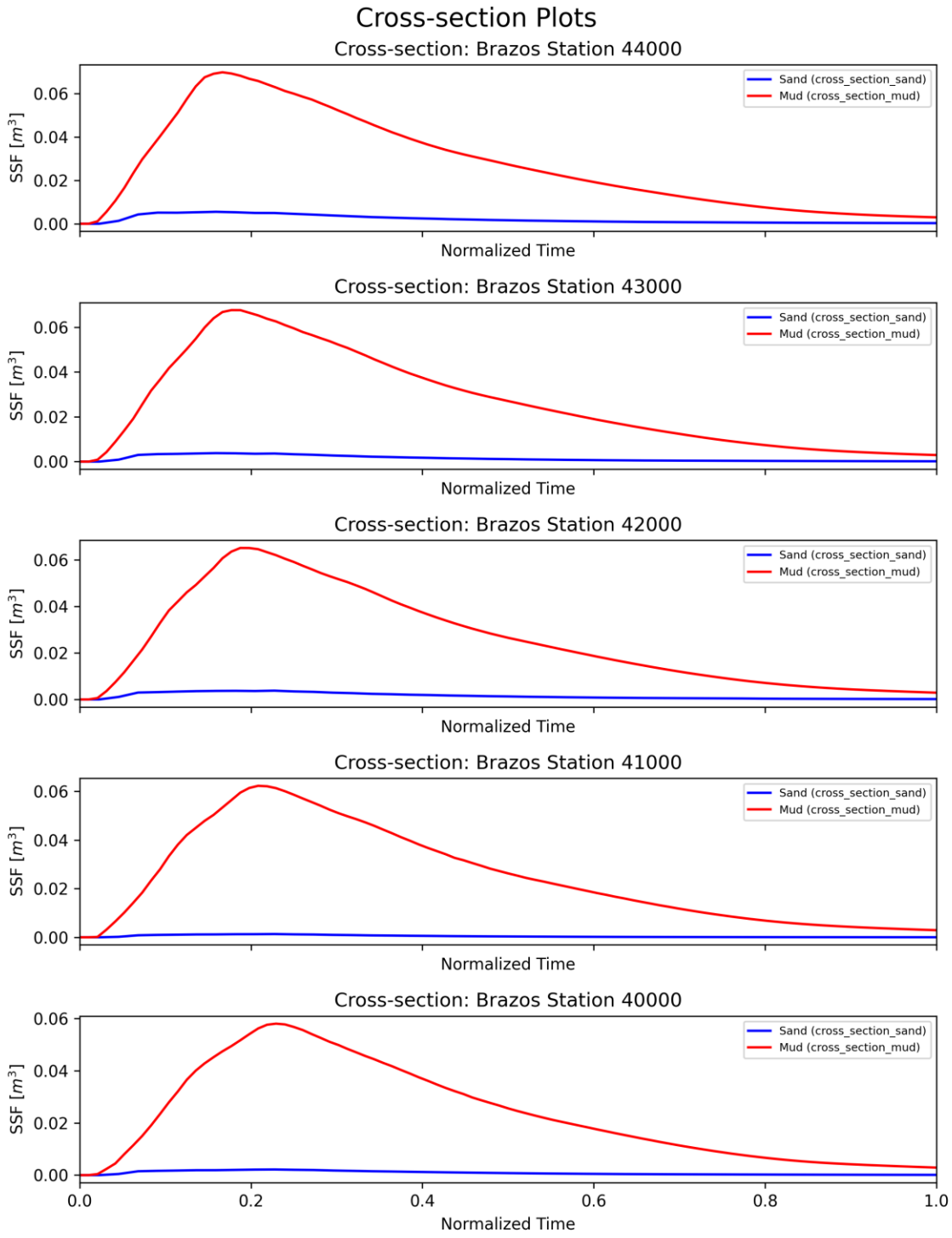
Cross-section Plots
Cross-section: Brazos Station 44000
Cross-section: Brazos Station 43000
Cross-section: Brazos Station 42000
Cross-section: Brazos Station 41000
Cross-section: Brazos Station 40000
Sand (cross_section_sand)
Mud (cross_section_mud)
SSF [m^3]
0.00
0.02
0.04
0.06
0.0
0.2
0.4
0.6
0.8
1.0
Normalized Time

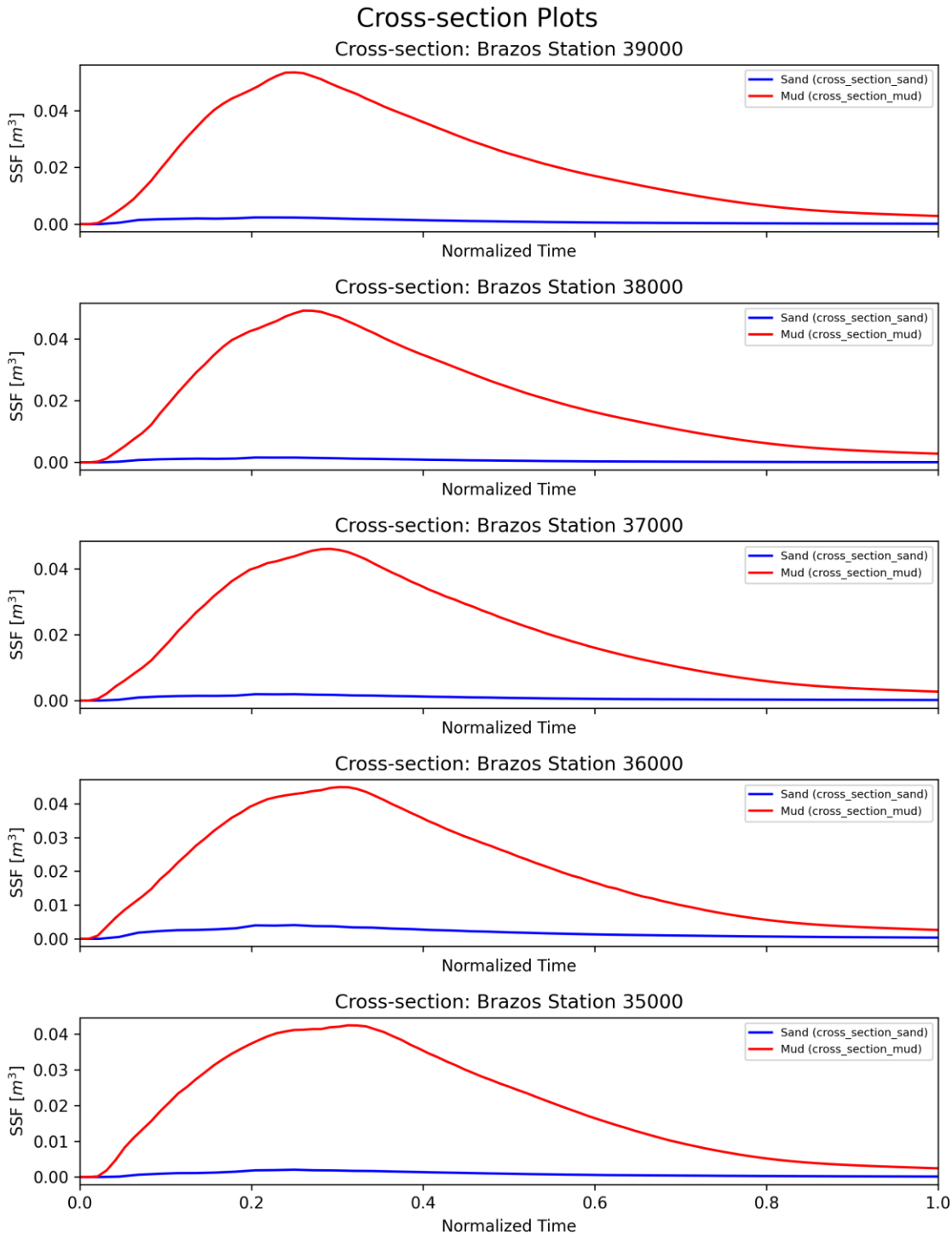
Cross-section Plots
Cross-section: Brazos Station 39000
Cross-section: Brazos Station 38000
Cross-section: Brazos Station 37000
Cross-section: Brazos Station 36000
Cross-section: Brazos Station 35000
Sand (cross_section_sand)
Mud (cross_section_mud)
SSF [m^3]
Normalized Time
0.00
0.01
0.02
0.03
0.04
0.0
0.2
0.4
0.6
0.8
1.0

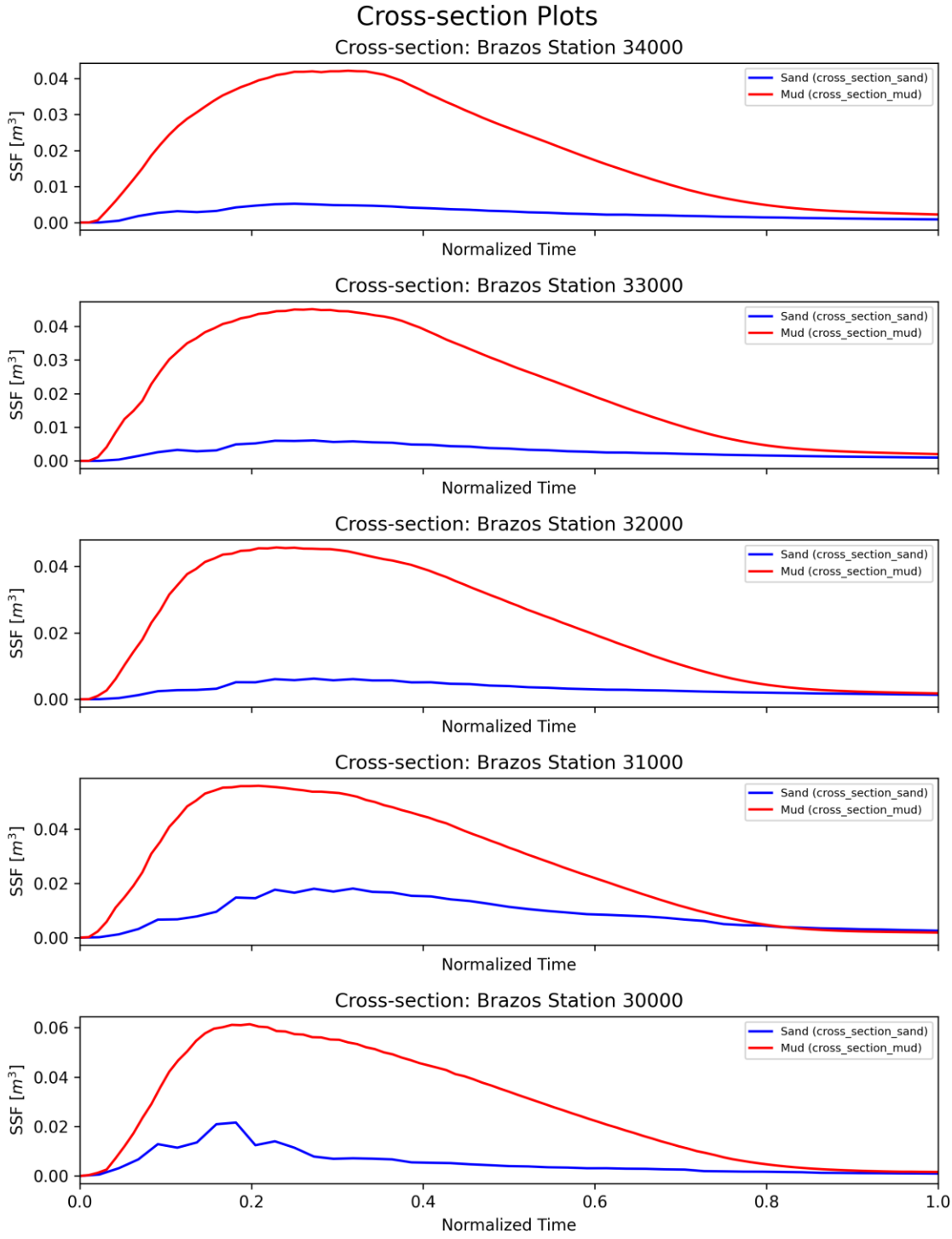
Cross-section Plots
Cross-section: Brazos Station 34000
Cross-section: Brazos Station 33000
Cross-section: Brazos Station 32000
Cross-section: Brazos Station 31000
Cross-section: Brazos Station 30000
Sand (cross_section_sand)
Mud (cross_section_mud)
SSF [m^3]
Normalized Time
0.00
0.01
0.02
0.03
0.04
0.06
0.0
0.2
0.4
0.6
0.8
1.0

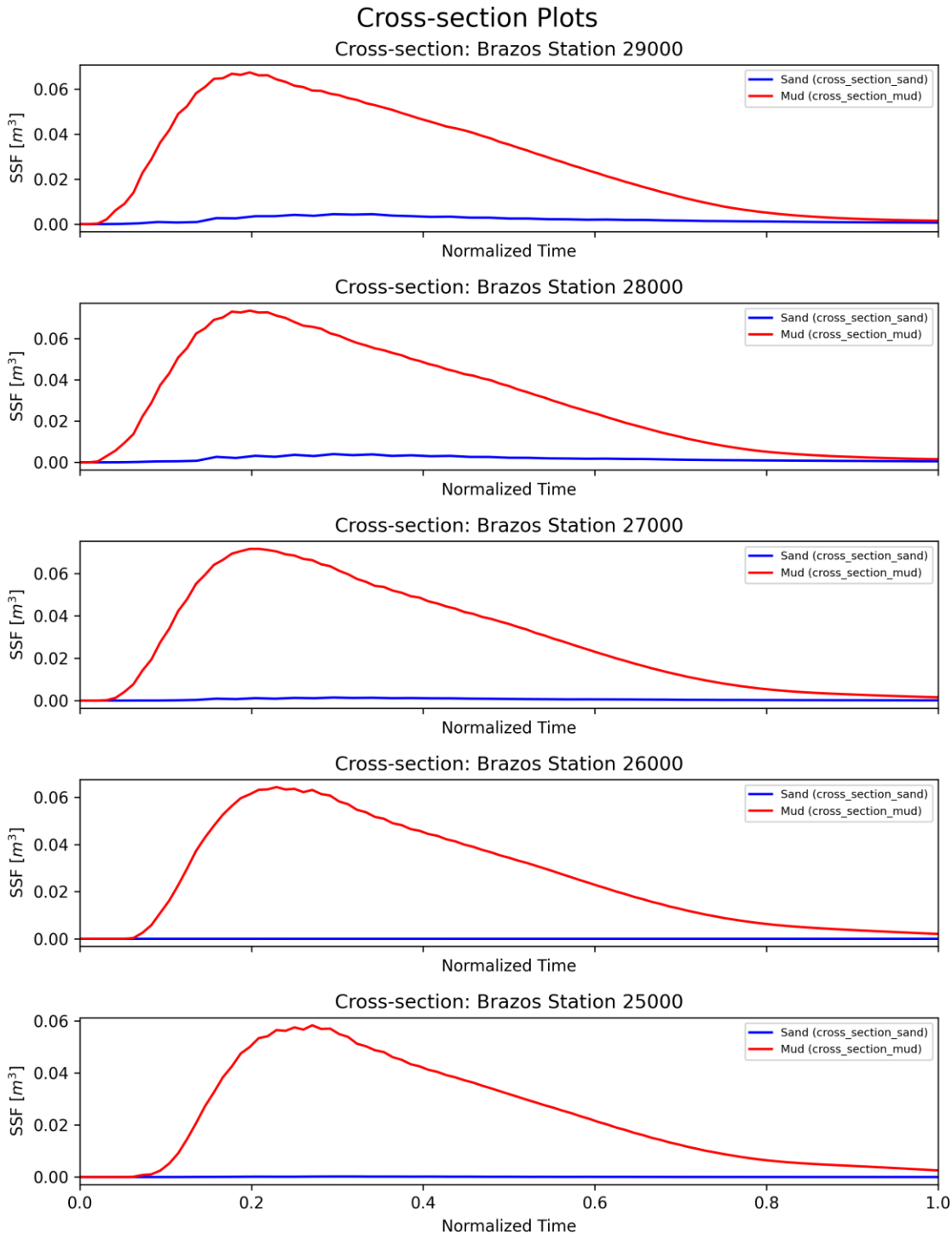
Cross-section Plots
Cross-section: Brazos Station 29000
Cross-section: Brazos Station 28000
Cross-section: Brazos Station 27000
Cross-section: Brazos Station 26000
Cross-section: Brazos Station 25000
Sand (cross_section_sand)
Mud (cross_section_mud)
SSF [m^3]
0.00
0.02
0.04
0.06
0.0
0.2
0.4
0.6
0.8
1.0
Normalized Time

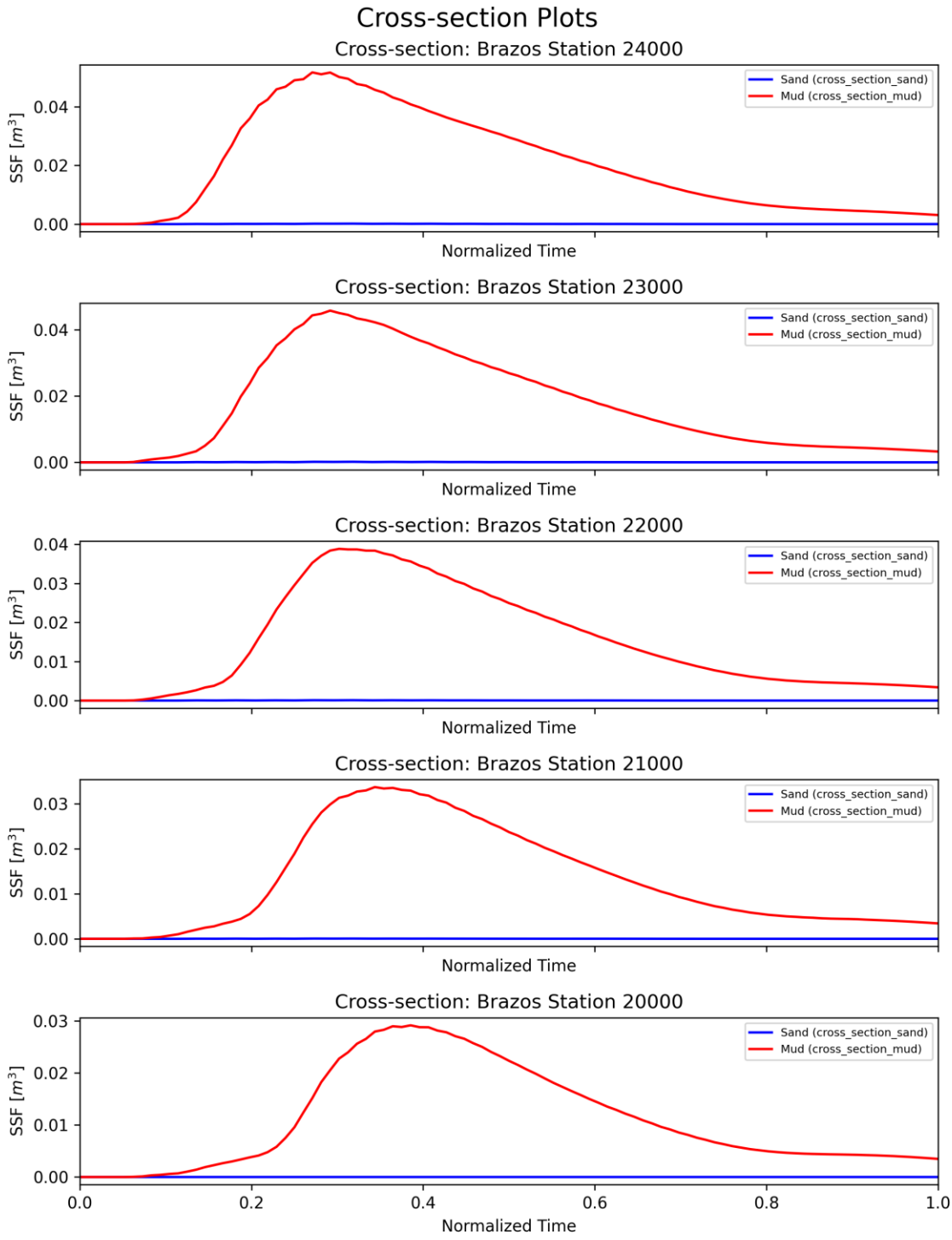
Cross-section Plots
Cross-section: Brazos Station 24000
Cross-section: Brazos Station 23000
Cross-section: Brazos Station 22000
Cross-section: Brazos Station 21000
Cross-section: Brazos Station 20000
Sand (cross_section_sand)
Mud (cross_section_mud)
SSF [m^3]
Normalized Time
0.00
0.01
0.02
0.03
0.04
0.0
0.2
0.4
0.6
0.8
1.0

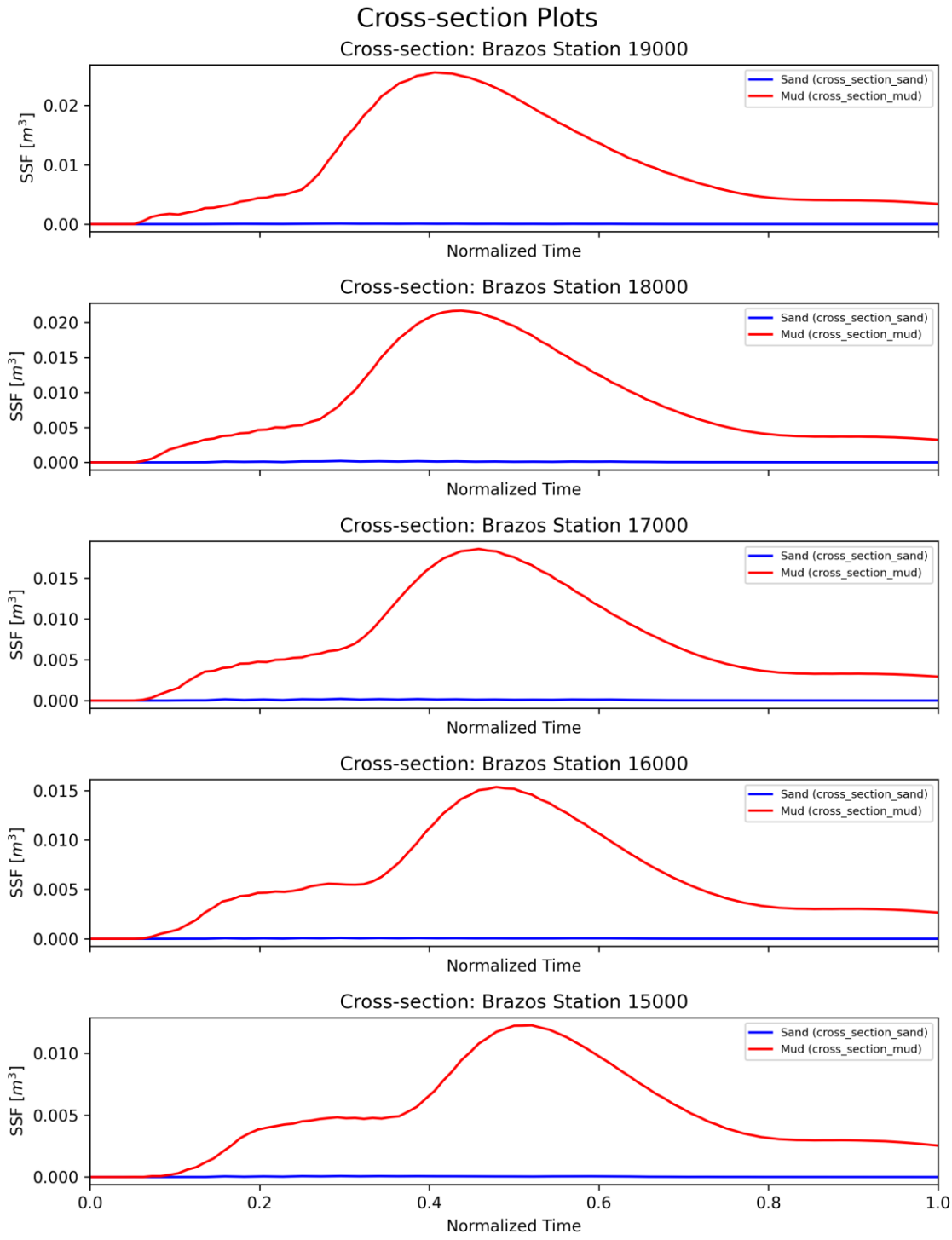
Cross-section Plots
Cross-section: Brazos Station 19000
Sand (cross_section_sand)
Mud (cross_section_mud)
SSF [m^3]
0.02
0.01
0.00
Normalized Time
Cross-section: Brazos Station 18000
Sand (cross_section_sand)
Mud (cross_section_mud)
SSF [m^3]
0.020
0.015
0.010
0.005
0.000
Normalized Time
Cross-section: Brazos Station 17000
Sand (cross_section_sand)
Mud (cross_section_mud)
SSF [m^3]
0.015
0.010
0.005
0.000
Normalized Time
Cross-section: Brazos Station 16000
Sand (cross_section_sand)
Mud (cross_section_mud)
SSF [m^3]
0.015
0.010
0.005
0.000
Normalized Time
Cross-section: Brazos Station 15000
Sand (cross_section_sand)
Mud (cross_section_mud)
SSF [m^3]
0.010
0.005
0.000
0.0
0.2
0.4
0.6
0.8
1.0
Normalized Time

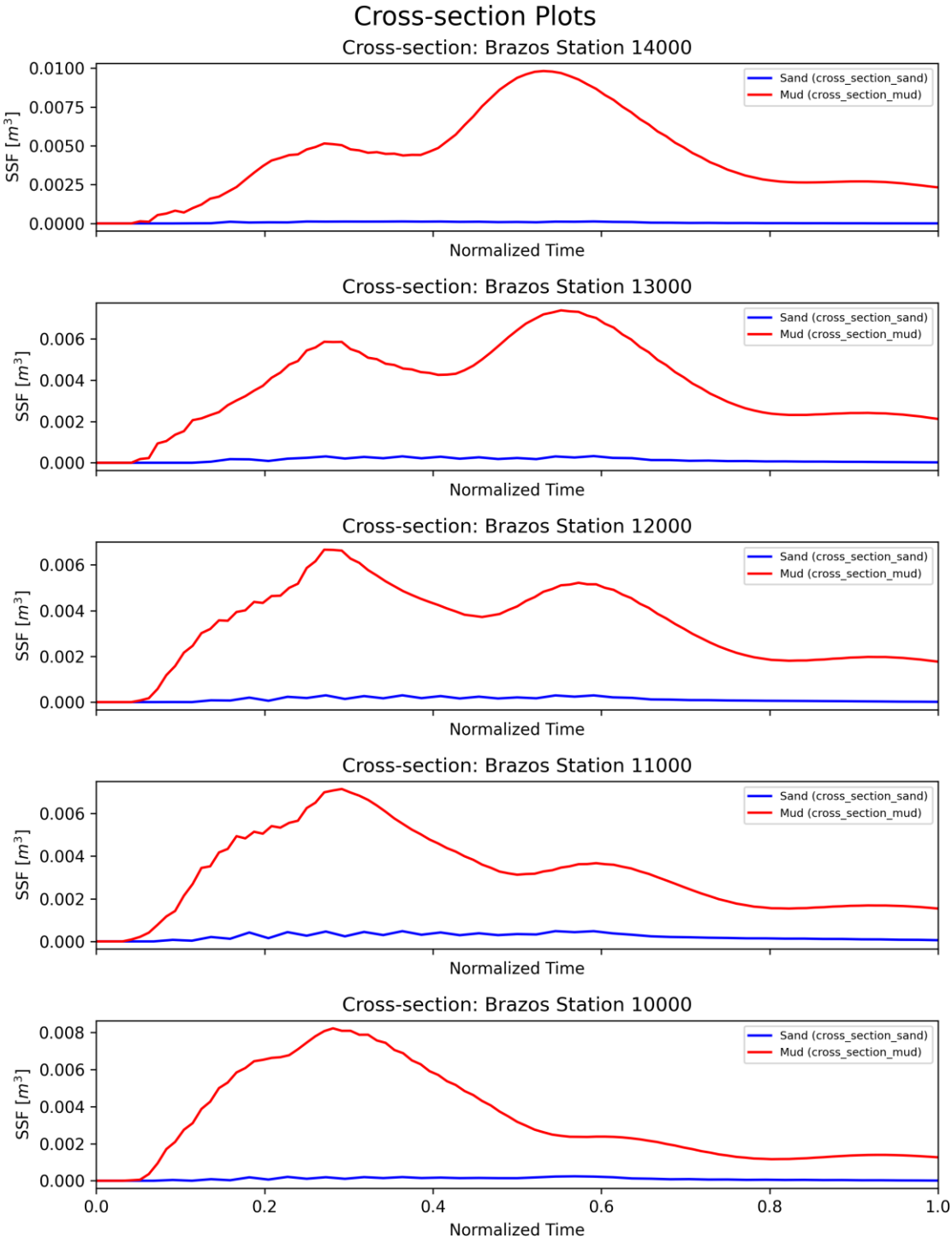
Cross-section Plots
Cross-section: Brazos Station 14000
Cross-section: Brazos Station 13000
Cross-section: Brazos Station 12000
Cross-section: Brazos Station 11000
Cross-section: Brazos Station 10000
Sand (cross_section_sand)
Mud (cross_section_mud)
SSF [m^3]
Normalized Time
0.0
0.2
0.4
0.6
0.8
1.0

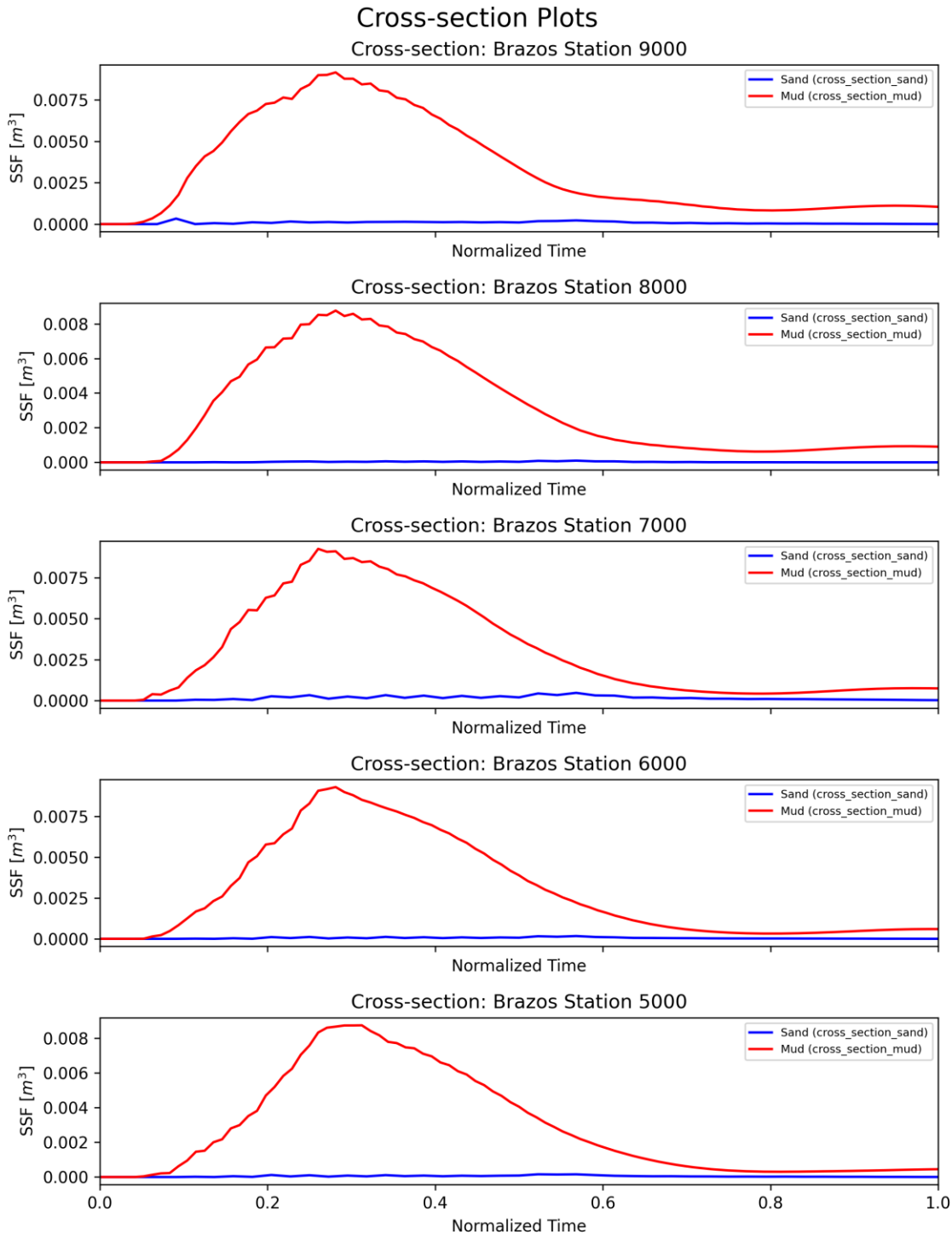
Cross-section Plots
Cross-section: Brazos Station 9000
Cross-section: Brazos Station 8000
Cross-section: Brazos Station 7000
Cross-section: Brazos Station 6000
Cross-section: Brazos Station 5000
Sand (cross_section_sand)
Mud (cross_section_mud)
SSF [m^3]
Normalized Time
0.0000
0.0025
0.0050
0.0075
0.000
0.002
0.004
0.006
0.008
0.0
0.2
0.4
0.6
0.8
1.0

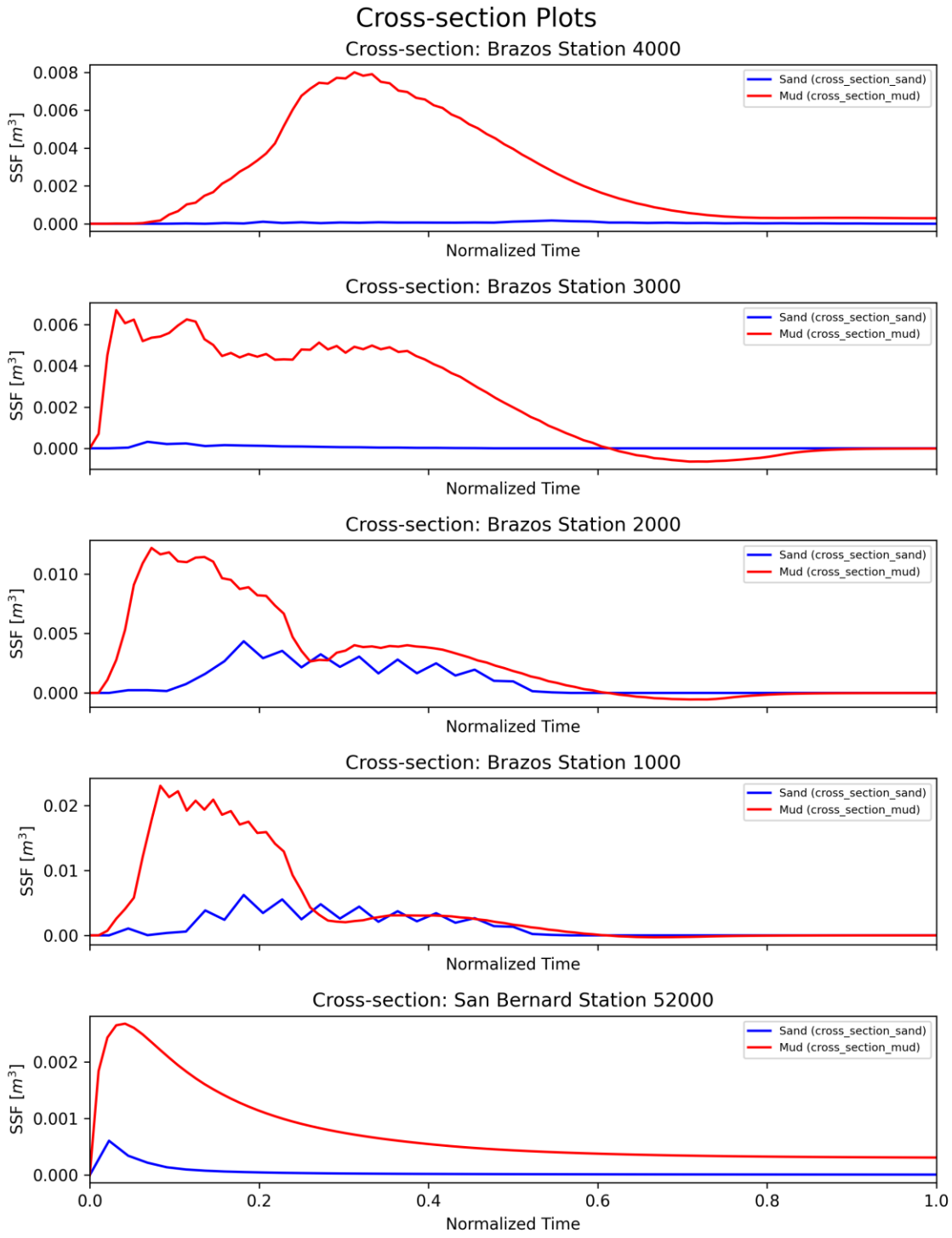
Cross-section Plots
Cross-section: Brazos Station 4000
Cross-section: Brazos Station 3000
Cross-section: Brazos Station 2000
Cross-section: Brazos Station 1000
Cross-section: San Bernard Station 52000
Sand (cross_section_sand)
Mud (cross_section_mud)
SSF [m^3]
Normalized Time

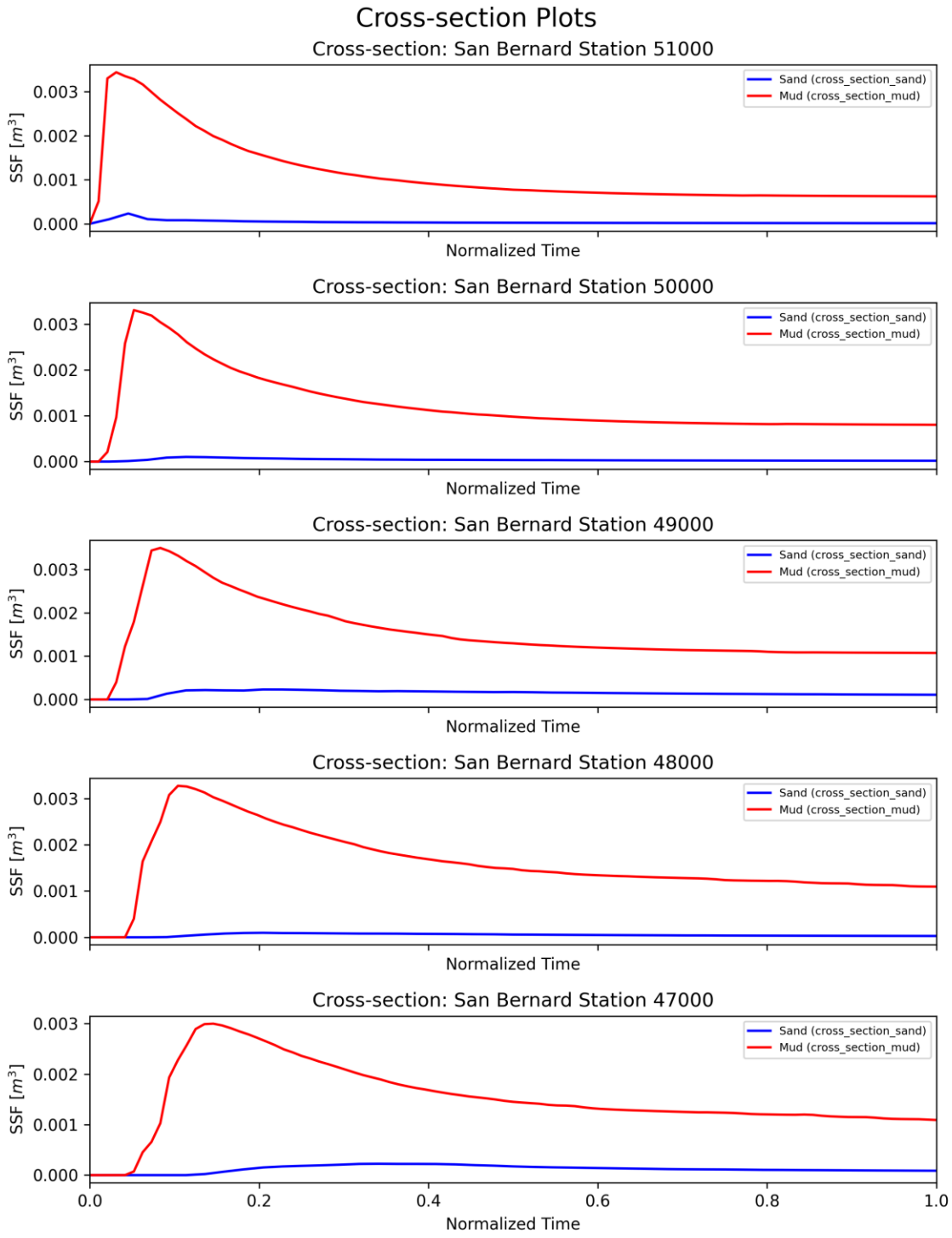
Cross-section Plots
Cross-section: San Bernard Station 51000
Cross-section: San Bernard Station 50000
Cross-section: San Bernard Station 49000
Cross-section: San Bernard Station 48000
Cross-section: San Bernard Station 47000
Sand (cross_section_sand)
Mud (cross_section_mud)
SSF [m^3]
0.000
0.001
0.002
0.003
0.0
0.2
0.4
0.6
0.8
1.0
Normalized Time

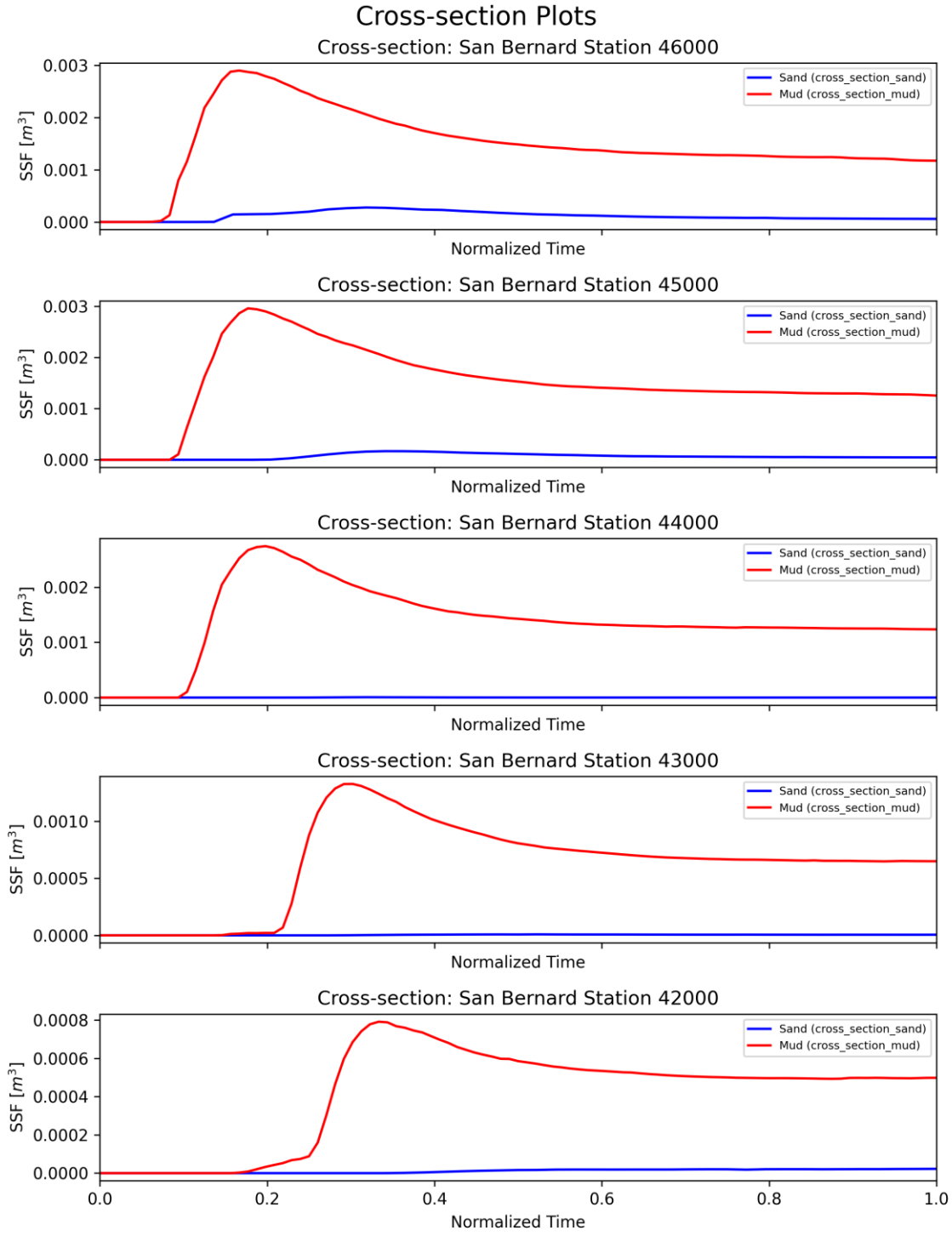
Cross-section Plots
Cross-section: San Bernard Station 46000
Cross-section: San Bernard Station 45000
Cross-section: San Bernard Station 44000
Cross-section: San Bernard Station 43000
Cross-section: San Bernard Station 42000
Sand (cross_section_sand)
Mud (cross_section_mud)
SSF [m^3]
Normalized Time
0.0
0.2
0.4
0.6
0.8
1.0

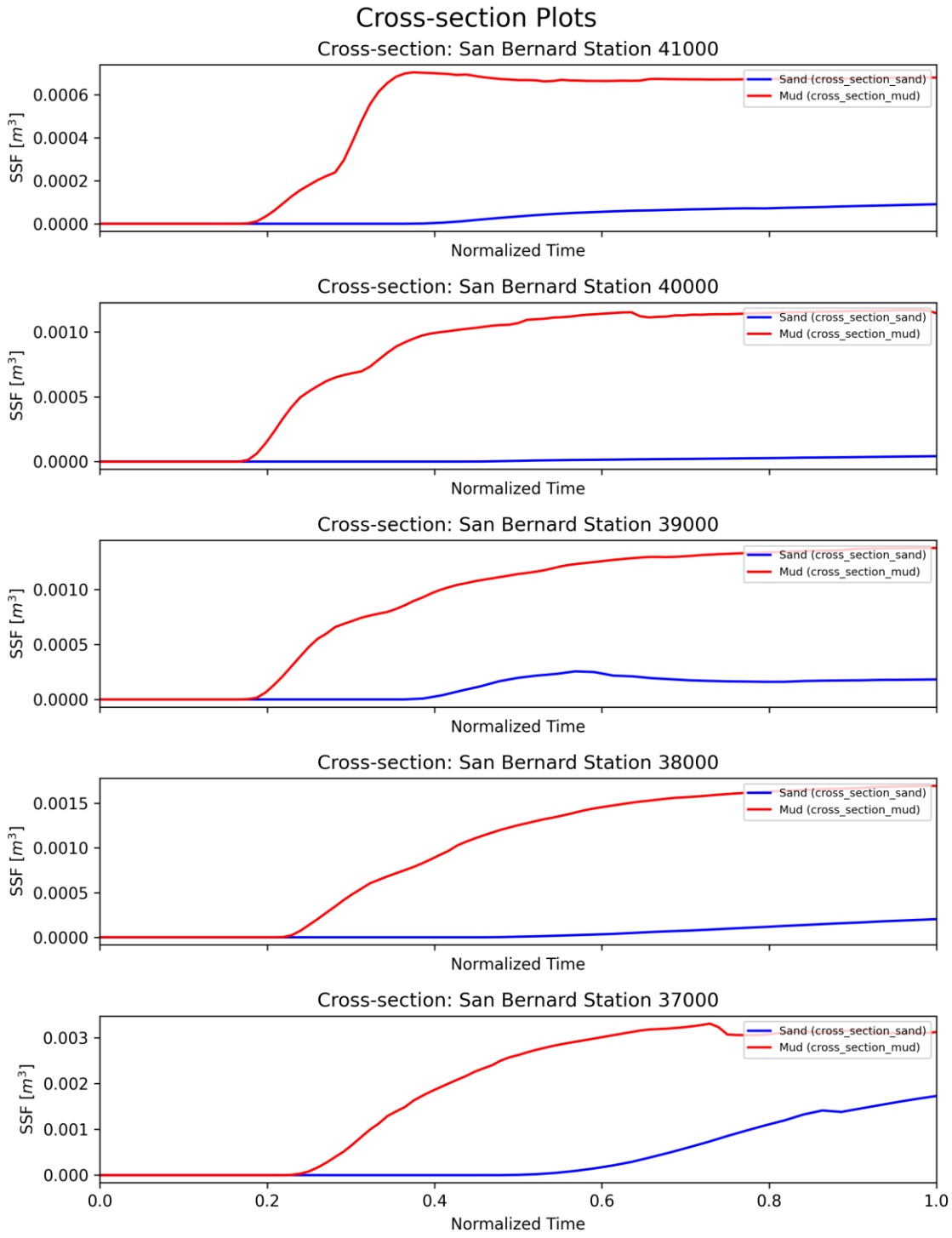
Cross-section Plots
Cross-section: San Bernard Station 41000
Cross-section: San Bernard Station 40000
Cross-section: San Bernard Station 39000
Cross-section: San Bernard Station 38000
Cross-section: San Bernard Station 37000
Sand (cross_section_sand)
Mud (cross_section_mud)
SSF [m^3]
Normalized Time
0.0000
0.0002
0.0004
0.0006
0.0005
0.0010
0.0015
0.001
0.002
0.003
0.000
0.0
0.2
0.4
0.6
0.8
1.0

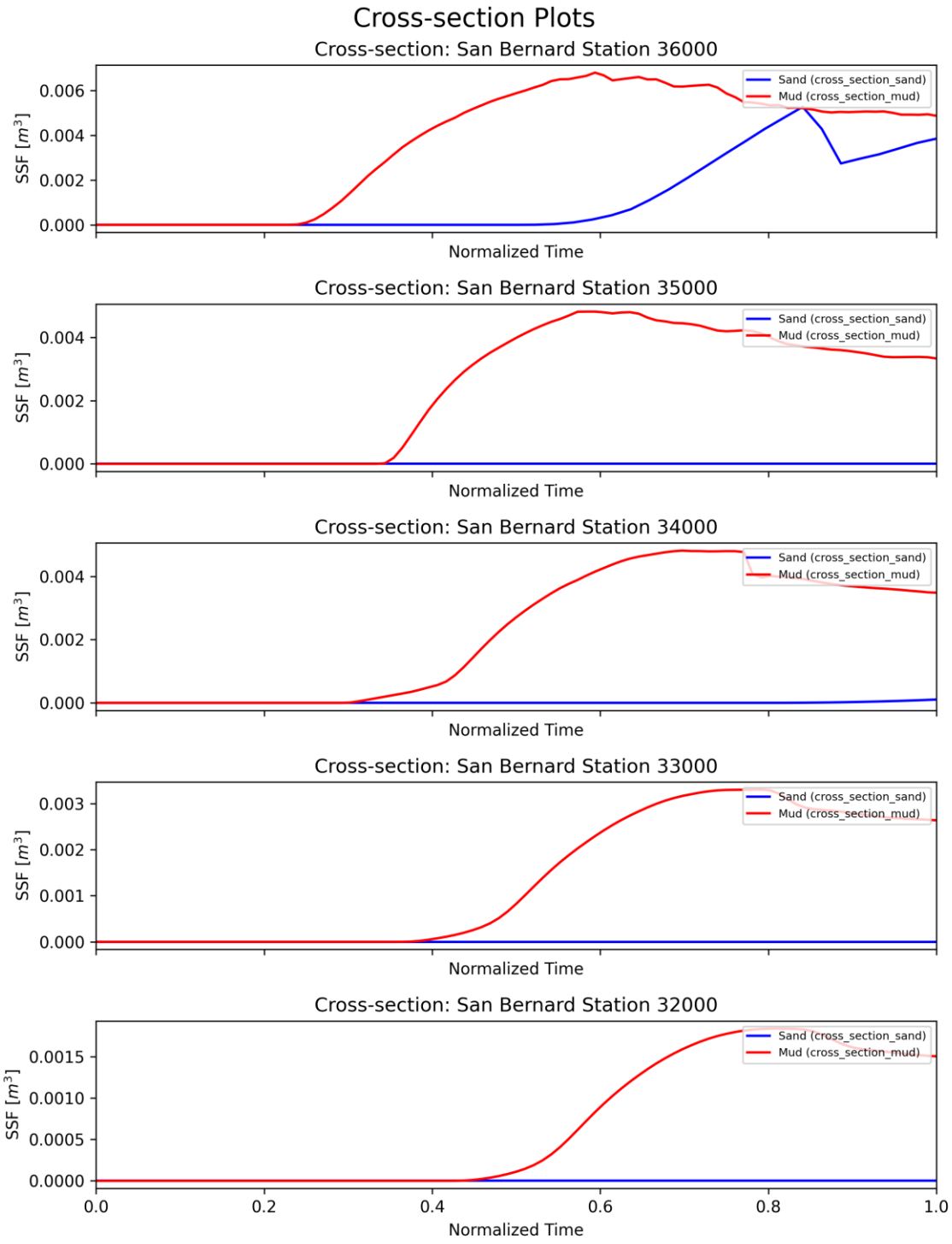
Cross-section Plots
Cross-section: San Bernard Station 36000
Cross-section: San Bernard Station 35000
Cross-section: San Bernard Station 34000
Cross-section: San Bernard Station 33000
Cross-section: San Bernard Station 32000
Sand (cross_section_sand)
Mud (cross_section_mud)
SSF [m^3]
Normalized Time
0.000
0.002
0.004
0.006
0.001
0.003
0.0000
0.0005
0.0010
0.0015
0.0
0.2
0.4
0.6
0.8
1.0

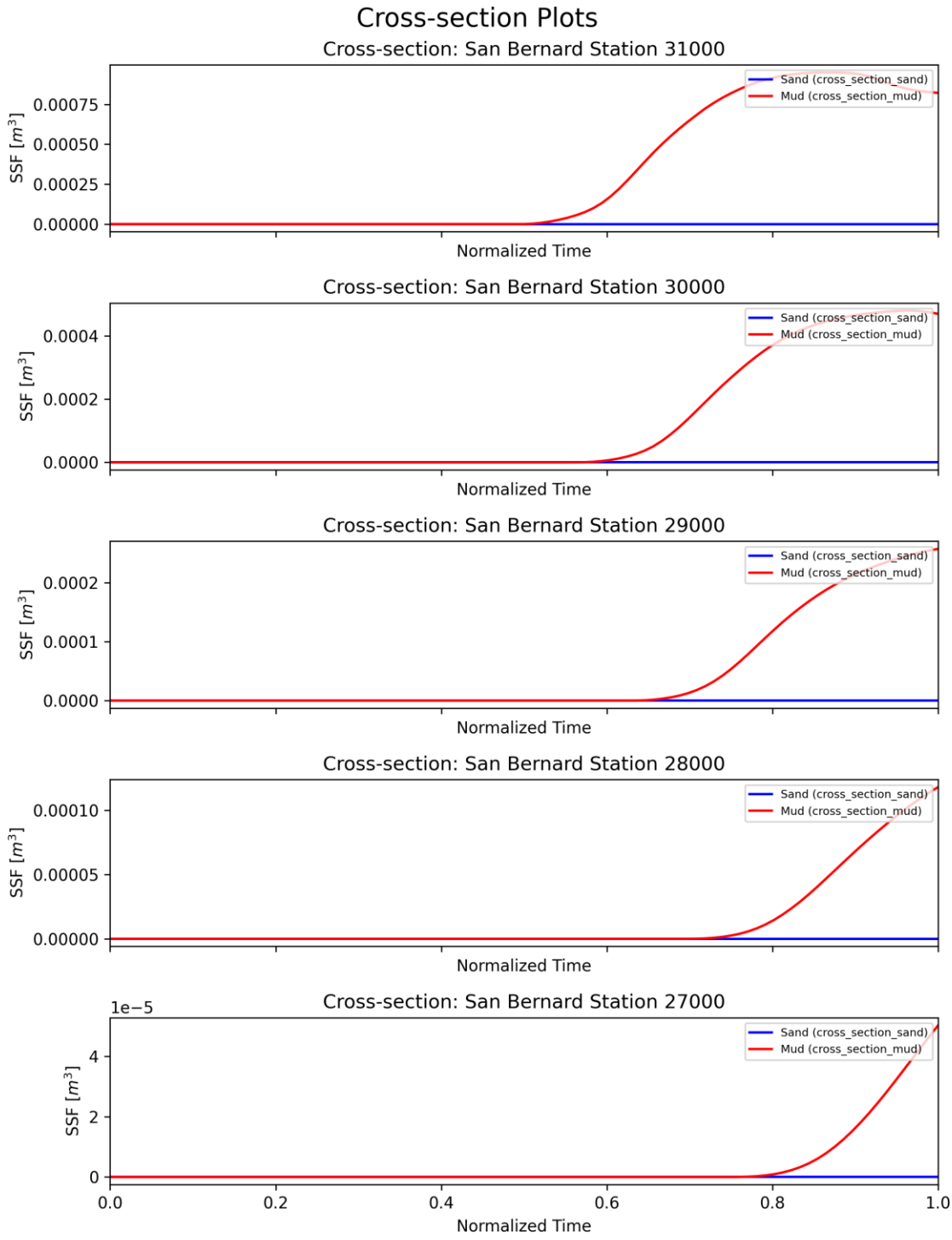
Cross-section Plots
Cross-section: San Bernard Station 31000
Sand (cross_section_sand)
Mud (cross_section_mud)
SSF [m^3]
0.00075
0.00050
0.00025
0.00000
Normalized Time
Cross-section: San Bernard Station 30000
Sand (cross_section_sand)
Mud (cross_section_mud)
SSF [m^3]
0.0004
0.0002
0.0000
Normalized Time
Cross-section: San Bernard Station 29000
Sand (cross_section_sand)
Mud (cross_section_mud)
SSF [m^3]
0.0002
0.0001
0.0000
Normalized Time
Cross-section: San Bernard Station 28000
Sand (cross_section_sand)
Mud (cross_section_mud)
SSF [m^3]
0.00010
0.00005
0.00000
Normalized Time
Cross-section: San Bernard Station 27000
1e−5
Sand (cross_section_sand)
Mud (cross_section_mud)
SSF [m^3]
4
2
0
0.0
0.2
0.4
0.6
0.8
1.0
Normalized Time

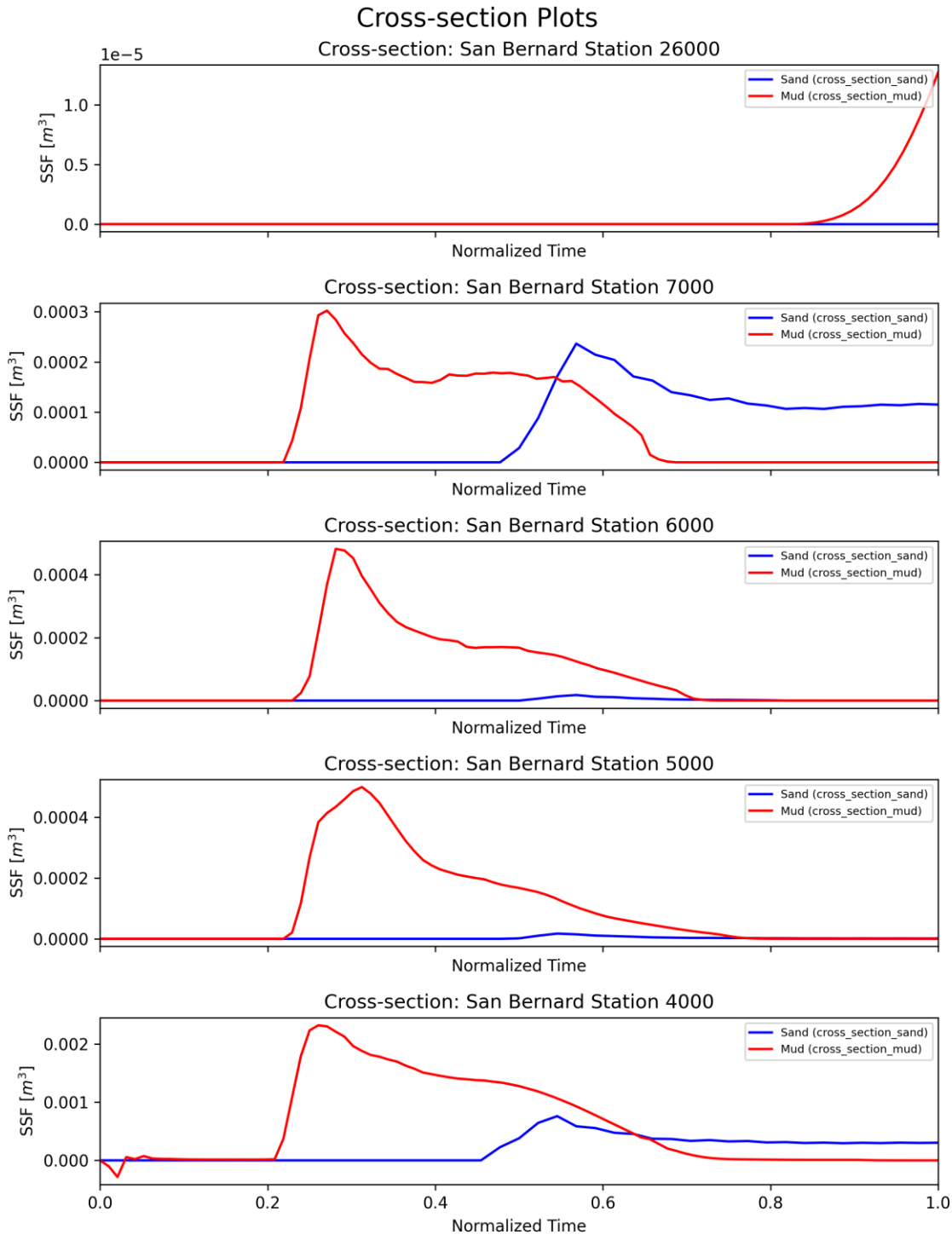
Cross-section Plots
Cross-section: San Bernard Station 26000
1e−5
SSF [m^3]
Normalized Time
Sand (cross_section_sand)
Mud (cross_section_mud)
Cross-section: San Bernard Station 7000
Cross-section: San Bernard Station 6000
Cross-section: San Bernard Station 5000
Cross-section: San Bernard Station 4000

APPENDIX J: THE EFFECT OF COHESIVE VS. NON-COHESIVE SEDIMENT IN COLORADO DOMAIN

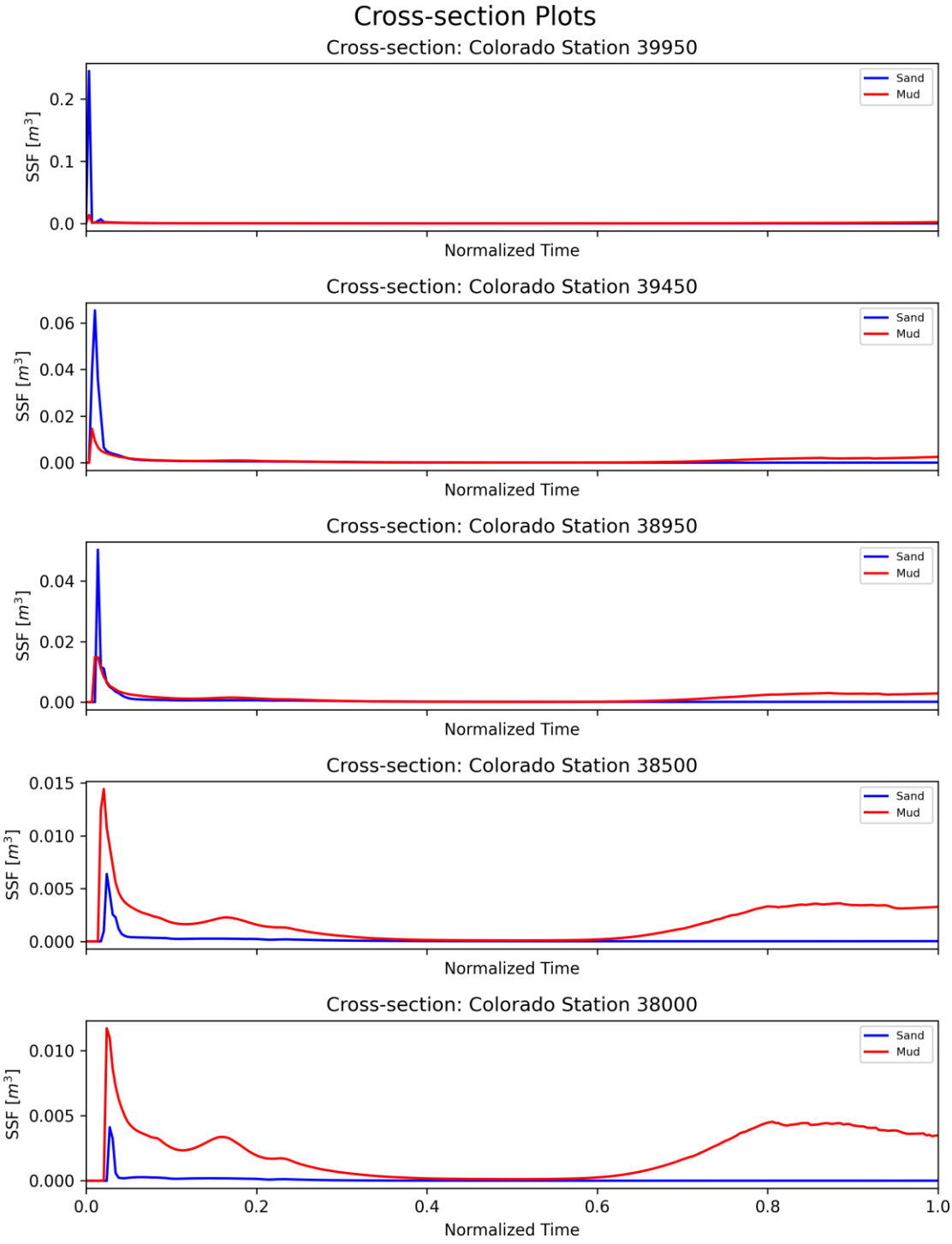
Cross-section Plots
Cross-section: Colorado Station 39950
Cross-section: Colorado Station 39450
Cross-section: Colorado Station 38950
Cross-section: Colorado Station 38500
Cross-section: Colorado Station 38000
Sand
Mud
SSF [m^3]
Normalized Time

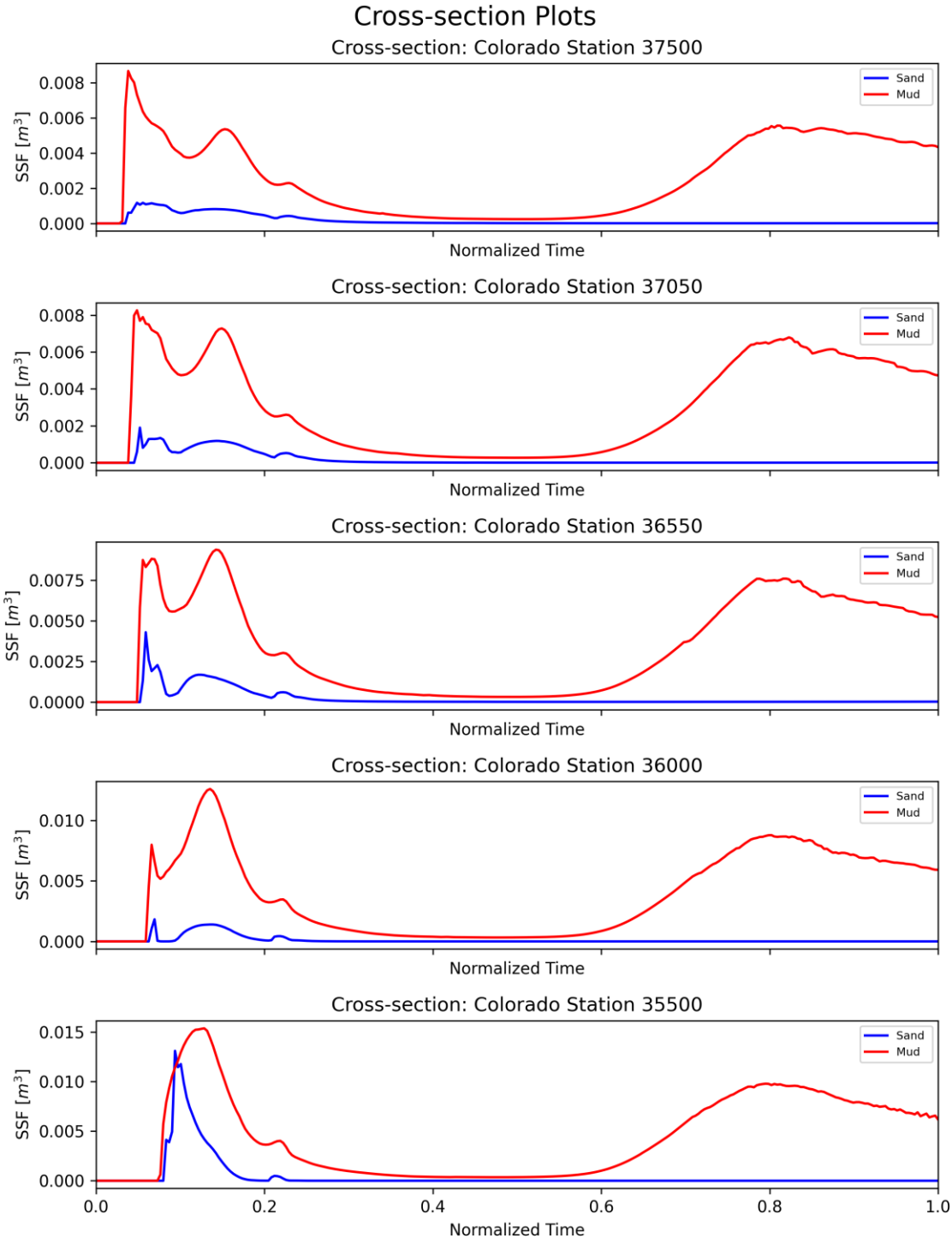
Cross-section Plots
Cross-section: Colorado Station 37500
Cross-section: Colorado Station 37050
Cross-section: Colorado Station 36550
Cross-section: Colorado Station 36000
Cross-section: Colorado Station 35500
Sand
Mud
SSF [m^3]
Normalized Time
0.008
0.006
0.004
0.002
0.000
0.0075
0.0050
0.0025
0.0000
0.010
0.005
0.015
0.0
0.2
0.4
0.6
0.8
1.0

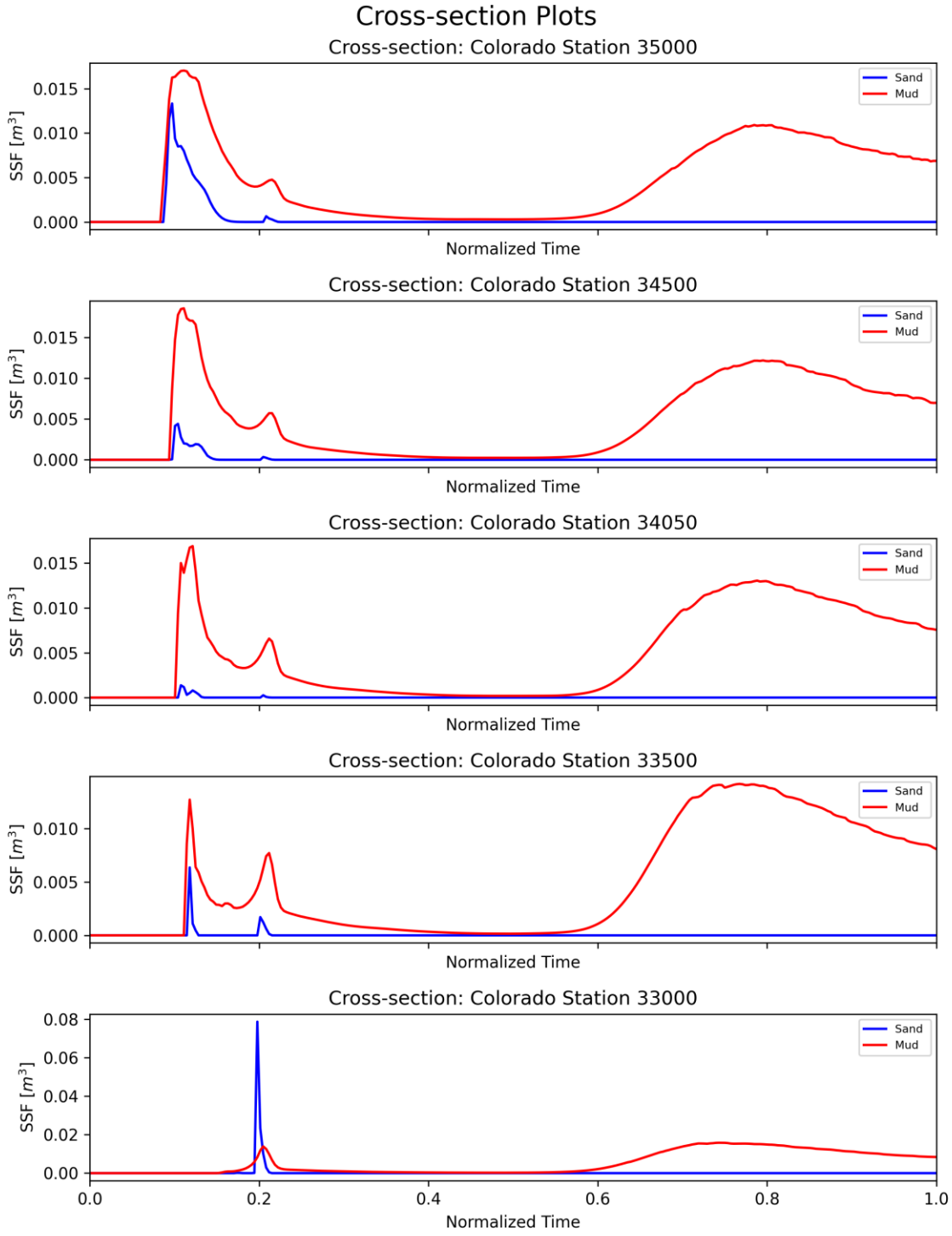
Cross-section Plots
Cross-section: Colorado Station 35000
Cross-section: Colorado Station 34500
Cross-section: Colorado Station 34050
Cross-section: Colorado Station 33500
Cross-section: Colorado Station 33000
Sand
Mud
SSF [m^3]
Normalized Time
0.000
0.005
0.010
0.015
0.00
0.02
0.04
0.06
0.08
0.0
0.2
0.4
0.6
0.8
1.0

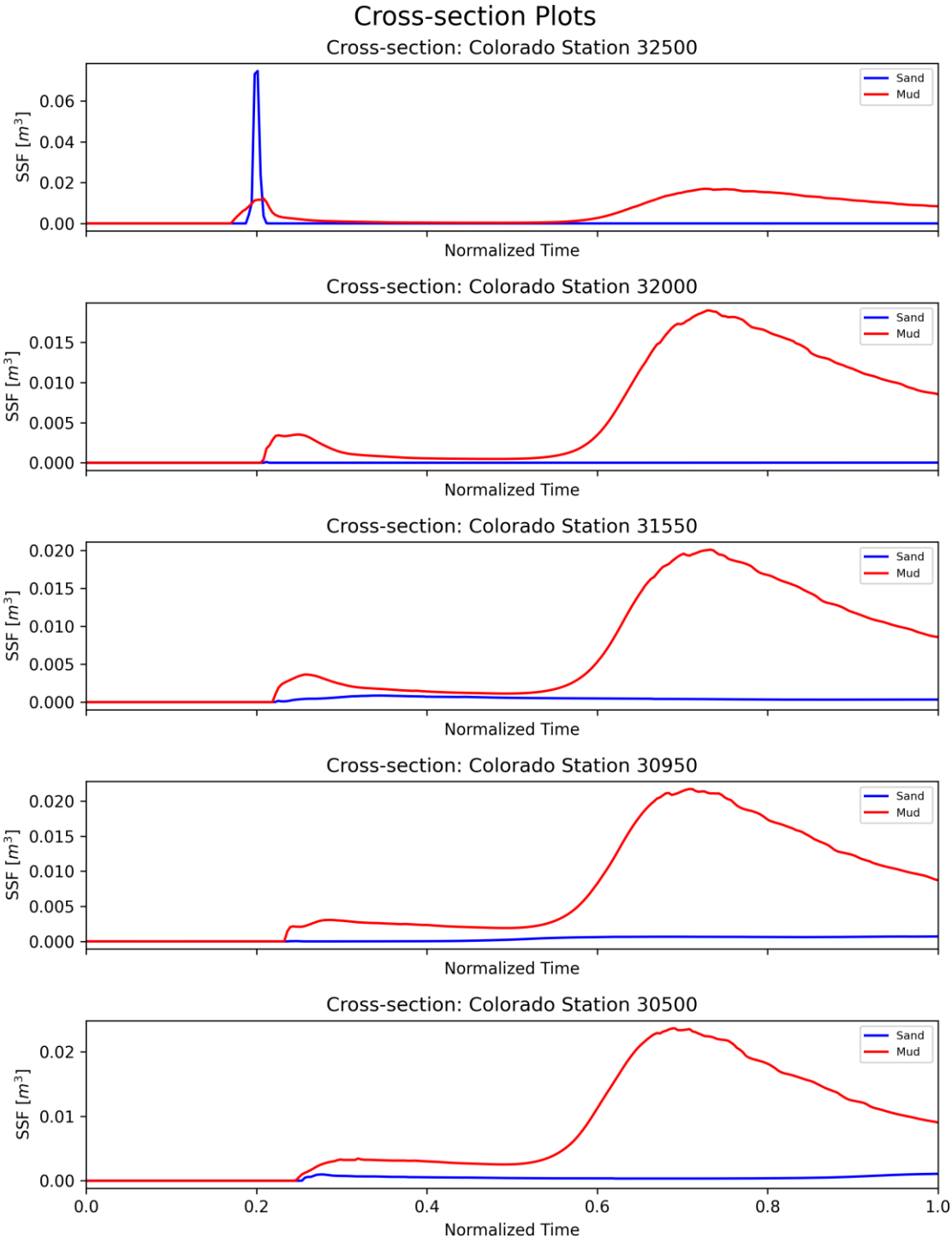
Cross-section Plots
Cross-section: Colorado Station 32500
Cross-section: Colorado Station 32000
Cross-section: Colorado Station 31550
Cross-section: Colorado Station 30950
Cross-section: Colorado Station 30500
Sand
Mud
SSF [m^3]
Normalized Time
0.00
0.02
0.04
0.06
0.000
0.005
0.010
0.015
0.020
0.0
0.2
0.4
0.6
0.8
1.0

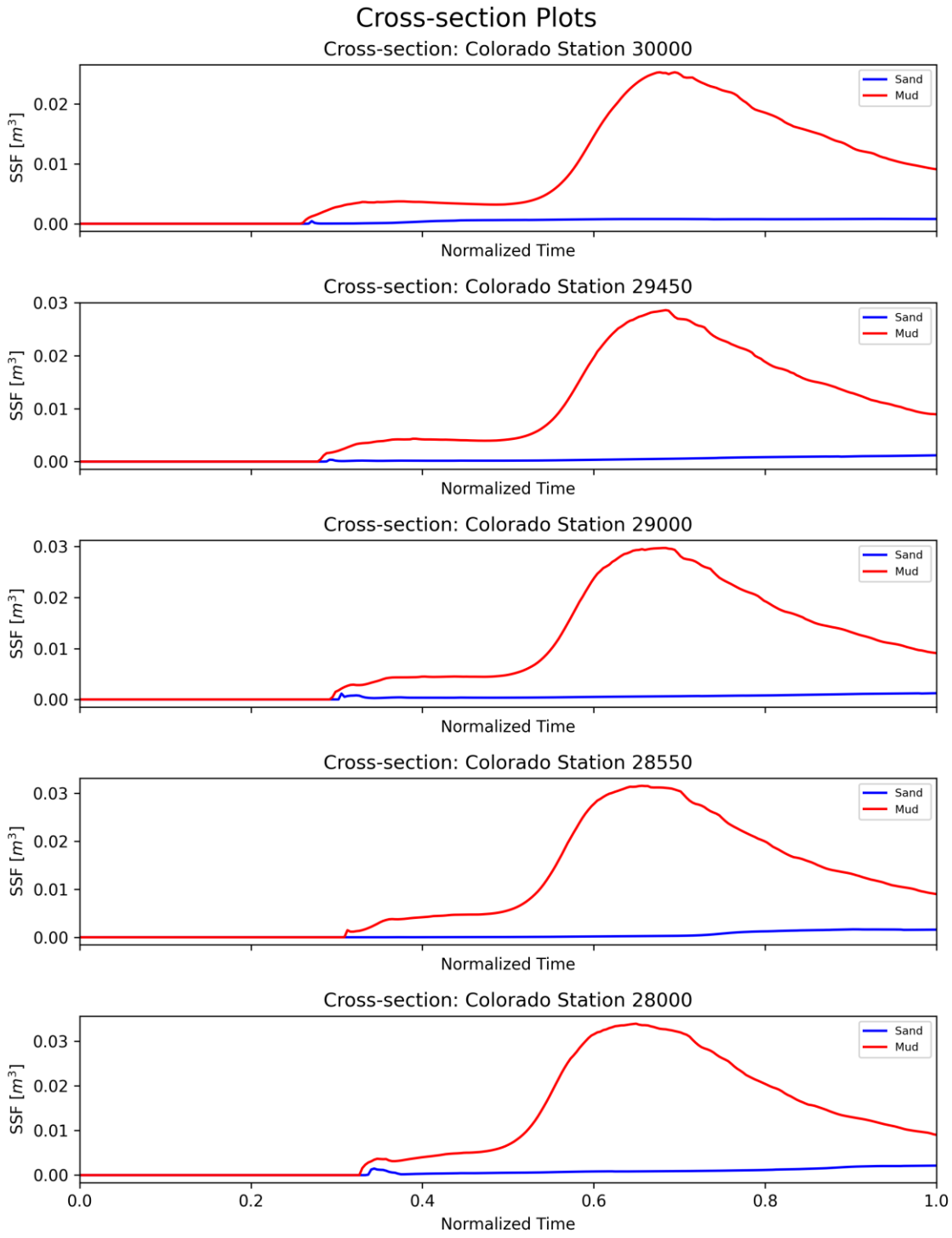
Cross-section Plots
Cross-section: Colorado Station 30000
Cross-section: Colorado Station 29450
Cross-section: Colorado Station 29000
Cross-section: Colorado Station 28550
Cross-section: Colorado Station 28000
Sand
Mud
SSF [m^3]
Normalized Time
0.00
0.01
0.02
0.03
0.0
0.2
0.4
0.6
0.8
1.0

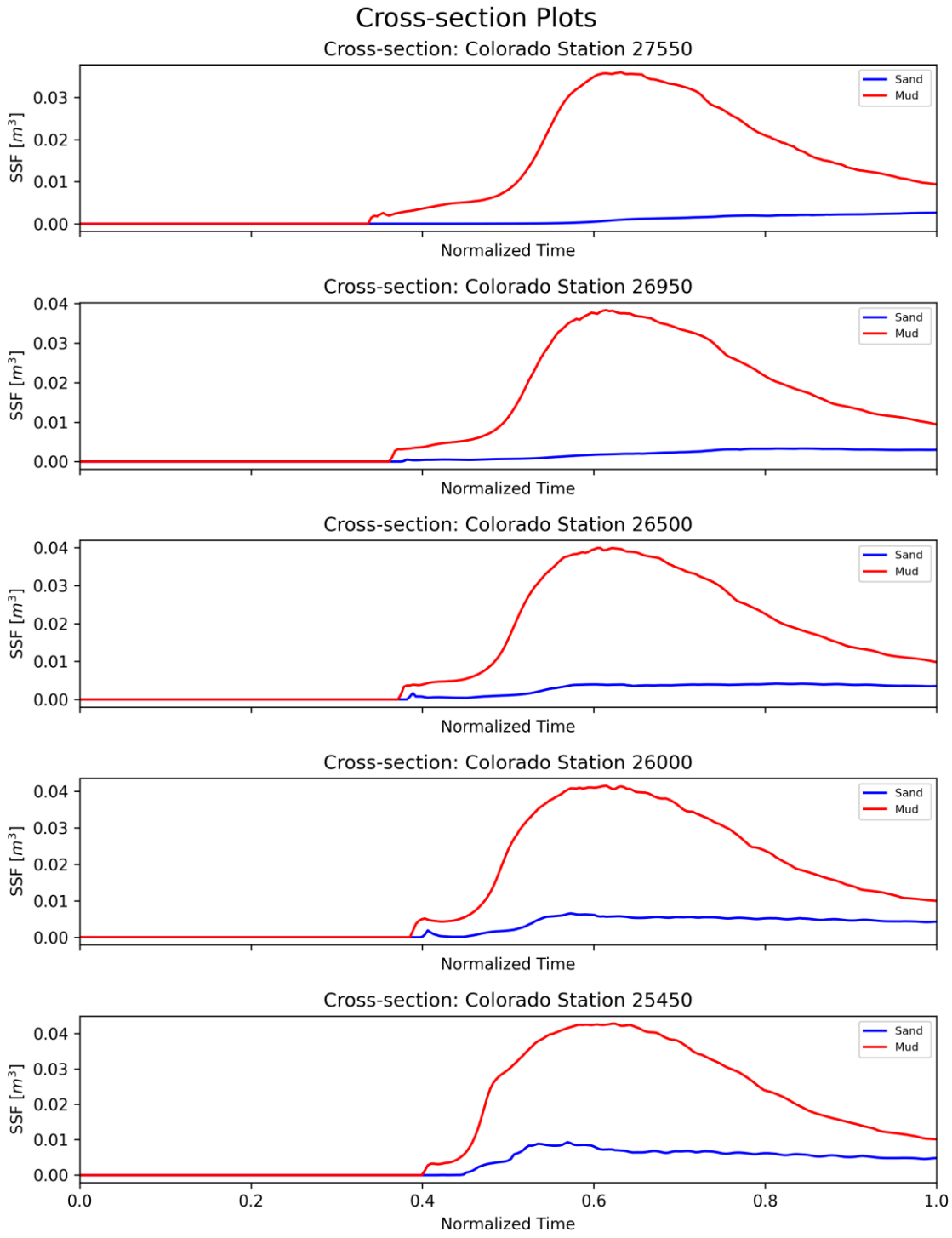
Cross-section Plots
Cross-section: Colorado Station 27550
Cross-section: Colorado Station 26950
Cross-section: Colorado Station 26500
Cross-section: Colorado Station 26000
Cross-section: Colorado Station 25450
Sand
Mud
SSF [m^3]
Normalized Time
0.00
0.01
0.02
0.03
0.04
0.0
0.2
0.4
0.6
0.8
1.0

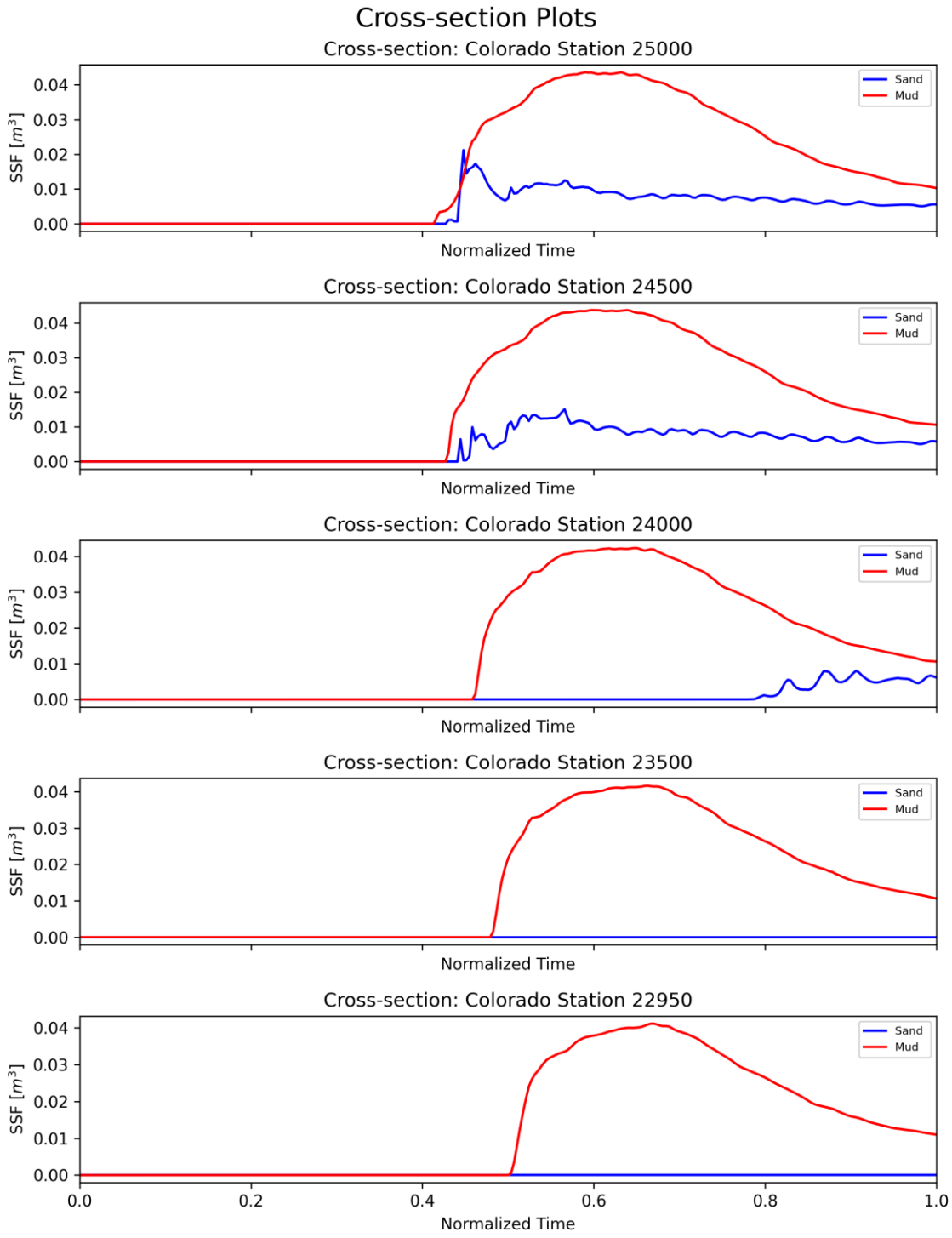
Cross-section Plots
Cross-section: Colorado Station 25000
Cross-section: Colorado Station 24500
Cross-section: Colorado Station 24000
Cross-section: Colorado Station 23500
Cross-section: Colorado Station 22950
Sand
Mud
SSF [m^3]
0.00
0.01
0.02
0.03
0.04
0.0
0.2
0.4
0.6
0.8
1.0
Normalized Time

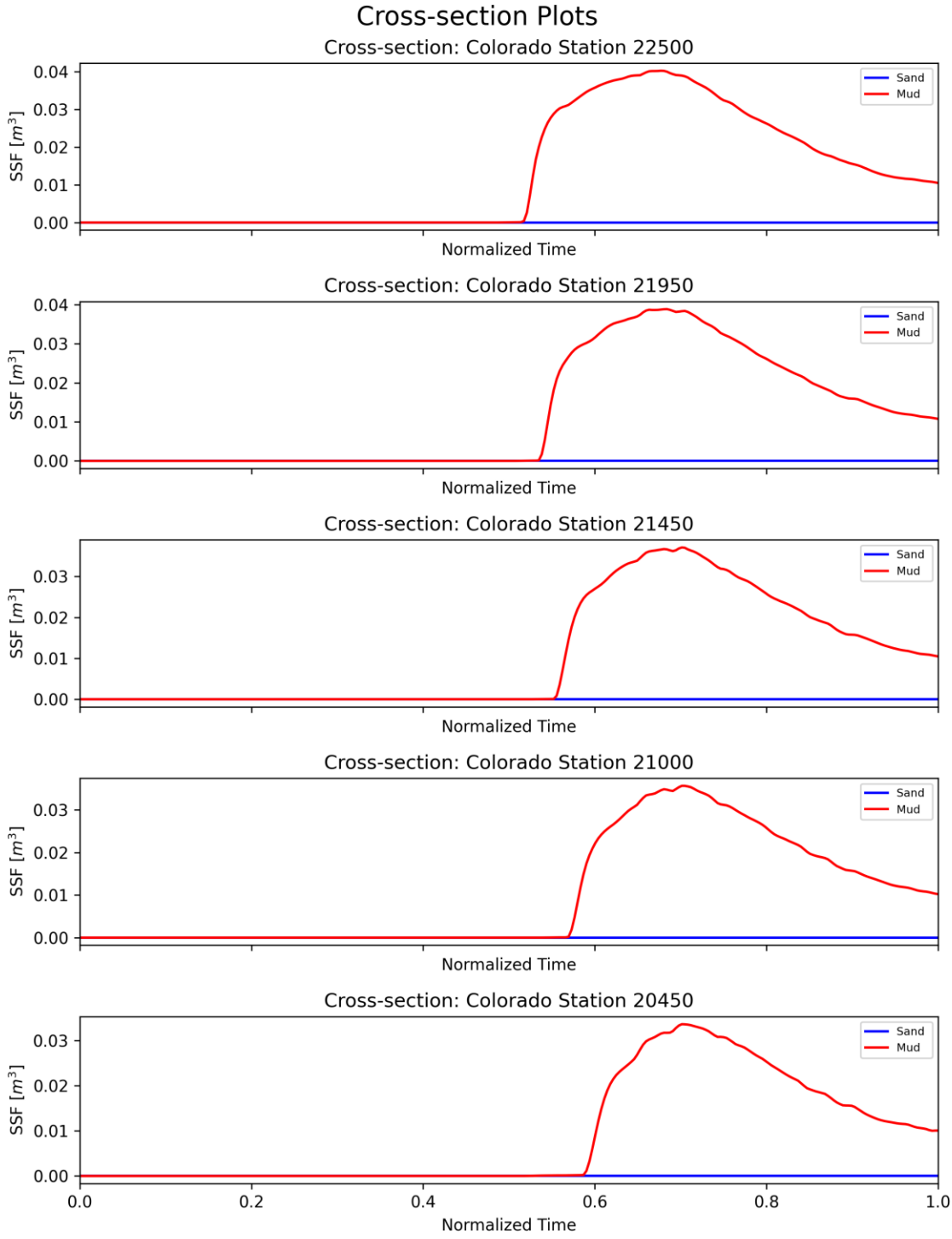
Cross-section Plots
Cross-section: Colorado Station 22500
Cross-section: Colorado Station 21950
Cross-section: Colorado Station 21450
Cross-section: Colorado Station 21000
Cross-section: Colorado Station 20450
Sand
Mud
SSF [m^3]
Normalized Time
0.00
0.01
0.02
0.03
0.04
0.0
0.2
0.4
0.6
0.8
1.0

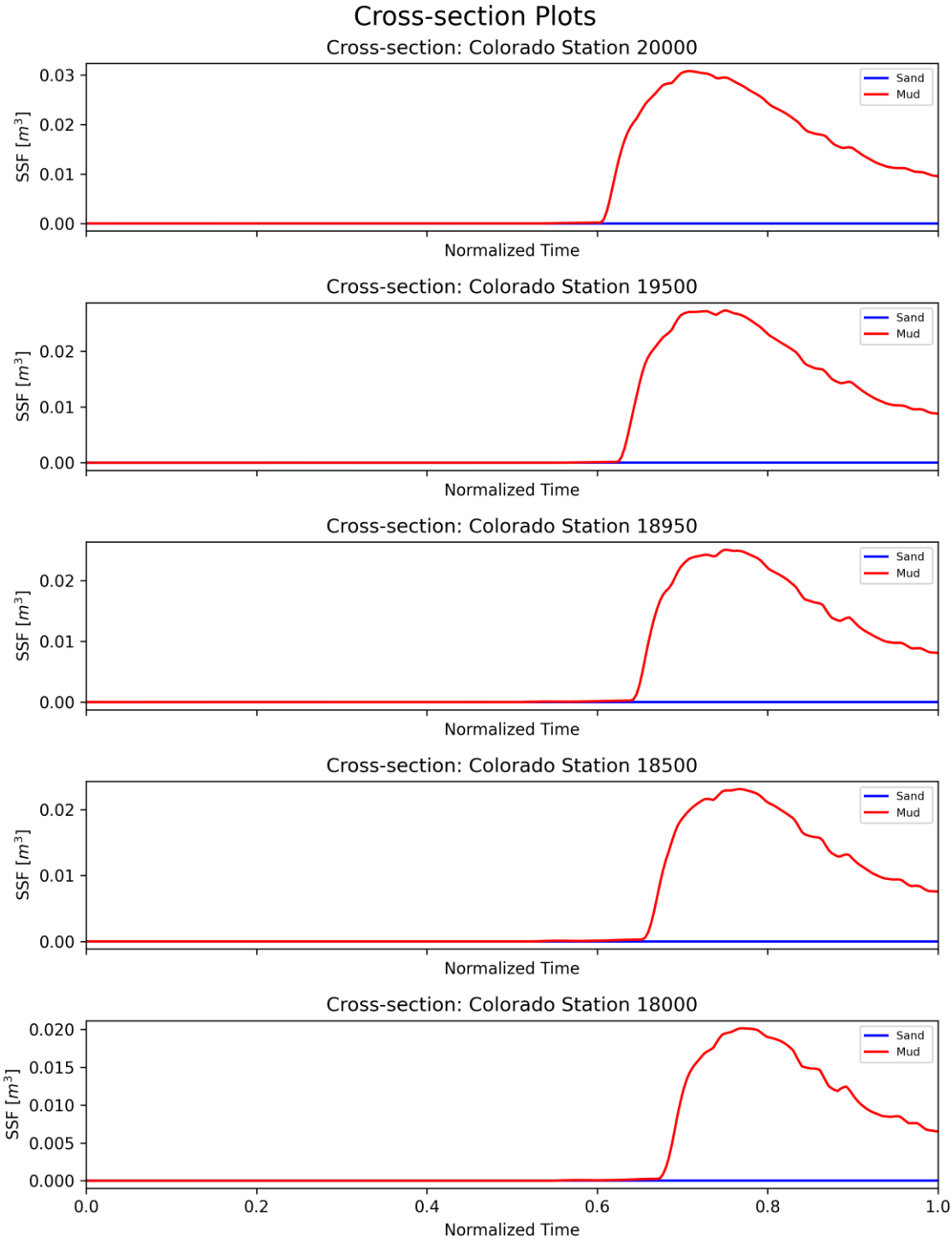
Cross-section Plots
Cross-section: Colorado Station 20000
Cross-section: Colorado Station 19500
Cross-section: Colorado Station 18950
Cross-section: Colorado Station 18500
Cross-section: Colorado Station 18000
SSF [m^3]
Normalized Time
Sand
Mud
0.03
0.02
0.01
0.00
0.020
0.015
0.010
0.005
0.000
0.0
0.2
0.4
0.6
0.8
1.0

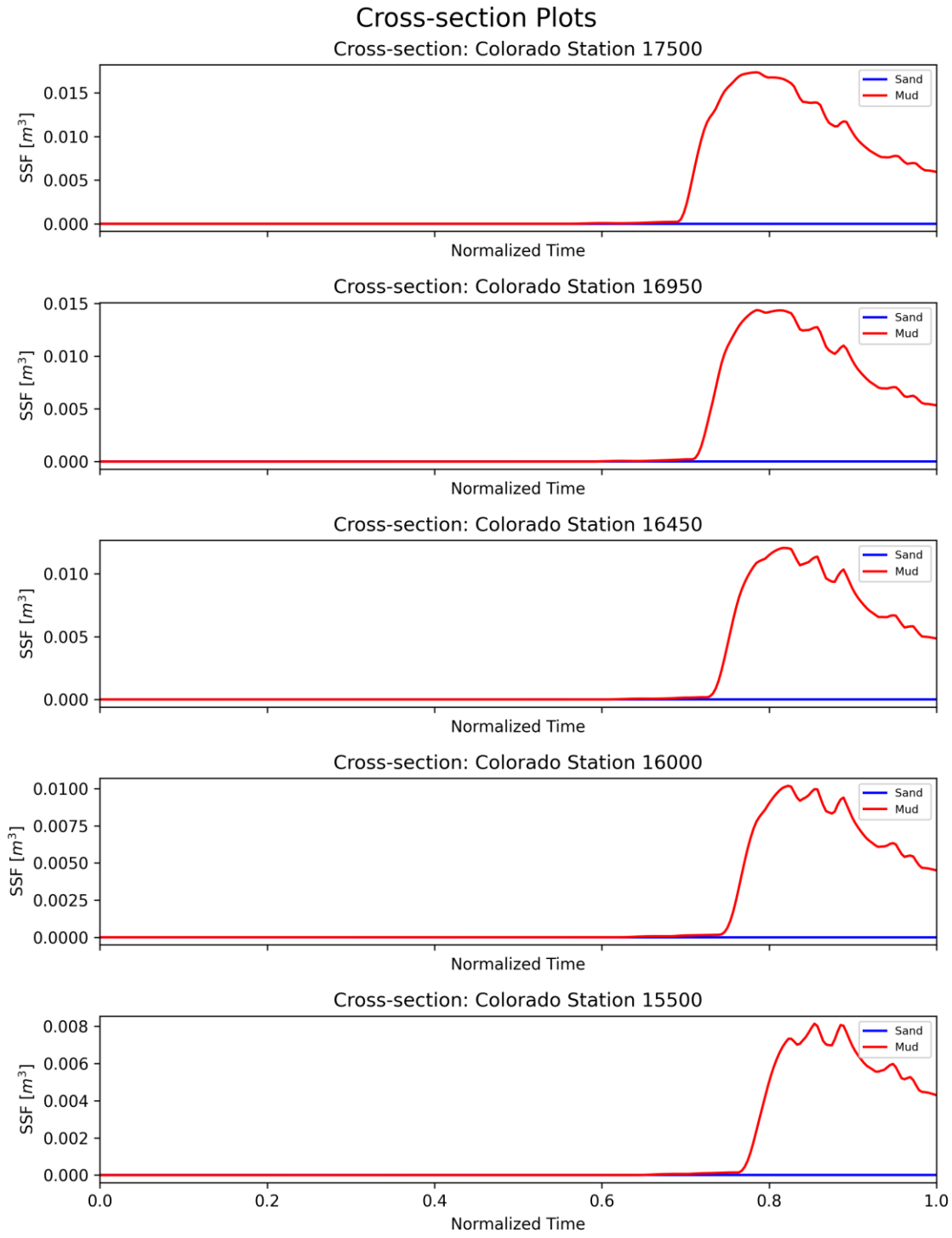
Cross-section Plots
Cross-section: Colorado Station 17500
Cross-section: Colorado Station 16950
Cross-section: Colorado Station 16450
Cross-section: Colorado Station 16000
Cross-section: Colorado Station 15500
SSF [m^3]
Normalized Time
Sand
Mud
0.015
0.010
0.005
0.000
0.0100
0.0075
0.0050
0.0025
0.0000
0.008
0.006
0.004
0.002
0.0
0.2
0.4
0.6
0.8
1.0

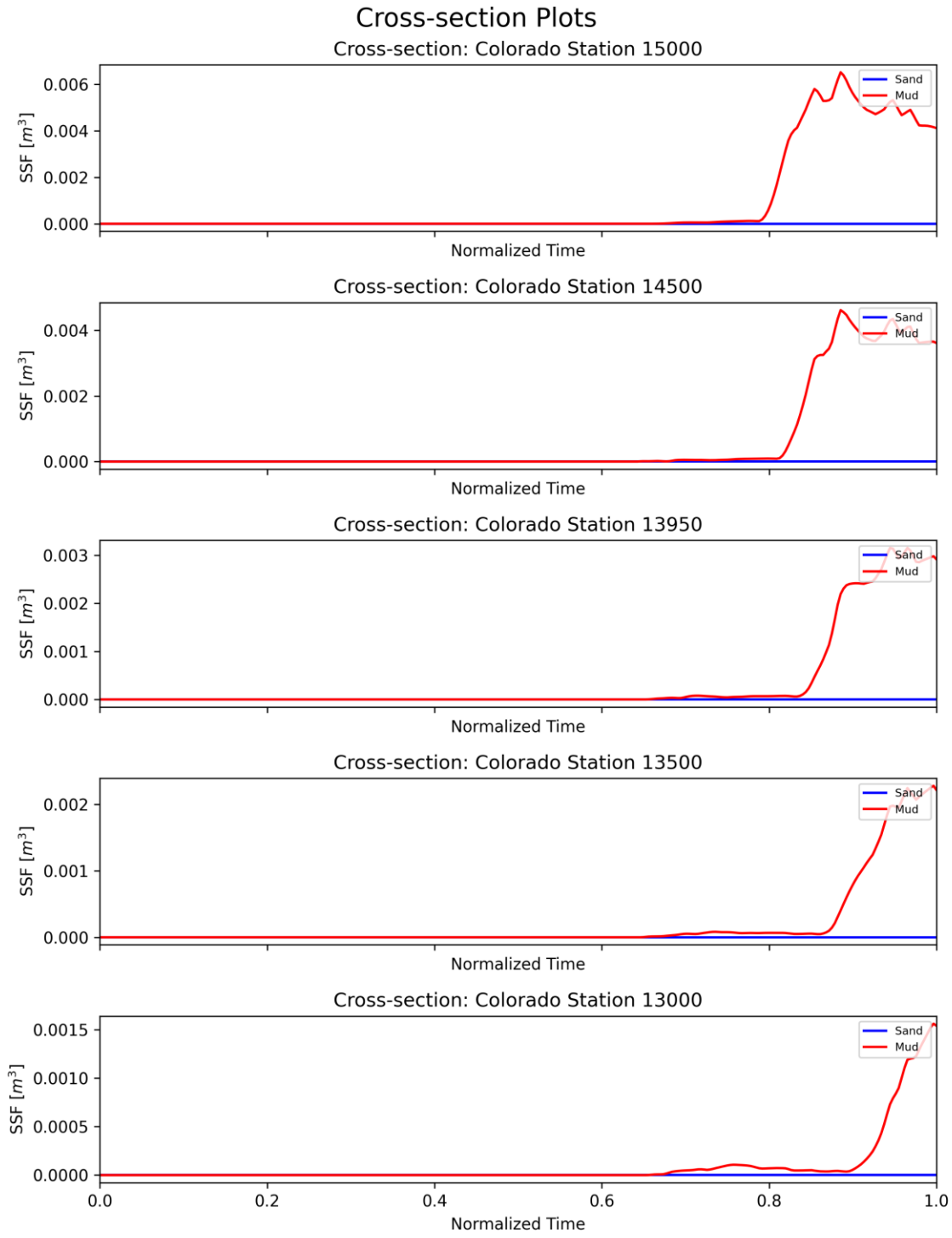
Cross-section Plots
Cross-section: Colorado Station 15000
SSF [m^3]
0.006
0.004
0.002
0.000
Sand
Mud
Normalized Time
Cross-section: Colorado Station 14500
SSF [m^3]
0.004
0.002
0.000
Sand
Mud
Normalized Time
Cross-section: Colorado Station 13950
SSF [m^3]
0.003
0.002
0.001
0.000
Sand
Mud
Normalized Time
Cross-section: Colorado Station 13500
SSF [m^3]
0.002
0.001
0.000
Sand
Mud
Normalized Time
Cross-section: Colorado Station 13000
SSF [m^3]
0.0015
0.0010
0.0005
0.0000
Sand
Mud
0.0
0.2
0.4
0.6
0.8
1.0
Normalized Time

APPENDIX K: THE EFFECT OF SEDIMENT INFLUX FROM UPSTREAM VS. NO SEDIMENT INFLUX

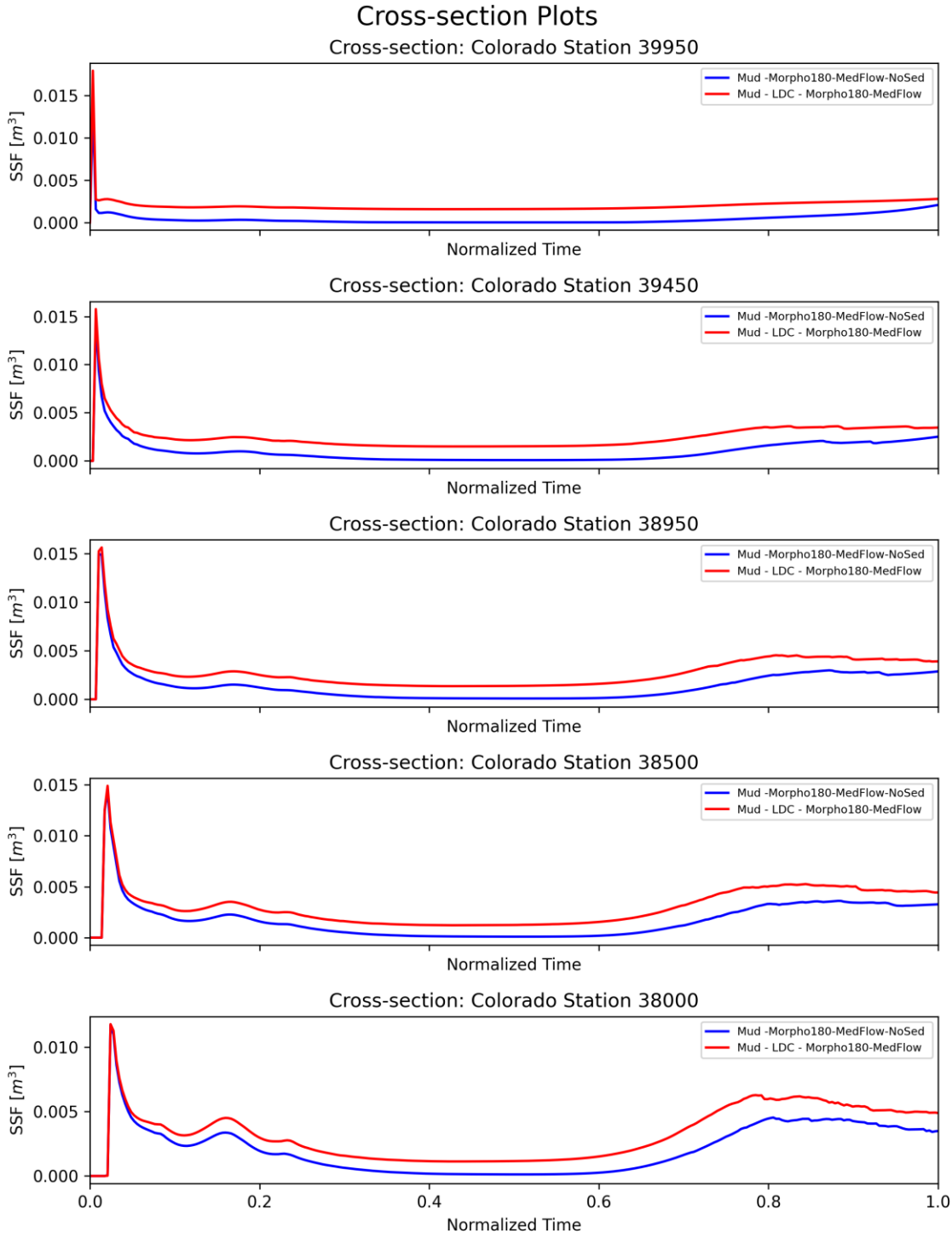
Cross-section Plots
Cross-section: Colorado Station 39950
Cross-section: Colorado Station 39450
Cross-section: Colorado Station 38950
Cross-section: Colorado Station 38500
Cross-section: Colorado Station 38000
Mud -Morpho180-MedFlow-NoSed
Mud - LDC - Morpho180-MedFlow
SSF [m^3]
Normalized Time
0.000
0.005
0.010
0.015
0.0
0.2
0.4
0.6
0.8
1.0

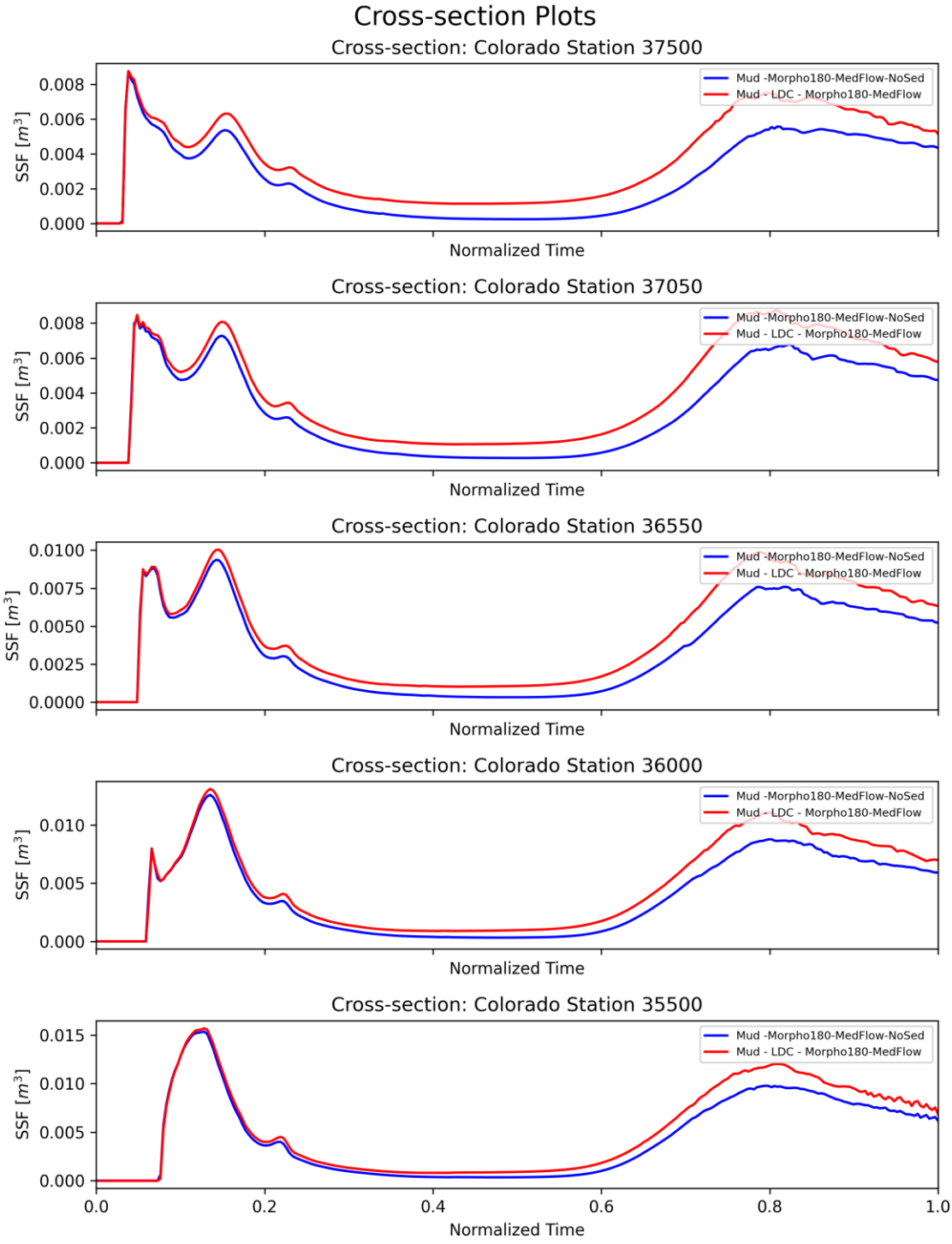
Cross-section Plots
Cross-section: Colorado Station 37500
Cross-section: Colorado Station 37050
Cross-section: Colorado Station 36550
Cross-section: Colorado Station 36000
Cross-section: Colorado Station 35500
Mud -Morpho180-MedFlow-NoSed
Mud - LDC - Morpho180-MedFlow
SSF [m^3]
Normalized Time

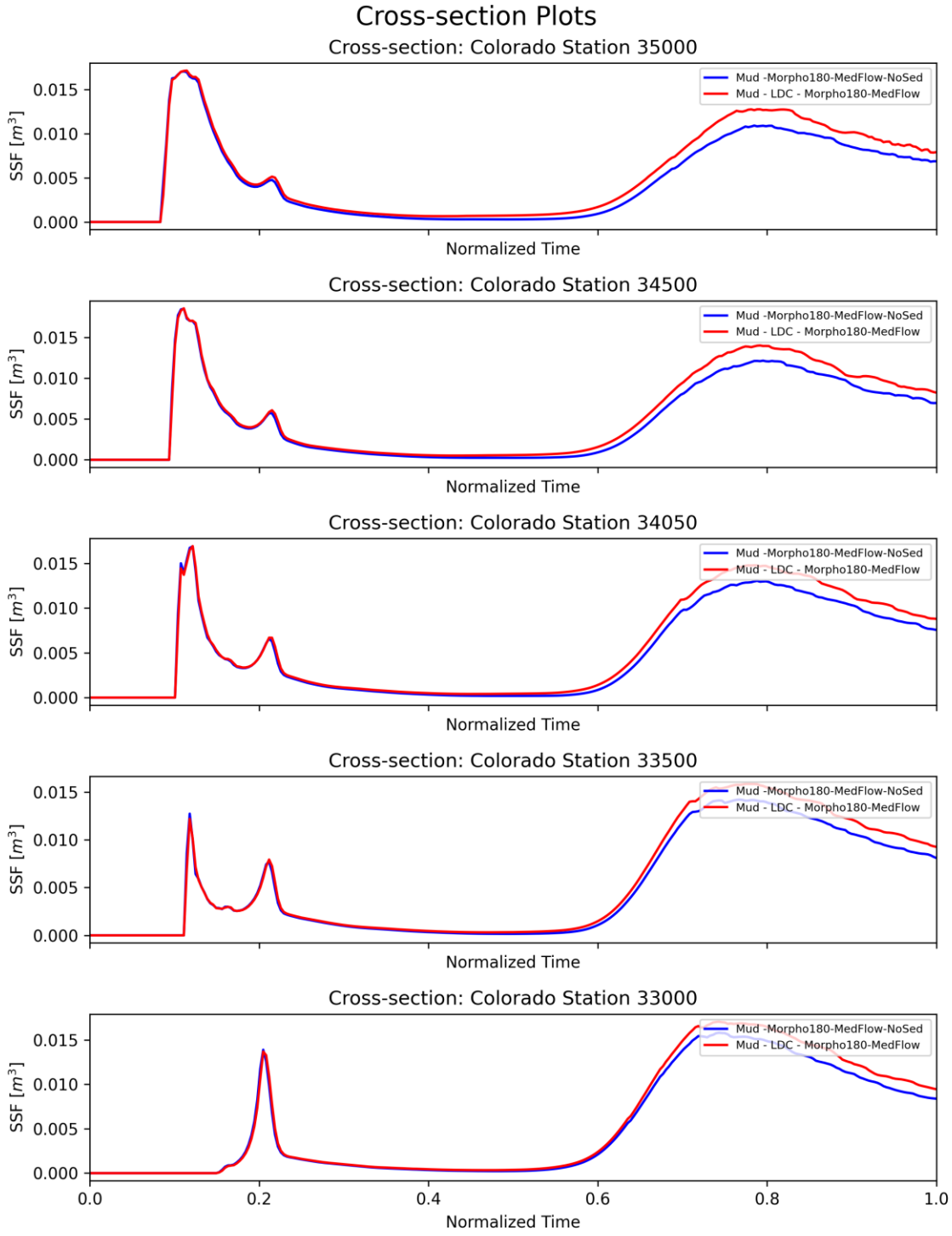
Cross-section Plots
Cross-section: Colorado Station 35000
Cross-section: Colorado Station 34500
Cross-section: Colorado Station 34050
Cross-section: Colorado Station 33500
Cross-section: Colorado Station 33000
Mud -Morpho180-MedFlow-NoSed
Mud - LDC - Morpho180-MedFlow
SSF [m^3]
0.000
0.005
0.010
0.015
0.0
0.2
0.4
0.6
0.8
1.0
Normalized Time

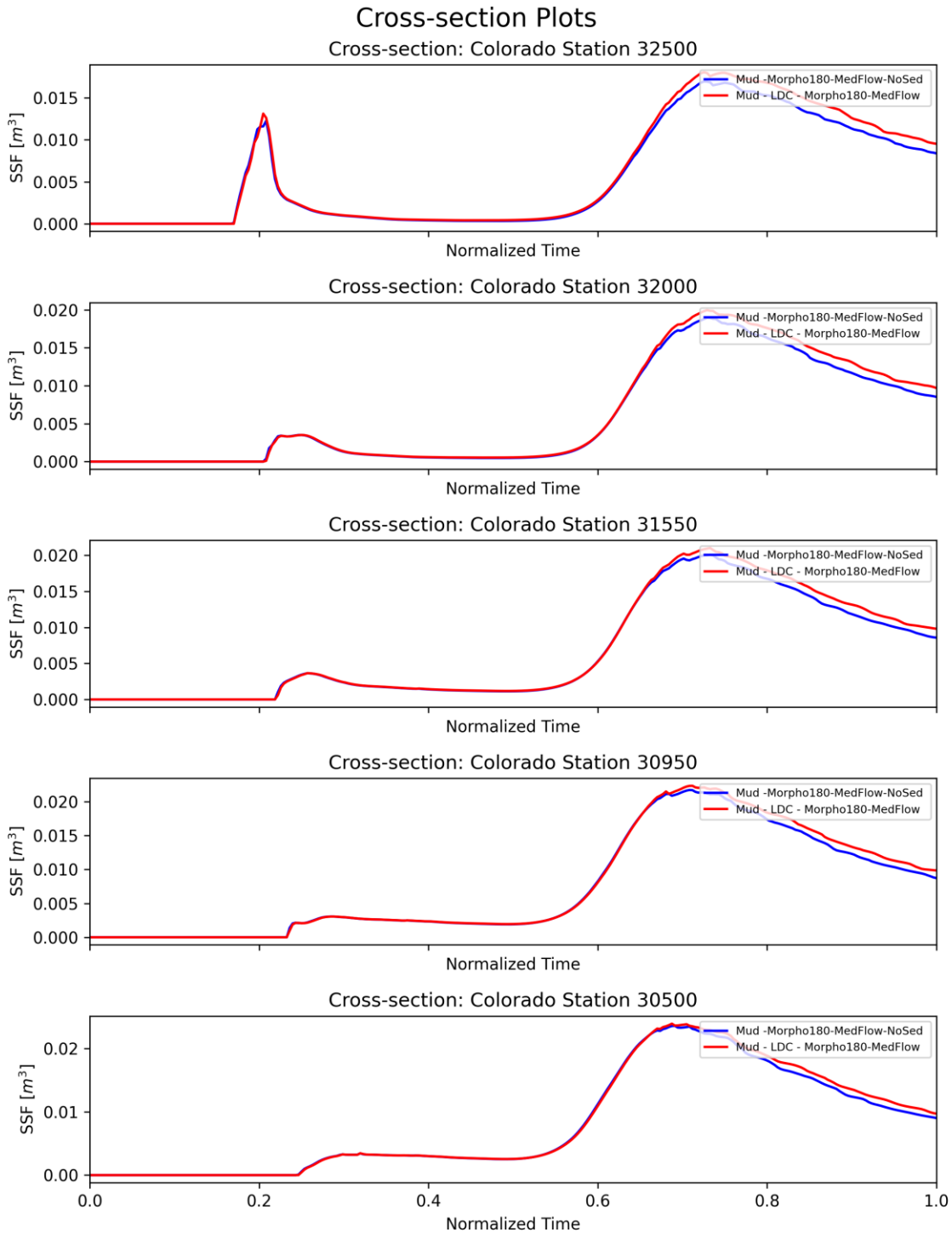
Cross-section Plots
Cross-section: Colorado Station 32500
Cross-section: Colorado Station 32000
Cross-section: Colorado Station 31550
Cross-section: Colorado Station 30950
Cross-section: Colorado Station 30500
Mud -Morpho180-MedFlow-NoSed
Mud - LDC - Morpho180-MedFlow
SSF [m^3]
Normalized Time

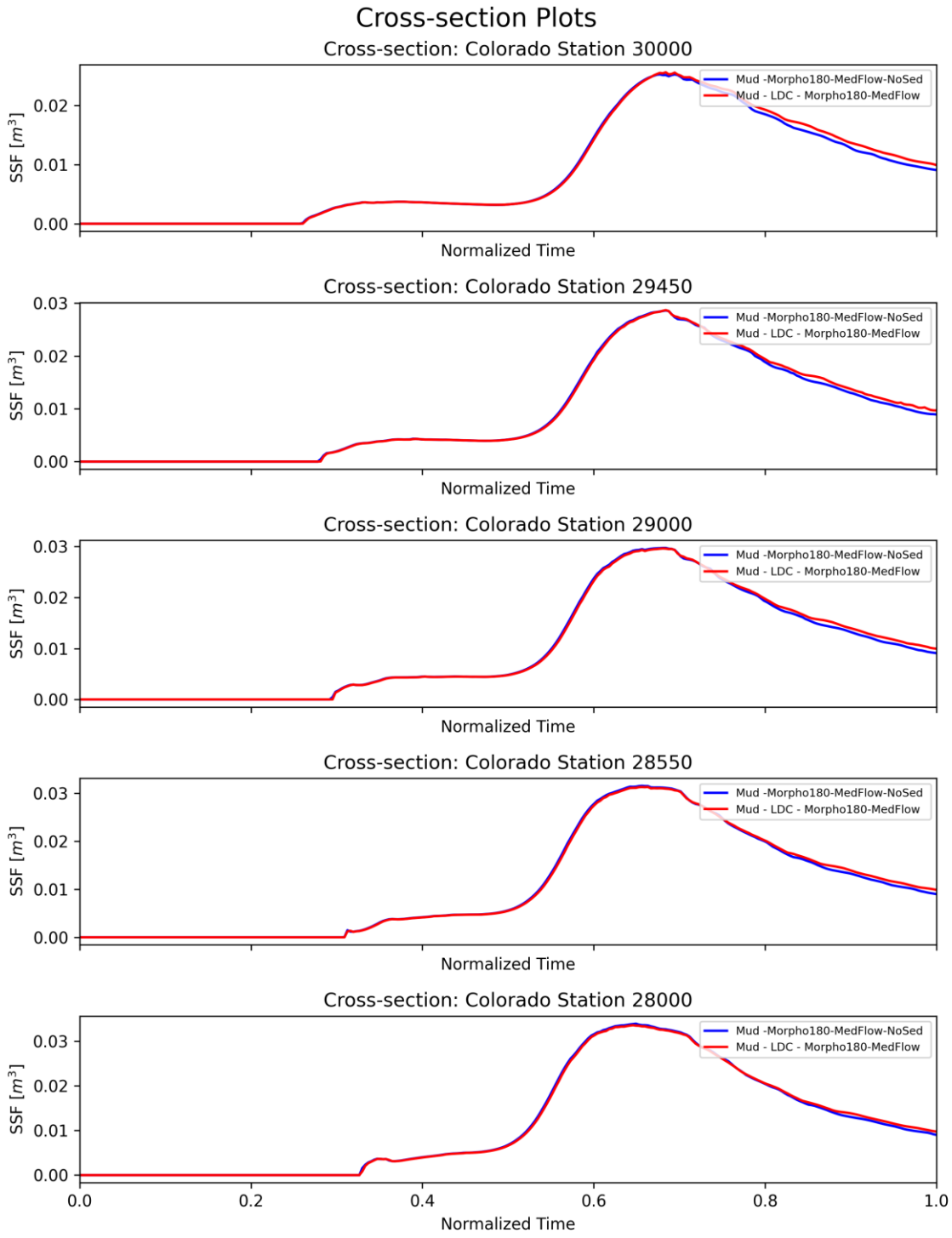
Cross-section Plots
Cross-section: Colorado Station 30000
Cross-section: Colorado Station 29450
Cross-section: Colorado Station 29000
Cross-section: Colorado Station 28550
Cross-section: Colorado Station 28000
Mud -Morpho180-MedFlow-NoSed
Mud - LDC - Morpho180-MedFlow
SSF [m^3]
Normalized Time
0.00
0.01
0.02
0.03
0.0
0.2
0.4
0.6
0.8
1.0

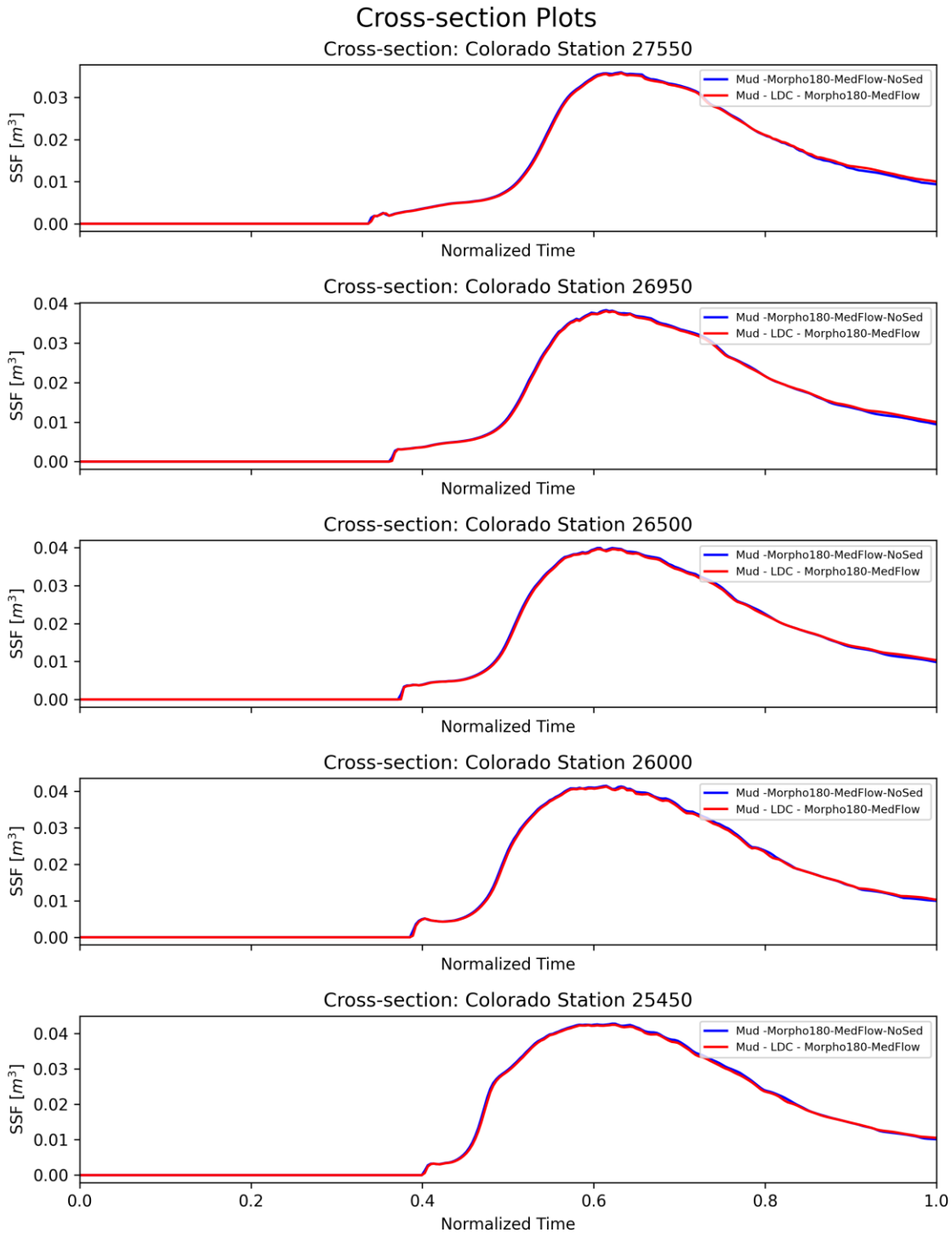
Cross-section Plots
Cross-section: Colorado Station 27550
Cross-section: Colorado Station 26950
Cross-section: Colorado Station 26500
Cross-section: Colorado Station 26000
Cross-section: Colorado Station 25450
Mud -Morpho180-MedFlow-NoSed
Mud - LDC - Morpho180-MedFlow
SSF [m^3]
Normalized Time
0.00
0.01
0.02
0.03
0.04
0.0
0.2
0.4
0.6
0.8
1.0

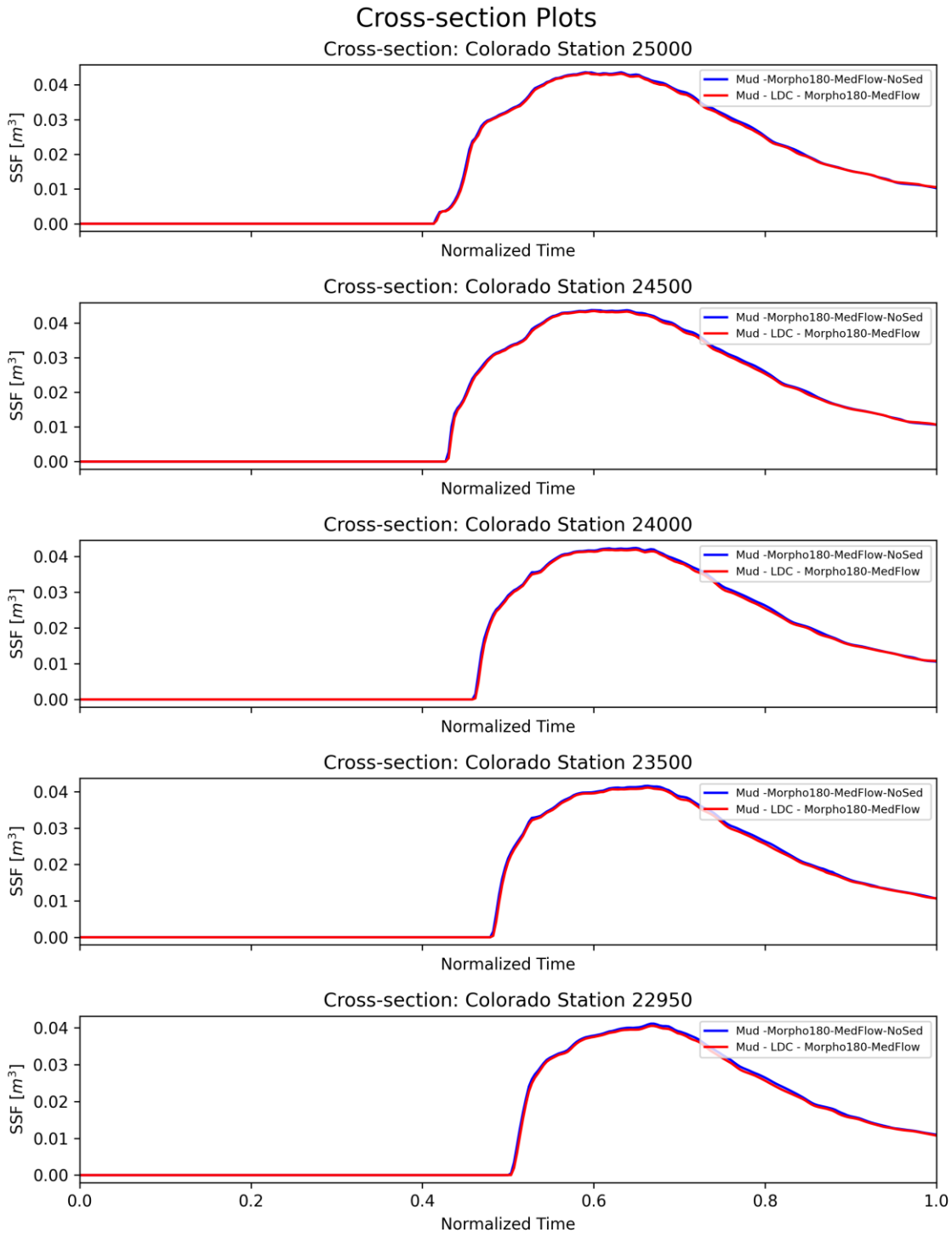
Cross-section Plots
Cross-section: Colorado Station 25000
Cross-section: Colorado Station 24500
Cross-section: Colorado Station 24000
Cross-section: Colorado Station 23500
Cross-section: Colorado Station 22950
Mud -Morpho180-MedFlow-NoSed
Mud - LDC - Morpho180-MedFlow
SSF [m^3]
0.00
0.01
0.02
0.03
0.04
0.0
0.2
0.4
0.6
0.8
1.0
Normalized Time

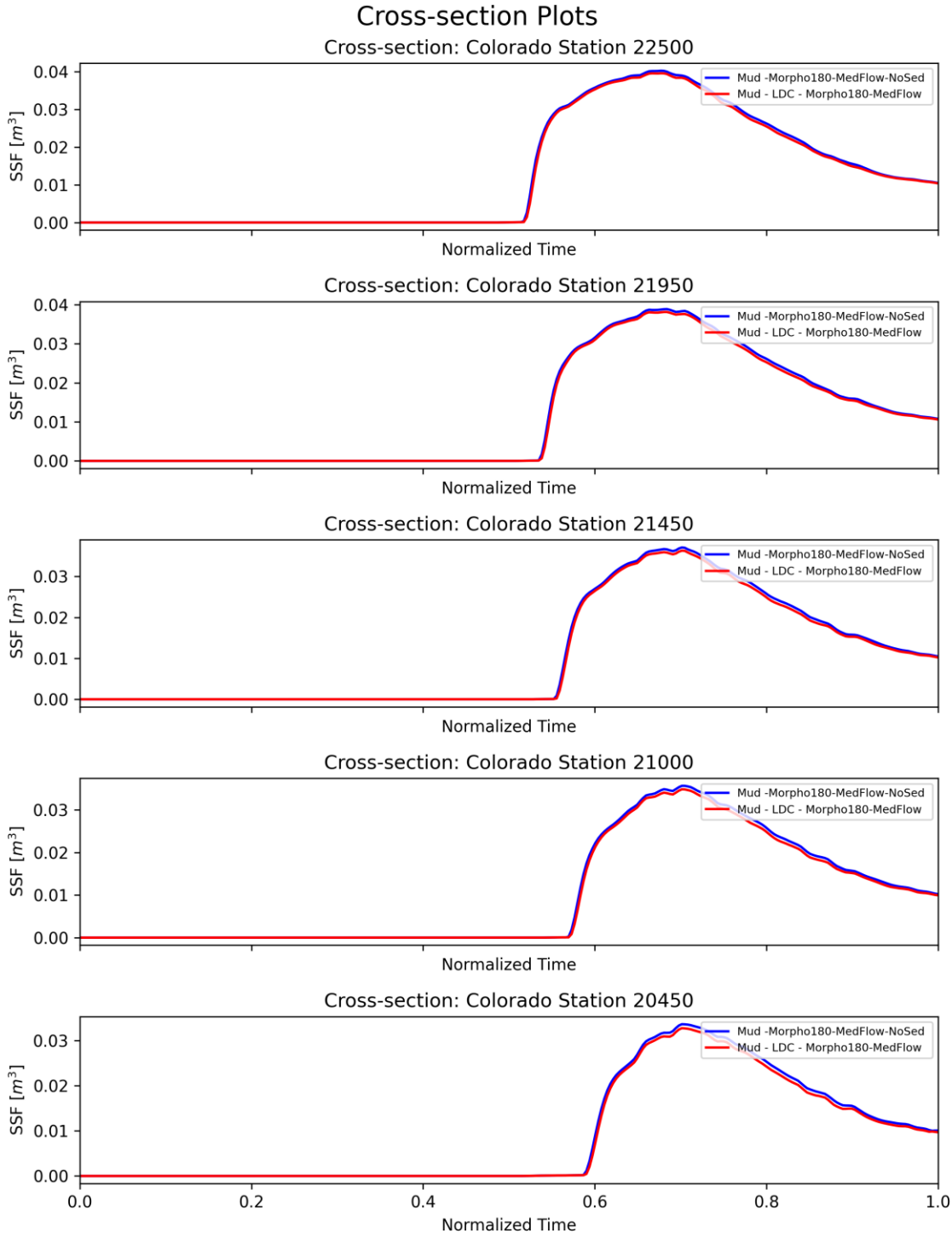
Cross-section Plots
Cross-section: Colorado Station 22500
Cross-section: Colorado Station 21950
Cross-section: Colorado Station 21450
Cross-section: Colorado Station 21000
Cross-section: Colorado Station 20450
Mud -Morpho180-MedFlow-NoSed
Mud - LDC - Morpho180-MedFlow
SSF [m^3]
Normalized Time
0.00
0.01
0.02
0.03
0.04
0.0
0.2
0.4
0.6
0.8
1.0

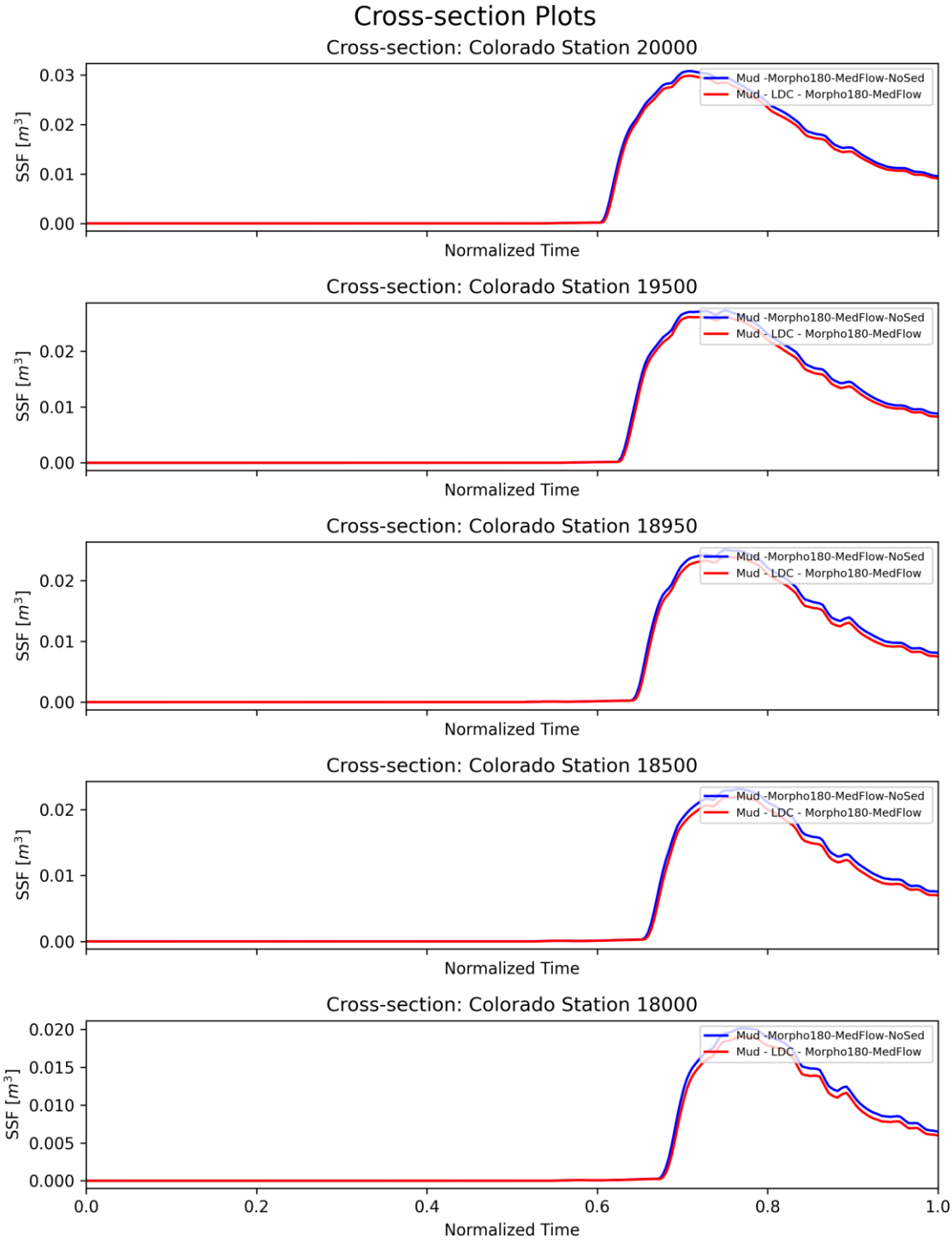
Cross-section Plots
Cross-section: Colorado Station 20000
Cross-section: Colorado Station 19500
Cross-section: Colorado Station 18950
Cross-section: Colorado Station 18500
Cross-section: Colorado Station 18000
Mud -Morpho180-MedFlow-NoSed
Mud - LDC - Morpho180-MedFlow
SSF [m^3]
Normalized Time

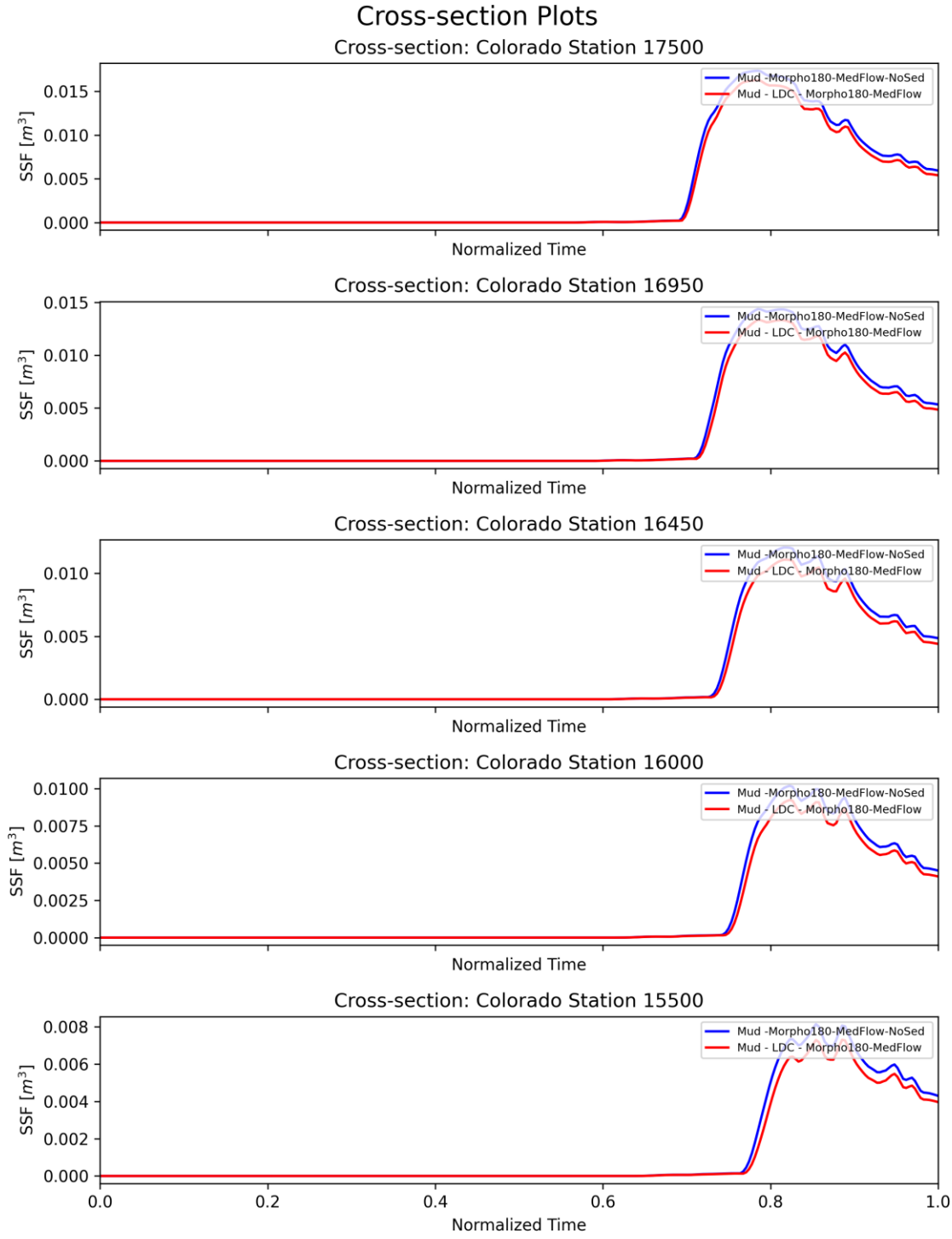
Cross-section Plots
Cross-section: Colorado Station 17500
Cross-section: Colorado Station 16950
Cross-section: Colorado Station 16450
Cross-section: Colorado Station 16000
Cross-section: Colorado Station 15500
Mud -Morpho180-MedFlow-NoSed
Mud - LDC - Morpho180-MedFlow
SSF [m^3]
Normalized Time

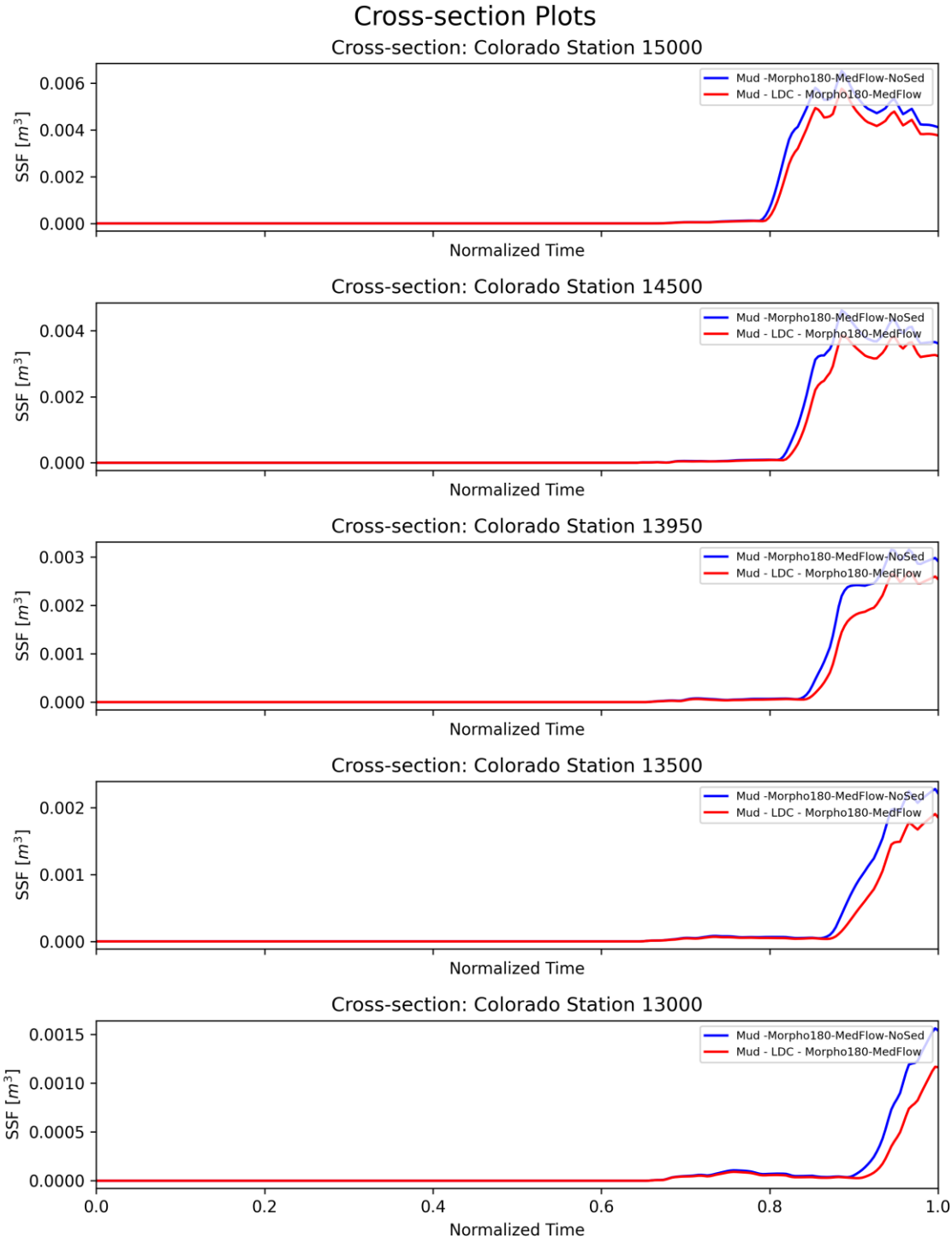
Cross-section Plots
Cross-section: Colorado Station 15000
Mud -Morpho180-MedFlow-NoSed
Mud - LDC - Morpho180-MedFlow
SSF [m^3]
0.006
0.004
0.002
0.000
Normalized Time
Cross-section: Colorado Station 14500
Mud -Morpho180-MedFlow-NoSed
Mud - LDC - Morpho180-MedFlow
SSF [m^3]
0.004
0.002
0.000
Normalized Time
Cross-section: Colorado Station 13950
Mud -Morpho180-MedFlow-NoSed
Mud - LDC - Morpho180-MedFlow
SSF [m^3]
0.003
0.002
0.001
0.000
Normalized Time
Cross-section: Colorado Station 13500
Mud -Morpho180-MedFlow-NoSed
Mud - LDC - Morpho180-MedFlow
SSF [m^3]
0.002
0.001
0.000
Normalized Time
Cross-section: Colorado Station 13000
Mud -Morpho180-MedFlow-NoSed
Mud - LDC - Morpho180-MedFlow
SSF [m^3]
0.0015
0.0010
0.0005
0.0000
0.0
0.2
0.4
0.6
0.8
1.0
Normalized Time

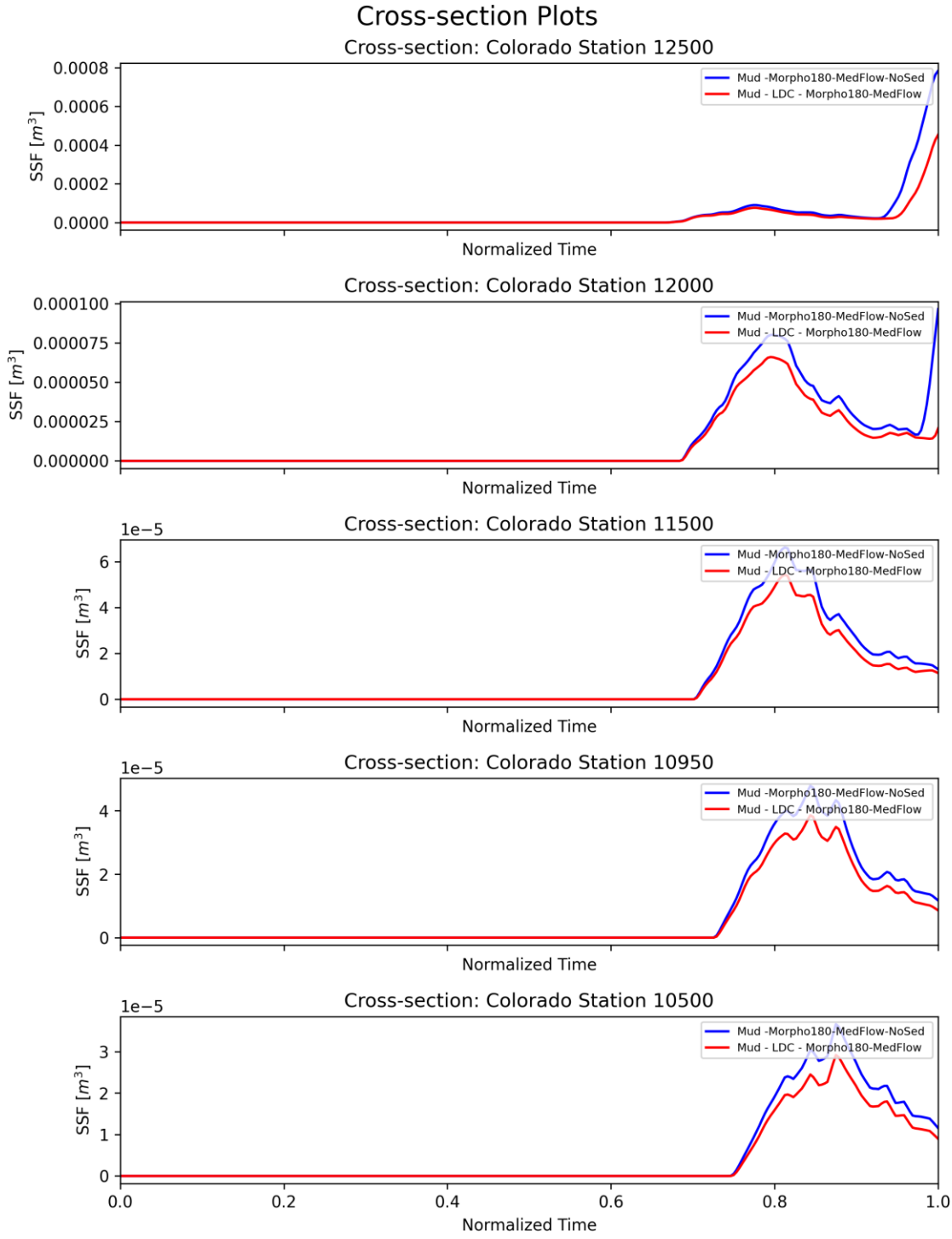
Cross-section Plots
Cross-section: Colorado Station 12500
Mud -Morpho180-MedFlow-NoSed
Mud - LDC - Morpho180-MedFlow
SSF [m^3]
0.0008
0.0006
0.0004
0.0002
0.0000
Normalized Time
Cross-section: Colorado Station 12000
Mud -Morpho180-MedFlow-NoSed
Mud - LDC - Morpho180-MedFlow
SSF [m^3]
0.000100
0.000075
0.000050
0.000025
0.000000
Normalized Time
Cross-section: Colorado Station 11500
1e−5
Mud -Morpho180-MedFlow-NoSed
Mud - LDC - Morpho180-MedFlow
SSF [m^3]
6
4
2
0
Normalized Time
Cross-section: Colorado Station 10950
1e−5
Mud -Morpho180-MedFlow-NoSed
Mud - LDC - Morpho180-MedFlow
SSF [m^3]
4
2
0
Normalized Time
Cross-section: Colorado Station 10500
1e−5
Mud -Morpho180-MedFlow-NoSed
Mud - LDC - Morpho180-MedFlow
SSF [m^3]
3
2
1
0
0.0
0.2
0.4
0.6
0.8
1.0
Normalized Time

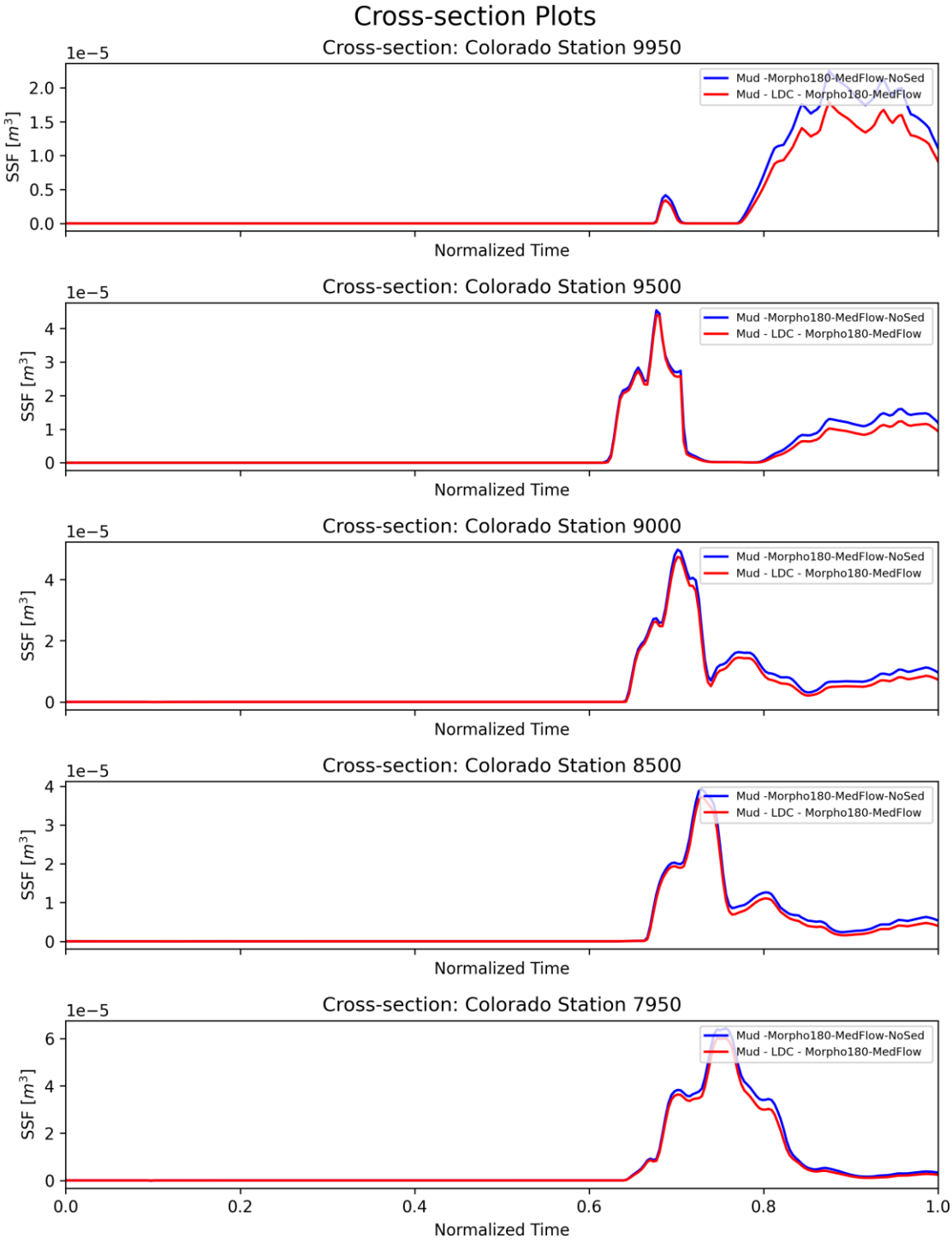
Cross-section Plots
Cross-section: Colorado Station 9950
Cross-section: Colorado Station 9500
Cross-section: Colorado Station 9000
Cross-section: Colorado Station 8500
Cross-section: Colorado Station 7950
1e−5
SSF [m^3]
Normalized Time
Mud -Morpho180-MedFlow-NoSed
Mud - LDC - Morpho180-MedFlow

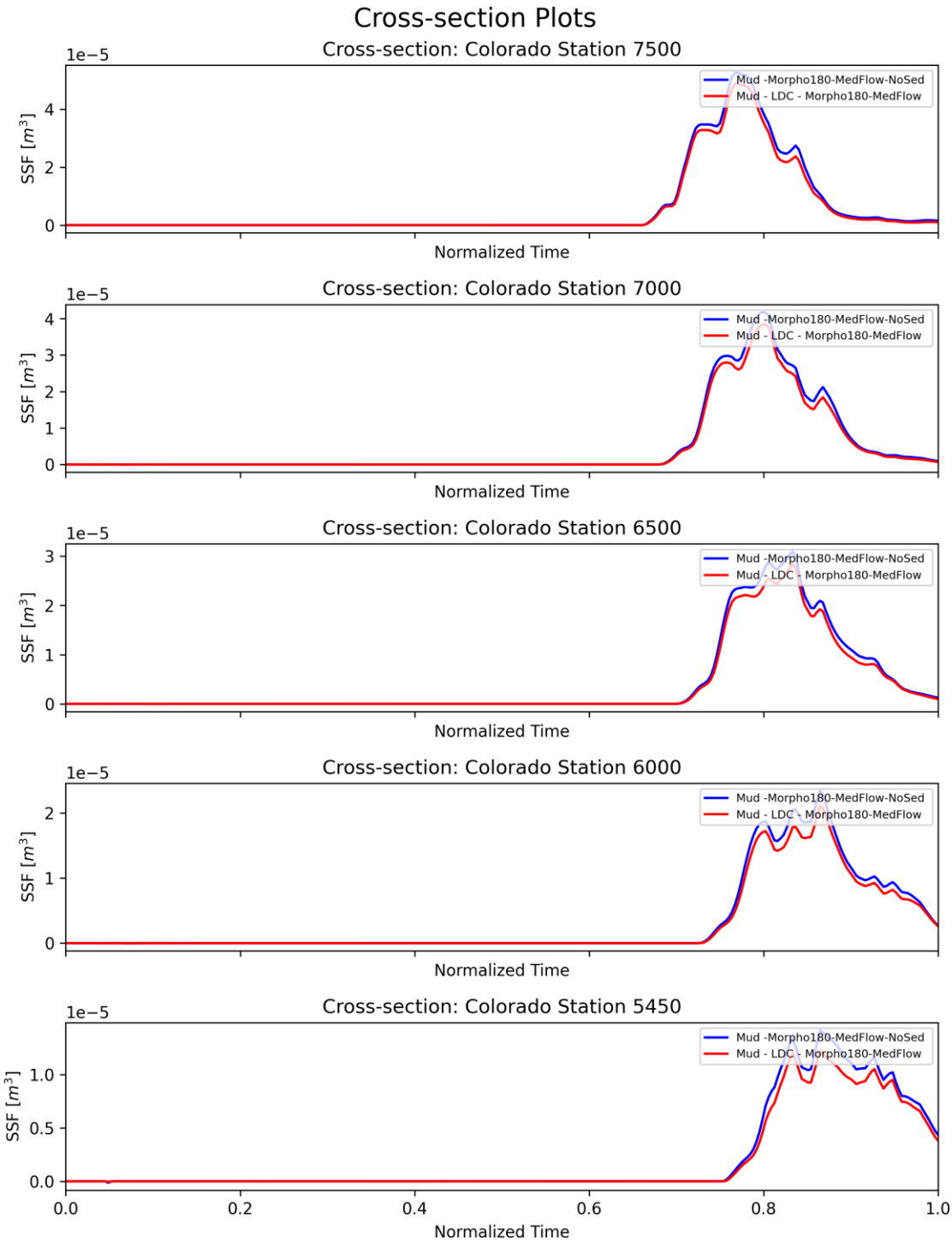
Cross-section Plots
Cross-section: Colorado Station 7500
Cross-section: Colorado Station 7000
Cross-section: Colorado Station 6500
Cross-section: Colorado Station 6000
Cross-section: Colorado Station 5450
1e−5
SSF [m^3]
Normalized Time
Mud -Morpho180-MedFlow-NoSed
Mud - LDC - Morpho180-MedFlow

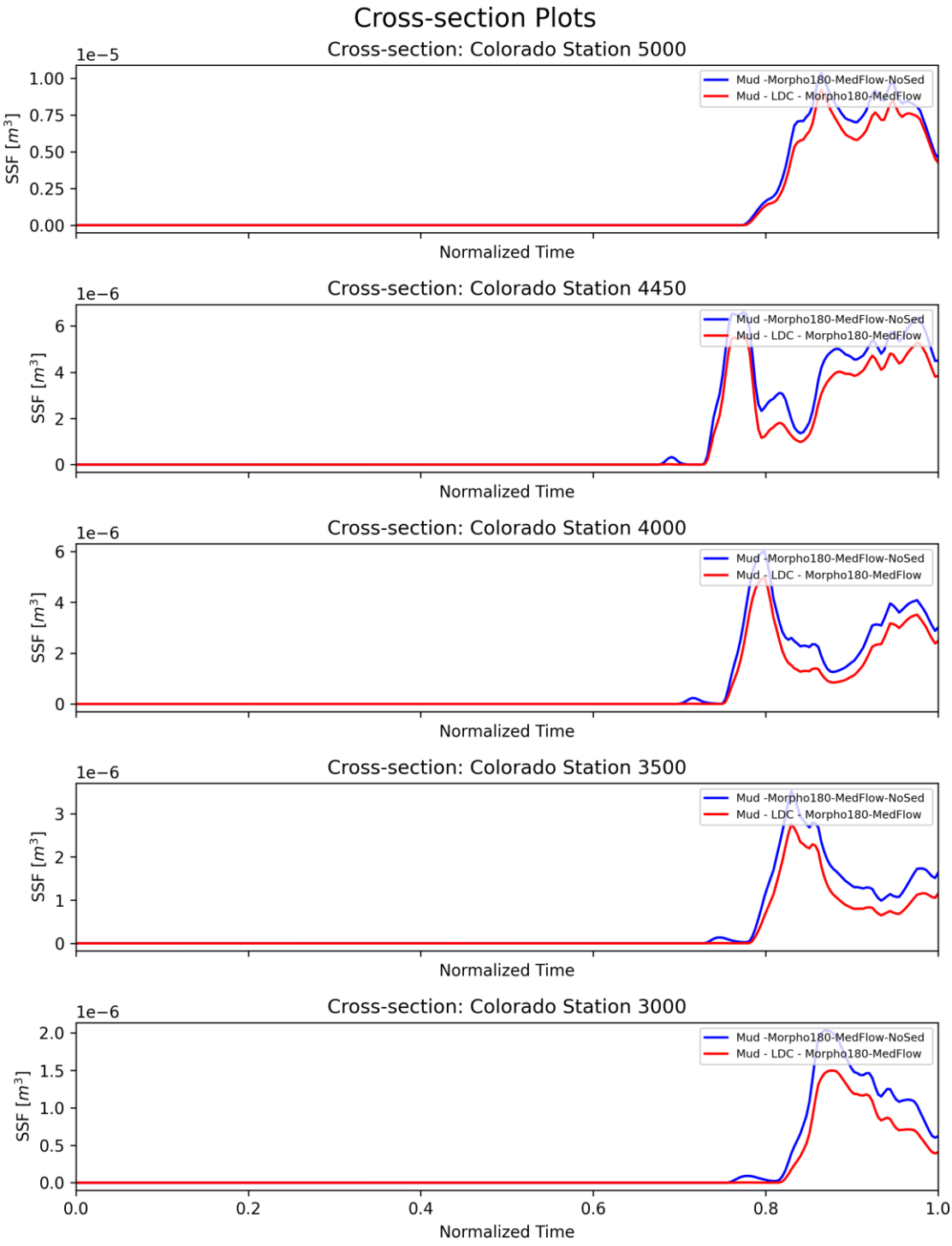
Cross-section Plots
Cross-section: Colorado Station 5000
1e−5
SSF [m^3]
Normalized Time
Cross-section: Colorado Station 4450
1e−6
SSF [m^3]
Normalized Time
Cross-section: Colorado Station 4000
1e−6
SSF [m^3]
Normalized Time
Cross-section: Colorado Station 3500
1e−6
SSF [m^3]
Normalized Time
Cross-section: Colorado Station 3000
1e−6
SSF [m^3]
Normalized Time
Mud -Morpho180-MedFlow-NoSed
Mud - LDC - Morpho180-MedFlow

APPENDIX L: THE EFFECT OF FLOODS IN COLORADO DOMAIN

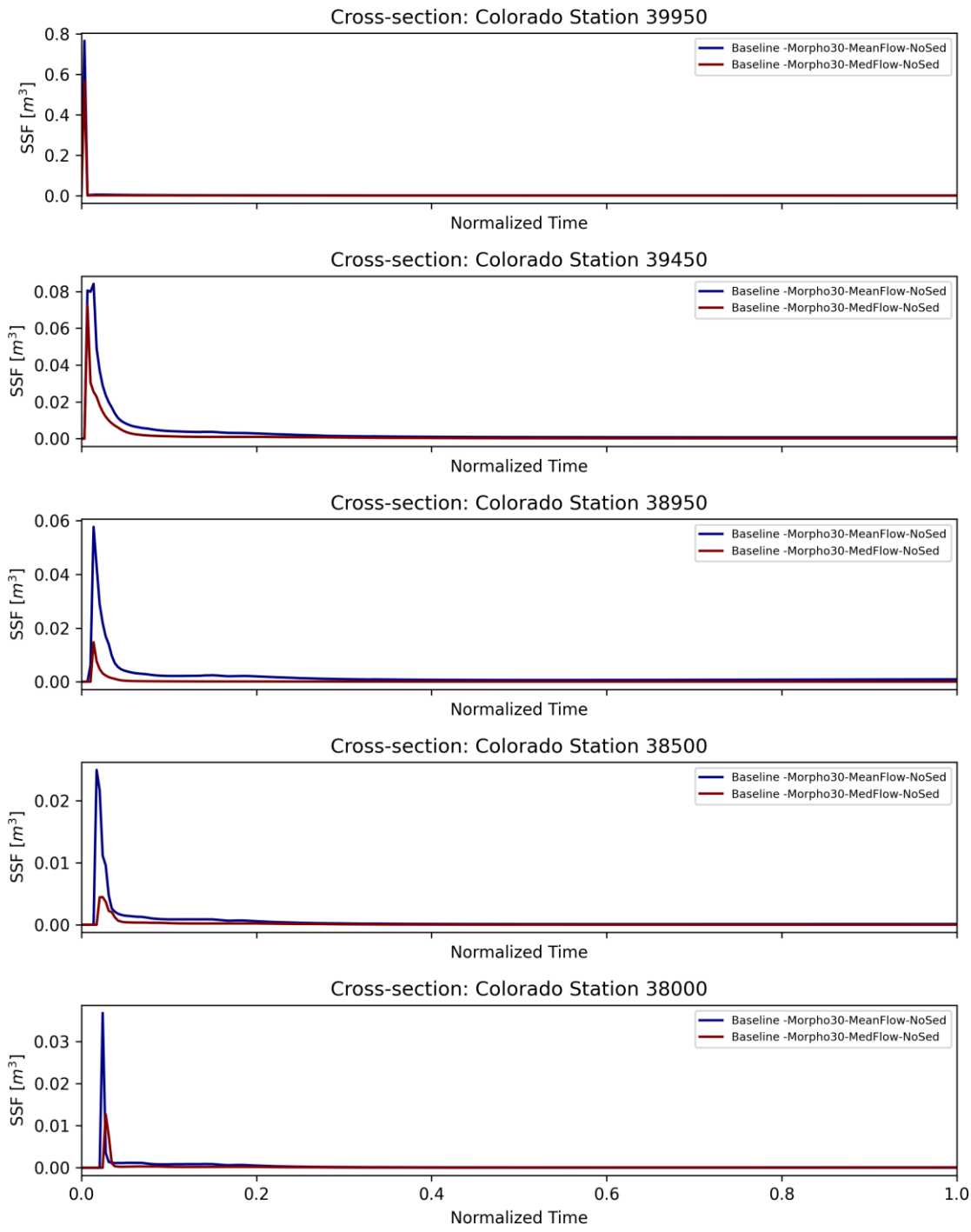
Cross-section Plots
Cross-section: Colorado Station 39950
Cross-section: Colorado Station 39450
Cross-section: Colorado Station 38950
Cross-section: Colorado Station 38500
Cross-section: Colorado Station 38000
Baseline -Morpho30-MeanFlow-NoSed
Baseline -Morpho30-MedFlow-NoSed
SSF [m^3]
Normalized Time

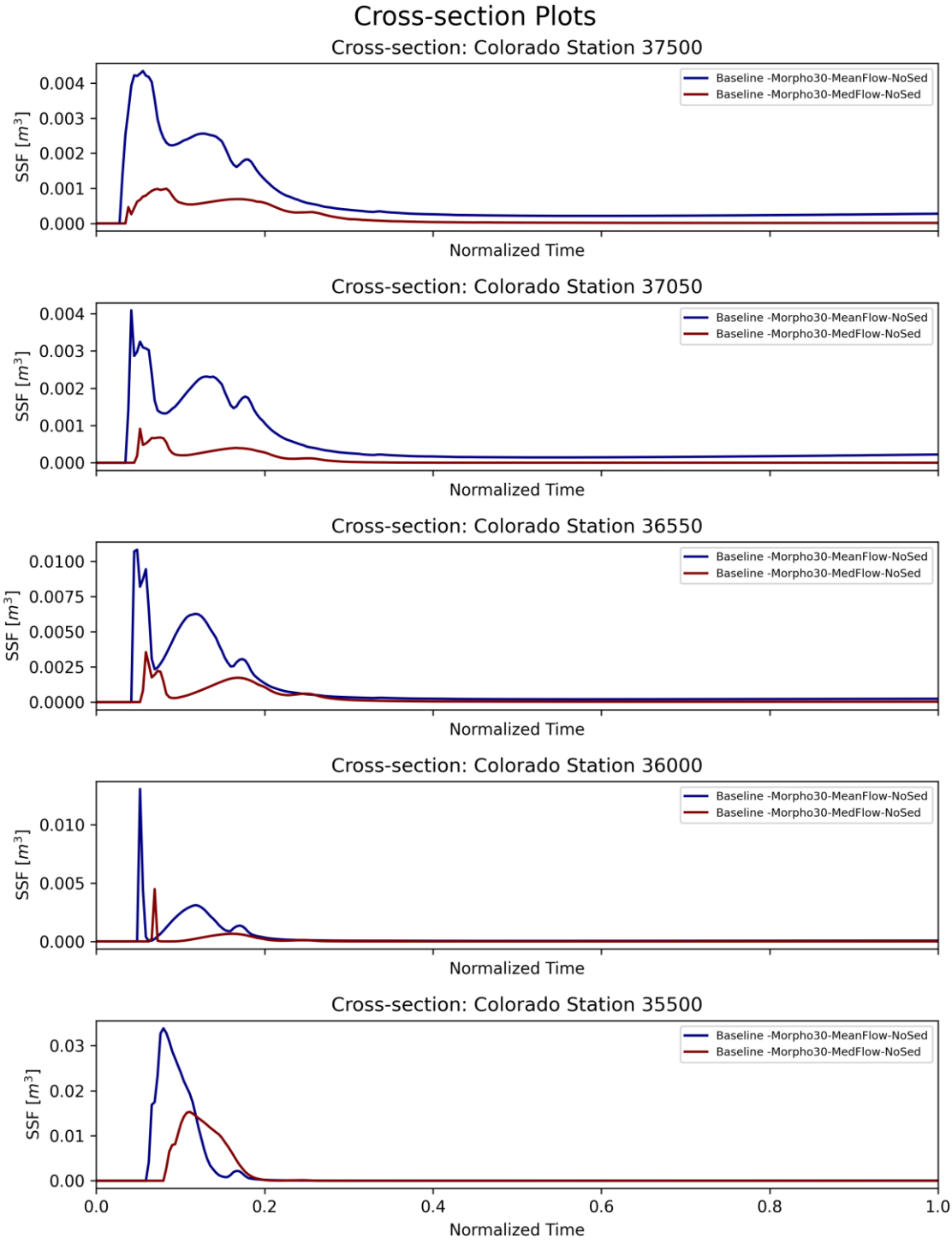
Cross-section Plots
Cross-section: Colorado Station 37500
Baseline -Morpho30-MeanFlow-NoSed
Baseline -Morpho30-MedFlow-NoSed
SSF [m^3]
0.004
0.003
0.002
0.001
0.000
Normalized Time
Cross-section: Colorado Station 37050
Baseline -Morpho30-MeanFlow-NoSed
Baseline -Morpho30-MedFlow-NoSed
SSF [m^3]
0.004
0.003
0.002
0.001
0.000
Normalized Time
Cross-section: Colorado Station 36550
Baseline -Morpho30-MeanFlow-NoSed
Baseline -Morpho30-MedFlow-NoSed
SSF [m^3]
0.0100
0.0075
0.0050
0.0025
0.0000
Normalized Time
Cross-section: Colorado Station 36000
Baseline -Morpho30-MeanFlow-NoSed
Baseline -Morpho30-MedFlow-NoSed
SSF [m^3]
0.010
0.005
0.000
Normalized Time
Cross-section: Colorado Station 35500
Baseline -Morpho30-MeanFlow-NoSed
Baseline -Morpho30-MedFlow-NoSed
SSF [m^3]
0.03
0.02
0.01
0.00
0.0
0.2
0.4
0.6
0.8
1.0
Normalized Time

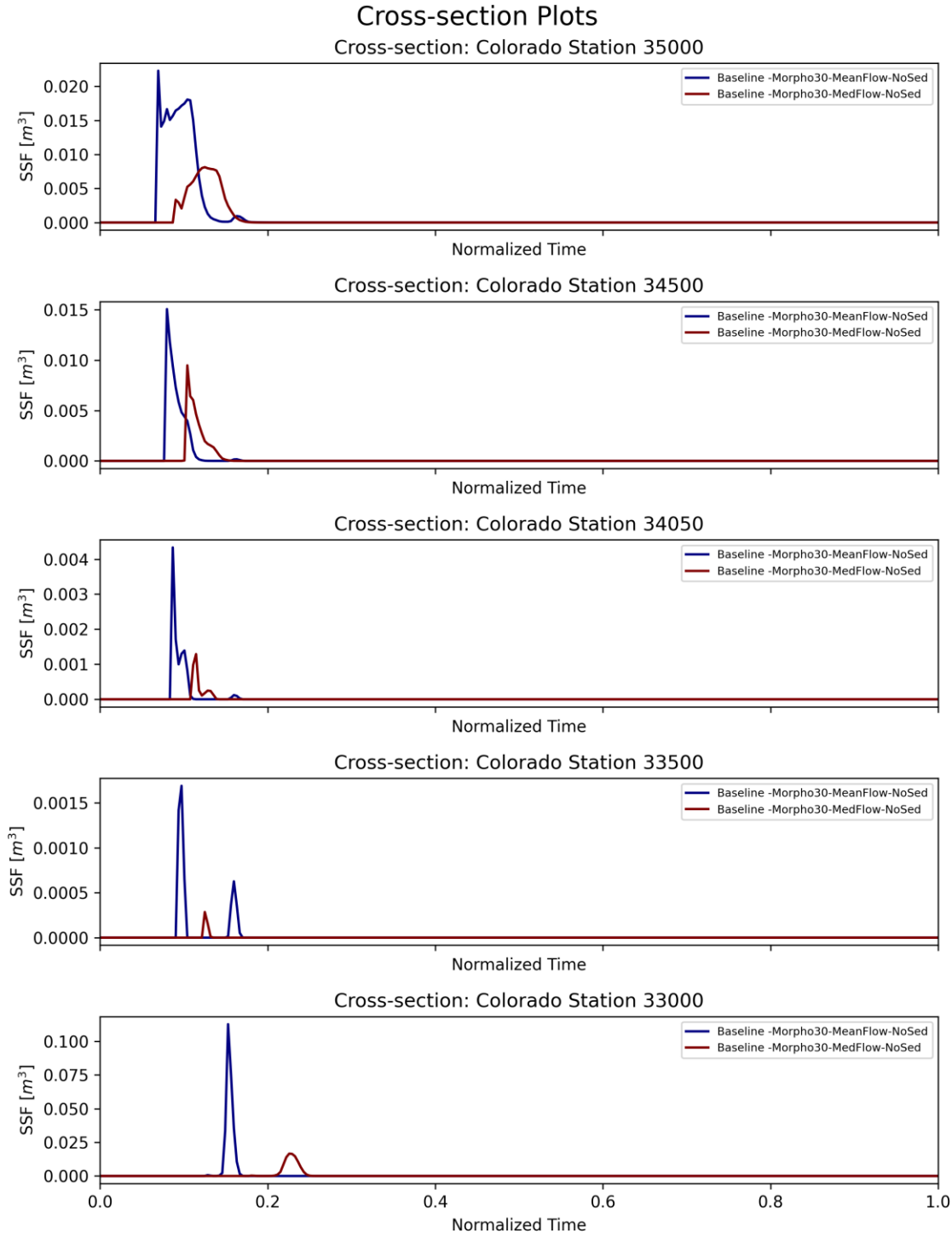
Cross-section Plots
Cross-section: Colorado Station 35000
Baseline -Morpho30-MeanFlow-NoSed
Baseline -Morpho30-MedFlow-NoSed
SSF [m^3]
0.020
0.015
0.010
0.005
0.000
Normalized Time
Cross-section: Colorado Station 34500
Baseline -Morpho30-MeanFlow-NoSed
Baseline -Morpho30-MedFlow-NoSed
SSF [m^3]
0.015
0.010
0.005
0.000
Normalized Time
Cross-section: Colorado Station 34050
Baseline -Morpho30-MeanFlow-NoSed
Baseline -Morpho30-MedFlow-NoSed
SSF [m^3]
0.004
0.003
0.002
0.001
0.000
Normalized Time
Cross-section: Colorado Station 33500
Baseline -Morpho30-MeanFlow-NoSed
Baseline -Morpho30-MedFlow-NoSed
SSF [m^3]
0.0015
0.0010
0.0005
0.0000
Normalized Time
Cross-section: Colorado Station 33000
Baseline -Morpho30-MeanFlow-NoSed
Baseline -Morpho30-MedFlow-NoSed
SSF [m^3]
0.100
0.075
0.050
0.025
0.000
0.0
0.2
0.4
0.6
0.8
1.0
Normalized Time

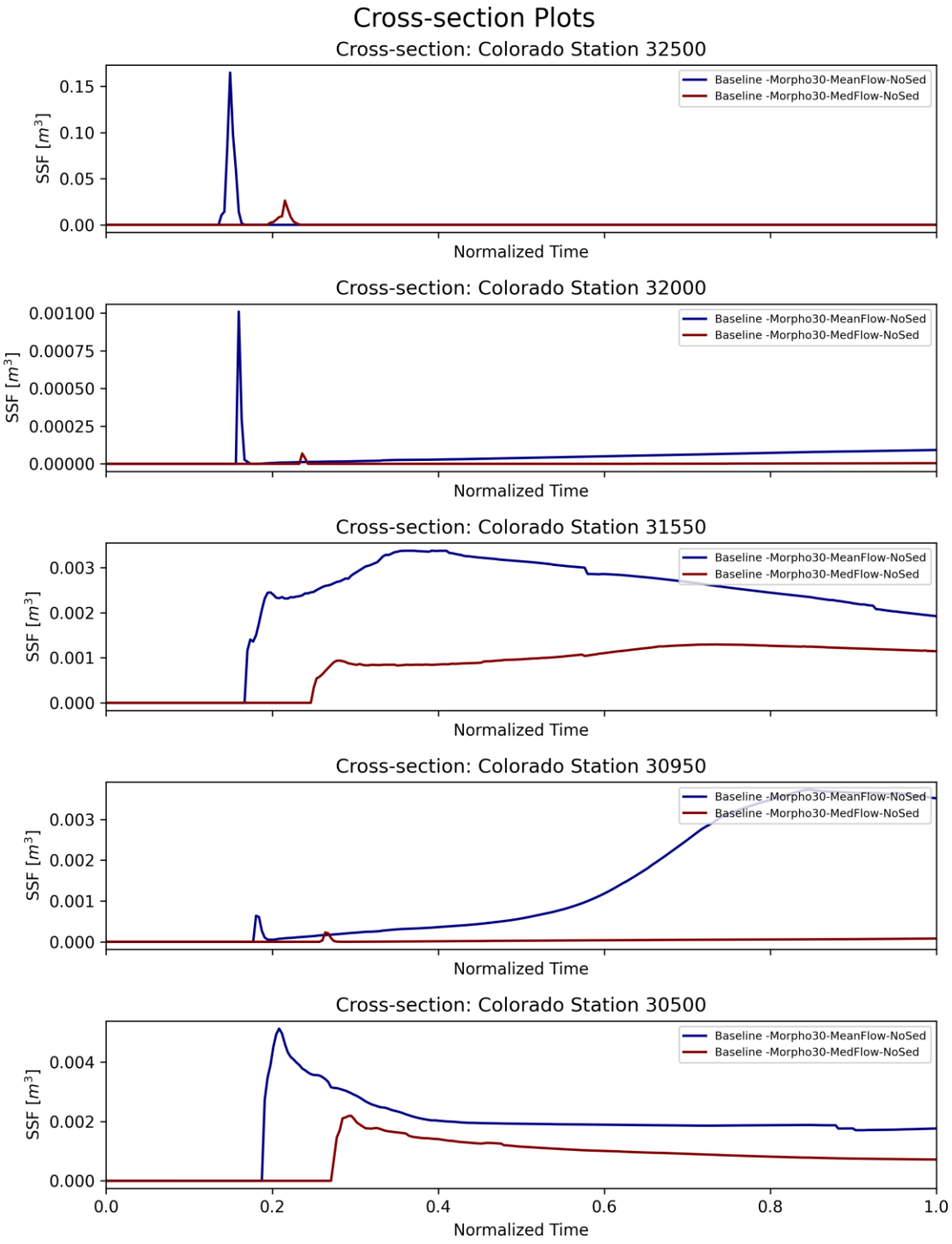
Cross-section Plots
Cross-section: Colorado Station 32500
Baseline -Morpho30-MeanFlow-NoSed
Baseline -Morpho30-MedFlow-NoSed
SSF [m^3]
0.15
0.10
0.05
0.00
Normalized Time
Cross-section: Colorado Station 32000
0.00100
0.00075
0.00050
0.00025
0.00000
Cross-section: Colorado Station 31550
0.003
0.002
0.001
0.000
Cross-section: Colorado Station 30950
Cross-section: Colorado Station 30500
0.004
0.0
0.2
0.4
0.6
0.8
1.0

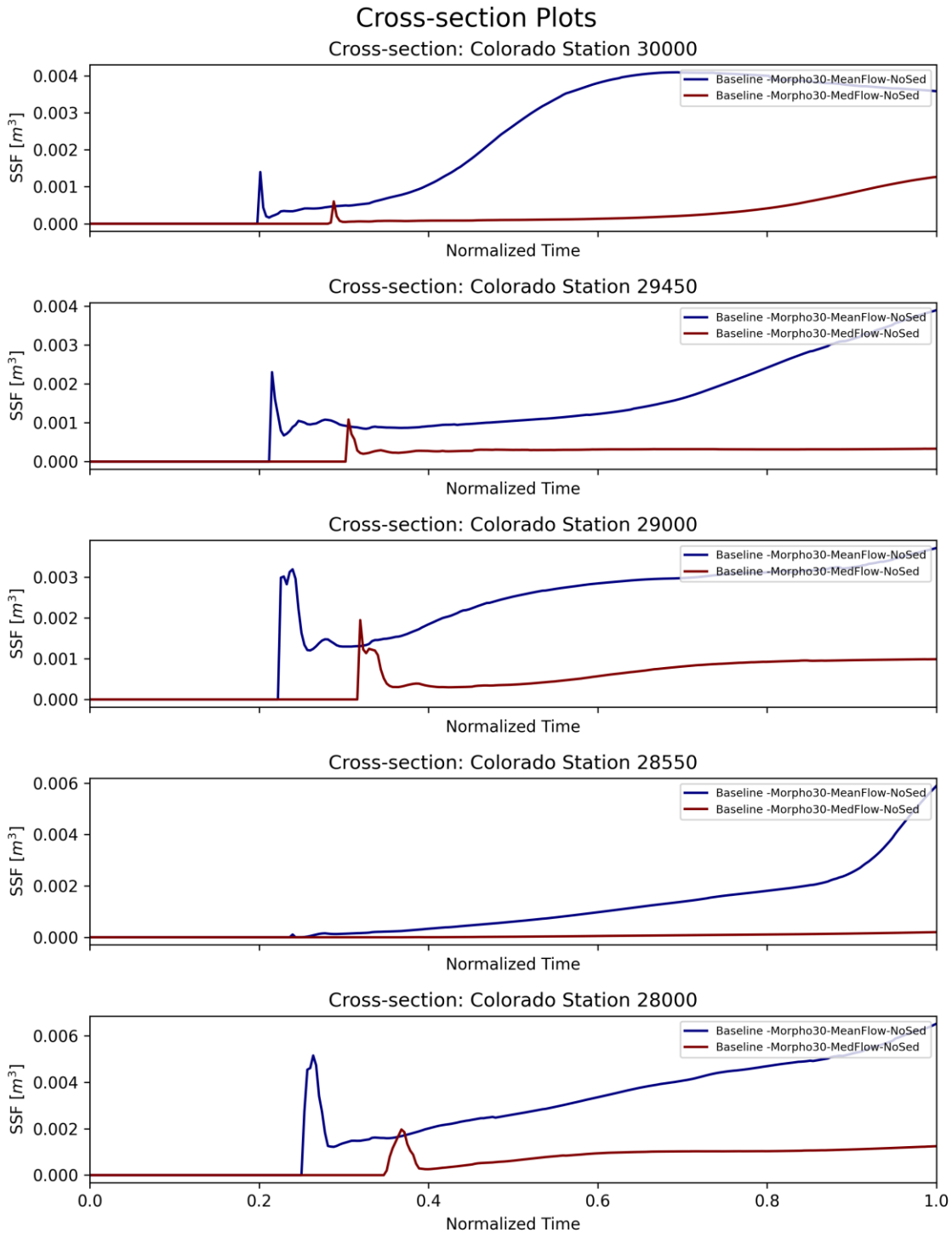
Cross-section Plots
Cross-section: Colorado Station 30000
Cross-section: Colorado Station 29450
Cross-section: Colorado Station 29000
Cross-section: Colorado Station 28550
Cross-section: Colorado Station 28000
Baseline -Morpho30-MeanFlow-NoSed
Baseline -Morpho30-MedFlow-NoSed
SSF [m^3]
Normalized Time
0.000
0.001
0.002
0.003
0.004
0.006
0.0
0.2
0.4
0.6
0.8
1.0

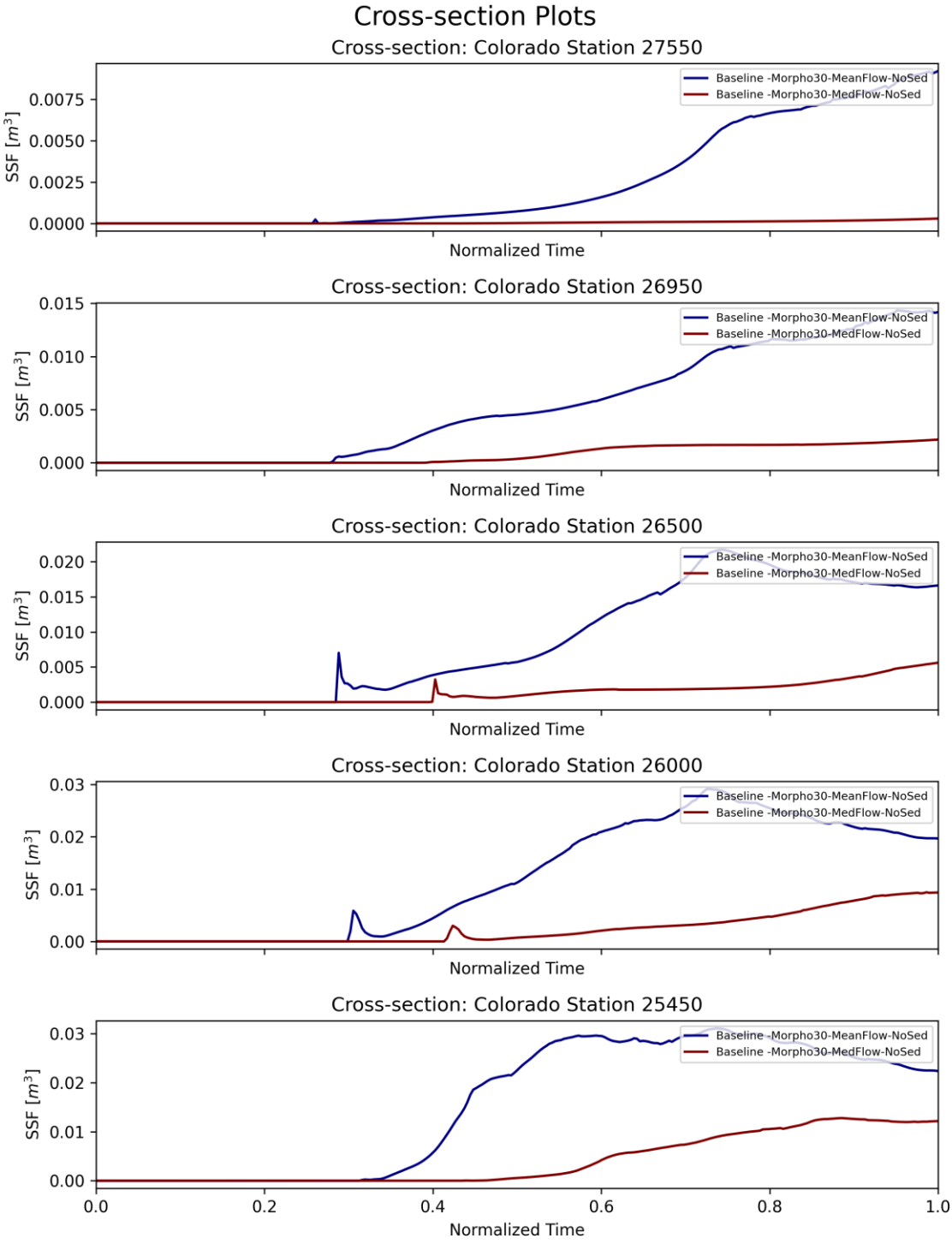
Cross-section Plots
Cross-section: Colorado Station 27550
Baseline -Morpho30-MeanFlow-NoSed
Baseline -Morpho30-MedFlow-NoSed
SSF [m^3]
0.0075
0.0050
0.0025
0.0000
Normalized Time
Cross-section: Colorado Station 26950
0.015
0.010
0.005
0.000
Cross-section: Colorado Station 26500
0.020
Cross-section: Colorado Station 26000
0.03
0.02
0.01
0.00
Cross-section: Colorado Station 25450
0.0
0.2
0.4
0.6
0.8
1.0

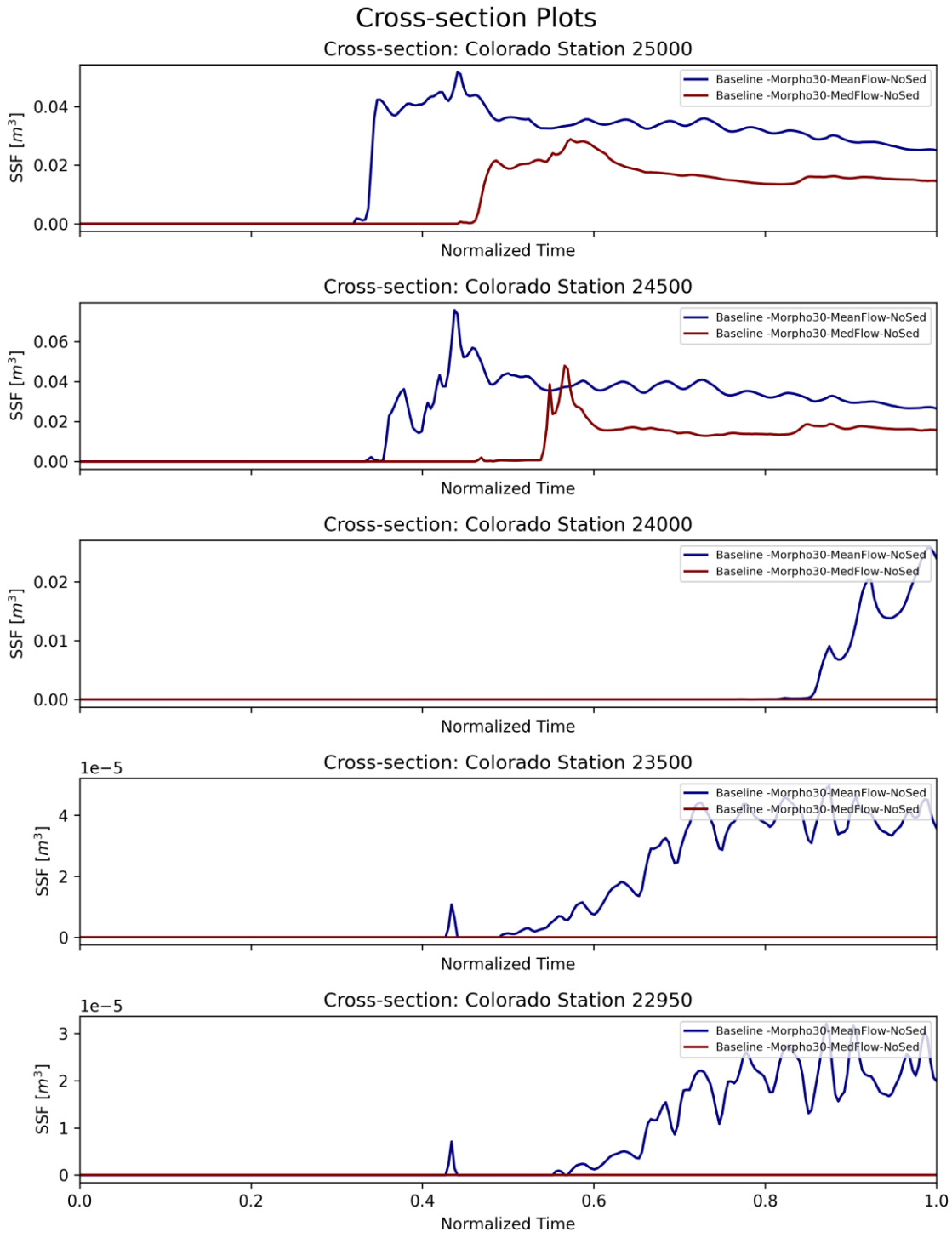
Cross-section Plots
Cross-section: Colorado Station 25000
Cross-section: Colorado Station 24500
Cross-section: Colorado Station 24000
Cross-section: Colorado Station 23500
Cross-section: Colorado Station 22950
Baseline -Morpho30-MeanFlow-NoSed
Baseline -Morpho30-MedFlow-NoSed
SSF [m^3]
Normalized Time
1e−5

UNIVERSITY OF TEXAS ARLINGTON

COASTAL MANAGEMENT PROGRAM – CYCLE 26

BEST PRACTICES IN MODELING SEDIMENT TRANSPORT AND BUDGET ALONG THE TEXAS COAST (CONTRACT NO. 23-020-018-D867)

Task 4: Guidelines for Best Practices

Prepared for:

Texas General Land Office

1700 N. Congress Avenue, Mail Code 158

Austin, TX 78701

Submitted by:

Behzad Nazari, Ph.D., P.E.

Yu Zhang, Ph.D., P.E.

Habib Ahmari, Ph.D., P.E.

The University of Texas at Arlington, Arlington, Texas, USA

September 2024

EXECUTIVE SUMMARY

This report addresses the Task 4 of the Texas General Land Office Project: COASTAL MANAGEMENT PROGRAM – CYCLE 26 BEST PRACTICES IN MODELING SEDIMENT TRANSPORT AND BUDGET ALONG THE TEXAS COAST, focusing on the best practices in modeling sediment transport and budget along the Texas Coast. Building upon previous tasks, it addresses the significant variability in sediment budget and yield estimates, highlighting the challenges faced by coastal managers and engineers in decision-making processes. The study emphasizes the importance of a holistic approach in coastal management, illustrated through case studies of unintended consequences resulting from narrowly focused interventions. It also acknowledges the limitations of purely data-driven management efforts, noting that while more data is beneficial, most collection campaigns provide only snapshots of dynamic coastal systems. Central to the report's findings is the critical role of sediment transport modeling in complementing data collection, while recognizing the inherent challenges in modeling complex coastal systems. The study outlines key considerations in sediment transport modeling, including the need for analyzing multiple scenarios, choosing appropriate modeling platforms, and setting realistic expectations for model capabilities. It also addresses important factors such as scale issues, limitations of stationarity assumptions, the incorporation of sea level rise, and the integration of local coastal features.

The report recommends adopting a comprehensive approach that integrates thorough data collection with targeted, scenario-based modeling techniques. By considering multiple scenarios and employing state-of-the-art modeling approaches, coastal managers and engineers can better recognize the uncertainties inherent in coastal systems and work towards more effective and sustainable coastal management strategies. This study underscores the complex nature of sediment transport in coastal environments and the need for adaptive, flexible approaches in coastal planning and decision-making. It provides valuable insights for stakeholders involved in the sustainable development and protection of the Texas Coast, emphasizing the importance of integrating various data sources and modeling techniques to develop the most reliable estimates possible.

Table of Contents

Executive Summary 2

1. Introduction 4

1.1 Project Overview 4

1.2 Summary of Previous Tasks 4

1.3 Importance of Sediment Transport Modeling 6

1.4 Task 4 Overview and Report Structure 8

2. The Need for a Holistic Approach in Coastal Management 8

2.1 Minimizing the Chances of Unintended Consequences 8

2.2 Historical Lessons in Coastal Management 9

2.3 Limitations of Data-driven Approaches 10

3. Key Considerations in Sediment Transport Modeling 12

3.1 Analyzing Multiple Scenarios 12

3.2 Choosing the Appropriate Modeling Platform 13

3.3 Setting Realistic Expectations for Model Capabilities 14

3.4 Selecting Relevant Processes for Modeling 16

3.5 Determining Sediment Influx Entry Points 17

3.6 Representing Flow-Sediment Load Relationships 17

3.7 Addressing Scale Issues 18

3.8 Recognizing Limitations of Stationarity Assumptions 20

3.9 Incorporating Sea Level Rise 21

3.10 Integrating Local Coastal Features 22

3.11 Addressing Wave Input and Nearshore Transformation 24

4. Conclusions 24

1. INTRODUCTION

1.1 Project Overview

Coastal environments, particularly sedimentary coasts and barrier systems found along the Gulf of Mexico, are dynamic and complex interfaces between land and sea. The intricate interaction of hydrodynamics, sediment movement, and geomorphological changes presents significant challenges in coastal management. Understanding and predicting sediment transport is necessary for sustainable coastal development and protection, as it fundamentally influences coastal behavior and evolution. This document is the report for Task 4 of the project "COASTAL MANAGEMENT PROGRAM – CYCLE 26 BEST PRACTICES IN MODELING SEDIMENT TRANSPORT AND BUDGET ALONG THE TEXAS COAST." This GLO Sediment Management Plan project examined the complexities of sediment transport estimates and modeling, the uncertainties involved and challenges in accurately predicting sediment delivery to the Gulf which thereby affects coastal projects. Before elaborating on the details of Task 4, a brief summary of the previous tasks will be provided to establish context and highlight the project's progression.

1.2 Summary of Previous Tasks

Task 1 of this project conducted a comprehensive review of recent literature on sediment budget studies along the Texas Coast. This review aimed to analyze assessments of major waterbodies, scrutinize methodologies, and identify gaps in existing research. The study focused on eleven waterbody systems that drain into the Gulf of Mexico, including major rivers flowing into the Texas Coast and natural and built passes.

For each system, the review provided detailed descriptions of watershed characteristics, daily flow statistics, annual sediment yield, and information on sediment input from rivers. It also examined sediment input from shoreline erosion and deposition rates where available. The study identified three distinct approaches used for sediment budget analysis along the Texas Coast: quantitative methods, geomorphological models, and field surveys and sampling.

Key findings highlighted significant gaps and uncertainties in sediment data, including limited historical sediment data from USGS gauges, uncertainties in estimating sediment inputs from fluvial sources and coastal shoreline erosion, and limited available data on sediment outputs due to dredging and longshore transport. The review emphasized the need for enhanced methodologies, data integration, and collaborative research efforts to improve the accuracy of

sediment budgeting along the Texas Coast, which is crucial for informed coastal management strategies in the face of ongoing environmental changes and anthropogenic activities.

Task 2 of this project conducted a literature review on the current state of practice in sediment dynamics modeling in coastal areas. The study examined common frameworks for modeling sediment dynamics in coastal rivers and estuaries, identified the advantages and shortcomings of widely used hydro-morphodynamic models, and explored uncertainties and errors in current sediment transport modeling practices.

The review compared quantitative sediment budget models with hydro-geomorphological models, highlighting their respective strengths and limitations. It provided a detailed assessment of nine widely-used hydro-geomorphological models (Delft3D, TELEMAC, MIKE 21, ADCIRC, XBeach, LITPAK, CoSMoS, GENESIS, and SBEACH), focusing on their application in coastal settings and their ability to simulate complex interactions between hydrodynamics, sediment transport, and morphological changes.

The study emphasized the importance of selecting appropriate models based on project requirements and environmental conditions. It also identified potential areas for future improvement in sediment dynamics modeling. This review offers valuable insights for researchers and coastal managers in choosing and applying suitable models for sediment transport studies in coastal areas.

Task 3 of this project focused on morphodynamical scenario analyses for the Brazos River and the Colorado River, contributing to the Texas General Land Office (GLO) Sediment Management Program. The study employed advanced numerical modeling techniques, specifically the Delft3D Flexible Mesh software, to investigate the complexities of sediment transport modeling in these coastal areas.

The research explored various scenarios to highlight uncertainties and potential variability in the results of current sediment transport modeling practices. Key findings included the significant impact of factors such as morphological acceleration, selection of representative flow, sediment type (mud versus sand), and the use of lumped versus spatially variable sediment influx on sediment transport patterns.

The study demonstrated that current morphodynamical models can simulate complex phenomena like the opening of a river mouth during a hurricane, but also discussed remaining challenges. It highlighted the limitations of current approaches to determining representative flows and

proposed using duration-based flow values with morphological acceleration as a potentially more robust method for long-term simulations.

Importantly, the research emphasized the need for caution when interpreting results from morphologically accelerated models and recommended more comprehensive data collection efforts, particularly for sediment composition and distributed sediment inputs along river reaches. These findings provide insights to inform future studies and improve decision-making processes for coastal management projects in Texas and similar coastal environments.

1.3 Importance of Sediment Transport Modeling

Sediment transport modeling is key for effective coastal management and river system analysis. As previously mentioned, an effective modeling campaign is essential in planning large coastal projects, for better understanding project areas' behavior, predicting and managing future changes, and adapting policies for sustainable development and protection of coastal areas. Many past coastal projects were completed without adequate data or knowledge of coastal processes, leading to unforeseen consequences [1], [2]. These have often not been due to negligence or lack of trying. Flow and sediment dynamics occur across various spatial and temporal scales [3], from individual grain movements to large-scale geomorphological changes over decades. These processes are influenced by climate conditions, land use changes, engineering interventions, and extreme events.

Employing modeling frameworks helps evaluate the impact of natural complexities coupled with human interventions. Constructions such as navigational channels, jetties, or coastal armoring can significantly interfere with natural sediment transport processes, disrupting adjacent beaches and altering coastal morphology [2]. In the context of climate change and rising sea levels, accurate sediment transport modeling becomes even more crucial for predicting future coastal changes [4], planning adaptation strategies, and designing resilient coastal infrastructure. Many of these long-term plans require an estimate of how much sediment is available in the system, also known as sediment budget. In addition, investing in modeling efforts can be a cost-effective way to scope a range of possible solutions to coastal problems such as beach erosion, navigational channel deposition, flooding and other coastal related challenges.

Estimating sediment delivery to the coast is a complex process that often yields significantly different results depending on the methods and analyses used [5]. This variability stems from the intricate nature of sediment transport systems and the numerous assumptions required in any estimation approach.

The process of sediment delivery to the coast can be broadly divided into two main components. The first involves quantifying how much sediment enters rivers and water bodies from the surrounding landscape. This is influenced by factors such as rainfall patterns, soil types, land use, topography, and vegetation cover. Methods for estimating this input range from simple empirical equations to complex physically-based models, each with its own set of assumptions and limitations.

The second component focuses on how these sediments move through the channel system and other connected water bodies, undergoing sink and sources processes of erosion, deposition, and transport along their path to the coast. This phase is equally complex, involving interactions between water flow, channel morphology, and sediment characteristics. Factors such as river discharge, flow velocity, channel geometry, and sediment grain size all play central roles in determining sediment movement.

Estimates of sediment delivery often vary widely due to the wide range of components, and interactions among these factors [5]. For instance, different sampling techniques, temporal and spatial scales of measurement, and modeling approaches can lead to divergent results. The choice of scales for analysis can also significantly impact results, as sediment transport can vary considerably between normal conditions and extreme events and floods [6].

Furthermore, human interventions such as dams, land-use changes, and river engineering works add exponential layers of complexity to these estimates [7]. These alterations can significantly modify natural sediment transport patterns, making historical data less reliable for future projections.

Despite the intrinsic challenges and uncertainties involved, these estimates of sediment yield are still recommended due to the very substantial impact they have on coastal processes. This sediment influx plays a vital role in maintaining beaches, barrier islands, and deltas, as well as influencing coastal ecosystems and water quality. Underestimating or overestimating sediment delivery can lead to misinformed coastal management decisions, potentially exacerbating issues like coastal erosion or excessive sedimentation in ports and harbors.

Given these challenges, researchers and coastal managers must often use multiple methods and integrate various data sources to develop the most reliable estimates possible. This might involve combining field measurements, remote sensing data, historical records, and advanced modeling techniques. Despite these efforts, a degree of uncertainty in sediment delivery estimates remains

an inherent aspect of coastal sediment management, underscoring the need for adaptive and flexible approaches in coastal planning and decision-making.

1.4 Task 4 Overview and Report Structure

Task 4, the focus of this document, builds on the previous tasks and findings that confirmed the considerable variability in sediment budget and yield estimates, highlighting how different methods, analyses, and assumptions can lead to divergent results, complicating decision-making for coastal managers and engineers.

In the following sections, we will present a series of case studies that demonstrate the real-world implications and the consequences of inadequate understanding sediment transport processes or modeling. These examples serve as cautionary tales, showing how coastal projects built without sufficient data or understanding of coastal processes can lead to unforeseen and often problematic outcomes. We also address the shortcomings of purely data-driven management efforts, noting that while more data is an obvious solution, most collection campaigns provide only snapshots of the dynamic and non-stationary nature of coastal system. This limitation underscores the importance of modeling in complementing data, while also acknowledging the challenges inherent in modeling such complex systems.

This report concludes with recommendations for best practices in sediment transport modeling. These include adopting a comprehensive approach that integrates thorough data collection with thoughtful, scenario-based modeling techniques. By considering multiple scenarios and employing state-of-the-art modeling approaches, coastal managers and engineers can use their best available tools to better recognize the uncertainties inherent in coastal systems and work towards more effective and sustainable coastal management strategies.

2. THE NEED FOR A HOLISTIC APPROACH IN COASTAL MANAGEMENT

2.1 Minimizing the Chances of Unintended Consequences

It is a very common occurrence that a coastal project has shown adverse impacts beyond its intended geographical domain [2]. This need for coordination before various coastal projects and multi-objective optimization to meet often competing sectors of economy, ecosystem, environment, navigation, sustainability, and natural hazard protection is not a trivial task. Sediment transport modeling can offer insights to better inform such complicated management decision making. For example, beach nourishment as one of the most common objectives of coastal projects, demonstrates the need for accurate modeling to understand and predict coastal behavior [8]. In the long-term, two known processes diminish the expected gained beach width:

the equilibration of the on-offshore beach profile and longshore spreading. The equilibration occurs on a shorter time scale of months or years, involving a transfer of sand from the dry beach to offshore areas to form an equilibrium profile. Longshore spreading causes sand to spread out in alongshore directions over several years to decades. Understanding these processes through modeling is important for planning periodic renourishment and maintaining long-term beach protection.

2.2 Historical Lessons in Coastal Management

The literature shows many case studies that highlight the critical importance of a holistic approach when developing coastal management strategies [2]. A recent study examined the complex interplay between various shoreline protection strategies and sea-level rise scenarios in San Francisco Bay, California [1]. Their analysis showed significant unintended consequences of localized flood protection measures that protecting individual shoreline segments, ranging from 5 to 75 kilometers in length, can have far-reaching impacts beyond the immediate area. In some cases, these localized interventions led to increased flooding in other regions, with volumes reaching up to 36 million cubic meters for a single flood event. The economic consequences of such displaced flooding are substantial, potentially causing up to $723 million in damage elsewhere. Most strikingly, the research uncovered instances where the regional flood damage resulting from localized protection measures actually exceeded the damages prevented [1]. This finding underscores the interconnected nature of coastal systems and the potential for well-intentioned but narrowly focused interventions to exacerbate overall risks. Coastal engineering textbooks cite many such examples.

The case of Ponce de Leon Inlet in Florida [2] is among those examples that clearly illustrates the complexities of coastal engineering projects. In 1970, a weir jetty system was constructed, including a weir in the updrift jetty and a deposition basin. However, the project encountered significant problems, including structural issues with the weir section, erosion of the valuable updrift beach, and migration of the inlet channel into the deposition basin. These issues led to public pressure and eventual modification of the project, highlighting the importance of comprehensive sediment transport modeling in project design and prediction of outcomes.

Port Orford in Oregon [2] demonstrates the importance of understanding equilibrium in both planform and profile when designing coastal engineering projects. A protective structure built on a rocky ledge in 1965 to increase sheltering at a loading pier had unintended consequences. It disrupted the planform equilibrium of the embayment, caused shoreline advancement and

shoaling at the pier, and led to sand being drawn predominantly from the south. This example underscores the need for thorough understanding of the forces in balance in natural coastal systems before intervening.

The Santa Barbara Harbor [2] case exemplifies the principle of Environmental Unity, showing how a single change can have far-reaching consequences. The L-shaped breakwater completed around 1929 interrupted the natural flow of sand along the shoreline, leading to the formation of a wide beach west of the breakwater and a problematic sand spit within the harbor. It also triggered substantial coastal erosion in nearby areas, necessitating ongoing dredging efforts and additional protective measures along the affected coastline.

These historical cases highlight the long-term impacts that must be considered in coastal development projects, which can be better predicted through advanced sediment transport modeling.

2.3 Limitations of Data-driven Approaches

Data plays a fundamental role in understanding and predicting sediment transport processes. Due to the complexities involved in coastal systems, many different types of data are required, including bathymetry, flow characteristics of discharge and water levels, wave characteristics, current velocities, sediment grain sizes, and meteorological conditions. Biological and chemical data may also be necessary in some cases, especially when dealing with cohesive sediments or in estuarine environments.

However, having abundant data alone is not sufficient to fully understand the intricacies of sediment behavior in coastal systems. The challenge lies in capturing all the various combinations of regimes and scenarios that occur in coastal and riverine environments. Most data collection campaigns collecting sediment information are limited to isolated points in the area and are conducted only a limited number of times, providing snapshots rather than continuous observations. While some long-term collection efforts exist in rare cases, even these are typically confined to certain geographical locations and fail to capture the overall big picture of sediment dynamics across an entire system interconnected process.

This limitation in data coverage and temporal resolution is precisely why modeling becomes so essential in projects that require sediment transport studies. Models allow us to interpolate and extrapolate from limited data points, providing insights into areas and time periods where direct measurements are not available. They help us understand the broader patterns and trends in sediment movement that may not be apparent from discrete data points alone and predict the

general behavior of the system in the future due to many controlling phenomena that have not occurred yet.

However, modeling itself comes with its own set of challenges [10]. The physics of sediment transport is not fully understood in all scenarios, particularly in complex environments with mixed sediment types or in the presence of interconnected networks of man-made channels and coastal structures. This leads to uncertainties in the mathematical representations used in models. Moreover, the many available equations predicting sediment transport are diverse, often highly non-linear and sensitive to initial conditions, making them challenging to implement accurately. The configuration of models also requires careful consideration, as choices in computational aspects such as computational grid, time steps, and boundary conditions can significantly impact results.

Given these challenges in both data collection and modeling, one can argue the best approach is to prepare the process-based models with as much data as possible while acknowledging limitations. The outcomes of such analysis should then be used to inform the rest of modeling efforts, but not as a sole source of certainty. Instead, modelers should make reasonable assumptions about the range of possible conditions and parameters that are not fully captured by collected data. By running models for these ranges of possibilities, they can obtain bands or envelopes within which the system is more likely to operate, rather than trying to predict exact outcomes, which seems impossible within the current technological landscape.

This approach of using data-informed modeling to explore a range of scenarios has several advantages. First, it acknowledges the inherent uncertainties in both our data and current understanding of sediment transport processes. Second, it provides decision-makers with a more realistic view of possible outcomes, allowing for more nature-representative planning and design. Finally, this method can highlight potential "red flags" that could be indicative of scenarios or outcomes that may require additional investigation.

For example, if model results consistently show extreme erosion under certain conditions, even at the lower end of the probability spectrum, this might flag the need for more detailed study of those specific conditions or the consideration of preventative measures in coastal management plans.

In the end, while comprehensive data collection remains a cornerstone of sediment transport studies, its integration with scenario-based modeling approaches offers a promising path forward in this complex field. This combined approach allows managers and stakeholders to make the

best use of limited data, account for uncertainties, and provide meaningful insights to guide coastal and riverine management decisions.

3. KEY CONSIDERATIONS IN SEDIMENT TRANSPORT MODELING

This section explores a range of important considerations in sediment transport modeling, drawing from lessons learned in this project and the study of related works. While not exhaustive, these aspects represent important factors that modelers should take into account when developing and applying sediment transport models in various coastal and riverine contexts.

3.1 Analyzing Multiple Scenarios

Analyzing multiple scenarios allows modelers to explore a range of potential outcomes, from baseline conditions to gradual environmental changes and extreme events. This comprehensive approach provides a general understanding of how different factors interact over time, enabling planners to identify robust strategies that perform well across various possible outcomes and to anticipate unexpected consequences that might arise from seemingly straightforward interventions.

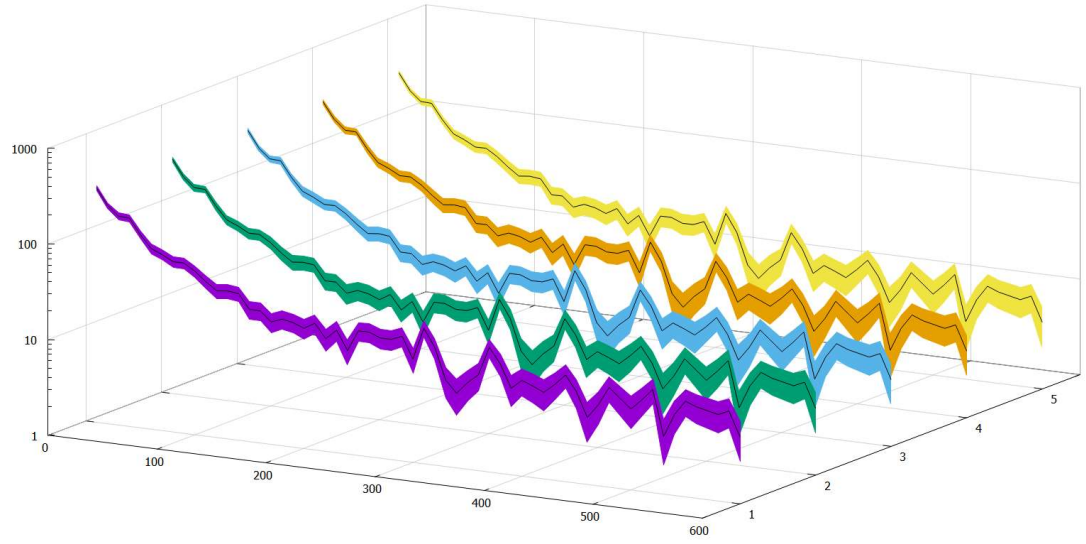

Figure 1 Scenario analysis can enhance forecasts for the complex nature of sediment transport

The scope of the modeling scenarios can be narrowed down based on the specifics of each project. When modeling the effects of coastal armoring, both short-term protection benefits and long-term impacts on adjacent beaches and offshore profiles should be considered. For navigational projects, careful modeling of the trade-offs between initial capital costs (e.g., dredging) and subsequent maintenance costs could become beneficial.

Building flexibility into modeling based on the type of coastal project being addressed allows for adjustments based on observed behaviors, helping to mitigate unforeseen consequences. Accordingly, following a very rigid modeling framework may not be adequate for the wide diversity of processes in coastal environments.

Differentiating between sediment types, particularly cohesive and non-cohesive sediments, is important as they behave differently under various hydraulic conditions. Using field measurements, including techniques such as monitoring deposition in test pits or installing suspended sediment traps, enhances the reliability of modeling efforts.

3.2 Choosing the Appropriate Modeling Platform

Sediment budget studies are essential for understanding sediment behavior in coastal watersheds, providing insights into sediment mobilization, transfer, and storage at the catchment scale. However, modeling the complete journey of sediments in a single platform is most likely not a feasible task. Sediment budgets typically account for sediment contributions from hillslopes, gullies, and riverbanks [11]. The complex interactions between these sources vary significantly with catchment size and characteristics, making accurate sediment yield estimations challenging. Larger catchments often see reduced contributions from surface sources due to increased sediment transit time and more opportunities for deposition. Conversely, riverbank erosion through mass failure, fluvial erosion, and weathering processes may become more prominent in larger catchments [11]. This dynamic interplay between erosion and deposition significantly impacts the balance of sediment contributions from different sources to total catchment loads.

Accurately differentiating between upland and riverine sediment sources is a complex task that requires advanced fingerprinting techniques [11]. These methods employ a range of tracers, including radionuclides, mineral magnetism, spectrocolorimetry, compound-specific stable isotopes, and environmental DNA. Newer approaches also utilize phytoliths and color-based tracing. Studies using these techniques have revealed that riverbank contributions to sediment yield can vary dramatically, ranging from as low as 3.6% to as high as 93.6% of the total sediment budget.

This variability in sediment sources presents significant challenges for modeling sediment budgets and yields. Watershed-scale models like SWAT are designed for long-term simulations at low spatial resolutions, making them suitable for modeling sediment at the watershed level. However, these models struggle with event-based simulations and complex flow dynamics [12],

particularly in coastal regions prone to tides, storms, and flooding. They also fail to accurately simulate the bidirectional flow and sediment movement in coastal areas [12]. The spatial and temporal scales of these models are usually too coarse to make them a good candidate for analyzing the impact of local coastal projects.

Hydrodynamic and morphodynamic models such as those reviewed in Task 2 of this project are better at simulating detailed sediment transport dynamics in specific water bodies, including rivers, estuaries, and coastal areas. These models can handle complex flows and sediment movement, but their high computational cost typically limits them to shorter simulation periods. While effective for tidal cycles or storm events, they are generally less suitable for analyzing sediment sources at the watershed scale.

Given these limitations, an ideal approach may involve combining watershed-scale models with hydrodynamic models to provide a comprehensive analysis of sediment dynamics from watershed to coast. However, implementing such a coupled strategy is challenging and heavily dependent on data availability. Many coastal watersheds face significant limitations in hydrological and sediment data, which can be periodic, spatial, or temporal in nature. These data constraints further complicate and delay modeling efforts.

Ultimately, to improve modeling of sediment dynamics, long-term monitoring of turbidity and sediment loads at representative gauge stations is crucial. This data would allow for a more thorough examination of variability and distribution patterns, leading to more accurate and improved coastal management strategies.

3.3 Setting Realistic Expectations for Model Capabilities

Sediment transport processes are inherently complex and notoriously difficult to simulate and predict precisely using mathematical equations [13]. However, this complexity is precisely why process-based models often prove more capable than those relying solely on data. As previously discussed, no matter how extensive, available data is rarely sufficient to capture the full range of coastal dynamics.

Mathematical models for coastal processes involving sediment transport face similar challenges to river models. These models are complex semi-empirical tools that provide valuable insights but have significant limitations [14]. Like river models, coastal sediment transport models are not closed systems and require substantial empiricism to complete governing equations and boundary conditions. This reliance on empirical data complicates rigorous verification.

Despite these limitations, sediment transport models are useful advancements over simpler methods, incorporating improved understanding of coastal physics. However, their predictive capability is often overstated. Overestimating these models' predictive role can lead to misguided coastal management decisions.

To improve sediment transport modeling, strategic studies are needed to define benchmark processes and assess individual model components. Developing systematic guidelines could optimize model-based decision-making in riverine and coastal environments.

Process-based mathematical sediment transport models should be used with a clear understanding of their limitations and not be mistaken for infallible predictive tools in complex coastal systems [14]. While not perfect, they can provide valuable insights into the directions of erosion and deposition, as well as general behavioral patterns with reasonable accuracy. These models incorporate fundamental physical principles, allowing them to extrapolate beyond the limits of available data and provide meaningful predictions even in novel scenarios.

The calibration and verification/validation methodology in sediment transport modeling is often problematic and misrepresented [14]. Terms like “verification” and “validation” overstate model performance, potentially misleading decision-makers and the public. In reality, this process only demonstrates that a model with specific parameter combinations can match certain observations. Claiming predictive capability based on such limited agreement, without considering overall performance indicators, is risky [14], especially in complex coastal systems. The dynamic nature of these environments means that a model's ability to fit past data does not guarantee accurate predictions of future conditions, particularly under changing environmental scenarios. This limitation is crucial to recognize when applying sediment transport models to coastal management decisions.

Understanding the strengths and limitations of different model types is crucial. For instance, there are significant differences between morphological models focused on coastal processes and watershed-level sediment yield estimates. While some integration between these approaches is possible, they cannot be used interchangeably. Morphological models are better for simulating nearshore processes and shoreline changes, while watershed models are better suited for estimating sediment delivery from river systems.

In practice, the most effective approach often involves using multiple models in combination, each addressing specific aspects of the sediment transport system. This multi-model approach

can provide a more comprehensive understanding of sediment dynamics across different spatial and temporal scales.

Ultimately, while sediment transport models have made significant advancements, it is important to maintain realistic expectations [14]. These models are tools for understanding and exploring physical processes under simplifying assumptions rather than for high reliability deterministic prediction. Their value lies in their ability to inform decision-making by identifying potential trends, vulnerabilities, and responses to different scenarios, rather than in providing exact forecasts of future conditions.

3.4 Selecting Relevant Processes for Modeling

An integrated two-way coupling of hydrodynamics, sediment transport processes is usually considered a morphodynamic model. Ideally, this model is not just a standardized simulation tool; it is customized as a sophisticated integration of various coastal processes and features, designed to predict and understand the long-term evolution of coastlines. The methodologies employed, from wave input handling to the simulation of morphological tide, are all geared towards creating a tool that is robust and also intricately aligned with the complex realities of coastal dynamics. However, many times such a comprehensive model development may not be feasible due to time or budget constraints. Therefore, many influential controlling processes might be overlooked inadvertently. This is inevitable unless the neglected processes are integral to the project. In that case, a careful consideration of modeling frameworks are required to arrive at an optimal tradeoff between accuracy and availability of resources.

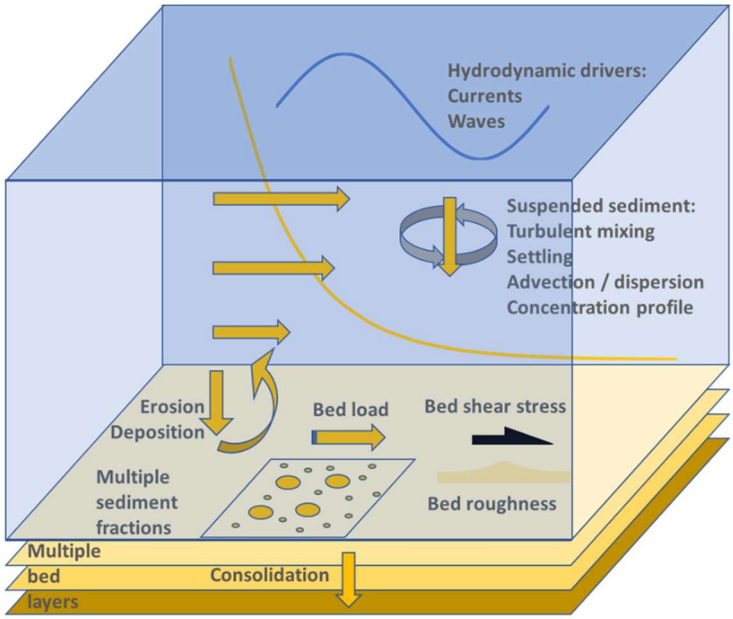

Figure 2 Many processes are involved in flow- sediment dynamics [15]

3.5 Determining Sediment Influx Entry Points

The sand that constitutes much of the Texas shoreline along the Gulf of Mexico is in continual motion. Tides, storm surges, wave action, wind, river processes, and longshore (littoral) drift act upon the sand and transport it along the shoreline to form and erode beaches, barrier islands, and peninsulas. Some of the sand supplied to this process originates in upland areas and is transported to the Gulf of Mexico by rivers and streams. Most of these rivers and streams discharge into bays or estuaries, which eventually will fill with sediment.

Shoreline changes in the form of beach erosion are aggravated by decreased sand input to the coast from the rivers because of alterations to the rivers and their drainage basin. The transport of sediment in most rivers is affected by many interdependent factors along the main stem and tributaries, basin hydrology (particularly extreme events), water-resource development, and human activities. This complex interplay of factors highlights the challenges in accurately predicting and managing sediment transport from rivers to coastal areas, underscoring the need for comprehensive, system-wide approaches.

Without considering this upstream contribution, efforts to manage coastal erosion, deposition, and overall shoreline stability may be incomplete or ineffective, potentially leading to unintended consequences along the coast. Any major project affecting coastal environments must consider the spectrum of riverine and coastal interactions to ensure sustainability and minimize unforeseen impacts. Ignoring these broader influences can lead to significant and potentially irreversible changes in coastline morphology, emphasizing the importance of a holistic perspective in managing coastal regions.

3.6 Representing Flow-Sediment Load Relationships

Sediment inflow under various flow regimes is typically prescribed as boundary conditions in hydrodynamic and sediment transport models, often in the form of sediment discharge relations or Load Duration Curves (LDCs). While LDCs aim to represent sediment loads across various flow conditions, they can be oversimplified and may not capture the full complexity of sediment transport processes. Here are some key issues to consider:

- Complex flow patterns: LDCs can oversimplify flow dynamics by not accounting for various complex flow patterns. For example:
    - Reverse flows in tidally influenced gauges
    - Differences between floodplain and main channel flows during high water events

    - Secondary currents in meandering river sections
    - Flow variations due to in-stream structures or natural obstacles
- Misrepresentation of high flows: LDCs often assume a consistent increase of sediment load as a function of discharge. However, in reality, there could be a supply-limited cap during extreme events, leading to overestimation of sediment transport.
- Hysteresis effects: Sediment transport can exhibit hysteresis, where the sediment concentration differs between the rising and falling limbs of a flood hydrograph. This occurs because loose sediment may be depleted during the rising limb, leaving the bed too armored for significant transport during the falling limb, even at the same discharge.
- Seasonality: LDCs typically do not account for seasonal variations in sediment transport, which can be significant due to changes in vegetation cover, soil moisture, and land use practices.
- Particle size distribution: LDCs often cannot adequately represent the full range of particle sizes present in a system, which can lead to inaccuracies in transport estimates.
- Bed forms and channel morphology: The presence and evolution of bed forms, as well as changes in channel morphology, can significantly affect sediment transport but are not typically captured in LDCs.
- Anthropogenic influences: Human activities such as dam operations, land use changes, or dredging can alter sediment dynamics in ways that are not reflected in a single LDC.

These complexities highlight the challenges in accurately representing sediment transport in coastal and riverine systems. They emphasize the need for careful consideration and potentially more sophisticated approaches when using LDCs in sediment transport modeling, especially in complex coastal environments.

3.7 Addressing Scale Issues

Accurately representing long-term sediment regimes by analyzing historical data is key, as is incorporating the effects of environmental stressors such as climate change, sea-level rise, and changes in land use. Modern models can account for temporal and spatial variability in sediment supply and transport across different timescales and spatial scales ([4], [9], [13]), and also consider the impacts of extreme hydrological events on sediment transport and coastal morphology. However, the scales at which the long-term effects are considered are different from event level analysis. Usually, large flooding events contain enough energy to create morphological changes and most of morphodynamical models can replicate this. However,

forecasting long-term morphological changes in non-extreme flow conditions face a scale discrepancy obstacle.

Addressing the inherent disparity between hydrodynamic and morphodynamic time scales is a challenge in coastal modeling. Modelers can tackle this by implementing a “morphological acceleration factor” [16]. This factor is usually not arbitrarily chosen; it is calculated to bridge the gap between the time scales, enabling us to simulate long-term coastal morphodynamics efficiently and accurately.

In addition to storm generated wave dynamics, tidal action plays a substantial role in shaping coastlines. Advanced modeling approaches include the simulation of “morphological tide” [17], a concept pivotal in understanding and predicting the long-term effects of tidal forces on coastal morphology based on a repetitive tidal pattern. This aspect ensures that the model is not just wave-centric but offers a comprehensive view of coastal dynamics. These concepts are relatively new. Although they have shown very promising results and seem to be essential in effective coastal management, their use requires additional consideration and careful trail and error.

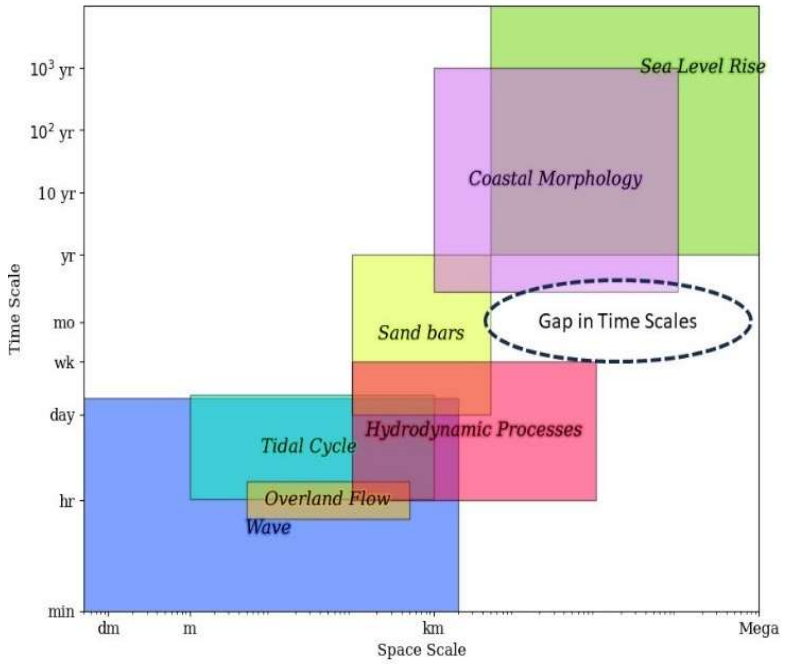

Fig. 3. Typical spatiotemporal scales of coastal processes, the discrepancy and the need for morphological acceleration.

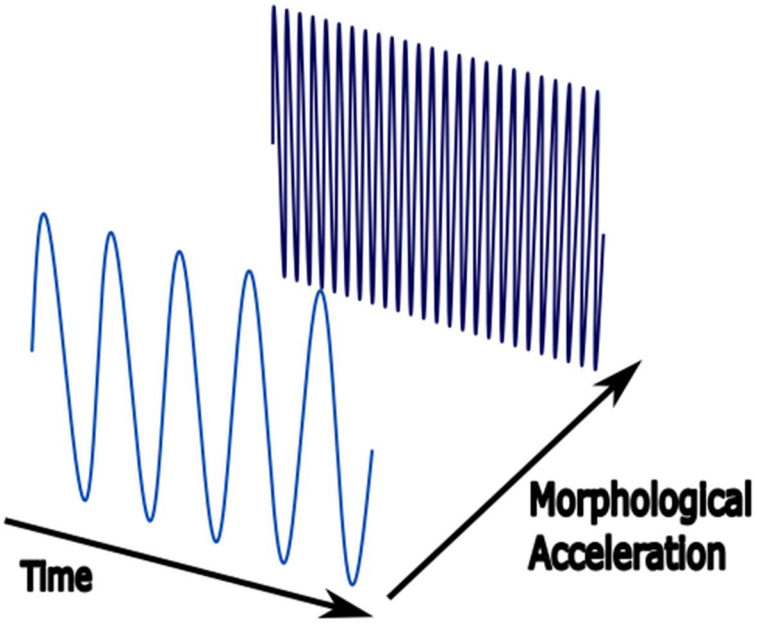

Figure 4 Morphological acceleration acts as a compression filter.

3.8 Recognizing Limitations of Stationarity Assumptions

Stationarity in sediment transport regimes is a decisive concept that is often overlooked in river and coastal management studies. The sediment transport regime in rivers is a complex process influenced by numerous, constantly changing factors [18]. This complexity is particularly evident in Texas rivers and their impact on the Gulf of Mexico coastline ([8], [9]). Potential sources of change in sand transport include the effects of reservoir construction, changes in land use, and instream sand and gravel mining. However, interpreting these changes is not always straightforward.

Extensive reservoir construction typically reduces sand transport by trapping sediment and reducing the magnitude of peak discharges. Yet, this reduction may be offset by increases associated with tributary sediment inflow and localized bank erosion [9]. These compensatory mechanisms highlight the non-linear nature of sediment transport systems and the challenges in predicting their behavior.

The combination of limited data availability and long-term changes in morphological regimes introduces additional uncertainty in sediment transport studies. This challenge is compounded by the fact that sediment data are usually sparse and potentially altering over time. The scarcity of

data creates gaps in our understanding of sediment dynamics, while long-term morphological changes can render even the available data inconsistent or outdated.

Given these complexities, it might be more informative to analyze periods with fewer changes separately in sediment transport modeling. Grouping behavior collectively over long periods overlooks important nuances and may result in very inaccurate or outdated estimates. This approach recognizes that the assumption of stationarity – the idea that natural systems fluctuate within an unchanging envelope of variability – may not hold true for sediment transport regimes over extended periods.

3.9 Incorporating Sea Level Rise

Building on our discussion of non-stationarity in sediment transport processes, we now turn to a related and even more significant long-term factor: sea level rise. While non-stationarity describes changes in system behavior over time, sea level rise represents a persistent, directional shift that fundamentally alters coastal environments [4]. This phenomenon amplifies the challenges of non-stationarity, making it crucial to consider in long-term coastal management and modeling efforts.

In Texas coastline, three major river deltas - Rio Grande, Brazos-Colorado, and Trinity have been significant sediment sources throughout the Holocene period, but their influence is now being reshaped by both historical changes in sediment supply and the ongoing effects of sea level rise. As sediment supply from these rivers decreased over time, wave action began eroding the deltaic headlands, redistributing sediments along the coast [8].

This process of shoreface erosion and longshore sediment transport has been instrumental in shaping the Texas coastline and its barrier islands. The Texas coastline alternates between deltaic headlands, where rivers deposit sediment into the sea, and interdeltaic embayments, which are the curved sections of coast between these headlands. This arrangement creates a complex sediment transport system along the shore.

At each deltaic headland, sediment transport tends to move in both directions along the coast away from where the river meets the sea. This happens because these areas are more exposed to waves coming from different directions. In the interdeltaic embayments, the pattern is different. Here, longshore currents carrying sediment from the neighboring deltaic areas often meet, leading to sediment accumulation in these curved sections of the coast [8].

This pattern of sediment moving away from deltas and gathering in the embayments creates a dynamic system of sand movement along the coast. This process plays a significant role in shaping and maintaining barrier islands and other coastal features.

In the context of sea-level rise, understanding these long-term sediment dynamics becomes even more critical for coastal modeling and management. Sea-level rise can accelerate coastal erosion, potentially altering the delicate balance of sediment supply and distribution that has shaped the coast over millennia. It may lead to increased flooding of low-lying deltaic areas, changing patterns of sediment deposition and erosion.

Moreover, as sea levels rise, the wave base will shift, potentially affecting the depth to which shoreface erosion occurs. This could alter the volume and characteristics of sediment available for longshore transport and barrier island maintenance. The convergence zones of sediment transport may also shift, impacting the distribution of sand along the coast.

These long-term processes underscore the importance of incorporating sea-level rise scenarios in sediment transport modeling [4]. Models in support of important long-term projects need to account not only for current sediment dynamics but also for how these dynamics might change under different sea-level conditions. This approach can provide more accurate predictions of future coastal morphology and inform more effective strategies for coastal management and adaptation to changing dynamics.

3.10 Integrating Local Coastal Features

Coastal environments exhibit a rich variety of local features that significantly influence sediment dynamics [2]. When designing coastal projects, it is essential to consider the interaction between different coastal features such as tidal inlets, barrier islands, and estuaries. Models must accurately represent the hydrodynamic and sedimentological effects of these structures to predict their impact on beach morphology.

Nearshore bathymetry, for instance, plays a critical role in wave transformation and sediment movement. The presence of sandbars, troughs, and rip channels creates complex patterns of wave breaking and nearshore currents, directly affecting sediment transport patterns.

Coastal structures such as groins, jetties, and seawalls interact with natural processes, often altering local sediment transport pathways. These structures can create areas of accretion and erosion, changing the shoreline configuration over time.

The composition of beach and nearshore sediments is another important local factor. Variations in grain size, sorting, and mineralogy along the coast can lead to differential erosion and deposition patterns.

Figure 5 Intricate configuration of flow and sediment pathways near Matagorda Bay inlet

Coastal vegetation plays a vital role in stabilizing the shoreline and trapping flow related in addition to wind-blown sand. The interaction between vegetation and sediment transport is complex, involving feedback mechanisms that can lead to the formation and maintenance of coastal dunes.

Tidal inlets and estuaries represent dynamic zones of sediment exchange between the open coast and back-barrier environments. The ebb and flood tidal deltas associated with these features are important reservoirs of sediment that can significantly influence adjacent shorelines.

Incorporating these local features and processes into sediment transport models requires a multi-scale approach. Models must be capable of resolving fine-scale processes while also capturing larger-scale coastal behavior. This often involves coupling different types of models, such as wave, current, and morphological models, for developing targeted coastal management strategies.

3.11 Addressing Wave Input and Nearshore Transformation

A critical aspect of coastal modeling is handling of incoming wave and swell, and consideration of how they interact with the coastal topography, affecting sediment transport and shoreline morphology.

For smaller scale projects, a common method is to include wave results from a larger domain at the boundary of smaller model domains, ensuring that the input is both accurate and representative of larger-scale dynamics while achieving efficiency as local near shore wave transformation can be simulated many times focusing on the study area. This approach ensures that our simulations are both globally relevant and locally precise, capturing the unique dynamics at play in specific coastal areas.

4. CONCLUSIONS

This report explored the complexities and best practices in modeling sediment transport and budget along the Texas Coast, highlighting the critical importance of a holistic approach in coastal management. Through the discussion of various case studies and analysis of modeling techniques, the report emphasized the intricate nature of coastal systems and the challenges inherent in predicting their behavior.

The variability in sediment budget and yield estimates, as shown in this study, emphasizes the need for caution when interpreting model results and making management decisions. The findings indicate that while data collection is crucial, it often provides only snapshots of a dynamic system. Thus, the integration of comprehensive data with advanced modeling techniques emerges as a key strategy for understanding and managing coastal environments effectively.

The analysis of different modeling approaches, from watershed-scale to hydrodynamic models, shows the importance of selecting appropriate tools for specific contexts. The report highlighted the need to consider multiple scenarios, incorporate local coastal features, and account for long-term factors such as sea-level rise in modeling efforts. The limitations of assuming stationarity in sediment transport regimes were addressed, pointing to the need for adaptive management strategies.

Looking forward, the findings of this report can be used by coastal managers, engineers, and policymakers. By adopting a comprehensive approach that combines thorough data collection with targeted, scenario-based modeling techniques, stakeholders can better navigate the

uncertainties inherent in coastal systems. This approach enables more informed decision-making, potentially leading to more sustainable and effective coastal management strategies.

5. REFERENCES

[1] M. A. Hummel, R. Griffin, K. Arkema, and A. D. Guerry, "Economic evaluation of sea-level rise adaptation strongly influenced by hydrodynamic feedbacks," *Proc. Natl. Acad. Sci. U.S.A.*, vol. 118, no. 29, p. e2025961118, Jul. 2021, doi: 10.1073/pnas.2025961118.

[2] R. G. Dean and R. A. Dalrymple, *Coastal Processes with Engineering Applications*. Cambridge, UNITED KINGDOM: Cambridge University Press, 2004. Accessed: Sep. 13, 2024.

[3] L. Zhu, W. Gong, H. Zhang, W. Huang, and R. Zhang, "Numerical study of sediment transport time scales in an ebb-dominated waterway," *Journal of Hydrology*, vol. 591, p. 125299, 2020.

[4] D. M. FitzGerald, M. S. Fenster, B. A. Argow, and I. V. Buynevich, "Coastal Impacts Due to Sea-Level Rise," *Annu. Rev. Earth Planet. Sci.*, vol. 36, no. 1, pp. 601–647, May 2008, doi: 10.1146/annurev.earth.35.031306.140139.

[5] M. C. Slattery and J. D. Phillips, "Controls on sediment delivery in coastal plain rivers," *Journal of environmental Management*, vol. 92, no. 2, pp. 284–289, 2011.

[6] M. Karimaee Tabarestani and A. R. Zarrati, "Sediment transport during flood event: a review," *Int. J. Environ. Sci. Technol.*, vol. 12, no. 2, pp. 775–788, Feb. 2015, doi: 10.1007/s13762-014-0689-6.

[7] C. Zarfl and A. Lucía, "The connectivity between soil erosion and sediment entrapment in reservoirs," *Current Opinion in Environmental Science & Health*, vol. 5, pp. 53–59, 2018.

[8] M. R. Dhanak and N. I. Xiros, *Springer handbook of ocean engineering*. Springer, 2016. Accessed: Aug. 27, 2024.

[9] D. D. Dunn and T. H. Raines, *Indications and potential sources of change in sand transport in the Brazos River, Texas*. US Department of the Interior, US Geological Survey, 2001. Accessed: Sep. 16, 2024.

[10] D. Vázquez-Tarrío *et al.*, "Effects of sediment transport on flood hazards: Lessons learned and remaining challenges," *Geomorphology*, vol. 446, p. 108976, 2024.

[11] G. Abbas, S. Jomaa, A. Bronstert, and M. Rode, "Downstream changes in riverbank sediment sources and the effect of catchment size," *Journal of Hydrology: Regional Studies*, vol. 46, p. 101340, 2023.

[12] P. Upadhyay, A. Linhoss, C. Kelble, S. Ashby, N. Murphy, and P. B. Parajuli, "Applications of the SWAT model for coastal watersheds: review and recommendations," *Journal of the ASABE*, vol. 65, no. 2, pp. 453–469, 2022.

[13] K. Vercruysse, R. C. Grabowski, and R. J. Rickson, "Suspended sediment transport dynamics in rivers: Multi-scale drivers of temporal variation," *Earth-Science Reviews*, vol. 166, pp. 38–52, 2017.

[14] Z. Cao and P. A. Carling, "Mathematical modelling of alluvial rivers: reality and myth. Part 2: Special issues," *Proceedings of the Institution of Civil Engineers - Water and Maritime Engineering*, vol. 154, no. 4, pp. 297–307, Dec. 2002, doi: 10.1680/wame.2002.154.4.297.

[15] "2D and 3D Sediment Transport and Morphological Modelling - Video," Australian Water School. Accessed: Sep. 13, 2024.

[16] J. A. Morgan, N. Kumar, A. R. Horner-Devine, S. Ahrendt, E. Istanbullouglu, and C. Bandaragoda, "The use of a morphological acceleration factor in the simulation of large-scale fluvial morphodynamics," *Geomorphology*, vol. 356, p. 107088, 2020.

[17] M. Fayyaz, M. Shafieefar, and A. Dastgheib, “Evaluation of the effects of sediment characteristics on long-term estuarine morphological modelling driven by waves and tides,” *Applied Ocean Research*, vol. 92, p. 101919, 2019.
[18] T. J. Coulthard, J. Lewin, and M. G. Macklin, “12 Non-stationarity of basin scale sediment delivery in response to climate change,” *Developments in Earth Surface Processes*, vol. 11, pp. 315–331, 2007.